Physico-chemical stabilization processes for inorganic contaminants in alternative materials

Bader Bouzar

N° d'ordre : ***XXX*** *(à ne mettre qu'après la délivrance du doctorat)*

IMT Nord Europe

UNIVERSITE DE LILLE

THÈSE

présentée en vue
d'obtenir le grade de

DOCTEUR

en
Sciences pour l'ingénieur
Spécialité : Génie Civil
par

Bader BOUZAR

DOCTORAT DE L'UNIVERSITÉ DE LILLE
DÉLIVRÉ PAR L'IMT Nord Europe

Titre de la thèse :

Physico-chemical stabilization processes for inorganic contaminants in alternative materials

Soutenue le 16/11/2022 devant le jury d'examen :

Président	*Nor-Edine ABRIAK, Professeur, IMT Nord Europe*
Rapportrice	*Fabienne BARAUD, Enseignante chercheuse-HDR, Université de Caen*
Rapporteur	*Khalil HANNA, Professeur, Ecole de Chimie de Rennes*
Examinatrice	*Anne PANTET, Professeure, Université du Havre*
Examinatrice	*Charlotte HUREL, Maître assistant-HDR, Université Côte d'Azur*
Directeur de thèse	*Yannick MAMINDY-PAJANY, Maître assistant-HDR, IMT Nord Europe*

Laboratoire d'accueil : Laboratoire du Département Génie Civil et Environnemental de l'IMT Nord Europe École Doctorale SPI 072 (Univ. Lille, Univ. Artois, ULCO, Univ. Polyt. Hauts de Fr., Centrale Lille, IMT Nord Europe)

Summary

Table list……..…..7
Figures list……..…...8
Abstract…….……9
Résumé…….…...…10
Remerciments……11
General introduction……..……...12
Chapter 1 : State of the art ……..……..14
1 Waste management in France 15
1.1 History and definition 15
1.2 Waste Framework Directive (2008/98/EC) 15
1.3 Hazardous and non-hazardous waste 16
1.4 Inert nature of non-hazardous waste 16
1.5 Waste list 16
1.6 Inert Waste Storage Installations 16
1.7 Waste status 18
2 Description of polluted mineral waste 18
2.1 Fly Ash 18
2.1.1 Source 19
2.1.2 Composition 19
2.2 Coal fly ash 20
2.2.1 Source and production 20
2.2.2 Chemical composition 22
2.2.3 Physical characteristics 22
2.2.4 Environmental characteristics 23
2.3 Biomass fly ash 23
2.3.1 Source and production 23
2.3.2 Physical and chemical properties 24
2.3.2.1 Biomass type 24
2.3.3 Biomass fly ash chemical composition 25
2.4 Paper waste ash 26
2.4.1 Physical characteristics 26
2.4.2 Chemical composition of paper mill fly ash 26
2.4.3 Mineralogical characteristics 28
2.5 Sediment 28

2.5.1 Origin and problematic of sediments 28
2.5.2 Fluvial sediments 29
2.5.3 Marine sediments 29
2.5.4 Sediment composition 29
2.5.4.1 Mineral phase 30
2.5.4.2 Inorganic phase 30
2.5.4.3 Organic phase 30
2.5.4.4 Liquid phase 30
2.5.4.5 Sediment particle size 31
2.5.5 Issues related to the management of dredged sediments 31
2.5.5.1 Pollutants in sediments 31
2.5.5.2 Organic pollutants 32
2.5.5.3 Metallic and metalloids trace elements (MMTE) 32
2.5.6 Dredging technology 34
2.5.7 Dredging techniques 34
2.5.7.1 Quantity of dredged material 34
2.5.7.2 Regulatory aspects of dredged material management 35
2.5.7.3 Immersion regulations 35
2.5.7.4 Landfill regulations 36
2.5.8 Treatment 36
2.6 Shooting range soil 36
2.6.1 Identification of environmental problems in the fields 37
2.6.2 Pollution in the vicinity of shooting installations 38
2.6.3 Contamination at small arms shooting sites 39
2.6.4 Metal toxicity 40
2.6.5 Availability of metals in soils and hazardousness 40
2.6.6 Elimination of shooting range soil 41
3 Physico-chemical stabilization of mineral waste 42
3.1 Retention mechanisms 43
3.1.1 Role of physico-chemical parameters 44
3.2 Alkaline waste carbonation technology 44
3.2.1 Carbonation mechanisms 45
3.2.2 Carbonation-influencing parameters 47

3.2.3 Environmental interest 47
3.2.4 Carbonation stabilization of alkaline waste 48
3.3 Geopolymers technology 50
3.3.1 Geopolymerization 51
3.3.2 Parameter influencing geopolymerization 53
3.3.2.1 Influence of alumino-silicate source 53
3.3.2.2 Influence of water quantity 53
3.3.2.3 Influence of the alkali cation 54
3.3.2.4 Influence of the Si/Al ratio 54
3.3.2.5 Influence of treatment parameters 55
3.3.2.6 Influence of time 55
3.3.3 Encapsulation of waste using geopolymerization 55
3.3.4 Immobilization of pollutants in geopolymeric matrices 56
3.4 Hydraulic binder technology 59
3.4.1 Cement constitution 59
3.4.2 Cement hydration 60
3.4.2.1 Immobilization in C-S-H 61
3.4.2.2 Immobilization in ettringite 61
3.4.2.3 Immobilization in calcium monosulfoaluminate hydrate 61
3.4.3 Concrete application examples 61
3.4.4 Limitations of the stabilization/solidification process 62
3.5 Amendment technology 62
3.5.1 Anion stabilization by adsorbent amendments 63
3.5.2 Layered double hydroxides (LDH) 64
3.5.2.1 Structure and characteristics 64
3.5.3 Synthesis 65
3.5.3.1 Co-precipitation 65
3.5.3.2 Anion exchange 66
3.5.4 Applications 66
4 Description of the mineral waste valorization processes 67
4.1 Sediment valorization in civil engineering 68
4.1.1 Marine sediments valorization in road technique 69
4.1.2 Marine sediments valorization in artificial aggregates 69

4.1.3 Marine sediments valorization in mortar and concrete production 70
4.1.4 Marine sediments valorization in landscape eco-model 71
4.2 Fly ash valorization in civil engineering 71
4.2.1 Ash valorization in the field of construction and public works 71
4.2.2 Fly ash valorization in the wastewater treatment sector 72
4.2.3 Phosphorus removal from filter materials 72
4.2.4 Ash valorization into lightweight aggregates 73
Chapter 2: Pilot-scale natural carbonation of waste paper fly ash for stabilization of Ba and Pb……..97
Chapter 3: Manufacture and characterization of carbonated lightweight aggregates from waste paper fly ash……126
Chapter 4: Innovative reuse of fly ashes for treatment of contaminated river sediments: Synthesis of Layered Double Hydroxides (LDH) and chemical performance……..142
Chapter 5: Immobilization study of As, Cr, Mo, Pb, Sb, Se and Zn in geopolymer matrix: application to shooting range soil and biomass fly ash……...166
Chapter 6: Phosphorus removal from real and synthetic wastewater using biomass bottom ash...…189
General conclusion……...……...208
Perspectives……..212
Appendix……...…213

TABLE LIST

TABLE 1.HAZARD CRITERIA DEFINED IN REGULATION 1357/2014/EU (REPLACING ANNEX III OF DIRECTIVE 2008/98/EC) 16
TABLE 2. THE DIFFERENT PARAMETERS FOR WASTE AND ELUATE FOR EACH LANDFILL FACILITY WASTE 17
TABLE 3. CHEMICAL COMPOSITION OF FLY ASH OBTAINED FROM DIFFERENT TYPES OF COAL (TOKYAY 2016) 22
TABLE 4. BIOMASS ASH PRODUCTION IN 2014 AND 2020 (BOULDAY ET MARCOVECCHIO 2016) 24
TABLE 5. CHEMICAL COMPOSITION OF BIOMASS FLY ASH FROM DIFFERENT WOOD SPECIES (CHEAH ET RAMLI 2011) 25
TABLE 6. CHEMICAL COMPOSITION OF PAPER MILLS ASH 27
TABLE 7. TOTAL METALLIC TRACE ELEMENT AND METALLOID CONTENT IN THE ASH STUDIED BY SEGUI (2011) 27
TABLE 8. PARTICLE SIZE CLASSIFICATION OF SOILS ACCORDING TO THE GTR GUIDE 31
TABLE 9. CLASSIFICATION OF METALLIC TRACE ELEMENTS AND METALLOIDS ACCORDING TO THEIR TOXICITY AND AVAILABILITY (DELABRE 1985) 33
TABLE 10. RELATIVE LEVELS OF TRACE ELEMENTS AND TRACE COMPOUNDS (MG/KG DRY SEDIMENT ON THE FRACTION BELOW 2MM) 35
TABLE 11. DISPOSAL ROUTES ACCORDING TO LEAD AND ANTIMONY CONTENT 41
TABLE 12. EQUILIBRIUM CONSTANTS AT 25°C AND 1 ATM (COWIE ET GLASSER 1992) 45
TABLE 13. DESCRIPTION OF WASTES TESTED FOR CARBONATION 49
TABLE 14. LEACHING OF MMTE (MG/L) FROM GEOPOLYMER MATRIX CONTAINING SOLIDIFIED MMTE NITRATES-INTERSOLIDIFICATION (VALUES IN BRACKETS GIVE CALCULATED % LEACHING) 58
TABLE 15. PORTLAND CEMENT CHEMICAL COMPOSITION 60
TABLE 16. PRODUCTION OF HYDRATED PHASES FROM THE ANHYDROUS PHASES OF CEM I 60
TABLE 17. INORGANIC AND ORGANIC AMENDMENTS COMMONLY USED FOR TRACE ELEMENT IMMOBILIZATION 63
TABLE 18. ANION ADSORPTION BY DIFFERENT LDH 66
TABLE 19. MARINE SEDIMENT VALORIZATION CHANNELS 68
TABLE 20. PHOSPHORUS REMOVAL BY MINERAL WASTE 73
TABLE 21. WASTE MATERIALS PROPOSED IN THE LITERATURE FOR LWA PRODUCTION 74

FIGURES LIST

FIGURE 1. WASTE MANAGEMENT OPERATIONS HIERARCHY (ARTICLE L541-1 OF THE ENVIRONMENTAL CODE) 18
FIGURE 2. PRINCIPLE OF FLY ASH PRODUCTION 19
FIGURE 3. OPERATION MODE OF A COAL-FIRED POWER PLANT (ELECTRABEL, 2016) 20
FIGURE 4. FLY ASH PRODUCTION IN EUROPE IN 2002 AND 2016 (AYRINHAC 2005; ECOBA 2016) 22
FIGURE 5. DIFFERENT TYPES OF BIOMASSES 25
FIGURE 6. QUANTITIES OF MARINE SEDIMENTS DREDGED IN FRANCE IN 2010 (RAUJOUAN ET LE GUYADER 2010) 29
FIGURE 7. SEDIMENT FAT 34
FIGURE 8. SHOOTING RANGES 37
FIGURE 9. SMALL ARMS PROJECTILE 37
FIGURE 10. LEAD POLLUTION FROM SHOOTING IN INSTALLATION 39
FIGURE 11. PRINCIPAL INTERACTIONS BETWEEN AN ATOM OR MOLECULE AND A SOLID AT THE SOLID/LIQUID INTERFACE (MANCEAU, MARCUS, ET TAMURA 2002).. 43
FIGURE 12. CARBONATE SYSTEM SPECIATION AS A FUNCTION OF PH 46
FIGURE 13. ILLUSTRATION OF THE PORTLANDITE CARBONATION MECHANISM (THIERY 2006) 47
FIGURE 14. EVOLUTION OF THE CONDITION OF AMPHOTERIC METAL HYDROXIDES AS A FUNCTION OF PH 48
FIGURE 15. GENERAL STRUCTURE OF A SODIUM GEOPOLYMER (ROWLES ET AL. 2007) 51
FIGURE 16. GEOPOLYMERIZATION MODEL (PSWM DUXSON ET AL. 2007) 53
FIGURE 17. MAIN CEMENT PHASES MORPHOLOGY (JUAN-ORTEGA-CEMENTS SPECIALIST) 60
FIGURE 18. SCHEMATIC REPRESENTATION OF THE LDH STRUCTURE (VAYSSE 2001) 65
FIGURE 19. IMPLEMENTATION OF THE FREYCINET 12 ROAD BASED ON DREDGED SEDIMENTS AT GPMD (ACHOUR 2013). 69
FIGURE 20. AGGREGATE CONSUMPTION IN CIVIL ENGINEERING (UNPG) 70
FIGURE 21. MARINE SEDIMENT-BASED AGGREGATES (BRAKNI 2008) 70
FIGURE 22. ECO-LANDSCAPED MERLON AT THE GPMD 71

Abstract

The management of industrial waste and by-products is a major challenge for the socio-economic actors of territories. Indeed, the systematic use of disposal option in specific storage facilities is becoming increasingly expensive depending on the nature of the waste, which forces operators in the sector to turn to innovative treatments that ensure the environmental safety of these materials in case of disposal or recovery. This strategy contributes to the reduction of pollutant emissions into the environment and to the preservation of non-renewable natural resources when a recycling scenario is considered.

The objective of this thesis work is to study the efficiency of different physicochemical stabilization processes on the immobilization of inorganic contaminants within mineral wastes such as river dredging sediments, fly ash and bottom ash from biomass thermal power plants, fly ash from paper mill sludge, and soil shooting ranges. In the first part of the study, various stabilization processes were applied to the most contaminated wastes (river sediments, shooting range sand, and biomass fly ash) in order allowing their disposal in storage facilities. In a second part, bottom ash from thermal power plants were reused as an adsorbent substrate for wastewater dephosphatation and fly ash from paper mill sludge combustion as artificial lightweight aggregates for incorporation into backfill or concrete/mortar.

Keyword: Mineral waste, Physico-chemical stabilization, Environmental acceptability, Waste storage installation, Material recovery, Lightweight aggregates, Dredging sediment, Soil shooting range, Fly ash, Bottom ash from thermal power plants.

Résumé

La gestion des déchets et sous-produits industriels constitue un enjeu majeur pour les acteurs socio-économiques du territoire. En effet, le recours systématique aux filières d'élimination en installation de stockage de déchets devient de plus en plus onéreux en fonction de la nature des déchets, ce qui oblige les opérateurs du secteur à s'orienter vers des traitements innovants permettant de garantir l'innocuité environnementale de ces matériaux en cas d'élimination ou de valorisation. Cette stratégie contribue à la réduction des émissions en substances polluantes dans l'environnement et à la préservation des ressources naturelles non renouvelables lorsque qu'un scénario de recyclage est envisagé.

Ce travail de thèse a pour objectif d'étudier l'efficacité de différents procédés de stabilisation physico-chimique sur l'immobilisation de contaminants inorganiques présents dans des déchets minéraux. Ainsi, des sédiments de dragage fluviaux, des cendres et des mâchefers de centrales thermiques à biomasse, des cendres volantes de boues de papeterie et des sables de champs de tir, présentant un caractère non inerte ont été prioritairement sélectionnés pour la réalisation de cette étude. Dans le premier volet de l'étude, les sédiments fluviaux, le sable de champs de tir, et les cendres volantes de biomasse ont été stabilisés par divers procédés physico-chimiques dans la perspective d'une élimination en installations de stockage. Dans un second volet, les mâchefers de centrales thermiques ont été réutilisés en tant que substrat adsorbant pour la déphosphatation des eaux usées et les cendres volantes issues de la combustion de boues de papeterie ont été granulées pour confectionner des granulats légers artificiels susceptibles d'être réutilisés en remblais ou dans des bétons/mortiers.

Mots clés : Déchets minéraux, Stabilisation physico-chimique, Acceptabilité environnementale, Installation de stockage de déchets, Valorisation matière, Granulats légers, Sédiment de dragage, Sol de champs de tir, Cendres volantes, Mâchefers de centrales thermiques.

Remerciements

Avant tout, je vous remercie, vous, qui venez de lire mon manuscrit de thèse et je remercie également tous ceux qui m'ont soutenu pour arriver à ce travail. Merci à mon père ma mère et mon frère qui m'ont donné tout le courage et l'amour dont j'avais besoin pendant ces trois ans de thèse. Vous avez essayé d'exécuter tous mes vœux et tous mes besoins et j'espérais réaliser votre rêve actuellement. Merci aussi à toute personne qui a contribué, de loin ou de près, à réaliser ce travail.

Merci à mon directeur de thèse, Yannick MAMINDY-PAJANY, pour ces efforts et sa présence en première ligne de cette thèse de doctorat, et d'avoir suivi mes travaux de thèse de bout en bout, et surtout pour ses conseils, sa bienveillance et son investissement permanent.

Je remercie Fabienne BARAUD, Enseignante chercheuse à Université de Caen, et Khalil HANNA, Professeur à Ecole de Chimie de Rennes, rapporteurs de thèse. Mes remerciements vont également à Nor-Edine ABRIAK, Professeur à IMT Nord Europe, Anne PANTET, Professeure à Université du Havre et Charlotte HUREL, Maître assistant-HDR à Université Côte d'Azur, d'avoir accepté l'invitation pour assister à mon jury en tant qu'examinateurs et pour leurs échanges enrichissants.

Mes remerciements vont à tous les doctorants et les assistants du LGCgE – IMT Lille Douai. Merci à Johanna, Guillaume et Mickaël pour leurs conseils et leurs disponibilités durant mes travaux pratiques. Merci également à ceux avec qui j'ai collaboré : Salim, Yassine, Abdelhadi, Amine, Morgan, Ali, Mhamed, Zeinab... Et je dédie ce travail à tous les anonymes : amis, camarades, étudiants que je n'ai pas cités mais qui ont contribué à la réussite de ce travail par leur soutien et leur présence. Ils se reconnaîtront.

Merci!

General introduction

For decades, several environmental issues such as global warming, environmental pollution or loss of biodiversity have emerged worldwide. This prompted industrial countries, particularly in Europe, to commit to the transition towards a circular economic model contributing to sustainable development. Waste management represents one of the main axes to promote the circular economy, in particular by reinforcing its reuse, recycling and recovery.

In France, several hundred million tons of waste are generated annually by the building and public works sector, industry and dredging operations. The management of these large quantities of waste is becoming increasingly restrictive and represents a major technical, economic and environmental challenge. This is mainly due to the saturation of the disposal sites, the highly heterogeneous physico-chemical characteristics of the waste and the presence of organic and inorganic contaminants in their matrices which can constitute a risk for the environment. The development of urban, industrial and agricultural activities during the last decades has led to many pollution problems, especially in metallic and metalloid trace elements (MMTE) and anionic compounds. These pollutants can be released by the weathering of natural rocks and/or by various anthropogenic sources. Due to their retention capacity, alternative materials such as soils or sediments are real traps for chemical substances coming from many human activities (mining, smelting, agriculture or transportation, etc.). A material is generally considered "polluted" when it contains one or more contaminants likely to cause biological, physical or chemical alterations in the various environmental compartments.

Once in the materials and depending on the physicochemical conditions, inorganic pollutants can either be "trapped" by the solid phase through different fixation/retention mechanisms (precipitation, adsorption...) on surface sites, or, if present in the interstitial solution of the material, be "transferred" to other environmental compartments such as surface water, groundwater or living organisms. Some inorganic pollutants such as Cu and Zn are an integral part of biogeochemical cycles (trace elements) and become toxic only at high levels, while others, such as As, Mo, Pb, Sb, ... are toxic at low levels for the trophic chain. It is recognized that the mobility, bioavailability and toxicity of inorganic pollutants depend more on their chemical forms than on their total concentration.

The search for alternatives within a sustainable development perspective remains essential. However, for each waste type and industrial by-products, several remediation and treatment ways have been developed, as well as their valorization, notably in the field of civil engineering. In France, the construction and maintenance of overland roads represent one of the major concerns. Thus, the public works sector consumes millions of tons of mineral aggregates every year. Similarly, millions of tons of hydraulic binders are manufactured annually, part of which is dedicated to the treatment of soil and road sub-layers. Also, an alternative to maintain the extensive character of the classical French system has been developed, the use of these industrial by-products as a low-cost adsorbent to remove P from wastewater in the treatment plants.

In the present thesis, the efficiency of different physicochemical stabilization processes was evaluated for various inorganic substances coming from sedimentary or soil matrices or fly ash in the perspective of their elimination or valorization. The thesis manuscript is structured in six chapters:

- The first chapter is dedicated to the state of art which presents in first a synthesis of the waste management problematic in France. Then a bibliography is presented on the different wastes, such as: fly ash (waste paper fly ash (WPFA), biomass fly ash (BFA) and biomass bottom ash (BBA), dredging sediments and shooting range soil (SRS). The analysis focuses on the management, source, main technical and environmental characteristics as well as the main

valorization ways of each waste (lightweight aggregates, road construction, use as reaction filter for P retention in wastewater treatment plants...). In a second part, the presentation of the remediation technologies and/or physicochemical stabilization of pollutants and the parameters that influence each technology used. The studied stabilization technologies are the following: hydraulic binders and geopolymers, amendments, natural and accelerated carbonation.

- The second chapter focuses on a new concept of natural carbonation at pilot scale of waste paper fly ash (WPFA) considered as a hazardous waste due to the concentration of Barium (Ba), Lead (Pb). The carbonation process allows both the stabilization of Ba and Pb in the WPFA while optimizing the reduction of liquid and solid wastes. The application of this concept required different phases of research including the optimization of carbonation parameters such as the Liquid/Solid ratio (L/S), humidity rate, temperature, carbon dioxide (CO_2) concentration and the treatment of the percolation water at the process end. Then, physicochemical and environmental analyses were performed to study the carbonation evolution in time and its effect on the chemical and mineralogical properties of the WPFA.
- The third chapter was devoted to the valorization of WPFA as lightweight aggregates (LWA). A presentation of the raw materials and the method used for the wet agglomeration process is described. Then, a study of manufacturing optimization of lightweight aggregates such as the liquid/solid ratio (L/S), the rotation modes between the steel pan and the turbine, the rotation speed of the steel pan, the granulation time, in order to improve the mass percentage of the targeted LWA (2-16 mm). Then, accelerated carbonation was performed in order to immobilize Pb and Ba in LWAs, and to improve the physicochemical properties such as porosity, water absorption, specific surface area, mechanical strength, thermal conductivity and leaching characteristics.
- The fourth chapter presents an innovative valorization pathway of waste paper fly ash (WPFA) and biomass fly ash (BFA) by reusing them for the treatment of river sediments from Noyelles-Sous-Lens (NSL) contaminated by antimony (Sb), zinc (Zn) and sulfates (SO_4^{2-}). Fly ash is used as a precursor for the synthesis of layered double hydroxides (LDH). Subsequently, the LDHs were characterized for the stabilization of contaminants in the NSL sediment. The stabilization of the contaminants in the NSL sediment was tested in a batch and columns reactors.
- The 5th chapter presents a study concerning the stabilization of wastes (SRS and BFA) considered as hazardous in geopolymeric matrices followed by an accelerated carbonation in an aqueous phase in order to immobilize Pb and Sb in SRS and Mo, Cr, Se, Pb, Zn in BFA. The synthesis of geopolymers consists of an alkaline activation of aluminosilicate materials (metakaolin) at ambient temperature. An optimization study of the different geopolymer formulation parameters such as water/solid ratio (W/S), $NaOH/Na_2SiO_3$, metakaolin/waste, curing condition (before and after carbonation) has been carried out, in order to improve the encapsulation of the two wastes, more precisely the immobilization of the MMTE, the mechanical strength and the resistance in acidic environment... etc.
- The last chapter was mainly devoted to the study of phosphorus adsorption processes by two types of biomass bottom ash (BBA) from the Haute-de-France region. The final objective is an application of these materials as filtering mass for the phosphorus retention of wastewater in treatment plants. In a first step, the phosphorus reactivity has been studied in relation to the two BBA_s in batch and column reactors. The influence of different physicochemical parameters was characterized such as chemical composition, specific surface, particle size, initial P concentration, contact time and pH. Finally, phosphorus speciation was studied onto the filters after adsorption in order to check the efficiency of the process.

Chapter 1:

State of the art

1 Waste management in France

The Management of the different types of industrial waste and by-products appears is an important issue both from an economic and environmental viewpoint. The storage of these materials is costly and all alternative solutions are therefore worth studying. In addition, their recycling, reuse or re-utilization could help preserve non-renewable natural resources, which is not negligible in the midst of a climate emergency.

Consequently, and in a logic of sustainable development, the stabilization and/or intelligent valorization of waste becomes a necessity. The civil and environmental engineering sector represents an interesting and viable field for the recovery of mineral waste in the form of natural, recycled or even artificial aggregates.

This bibliographic chapter aims to show the challenge of managing five industrial wastes and by-products (dredged sediments, biomass ash, non-hazardous fly ash, wastepaper fly ash and shooting range sand) in order to reduce the environmental impacts linked mainly to their disposal. This waste management makes it possible to preserve natural resources by stabilizing on one side the materials of non and/or dangerous character (sediment, shooting range sand, biomass ash) for storage and on other side by valorizing certain material in the fillers of wastewater treatment (bottom ash) or the manufacture of aggregates (paper mill fly ash).

Initially, this bibliographical section will deal with waste management in the widest sense of the term, then the various wastes used in this thesis will be presented, explaining the information relating to their deposits, their characteristics and their recovery methods. The last part will be devoted to the two recovery methods selected for this study, specifically: the manufacture of lightweight aggregates and the elimination of phosphorus from wastewater

1.1 History and definition

Since the 1970s, actions have been focused on solving the problem of waste management, especially after the development of the consumer society and the increase in waste production **(ALBAREDA et al., 2009)**.

It was also in the 1970s that the Ministry of the Environment was created and the notion of Installations Classified for the Protection of the Environment (ICPE) was considered on a national basis. These installations are based on strict specifications in order to treat waste in appropriate environmental conditions **(ALBAREDA et al., 2009)**.

According to the law of 15 July 1975, " all residues of a production, transformation or use process, all substances, materials, products or, more generally, all movable property abandoned or intended for abandonment by its holder " is defined as waste.

1.2 Waste Framework Directive (2008/98/EC)

Directive 2008/98/EC of the European Parliament and of the Council of 19 November 2008 is referred to as the "Waste Framework Directive". This directive defines the concepts of waste and the appropriate management of waste in the European Union. It also establishes a set of rules for its collection, transport, recovery and disposal. This European directive and other international and European regulations are transposed into French law in the Environmental Code.

1.3 Hazardous and non-hazardous waste

The hazardousness of a waste is assessed according to 15 hazard properties listed in Regulation 1357/2014/EU (replacing Annex III of Directive 2008/98/EC). Since 1 June 2015, these properties are called HP1 to HP15 **(Table 1)**. If the waste has at least one of the criteria listed in **Table 1**, then it is classified as hazardous. The management of such a waste is either by treatment to make it non-hazardous, by incineration or by storage in specific hazardous waste facilities. Conversely, non-hazardous waste is defined as waste that does not exhibit any of the properties that make it hazardous.

1.4 Inert nature of non-hazardous waste

According to article R.541-8 of the Environmental Code, among the non-hazardous wastes without any property from HP1 to HP15, the category of inert waste is included. Indeed, an inert waste is defined according to article R.541-8 of the Environmental Code as " all waste which does not undergo any significant physical, chemical or biological modification, which does not decompose, does not burn, does not produce any physical or chemical reaction, is not biodegradable and does not deteriorate the materials with which it comes into contact in a fashion liable to cause harm to the environment or human health ".

1.5 Waste list

The waste list, according to the French regulation on risk prevention and environmental protection, is reported in the Community decision n° 2000/532/CE which replaces the decision 94/3/CE. The different types of waste on the list are presented by a six-digit code and hazardous waste is distinguished by an asterisk (*). Some wastes have a "mirror entry" thus they represent two possible classification options according to their hazardous properties.

Table 1. Hazard criteria defined in Regulation 1357/2014/EU (replacing Annex III of Directive 2008/98/EC)

Properties	Characteristics
HP1	Explosif
HP2	Combustible
HP3	Flammable
HP4	Irritant - irritation to the skin and eye damage
HP5	Specific target organ toxicity (STOT) / Aspiration toxicity
HP6	Acute toxicity
HP7	Carcinogenic
HP8	Abrasive
HP9	Infectious
HP10	Reproductive toxicity
HP11	Mutagenic
HP12	Release of an acutely toxic gas
HP13	Sensitizer
HP14	Ecotoxic
HP15	Waste capable of exhibiting one of the above-mentioned hazardous properties which is not directly present in the original waste

1.6 Inert Waste Storage Installations

Concerning Inert Waste Storage Installations (IWSI), the decree of 28 October 2010, which is replaced by the decree of 12 December 2014, specifies the thresholds to be respected in terms of total content and leached elements (NF EN 12457-2). Some flexibility can be noted: when the thresholds for

chlorides, sulphates or the soluble fraction are not respected in the eluate, the waste can be admitted to an IWSI provided that it respects either the chloride and sulphate limits or the soluble fraction limit.

Exceeding the limits for IWSI, the waste can be admitted to a Non-Hazardous Waste Storage Installation (NHWSI) provided that it complies with the thresholds set out in the Order of 9 September 1997 (replaced by the Order of 12 March 2012, itself replaced by the Order of 15 February 2016) **(Table 2)**. The admission of waste classified as hazardous according to the properties HP1 to HP15 is limited by compliance with the limits defined by the Order of 30 December 2002 (replaced by the Order of 10 October 2012).

Table 2. The different parameters for waste and eluate for each landfill facility waste

	IWSI	NIWSI	HWSI
Metallic trace elements and metalloids (mg/kg)			
Arsenic	0.5	2	25
Barium	20	100	300
Chrome	0.5	10	70
Copper	2	50	100
Molybdenum	0.5	10	30
Nickel	0.4	10	40
Lead	0.5	10	50
Zinc	4	50	200
Cadmium	0.04	1	5
Mercury	0.01	0.2	2
Antimony	0.06	0.7	5
Selenium	0.1	0.5	7
Another parameter (mg/kg)			
TOC	500	800	1 000
Soluble fraction	4 000	60 000	100 000
Chlorides	800	15 000	25 000
Fluorides	10	150	500
Phenol indice	1	3	1 000
Organic pollutant (mg/kg)			
TOC on the raw	30 000	50 000	100 000
PAH	50	-	-
PCB	1	-	-
TBT	6	-	-

According to Article L541-1-1 of the Environmental Code, recovery is defined as any operation aimed at using a waste for useful purposes by substituting a substance, material or product. In fact, in order for treatment processes to be qualified as recovery and not elimination, they must aim at a subsequent use of the treated waste.

In contrast, recycling includes all recovery processes except energy recovery, operations to transform waste into fuel and landfill operations. Reuse is a part of recycling where the waste is used for its original purpose. Article L 541-1 of the Environmental Code describes the hierarchy of waste treatment methods in order of priority **(Figure 1)**.

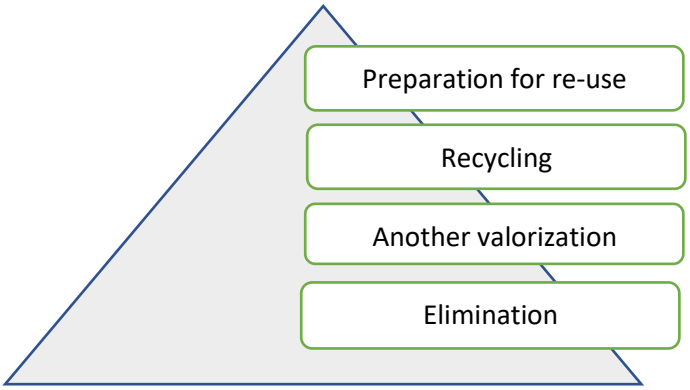

Figure 1. Waste management operations hierarchy (Article L541-1 of the Environmental Code)

Depending on the type of recycling process desired, the waste must meet geotechnical and mechanical criteria defined in application-specific specifications. From an environmental viewpoint, and in the case where the regulatory framework is defined, the environmental criteria to be respected for a recovery method are described there. Conversely, in the absence of a regulatory framework, it is necessary to verify the environmental harmlessness of the recovery facility by defining a scientific methodology in accordance with the European standard NF EN 12920+A1.

1.7 Waste status

French environmental laws are adapted to promote the integration of waste into the circular economy concept, by taking several decisions and actions that encourage the recovery of waste. Indeed, the removal of waste status allows a material that has been treated and recovered to no longer be considered as waste if the waste meets the following criteria:

- Use: it must be applied for specific purposes;
- Market: it must satisfy a demand in the market;
- Technical: it complies with the technical requirements, legislation and standards in force;
- Health and environment: it has no harmful impact on either the environment or human health.

Prior to 1 April 2021, the removal of waste from the waste status required a passage through an ICPE or an IOTA (Installations, Works, and Activities provided for under the water legislation) in order to ensure the treatment and recovery process. From 1 April 2021, the decree n° 2021-380 on the exit from waste status allows all producers or holders of waste to ask the competent authority to set criteria in order for the waste they produce or hold to cease to have waste status

2 Description of polluted mineral waste

2.1 Fly Ash

The term "fly ash" was coined around 1930 by the electric power industry as the quantities recovered from coal residues in thermal power plants became increasingly important **(Karouite 2003)**. Overall, the most common definitions of fly ash are similar. **Jarrige (1971)** noted that ash is the solid residue from the combustion of coal (coal, lignite, anthracite). For the purpose of generating electricity in thermal power plants, fly ash is the main by-product of fine solid waste, which results from the combustion of a predominantly carbonaceous fossil material of plant origin (coal) **(Moufti et Mountadar 2004; Ayrinhac 2005)**. **Karouite (2003)** also noted that fly ash is a fine particle collected during the dedusting of gases resulting from the combustion of pulverized coal, used in thermal power plants.

2.1.1 Source

The combustion of a solid fossil combustible, which is previously pulverized to produce vapor and injected into the combustion chamber in thermal power plants, leads to two types of by-products: bottom ash and fly ash. It should be noted that for the moment the fuel is mainly coal, which remains an essential source of energy for the production of electricity in the world and will be the last of the available carbon energies if consumption grows at the current rate **(Ayrinhac 2005)**.

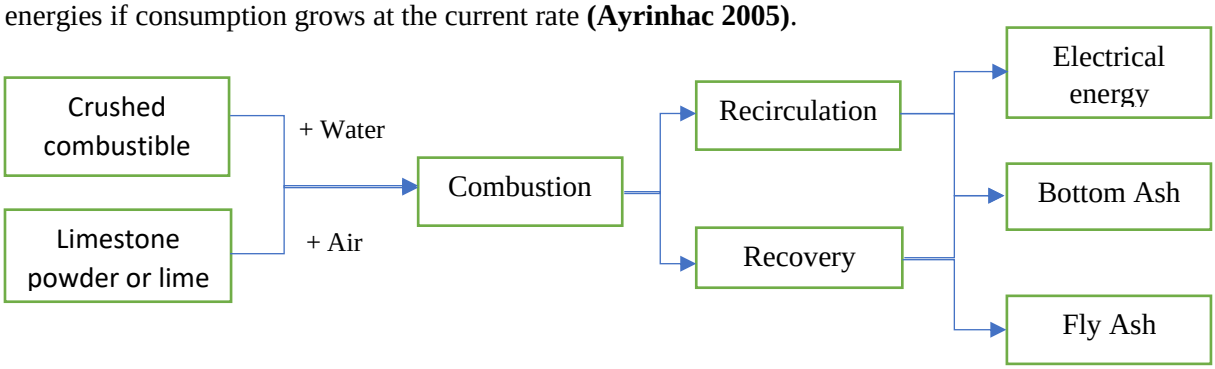

Figure 2. Principle of fly ash production

2.1.2 Composition

The composition of fly ash, which varies in color from brown to grey and black depending on the amount of unburnt carbon, is related to the different types of combustibles and the different combustion processes used in thermal power plants. For the coal and/or biomass fly ash, the most common mineral constituents are clay minerals (illite and kaolinite), sulphides (pyrite and marcasite), carbonates (dolomite, ankerite, calcite and siderite) and quartz (SiO_2) **(Scheetz et Earle 1998)**. Generally, fly ash can be classified into two main families according to its chemical composition, with the main elements being: silicon, aluminum, iron, calcium and magnesium.

- Silica-alumina fly ash (SiO_2+Al_2O_3): It is a grey to black powder depending on the unburnt and iron oxide content **(Karouite 2003)**. It does not exist when the combustible is not coal (for example: petroleum coke) **(Ayrinhac 2005)**. The fly ash must contain mainly reactive silica SiO_2 and alumina Al_2O_3, but it must also contain other oxides, e.g. iron oxides (Fe_2O_3 and Fe_3O_4), lime (CaO), magnesia (MgO) and sulphur dioxide (SO_3). In particular, the proportion of reactive lime CaO must be less than 5% by mass, and that of reactive silica must be superior or equivalent to 25% by mass **(Karouite 2003)**. According to **NF P 98-110** ("Products"), the high sulphate (>2.5%) and sulphur (>8%) content does not allow this fly ash to be considered as silico-aluminous ash in the case of use in pavement foundations. Moreover, the carbon content is admissible when the loss on ignition at 1000°C is less than or equal to 8%, and the pH of silico-aluminous fly ash is around 10.
- Sulpho-calcic fly ash (SO_3+CaO): Its main characteristic is that it has a high lime (CaO) and sulphur dioxide (SO_3) content compared to silica-alumina fly ash. Sulpho-calcic fly ash, which is the residue of flue gas desulphurization, has a much higher CaO content than silico-aluminous fly ash. It essentially contains reactive lime, reactive silica and alumina, and is therefore susceptible to binding in the presence of water. As such, Sulpho-calcic fly ash can be considered as a real cement as it is close to clinkers. The reactive lime content must be equal to or higher than 5% by mass, and fly ash containing 5 and 15% reactive lime must contain more than 25% reactive silica by mass ("Products").

2.2 Coal fly ash

2.2.1 Source and production

Classic fly ash is a by-product of coal combustion in coal-fired power plants. Pulverized coal is combustion in boilers of thermoelectric power plants with or without co-combustibles. As a result of this combustion, fine particles are extracted: fly ash. Fly ash obtained in this manner only can be used as a constituent of cement. In Europe, several organizations are studying the precautions to be followed when recovering this type of waste, such as ECOBA (European Coal Ash Producers Association) **(Ecoba 2016)** and IEA Coal research (International Energy Association) **(Balakrishnan et al. 2017; Rajamma et al. 2015; Ayrinhac 2005)**

A coal power plant is equipped with a purification system that removes sulphur dioxide (SO_2) and nitrogen oxide (NO_X) from the flue gas before it exits the chimney. The fine dust, referred to as fly ash, is collected in hoppers by an electrostatic precipitator, located at point 10 in Fig 2 **(Electrabel, 2016**).

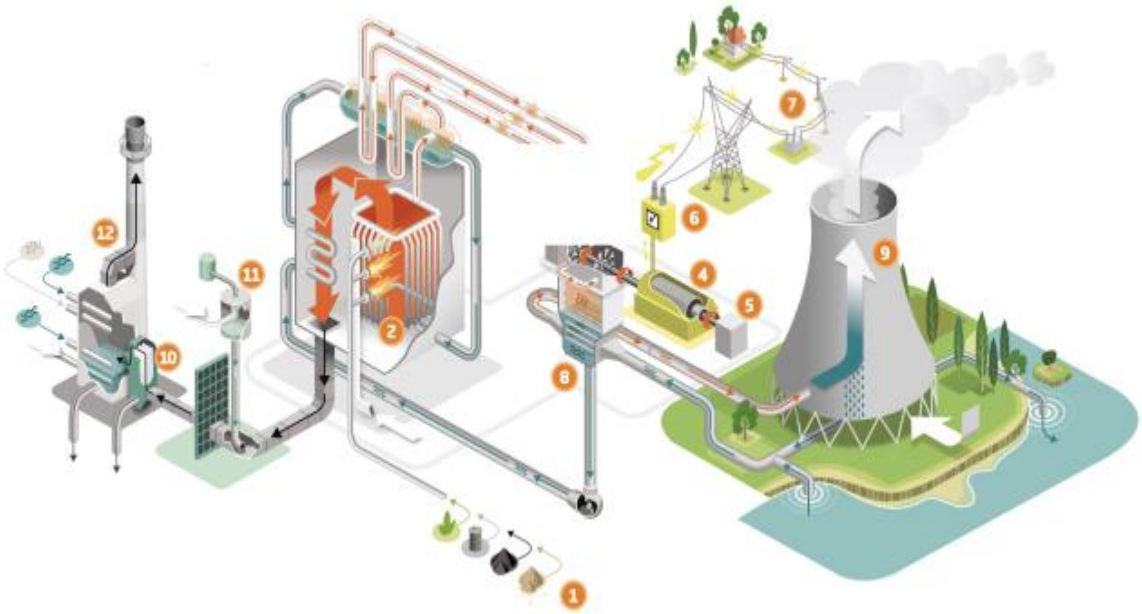

1-	**Combustible**	6-	**Transformer**	11-	**Denitrification**
2-	**Steam boiler**	7-	**High-voltage line**	12-	**Desulphurization**
3-	**Steam turbine**	8-	**Capacitor**		
4-	**Alternator**	9-	**Cooling tower**		
5-	**Exciter**	10-	**Electrostatic precipitator**		

Figure 3. Operation mode of a coal-fired power plant (Electrabel, 2016)

Coal ash is produced as a result of coal combustion in power plants. Globally, results show that fly ash production is proportional to coal production. However, it should be borne in mind that there are several coal combustion products and not all fly ash can be exploited.

The combustion products of coal are multiple as coal has different mineral components and combustion can be performed using different techniques. The different products of coal combustion are the following **(Ayrinhac 2005; Ecoba 2016)**:

- Fly ash: Fly ash is obtained from electrostatic or mechanical precipitation upstream of the stack and then cooled. Fly ash is a dusty particle from the flue gas of coal or lignite-fired furnaces at

a temperature of 1100 to 1400 ◦C. Fly ash is in the form of a fine powder, composed mainly of spherical glassy particles. Depending on the type of boiler and the type of coal, fly ash produced is siliceous or calcareous with pozzolanic and/or latent hydraulic properties.

- Desulphurization gypsum: Gypsum is a naturally occurring gypsum product which is obtained by wet desulphurization of flue gases and special treatment of the adsorbed products.
- FBC ash: Fluidized bed combustion ash is produced in fluidized bed combustion boilers. This technique involves a combination of coal combustion and flue gas desulphurization in the boiler at temperatures of 800 to 900 ◦C. This ash is rich in lime and Sulphur. - Boiler slag.
- Bottom ash: Bottom ash consists of granular material removed from the floor of dry boilers. This type of ash is much coarser than fly ash, yet it is also formed during the combustion of coal.
- Flue gas cleaning products
- Boiler slag

Every year, ECOBA carries out a statistical survey on the production and use of coal combustion products in Europe. Unfortunately, the data are not available for all European countries, as some countries are not members of ECOBA or the figures of the member states are simply not available. The production data is therefore verified by statistical figures on coal consumption. These figures also cover the production and use of fly ash.

ECOBA statistics on fly ash production in EU countries in 2002 and 2016 are presented in Figure 4. The production of coal combustion products changes every year. About 63 million tons were produced in 2002, while 40 million tons were produced in 2016. Of all the waste, the proportion of fly ash production is 67% in 2002, or 42 million tons, and 64%, or 26 million tons, in 2016. During coal combustion, fly ash represents the largest amount of combustion product **(Ayrinhac 2005; Ecoba 2016)**.

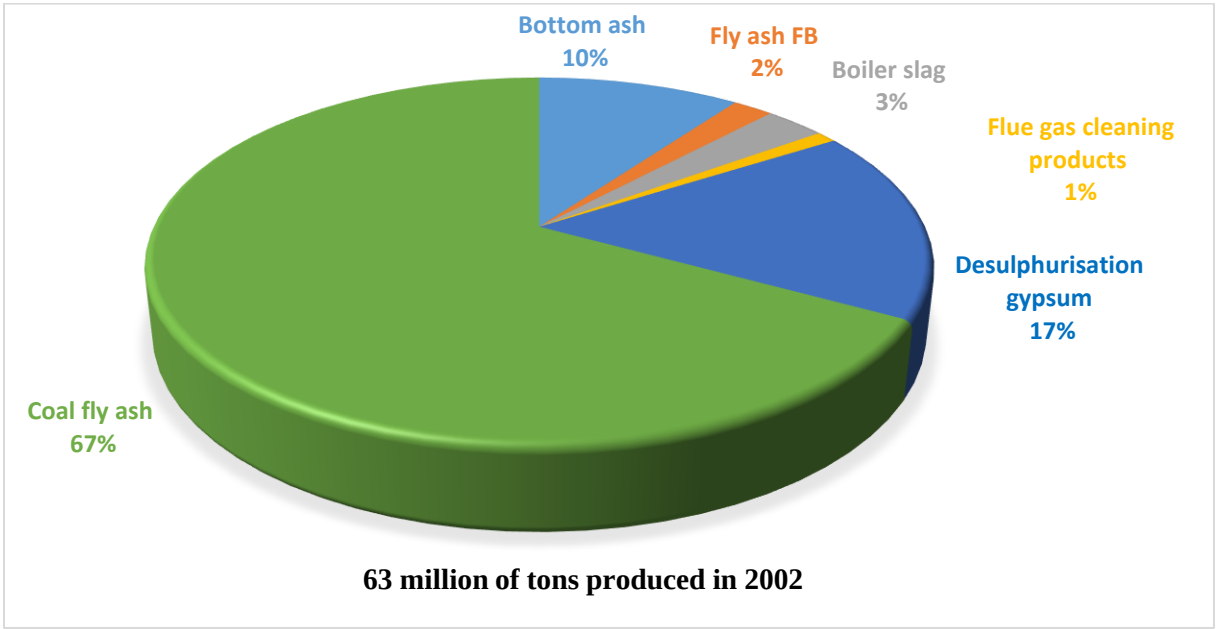

63 million of tons produced in 2002

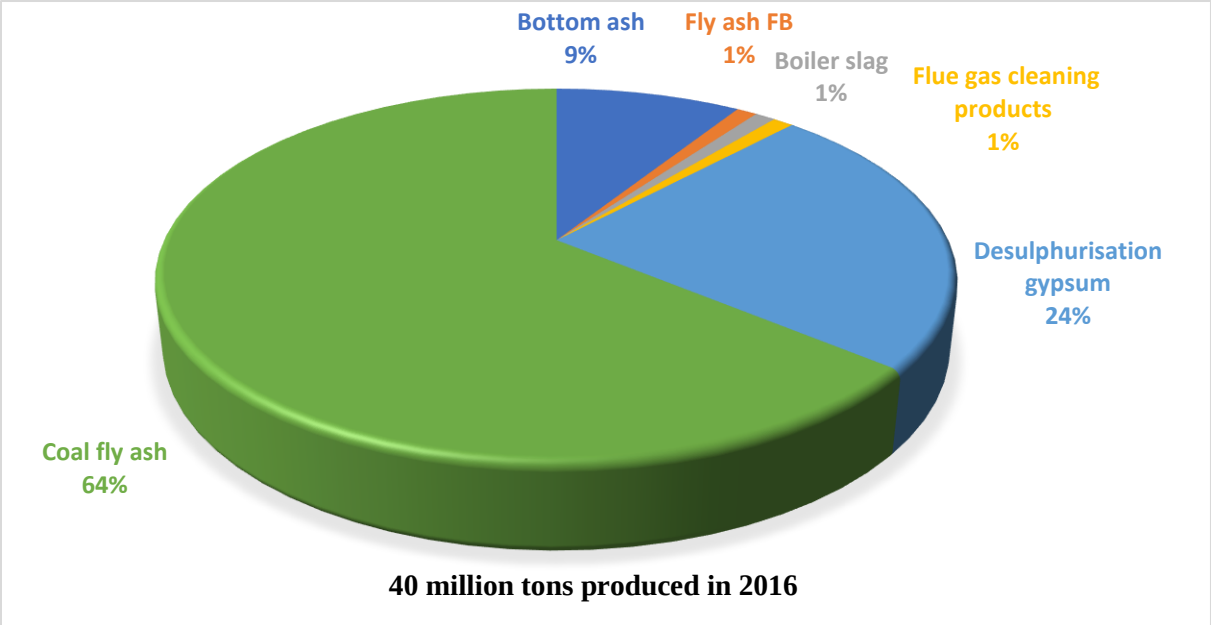

Figure 4. Fly ash production in Europe in 2002 and 2016 (Ayrinhac 2005; Ecoba 2016)

2.2.2 Chemical composition

The chemical composition of a variety of fly ashes obtained from different types of coal is presented in Table 3.

Table 3. Chemical composition of fly ash obtained from different types of coal (Tokyay 2016)

Oxide (%)	Type of coal used to produce fly ash			
	Anthracite	Bituminous	Sub-bituminous	Lignite
SiO_2	47-68	7-68	17-58	6-45
Al_2O_3	25-43	4-39	4-35	6-23
Fe_2O_3	2-10	2-44	3-19	1-18
CaO	0-4	1-36	2-45	15-44
MgO	0-1	0-4	0-8	3-12
Na_2O	-	0-3	-	0-11
K_2O	-	0-4	-	0-2
SO_3	0-1	0-32	3-16	6-32

The chemical composition of fly ash is determined by the types and relative proportions of mineral materials present in the coal used. Silica (SiO_2), alumina (Al_2O_3), iron oxide (Fe_2O_3), lime (CaO) and magnesia (MgO) constitute over 85% of most fly ash. In general, fly ash from the combustion of lignite and sub-bituminous coals contains more lime than fly ash from bituminous coals and anthracite **(Tokyay 2016)**.

2.2.3 Physical characteristics

Pulverized coal fly ash is a fine powder containing many spherical particles. The particle size of the ash generally ranges from 0.5 to about 300 micrometers, with the larger particles being agglomerated particles or unburnt material. Scanning electron microscope results have shown that the spherical particles of coal fly ash are in the range of 1 to 150 micrometers, while the irregular particles are often larger **(Ramezanianpour et al. 2009; Wesche 1991)**.

Concerning the specific surface, values from the literature are measured by different methods and show very different values depending on the technique used. The values obtained on fly ash by the BET method (Brunauer-Emmett-Teller nitrogen absorption technique) vary from 4800 to 89 000 cm^2/g and are 2 to 20 times higher than those obtained by the Blaine method **(Plowman et Cabrera 1981)**, which is the one most used in France. The Blaine method gives coal fly ash specific surface areas that generally vary between 2200 and 5500 cm^2 /g, but can also be below or above this in some cases **(Wesche 1991)**. It should be noted that the difference in value between the Blaine and BET methods is due to the fact that the BET technique measures the total voids present on the surface of the particles.

In common with other physico-chemical properties, the real density of an ash is highly variable depending on its origin and that of the coal from which it is derived. Studies on 11 fly ash from thermal power plants have shown variations in real density (from 1.9 to 2.96g/cm^3) and Blaine specific surface area (from 1980 to 5810 g/cm^3) depending on the type of coal used **(Carette et Malhotra 1984)**.

2.2.4 Environmental characteristics

The solubility of the elements contained in fly ash depends on the phases to which they are bound (glassy or crystallized phase) and the conditions (pH, temperature...) to which they are exposed **(Blissett et Rowson 2012)**.

The pH of fly ash ranges from 4.5 to 12.0, according to the Sulphur content of the original coal as well as its content of calcium and magnesium hydroxides and carbonates which depend on the combustion process **(François, Hirczak, et Senil 2006; Jambhulkar et Juwarkar 2009; Pandey et Singh 2010)**. Studies have shown that the acidity of the eluate from fly ash will depend on the Ca/S ratio. Indeed, if this ratio is lower than 2.5, the eluate will be acidic and if Ca/S is higher than this value, the eluate will be alkaline **(Pandey et Singh 2010; Ainsworth et Rai 1987)**. As shown in the reference sample proposed by the National Institute of Standards and Technology [NIST, Gaithersburg, USA], with a Ca/S ratio of 7.5, the effect via pH has a significant consequence on the leachability of fly ash **(Izquierdo et Querol 2012)**. It was observed that in the pH 7-10 zone, the elements Cd, Co, Cu, Fe, Mg, Mn, Ni, Pb, Si, Ti, U and Zn have minimal solubility in contrast to the anions As, Cr, Se, V and W which have maximum solubility even though the presence of Ca reduces the release of As and V **(Izquierdo et Querol 2012)**. The leaching of fly ash (class C) from thermal power plants shows that it first releases the salts KCl, $BaCrO_4$, NaCl, $CaSO_4.H_2O$ **(Tiruta-Barna, Rakotoarisoa, et Mehu 2006)**. According to the studies of **Lapa et al. (2007) and Tiruta-Barna, et al (2006)**, the leaching method recommended by the EN12457-2 standard led to a low solubility of trace elements (As, Cd, Hg, Ni, Pb and Zn) in fly ash from fluidized bed **(Lapa et al. 2007a)** and bottom ash **boilers (Tiruta-Barna, Rakotoarisoa, et Mehu 2006)**.

2.3 Biomass fly ash

2.3.1 Source and production

Biomass usually originates from wood waste of forests, farm waste or waste from the agri-food industry **(Berra, Mangialardi, et Paolini 2015)**. Not all biomass waste is the same and not all biomass waste has the same potential. For example, wood waste is preferred to other biomass such as grass and agricultural waste because incineration of wood waste generates less fly ash **(Cheah et Ramli 2011)**. The aim is obviously to produce as little waste as possible to have fewer storage and recycling problems.

At the European level, the production of biomass fly ash has been increasing year after year, as shown in **Table 4**. Biomass fly ash is derived from solid biomass used in dedicated and collective boiler rooms, industries and cogeneration. Firewood ash is excluded.

Table 4. Biomass ash production in 2014 and 2020 (Boulday et Marcovecchio 2016)

	2014	2020
Mass of combustible (millions of tons)	145	2.8
Mass of biomass fly ash (millions of tons)	270	5.5

Similar to coal fly ash, the use of biomass fly ash has many advantages. In Europe, the demand for renewable energy is growing due to the pressure on the global environment and energy. Diversification of energy supply is becoming essential. Renewable energy resources are a necessary alternative and have the advantage of being CO_2 neutral **(Rajamma et al. 2009).**

Biomass fly ash is an industrial by-product of the energy industries and has significant potential for use as a pozzolanic mineral admixture and as an activator or binder for cement composite materials. At present, biomass fly ash is not yet widely used commercially, unlike coal fly ash. Most biomass fly ash produced by power plants is either landfilled or recycled on fields or forests, and often this happens without any form of control **(Rajamma et al. 2015)**.

Biomass fly ash is different from coal fly ash as it is derived from different combustible (S. Wang, Baxter, et Fonseca 2008). Biomass ash differs from coal fly ash mainly in its chemistry and mineralogy **(Rajamma et al. 2009)**. Compared to coal fly ash, biomass fly ash contains a lot of calcium oxide (CaO), silica (SiO_2) and alumina (Al_2O_3) and little iron oxide (Fe_2O_3) **(Esteves et al. 2012)**.

In Europe, there is currently no standard allowing the incorporation of biomass fly ash into cement. Only Switzerland authorizes the use of fly ash in cement subject to limits on the content of metals such as zinc. However, the EN-450 standard allows the use of fly ash in concrete if it is derived from the co-combustion of combustibles that contain a maximum of 50% biomass **(Boulday et Marcovecchio 2016)**. Co-combustion has been designed to modernize existing coal-fired power plants and reduce their CO_2 emissions. When biomass is introduced into the combustible of these power plants, it decreases their CO_2 emissions and reduces their contribution to the greenhouse effect. Biomass also has lower sulphur levels than combustible materials and therefore contributes to reducing sulphurous gas emissions. However, the substitution of biomass for a part of the combustible has impacts on the operation of the plants. When the biomass content is less than 10% by mass, the installation does not require major modification. For higher contents, more significant modifications are required **(CAILLAT et al. 2010)**.

2.3.2 Physical and chemical properties

The quality and characteristics of biomass fly ash are influenced by many factor **(Rajamma et al. 2009; Cheah et Ramli 2011)**:

2.3.2.1 Biomass type

The characteristics of biomass fly ash depend on the biomass used, such as grass, wood, bark, ... **(Figure 5)** The type of biomass used has an impact on the chemical and physical properties of the fly ash produced. The chemical composition, such as silica (SiO_2), alumina (Al_2O_3), iron oxide (Fe_2O_3) and quicklime (CaO) varies considerably between tree species.

Figure 5. Different types of biomasses

2.3.3 Biomass fly ash chemical composition

Variations in the chemical composition of ash produced from different tree species are listed in table 5 **(Rajamma et al. 2009; Cheah et Ramli 2011)**. The performance of woody biomass fly ash as a mineral mixture is highly dependent on its physico-chemical characteristics which, in turn, depend on the type of woody biomass and the type of combustion adopted in the thermal power plant **(Berra, Mangialardi, et Paolini 2015)**.

Table 5. Chemical composition of biomass fly ash from different wood species (Cheah et Ramli 2011)

Biomass group. sub-group and variety	SiO_2	CaO	K_20	P_2O_5	Al_2O_3	Mg0	Fe_2O_3	SO_3	Na_2O	TiO_2
Wood and woody biomass										
Alder-fir sawdust	37.49	26.41	6.1	2.02	12.23	4.04	8.09	0.83	1.81	0.98
Balsam bark	26.06	45.76	10.7	4.27	1.91	2.33	1.65	2.86	2.65	0.21
Beech bark	12.4	6.82	2.6	23	0.12	11.5	1.1	0.8	0.9	0.1
Birch bark	4.38	69.06	8.99	4.13	0.55	5.92	2.24	2.75	1.85	0.13
Christmas trees	39.91	9.75	8.06	2.46	15.12	2.59	9.54	11.66	0.54	0.37
Elm bark	*4.48*	83.46	5.47	1.62	0.12	2.49	0.37	1	0.87	0.12
Eucalyptus bark	10.04	57.74	9.29	2.35	3.1	10.91	1.12	3.47	1.86	0.12
Fir mill residue	19.26	15.1	8.89	3.65	5.02	5.83	8.36	3.72	29.82	0.35
Forest residue	20.65	47.55	10.23	5.05	2.99	7.2	1.42	2.91	1.6	0.4
Hemlock bark	2.34	59.62	5.12	11.12	2.34	14.57	1.45	2.11	1.12	0.11
Land clearing wood	65.82	5.79	2.19	0.66	14.85	1.81	1.21	0.36	2.7	0.55
Maple bark	8.95	67.36	7.03	0.79	3.98	6.59	1.43	1.99	1.76	0.12
Oak sawdust	29.93	15.56	31.99	1.9	4.27	5.92	4.2	3.84	2	0.39
Oak wood	48.95	17.48	9.49	1.8	9.49	1.1	8.49	2.6	0.5	0.1
Olive wood	10.24	41.47	25.16	10.75	2.02	3.03	0.88	2.65	3.67	0.13
Pine bark	9.2	56.83	7.78	5.02	7.2	6.19	2.79	2.83	1.97	0.19
Pine chips	68.18	7.89	4.51	156	7.09	243	5.45	1.19	12	0.55
Pine pruning	7.76	44.1	22.32	5.73	2.75	11.33	1.25	4.18	0.42	0.17
Pine sawdust	9.71	48.88	14.38	6.08	2.34	13.8	2.1	2.22	0.35	0.14
Poplar	3.87	57.33	1833	025	0.68	13.11	1.16	3.77	0.22	02

Poplar bark	1.86	77.31	8.93	2.48	0.62	2.36	0.74	0.74	4.84	0.12
Sawdust	26.17	44.11	10.83	2.27	4.53	5.34	1.82	2.05	2.48	0.4
Spruce bark	6.13	72.39	7.22	2.69	0.68	4.97	1.9	1.88	2.02	0.12
Spruce wood	49.3	17.2	9.6	1.9	9.4	1.1	8.3	2.6	0.5	0.1
Tamarack bark	7.77	53.5	5.64	5	8.94	9.04	3.83	2.77	3.4	0.11
Willow	6.1	46.09	23.4	13.01	1.96	4.03	0.74	3	1.61	0.06
Wood	23.15	37.35	11.59	2.9	5.75	7.26	3.27	9.95	2.57	12
Wood residue	53.15	11.66	4.25	1.37	12.64	3.06	6.24	1.99	4.47	0.57
Mean	22.22	43.03	10.75	3.48	5.09	6.07	3.44	2.78	2.85	0.29

2.4 Paper waste ash

This fly ash is derived from the combustion of biomass waste from the paper industry. Three types of waste are typically co-incinerated: water treatment sludge used in papermaking, de-inking sludge, and paper mill waste (wood, waste paper, etc.).

Since the nineties, France has been committed, along with 170 other countries, to promoting sustainable forest management at the United Nations Conference on Environment and Development in Rio (Earth Summit) **(TERRE 1992)**. Industrialists were therefore invited to develop paper recycling to combat the excessive demand for wood. However, new wastes (pulp processing sludge and de-inking sludge) are produced during recycling operations, creating new challenges. For example, paper manufacturers have found combustible material for their boilers in these sludges (with high calorific value), which constitutes an important recovery channel limiting the need for disposal **(Flourat 2020)**. When these residues are co-incinerated with biomass, new waste is generated: paper waste ash.

In France, two of the twelve paper mills equipped with biomass boilers use paper mill sludge as a substitute for biomass up to 60% **(Flourat 2020)**. The physico-chemical properties of this ash depend mainly on the combustibles used by the boilers of the paper production and/or recycling plants. The production of fly ash from the 2 paper mills recycling sludge in their boiler is about 120 000 tones/year. The amount produced differs between the recycling and paper production facilities. It depends mainly on the thermal power of the boilers and the nature of the inputs as well as on the production capacity in the paper industries.

2.4.1 Physical characteristics

Paper mill ash like other fly ashes from coal, biomass and non-hazardous waste incineration are fine powders with a wide particle size distribution ranging from 1 to 300 µm (R. García et al. 2008; Bai et al. 2003; Segui 2011; Davidenko 2015). Paper mill ashes are very heterogeneous. SEM observations show that it is formed of more or less spherical particles with a porous and agglomerated structure **(Mozaffari et al. 2009; Segui 2011; Davidenko 2015)**. This porosity can lead to problems when the ash is introduced into a cementitious matrix due to the increased water demand.

In the literature, few studies specify the actual density and specific surface area of paper mill ash. In that of **(Frías et al. 2008)**, the ash had a BET specific surface area of 8.7 m²/g **(Frías et al. 2008)** while the ash studied by **Davidenko (2015)** showed lower finenesses (between 2.71 and 4.98 m^2 /g) [117]. Generally, the actual ash densities are between 2.5 and 2.9 g/cm^3 **(Bai et al. 2003; Segui 2011; Davidenko 2015)**.

2.4.2 Chemical composition of paper mill fly ash

The chemical compositions of the ash result from the compositions of the mineral charges (kaolin, natural or precipitated calcium carbonate, titanium dioxide, talc, colloidal silica) used as pigment in paper and inks but also from the coagulating agents used during the de-inking stage of the recycling sludge.

Table 6 below summarizes the chemical compositions of ash produced in the UK **(Bai et al. 2003; Mozaffari et al. 2009; 2006)** and Spain **(Frías et al. 2008; Vegas et al. 2009)**. The Spanish ashes studied by Frias and Vegas are from laboratory tests and not from current production as they seek to understand their formation modes and thus consider modifying the combustion process for their reuse.

Table 6. Chemical composition of paper mills ash

Oxyde	CaO	SiO_2	Al_2O_3	MgO	Fe_2O_3	K_2O	TiO_2	P_2O_5	Na_2O	MnO	SO_3	LOI
(Bai et al. 2003)	43.5	25.7	18.9	5.2	0.9	1.3	0.7	0.5	1.6	0.04	1.1	1.2
(Mozaffari et al. 2006)	40.2	22.3	14.6	2.4	0.6	0.4	0.3	0.2	0.1	-	0.3	18.5
(Banfill et Frias 2007)	36.5	21.6	14.4	2.4	0.5	0.4	0.3	0.2	0.1	-	0.3	23.2
(Vegas et al. 2009)	31.4	30.2	18	2.7	0.7	0.3	0.4	-	0.2	-	0.3	15

Paper mill ash is mainly composed of calcium, silicon and aluminum: together they represent between 70 and 90% of the material. Concentrations of other major elements are low (less than 2%) except for MgO, which can reach a content of 5%. Sulphate (SO_3) levels are below 1% except for the ash studied by **Bai et al. (2003)** et **Mozaffari et al. (2009)**. The high values (between 14.5 and 23.5%) of loss on ignition reflect the decarbonation of the calcite present but also the combustion of unburnt organic compounds initially contained in the paper mill sludge (notably cellulose). The low value (1.2%) proposed by **Bai et al. (2003)** et **Mozaffari et al. (2006)** is certainly due to the temperature used for the test. Indeed, the authors did not specify this temperature and it is possible that the loss on ignition was measured at a temperature of 550°C (as is sometimes the case). In this case, the temperature is not high enough to cause the decarbonation of the calcite, and the loss of mass is only the result of the combustion of the unburnt organic matter.

Concerning free lime, its value varies between 2.7 and 5%. This parameter is very important as it can lead to swelling in early life when ash is used as a partial replacement for cement **(Bai et al. 2003)**. Similarly, the rapid hydration of free lime when ash is mixed with water leads to rapid setting of the paste, loss of strength and cracking **(Davidenko 2015)**.

Only the study by **Segui (2011)** takes into consideration the environmental aspect of fly ash recovery from paper mills. Table 16 shows that the inorganic contaminants present in fly ash are mainly zinc (1389 mg/kg), barium (1238 mg/kg) and lead (796 mg/kg). To date, there is no specific guidance for the assessment of the environmental acceptability of paper mill fly ash or materials made from these industrial by-products. Therefore, it is necessary to refer to the methodological guide **(« Acceptabilité de matériaux alternatifs en technique routière - Evaluation environnementale » s. d.)** to validate their environmental harmlessness according to standardised leaching tests. In the ashes studied by **Segui (2011)**, the concentration of barium in the eluates exceeded the thresholds of the methodological guide, which led to a limitation of their use.

Table 7. Total metallic trace element and metalloid content in the ash studied by Segui (2011)

Metallic trace elements and metalloids	**As**	**Ba**	**Cr**	**Cu**	**Mo**	**Ni**	**Pb**	**Zn**

Concentration (mg/kg)	11.1	1238	117.5	312.8	3.6	50.3	795.9	1389

2.4.3 Mineralogical characteristics

Depending on the origin of the ash listed in Table 5, two mineralogical families appear. The ash contains metakaolin, phyllosilicates, quartz, talc and calcite (Spanish studies **(Frías et al. 2008; de la Villa et al. 2007)** plus that of **(Pera et Amrouz 1998)**): **Pera et Amrouz** were the first to show that calcination of deinking sludge at 700°C to 750°C for two hours in the laboratory produces a highly reactive metakaolin **(Pera et Amrouz 1998)**. These results have been confirmed by the numerous works of **(Frías et al. 2008; de la Villa et al. 2007)**. The presence of metakaolin in these ashes is of interest in the cement industry as it gives the ashes a high pozzolanic potential.

The ash contains about 5% free lime, calcium carbonate, an amorphous phase and hydraulic minerals (α′-C2S and bredigite) as well as inert elements (gehlenite, anorthite and quartz) as in the English sample studied by **Bai et al. (2003) et Mozaffari et al. (2009)**. These ashes can be used in the cement matrix because the quicklime and calcium silicates they contain are hydraulic minerals. In laboratory studies, **Koshikawa** and **Isogai** tried to understand the changes in deinking sludge during incineration **(Koshikawa et Isogai 2004)**. They obtained the same type of mineralogy as the English ash when burnt for one hour at 1000°C. At 800°C, the majority mineral in the ash was talc.

2.5 Sediment

2.5.1 Origin and problematic of sediments

According to the geological dictionary, sediments are defined as a set of particles of varying size or precipitated matter that have separately undergone a certain amount of transport **(Foucault et Raoult 1980)**. Sediment particles can originate from the erosion of rocks and soils or result from chemical precipitation (precipitation of salts such as chlorides and sulphates) and biochemical precipitation (accumulation of skeletons of living organisms, shells). Sediments transported in water have an important role in the transport and fate of pollutants. Toxic substances can be attached to or absorbed by sediment particles and then transported and deposited in another environment. Accumulation of sediments in rivers or lakes can cause the water depth to decrease, making navigation difficult or impossible. Some of the sediment may have to be dredged to provide access to a river or harbor, which can release contaminants into the environment. For this reason, sediment removal is a major problem for harbor and waterway managers.

Two types of sediments are distinguished, marine and river sediments. According to **(SCHNEIDER 2001)**, sediments have three main origins: endogenous, exogenous and diagenesis or neo-formation.

- ***Endogenous origin:*** This is all the debris resulting from the decomposition of large plant macrophytes inhabiting aquatic ecosystems, phanerogams and the corpses of microphytes and animals. In general, all particles come from the indigenous production of the environment.
- ***Exogenous origin:*** they can be of natural or anthropogenic origin. These are particles resulting from water runoff or transported by the wind, they come from soil erosion, the decomposition of organic matter, micropollutants linked to agricultural, industrial and domestic waste.
- ***Diagenesis or neo-formation origin:*** this corresponds to all the alteration, precipitation, biochemical and physico-chemical transformation phenomena that occur in a sedimentation basin and during sedimentation.

The accumulation of these sediments in ports, access channels, canals, rivers and streams prevent the circulation of boats and disturbs the physico-chemical balance of the water quality. Dredging is an essential operation in order to re-establish the minimum draught, the restoration of the natural

environment, as well as to avoid several problems such as: flooding, algae proliferation (fight against eutrophication), and the collapse of banks **(SCHNEIDER 2001)**. Generally, there are two main techniques often used to carry out cleaning: the hydraulic method and the mechanical method.

2.5.2 Fluvial sediments

The French fluvial network comprises more than 525,000 km of waterways, 8,500 km of which are considered navigable **(Capilla 2005)**. The decrease in navigation depth or the risk of flooding requires maintenance operations **(Romero 1999)**. Cleaning operations are the responsibility of the State through the:

- VNF (Voies Navigables de France) for navigable waterways;
- Ports Autonomes Fluviaux (e.g. the autonomous port of Paris ;
- Public establishments such as the Compagnie Nationale du Rhône (CNR) ;

According to a survey carried out by the navigation service of the Hauts-de-France region, approximately 6 million m^3 of fluvial sediments are dredged each year. The destination of these quantities of sediment depends on their degree of pollution: 70% is deposited or placed in strips on the banks, 10% is reused in the public domain, 7% is spread and the rest is used for various purposes (embankments, dumping, etc.) **(Chassiot et al. 2017)**.

2.5.3 Marine sediments

According to surveys and statistics carried out by the Center for Maritime and River Technical Studies (CMRTS), the quantity of marine sediments dredged in France in 2010 represented a total of 18.6 million tons of dry matter, a decrease of 44% compared to that recorded in 2009, which was 33.56 million tons (a difference mainly due to the work carried out in 2009 in the large seaports of Le Havre and Marseille, which was not repeated in 2010**) (Raujouan et Le Guyader 2010)**. The marine sediments are mainly from France the 7 major seaports **Figure 6**, in particular the ports of Dunkirk, Le Havre, Rouen, Nantes, La Rochelle, Bordeaux and Marseille, which together account for 15.2 million tons of dredged sediments, i.e. 82% of the total dredged **(Raujouan et Le Guyader 2010)**.

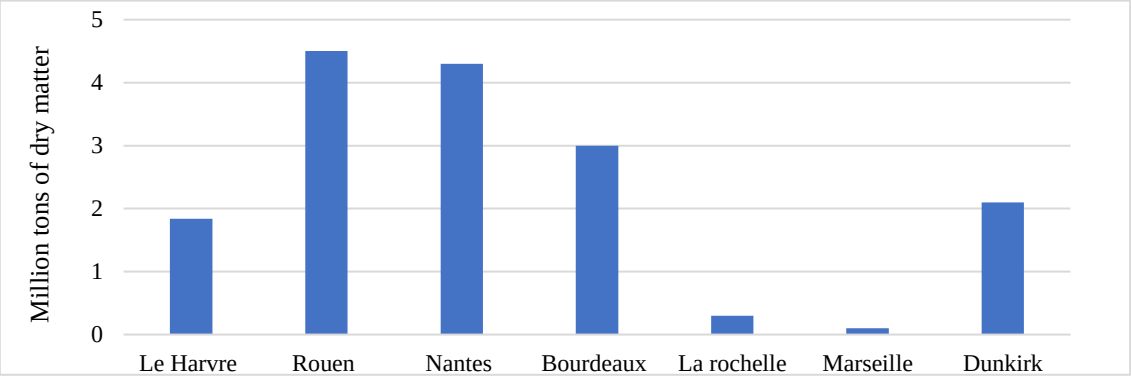

Figure 6. Quantities of marine sediments dredged in France in 2010 (Raujouan et Le Guyader 2010)

2.5.4 Sediment composition

In general, sediments are characterized mainly by: their mineral composition, their grain size, their organic matter and water content. Sediments are made up of three elements **(Artois-Picardie 2001)**:

- The mineral matrix with particles larger than 2µm (quartz, feldspars...) ;
- The clay, fraction inferior to 2 µm (kaolinite, illite...);

- The organic fraction (plant debris, humid acids...);
- The amount of water present in different forms.

2.5.4.1 Mineral phase

Mineral elements essentially influence the physical, chemical and mechanical characteristics of sediments. In sediments, the mineral composition is diverse depending on their origin **(SCHNEIDER 2001)**:

- Terrigenous sediments resulting from soil erosion: boulders, pebbles, gravel and sand;
- Quartz sands (silica) or silicate sands (mica, feldspar), accompanied by heavy minerals (amphiboles, garnets, kyanite...), and calcareous sands;
- The finest particles (silts, sludges and muds) are composed of clay minerals of terrigenous origin, and also the skeletons of endogenous origin organisms.

2.5.4.2 Inorganic phase

Clays are sedimentary rocks, composed of aluminum silicates of varying degrees of hydration, which exist in a layered structure (phyllosilicates) or in a fibrous structure (sepiolite and palygorskite). The origin of the minerals depends on the climate: inheritance (from the source rock), transformation (from other clay minerals), neo-formation (from ions transported by soil water). The most common minerals in clays are therefore kaolinite, halloysite, montmorillonite, illite and vermiculite. The crystalline structure in layers allows the hydration of clays with a swelling phenomenon. The suppleness of the bonds between the layers allows the clays to have a very high plasticity. The negative charges of the clays are neutralized by compensating cations, which can be exchanged with those present and the heavy metals in the medium. The fine sediment thus has the property to capture, retain and accumulate pollutants. Therefore, it can be said that the properties of clay minerals are due to the layered structure, the small size and the negative charge of the particles.

2.5.4.3 Organic phase

Concerning organic matter, all-natural organic compounds are found in sediments. Organic matter is the carbonaceous material, water is the main component besides carbon. The elements hydrogen, oxygen, nitrogen, phosphorus, sulphur, and iron etc. are also found. In general, plants, algae, animals, biosynthesis from microflora, and humid colloids are considered for the origin of organic constituents. The organic fraction comprises two categories: non-humid substances and humid substances. It is the humid substance that colors the sediment black and interacts with the dissolved mineral compound such as metal ions. **Colin (2003)** indicated that humid substances can constitute between 85% and 90% of the total organic fraction of soil. The proportion of organic matter in the dry matter of sediments varies from 2% for river sands to 90% in the case of peat **(SCHNEIDER 2001)**. The proportion of organic matter is usually in the order of 2% to 10% for sediments of white-water rivers and is made up of 60% of humid compounds **(SCHNEIDER 2001)**.

2.5.4.4 Liquid phase

Finally, the nature of the water in the sediment needs to be analyzed, and water is a very important component of the sediment. Normally, water can be considered to fall into five categories:

- Free water which is not bound to the fines.
- Capillary water which is bound to the fines by capillary forces.
- Colloidal water which hydrates the colloid.
- Intercellular water which is chemically bound to the surface of the particles and forms a film around them.

- Water that participates in the hydration reaction to form the hydrated substances.

Free water can be easily removed by simple decantation, and capillary and colloidal water by mechanical solid-liquid separation processes. Intercellular water and water involved in the reaction can be removed by thermal processes.

2.5.4.5 Sediment particle size

The particle size analysis determines the granular characteristics of materials and their statistical size distribution of a population of elements. The grain size frequency distribution explains the distribution of sediments in an aquatic environment. **Table 8** details the particle size classification of sediments.

Table 8. Particle size classification of soils according to the GTR guide

Particle size fraction	Denomination
> 200 mm	Rockfill
20 mm to 200 mm	Rocks
2 mm to 20 mm	Gravels
63 µm to 2 mm	Sands
2 µm to 63 µm	Silts
0 to 2 µm	Clays

In terms of granulometry, the fine fraction is characterized by silts and clays with significant cohesion. Thus, this fine fraction generally induces a complex behavior caused by interactions between mineral particles, water contained in the medium, ions and organic elements **(Dubois 2006)**. Several researchers have shown that fine particles in sediments trap heavy metals (**Péna et Picot 1991)** and most contaminations are fixed in the fine fractions rather than in the other granulometric classes **(Mkahal et al. 2022; Tran 2009).**

2.5.5 Issues related to the management of dredged sediments

2.5.5.1 Pollutants in sediments

Discharges from industrial, urban and agricultural activities are the main source of contamination of dredged sediments. Indeed, these activities are the source of many substances of a proven toxic nature: heavy metals, polycyclic aromatic hydrocarbons (PAHs), organochlorines, organotins, pesticides and various biocides **(Alzieu 1999)**. Due to the fine nature of sediments, they constitute the final refuge for the various pollutants: it has been proven that toxic substances are mainly concentrated in the fine part (< 45 µm) **(Noppe 1996; Gosselin, Blackburn, et Bergeron 1999)** and in the OM, which manages to immobilise organic pollutants and heavy metals **(Alzieu 1999; Xiaofeng Zhao et al. 2011)**. The problem of the mobility of toxic elements and their effects on living organisms is caused when their physico-chemical environment is disturbed, particularly by dredging, immersion or disposal operations.

According to **Alzieu (1999)**, the main physico-chemical characteristics of the dredged materials, which control the interactions between the sediment and the toxic substances are:

- The quantity and type of fine particles (pelites)
- The pH
- The quantity and nature of the cations and anions present;
- The Redox potential: a measure of the reactivity between chemical species;
- The Organic matter content (especially humid acids)
- The degree of salinity.

2.5.5.2 *Organic pollutants*

Organic pollutants are mostly carcinogenic and can constitute a real danger to human health. According to **(Dia 2013)**, the degree of risk associated with these substances depends mainly on the pollutant's nature, the level of toxicity and the mode of exposure. The main organic pollutants usually found in dredged sediments are tributyltin (TBT), polychlorinated biphenyls (PCB) and PAHs.

Tributyltin (TBT)

TBT is used as an active material in antifouling paints applied to harbor and roadstead buildings and to the hulls of ships to protect them from attachment by living organisms. It is degradable in water by microbiological and photolytic action, and its lifetime measured under environmental conditions varies from a few days to a few weeks. In sediments, TBT is much more stable and can persist for several years **(Alzieu 1999)**. The degradation of TBT in the environment releases two products, dibutyltin (DBT) and monobutyltin (MBT). These two substances are also toxic but their toxicity is less than that of TBT **(Zeraoui 2020)**. TBT belongs to the family of organotin compounds listed in the OSPAR Convention[1] **(OSPAR Commission)**, which requires the elimination of these products from all ships from 1 January 2008 unless they are prevented from escaping by a coating **(Zeraoui 2020)**. It is important to note that TBTs are highly toxic and can cause disturbances to living marine organisms even at very low concentrations.

Polychlorinated biphenyls (PCB)

PCBs are a family of synthetic chemical molecules belonging to the group of organochlorines with the chemical formula C10H(10-n)Cln. This group includes more than 209 congeners. Before their effect on the environment was proven, PCBs were widely used as additives in several products such as paints, inks and primers for wall covering **(Alzieu 1999)**. PCBs are exclusively of anthropogenic origin. According to **Alzieu (1999)**, the sources of PCBs are potentially urban discharges, used equipment landfills, activities related to the recovery of ferrous materials and losses due to the filling and reprocessing of closed systems. PCBs contaminate the entire food chain up to humans and can have a chronic health effect such as immune suppression, inflammatory response, and endocrine effects to varying degrees. In 2016, IARC2 classified PCBs (Group 1) as a carcinogen **(Zeraoui 2020)**.

Polycyclic aromatic hydrocarbons (PAHs)

PAHs are a family of molecules composed only of carbon and hydrogen, and are mainly of pyrolytic origin - resulting from the incomplete combustion of OM at high temperature (fuel, wood, etc.) - or petrogenic origin - i.e. the result of the slow mutation (over several million years) of OM during diagenesis and catagenesis, which are the mechanisms of oil production in the deepest part of the sedimentary environment **(Mazeas 2004)**. Indeed, oil contains between 0.2 and 7% PAHs which are also found in fuels **(Léauté 2008)**. PAHs are commonly poorly soluble in water; therefore, they associate with hydrophobic regions of OM through the process of adsorption and thus the soil serves as a storage reservoir for PAHs **(Mazeas 2004)**. Depending on the source of the PAHs, they can be present in more than 100 different compounds. In general, the 16 PAHs classified by the EPA[3] as priority pollutants are checked during the environmental assessment of sediments **(Zeraoui 2020)**.

2.5.5.3 *Metallic and metalloids trace elements (MMTE)*

Heavy metals, commonly referred to as " metallic and metalloids trace elements " (MMTEs) because of their low quantity in the soil, do not have a unanimously recognised scientific definition, some authors defining them according to their minimum density and others according to their atomic number or mass

[1] OSPAR: Convention for the Protection of the Marine Environment of the North-East Atlantic, September 1992.
[2] IARC: International Agency for Research on Cancer
[3] EPA : Environmental Protection Agency

(Elghali et al. 2019; Duffus 2002) . According to **Delabre (1985)**, the origin of metallic trace elements and metalloids present in sediments can be divided into two groups:

- Metallic trace elements and metalloids of natural origin: they result from the erosion of rocks or the leaching of soils where they are present in their natural state;
- Metallic trace elements and metalloids of anthropogenic origin: they are derived from human activity such as the extraction and processing of ores, the use of metals and metallic compounds, the combustion of fossil fuels, the leaching of metals from refuse and solid waste landfills, rainwater and wastewater discharges from highly urbanised areas, etc.

Metallic trace elements and metalloids, as for organic matter, are distributed in the various fractions of the sediments. Heavy metals related to precipitation phenomena are present in different forms: complexes, ions, adsorbed on the surface of particles, and can be fixed on mineral particles and organic matter in sediments. In the present work, the main sectors and sources are presented below **(Alzieu 1999)**.

- Arsenic (As) : L'extraction, le transport et le traitement métallurgique ; les rejets liquides ou solides et les émissions atmosphériques ; la combustion du charbon ; production de trioxyde d'arsenic.
- Cadmium (Cd) : La fabrication des batteries, pigment ; le traitement de surface des aciers ; la stabilisation des matières plastiques ; la composition des alliages non ferreux.
- Chrome (Cr) : L'extraction de la chromite, minerai de fer et de chrome ; la métallurgie ; des matériaux réfractaires ; l'industrie chimique.
- Cuivre (Cu): L'industrie électrique; l'utilisation de l'oxyde Cu_2O comme matière active des peintures antisalissures marines.
- Mercury (Hg): The manufacture and use of catalysts, fungicides, pigments and mercury compounds, mercury batteries, the manufacture of chlorine by electrolysis on a mercury cathode, the processing of non-ferrous ores, waste incineration and coal combustion.
- Nickel (Ni): Fossil fuel use; non-ferrous metal production; volcanic activity; wind erosion.
- Lead (Pb): The use of tetraethyl lead as an additive to anti-knock fuels; battery manufacture; petrol; atmospheric emissions.
- Zinc (Zn): The dissolution of pure zinc masses attached to boat sinks; certain antifouling paints.

Once the tolerance threshold is exceeded, metallic trace elements and metalloids can be considered toxic **(SCHNEIDER 2001)**. The toxicological impact of metallic trace elements and metalloids depends on their concentration, the environmental context, their chemical form and the possibility of passage through the living chain. For example, the absorption of lead causes lead poisoning, but lead is considered biocompatible and used in surgery or dentistry. The different metals and metalloids have been classified according to their toxicity and availability in the environment **(Table 9)**.

Table 9. Classification of metallic trace elements and metalloids according to their toxicity and availability (Delabre 1985)

Non-toxic elements			Toxic elements		Highly toxic elements		
Na	C	F	Ti	Ga	Be	As	Au
K	P	Li	Hf	La	Co	Te	Sb
Mg	Fe	Rb	Zr	Os	Ni	Pb	Bi
Ca	S	Sr	W	Rh	Cu	Ag	
H	Cl	Al	Nb	Ir	Zn	Cd	
O	Br	Si	Ta	Ru	Sn	Pt	
N			Re	Ba	Se	Hg	

2.5.6 Dredging technology

Dredging is an operation that consists of removing materials (sand, gravel, limestone) from the sea bed. Dredging procedures vary according to the zone, the type of dredging work and the nature of the sediment to be dredged. Classically, three types of dredging are distinguished: deepening dredging, dredging for the development of new port areas and maintenance dredging **(Foucher 2005)**. Deepening dredging is undertaken when there is a need to modernize ports and to adapt navigation weirs. Periodic maintenance dredging aims to extract sediments that have settled and interfere with navigation in the access channels of seaports and estuaries, and in the docks. Dredging for the construction of new port areas concerns the displacement of volumes of various materials (sand, clay, gravel).

In terms of equipment, a general distinction is made between mechanical, hydraulic and pneumatic dredges **(CETMEF 2000)**. There are several types of dredgers, and the classification of dredges is presented in **Figure 7**. Mechanical dredges are used in areas that are difficult to access (dock edges, narrow basins) and can work to depths of 25 m (bucket dredge) to 30 m (clamshell dredge) **(Foucher 2005)**. Hydraulic dredges are based on the principle of the centrifugal water pump and operate by creating a vacuum at the pump inlet. The atmospheric pressure in the water forces the mixture to follow the suction line, which is the only available trajectory **(Foucher 2005)**. Hydraulic dredging is the most commonly used method, which includes the following categories: stationary or simple suction hopper dredger, cutter suction dredger, trailing suction hopper dredger or more commonly known as a running suction dredger, sweeping dredger, disc cutter dredger and screw dredger **(Foucher 2005)**. The pneumatic dredger is particularly adapted to dredge contaminated sediments, and the material is then evacuated by barge or floating pipe **(Foucher 2005)**.

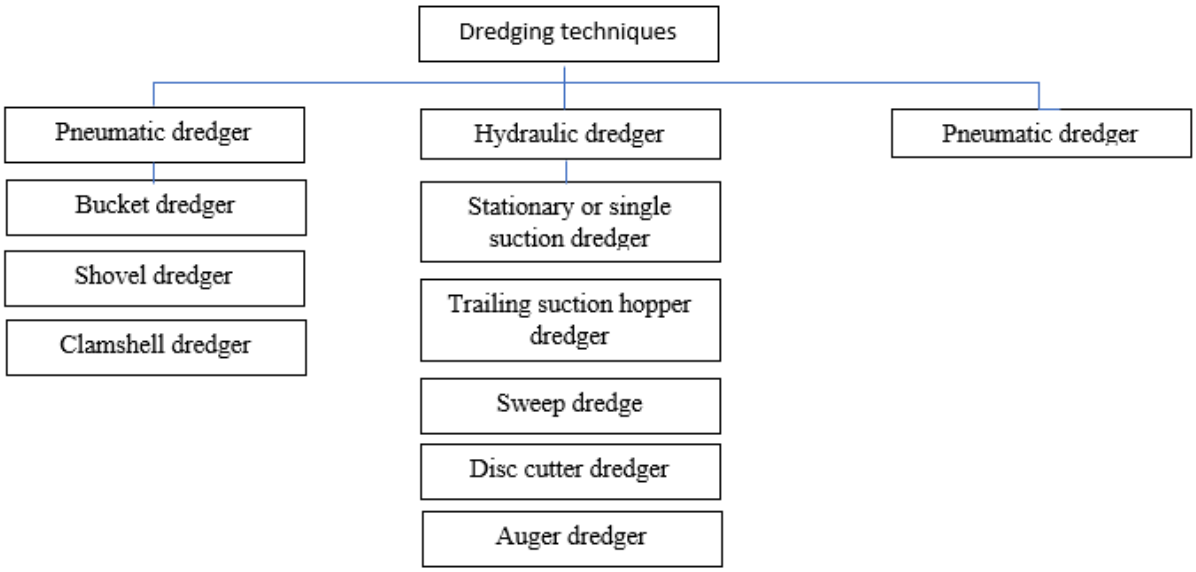

Figure 7. Sediment fat

2.5.7 Dredging techniques

2.5.7.1 Quantity of dredged material

In European countries, especially France, a large amount of material has to be dredged annually from the seabed, rivers, lakes and ports by dredgers. The dredging activity is carried out either to carry out

port engineering works or to exploit the dredged material. The situation of dredging of sediments in many European countries is carried out by the annual survey of the OSPAR Commission. In France, there are 69 commercial and fishing ports, including 17 metropolitan ports of national interest and 6 autonomous ports. Each year, between 25 and 45 million tons of dry sediment are dredged for port maintenance. In the five major maritime ports: Dunkirk, Calais, Boulogne, Le Havre and La Rochelle, an average annual volume of about 4 million tons is dredged. In the three estuary ports (Rouen, Nantes Saint-Nazaire and Bordeaux), an average annual volume of about 15 million tons of sediment is dredged. But dredging in the ports of Lorient, Sète and Port la Nouvelle is negligible in terms of quantity. The total quantities of sediments dredged in French ports are respectively 20440, 27354 and 43424 thousand Tons in 2001, 2002 and 2003.

2.5.7.2 Regulatory aspects of dredged material management

Dredging, dumping or land-based management of sediments are subject to evolving national and international regulations recommending good environmental practices and whose objectives are the prevention and protection of the environment and aquatic environments and the preservation of biodiversity.

In France, the regulations apply to the different levels of dredging sediment management. Depending on whether the management method is by immersion or by management on land, and whether the dredged materials are of maritime or river origin, the regulations that apply and the thresholds established are no longer the same. Indeed, the procedure for managing sediments immediately after dredging is faced with the various possible disposal channels and the notion of waste defined in article L 541-1 of the environmental code, which stipulates that all sediments, once extracted from their environment, are considered as waste.

2.5.7.3 Immersion regulations

Dumping at sea is another method of disposal that contributes to the elimination of waste. This method is only applicable to materials with little or no pollution. For contaminated sediments, one of the methods already considered and adopted is confinement in an aquatic environment, in a site where the hydrodynamic conditions ensure the stability of the dredged materials **(Boutouil 1998)**.

In France, regulations apply to the different levels of dredged material management. Depending on whether the management method is by immersion or by management on land, and whether the dredged materials are of maritime or river origin, the regulations that apply and the thresholds established are no longer the same. Indeed, the procedure for managing sediments immediately after dredging is faced with the various possible disposal channels and the notion of waste defined in article L 541-1 of the Environmental Code, which stipulates that all sediments, once extracted from their environment, are considered as waste. The degree of contamination of dredged sediments intended for dumping is assessed against reference values according to **Table 10**.

Table 10. Relative levels of trace elements and trace compounds (mg/kg dry sediment on the fraction below 2mm)

Pollutants (mg/kg)	Level 1	Level 2
Arsenic	25	50
Chrome	90	180
Copper	45	90
Nickel	37	74
Lead	100	200
Zinc	276	552

Cadmium	1.2	2.4
Mercury	0.4	0.8
PCB	0.5	1

Level 1 (N1): below which dredging and dumping operations would be allowed without further study: the potential impact is considered neutral or negligible, as the observed values are found to be comparable to environmental "background".

Level 2 (N2): above which dumping operations are likely to be prohibited provided that such prohibition is the least environmentally damaging management option: further investigation is generally required as there are indications of a potential impact of the operation. A thorough impact assessment is then considered essential.

2.5.7.4 Landfill regulations

A decision was taken by the Council of the European Union on 19 December 2002 **(JOCE 16 janvier 2003)** establishing criteria and procedures for the acceptance of waste at landfills. This document defines three types of landfills: inert, non-hazardous and hazardous waste. Pollution thresholds have been specified to determine whether waste is suitable for landfill for materials **(Table 2)**. It should be noted that these criteria are largely based on leaching and percolation tests **(Order of 12 December 2014)**.

- Inert Waste Storage Installations (IWSI) whose acceptability criteria are defined in the decree of 28 October 2010 on inert waste;
- Non-Hazardous Waste Storage Installations (NIWSI): these installations are regulated by the decree of 9 September 1997;
- Hazardous Waste Storage Installations (HWSI): these are subject to the decree of 30 December 2002, and in the event that the thresholds presented in **Table 2** are exceeded, treatments must be applied to the sediments before storage.

2.5.8 Treatment

The treatment of sediments using several methods has many advantages: destroying, extracting, immobilizing or neutralizing contaminants. These methods are developing and evolving due to technological advances. Nevertheless, it is difficult to establish an exhaustive list of all treatment methods. It is necessary to pre-treat sediments for storage, reclamation and treatment. For example, their water content can be reduced by decanting and air drying. According to **Boucard (2006); Zoubeir et al. (2007)** and **Artois-Picardie (2001)**, the main processes and techniques are: physico-chemical treatment, thermal inserting, biological treatment and immobilization. It is important to consider several criteria in order to evaluate the performance of treatments: technical, socio-economic and environmental factors.

2.6 Shooting range soil

The military training activities that occur on military bases, such as small- and large-caliber firing exercises, can lead to the release of contaminants into the environment, particularly metals. Lead (Pb) together with antimony (Sb), copper (Cu) and zinc (Zn) are present in most small arms ammunition. The core of the bullet accounts for approximately 95% of the total bullet mass and consists of a Pb-Sb alloy. The outer cover of the bullets is made of Cu-Zn alloy and represents approximately 5% of the total bullet mass.

The large quantities of bullets shot at the hundreds of French military shooting sites therefore lead to very high levels of Pb, Cu, Sb and Zn pollution in the soils of the stopes. Not only can wildlife in the vicinity of the shooting sites be exposed to these high concentrations of metals, but military personnel who frequent the sites during exercises as well as personnel who carry out maintenance on the sites can also be exposed to the contaminants via fine metal particles carried by the wind **(Fig 8)**. These particles could also affect the surrounding flora. Soil contamination could also affect the interstitial water in the unsaturated zone and possibly the quality of the groundwater. For these reasons, it is important to examine the environmental impacts of French small arms shooting sites.

Figure 8. Shooting ranges

2.6.1 Identification of environmental problems in the fields

As explained above, shooting practice is an essential element in the preparation of French Forces soldiers for their tasks. However, this practice can have adverse effects on the sustainability of a small arms range, as this activity introduces contaminants into the environment when projectiles are fired.

Brochu et al. (2011) estimate that military training sites, such as small arms ranges, are the most contaminated due to the accumulation of contaminants over limited areas. This accumulation of contaminants occurs when soldiers practices live shooting. Soldiers use projectiles that, when fired, project a bullet at high velocity towards a specific target. Figure 9 shows the four components of a small arms projectile, the bullet, the case, the charge (inside the case) and the primer.

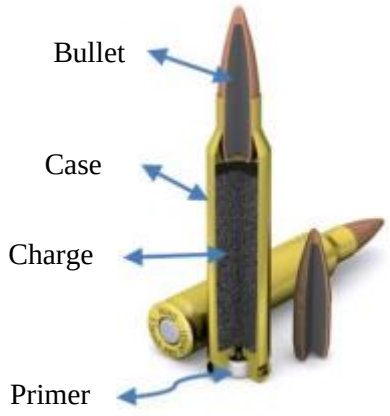

Figure 9. Small arms projectile

The bullet is the front part of the projectile that is ejected towards the target. The exact composition of the metals contained in the bullet varies according to each manufacturer's specifications. Each bullet contains a mixture of several metals, including lead, copper, zinc and antimony **(Marois et al. 2004)**. Lead forms the core of the bullet and varies in quantity depending on the type of bullet used. For example, a 5.56mm bullet contains 93.1% lead, 1.9% antimony, 4.5% copper and 0.5% zinc **(Laporte-Saumure 2010)**. The antimony is used to harden the bullet, while the copper and zinc are used to coat the bullet core **(Laporte-Saumure 2010)**. The casing is the largest part of the projectile. It is made of copper, zinc and nickel **(Marois et al. 2004)**. The charge is located inside the case and contains energetic material that burns very rapidly to cause a violent expansion of gases that ejects the bullet **(Nations Unis 1999)**. The energetic materials causing this combustion and rapid gas expansion are an amalgam of nitrocellulose, nitroglycerin, dibutylphthalate, graphite and dinitrotoluene (DNT) **(Marois et al. 2004)**.

2.6.2 Pollution in the vicinity of shooting installations

The practice of shooting pollutes the ground when whole projectiles penetrate directly into the bullet-proof mound and when shrapnel and metal dust produced on impact penetrate into the surrounding soil. Pollution in the vicinity of shooting installations can be subdivided into distinct sectors according to its extent. It has been customary to distinguish between a limited and highly polluted "sector A" and a less polluted "sector B". The following example illustrates the pollution to be expected in sectors A and B of a 300 m shooting installation (Figure 10).

- Sector A includes the bulletproof mound and the target area, as well as a band of terrain approximately 5-10m wide surrounding the mound. The most significant pollution is found directly behind the targets in the various impact zones. More than 20 g of projectiles or projectile fragments can be found per kg of soil. The lead content is therefore of the same order of magnitude as in some mineable lead ores. Pollution in the rest of sector A is mainly due to stray projectiles, fragments, ricochets and deflections. It is generally above 1000 mg Pb/kg.
- Sector B comprises the area adjacent to the bullet-proof mound, referred to as the "close zone". Pollution here varies between 200 and 1000 mg Pb/kg. It is attributable to the dispersion of projectile fragments during the impact and gradually decreases towards the outside. The extent of soil pollution due to this dispersion depends mainly on the nature of the shock-absorbing materials forming the mound (sand, stones, wood), local aerological conditions, the topography and the maintenance of the installation (fired projectiles that explode when they hit old projectiles).
- The areas furthest away from the bullet-proof mound usually only contain concentrations below 200 mg Pb/kg. This pollution has no health consequences and does not require any measures such as land use restrictions.

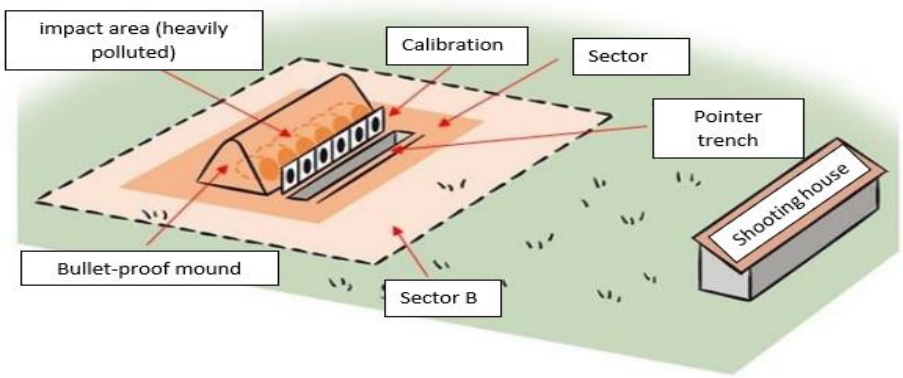

Figure 10. Lead pollution from shooting in installation

2.6.3 Contamination at small arms shooting sites

In recent years various characterization studies of small arms shooting sites have been carried out. These studies have been carried out on military or civilian shooting sites (i.e. recreational shooting sites). They focus on the quantification of Pb contents and on the alteration products of the initial metallic Pb. Among the many studies characterizing Pb levels at small arms shooting sites are those of **Manninen et Tanskanen (1993)**, who found total Pb levels of 54,000 mg/kg soil; **Mellor et McCartney (1994),** with maximum levels of 10,620 mg/kg soil; **Lin (1996)** who found total Pb levels of 3,400 mg/kg soil; **Lin (1996)** who reported total Pb levels up to 24,500 mg/kg soil; **Stansley et Roscoe (1996)** who observed total Pb levels up to 75,000 mg/kg soil; **(Murray et al. 1997)**, with maximum levels of 2256 mg/kg soil; **(Rooney et al 1999)**, who observed maximum total Pb levels of 6724 mg/kg soil; and finally **Clausen et Korte (2009)** observed maximum Pb levels of up to 97,600 mg/kg. Other studies (e.g.**Lin 1996; Corinne P. Rooney et al 2007; Cao et al. 2003**) focused on the analysis of the composition of weathering crusts developing on bullet fragments in soil. These studies reveal that the main weathering products of the bales and bale residues are hydrocerusite ($Pb_3(CO_3)_2(OH)_2$), cerussite ($PbCO_3$), litharge (PbO), anglesite ($PbSO_4$) and hydroxypyromorphite ($Pb_{10}(PO_4)_6(OH)_2$). The identification of the different secondary Pb mineral phases present in soils is important, as these mineral phases are characterized by distinct solubilities and Pb present in the soil of shooting sites has a strong tendency to react with these phases and to be found within these minerals (Z. Lin 1996). According to **Hardison Jr et al. (2004)**, the abrasion of bullets when they contact the mound soil results in the formation of significant amounts of fine metallic Pb particles. These fine Pb particles can rapidly transform into Pb compounds that are more reactive than the metallic Pb originally present in the soils. **Rooney et al (2007)** carried out an experiment to evaluate the rate of oxidation of Pb in an incubator mound soil and found that visible weathering crusts had developed on Pb particles in the mound soil after only 6 months. Although many studies have focused on Pb contamination at shooting sites, some studies have also addressed Cu, Zn and Sb contamination associated with the small arms shooting site (e.g. **Johnson et al. 2005**; **Thorbjornsen et Myers 2007**; **Ackermann et al. 2009**; **Bannon et al. 2009**; **Clausen et Korte 2009**).

The Sb pollution is also significant in this type of soil. Concentrations of 437 mg Sb/ kg have been found in shooting range soils **(Spuller et al 2007)**, while other concentrations ranging from 35 to 17,500 mg Sb/kg were measured in another shooting range soil **(Johnson et al. 2005)**. **Laporte-Saumure (2010)** found values of 80 to 2660 mg Sb/kg. The Sb contamination of shooting ranges tends to be high at the soil surface **(Johnson et al. 2005)** and decreases with depth **(Filella et al 2002)**.

Ampleman et al. (2009) reported lead levels of 6,140 mg/kg, antimony levels of 69.6 mg/kg, copper levels of 227 mg/kg, and zinc levels of 33 mg/kg when sampling the Alpha Range at the Meaford military base in Ontario. All of these amounts are above the Canadian Council of Ministers of the Environment **(CCME)** industrial soil quality criteria of 600 mg/kg for lead, 40 mg/kg for antimony, 91 mg/kg for copper and 360 mg/kg for zinc. **Diaz et al. (2008)** report similar results to **Ampleman et al. (2009)** for the types of metals found in the Range 1 stop mound at the Wainwright Military Base in Alberta. However, the metal levels are higher: 66,100 mg/kg lead, 932 mg/kg antimony, 6,740 mg/kg copper and 715 mg/kg zinc.

2.6.4 Metal toxicity

Pb is problematic in terms of its toxicity. In humans, Pb has degenerative effects on the nervous system **(Schwartz et al. 1988; Davis et al. 2003; CCME.; Hardison Jr et al. 2004).** Lead poisoning is an acute or chronic poisoning by Pb. **Davies (1995)** demonstrated a direct relationship between Pb in soils and dusts and Pb levels in human blood. Pb can cause high blood pressure, as well as fertility problems and liver and kidney damage **(Davydova 2005)**. **Xintara (1992)** points out that in large US cities, there are an estimated 10 to 25 million children with blood Pb levels too high to be considered healthy (health problems such as anemia and neurotoxicity). These children, especially those aged 2 to 4, are exposed to Pb via oral ingestion of contaminated soil (pica eating phenomenon; **Xintara 1992**).

Antimony is also identified as a pollutant that can cause health problems in humans **(Ackermann et al. 2009)** and is classified as a potential carcinogen by the International Agency for Research on Cancer **(International Agency for Research on Cancer 1989)**. Ingestion of Sb can lead to irritation of the digestive system, growth retardation in mammals, and fertility problems in women.

Cu and Zn are essential trace elements that must be present in the human diet to maintain normal physiological functions **(Goldhaber 2003)**. However, at high levels Cu and Zn can become toxic to both humans and plants. High levels of Cu in the blood can cause abdominal pain, diarrhea and when combined with certain genetic factors, liver damage. High levels of Zn have been associated with gastrointestinal irritation and vomiting **(Tanner 1998; Goldhaber 2003).** At high levels, both Cu and Zn are damaging to plants, slowing down their growth **(Gallego et al 1996; Prasad et al 1999, CCME)**

2.6.5 Availability of metals in soils and hazardousness

The potential availability of metals from contaminated soil can be characterized in two main ways: (1) by directly measuring metal concentrations in soil pore water (in situ) and (2) by laboratory leaching tests, i.e. ex situ.

Few studies have characterized the water quality at small arms shooting sites by in situ sampling. However, **Clausen et Korte (2009)** sampled the interstitial water at US military small arms shooting sites using porous ceramic suction lysimeters. They concluded that Zn was potentially more mobile than Pb and that Sb and Zn concentrations should be monitored in pore water at small arms shooting sites.

There are numerous laboratories leaching tests to characterize the availability of metals in soils or solid residues. These tests are used to determine whether these soils or residues are hazardous wastes. The concentrations of metals leached in these different tests are compared to defined limits to determine whether or not the waste is hazardous **(Tables 10)**. Concentrations above the limits indicate that the soil or residue is considered hazardous and must be treated before disposal, or can only be landfilled in special sites reserved for this type of hazardous waste, such as the Saint Nazaire site (Soil used in this study). It should be noted that in France, the potential hazardousness of soils or residues is mainly determined by the concentrations of metals in the soil. Indeed, the standard NF EN 12457-2 and the

HP1-HP15 criteria, respectively, are defined as the limit for soil landfill and waste hazardousness. In the USA, the Toxicity Characteristic Leaching Procedure (**TCLP 1992**) and the Synthetic Precipitation Leaching Procedure are frequently used.

Other tests such as the Extraction Procedure (EP) Toxicity Test and the American Society for Testing Material water test are also used. In Australia, tests such as AS 4439.2-1997 and AS 4439.3-1997 from Australian Standards are used. In Europe many other tests are used in different countries. For example, in the Netherlands the NEN 7341 and NEN 7349 tests are used.

2.6.6 Elimination of shooting range soil

When planning the remediation project, the polluted areas and their contents must be precisely delimited in order to ensure that the subsequent sorting of the materials to be disposed of is environmentally sound and cost-effective. The crucial parameter for the choice of disposal route is usually the lead content of the polluted materials. The table presents the conditions for the valorization or disposal of shooting range soils by the Federal Office for the Environment (OFEV) in Switzerland (Table 11).

Table 11. Disposal routes according to lead and antimony content

	Lead/antimony content	Disposal route	Motive or indication
Excavated earthen material (top soil layer)	0-50 mg Pb/kg	Left in place; reuse as unpolluted soil material	Top layer of unpolluted soil, to be recovered as far as possible
	50-200 mg Pb/kg	Left in place; reuse as low-pollution soil material	Considered as little polluted earth materials, to be recovered if possible on site according to the principle of regrouping what is similar.
	>200 mg Pb/kg	Disposal according to OLED*	Heavily polluted soil materials that cannot be reused, to be disposed of in accordance with the OLED.
Mineral excavation materials (subsoil)	0-50 mg Pb/kg	Disposal as unpolluted excavation material	Mineral materials up to a lead content of 50 mg/kg, considered unpolluted, to be recovered as far as possible to save resources.
	50-250 mg Pb/kg	Disposal as low-pollution excavation material	Mineral materials up to a lead content of 250 mg/kg, considered to be slightly polluted, reusable in many areas, to be recovered as far as possible to save resources.
	250-500 mg Pb/kg	Recovery on site or as construction material in a B-E landfill construction material in a B-E landfill or storage in a B landfill or use as raw material for the production of cement clinker	Mineral materials with a lead content of up to 500 mg/kg: recovery in accordance with Art. 19, para. 3, OLED or use in the manufacture of cement and concrete or storage in a type B landfill, OLED.

	500-2000 mg Pb/kg and max 500 mg Sb/kg	Storage in a type D landfill	Mineral materials up to a lead content of 2000 mg/kg storage in a Type D landfill. The antimony content of the ammunition used on the site during its entire operational life is usually not known precisely. Materials intended for storage in a Type D landfill may have lead contents of more than 1000 mg/kg in combination with antimony contents in the projectiles of more than 5% (relative to lead), which may result in concentrations of more than 50 mg Sb/kg, prohibiting direct storage in a Type D landfill and requiring prior treatment. The OFEV therefore recommends that antimony should always be measured, i.e. the antimony/lead ratio should be determined, when analyzing waste disposal according to OLED.
	>2000 mg Pb/kg or > 50mg Sb/kg	Treatment (soil washing as a general rule)	Materials with a lead content >2000 mg/kg or antimony content >50 mg/kg, which may not be landfilled as such, but which must be treated beforehand (to lower their concentration). Lead recovered from soil washing can be valorized. The treatment of highly polluted mineral materials is not only technically feasible and ecologically sensible, but also economically feasible. It would also be theoretically possible - but in practice too expensive - to store these materials in an underground dump.

3 Physico-chemical stabilization of mineral waste

Stabilization is defined as the process of reducing the hazardous potential and leachability of a material (fly ash, soil...) by converting its contaminants into less soluble, mobile or toxic forms. The notion of stabilization is often associated with the notion of solidification; the term stabilization/solidification (S/S) is used. Solidification transforms a material into a solid monolith with high physical integrity and structural homogeneity. Solidification does not necessarily directly involve a chemical reaction between the waste and the solidifying agent: it can be a mechanical entrapment of the waste in the solid. Similarly, for stabilization, which may only be a change in the environment (such as a change in pH) **(Conner et Hoeffner 1998; Wiles 1987)**. It is important to emphasize that stabilization does not necessarily imply solidification; but that while solidification does not necessarily imply stabilization in the strict sense of the word, it can reduce the leachability of the material by reducing its exposed surface area or by changing its water properties.

In this section, we will first describe the physico-chemical mechanisms responsible for the retention of trace metals and metalloids in the solid. Secondly, we will give examples of applications in the field of stabilization of trace metals and metalloids in contaminated soils as well as in industrial waste. Only the

contaminant stabilization methods used in this study (geo-polymerization, stabilization-solidification with hydraulic binders, carbonation of alkaline wastes and dephosphatation) will be discussed here, but not the remediation methods that consist of removing the contaminants from the material by means of dynamic processes.

3.1 Retention mechanisms

In this section, we will present the principal physico-chemical mechanisms responsible for the retention of metallic and metalloid trace elements in solids. **Figure 11 (Manceau, Marcus, et Tamura 2002)** illustrates the main interactions between an atom (or a molecule) and a solid. The physico-chemical processes at the solid/liquid interface, which can allow the trapping of metallic and metalloid trace elements, are the following:

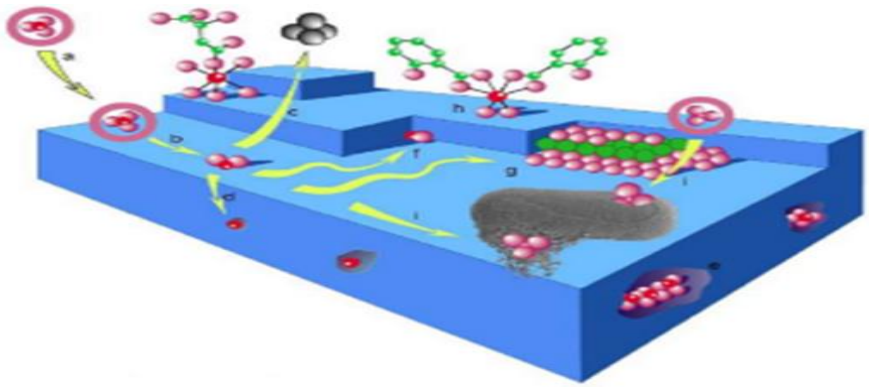

Figure 11. Principal interactions between an atom or molecule and a solid at the solid/liquid interface (Manceau, Marcus, et Tamura 2002). a) adsorption or physisorption; b) chemisorption; c) detachment; d) absorption or inclusion (case of ions having a similar radius and charge to one of the ions of the crystal); e) occlusion (pocket of impurity literally trapped inside the growing crystal); f) attachment of a complex molecule; g) hetero-nucleation (epitaxial growth); h) organo-mineral complexation; i) complexation with bacterial exopolymers.

- Adsorption: surface phenomenon by which atoms or molecules attach to the solid surface of a substrate through various processes. Some minerals, such as clays or zeolites, are excellent adsorbents, due to their very large specific surfaces. Desorption is the reverse transformation of adsorption, whereby the adsorbed molecules or atoms are detached from the substrate. There are two types of adsorption, depending on the mechanisms involved:
  - Physical adsorption (or physisorption): It is due to the electrostatic attraction of a solute by a polarized surface, in order to maintain electroneutrality. The binding energies involved are relatively low, of the Van der Waals force type. The species adsorbed in this process retain the water molecules associated with them. Several layers of atoms or molecules can be deposited in this manner. Physical adsorption is generally easily reversible **(Manceau, Marcus, et Tamura 2002)**. The ability of a material to retain cations by physical adsorption is called C.E.C. (cation exchange capacity).
  - Chemical adsorption (or chemisorption): In this case, the molecule adheres to the surface by ionic or covalent bonds. It is often not easily reversible and engenders a mono-molecular layer. This binding is specific, i.e. it is only possible between elements with a suitable electronic configuration **(Sigg, Behra, et Stumm 2001)**. Surface complexation occurs when a metal ion reacts with an anionic group that functions as an inorganic ligand (e.g. OH^-, Cl^-, SO_4^-, CO_3^{2-}); thus, these surface sites form chemical bonds with the ions in solution.

- Precipitation: It is the passage of a species from a dissolved state to a solid state. The metals can precipitate in pore water or on the surface of solid particles. In a natural environment, metals precipitate mainly as hydroxides, carbonates, phosphates or sulphides.
- Substitution in the crystal lattice: An atom can substitute for another in the crystal lattice; its charge and size must then be similar. This is for example, the case of a metal ion incorporated into the crystal lattice during its precipitation, or which diffuses into the solid to replace a void or an atom of the solid.
- Inclusion (mechanical entrapment): This refers to impurities mechanically trapped in non-open pores during mineral growth. This can be in dissolved or solid form.
- Diffusion into the crystal lattice: Once adsorbed on the surface, a cation can diffuse into the crystal lattice and fill the lacunae in the lattice, or substitute for the ions present. This process will occur if the ionic radius of the cation in question is close to the size of the cavity or the substituted cation.

A metallic element retained on the surface of a material (physisorption, complexation, precipitation, chemisorption) will be more rapidly put into solution and therefore present a greater risk of toxicity than if it is inserted into the crystalline lattice of the material **(Benard 2003)**.

3.1.1 Role of physico-chemical parameters

The pH has a very important role in the mobility of metals. An acidic pH leads to solution of metal salts, solution of retention phases, desorption of cations and adsorption of anions **(Lions 2004)**. Solubility therefore decreases as the pH increases, passes through a minimum, and then increases when the element is in anionic form. Some metals are relatively mobile depending on their redox state. For example, chromium is considered toxic and mobile in its Cr(VI) form, but not in its Cr(III) form. Redox conditions can influence the mobility of an element in three different manners **(Blanchard 2000)**: (i) change in the oxidation state of the element themselves, (ii) change in the oxidation state of elements bonding with the element itself to form a complex and (iii) formation or dissolution of carrier phases of the trace element (e.g. hydroxide). Between 10 and 30°C, temperature has only a negligible direct effect on the mobility of metals **(Serpaud et al. 1994)**. However, in the presence of organic matter, it can have an indirect role, for example by increasing its degradation, which can produce acid and complexing substances **(Lions 2004)**. It can also affect bacterial activity. The action of micro-organisms can lead to solubilization (production of acid and complexing compounds etc.) or solubilization (formation of insoluble metal sulphides, bioaccumulation and bio-sorption by micro-organisms) of metallic trace elements and metalloids. The effect of competition on surface sites between metals or between metals and major cations can also be important. For example, it has been shown that the presence of calcium strongly reduces the retention of iron and manganese on zeolites **(Jacobs, Syers, et Keeney 1970)**.

3.2 Alkaline waste carbonation technology

Carbonation is a natural phenomenon due to the dissolution of carbon dioxide from the air in the interstitial solution of the material (a porous medium more or less saturated with water). The effect of CO_2 appears at low concentrations (such as those found in the atmosphere, where the volume fraction of CO_2 is of the order of 0.04% and can reach up to 1% in some very poorly ventilated places **(Thiery 2006)**). Depending on the saturation state of the material, CO_2 diffuses in dissolved form (100% saturated material) or in gaseous form (unsaturated or slightly saturated material) **(Drouet 2010)**. The passage of CO_2 into solution leads to a drop in the pH of the interstitial solution. This leads to an acid-base reaction with basic compounds such as portlandite and hydrates leading to mineralogical and microstructural changes; i.e. the main hydrates of alkaline wastes dissolve and calcium carbonates

precipitate **(Houst 1993)**. These chemical reactions are at the origin of the modification of the properties of the carbonated zone which can directly impact the durability of the structure with respect to its environment. Thus, for decades, carbonation has been a widely studied phenomenon. In particular, because it leads to the physico-chemical stabilization of metallic and metalloid elements, when the pH drops from around 13.5 to a value below 10, the speciation of elements changes, as does the precipitation in the form of carbonates of certain elements such as Pb, Ba and Zn.

3.2.1 Carbonation mechanisms

Numerous studies have shown that carbonation of alkaline wastes leads to the precipitation of numerous mineral phases. Calcite (calcium carbonate) is clearly the most common mineral present in these neoformations. It precipitates in association with other trace minerals such as quartz and some sulphates. The main compound that forms calcite is portlandite (calcium hydroxide) **(Freyssinet 1998; Garrabrants et al. 2002)**.

In the pores, on contact with water, carbon dioxide dissolves *(The dissolution of CO_2 is governed by Henry's law ''at constant temperature and saturation, the amount of gas dissolved in a liquid is proportional to the partial pressure of the gas on the liquid'')* to the extent that the water/CO_2 contact time is long enough to form carbonic acid (H_2CO_3) which in turn reacts to form the hydrogen carbonate ion (commonly called the bicarbonate ion) (HCO^-) **(Eq-1)** and the carbonate ion (CO_3^{2-} **) (Harned et Davis Jr 1943)**.

$$CO_2\ (g) + H_2O \longrightarrow H_2CO_3 \qquad \text{Eq (1)}$$

$$H_2CO_3 \longrightarrow HCO_3^- + H^+ \qquad \text{Eq (2)}$$

$$HCO_3^- \longrightarrow CO_3^{2-} + H^+ \qquad \text{Eq (3)}$$

Carbonic acid only exists in the indicated form in very low concentrations under normal conditions. Moreover, when it dissolves, CO_2 reacts with water to a greater or lesser extent. The formulation given (H_2CO_3) is therefore a simplification of the writing. To write the concentration of dissolved CO_2, the notation $[H_2CO_3]$ * is used, with $[H_2CO_3]$*= aqueous CO_2 + H_2CO_3 **(Legendre 2021)**.

In water, carbonic acid behaves as a weak diacid whose dissociation constants Ka1 and Ka2, associated with (Eq-2) and (Eq-3) respectively, are indicated by their pKa (for the temperature of 25ºC). The values of pKa1 and pKa2 are given in **Table 12**.

Table 12. Equilibrium constants at 25°C and 1 atm (Cowie et Glasser 1992)

Temperature (°C)	pK_{a1} (CO_2, H_2O/HCO_3^-)	pK_{a2} (HCO_3^-/ CO_3^{2-})
25	6.37	10.33

At equilibrium, the acidities of the species H_2CO_3* (Eq-1), HCO_3^- (Eq-2) and CO_3^{2-} (Eq-3) have different domains of predominance which can be plotted as a function of pH (Figure 12). For this purpose, it is sufficient to express the concentrations of the species $[HCO_3^-]$, $[CO_3^{2-}]$ and $[H_2CO_3$*] as a function of the total CO_2 concentration.

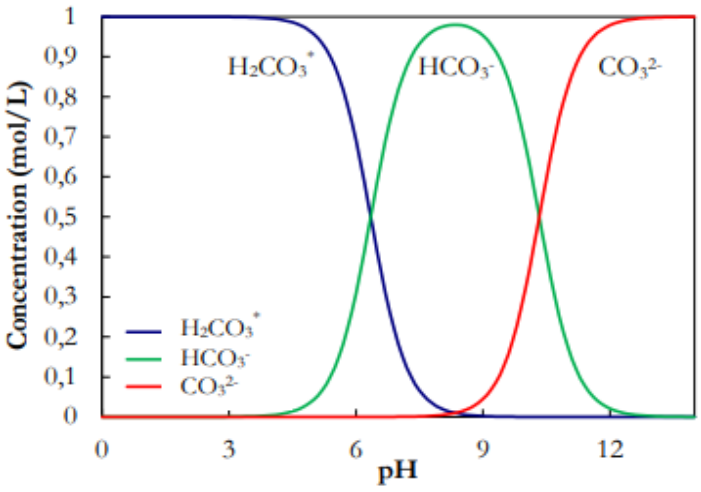

Figure 12. Carbonate system speciation as a function of pH

During the carbonation of the alkaline waste, the pH of the pore solution evolves from a highly basic value (around 13.5) to a value close to 9. Based on the high pH of the pore solution, it can be considered that the CO_3^{2-} species is the majority dissolved carbonate species present in the alkaline carbonated waste. Since the main compound to form calcite is portlandite, the carbonation reaction process can be described in a simplified way by the balance equation **(Eq-4)**.

$$Ca(OH)_2 + H_2CO_3^* \longrightarrow CaCO_3 + 2H_2O \quad \text{(Eq-4)}$$

The carbonation mechanism of portlandite is illustrated in **Figure 13**, associated with reactions (Eq-5) to (Eq-9).

Specifically, the dissolution of portlandite according to equation (Eq-7) causes the release of calcium (Ca^{2+}) and hydroxyl (OH^-) ions. The hydroxyls neutralize the dissolved CO_2 to form carbonates. The released calcium ions precipitate with carbonate ions to form calcium carbonates according to reaction (Eq-10).

$$Ca^{2+} + CO_3^{2-} \longrightarrow CaCO_3 \quad \text{(Eq-10)}$$

Some authors identify the presence of residual portlandite (i.e. incomplete dissolution of portlandite) despite an advanced carbonation time. It is attributed to the presence of a protective gangue of calcium carbonates formed on the surface of the portlandite crystals **(Swenson et Sereda 1968; Groves, Rodway, et Richardson 1990)**.

The precipitated carbonates occur as multipolar solid solutions such as Ca, Ba, Fe, Pb, Zn or Mg, with the majority carbonate being calcite ($CaCO_3$). The main consequence of carbonation is a drop in the pH of the leachate, which leads to an immobilization of part of the pollutant potential.

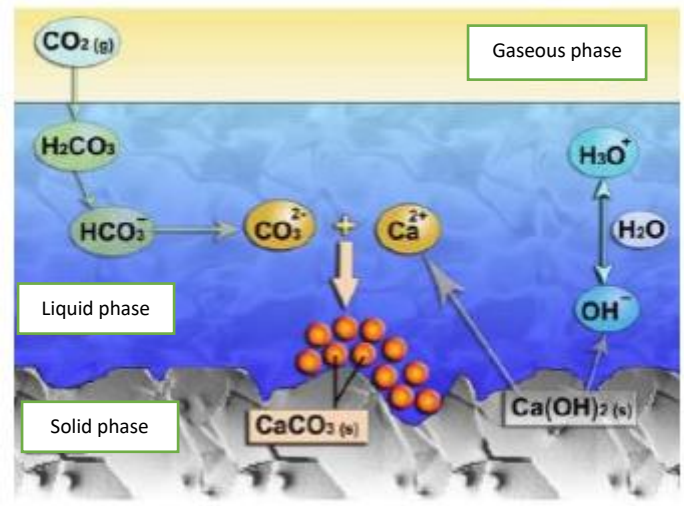

$CO_2\ (g) + H_2O \rightarrow H_2CO_3$ Eq (5)

$HCO_3^- \rightarrow CO_3^{2-} + H^+$ Eq (6)

$Ca(OH)_2 \rightarrow Ca^{2+} + 2OH^-$ Eq (7)

$Ca^{2+} + CO_3^{2+} \leftrightarrow CaCO_3$ Eq (8)

$Ca^{2+} + CO_3^{2-} \leftrightarrow CaCO_3$ Eq (9)

Figure 13. Illustration of the portlandite carbonation mechanism (Thiery 2006)

3.2.2 Carbonation-influencing parameters

The mechanism of carbonation is influenced by factors internal and external to the material. The internal factors are the water/material ratio, the chemical composition of the material and the internal relative humidity while the external factors include relative humidity, temperature, carbon dioxide concentration, and surface texture **(A. Neville 2003; A. M. Neville 2004)**.

The most favorable temperature and humidity for maximum carbonation vary between 20-25°C and 50-70%, respectively **(A. Neville 2003; A. M. Neville 2004)**. Indeed, the carbonation process requires that the material is neither totally saturated in order for the CO_2 to diffuse nor totally dry for the CO_2 to dissolve in the pore solution **(Thiery 2006)**.

3.2.3 Environmental interest

The environmental impact of solid incineration residues is mainly related to their capacity to release, upon contact with water, a number of chemical elements, including soluble salts and metallic and metalloid trace elements.

The carbonation process has an important role in the immobilization of certain metallic trace elements and metalloids within the matrix of alkaline waste. The initial pH of the alkaline waste, at the furnace outlet, is generally between 11 and 12.5. At these pH values, all the amphoteric metals (Pb, Zn, etc.) are in the form of soluble hydroxides. Carbonation then induces a decrease in pH to 8-9. This pH range corresponds to a solution containing carbonate (CO_3^{2-}) and hydrogen carbonate (HCO_3^-) ions. At such a pH, the amphoteric metals become insoluble **(Figure 14)** and are trapped in the alkaline waste.

This observation is verified by the studies carried out at BRGM on the evolution of MIOM subjected to meteoric alteration, which stress the importance of the carbonation process for the stabilization of certain metals (Pb, Zn, Cd) in these products **(Freyssinet 1998)**. Carbonation therefore has a beneficial role and reduces the environmental impact, mainly through the drop in pH that it causes.

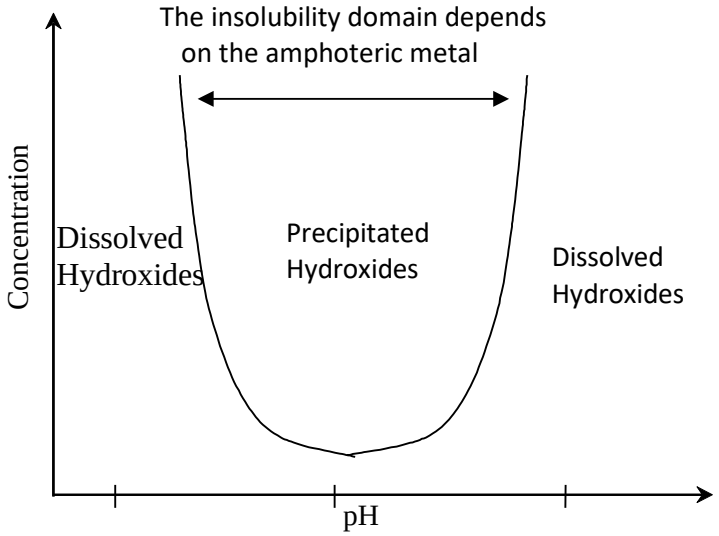

Figure 14. Evolution of the condition of amphoteric metal hydroxides as a function of pH

3.2.4 Carbonation stabilization of alkaline waste

Carbonation is a very important reaction in alkaline residues and occurs as a result of previous oxidations and hydrolysis. The process is a long term one and depends on many parameters such as permeability, water content, mineral composition of the material, CO_2 concentration, relative humidity and temperature of the surrounding air. The long-term behavior has been studied by many authors both by simulation and by field studies ('full-scale' specifically for bottom ash).

Some authors have simulated carbonation by modelling pollutant release curves obtained by column percolation and/or by studying leachates from storage areas **(Belevi et Baccini 1991; C. Lu 1996; Baranger et al. 1999)**. These studies have shown that a limited proportion of the total metal content leaches out rapidly at the start of storage.

Buchholz et Landsberger (1993) have highlighted the importance of changes in the mineral and organic composition of ash over the longer term (hundreds to thousands of years) depending on the conditions imposed by the environment. Under reducing conditions, metals are often bound to sulphides, while under oxidizing conditions they can be degraded and thus leached. However, the formation of ferric oxy-hydroxides with high adsorption capacities significantly reduces this mobility. In addition, they estimated that carbonation and oxidation become much slower at depth of storage than at the surface.

Ecke, Menad, et Lagerkvist (2003); Du et al. (2016); Xu et Yi (2022) experimented the carbonation of fly ash in the laboratory to study the impact on the mobilization of metals including Pb, Zn, Cr and Cd. A total of four variables were tested, CO_2 flow rate (g); temperature, time and water addition (humidity). The availability of critical elements such as Pb and Zn would be reduced, while Cr would be demobilized with the addition of water and then remobilized over time by the oxidizing conditions of the treatment. Unlike the previous metals, the mobility of Cd increases during treatment, leading to contamination risks.

Other authors have worked specifically on bottom ash. **Knight, Cheeseman, et Rogers (1999)**studied the storage of bottom ash on a mineral support covered with a geomembrane. In these reducing conditions of the anaerobic environment, it was observed that bacteria belonging to the thiobacillus genus were present, which lowered the pH of the surface of the slag while favoring the appearance of more acidophilic bacteria such as T. thiooxidans, which are responsible for the release of metal pollutants. **Pascual et al. (1994)** showed an increase in the concentration of $CaCO_3$ in several stocks of

open bottom ash, which indicates the carbonation of the bottom ash. Temperature increases (up to 80°C) caused by oxidation and/or hydrolysis reactions of unburnt materials were also observed. Carbonation is said to be almost complete after three months of storage in the open air. The release of metallic pollutants in the bottom ash leachate would then be minimal. Only the chlorides (Cl^-) would still be mobilized in significant quantities after three months. The work carried out by **Freyssinet (1998)** completes the previous study. Indeed, this team characterized the transformation mechanisms of a bottom ash stockpile subjected to climatic conditions in France. In the pore water of the stockpile, calcium and sulphates are dissolved in the form of complexes ($CaOH^+$, $CaCO_3$(aq), $CaSO_4$ (aq), $NaSO_4^-$, KSO_4^-) while in the leachate (elution water flowing by gravity under a pile of residue), calcium is present in the form of Ca^{2+}(80%). The metals (Fe, Cu, Pb, Zn) dissolved in the pore water are mainly bound to hydroxide ions, whereas in the leachate, Cu and Pb are associated with chlorides and Zn is in its free form (Zn^{2+}). They highlighted the predominant neo-formed phase after maturation of the bottom ash corresponding to calcite. After five months, the period necessary for maturation, 80% of the calcium, copper, sodium and chlorine that could be mobilized are leached and after 16 months, 86% of the mobilizable material is removed, including 35% of total chlorides. Stabilization by carbonation is one of the techniques currently being studied. The application of this technique has been considerably exploited in France with MIOM (Mâchefers d'Incinération d'Ordures Ménagères) since their use in road techniques must be preceded by a maturation period. The efficiency of this technique seems to be recognized but in the long term. In the short term, the presence of metals in the leachate is observed from the first rainfall **(Choi et Shin 2020)**. The current state of laboratory research on the stabilization by carbonation of RCPA (North America) or REFIOM (Residues d'Épuration des Fumes d'Incinération d'Ordures Ménagères, in Europe) does not allow us to stipulate the effectiveness of this treatment in the short term. Indeed, the short-term leaching of metals, particularly Cd, is still problematic **(Ecke, Menad, et Lagerkvist 2003)**. **Table 13** Show wastes tested for carbonation.

Table 13. Description of wastes tested for carbonation

Waste	Description	Issues	Management method	Volume (UK annual)
Bauxite (BX)	By-product of the Bayer aluminum manufacturing process **(« Brunori et al,2005.; Gunning, Hills, et Carey 2010)**	Alkalinity, volume **(Yalçın et Sevinç 2000; Brunori et al. 2005)**	Mostly stockpiled or landfilled **(Kalkan 2006)**	Not available
Biomass ash (BA)	Ash from the incineration of the pressed plant fibre residue (Rape Cake) after oil extraction	Disposal issues with increasing use of biodiesel	Landspreading, new disposal routes being sought	31,000 tons **(McKay, Hudson, et Hudson 2003)**
Cement kiln/ bypass dusts (CKD/CBD)	Alkali-rich dusts removed from kiln exhaust gasses **(Sreekrishnavilasam, King, et Santagata 2006; Singh, Bhattacharjee, et Shukla 1995)**	Dusts are regarded as being a health hazard **(Baghdadi, Fatani, et Sabban 1995)**	Landfilled, but increasing reused **(Taha et al. 2002; Ryou 2004)**	45,456 tons (sent to landfill) **(Oggioni, Riccardi, et Toninelli 2011)**
Clinical waste incineration ash (CWIA)	Ash from the incineration of hazardous medical materials in specialized incinerators **(Blenkharn 2005)**	Heavy metal content; Ar, Cd, Cr, Hg, Pb **(Delay, Swithenbank, et Argent 2001)**	Sent to hazardous landfill **(Wheatley et Sadhra 2004)**	123,000 tons (before incineration) **(X. Li et al. 2007)**
Municipal solid waste incineration (MSWI) ash	Incineration of domestic waste reduces weight by about 70%. MSWIs include coarse bottom	Heavy metals in non-hazardous bottom ash. High concentrations of	Fly ashes are landfilled. Thirty-eight percent of bottom ashes are landfilled, with the	5 million tons (before incineration) **(X. Li et al. 2007)**

	ashes (MSWI-BA) and fine fly ashes (MSWI-FA) **(X. Li et al. 2007)**	heavy metals in hazardous fly ashes **(Ecke 2003)**	remainder recycled as aggregate and bulk fill **(X. Li et al. 2007)**	
Paper sludge incineration ash (PSIA)	Fine ash residue from incineration of paper making wastewater sludge containing residual fibres, fillers and chemicals (**Gunning, Hills, et Carey 2010; Boni, D'Aprile, et De Casa 2004)**	Sludges may contain a variety of chemicals and traces of heavy metals. The ashes are highly alkaline **(Xiao, Ma, et Sarigumba 1999)**	Landspreading (unlikely to continue in the UK), incineration or landfilling **(Gunning, Hills, et Carey 2010)**	130,000 tons **(Rubin et al. 2007)**
Pulverized fuel ash (PFA)	Fine ash electrostatically separated from the flue gases of coalfired power stations **(Sims, Rogner, et Gregory 2003)**	PFA is considered non-hazardous **(Coventry, Woolveridge, et Hillier 1999)**	About 50% of PFA is landfilled, the remainder is used in construction **(Thomas et Matthews 1991)**	5 million tons, 2.3 million tons available **(Mankelow et al. 2007)**
Sewage sludge ash (SSA)	Fine ash from incineration sewage sludge from the domestic and industrial wastewater treatment process **(Cyr, Coutand, et Clastres 2007a; Mohan et al. 2006)**	Contains As, Cd, Cr, Cu, Hg, Pb, Zn and cyanide **(Lapa et al. 2007b)**	The ash is landfilled **(Cheeseman et Virdi 2005a)**	100,000 tons **(Gunn 2004)**
Steel wastewater sludge (SWS)	Metallic sludge from steel manufacture. One ton of steel produces 2–4 tons of slags, dusts, ashes and sludges **(Das et al. 2007)**	Contain lead, chromium, cadmium, zinc, oil and grease **(Wilson, Velis, et Cheeseman 2006)**	Sludges are stabilized and sent to hazardous landfill **(Wilson, Velis, et Cheeseman 2006)**	1.4 million tons (total waste including sludge **(Dawley, Stenning, et Pike 2008)**
Wood ash (WA)	Coarse ash derived from combined electricity and heat generation plants using sustainable wood sources **(Pitman 2006)**	Alkalinity and handling problems **(Górecka, Chojnacka, et Górecki 2006)**	Primarily destined for landspreading. Possible use as a cement replacement **(Abdullahi 2006)**	31,000 tons **(McKay, Hudson, et Hudson 2003)**

In the context of the Haute-France region's incinerator, the management of fly ash from the combustion of paper sludge with waste biomass is subject to the regulation on residual materials. In order to meet the requirements of this regulation, the Haute France region has mandated the company IMT Nord Europe to stabilize the fly ash. Once stabilized, the ash is buried with other eligible waste materials in a technical landfill site or recovered in the civil engineering sector if it meets the environmental criteria. The mandate of our research was mainly to develop a process for the stabilization of metals (Pb and Pb) by carbonation in order to landfill or valorize the ash once treated. The study of ash stabilization by maturation was a possible option due to the legislation in force in France. Furthermore, certain aspects such as heavy snowfall, significant temperature variations and the hazardous nature of the ash suggest that metallic trace elements and metalloids will be leached out in the short term.

3.3 Geopolymers technology

The reaction of an alumino-silicate source at room temperature with a highly concentrated alkali silicate solution, under certain concentration conditions, results in the formation of an amorphous, mesoporous, low-calcium solid monolith referred to as a geopolymer. This term was coined in the 1970s in reference to mineral or inorganic polymers **(Davidovits 1991)**. Geopolymers have a network structure of aluminate and silicate tetrahedra **(Figure 15)**. The aluminum is in tetrahedral co-ordination; this results

in a charge deficit in the structure. An off-lattice alkali cation compensates for the negative charge of the AlO_4 group. If these cations are in excess, they migrate to the surface and are carbonated by the ambient atmosphere **(Barbosa et al. 2000)**. The Alkali/Aluminum atomic ratio must therefore remain equal to 1 to obtain a pure phase.

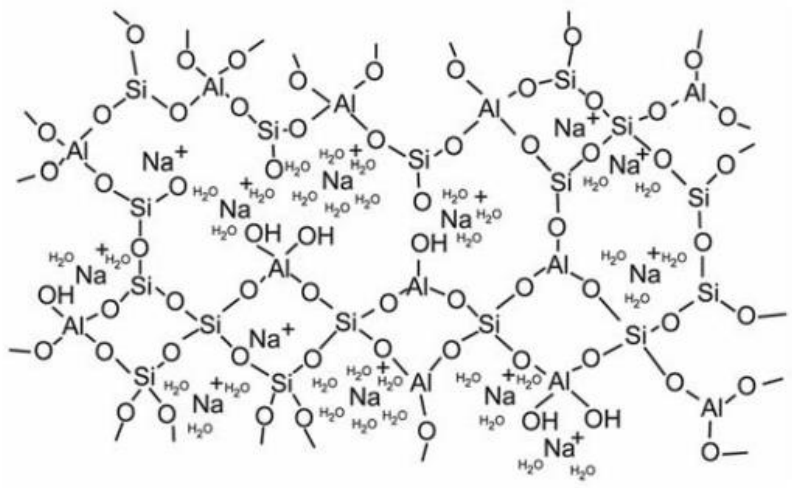

Figure 15. General structure of a sodium geopolymer (Rowles et al. 2007)

Geopolymers are considered to be the amorphous analogues of zeolites. The zeolites are crystallized microporous alumino-silicate materials. Under certain conditions, they can appear within the geopolymeric gel **(Provis et al. 2005; Breck et Breck 1973)**.

The empirical formula for a geopolymer is presented below:

$$Mn\ –[(SiO_2)z – AlO_2\text{-}]n,\ w\ H_2O$$

where M is a monovalent cation (Na, K or Cs), n is the degree of polycondensation, w is the amount of water and z is the Si/Al ratio. Varying the amounts of silica, water or the nature of the compensating alkali cation, geopolymers with different structural properties can be synthesized. In practice, when preparing a geopolymer, the formulation parameters to be varied are the ratios: SiO_2 / M_2O and H_2O / M_2O. However, it is important to remain within the range of existence of geopolymers **(Prud'Homme et al. 2013)**.

3.3.1 Geopolymerization

The exact mechanism of geopolymerization is not yet well understood, mainly because of the high speed of the reaction. However, most authors suggest that it is a dissolution mechanism of the compounds used (such as volatile ash or metakaolin) followed by a polycondensation in the form of a gel.

The starting materials are solid materials containing silicates and aluminates to which an alkaline solution is added. It is the alumina and silicate that react with the hydroxide and then with each other to form polymer chains. Therefore, silicon-rich materials (such as fly ash) and aluminum-rich materials (such as kaolin) fulfil the condition for geopolymerization. The most commonly used alkaline activator solution in geopolymerization is a combination of sodium hydroxide (NaOH) or potassium hydroxide (KOH) with sodium silicate (Na_2SiO_3) or potassium silicate (K_2SiO_3) **(Davidovits 1999; Barbosa, MacKenzie, et Thaumaturgo 2000; H. Xu et Van Deventer 2002)**. The sodium or potassium silicate

brings a soluble silicate into the system, which favors the reactions. For this reason, the addition of one of these two components is favorable compared to the use of alkali hydroxides alone. **Palomo et al (1999)** concluded that the type of alkaline liquid has a very important role in the polymerization process. OH^- acts as a catalyst for the reaction and the metal cation serves to balance the negative charge carried by the tetrahedral aluminum.

The alkaline activation process was first studied in detail by **Davidovits (1999)** who developed and patented a binder obtained from the alkaline activation of metakaolin. The mechanism of geopolymer formation has also been described by **(H. Xu et Van Deventer 2002; Fernández-Jiménez, Palomo, et Criado 2005; Němeček 2009)**. The following list divides the formation of geopolymers from fly ash into three stages **(Němeček 2009; Davidovits 1999; Fernández-Jiménez, Palomo, et Criado 2005)**:

Step 1: Dissolution - is the chemical attack of the highly alkaline liquid medium on the fly ash particles. Hydrolysis of the alkaline solution is followed by the breaking of the Si-O-Si and Si-O-Al bonds of the mineral to form reactive $Si(OH)_4^-$ and $Al(OH)_4^-$ precursors in solution. These precursors condense and precipitate out of the zeolite product. The process then leaves the fly ash in spherical form with trapped gas. The dissolution process partially opens the internal porosity and the alkaline solution can penetrate the ash particles. The diluted components are mainly based on Al and Si. The mixture carries a negative charge due to the substitution of a Si^{4+} cation by an Al^{3+} cation (associated with the hydroxide). This electronic imbalance is compensated by an alkaline cation (Na^+, K^+, Ca^{2+}). There is not enough time or space for the resulting gel to evolve into a well-crystallised structure **(Fernández-Jiménez, Palomo, et Criado 2005; Fernández-Jiménez et al. 2006; Fernández-Jiménez, Palomo, et Criado 2005; Davidovits 1999; H. Xu et Van Deventer 2002)**

Step 2: Reorganization / creation of monomers - After dissolution, the Al and Si based ionic precursors are transported into the highly alkaline environment. They react with part of water and alkali, forming monomer units that start to form nuclei. **Fernández-Jiménez et al. (2006); Fernández-Jiménez et al (2005)** show that around the fly ash particles a metastable aluminum-based gel originating from the fly ash was formed. It should be noted that water in the geopolymer system does not have any indispensable role for the reaction, contrary to ordinary cement. Water is probably only used for the workability of the mixture during handling **(Fernández-Jiménez et al. 2006; Fernández-Jiménez, Palomo, et Criado 2005; Davidovits 1999; H. Xu et Van Deventer 2002)**.

Step 3: Polycondensation / Polymerization - The third stage of polymerization occurs when the nuclei reach a larger size and when the concentration of precursors becomes higher than the saturation concentration. The gel creates a barrier around the ash particles and prevents the alkaline solution from penetrating. At this point the soluble silicate is incorporated into the gel. During this step, some water (~40 wt%) is released by evaporation **(Fernández-Jiménez et al. 2006; 2006; Davidovits 1999; H. Xu et Van Deventer 2002)**. The water remaining in the system is not evaporable below 1050°C **(Fang et Kayali 2013)**. A final reaction step leads to a three-dimensional polymer chain and ring structure composed of Si-O-Al-O. During this phase, the development of the pore structure begins and lasts longer than in the case of ordinary cement **(Ma, Hu, et Ye 2013)**. The final product of geopolymerization is an amorphous cement-like material. Nevertheless, several authors have suggested the existence of semi-crystalline or polycrystalline phases, especially when no silica source is dissolved in the alkaline solution.

In **Figure 16** a model described by **Duxson et al. (2007)**is presented. The process is explained using the different reaction mechanisms as already explained in the previous section in three steps. However, these three steps can overlap with each other and occur almost simultaneously, making it difficult to isolate

and examine each of them separately (Angel Palomo, Grutzeck, et Blanco 1999). The kinetics of each step and then the properties of the geopolymers depend on several factors such as the type of aluminosilicate source, the solid/liquid ratio, the silicate and alkali concentrations (pH), etc.

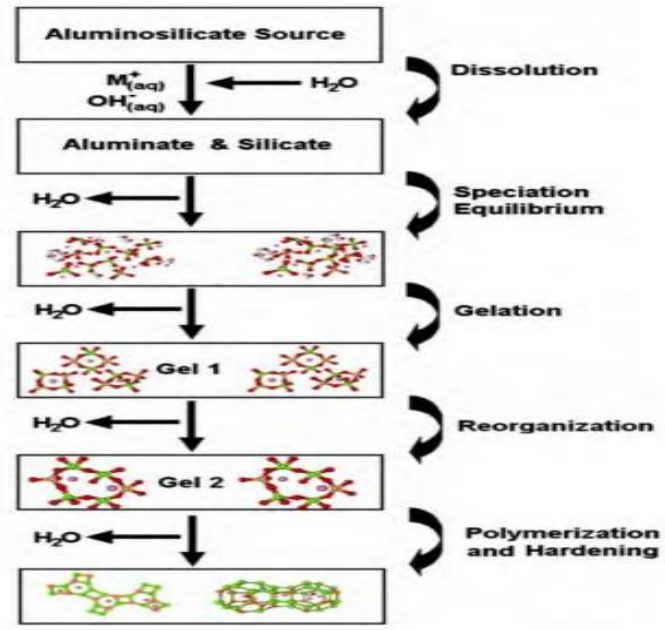

Figure 16. Geopolymerization model (PSWM Duxson et al. 2007)

3.3.2 Parameter influencing geopolymerization

Several parameters can influence the characteristics of the formulated geopolymers, among these parameters are:

- Influence of alumino-silicate source
- Influence of water quantity
- Influence of the alkali cation
- Influence of the Si/Al ratio
- Influence of cure parameters
- Influence of time

3.3.2.1 Influence of alumino-silicate source

The properties of geopolymers synthesized from the two most used alumino-silicate sources (metakaolin and fly ash) are likely to vary. The mechanical properties of metakaolin geopolymers are often superior to those of fly ash geopolymers. The porosity also differs. In general, the structure has more isolated pores with metakaolin and more interconnected ones for fly ash. These differences must be put into perspective in view of the possible variations for each type of geopolymer according to the starting formulation.

3.3.2.2 Influence of water quantity

The polymerization process is influenced by the water quantity used during the geopolymer synthesis. This must not be too low in order to mix the reagents correctly and allow ionic transfer. It should not be too high either, in order not to dilute the reagents, slow down the encounter of the oligomers and thus slow down the polymerization **(Barbosa, MacKenzie, et Thaumaturgo 2000)**. An excess of water

leads to a significant loss of mechanical strength. Moreover, as water does not participate in the geopolymerization reaction, it is possible that an excess of water will lead to the appearance of larger pores and a larger pore volume **(Steveson et Sagoe-Crentsil 2005)**.

3.3.2.3 Influence of the alkali cation

During geopolymerization, the alkali metal has a role in shaping the structure of the geopolymer, since it compensates the negative charge of the aluminates and thus ensures its stability. Its nature affects all stages of geopolymerization: from dissolution to gel hardening and even the possible crystallization of zeolites. It influences, among other things, the number and size of oligomers in solution.

In the case of a sodium hydroxide-based activation solution, dissolution is rapid and the oligomers formed are large but less numerous. In the case of a potassium-based activation solution, the opposite is the case, dissolution is slower and the oligomers are smaller in size but more numerous. The polymerization is then more efficient **(H. Xu et van Deventer 2003)**.

A study on the dissolution of metakaolin by alkali hydroxide solutions has been carried out **(Steins et al. 2012)**. The use of different alkali ions (Na, K and Cs) shows that dissolution occurs more rapidly for small alkali ions. It is therefore faster for Na than K or Cs. On the contrary, the silicate species are more polymerized and the alumino-silicate oligomers formed are more numerous and smaller in size for large cations. This is due to the difference in electronic charge density between cations. More globally, this study shows that the local organization, as well as the gelling and consolidation steps of the geopolymer are modified according to the hydration energy and the organization of the hydration sphere of the alkali used. Moreover, other studies by the same author show that the final properties of geopolymers are also modified **(Steins 2014; Steins et al. 2014)**. A potassium geopolymer has a larger specific surface area than a sodium geopolymer; its average pore size is smaller and the pores are present in greater numbers.

Finally, several studies **(Van Jaarsveld et Van Deventer 1999; H. Xu et Van Deventer 2000)** have shown that potassium-based geopolymers would have a higher compressive strength related to a higher degree of polycondensation using potash **(Phair et Van Deventer 2002)**. This difference would be induced by the size of the cation, since the water molecules would organize themselves more effectively with small cations **(McCormick et Bell 1989)**.

3.3.2.4 Influence of the Si/Al ratio

The Si/Al ratio is an important parameter in the formulation of a geopolymer. In the concentration range allowing the formation of geopolymers, when the silica content increases, the metakaolin is less well dissolved but the polymerization is more efficient. This can have an impact on the properties, notably mechanical, of the geopolymer **(Peter Duxson et al. 2005)**. The porosity is also modified. For a Si/Al ratio ranging from 1.15 to 2.15, the pore volume decreases from 0.206 to 0.082 cm^3/g **(Peter Duxson et al. 2005)**.

Peter Duxson et al. (2005) also demonstrated the relationship between Si/Al ratio and mechanical properties for geopolymers synthesized from metakaolin and a sodium silicate solution. The authors suggest an explanation linking microstructure and mechanical strength. Indeed, the variations of the mechanical strength can often be explained by the microstructure of the material as in metals, glasses or ceramics. For a Si/Al ratio lower than 1.4, they observe large interconnected pores, the presence of destructuring precipitates and traces of unreacted materials. The resulting mechanical strength and Young's modulus are low. For Si/Al above 1.65, they observe smaller isolated pores and a more homogeneous binder. The optimum strength is found for a Si/Al ratio of 1.9 and also corresponds to a slight decrease in porosity. Beyond this ratio, the mechanical strength would decrease because this

modification is to the detriment of the Si-O-Al bridges which would ensure the crosslinking of the lattice. In fact, the decrease in mechanical strength beyond a Si/Al ratio of 1.9 can also be explained by a faster setting of the geopolymer and thus an early decrease in the mobility of the reactants. Furthermore, as the Si/Al ratio increases, the metakaolin is less dissolved. The proportion of unreacted material is then higher. This effect would counterbalance the effect of more Si-O-Si bridges.

3.3.2.5 Influence of treatment parameters

Temperature, relative humidity and cure time are the main parameters to be fixed. Temperature has the effect of accelerating the kinetics of geopolymerization reactions. For this reason, geopolymers can be stored at temperatures between 50°C and 80°C after mixing (addition of the alumino-silicate source) **(Palomo et al. 1999)**. However, special precautions must be considered concerning water loss. This acceleration of the reactions has an influence on the final properties of the material, e.g. the mechanical strengths **(Bakharev 2005)**. At room temperature, the reactions are not accelerated and the mechanical strengths are therefore lower. Conversely, at too high a temperature, the geopolymer can fissure and this can have a negative effect on the physical properties **(Van Jaarsveld et al 2002)**. The cracking can also be caused by drying a geopolymer too quickly **(Mo et al. 2014)**. This usually occurs when the geopolymer is not sealed at the time of curing and placed in an environment with a relative humidity between 30 and 70% **(Perera et al. 2007)**. Another experience shows that curing at elevated temperature does not improve the mechanical strengths if the cure is very short (1 h). A longer cure (4 h) is necessary to observe an effect **(Rovnaník 2010)**. This experiment was carried out over a larger temperature range: between 10 and 80 °C. Cures between 40 and 80 °C lasted 4 h. The cure at room temperature is carried out until the sample is analyzed. The cure at 10 °C again demonstrates the influence of temperature. At low temperatures, the geopolymerization reaction is slowed down. Compressive strength measurements after one and three days are therefore not possible because the sample is not yet cured.

3.3.2.6 Influence of time

A recent study highlighted the changes observed in porosity (pore size, volume and specific surface) between 3 days and 6 months after their synthesis **(Steins et al. 2014)**. Two different geopolymers, one sodium and the other potassium, were compared. These two materials were analyzed by nitrogen adsorption measurements in order to characterize the evolution of porosity and specific surface. Regardless of the nature of the alkali cation, the pore volume and specific surface of both geopolymers decreased between 3 days and 6 months after their synthesis **(Steins et al. 2014)**.

Another study confirms that, whatever the cure undergone by the samples, the porosity tends to decrease over time **(Rovnaník 2010)**. In contrast to the previous study, however, this one was carried out only in the first 28 days after the geopolymer synthesis.

3.3.3 Encapsulation of waste using geopolymerization

An initial attempt to understand the principle of geopolymerization was made using metakaolin because it is easier to keep the Si/Al ratio at a desired value **(Gourley 2003)**. However, for the manufacture of mass concrete, metakaolin is expensive. In recent years, much more fundamental research on geopolymers has been conducted. The interest of geopolymers in different applications has increased, in particular for waste encapsulation. The geopolymeric structure has been tested for the incorporation of nuclear waste **(Malek et al. 1986; Blackford 2007; Pereira, Linden, et Weinberg 2007)**. The incorporation of UO_2 mixed with ZrO_2, P_2O_5, Fe_2O_3, SrO and CeO_2 into the geopolymeric structure resulted in sufficient chemical resistance, despite the presence of sodium and phosphate phases which are rather soluble.

Several industrial wastes and by-products studied in the past were mostly low in calcium such as Class F (ASTM) fly ash **(Palomo et al. 1999; Swanepoel et Strydom 2002)**, combination of fly ash and metakaolin **(Van Jaarsveld, Van Deventer, et Lukey 2002; Swanepoel et Strydom 2002**) and combination of bottom ash and metakaolin **(Yip, Lukey, et Van Deventer 2004; Cheng et Chen 2003)**. **Barbosa et al (2000)** observed the nature of the aluminosilicate source to produce geopolymers and the influence of calcium in the system. It has been shown that calcined raw materials, such as fly ash or slag, show a higher final compressive strength when compared to those made using non-calcined materials such as clay, mine tailings and minerals of natural origin **(Barbosa et al., 2000)**. Different researches show that calcium improves the mechanical properties of geopolymers by accelerating the curing process **(H. Xu et Van Deventer 2000; Yip, Lukey, et Van Deventer 2004; Temuujin, Van Riessen, et Williams 2009)**. On the contrary, **Gourley (2003)** concluded that fly ash with a low calcium content is preferable, as the presence of calcium in large quantities can interfere with the polymerization process and modify the microstructure to the detriment of the final product properties. **Fernández-Jiménez et al. (2006); Fernández-Jiménez, Palomo, et Criado (2005)** also presented an ideal blend for obtaining high mechanical properties, containing 40-50 wt% silicate and relatively little CaO. However, **H. Xu et Van Deventer (2002)** studied the effect of the addition of clinker on the structure of metakaolin-based geopolymer. They found that the use of a combination of calcium-rich material (e.g. fly ash) with calcium-poor material (e.g. kaolinite or clay and albite) leads to a significant improvement in compressive strength and reduction in reaction time.

3.3.4 Immobilization of pollutants in geopolymeric matrices

As indicated in the previous sections on hazardous waste matrices, the immobilization of metallic trace elements and metalloids must be durable and resistant to leaching.

Studies have shown that geopolymeric materials can undergo aggressive conditions for several months without surface alteration, contrary to Porthland cement. The alkaline reaction during the formation of geopolymers influences the density, limits the infiltration of acid and sulphate elements into the geopolymer system and thus prevents potential degradation. The resistance against chemical attack is important from the aspect of the release of toxic elements into the environment, as for example by degradation of the structure by hydro-meteorological conditions when the pH can drop to a value of 3. Davidovits (1999) analyzed the chemical resistance of geopolymers and at the same time the resistance of Portland cement using 5% HCl and 5% H_2SO_4. The results revealed that the geopolymers do not show any significant change unlike Portland cements. **Stene-Johansen et al (2005)** used sulphate and acid exposure as a leaching test. Samples with silicate-rich fly ash were immersed in 0.5-2% sulphuric acid and 5% sulphate solution for 1-12 months. The results showed that the geopolymer has excellent resistance in a sulphate environment. On the other hand, the acid attack damaged the surface of the specimens and significantly reduced the compressive strength. The strength evaluation of the geopolymer to sulphuric acid attack with a concentration of 10% was studied by **Song et al. (2005)**. The sample was leached for 2 months. Na^+ and Al^{3+} ions were leached out, but the surface observed with a scanning microscope showed no degradation. It was observed that the increase in chemical resistance of geopolymers is related to the calcium content. According t**o Buchwald et al. (2005)**, the addition of CaOH does not show any deterioration on the structure nor an increase of the elements released after leaching. However, the majority of studies focus on the chemical resistance of geopolymers using low calcium REFIOM. In this thesis, we work with two types of materials, the first one is a biomass fly ash which has a high CaO content and the second material is a shooting range soil, thereafter we observe the different parameters that could improve the immobilization efficiency of metallic and metalloid trace elements.

Two possibilities exist for the immobilization of metallic and metalloid trace elements. One possibility is physical immobilization by capturing the toxic elements in the empty pore space in the solid matrix. Another possibility is the immobilization of metallic and metalloid trace elements by their replacement with a component of the same valency. The function of Pb^{2+}, Zn^{2+} or Cr^{3+} will be to compensate the negative charge of aluminum. Metallic trace elements and metalloids such as Pb, Zn have two (divalent) cations, which is identical to Ca. We can assume that these trace metals could replace Ca during the structuring of the matrix. Ca^{2+} would behave like Na+ i.e. it would compensate the negative charge of the aluminum ion **(Fang et Kayali 2013)** which forms a tetravalent hydroxide ($Al(OH)_4$). This favors the CaO-rich biomass fly ash with which we work in this thesis. A study on the fixation of metallic and metalloid trace elements in geopolymeric materials based on lignite fly ash was carried out by **MINAØÍKOVÁ et ŠKVÁRA (2006)**. They looked at the immobilization efficiency of Cd, Cu, Cr, Pb and Zn against leaching in deionized water and then carried out analyses by atomic absorption spectrometry. The leaching values were different for each metal. The most promising immobilization results were for zinc, which cannot be solidified in Porthland cement. For the other metals (Pb, Cd ...) the Porthland cement matrix exhibited improved leaching results compared to geopolymers. The metallic trace elements and metalloids present in the Ca-rich geopolymer are contained in the C-S-H phase, more precisely there is a creation of calcium and metal hydrides. Similar to the results of **H. Xu et Van Deventer (2002)**, they concluded that by adding calcium (in the form of MIOM, or gypsum) to fly ash (rich in Si), the leaching results of the geopolymers were improved **by MINAØÍKOVÁ et ŠKVÁRA (2006)**. It was observed that the addition of metallic trace elements and metalloids did not cause the formation of new crystalline phases.

Palomo et Palacios (2003) proposed the following three possibilities for incorporating Pb into the C-S-H system:

Addition: C-S-H + Pb → Pb-C-S-H (Eq 11)

Substitution: C-S-H + Pb → Pb-S-H + Ca (Eq 12)

Précipitation de nouveaux composants : Pb + OH + Ca + SO_4 → mélange de sels (Eq 13)

The chemical resistance is then dependent on the solubilities of the new components. In case of geopolymers, the solubility is dependent on the components that are formed during the alkaline reaction. For example, the immobilization capacity of metallic and metalloid trace elements (Pb and Cu) in geopolymers based on silicate-rich sources, was observed by **Yunsheng et al. (2007)** Their content in the mixture was 0.1-0.3 wt.% by adding $Pb(NO_3)_2$ and $Cu(NO_3)_2$. The incorporation efficiency was determined by TCLP at 98.5%. The addition of the $Pb(NO_3)_2$ composition into the system with sufficient silicates formed a Pb_3SiO_5 compound. This compound is able to immobilize lead durably, as it is highly insoluble **(Ogundiran et al. 2013)**. The influence of different parameters on the immobilization of metallic and metalloid trace elements (Mn, Zn, Pb, Cu, Fe and Ni) has been observed in India by **Srivastava et al. (2008)** . The synthesis of geopolymers was carried out from silicate-rich REFIOM. The low pH caused the highest release of metallic trace elements and metalloids. The order in the ability to bind metallic and metalloid trace elements was as follows: Zn > Mn > Fe > Ni > Pb. Depending on the pH, the immobilization efficiency of Pb can vary from 20% (pH=4) to 99% with the influence of the composition. Zinc seems to be an easily immobilized metal, which is in contradiction with the results of **MINAØÍKOVÁ et ŠKVÁRA (2006)**. Geopolymers have a high potential for the immobilization of toxic metals in their structure. There is a large possibility of encapsulation in the geopolymer structure with excellent results on leaching **(Luna et al. 2007)**. However, samples containing kaolin and metakaolin, when exposed to leaching, released excess metallic and metalloid trace elements, therefore

they are not recommended as a source of geopolymers for the encapsulation of metallic and metalloid trace elements. **Table 14** reports the leaching results of certain elements (Cu^{2+}, Pb^{2+}, Cr^{6+}, Cd^{2+}, Cr^{3+} and Ni^{2+}) from different waste-based geopolymers.

Table 14. Leaching of MMTE (mg/L) from geopolymer matrix containing solidified MMTE nitrates-intersolidification (values in brackets give calculated % leaching)

GP matrix	Leaching test	Mass % of metal solidified	Cu(II) (mg/kg)	Pb(II) (mg/kg)	Cr(VI) (mg/kg)	Cd(II) (mg/kg)	Cr (III) (mg/kg)	Ni (II) (mg/kg)	Ref.
FA/MK	TCLP, pH 3, 24 h	0.1	22 (55)	23 (58)					**(Van Jaarsveld, Van Deventer, et Schwartzman 1999)**
FA/kaolin			26.1 (65)	9.1 (23)					
FA/kaolin	TCLP, 28 days	0.5	85.7 (43)	8.5 (43)					**(Phair, Van Deventer, et Smith 2004)**
FA/MK			101 (51)	17.5 (9)					
FA/feldspar			116 (58)	11 (6)					
FA			113 (57)	7.5 (4)					
MK/FA	TCLP, pH 3, 24 h HCl solution, pH 3	0.1	17 (125) 8 (59)	17 (68) 3 (12)					**(Van Jaarsveld, Van Deventer, et Lukey 2004)**
Kaolin/FA	TCLP, pH 3, 24 h HCl solution, pH 3		9 (67) 17 (125)	7 (28) 10 (40)					
FA/MK	TCLP	0.1	0.0075	0.0025		0.020	0.001		**(J. Z. Xu et al. 2006)**
BFS/MK(1:1)	TCLP, 24 h	0.1 0.2 0.3	0.176 (0.44) 0.384 (0.48) 0.396 (0.33)	0.292 (0.73) 0.864 (0.72) 0.192 (0.16)					**(Yunsheng et al. 2007)**
FA	H_2SO_4, pH 1, 90 days 5% $MgSO_4$, 90 days 5% Na_2CO_3, 90 days Water, 90 days	0.5		(0.4) (0.0) (0.1) (0.004)	(88) (75) (78) (80)	(37) (0.02) (0.04)			**(J. Zhang et al. 2008, 2)**

MK, sodium silicate activator	Deionized water,L/S ratio 6 0.1 M HCl 0.1 M NaCl 1.0 M NaCl 0.1 M NaOH	0.1	22.1 (28.4) 15.0 (21.04) 11.3 (15.51) 7.4 (0.82) 14.3 (21.22)	10.3 (4.10) 7.5 (2.71) 4.7 (1.81) 18.1 (7.71) 7.1 (2.52)		20.5 (14.82) 10.7 (7.28) 7.7 (4.89) 10.0 (6.16) 7.7 (5.01)			**(Bassam I. El-Eswed, Aldagag, et Khalili 2017)**
Ferronickel slag	TCLP, pH 3 24 h	0.5 Nitrates 0.5 sulfate	25.5 (4) 46.6 (7)	7.9 (0.5) 9.0 (0.5)			0.3 0.1	34.7 47.3	**(Komnitsas, Zaharaki, et Bartzas 2013)**
FA	EN-12457-2 deionized water, 28 days	0 0.5 1.0		1.0 4.0 (0.8) 7.0 (1.4)					**(Nikolić et al. 2014)**
Mechanically activated FA		0 0.5 1.0		0.5 0.9 (0.2) 1.0 (0.2)					
FA		0.5 1.0 2.0			126 (25) 338 (34) 735 (37)				**(B. I. El-Eswed et al. 2015)**
Mechanically activated FA		0.5 1.0 2.0			44 (9) 219 (22) 530 (27)				
USEPA TCLP allowed limit (mg/L)				5	5	1	5		

3.4 Hydraulic binder technology

Hydraulic binders are very often used in the stabilization/solidification of waste. Indeed, due to their specific chemical properties (pH, substitution possibilities...), they are well documented to have a high immobilization potential **(Glasser 1993)**. These characteristics make it possible to obtain excellent results for the treatment of waste via the stabilization/solidification process while using small quantities of cement in the preparations. Among the hydraulic binders available, Portland cement is one of the most frequently used in waste treatment. The most significant contribution to waste immobilization is made by the hydrates formed during hydration. It has been shown that C-S-H, ettringite and hydrated calcium monosulfoaluminate have a dominant role in the stabilization/solidification process **(Glasser 1993; Gougar, Scheetz, et Roy 1996)**. The main mechanism of waste retention within these hydrates is substitution in the crystal lattice.

3.4.1 Cement constitution

The most important phases in COP are mainly dicalcium silicate ($2CaO,SiO_2$) noted C_2S or belite, tricalcium silicate ($3CaO,SiO_2$) noted C_3S or alite, tricalcium aluminate ($3CaO,Al_2O_3$) noted C_3A and tetracalcium alumino-ferrite ($4CaO,Al_2O_3,FeO_3$) noted C_4AF or ferrite. The incorporation of gypsum ($CaSO_4,2H_2O$) is necessary to delay the setting and thus increase the workability time. **Table 15** and **Figure 17** show the main phases present in cement **(Begarin 2012)**.

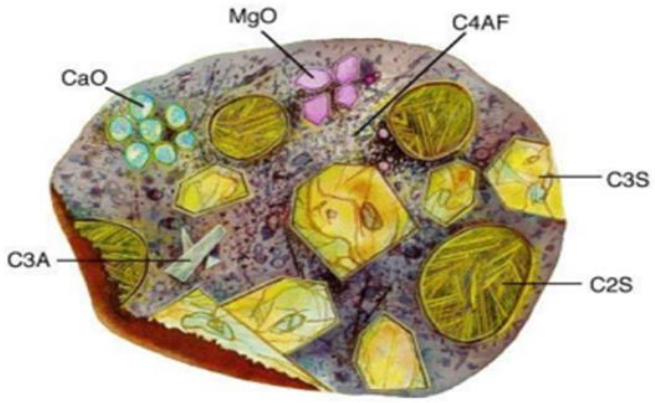

Figure 17. Main cement phases morphology (Juan-Ortega-cements specialist)

Table 15. Portland cement chemical composition

Constituent	Abbreviation	ΔH1 (J/g)	Mass percentage
Tricalcium silicate	Ca_3SiO_5 or C_3S	-500	50-70
Dicalcium silicate	Ca_2SiO_4 or C_2S	-250	15-30
Tricalcium aluminate	$Ca_3Al_2O_6$ or C_3A	-1350	5-10
Alumino-ferrite tetracalcic	$Ca_4Al_2FeO_{10}$ or C_4AF	-	5-15
Calcium sulphate	$CaSO_4$	-	5

3.4.2 Cement hydration

The reaction between water and COP, as for all chemical reactions, follows thermodynamic and kinetic laws. The reactions produced with water are mainly related to different phases of the cement.

The alumina phases show a high chemical reactivity in water, implying a rapid stiffening of the paste and low mechanical resistances. This disadvantage is due to the precipitation of calcium hydroaluminates. To solve this problem of rapid setting, cement manufacturers add calcium sulfate to the clinker which favors the formation of calcium trisulfoaluminate ($(CaO)_6(Al_2O_3)(SO_3)_3$, $32H_2O$) (TSA) and calcium monosulfoaluminate ($(CaO)_3(Al_2O_3)(CaSO_4)$, $12H_2O$) (AFm) ettringites.

The main reactions during the cement hydration are given in **Table 16** and by the equations below **(Á. Palomo et al. 2015)** :

$$2\,C_3S + 6H \longrightarrow C\text{-}S\text{-}H + 3CH \qquad \text{Eq. 1-4}$$

$$2C_2S + 4H \longrightarrow C\text{-}S\text{-}H + CH \qquad \text{Eq. 1-5}$$

Table 16. Production of hydrated phases from the anhydrous phases of CEM I

Anhydrous	Hydrates
C_2S, C_3S	C-S-H; CH
C_3A	C_3AH_6, C_4AH_{13} In presence of gypsum (CEMI)

	$C_6As\bar{H}_{32}$ or TSA, $C_4AS\bar{H}_{12}$ ou AFm
C_4AF	$C_3(A,F)H_6$, $C_4(A,F)H_{13}$ In presence of gypsum (CEMI) $C_6(A,F)H_6$, $C_4(A,F)S3\bar{H}_{32}$, $C_4(A,F)S\bar{H}_{12}$

3.4.2.1 *Immobilization in C-S-H*

The ability to integrate foreign elements within C-S-H is very large. This seems to be due to the high variability of the existing C-S-H structure. Foreign elements can either substitute for calcium or silicon or integrate at the interleaflet level **(Dmitriev A.M. 1986)**.

Two main mechanisms of metal binding in C-S-H have been demonstrated by **Bhatty et West (1993)**. These are substitution and addition. Substitution corresponds to an exchange process between metal cations and the calcium constituting C-S-H. This reaction is often irreversible. The addition, as for it, can be made according to 2 methods. It can be either the integration of a metal in the structural layers of C-S-H or an adsorption of metal cations on the hydroxyl sites having lost a proton.

3.4.2.2 *Immobilization in ettringite*

The structure of ettringite allows many substitutions. Thus, it is possible to replace divalent calcium by many elements such as Sr(II), Ba(II) **(Bensted et Varma 1971)** or Pb(II) and Zn(II) **(Auer et al. 1995)**. Elements such as Fe(III), Cr(III) **(Buhlert et Kuzel 1971)**, Mn(III) and Ti(III) **(Bensted et Varma 1971)** can, for their part, replace trivalent aluminium.

However, the most interesting property of ettringite lies in its capacity to immobilize soluble anions. In fact, anions such as OH^-, CO_3^-, NO_3^-, SO_3^- or $B(OH)_4^-$ can replace sulfate ions **(Pollmann 1989; Kumarathasan et al. 1989; McCarthy, Hassett, et Bender 1991)**.

The amount of foreign elements actually incorporated in ettringite is variable. It is necessary to consider the solubility of the metal hydroxide compared to that of ettringite. Thus **Bensted et Varma (1971)** showed that $Ba(OH)_2$ precipitates before ettringite. Moreover, the ratio of concentrations in solution at the time of precipitation between Me/Ca, Me/Al and anion/SO_2^- is also very important

3.4.2.3 *Immobilization in calcium monosulfoaluminate hydrate*

The possibilities for substitutions within calcium monosulfoaluminate hydrate are numerous due in particular to the presence of the sulfate anion between the interfoliar planes. This substitution is particularly favorable because it offers few constraints in terms of size and charge for the foreign anion. Moreover, it is possible to perform, as for ettringite, substitutions at the calcium and aluminum positions.

3.4.3 Concrete application examples

The studies carried out have shown that it is possible to successfully immobilize a large number of wastes containing metallic and metalloid trace elements. Among the most comprehensive studies on this subject is that of **Akhter et al. (1990)**. The authors succeeded in stabilizing various soils contaminated with metallic trace elements and metalloids using the stabilization/solidification process. Thus, a first soil highly contaminated with Cd (10000 ppm) was stabilized by adding 10% Portland cement. After this treatment, the leached Cd content decreased from 338 to 0.48 ppm. A soil, contaminated by high levels of Cr (12200 ppm) was also successfully treated. The Cr content observed during the leaching tests was reduced from 441 ppm to less than 5 ppm after treatment. Finally, a soil containing 12200 ppm of arsenic was stabilized by adding 44% Portland cement. The leaching tests showed a decrease in the released As content from 420 ppm to 4.56 ppm once the soil was treated

Other wastes, such as sludge, could be treated in this manner. **Jones et al. (1992)** studied the effect of stabilization/solidification treatment with Portland cement on Ni-contaminated sludge (29 350 mg/kg). The Ni concentrations obtained after treatment were 0.083 mg/L instead of 149 for the raw material.

3.4.4 Limitations of the stabilization/solidification process

Although the applications for the conditioning and recovery of waste via the stabilization/solidification process are numerous, the treatment of certain wastes has proved to be problematic. Thus, **Bricka R.M., Cullinane M.J (1990)** encountered problems during the stabilization of a waste strongly contaminated in Hg (25900 ppm). The Hg concentrations leached after treatment (28.6 mg/L) were higher than those released by the original material (0.1 mg/L). The same type of problem was encountered a few years later by **Shin et al. (1992)** during tests conducted for the stabilization of sludge contaminated, in this case, by high Cu contents (74mg/g). The authors showed that the presence of copper totally inhibited the hydration of cement.

The limitations of the stabilization/solidification process are mainly due to the effects of certain trace elements on cement hydration. The literature lists a very significant number of studies on this subject (Poon et al. 1986; J. I. Bhatty et West 1993; Rossetti et Medici 1995; Nocuń-Wczelik et Ma\lolepszy 1995; Takahashi et al. 1973; Miller 1976; Tashiro et al. 1977; Arliguie et Grandet 1985; Olmo, Chacon, et Irabien 2001)**.**

3.5 Amendment technology

In-situ immobilization, was initially described for metal-contaminated waters using different sorbents (G. Guo, Zhou, et Ma 2006) . In the 1950s to 1970s, scientists realized that total content was not sufficient to assess metal contamination **(Kabata-Pendias 2000)**. Also, the growing awareness of the strong dependence between the toxicity of metals and their chemical forms (speciation) led to an increasing interest in immobilization (G. Guo, Zhou, et Ma 2006). In-situ immobilization covers a wide range of techniques and consists of reducing the labile fraction of ETs (the fraction that can be easily released into the soil solution) by adding a soil binding agent (amendment) **(Kumpiene, Lagerkvist, et Maurice 2008)**, while leaving the soil structure intact **(Panfili 2004)**. This technique consists in modifying the chemical state of the ETs by bringing into the soil surface horizons mineral or organic phases capable of adsorbing, complexing or co-precipitating the ETs in situ. This technique is also called chemical stabilization or assisted natural attenuation.

It does not eliminate the contaminants from the soil, but it does significantly reduce their transfer to the various environmental compartments (soil solution, groundwater, living organisms, especially plants, etc.). Thus, the immobilization of ETs presents a better environmental balance for the stabilization of large surfaces (e.g.: mining and agricultural activities) than excavating several thousands of tons and moving them over long distances and replacing them with clean soil. In such situations, immobilization may offer a more sustainable and cost-effective solution.

Since immobilization studies are often aimed at limiting plant contamination, limited attention has been focused on leaching of ETs to groundwater **(Alvarez-Ayuso et Garcıa-Sánchez 2003; Ruttens et al. 2006; Oste et al. 2001; Houben, Pircar, et Sonnet 2012; Hartley, Edwards, et Lepp 2004; González-Núñez et al. 2012)**. Yet a reduction in leaching of ETs could have a significant role in protecting groundwater and reducing dispersion of ETs **(Ruttens et al. 2006)**.

Among the disadvantages mentioned, it should be noted that the addition of these amendments to the soil can also immobilize the elements essential to living organisms. They can also modify the physical properties of soils, and thus affect transfers in solution.

3.5.1 Anion stabilization by adsorbent amendments

Water pollution is currently a major concern for both human health and the environment. Many organic or inorganic anions can contaminate water, such as anionic dyes, salicylic acid, benzoic acid, fluorides, sulphates, perchlorates, chromates and arsenates etc. A large number of works are devoted to the adsorption of cationic pollutants, but the supports adapted to interact with anionic contaminants are relatively less studied. Some types of adsorbent materials and their applications in anion adsorption are presented in this section **(Table 17)**.

Table 17. Inorganic and organic amendments commonly used for trace element immobilization

	Material	Trace elements	Type of fixing	Advantages	References
Organic amendments	Compost WWTP sludge	As, Cd, Cu, Ni, Pb,Zn,Cr	Complexation with organic matter	Improves soil quality	**(Kumpiene, Lagerkvist, et Maurice 2008; Lindsay et al. 2011)**
Liming		Cd, Cu, Ni, Pb, Zn, Cr, Hg	Precipitation as carbonates	Alkaline effect increases the mobility of anions	**(Geebelen et al. 2006; Ruttens et al. 2006**)
Aluminosilicates	Beringitis	Zn, Cd	Adsorption Coprecipitation Sequestration	High immobilization capacity	**(Sappin-Didier 1995)**
	Zeolites	Zn, Pb, As, Cu, Sb, Co, Ti, Cd	Adsorption	Alkaline capacity Increases CEC	**(Chunfeng et al. 2009; Shi et al. 2009)**
	Ashes	Cations	ETs precipitation by pH increase Increase of the specific soil surface	High immobilization capacity	**(Geebelen et al. 2006; Donatello, Fernández-Jiménez, et Palomo 2012; Mench et al. 2006)**
	Bridged clays	As, Ni	Substitution in the crystalline lattice	Increases CEC	**(Lenoble 2003)**
Oxides and oxyhroxides of Fe	Steel shot	As, Cd, Cu, Ni, Pb, Zn	Sorption on the exchange surface of oxides Secondary mineral coprecipitation	High surface reactivity	**(Sappin-Didier 1995; Kumpiene, Lagerkvist, et Maurice 2008; Kumpiene 2010;**

					Ruttens et al. 2006)
Oxides and oxyhroxides of Al and Mn		As, Pb, Cd, Zn, Cr	Specific adsorption Internal sphere complexes		**(Kumpiene 2010)**
Phosphates	Hydroxyapatite	Zn, Pb, Cu, Cd, As	Adsorption Surface complexation	Highly soluble Highly fixed	**(Oliva et al. 2012; Sneddon et al. 2006; Montinaro et al. 2008; Boisson et al. 1999)**
	Phosphate rocks	Zn, Pb, Cd, Cu	Adsorption Complexation	Coprecipitation	**(Basta et McGowen 2004)**

Generally, all solids have adsorbent properties, while only adsorbents with sufficient specific surface area can be of practical interest. The specific surface areas of industrial adsorbents are usually above 100 m^2/g. The most widely used industrial adsorbent is activated carbon. However, the use of biomaterials such as chitosan, alginates or layered double hydroxides, agricultural waste is tending to develop thanks to very low raw material costs and the possibility of preparation from renewable sources.

The choice of amendment used in this thesis for the stabilization of anions in sediments was based, in part, on the knowledge of the influence of minerals on the speciation of anionic elements in the sediment, and in part, on previous studies. In this section, in order to evaluate the effectiveness of anions in sediments, layered double hydroxides will be the only mineral amendments presented and used.

3.5.2 Layered double hydroxides (LDH)

Layered double hydroxides, also named anionic clays, are materials that are not very abundant in the natural state, but are easily synthesized in the laboratory **(Géraud 2006)**. They are the subject of many studies because of anionic exchange properties, adsorption capacities, use in heterogeneous catalysis and their pharmaceutical applications **(Tao et al. 2006; Vaysse 2001)**.

3.5.2.1 Structure and characteristics

The general formula of an LDH is: $[M^{II}_{1-y}L^{III}_{y}(OH)_2]^{y+}[X^{n-}_{y/n}.zH_2O]$. It is similar to the natural hydrotalcite $Mg_6Al_2(OH)_{16}(CO_3)$-$4H_2O$, in which divalent magnesium cations are replaced by trivalent aluminum cations.

The structure of LDH is of the brucite $(M,L)(OH)_2$ type. The metal cations surrounded by six oxygen atoms of hydroxyl groups form $(M,L)(OH)_6$ octahedra. The partial substitution of trivalent L cations for divalent M cations generates an excess of positive charges on the layers **(Figure 18)**. In order to compensate this excess of charges, anions accompanied by water molecules are inserted between the layers and allow the electroneutrality of the structure **(Vaysse 2001; Vial 2005)**.

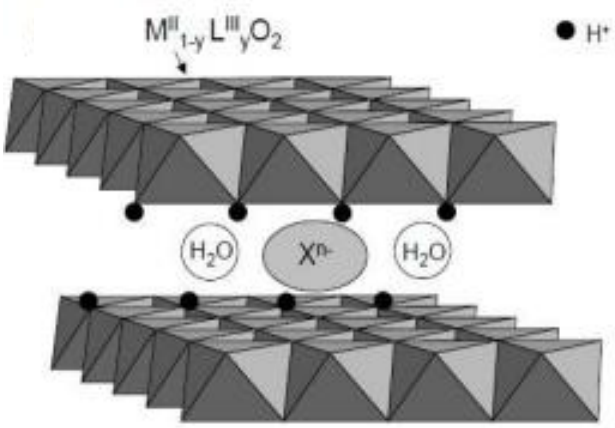

Figure 18. Schematic representation of the LDH structure (Vaysse 2001)

A wide variety of Double Lamellar Hydroxide compounds can be synthesized by varying:

- The chemical composition of the layered compound,
- The intercalated anion.

The chemical composition of the layer corresponds to the abbreviated formula [$M^{II}_{1-y}L^{III}$ y]. It is then possible to change the nature of the metal cations. Many divalent and trivalent metals can form the LDH layers. The most often synthesized layers are based on magnesium and aluminum, as in natural hydrotalcite. But other metals can also be used:

- Divalent metals: Zn^{2}+, Ni^{2+}, Cu^{2+}, Co^{2+}, Fe^{2+}, Ca^{2+}...
- Trivalent metals: Cr^{3+}, Fe^{3+}, Co^{3+}, Mn^{3+}, V^{3+}, Ga^{3+}...

A priori, no limitation exists in the intercalation of anions. However, it is necessary that the anions are stable under the experimental conditions and that there are no steric or geometric constraints. A wide variety of anionic species can fit into the interleaf space **(Rives, del Arco, et Martín 2014)** :

- Non-metallic oxo-anions (BO_3^{3-}, CO_3^{2-}, NO_3^- , $Si_2O_5^{2-}$, HPO_4^{2-}, SO_4^{2-}, ClO_4^-, AsO_4^{3-}, SeO_4^{2-}, BrO_4^-…)
- Halogens (F^-, Cl^-; Br^-, I^-)
- Oxometallate anions (VO_4^{3-}, CrO_4^{2-}, MnO_4^-, $V_{10}O_{28}^{6-}$, $Cr_2O_7^{2-}$, $Mo_7O_{24}^{6-}$)
- Cyanocomplexes $[Fe(CN)_6]^{4-}$, $[Co(CN)_6]^{4-}$, $[Mo(CN)_8]^{4-}$
- Organic anions (CH_3COO^-, $C_6H_5COO^-$, $C_{12}H_{25}COO^-$, $C_2O_4^{2-}$, $C_6H_5SO^{3-}$…)
- Anionic polymers (polyacrylate, polystyrene sulfonates, DNA strands ...) **(Desigaux et al. 2006)**.

3.5.3 Synthesis

Two main methods exist for the synthesis of LDH, co-precipitation and anion exchange

3.5.3.1 Co-precipitation

Co-precipitation is the most widely used method for synthesizing LDH. It consists of adding a basic species to a salt solution containing divalent and trivalent metal cations in order to achieve simultaneous precipitation of the metal cations **(Bocher et al. 2004; Tao et al. 2006)**.

The advantage of this method is that it allows control of several parameters during the synthesis such as, the molar ratio of divalent and trivalent metal cations, the concentration of metal salts, the reaction pH and the anionic species involved **(Olfs et al. 2009)**. However, some LDHs cannot be prepared by co-precipitation due to the complexation of anions by metals present in solution. In this case, another route, anion exchange, can be used for LDH synthesis **(Vaysse 2001)**.

3.5.3.2 Anion exchange

This method of synthesis is of high importance and may be the only possible route to obtain new LDH. It uses one of the main properties of LDH, i.e. ion exchange **(Mostarih 2006)**. The principle of this method consists in replacing the intercalated anionic species by another species having a higher affinity than the starting anion **(Géraud 2006)**. An order of decreasing affinity for mono- and divalent anions is proposed by **Vial (2005)**:

$OH^- > F^- > Cl^- > Br^- > NO_3^- > I^-$

$CO_3^{2-} > C_{10}H_4N_2O_8S^{2-} > SO_4^{2-}$

The synthesis is performed by dispersion of the precursor in the solution containing the anion to be exchanged in excess with agitation at room temperature.

3.5.4 Applications

Layered double hydroxides have many applications due to their variable composition, low synthesis cost, low toxicity and high specific surface area.

LDHs, due to their high specific surface area and the flexibility of the interleaflet space, have the ability to trap anions by surface adsorption and/or anion exchange. The anion exchange capacity depends on the nature of the anion present in the interleaflet and also on the charge density of the leaflets, i.e. the M^{II}/L^{III} molar ratio.

This ability to adsorb anions can be used in the field of soil or water remediation. Many studies are reported in the literature on the adsorption of dyes in aqueous solution **(de Sá, Cunha, et Nunes 2013; Extremera et al. 2012)**. Their removal capabilities for simple anions (F^-, Cl^-, Br^-, I^-) and complex anions (ClO_4^-, BF_4^-, CrO_4^-, SO_4^-) are also demonstrated in the literature **(Châtelet et al. 1996; Theiss et al. 2014)**. **Table 18** lists a number of literature references regarding anion adsorption.

Table 18. Anion adsorption by different LDH

Adsorbed anion	Adsorbent	Reference
Fluoride	LDH Mg/Al	**(Jimenez-Nunez et al. 2012)**
	LDH Mg/Al	**(Wan et al. 2015)**
	LDH Co/Al	**(Xin Zhao et al. 2015)**
	LDH Mg/Cr/Cl	**(Mandal et al. 2013)**
	LDH Mg/Fe/La	**(J. Wang et al. 2015)**
	LDH-Mg/Fe modified by CeO_2	**(T. Zhang et al. 2013)**
	LDH Zn/Cr	**(P. Koilraj et Kannan 2013)**
Phosphate	LDH/kaolin	**(Deng et Shi 2015)**
	ZnAl-LDH intercalated with pyromellitic acid	**(Yu et al. 2015)**
	Fe_3O_4/LDH composite	(L. Yan et al. 2015)
	LDH-Zn/bioceramic composite	**(X. Zhang et al. 2016)**
	LDH Mg/Al	**(Novillo et al. 2014)**
	Fe_3O_4/LDH Mg/Al/NO3	**(Paulmanickam Koilraj et Sasaki 2016)**

	Superparamagnetic particles modified by LDH	**(Drenkova-Tuhtan et al. 2013)**
	LDH Mg/Al composite and biochar	**(Islam et Patel 2011)**
	LDH Zn/Al et Mg/Al	**(Yang et al. 2014)**
Nitrate	LDH Mg/Al	**(Halajnia et al. 2013)**
	LDH Mg/Fe modified wheat straw	**(Xue et al. 2016)**
	LDH Mg/Fe and Mg/Al	**(Halajnia et al. 2012)**
	LDH Ca/Al/Cl	**(Islam et Patel 2011)**
	LDH Zn/Al	**(Islam et Patel 2010)**
	LDH Mg/Al	**(Wan et al. 2012)**
Chromate	Composite LDH Mg/Al et SiO_2	**(Perez et al. 2015)**
	LDH Mg/Al	**(W. Wang et al. 2014)**
	LDH-Ni/Fe	**(Y. Lu et al. 2016)**
	LDH Mg/Al	**(Khitous, Salem, et Halliche 2016)**
	LDH Ca-Al	**(Y. Li et al. 2013)**
	LDH Mg/Al/Cl	**(Yue et al. 2017)**
	LDH Co/Bi	**(Jaiswal et al. 2015)**
	LDH Mg/Al	**(Z. Zhang et al. 2014)**
	Graphene/ LDH Mg/Al	**(Yuan et al. 2013)**
	Different LDH type compounds Mg/Al or Mg/Zn/Al	**(Dudek et al. 2012)**
Arsenate	Hydrotalcite-Fe	**(Türk, Alp, et Deveci 2009)**
	LDH Mg/Al	**(Duan et al. 2016)**
	LDH Zn/Fe	**(Y. Lu et al. 2016)**
	LDH Mg/Fe	(D. Kang et al. 2013)
	LDH Zn/Al	**(Meng et al. 2016)**
	LDH Mg/Al nanocrystalline	**(Wu et al. 2013)**
	LDH Cu/Mg/Fe/La	**(Y. Guo et al. 2012)**
	LDH Mg/Al and Mg/Fe	**(Yoshida et al. 2015)**
	LDH Zn/Al/SO_4	**(Bagherifam et al. 2014)**
	LDH Mg/Fe	**(Caporale et al. 2013)**
	LDH Cu/Mg/Fe	**(Y. Guo et al. 2013)**
Sulfate	LDH Mg/Fe	**(Matusik et Rybka 2019)**
	LDH Zn/Al	**(Mahjoubi et al. 2017)**
	LDH Zn/Al	**(Ardau, Frau, et Lattanzi 2016)**
	LDH Mg/Al	**(Guimarães et al. 2019)**

4 Description of the mineral waste valorization processes

The important quantities of mineral wastes generated annually must be managed in environmentally friendly conditions. The French law favors this disposal method in order to ensure that only ultimate waste is kept in a storage installation.

Currently, almost all mineral wastes is immersed into the sea in the case of sediments or disposed of in landfill, in the case of fly ash. However, in the perspective of the evolution of the laws, mineral waste could be recovered in the construction and public works sector, as backfill sand, artificial aggregates, road gravel as sand concrete, or even in the treatment of wastewater**. (Abriak, Grégoire, et Bernard 2003; Ádám et al. 2007; Alqahtani et al. 2017)**. In civil engineering, the recovery of mineral waste is often envisaged in materials after treatment. The Douai School of Mines has therefore surrounded itself with various industrial, institutional and university partners in order to carry out research projects on the recovery of mineral waste in various forms: road techniques (sub-base, base course, etc.), artificial aggregates, concrete formulation, wastewater treatment, etc. In the process of this recovery and with the

updating and appearance of new regulations, the valorization generally follows the scheme: mineral waste valorization in compliance with regulatory, environmental and ecotoxicological requirements (Protocol HP14).

In this section we will describe the different valorization pathways of mineral waste (sediment, fly ash), focusing on two valorization routes used in this thesis: **(i)** the valorization of paper mill fly ash for the manufacture of lightweight aggregates; **(ii)** the valorization of biomass bottom ash as a reactive filter to remove phosphorus from wastewater

4.1 Sediment valorization in civil engineering

The large quantities of sediments generated each year must be managed in environmentally friendly conditions. This disposal method is favored by French law to ensure that only final waste is kept in a storage installation. Currently, almost all dredged material is dumped at sea.

The choice of a valorization pathway depends on several criteria such as the intrinsic characteristics of the sediment (degree of contamination, agronomic value, etc.), the impact on the environment, the cost, the regulations in force and societal acceptability. Several recovery methods can be envisaged **(Table 19)**.

Table 19. Marine sediment valorization channels

Sector	Conditions	Applicable regulations	Reference
Recovery in road techniques	Inert or non-hazardous sediment		Guide to road building Guide to the acceptability of alternative materials in road construction Environmental assessment Technical guide CFTR soil treatment with lime and/or hydraulic binders-applications to the reaction of pavement bases
Valuation in landscaping	Inert sediment or specific study according to EN 12920+A1		Order of 28 October 2010 on inert waste storage installations
Recovery by reinforcing the riverbanks	Inert or acceptable sediment in immersion	Environmental Code for discharge into surface waters (Article 214-1)	Order of 28 October 2010 on inert waste storage facilities Order of 9 August 2006 known as the "Geode" order

Quarry backfill	Inert sediment	Order of 22 September 1994 on quarry operations	Order of 28 October 2010 on inert waste storage facilities
Covering of a waste storage facility	Inert or non-hazardous sediment depending on use	Decree of 9 September 1997 on the storage of "non-dangerous" waste	Order of 28 October 2010 on inert waste storage installations
Maritime works	Inert sediment or specific study according to EN 12920+A1		Order of 28 October 2010 on inert waste storage installations
Construction products	Inert sediment or specific study according to EN 12920+A1		Order of 28 October 2010 on inert waste storage installations

4.1.1 Marine sediments valorization in road technique

The valorization of marine sediments in road techniques has been the subject of several studies. The laboratory of the School of Mines was one of the first laboratories in France to study this issue. As part of an initial approach to the use of marine sediments in road construction in 2005, the Douai School of Mines validated a methodological approach developed in the laboratory by creating an experimental bed with a surface area of 300 m² (50 m long and 6 m wide).

The purpose of this project was to validate an experimental technique by fulfilling the requirements of the standards and application guides in terms of mechanical and environmental aspects, to verify the feasibility of installing construction equipment, to achieve the proportions of marine sediments fixed in the laboratory and to monitor the evolution of the structure over a period of one year in terms of mechanical and environmental aspects **(Dubois 2006)**.

Figure 19. Implementation of the Freycinet 12 road based on dredged sediments at GPMD (Achour 2013).

Several studies have been carried out on the recovery of polluted sediments after treatment by industrial processes, in the field of road construction **(Scordia 2008; Tribout, Husson, et Nzihou 2011; Miraoui 2010; Dia 2013) (Figure 19).**

4.1.2 Marine sediments valorization in artificial aggregates

In France, aggregates consumption amounts to 376 million tons, mainly from land-based deposits **(UNPG) (Figure 20)**.

As access to land-based deposits has become increasingly difficult, aggregates producers have diversified their resources, notably to marine aggregates (marine sands and sediments). These materials

extracted from the sea have similar characteristics to those of unconsolidated rock aggregates extracted from land-based quarries. Thus, they represent a complementary resource, particularly for coastal regions and large urban centers that can be served by water. The cities of Dunkirk, Lille, Nantes and Bordeaux satisfy a large part of their material needs with marine aggregates.

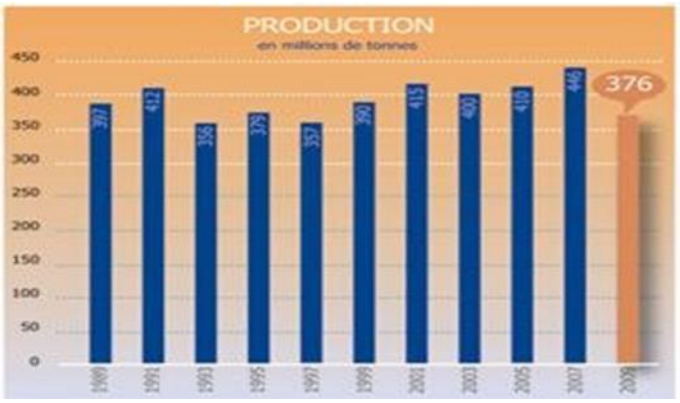

Figure 20. Aggregate consumption in civil engineering (UNPG)

This production represents 7 million tons per year which is 2% of the French aggregate production. In the case of sediments, the sandy fraction (marine sands) can be used directly as aggregate. In addition, fine sediments have been the subject of work for the production of aggregates **(Brakni 2008)**. The manufactured aggregates, which aim to fight against coastal erosion, will be the products of this sector. Artificial aggregates are made from marine sediments. These sediments are then integrated into a water and cement mixture to form a cement matrix **(Figure 21)**. These aggregates will be immersed in several applications (erosion control and dune stabilization or in the form of a wear layer, protection of the foot of jetties and dykes or possibly, depending on their characteristics, as a road sub-base).

Figure 21. Marine sediment-based aggregates (Brakni 2008)

4.1.3 Marine sediments valorization in mortar and concrete production

Agostini, Skoczylas, et Lafhaj (2007) studied the behavior of marine sediments treated by an industrial process in cementitious materials through the production of mortars. The laboratory study focused on the evaluation of the practical feasibility of incorporating sediments into mortar by studying the constraints related to the water absorption by the aggregates, the determination of the basic characteristics of the mortar (porosity, density), the evaluation of the curing conditions influences and

finally the study of the mechanical performances. Based on several formulation studies, the researchers demonstrated the feasibility of using treated sediments as a raw material for the production of cement matrix materials. Other studies on the valorization of marine sediment in a cementitious matrix were carried out by producing a sand concrete based on sediment. The study consisted in finding an optimal mixture between dredged sand and one or several additives with cement and water in order to obtain satisfactory mechanical characteristics. The dredged sand studied was of marine origin; it is the sand deposited at the West Harbour Master's Office of the Port Autonome de Dunkerque **(ZRI, ABRIAK, et BENZERZOUR, 2009)**. According to the authors, the results obtained showed the possibility of using dredged sand and fine sediment in sand concrete.

4.1.4 Marine sediments valorization in landscape eco-model

The valorization of non-immersible sediments in landscaped eco-modelled bunds represents a new approach to valorization in order to minimize the quantity of dredged sediments. As part of its sustainable development approach, the GPMD has developed five landscaped eco-modelled bunds to promote biodiversity **(Figure 22)**.

Figure 22. Eco-landscaped merlon at the GPMD

4.2 Fly ash valorization in civil engineering

Currently, most of the fly ash produced is stored in class I or II landfills **(Reijnders 2005)**. However, due to the constant increase in the amount of fly ash produced, and the shortage of landfill space, landfilling is increasingly considered an unsatisfactory management option. Furthermore, the use of ash for agricultural spreading is often not considered an acceptable management option, considering the concentration of pollutants, particularly metallic trace elements and metalloids, in the ash. Therefore, several countries have made provision for the stabilization of ash prior to landfill in order to immobilize the pollutants **(Reijnders 2005)**. Increasingly, it seems inevitable that the various techniques and possibilities for ash recovery will be developed. The different recovery techniques have been studied to a greater or lesser extent up to now, depending on the cost involved, while considering the regulatory context. In this section, the available ash recovery or treatment options will be described and analyzed in a more systematic manner.

4.2.1 Ash valorization in the field of construction and public works

The construction sector has been using by-products from other industrial sectors for many years, in particular the use of fly ash from thermal power stations. This fly ash has even become a material in its own right in the manufacture of concrete and provides it with special properties. In general, fly ash has pozzolanic properties. The pozzolanic activity of a material can be defined as the ability of the silicates and aluminates in that material to react, in the presence of water, with hydrated lime to form hydrates. The pozzolanic binder allows the formation of a wide range of hydrate products that contribute to the

binding and hardening of the material. The incorporation of such a material into concrete or mortar replaces part of the cement and thus allows a reduction in the cement supply.

Several combustion residues such as rice husk ash **(Povindar K. Mehta 1977; P. K. Mehta et Pirtz 1978)** and municipal solid waste ash **(Gress et al. 1991; Ali et Chang 1994; Van der Sloot, Kosson, et Hjelmar 2001; Nishida et al. 2001)** have been successfully used in construction. The incorporation of ash to replace cement or sand in cementitious materials is also reported in some recent studies (Cyr, Coutand, et Clastres 2007b; Monzó et al. 1996; 2003; Pan et al. 2003; Garcés et al. 2008; Wiebusch et al. 1998). It is generally accepted that from an economic and technical viewpoint, alternative materials such as coal fly ash and silica fume can be used as substitutes for traditional cement and/or aggregates.

4.2.2 Fly ash valorization in the wastewater treatment sector

In view of the current challenges, the elimination of phosphorus from water treatment plants is an imperative point to be ensured. In wastewater treatment plants, effluent phosphorus removal can be achieved in two different ways. It is possible to let the micro-organisms in the aeration tanks operate, which will assimilate and eliminate part of the phosphorus. However, when this solution is not possible, the operator is required to apply a physico-chemical treatment by adding reactive that will allow the precipitation of phosphorus. The present dephosphatation technique used in France in WWTPs consists of adding metal salts such as $FeCl_3$ or $AlCl_3$ or calcium hydroxide to form insoluble phosphate precipitates. However, it is essential to have a separation step to eliminate this precipitate formed, either at the inlet or at the outlet of the WWTP. In addition, several studies **(Esser, D., Ricard, B., Fernades, N., Merlin, G. 2004)** have demonstrated that the use of $FeCl_3$ can lead to phosphorus release when this precipitate is under reducing conditions due to the chemical instability of iron phosphate.

The use of reactive materials for phosphorus retention on a solid phase through adsorption and/or precipitation mechanisms is an alternative to maintain the extensive character of the classical French system **(Vohla et al. 2011; Akratos et Tsihrintzis 2007)**. Various types of materials rich in calcium have been used in P removal processes to precipitate hydroxyapatite ($Ca_{10}(PO_4)_6OH_2$) using low cost materials, among these materials are steel slag (Kostura, Kulveitová, et Leško 2005; E.-H. Kim et al. 2006; Korkusuz, Beklioğlu, et Demirer 2005), magnetite minerals **(Karapinar, Hoffmann, et Hahn 2004)**, limestone and calcite concrete **(Y. Song et al. 2006; P. Molle, A. Liénard, A. Grasmick, A. Iwema 2003)** , natural wastes and industrial by-products **(Y. Yan et al. 2014))**, fly ash and red mud (S Karaca et al. 2006; Y. Yan et al. 2014), these materials have been developed as low cost adsorbents to remove phosphorus from wastewater, the removal rates vary between 40% and 90%.

This sector has been the subject of studies focusing on technical aspects. The technical feasibility has been demonstrated in all cases (Cyr, Coutand, et Clastres 2007b) . However, in most cases, an environmental assessment has not been carried out. This step would be essential before any development on an industrial scale. Since the use of ash in wastewater treatment is one of the objectives of this thesis, this application case is presented in the following paragraph, this valorization pathway corresponds to the valorization of ash as a reactive filter to remove phosphorus from wastewater.

4.2.3 Phosphorus removal from filter materials

The summary of studies on phosphorus removal by various materials **(Vohla et al. 2011; Johansson 1999)** is presented in **Table 20**. The selection of each material in this table was based on the maximum phosphorus retention potential considered in the literature. The column and pilot/full scale studies were selected as more representative of the real conditions. Indeed, although the columns are generally fed

with synthetic effluent (distilled water or tap water), the pilot/full scale plants are mostly fed with secondary effluent.

However, the operating conditions and material composition of these studies vary. The evaluation criteria used in the publication by **Vohla et al. (2011)** are:

- The experimental time,
- The residence time,
- The mass percentage of calcium in the material,
- The input phosphorus concentration and the purification efficiency,
- The amount of phosphorus accumulated on the material.

Table 20. Phosphorus removal by mineral waste

Materials	Study type	P retention ($g.kg^{-1}$)	Reference
Apatite	Column Column	13.9 (550 d) 0.28-1.09 (24 h)	**(Molle et al. 2005)** **(Bellier, Chazarenc, et Comeau 2006)**
Bauxite	Batch Batch	0.355-0.612 0.82-2.95	**(Drizo et al. 1999)** **(Altundoğan et Tümen 2003)**
Limestone	Batch Batch	0.25-0.3 0.682	**(Jönsson et al. 2004; Drizo et al. 1999)**
Oyster shell	Batch Column	0.792 0.833	**(Seo et al. 2005)**
Dolomite	Batch	7.34-52.02	**(Semra Karaca et al. 2004)**
Dolomite and sand	Batch	0.121-0.168	**(Prochaska et Zouboulis 2006)**
FerooSorp	Batch Column	9.5 9.8	**(Molle 2003)**
Filtralite P™	Batch Full scale	2.5 3.89	**(Ádám et al. 2007; Ádám, Søvik, et Krogstad 2006)**
Gravel	Batch	3-3.6	**(Vohla et al. 2005)**
Blast Furnace	Column Batch	4.1-4.7 (630 d) 0.9 (730 d)	**(Prigent 2013)**
Sand	Full scale	0.04-0.97 (2920 d)	**(Vohla et al. 2007) (Del Bubba, Arias, et Brix 2003)**
Dolomite sand	Batch Column	0.7 1	**(Pant, Reddy, et Lemon 2001)**
Sand (Estonia)	Batch Full scale	2.45 0.05	**(Arias, Del Bubba, et Brix 2001)**
Shell sand	Column Batch Batch	3.5 0.8-8 9.6	**(Søvik et Kløve 2005; Roseth 2000; Ádám et al. 2007)**
Zeolite	Batch Batch	2.15 0.46	**(Sakadevan et Bavor 1998; Drizo et al. 1999)**

4.2.4 Ash valorization into lightweight aggregates

The production of lightweight aggregates represents a particularly interesting application for ash. For some applications, low density aggregates are more valuable than normal density aggregates **(Owens et Newman 1999)**. Natural aggregates generally have particle densities between 2.4 and 2.8 g/cm^3, while lightweight aggregates have densities between 0.8 and 2.0 g/cm^3.

Lightweight aggregates are therefore used to produce lightweight concrete and other lightweight construction products. They are also used in other applications such as lightweight geotechnical fill, insulation products, soil engineering, hydro-culture, drainage and filters. The low density also offers additional benefits such as higher thermal insulation and improved thermal inertia.

Certain studies (Cheeseman et Virdi 2005b; Javed I. Bhatty et Reid 1989) indicate the possibility of using ash for the manufacture of low-density aggregates, using relatively simple processing and low temperature sintering. The procedure presented for the manufacture of lightweight products containing the ash involves mixing the ash with a clay binder, then forming the pellets into spherical or plate-like shapes, and finally sintering them in a rotary tube furnace at temperatures between 1020°C and 1080°C. This method produces lightweight products which are then classified for use as aggregates according to the properties of concrete with lightweight aggregates (ASTM C330, USA). Studies report that aggregates made from the ash have a lower density than a commercially available lightweight aggregate. Also, the water absorption of ash-containing aggregates is lower. However, these aggregates have a compressive strength comparable to that of conventional aggregates. The major crystalline phases identified in these aggregates are quartz (SiO_2), whitlockite ($Ca_3(PO_4)_2$), a calcium magnesium phosphate ($Ca_7Mg_2P_6O_{24}$) and hematite (Fe_2O_3) **(Cheeseman et Virdi 2005b)**. The table 21 describes the wastes proposed in the literature for the manufacture of lightweight aggregates.

Table 21. Waste materials proposed in the literature for LWA production

Municipal solid wastes	Sewage sludge	**(Anh Tuan et al. 2014; Bia\lowiec et al. 2014)**
	Incinerator fly ash	**(Tan et al. 2013; Quina et al. 2014)**
	Sewage ash	**(K.-L. Lin 2006; Cheeseman et Virdi 2005b)**
	Water treatment	**(C. Huang, Pan, et Liu 2005; C.-H. Huang et Wang 2013)**
Mining and quarrying residues	Ornamental stones	**(Ducman et Mirtič 2009; K. Kim 2014)**
	Zeolite-rich rocks	**(Lotov 2012; Sokolova et Vereshagin 2010)**
	Natural aggregates	**(Volland et al. 2014; González-Corrochano, Alonso-Azcárate, et Rodas 2014)**
	Waste clay materials	**(Fakhfakh et al. 2007; W. Franus et al. 2011)**
	Ore beneficiation	**(Loutou et al. 2013; Christogerou, Kavas, et Angelopoulos 2014)**
	Other rocks	**(O. V. Kaz'mina et al. 2009; O. Kaz'mina et al. 2009)**
Coal power plant residues	Fly ash	**(Güneyisi et al. 2013; Zorić et al. 2012)**
	Bottom ash, slag	**(M. A. Kang et Kang 2013; Lee 2014)**
Mineral transformation industry	Soda-lime glass	**(Bernardo et al. 2010; Wei et al. 2011)**
	Ceramic tile polishing	**(Bernardin, da Silva, et Riella 2006; Ducman et Mirtič 2009)**
	Other ceramics & glasse	**(Sim et Kim 2010; Tang 2014)**
	Other sludges	**(Huifen et al. 2010; Ducman et Mirtič 2009)**
Sediments dredging	Water reservoirs	**(Liao, Huang, et Chen 2013; Chiou et Chen 2013)**
	Harbors	**(Wei et al. 2011; 2014; 2008)**
Metallurgical industry	Steel dust & slag	**(Wei et al. 2011; 2014; 2008)**
	Aluminium scrap	**(D. Bajare et al. 2012; Diana Bajare, Kazjonovs, et Korjakins 2013)**
	Wastewater treatment	**(Tay, Show, et Hong 2002; Tay, Hong, et Show 2000)**

Other sources	Air pollution	**(M. Franus, Bandura, et Franus 2014; Quina, Bordado, et Quinta-Ferreira 2014)**
	Agriculture and forestry	**(C. M. García et al. 2014; Chindaprasirt, Jaturapitakkul, et Rattanasak 2009)**
	Spent catalysers	**(S.-N. Jo et Kang 2012; S. N. Jo et al. 2012)**
	Construction and demolition	**(S. N. Jo et al. 2012; Mueller, Sokolova, et Vereshagin 2008)**

Reference

Abdullahi, M. 2006. « Characteristics of wood ash/OPC concrete ». *Leonardo Electronic Journal of Practices and Technologies* 8: 9-16.

Abriak, N. E., P. Grégoire, et F. Bernard. 2003. « Etude d'une grave routière à base de sable de dragage ». In *2nd International symposium on contaminated sediments, Québec, Canada*, 370-73.

« Acceptabilité de matériaux alternatifs en technique routière - Evaluation environnementale ». s. d. Cerema. Consulté le 8 mars 2022. http://www.cerema.fr/fr/centre-ressources/boutique/acceptabilite-materiaux-alternatifs-technique-routiere.

Achour, Raouf. 2013. « Valorisation et caractérisation de la durabilité d'un matériau routier et d'un béton à base de sédiments de dragage ». PhD Thesis, Université de Sherbrooke.

Ackermann, Sonia, Reto Gieré, Matthew Newville, et Juraj Majzlan. 2009. « Antimony sinks in the weathering crust of bullets from Swiss shooting ranges ». *Science of the Total Environment* 407 (5): 1669-82.

Ádám, Kinga, Tore Krogstad, Lasse Vråle, Anne Kristine Søvik, et Petter D. Jenssen. 2007. « Phosphorus Retention in the Filter Materials Shellsand and Filtralite P®—Batch and Column Experiment with Synthetic P Solution and Secondary Wastewater ». *Ecological Engineering* 29 (2): 200-208. https://doi.org/10.1016/j.ecoleng.2006.09.021.

Ádám, Kinga, Anne Kristine Søvik, et Tore Krogstad. 2006. « Sorption of phosphorous to Filtralite-PTM—The effect of different scales ». *Water Research* 40 (6): 1143-54.

Agostini, Franck, Frédéric Skoczylas, et Zoubeir Lafhaj. 2007. « About a possible valorisation in cementitious materials of polluted sediments after treatment ». *Cement and Concrete Composites* 29 (4): 270-78.

Ainsworth, Calvin C., et Dhanpat Rai. 1987. « Chemical characterization of fossil fuel combustion wastes ». Pacific Northwest Lab., Richland, WA (USA); Electric Power Research Inst ….

Akhter, H., L. G. Butler, S. Branz, F. K. Cartledge, et M. E. Tittlebaum. 1990. « Immobilization of As, Cd, Cr and Pb-containing soils by using cement or pozzolanic fixing agents ». *Journal of hazardous materials* 24 (2-3): 145-55.

Akratos, Christos S., et Vassilios A. Tsihrintzis. 2007. « Effect of Temperature, HRT, Vegetation and Porous Media on Removal Efficiency of Pilot-Scale Horizontal Subsurface Flow Constructed Wetlands ». *Ecological Engineering* 29 (2): 173-91. https://doi.org/10.1016/j.ecoleng.2006.06.013.

ALBAREDA, L., JM LOZANO, A. TENCATI, A. MIDTTUN, et F. PERRINI. s. d. « ADEME (AGENCE DE L'ENVIRONNEMENT ET DE LA MAITRISE DE L'ENERGIE)(2009), Évalutation des Resultats de la Reutilisation et du Recyclage des Emballages en Europe–Synthèse, marzo, http://www2. ademe. fr/servlet/getDoc? cid= 96&m= 3&id= 67529&p1= 02&p2= 05&ref= 17597. »

Ali, Mujahid T., et Wen F. Chang. 1994. « Strength properties of cement-stabilized municipal solid waste (MSW) incinerator ash masonry bricks ». *Materials Journal* 91 (3): 256-63.

Alqahtani, Fahad K., M. Iqbal Khan, Gurmel Ghataora, et Samir Dirar. 2017. « Production of recycled plastic aggregates and its utilization in concrete ». *Journal of materials in civil engineering* 29 (4): 04016248.

Altundoğan, H. Soner, et Fikret Tümen. 2003. « Removal of phosphates from aqueous solutions by using bauxite II: the activation study ». *Journal of Chemical Technology & Biotechnology: International Research in Process, Environmental & Clean Technology* 78 (7): 824-33.

Alvarez-Ayuso, E., et A. Garcıa-Sánchez. 2003. « Palygorskite as a feasible amendment to stabilize heavy metal polluted soils ». *Environmental pollution* 125 (3): 337-44.

Alzieu, Claude. 1999. *Dragages et environnement marin: état des connaissances= Dredging and marine environment: state of the art*.

Ampleman, Guy, Sonia Thiboutot, André Marois, et Annie Gagnon. 2009. « Evaluation of soil contamination by explosives and metals at the Land Force Central Area Training Centre (LFCA TC) Meaford, Ontario (Phase I) ». DEFENCE RESEARCH AND DEVELOPMENT CANADA VALCARTIER (QUEBEC).

Anh Tuan, Bui Le, Mewael Gebregiorgis Tesfamariam, Yuan-Yuan Chen, Chao-Lung Hwang, Kae-Long Lin, et Mung-Pei Young. 2014. « Production of lightweight aggregate from sewage sludge and reservoir sediment for high-flowing concrete ». *Journal of Construction Engineering and Management* 140 (5): 04014005.

Ardau, Carla, Franco Frau, et Pierfranco Lattanzi. 2016. « Antimony Removal from Aqueous Solutions by the Use of Zn-Al Sulphate Layered Double Hydroxide ». *Water, Air, & Soil Pollution* 227 (9): 344. https://doi.org/10.1007/s11270-016-3048-z.

Arias, C.A, M Del Bubba, et H Brix. 2001. « Phosphorus Removal by Sands for Use as Media in Subsurface Flow Constructed Reed Beds ». *Water Research* 35 (5): 1159-68. https://doi.org/10.1016/S0043-1354(00)00368-7.

Arliguie, G., et J. Grandet. 1985. « Etude par calorimetrie de l'hydratation du ciment Portland en presence de zinc ». *Cement and Concrete Research* 15 (5): 825-32.

Artois-Picardie, Agence de l'eau. 2001. *Méthodes de gestion et de réutilisation des sédiments pollués: inventaire détaillé technique et financier des méthodes de curage, de traitement et des usages possibles: logiciel d'aide à la décision pour la gestion des sédiments*.

Auer, S., H.-J. Kuzel, H. Pöllmann, et F. Sorrentino. 1995. « Investigation on MSW fly ash treatment by reactive calcium aluminates and phases formed ». *Cement and concrete research* 25 (6): 1347-59.

Ayrinhac, Fabien. 2005. « Valorisation des cendres volantes de chaudière à lit fluidisé circulant dans la filière du génie civil ». PhD Thesis, INSA de Toulouse.

Baghdadi, Z. A., M. N. Fatani, et N. A. Sabban. 1995. « Soil modification by cement kiln dust ». *Journal of Materials in Civil Engineering* 7 (4): 218-22.

Bagherifam, Saeed, Sridhar Komarneni, Amir Lakzian, Amir Fotovat, Reza Khorasani, Wenyan Huang, Jianfeng Ma, et Yujue Wang. 2014. « Evaluation of Zn–Al–SO4 layered double hydroxide for the removal of arsenite and arsenate from a simulated soil solution: isotherms and kinetics ». *Applied clay science* 95: 119-25.

Bai, J., A. Chaipanich, J. M. Kinuthia, M. O'farrell, B. B. Sabir, S. Wild, et M. H. Lewis. 2003. « Compressive strength and hydration of wastepaper sludge ash–ground granulated blastfurnace slag blended pastes ». *Cement and Concrete Research* 33 (8): 1189-1202.

Bajare, D., A. Korjakins, J. Kazjonovs, et I. Rozenstrauha. 2012. « Pore structure of lightweight clay aggregate incorporate with non-metallic products coming from aluminium scrap recycling industry ». *Journal of the European Ceramic Society* 32 (1): 141-48.

Bajare, Diana, Janis Kazjonovs, et Aleksandrs Korjakins. 2013. « Lightweight concrete with aggregates made by using industrial waste ». *Journal of Sustainable Architecture and Civil Engineering* 4 (5): 67-73.

Bakharev, T. 2005. « Geopolymeric materials prepared using Class F fly ash and elevated temperature curing ». *Cement and concrete research* 35 (6): 1224-32.

Balakrishnan, Balamohan, ASM Abdul Awal, Abdul Halid B. Abdullah, et M. Z. Hossain. 2017. « Flow properties and strength behaviour of masonry mortar incorporating high volume fly ash ». *GEOMATE Journal* 12 (31): 121-26.

Banfill, P., et Moisés Frias. 2007. « Rheology and conduction calorimetry of cement modified with calcined paper sludge ». *Cement and concrete research* 37 (2): 184-90.

Bannon, Desmond I., John W. Drexler, Genevieve M. Fent, Stan W. Casteel, Penelope J. Hunter, William J. Brattin, et Michael A. Major. 2009. « Evaluation of small arms range soils for metal contamination and lead bioavailability ». *Environmental science & technology* 43 (24): 9071-76.

Baranger, Ph, M. Azaroual, S. Lanini, P. Piantone, et Ph Freyssinet. 1999. « Modelling the weathering of a bottom-ash heap ». In *Stab & Env: stabilisation des déchets et environnement. Congrès*.

Barbosa, Valeria FF, Kenneth JD MacKenzie, et Clelio Thaumaturgo. 2000. « Synthesis and characterisation of materials based on inorganic polymers of alumina and silica: sodium polysialate polymers ». *International journal of inorganic materials* 2 (4): 309-17.

Basta, N. T., et S. L. McGowen. 2004. « Evaluation of chemical immobilization treatments for reducing heavy metal transport in a smelter-contaminated soil ». *Environmental pollution* 127 (1): 73-82.

Begarin, Farid. 2012. « Etude de paramètres endogènes et exogènes au ciment Portland ordinaire influençant l'hydratation de sa phase principale: le silicate tricalcique ». PhD Thesis, Université de Bourgogne.

Belevi, H., et P. Baccini. 1991. « Long-term assessment of leachates from municipal solid waste landfills and bottom ash monofills. » *J. RESOUR. MANAGE. TECHNOL.* 19 (2): 68-73.

Bellier, Nathalie, Florent Chazarenc, et Yves Comeau. 2006. « Phosphorus removal from wastewater by mineral apatite ». *Water research* 40 (15): 2965-71.

Benard, Anne. 2003. « Le plomb et le chrome dans les ciments: spéciation et modélisation du transfert au cours de la lixiviation ». PhD Thesis, Aix-Marseille 3.

Bensted, John, et S. Prakash Varma. 1971. « Studies of ettringite and its derivatives ». *Cement Technology* 2 (3): 73-77.

Bernardin, Adriano Michael, Márcio José da Silva, et Humberto Gracher Riella. 2006. « Characterization of cellular ceramics made by porcelain tile residues ». *Materials Science and Engineering: A* 437 (2): 222-25.

Bernardo, Enrico, Giovanni Scarinci, Paolo Bertuzzi, Piero Ercole, et Ludovico Ramon. 2010. « Recycling of waste glasses into partially crystallized glass foams ». *Journal of Porous Materials* 17 (3): 359-65.

Berra, Mario, Teresa Mangialardi, et Antonio Evangelista Paolini. 2015. « Reuse of woody biomass fly ash in cement-based materials ». *Construction and Building Materials* 76: 286-96.

Bhatty, J. I., et P. B. West. 1993. « Interaction of heavy metals in Portland cement stabilized waste systems: effects on paste hydration ». In *Proceedings of Emerging technologies symposium on cement and concrete in the global environment, PCA-SP114T, Skokie, Chicago, IL*, 3:1-13.

Bhatty, Javed I., et Kenneth J. Reid. 1989. « Lightweight aggregates from incinerated sludge ash ». *Waste management & research* 7 (4): 363-76.

Bia\lowiec, Andrzej, Wojciech Janczukowicz, Zygmunt M. Gusiatin, Arthur Thornton, Joanna Rodziewicz, et Magdalena Zielińska. 2014. « Recycling potential of air pollution control residue from sewage sludge thermal treatment as artificial lightweight aggregates ». *Waste management & research* 32 (3): 221-27.

Blackford, Jane R. 2007. « Sintering and microstructure of ice: a review ». *Journal of Physics D: Applied Physics* 40 (21): R355.

Blanchard, Claire. 2000. « Caractérisation de la mobilisation potentielle des polluants inorganiques dans les sols pollués ». PhD Thesis, Lyon, INSA.

Blenkharn, J. I. 2005. « Safe disposal and effective destruction of clinical wastes ». *Journal of Hospital Infection* 60 (4): 295-97.

Blissett, R. S., et N. A. Rowson. 2012. « A review of the multi-component utilisation of coal fly ash ». *Fuel* 97: 1-23.

Bocher, Florent, Antoine Géhin, Christian Ruby, Jaafar Ghanbaja, Mustapha Abdelmoula, et Jean-Marie R. Génin. 2004. « Coprecipitation of Fe (II–III) hydroxycarbonate green rust stabilised by phosphate adsorption ». *Solid State Sciences* 6 (1): 117-24.

Boisson, J., A. Ruttens, Michel Mench, et J. Vangronsveld. 1999. « Evaluation of hydroxyapatite as a metal immobilizing soil additive for the remediation of polluted soils. Part 1. Influence of hydroxyapatite on metal exchangeability in soil, plant growth and plant metal accumulation ». *Environmental pollution* 104 (2): 225-33.

Boni, Maria Rosaria, Laura D'Aprile, et Giancarlo De Casa. 2004. « Environmental quality of primary paper sludge ». *Journal of hazardous materials* 108 (1-2): 125-28.

Boucard, L. 2006. « Valorisation des sédiments fluviaux stabilisés ». PhD Thesis, Thèse de doctorat, Ecole Centrale de Lille.

Boulday, D., et F. Marcovecchio. 2016. « Management methods ash from combustion of biomass. Review of productions and associated methods-Final report ».

Boutouil, Mohamed. 1998. « Traitement des vases de dragage par solidification/stabilisation à base de ciment et additifs ». PhD Thesis, Le Havre.

Brakni, Samira. 2008. « Première approche vers une valorisation de granulats artificiels à base de sédiments de dragage portuaire: application en génie côtier ». PhD Thesis, Artois.

Breck, Donald W., et Donald Wesley Breck. 1973. *Zeolite molecular sieves: structure, chemistry, and use*. John Wiley & Sons.

Bricka R.M., Cullinane M.J. 1990. « Solidification/stabilisation as a best demonstrated available technology for resource conservation and recovery act wastes, in Remedial action, treatment, and disposal of hazardous waste ». *15th Annual Research Symposium Proceedings, Environmental Protection Agency*, p. 437-447 1990.

Brochu, S., S. Thiboutot, G. Ampleman, E. Diaz, I. Poulin, et R. Martel. 2011. « Canadian Approach to the Environmental Characterization and Risk Assessment of Military Training ». In *Environmental Chemistry of Explosives and Propellant Compounds in Soils and Marine Systems: Distributed Source Characterization and Remedial Technologies*, 49-76. ACS Publications.

Brunori, Claudia, Carlo Cremisini, Paolo Massanisso, Valentina Pinto, et Leonardo Torricelli. 2005. « Reuse of a treated red mud bauxite waste: studies on environmental compatibility ». *Journal of hazardous materials* 117 (1): 55-63.

« Brunori: Reuse of a treated red mud bauxite waste:... - Google Scholar ». s. d. Consulté le 21 avril 2022. https://scholar.google.com/scholar_lookup?title=Reuse%20of%20a%20treated%20red%20mud%20bauxite%20waste%3A%20studies%20on%20environmental%20compatibility&publication_year=2005&author=C.%20Brunori&author=C.%20Cremisini&author=P.%20Massanisso&author=V.%20Pinto&author=L.%20Torricelli.

Buchholz, B. A., et S. Landsberger. 1993. « Trace metal analysis of size-fractioned municipal solid waste incinerator fly ash and its leachates ». *Journal of Environmental Science & Health Part A* 28 (2): 423-41.

Buchwald, A., K. Dombrowski, et M. Weil. 2005. « The influence of calcium content on the performance of geopolymeric binder especially the resistance against acids ». *Proceedings of the world geopolymer*, 35-39.

Buhlert, R., et H. J. Kuzel. 1971. « Über den Einbau von Cr3+ und Fe3+ in Ettringit ». *Zement, Kalk, Gips* 2: 83-85.

CAILLAT, Sébastien, Esperanza PERDRIX, Karim TABET, et Benoît TAUPIN. 2010. « Cocombustion de charbon et de biomasse-Cas des chaudières industrielles ».

Cao, Xinde, Lena Q. Ma, Ming Chen, Donald W. Hardison Jr, et Willie G. Harris. 2003. « Weathering of lead bullets and their environmental effects at outdoor shooting ranges ». *Journal of environmental quality* 32 (2): 526-34.

Capilla, Xavier. 2005. « Dynamique de transfert du cadmium et du zinc au sein des dépôts de sédiments de curage végétalisés ». PhD Thesis, INPL-Institut National Polytechnique de Lorraine.

Caporale, A. G., M. Pigna, SMGG Azam, A. Sommella, M. A. Rao, et A. Violante. 2013. « Effect of competing ligands on the sorption/desorption of arsenite on/from Mg–Fe layered double hydroxides (Mg–Fe-LDH) ». *Chemical Engineering Journal* 225: 704-9.

Carette, G. G., et V. M. Malhotra. 1984. « Characterization of Canadian fly ashes and their performance in concrete ». *Division Report, MRP/MSL*, 84-137.

CETMEF. 2000. « Inventaire des techniques de dragage. » *32p*, avril 2000.

Chassiot, Léo, Pierre Francus, Arnaud De Coninck, Thibault Labarre, Danielle Cloutier, et Patrick Lajeunesse. 2017. « Distribution spatio-temporelle des polluants métalliques et organiques au sein des sédiments de la rivière Saint-Charles. »

Châtelet, L., J. Y. Bottero, J. Yvon, et A. Bouchelaghem. 1996. « Competition between monovalent and divalent anions for calcined and uncalcined hydrotalcite: anion exchange and adsorption sites ». *Colloids and Surfaces A: Physicochemical and Engineering Aspects* 111 (3): 167-75.

Cheah, Chee Ban, et Mahyuddin Ramli. 2011. « The implementation of wood waste ash as a partial cement replacement material in the production of structural grade concrete and mortar: An overview ». *Resources, Conservation and Recycling* 55 (7): 669-85.

Cheeseman, C. R., et G. S. Virdi. 2005a. « Properties and microstructure of lightweight aggregate produced from sintered sewage sludge ash ». *Resources, Conservation and Recycling* 45 (1): 18-30.

———. 2005b. « Properties and microstructure of lightweight aggregate produced from sintered sewage sludge ash ». *Resources, Conservation and Recycling* 45 (1): 18-30.

Cheng, T. W., et Y. S. Chen. 2003. « On formation of CaO–Al2O3–SiO2 glass–ceramics by vitrification of incinerator fly ash ». *Chemosphere* 51 (9): 817-24.

Chindaprasirt, P., C. Jaturapitakkul, et U. Rattanasak. 2009. « Influence of fineness of rice husk ash and additives on the properties of lightweight aggregate ». *Fuel* 88 (1): 158-62.

Chiou, I. J., et C. H. Chen. 2013. « Effects of waste-glass fineness on sintering of reservoir-sediment aggregates ». *Construction and Building Materials* 38: 987-93.

Choi, Jiyeon, et Won Sik Shin. 2020. « Application of Aqueous Carbonated Slags in the Immobilization of Heavy Metals in Field-Contaminated Soils ». *Environmental Engineering Research* 25 (3): 356-65. https://doi.org/10.4491/eer.2019.101.

Christogerou, A., T. Kavas, et G. N. Angelopoulos. 2014. « Synergy of boron containing solid wastes and fructose for the production of lightweight aggregates: microstructure and properties ». *Waste and Biomass Valorization* 5 (4): 733-41.

Chunfeng, Wang, L. I. Jiansheng, S. U. N. Xia, WANG Lianjun, et S. U. N. Xiuyun. 2009. « Evaluation of zeolites synthesized from fly ash as potential adsorbents for wastewater containing heavy metals ». *Journal of environmental sciences* 21 (1): 127-36.

Clausen, J. A. Y., et N. I. C. Korte. 2009. « The distribution of metals in soils and pore water at three US military training facilities ». *Soil and Sediment Contamination* 18 (5): 546-63.

Colin, David. 2003. « Valorisation de sédiments fins de dragage en technique routière ». PhD Thesis, Caen.

Conner, Jesse R., et Steve L. Hoeffner. 1998. « The history of stabilization/solidification technology ». *Critical reviews in environmental science and technology* 28 (4): 325-96.

Conseil, Décision du. 2003. « 33/CE du 19/12/2002 établissant les critères et procédures d'admission des déchets dans les décharges, conformément à l'article 16 et à l'annexe II de la Directive 1999/31 ». *CE (JOCE du 16/01/2003)*.

« Convention Text ». s. d. OSPAR Commission. Consulté le 14 mars 2022. https://www.ospar.org/convention/text.

Coventry, Stuart, Claire Woolveridge, et Shaun Hillier. 1999. *The reclaimed and recycled construction materials handbook*.

Cowie, J., et F. P. Glasser. 1992. « The reaction between cement and natural waters containing dissolved carbon dioxide ». *Advances in Cement Research* 4 (15): 119-34.

Cyr, Martin, Marie Coutand, et Pierre Clastres. 2007a. « Technological and environmental behavior of sewage sludge ash (SSA) in cement-based materials ». *Cement and Concrete Research* 37 (8): 1278-89.

———. 2007b. « Technological and environmental behavior of sewage sludge ash (SSA) in cement-based materials ». *Cement and Concrete Research* 37 (8): 1278-89.

Das, Biki, S. Prakash, P. S. R. Reddy, et Vibnuti N. Misra. 2007. « An overview of utilization of slag and sludge from steel industries ». *Resources, conservation and recycling* 50 (1): 40-57.

Davidenko, Tatyana. 2015. « Hydratation D'un Système Cimentaire Binaire Contenant Des Cendres Volantes de Biomasse ». PhD Thesis, Université de Sherbrooke.

Davidovits, Joseph. 1991. « Geopolymers: inorganic polymeric new materials ». *Journal of Thermal Analysis and calorimetry* 37 (8): 1633-56.

———. 1999. « Chemistry of geopolymeric systems, terminology ». In *Geopolymer*, 99:9-39. sn.

Davies, B.E. 1995. « Lead in Heaty metals in soil », 1995, B.J. Alloway, ed.Blackie Academic and Professional, London, UK, 206-223. édition.

Davis, Allen P., Mohammad Shokouhian, Himanshu Sharma, Christie Minami, et Derek Winogradoff. 2003. « Water quality improvement through bioretention: Lead, copper, and zinc removal ». *Water Environment Research* 75 (1): 73-82.

Davydova, S. 2005. « Heavy metals as toxicants in big cities ». *Microchemical Journal* 79 (1-2): 133-36.

Dawley, Stuart, Alison Stenning, et Andy Pike. 2008. « Mapping corporations, connecting communities: Remaking steel geographies in northern England and southern Poland ». *European Urban and Regional Studies* 15 (3): 265-87.

Del Bubba, M., C. A. Arias, et H. Brix. 2003. « Phosphorus adsorption maximum of sands for use as media in subsurface flow constructed reed beds as measured by the Langmuir isotherm ». *Water research* 37 (14): 3390-3400.

Delabre, Dominique. 1985. « Les métaux lourds dans les sédiments du littoral Nord de la France et leur disponibilité lors des rejets de dragages ». PhD Thesis, Lille 1.

Delay, I., J. Swithenbank, et B. B. Argent. 2001. « Prediction of the distribution of alkali and trace elements between the condensed and gaseous phases generated during clinical waste incineration ». *Journal of alloys and compounds* 320 (2): 282-95.

Deng, Lin, et Zhou Shi. 2015. « Synthesis and characterization of a novel Mg–Al hydrotalcite-loaded kaolin clay and its adsorption properties for phosphate in aqueous solution ». *Journal of Alloys and Compounds* 637: 188-96.

Desigaux, Léa, Malha Ben Belkacem, Peggy Richard, Joël Cellier, Philippe Léone, Laurent Cario, Fabrice Leroux, Christine Taviot-Guého, et Bruno Pitard. 2006. « Self-assembly and characterization of layered double hydroxide/DNA hybrids ». *Nano Letters* 6 (2): 199-204.

Dia, Moussa. 2013. « Traitement et valorisation de sédiments de dragage phosphatés en technique routière ». PhD Thesis, Artois.

Diaz, Emmanuela, Sylvie Brochu, Sonia Thiboutot, Guy Ampleman, Andre Marois, et Annie Gagnon. 2008. « Energetic Materials and Metals Contamination at CFB/ASU Wainwirght, Alberta Phase 1 ». DEFENCE RESEARCH AND DEVELOPMENT CANADA VALCARTIER (QUEBEC).

Dmitriev A.M. 1986. « Chimie physique du processus d'hydratation – Influence des éléments mineurs et des matières d'addition ». *International Congress on Cement Chemistry Proceedings,* p. 73-81 1986.

Donatello, Shane, Ana Fernández-Jiménez, et Angel Palomo. 2012. « An assessment of Mercury immobilisation in alkali activated fly ash (AAFA) cements ». *Journal of hazardous materials* 213: 207-15.

Drenkova-Tuhtan, Asya, Karl Mandel, Anja Paulus, Carsten Meyer, Frank Hutter, Carsten Gellermann, Gerhard Sextl, Matthias Franzreb, et Heidrun Steinmetz. 2013. « Phosphate recovery from wastewater using engineered superparamagnetic particles modified with layered double hydroxide ion exchangers ». *Water research* 47 (15): 5670-77.

Drizo, A., C. A. Frost, J. Grace, et K. A. Smith. 1999. « Physico-chemical screening of phosphate-removing substrates for use in constructed wetland systems ». *Water Research* 33 (17): 3595-3602.

Drouet, Emeline. 2010. « Impact de la température sur la carbonatation des matériaux cimentaires: prise en compte des transferts hydriques ». PhD Thesis, École normale supérieure de Cachan-ENS Cachan.

Du, Yan-Jun, Ming-Li Wei, Krishna R. Reddy, et Hao-liang Wu. 2016. « Effect of Carbonation on Leachability, Strength and Microstructural Characteristics of KMP Binder Stabilized Zn and Pb Contaminated Soils ». *Chemosphere* 144 (février): 1033-42. https://doi.org/10.1016/j.chemosphere.2015.09.082.

Duan, Shibo, Wei Ma, Zihong Cheng, Panpan Zong, Xuelong Sha, et Fanqing Meng. 2016. « Preparation of modified Mg/Al layered double hydroxide in saccharide system and its application to remove As (V) from glucose solution ». *Colloids and Surfaces A: Physicochemical and Engineering Aspects* 490: 250-57.

Dubois, V. 2006. « Caractérisation physico-mécanique et environnementale des sédiments marins. Application en technique routière ». *Ecole des Mines de Douai. Ph. D. diss*.

Ducman, Vilma, et Breda Mirtič. 2009. « The applicability of different waste materials for the production of lightweight aggregates ». *Waste Management* 29 (8): 2361-68.

Dudek, Barbara, Piotr Kuśtrowski, Anna Bia\las, Piotr Natkański, Zofia Piwowarska, Lucjan Chmielarz, Marek Kozak, et Marek Michalik. 2012. « Influence of textural and structural properties of MgAl and MgZnAl containing hydrotalcite derived oxides on Cr (VI) adsorption capacity ». *Materials Chemistry and Physics* 132 (2-3): 929-36.

Duffus, John H. 2002. « " Heavy metals" a meaningless term?(IUPAC Technical Report) ». *Pure and applied chemistry* 74 (5): 793-807.

Duxson, Peter, John L. Provis, Grant C. Lukey, Seth W. Mallicoat, Waltraud M. Kriven, et Jannie SJ Van Deventer. 2005. « Understanding the relationship between geopolymer composition, microstructure and mechanical properties ». *Colloids and Surfaces A: Physicochemical and Engineering Aspects* 269 (1-3): 47-58.

Duxson, PSWM, Seth W. Mallicoat, Grant C. Lukey, Waltraud M. Kriven, et Jannie SJ van Deventer. 2007. « The effect of alkali and Si/Al ratio on the development of mechanical properties of metakaolin-based geopolymers ». *Colloids and Surfaces A: Physicochemical and Engineering Aspects* 292 (1): 8-20.

Ecke, Holger. 2003. « Sequestration of metals in carbonated municipal solid waste incineration (MSWI) fly ash ». *Waste Management* 23 (7): 631-40.

Ecke, Holger, Nourreddine Menad, et Anders Lagerkvist. 2003. « Carbonation of municipal solid waste incineration fly ash and the impact on metal mobility ». *Journal of Environmental Engineering* 129 (5): 435-40.

Ecoba. 2016. « http://www.ecoba.com/ecobaccpprod.html ». *Accessed 13 May 2020.*, 2016.

El-Eswed, B. I., R. I. Yousef, M. Alshaaer, I. Hamadneh, S. I. Al-Gharabli, et F. Khalili. 2015. « Stabilization/solidification of heavy metals in kaolin/zeolite based geopolymers ». *International journal of mineral processing* 137: 34-42.

El-Eswed, Bassam I., Omar M. Aldagag, et Fawwaz I. Khalili. 2017. « Efficiency and mechanism of stabilization/solidification of Pb (II), Cd (II), Cu (II), Th (IV) and U (VI) in metakaolin based geopolymers ». *Applied Clay Science* 140: 148-56.

Elghali, Abdellatif, Mostafa Benzaazoua, Bruno Bussière, et Thomas Genty. 2019. « In situ effectiveness of alkaline and cementitious amendments to stabilize oxidized acid-generating tailings ». *Minerals* 9 (5): 314.

Esser, D., Ricard, B., Fernades, N., Merlin, G. 2004. « Physico-chemical phosphorus removal in vertical flow reed bed treatment plants. » *international Conference on Wetland Systems for Water Pollution Control. Avignon, France.*, 2004.

Esteves, T. C., R. Rajamma, D. Soares, A. S. Silva, V. M. Ferreira, et J. A. Labrincha. 2012. « Use of biomass fly ash for mitigation of alkali-silica reaction of cement mortars ». *Construction and Building Materials* 26 (1): 687-93.

Extremera, R., I. Pavlovic, M. R. Pérez, et C. Barriga. 2012. « Removal of acid orange 10 by calcined Mg/Al layered double hydroxides from water and recovery of the adsorbed dye ». *Chemical engineering journal* 213: 392-400.

Fakhfakh, Emna, W. Hajjaji, M. Medhioub, F. Rocha, A. López-Galindo, M. Setti, F. Kooli, F. Zargouni, et F. Jamoussi. 2007. « Effects of sand addition on production of lightweight aggregates from Tunisian smectite-rich clayey rocks ». *Applied Clay Science* 35 (3-4): 228-37.

Fang, Yuan, et Obada Kayali. 2013. « The fate of water in fly ash-based geopolymers ». *Construction and Building Materials* 39: 89-94.

Fernández-Jiménez, Ana, A. G. De La Torre, A. Palomo, G. López-Olmo, M. M. Alonso, et M. A. G. Aranda. 2006. « Quantitative determination of phases in the alkaline activation of fly ash. Part II: Degree of reaction ». *Fuel* 85 (14-15): 1960-69.

Fernández-Jiménez, Ana, A. Palomo, et M. Criado. 2005. « Microstructure development of alkali-activated fly ash cement: a descriptive model ». *Cement and concrete research* 35 (6): 1204-9.

Filella, Montserrat, Nelson Belzile, et Yu-Wei Chen. 2002. « Antimony in the environment: a review focused on natural waters: II. Relevant solution chemistry ». *Earth-Science Reviews* 59 (1-4): 265-85.

Flourat, Amandine. 2020. « Valorisation de co-produits de filières agroindustrielles, de la chimie verte aux applications ». PhD Thesis, Reims.

Foucault, Alain, et Jean Fran Raoult. 1980. *Dictionary of geology*. Masson.

Foucher, Jérôme. 2005. « Valorisation des déblais sableux de dragage portuaire en France métropolitaine ». *Final year project. ENTPE*, 1-66.

François, Hugues, Maud Hirczak, et Nicolas Senil. 2006. « Territoire et patrimoine: la co-construction d'une dynamique et de ses ressources ». *Revue dEconomie Regionale Urbaine*, n° 5: 683-700.

Franus, M., L. Bandura, et W. Franus. 2014. « Modification of the lightweight aggregate with the use of spent zeolite sorbents after the sorption of diesel fuel ». *Вісник Національного університету Львівська політехніка. Теорія і практика будівництва*, n° 781: 32-41.

Franus, Wojciech, Ma\lgorzata Franus, Jolanta Latosinska, et RAFA\l Wojcik. 2011. « USE OF SPENT GLAUCONITE IN LIGHTWEIGHT AGGREGATE PRODUCTION ». *Boletin De La Sociedad Espanola De Ceramica Y Vidrio* 50 (4): 193-200.

Freyssinet, Jacques. 1998. « L'indemnisation du chômage en Europe. Entre l'activation des dépenses pour l'emploi et la garantie de minima sociaux ». *Pauvreté et exclusion*, 69-92.

Frías, Moisés, Rosario García, Raquel Vigil, et Sergio Ferreiro. 2008. « Calcination of art paper sludge waste for the use as a supplementary cementing material ». *Applied Clay Science* 42 (1-2): 189-93.

Gallego, Susana M., Maria P. Benavides, et Maria L. Tomaro. 1996. « Effect of heavy metal ion excess on sunflower leaves: evidence for involvement of oxidative stress ». *Plant Science* 121 (2): 151-59.

Garcés, P., M. Pérez Carrión, E. García-Alcocel, J. Payá, J. Monzó, et M. V. Borrachero. 2008. « Mechanical and physical properties of cement blended with sewage sludge ash ». *Waste management* 28 (12): 2495-2502.

García, Carmen Martínez, Teresa Cotes Palomino, Francisco J. Iglesias Godino, et Francisco A. Corpas Iglesias. 2014. « Porosity of expanded clay manufactured with addition of sludge from the brewing industry ». *International Journal of Energy and Environmental Engineering* 5 (4): 341-47.

García, R., R. Vigil de la Villa, Iñigo Vegas, Moisés Frías, et MI Sánchez de Rojas. 2008. « The pozzolanic properties of paper sludge waste ». *Construction and Building Materials* 22 (7): 1484-90.

Garrabrants, A. C., F. Sanchez, C. Gervais, P. Moszkowicz, et D. S. Kosson. 2002. « The effect of storage in an inert atmosphere on the release of inorganic constituents during intermittent wetting of a cement-based material ». *Journal of hazardous materials* 91 (1-3): 159-85.

Geebelen, Wouter, Valérie Sappin-Didier, Ann Ruttens, Robert Carleer, Jan Yperman, Kwèlè Bongué-Boma, Michel Mench, Niels Van der Lelie, et Jaco Vangronsveld. 2006. « Evaluation of cyclonic ash, commercial Na-silicates, lime and phosphoric acid for metal immobilisation purposes in contaminated soils in Flanders (Belgium) ». *Environmental pollution* 144 (1): 32-39.

Géraud, Erwan. 2006. « Elaboration et caractérisation de matrices hydroxydes doubles lamellaires macroporeuses ». PhD Thesis, Université Blaise Pascal-Clermont-Ferrand II.

Glasser, F. P. 1993. « Chemistry of cement-solidified waste forms ». *Chemistry and microstructure of solidified waste forms*, 1-39.

Goldhaber, Susan B. 2003. « Trace element risk assessment: essentiality vs. toxicity ». *Regulatory toxicology and pharmacology* 38 (2): 232-42.

González-Corrochano, Beatriz, Jacinto Alonso-Azcárate, et Magdalena Rodas. 2014. « Effect of prefiring and firing dwell times on the properties of artificial lightweight aggregates ». *Construction and Building Materials* 53: 91-101.

González-Núñez, Raquel, María D. Alba, M. M. Orta, Miquel Vidal, et Anna Rigol. 2012. « Remediation of metal-contaminated soils with the addition of materials–Part II: Leaching tests to evaluate the efficiency of materials in the remediation of contaminated soils ». *Chemosphere* 87 (8): 829-37.

Górecka, H., K. Chojnacka, et H. Górecki. 2006. « The application of ICP-MS and ICP-OES in determination of micronutrients in wood ashes used as soil conditioners ». *Talanta* 70 (5): 950-56.

Gosselin, Anne, Denis Blackburn, et Mario Bergeron. 1999. *Protocole d'évaluation de la traitabilité des sédiments, des sols et des boues à l'aide des technologies minéralurgiques*. Environnement Canada.

Gougar, M. L. D., B. E. Scheetz, et D. M. Roy. 1996. « Ettringite and C S H Portland cement phases for waste ion immobilization: A review ». *Waste management* 16 (4): 295-303.

Gourley, J. T. 2003. « Geopolymers; opportunities for environmentally friendly construction materials ». In *Materials 2003 Conference: Adaptive Materials for a Modern Society, Sydney, Institute of Materials Engineering Australia*.

Gress, D. L., X. Zhang, S. Tarr, I. Pazienza, et T. T. Eighmy. 1991. « Municipal Solid Waste Combustion ASH as an Aggregate Substitute in Asfhaltic Concrete ». In *Studies in Environmental Science*, 48:161-75. Elsevier.

Groves, G. W., D. I. Rodway, et I. G. Richardson. 1990. « The carbonation of hardened cement pastes ». *Advances in Cement research* 3 (11): 117-25.

Guimarães, Damaris, Natasha C.M. da Rocha, Rafaela A.P. de Morais, Andréia De-Lazzari B.P. Resende, Rosa M.F. Lima, Geraldo M. da Costa, et Versiane A. Leão. 2019. « Precipitation of a Layered Double Hydroxide Comprising Mg2+ and Al3+ to Remove Sulphate Ions from Aqueous Solutions ». *Journal of Environmental Chemical Engineering* 7 (1): 102815. https://doi.org/10.1016/j.jece.2018.102815.

Güneyisi, Erhan, Mehmet Gesoğlu, Özgür Pürsünlü, et Kasım Mermerdaş. 2013. « Durability aspect of concretes composed of cold bonded and sintered fly ash lightweight aggregates ». *Composites Part B: Engineering* 53: 258-66.

Gunn, A. P. 2004. *Use of sewage sludge in construction*. Vol. 608. Ciria.

Gunning, Peter J., Colin D. Hills, et Paula J. Carey. 2010. « Accelerated carbonation treatment of industrial wastes ». *Waste management* 30 (6): 1081-90.

Guo, Guanlin, Qixing Zhou, et Lene Q. Ma. 2006. « Availability and assessment of fixing additives for the in situ remediation of heavy metal contaminated soils: a review ». *Environmental monitoring and assessment* 116 (1): 513-28.

Guo, Yanwei, Zhiliang Zhu, Yanling Qiu, et Jianfu Zhao. 2012. « Adsorption of arsenate on Cu/Mg/Fe/La layered double hydroxide from aqueous solutions ». *Journal of hazardous materials* 239: 279-88.

———. 2013. « Synthesis of mesoporous Cu/Mg/Fe layered double hydroxide and its adsorption performance for arsenate in aqueous solutions ». *Journal of Environmental Sciences* 25 (5): 944-53.

Halajnia, Akram, S. Oustan, N. Najafi, A. R. Khataee, et Amir Lakzian. 2013. « Adsorption–desorption characteristics of nitrate, phosphate and sulfate on Mg–Al layered double hydroxide ». *Applied Clay Science* 80: 305-12.

Halajnia, Akram, S. Oustan, Nosratollah Najafi, A. R. Khataee, et Amir Lakzian. 2012. « The adsorption characteristics of nitrate on Mg–Fe and Mg–Al layered double hydroxides in a simulated soil solution ». *Applied Clay Science* 70: 28-36.

Hardison Jr, Donald W., Lena Q. Ma, Thomas Luongo, et Willie G. Harris. 2004. « Lead contamination in shooting range soils from abrasion of lead bullets and subsequent weathering ». *Science of the Total Environment* 328 (1-3): 175-83.

Harned, Herbert S., et Raymond Davis Jr. 1943. « The ionization constant of carbonic acid in water and the solubility of carbon dioxide in water and aqueous salt solutions from 0 to 50 ». *Journal of the American Chemical Society* 65 (10): 2030-37.

Hartley, William, Robert Edwards, et Nicholas W. Lepp. 2004. « Arsenic and heavy metal mobility in iron oxide-amended contaminated soils as evaluated by short-and long-term leaching tests ». *Environmental pollution* 131 (3): 495-504.

Houben, David, Jonathan Pircar, et Philippe Sonnet. 2012. « Heavy metal immobilization by cost-effective amendments in a contaminated soil: effects on metal leaching and phytoavailability ». *Journal of Geochemical Exploration* 123: 87-94.

Houst, Yves Freddy. 1993. « Diffusion de gaz, carbonatation et retrait de la pâte de ciment durcie ». EPFL.

Huang, Chihpin, Jill Ruhsing Pan, et Yaorey Liu. 2005. « Mixing water treatment residual with excavation waste soil in brick and artificial aggregate making ». *Journal of environmental engineering* 131 (2): 272-77.

Huang, Chung-Ho, et Shun-Yuan Wang. 2013. « Application of water treatment sludge in the manufacturing of lightweight aggregate ». *Construction and Building Materials* 43: 174-83.

Huifen, Yang, Dang Chunge, Liang Wentao, et Ma Wen. 2010. « Utilization of red mud for the preparation of lightweight aggregates ». In *2010 International Conference on Digital Manufacturing & Automation*, 2:883-86. IEEE.

International Agency for Research on Cancer. 1989, 1989, IARC Monograph 47,Lyon, France. édition.

Islam, Mahamudur, et Rajkishore Patel. 2010. « Synthesis and physicochemical characterization of Zn/Al chloride layered double hydroxide and evaluation of its nitrate removal efficiency ». *Desalination* 256 (1-3): 120-28.

———. 2011. « Physicochemical characterization and adsorption behavior of Ca/Al chloride hydrotalcite-like compound towards removal of nitrate ». *Journal of hazardous materials* 190 (1-3): 659-68.

Izquierdo, Maria, et Xavier Querol. 2012. « Leaching behaviour of elements from coal combustion fly ash: an overview ». *International Journal of Coal Geology* 94: 54-66.

Jacobs, L. W., J. K. Syers, et D. R. Keeney. 1970. « Arsenic sorption by soils ». *Soil Science Society of America Journal* 34 (5): 750-54.

Jaiswal, Amita, Raj Mani, Sushmita Banerjee, Ravindra Kumar Gautam, et M. C. Chattopadhyaya. 2015. « Synthesis of novel nano-layered double hydroxide by urea hydrolysis method and their application in removal of chromium (VI) from aqueous solution: Kinetic, thermodynamic and equilibrium studies ». *Journal of Molecular Liquids* 202: 52-61.

Jambhulkar, Hemlata P., et Asha A. Juwarkar. 2009. « Assessment of bioaccumulation of heavy metals by different plant species grown on fly ash dump ». *Ecotoxicology and Environmental Safety* 72 (4): 1122-28.

Jarrige, Adolphe. 1971. « LES CENDRES VOLANTES PROPRIETES-APPLICATIONS INDUSTRIELLES ».

Jimenez-Nunez, M. L., M. Solache-Rios, J. Chavez-Garduno, et M. T. Olguin-Gutierrez. 2012. « Effect of grain size and interfering anion species on the removal of fluoride by hydrotalcite-like compounds ». *Chemical Engineering Journal* 181: 371-75.

Jo, Si Nae, Yoo Tack Kim, Seung Gu Kang, et Chang Sam Kim. 2012. « Properties of artificial lightweight aggregates (ALAs) made of dredged soil mixed with waste catalyst slag ». In *Applied Mechanics and Materials*, 174:1079-85. Trans Tech Publ.

Jo, Si-Nae, et Seung-Gu Kang. 2012. « A study on the properties of artificial aggregates containing bottom ash from the power plant and waste catalyst slag ». *Journal of the Korean Crystal Growth and Crystal Technology* 22 (4): 200-206.

Johansson, Lena. 1999. « Industrial by-products and natural substrata as phosphorus sorbents ». *Environmental Technology* 20 (3): 309-16.

Johnson, C. Annette, Hermann Moench, Paul Wersin, Pia Kugler, et Christoph Wenger. 2005. « Solubility of antimony and other elements in samples taken from shooting ranges ». *Journal of environmental quality* 34 (1): 248-54.

Jones, Larry W., RMark Bricka, et M. J. Cullinane. 1992. « Effects of selected waste constituents on solidified/stabilized waste leachability ». In *Stabilization and Solidification of Hazardous, Radioactive, and Mixed Wastes: 2nd volume*. ASTM International.

Jönsson, Håkan, Anna Richert Stintzing, Björn Vinnerås, et Eva Salomon. 2004. *Guidelines on the use of urine and faeces in crop production*. EcoSanRes Programme.

Kabata-Pendias, Alina. 2000. *Trace elements in soils and plants*. CRC press.

Kalkan, Ekrem. 2006. « Utilization of red mud as a stabilization material for the preparation of clay liners ». *Engineering geology* 87 (3-4): 220-29.

Kang, Dongjuan, Xiaolin Yu, Shengrui Tong, Maofa Ge, Junchao Zuo, Changyan Cao, et Weiguo Song. 2013. « Performance and mechanism of Mg/Fe layered double hydroxides for fluoride and arsenate removal from aqueous solution ». *Chemical Engineering Journal* 228: 731-40.

Kang, Min A., et Seunggu Kang. 2013. « Effect of activated carbon on bloating properties of artificial lightweight aggregates containing coal reject ash and bottom ash ». *Journal of the Korean Crystal Growth and Crystal Technology* 23 (4): 201-6.

Karaca, S, A Gurses, M Ejder, et M Acikyildiz. 2006. « Adsorptive Removal of Phosphate from Aqueous Solutions Using Raw and Calcinated Dolomite ». *Journal of Hazardous Materials* 128 (2-3): 273-79. https://doi.org/10.1016/j.jhazmat.2005.08.003.

Karaca, Semra, A. Gürses, M. Ejder, et M. Açıkyıldız. 2004. « Kinetic modeling of liquid-phase adsorption of phosphate on dolomite ». *Journal of Colloid and Interface Science* 277 (2): 257-63.

Karapinar, Nuray, Erhard Hoffmann, et Hermann H Hahn. 2004. « Magnetite Seeded Precipitation of Phosphate ». *Water Research* 38 (13): 3059-66. https://doi.org/10.1016/j.watres.2004.04.042.

Karouite, Azddine. 2003. « Utilisation des cendres volantes pour la prévention des désordres dus à l'alcali-réaction ». *Ecole HASSANIA des Travaux publics*.

Kaz'mina, O. V., V. I. Vereshchagin, A. N. Abiyaka, et Yu V. Popletneva. 2009. « Viscosity evaluation for glass and glass crystal compositions in their foaming temperature range ». *Glass and Ceramics* 66 (7): 236-39.

Kaz'mina, O., V. Vereshchagin, B. Semukhin, et A. Abiyaka. 2009. « Low-temperature synthesis of granular glass from mixes based on silica-alumina-containing components for obtaining foam materials. » *Glass & Ceramics* 66.

Khitous, Mohamed, Zineb Salem, et Djamila Halliche. 2016. « Effect of interlayer anions on chromium removal using Mg–Al layered double hydroxides: kinetic, equilibrium and thermodynamic studies ». *Chinese Journal of Chemical Engineering* 24 (4): 433-45.

Kim, Eung-Ho, Dong-Woo Lee, Hwan-Kook Hwang, et Soobin Yim. 2006. « Recovery of Phosphates from Wastewater Using Converter Slag: Kinetics Analysis of a Completely Mixed Phosphorus Crystallization Process ». *Chemosphere* 63 (2): 192-201. https://doi.org/10.1016/j.chemosphere.2005.08.029.

Kim, Kangduk. 2014. « The fabrication of artificial fine aggregates using stone sludge and spent bleaching clay ». *Journal of the Korean Ceramic Society* 51 (5): 492-97.

Knight, J., C. Cheeseman, et R. Rogers. 1999. « Microbial influenced degradation of solidified wastes ». In *Stab & Env: stabilisation des déchets et environnement. Congrès*.

Koilraj, P., et S. Kannan. 2013. « Aqueous fluoride removal using ZnCr layered double hydroxides and their polymeric composites: Batch and column studies ». *Chemical Engineering Journal* 234: 406-15.

Koilraj, Paulmanickam, et Keiko Sasaki. 2016. « Fe3O4/MgAl-NO3 layered double hydroxide as a magnetically separable sorbent for the remediation of aqueous phosphate ». *Journal of environmental chemical engineering* 4 (1): 984-91.

Komnitsas, Kostas, Dimitra Zaharaki, et Georgios Bartzas. 2013. « Effect of sulphate and nitrate anions on heavy metal immobilisation in ferronickel slag geopolymers ». *Applied clay science* 73: 103-9.

Korkusuz, E. Asuman, Meryem Beklioğlu, et Göksel N. Demirer. 2005. « Comparison of the Treatment Performances of Blast Furnace Slag-Based and Gravel-Based Vertical Flow Wetlands Operated Identically for Domestic Wastewater Treatment in Turkey ». *Ecological Engineering* 24 (3): 185-98. https://doi.org/10.1016/j.ecoleng.2004.10.002.

Koshikawa, Masaya, et Akira Isogai. 2004. « Analyses of incinerated ash of paper sludge: comparison with incinerated ash of municipal solid waste ». *Journal of material cycles and waste management* 6 (1): 64-72.

Kostura, Bruno, Hana Kulveitová, et Juraj Leško. 2005. « Blast Furnace Slags as Sorbents of Phosphate from Water Solutions ». *Water Research* 39 (9): 1795-1802. https://doi.org/10.1016/j.watres.2005.03.010.

Kumarathasan, Premkumari, Gregory J. McCarthy, David J. Hassett, et Debra F. Pflughoeft-Hassett. 1989. « Oxyanion substituted ettringites: synthesis and characterization; and their potential role in immobilization of As, B, Cr, Se and V ». *MRS Online Proceedings Library (OPL)* 178.

Kumpiene, Jurate. 2010. « Trace element immobilization in soil using amendments ». *Trace elements in soils*, 353-79.

Kumpiene, Jurate, Anders Lagerkvist, et Christian Maurice. 2008. « Stabilization of As, Cr, Cu, Pb and Zn in soil using amendments–a review ». *Waste management* 28 (1): 215-25.

Lapa, N., R. Barbosa, M. H. Lopes, B. Mendes, P. Abelha, IJSO Gulyurtlu, et J. Santos Oliveira. 2007a. « Chemical and ecotoxicological characterization of ashes obtained from sewage sludge combustion in a fluidised-bed reactor ». *Journal of hazardous materials* 147 (1-2): 175-83.

———. 2007b. « Chemical and ecotoxicological characterization of ashes obtained from sewage sludge combustion in a fluidised-bed reactor ». *Journal of hazardous materials* 147 (1-2): 175-83.

Laporte-Saumure, Mathieu. 2010. « Caractérisation de sites de tir à l'arme légère militaires canadiens, enlèvement des métaux et suivi hydrogéologique des contaminants. » PhD Thesis, Université du Québec, Institut national de la recherche scientifique.

Léauté, Frédérique. 2008. « Biogéochimie des contaminants organiques HAP, PCB et pesticides organochlorés dans les sédiments de l'étang de Thau ». PhD Thesis, Université Pierre et Marie Curie-Paris VI.

Lee, Ki Gang. 2014. « Bloating mechanism for coal ash with iron oxide ». *Journal of the Korean Crystal Growth and Crystal Technology* 24 (2): 77-83.

Legendre, André. 2021. « Chapitre 8. Les gaz à effet de serre, le cycle du carbone et Gaïa ». In *L'homme est-il responsable du réchauffement climatique?*, 175-210. EDP Sciences.

Lenoble, Véronique. 2003. « Elimination de l'Arsenic pour la production d'eau potable: oxydation chimique et adsorption sur des substrats solides innovants ». PhD Thesis, Université de Limoges.

Li, Xiaomin, Marta Fernández Bertos, Colin D. Hills, Paula J. Carey, et Stef Simon. 2007. « Accelerated carbonation of municipal solid waste incineration fly ashes ». *Waste management* 27 (9): 1200-1206.

Li, Yanlin, Jun Wang, Zhanshuang Li, Qi Liu, Jingyuan Liu, Lianhe Liu, Xiaofei Zhang, et Jing Yu. 2013. « Ultrasound assisted synthesis of Ca–Al hydrotalcite for U (VI) and Cr (VI) adsorption ». *Chemical engineering journal* 218: 295-302.

Liao, Yi-Chong, Chi-Yen Huang, et Yen-Ming Chen. 2013. « Lightweight aggregates from water reservoir sediment with added sodium hydroxide ». *Construction and Building Materials* 46: 79-85.

LIEU, AU. s. d. « Guide concernant l'application propre à un lieu des Recommandations pour la qualité des eaux au Canada: procédures d'établissement d'objectifs numériques de qualité de l'eau Table des matières ».

Lin, Kae-Long. 2006. « Mineralogy andMicrostructures of Sintered Sewage Sludge Ash as Lightweight Aggregates ». *Journal of Industrial and Engineering Chemistry* 12 (3): 425-29.

Lin, Zhixun. 1996. « Secondary mineral phases of metallic lead in soils of shooting ranges from Örebro County, Sweden ». *Environmental Geology* 27 (4): 370-75.

Lindsay, Matthew BJ, David W. Blowes, Carol J. Ptacek, et Peter D. Condon. 2011. « Transport and attenuation of metal (loid) s in mine tailings amended with organic carbon: Column experiments ». *Journal of contaminant hydrology* 125 (1-4): 26-38.

Lions, Julie. 2004. « Etude hydrogéochimique de la mobilité de polluants inorganiques dans des sédiments de curage mis en dépôt: expérimentations, étude in situ et modélisations ». PhD Thesis.

Lotov, V. A. 2012. « Making foam glass based on natural and technogenic aluminosilicates ». *Glass and ceramics* 68 (9): 302-5.

Loutou, M., M. Hajjaji, M. Mansori, C. Favotto, et R. Hakkou. 2013. « Phosphate sludge: thermal transformation and use as lightweight aggregate material ». *Journal of environmental management* 130: 354-60.

Lu, Chungsying. 1996. « A model of leaching behaviour from MSW incinerator residue landfills ». *Waste management & research* 14 (1): 51-70.

Lu, Yi, Bin Jiang, Liang Fang, Faling Ling, Jiemei Gao, Fang Wu, et Xihua Zhang. 2016. « High performance NiFe layered double hydroxide for methyl orange dye and Cr (VI) adsorption ». *Chemosphere* 152: 415-22.

Luna, Y., X. Querol, D. Antenucci, El-Aid Jdid, C. Fernández, et J. Vale. 2007. « Immobilization of a metallurgical waste using fly ash-based geopolymers ». *World of Coal Ash (WOCA); May*, 7-10.

Ma, Y., J. Hu, et G. Ye. 2013. « The pore structure and permeability of alkali activated fly ash ». *Fuel* 104: 771-80.

Mahjoubi, Fatima Zahra, Abderrahim Khalidi, Mohamed Abdennouri, et Noureddine Barka. 2017. « Zn–Al layered double hydroxides intercalated with carbonate, nitrate, chloride and sulphate ions: Synthesis, characterisation and dye removal properties ». *Journal of Taibah University for Science* 11 (1): 90-100. https://doi.org/10.1016/j.jtusci.2015.10.007.

Malek, Thomas R., Jonathan D. Ashwell, Ronald N. Germain, Ethan M. Shevach, et Jim Miller. 1986. « The murine interleukin-2 receptor: biochemical structure and regulation of expression ». *Immunological reviews* 92 (1): 81-102.

Manceau, Alain, Matthew A. Marcus, et Nobumichi Tamura. 2002. « Quantitative speciation of heavy metals in soils and sediments by synchrotron X-ray techniques ». *Reviews in mineralogy and geochemistry* 49 (1): 341-428.

Mandal, Sandip, Swagatika Tripathy, Tapswani Padhi, Manoj Kumar Sahu, et Raj Kishore Patel. 2013. « Removal efficiency of fluoride by novel Mg-Cr-Cl layered double hydroxide by batch process from water ». *Journal of Environmental Sciences* 25 (5): 993-1000.

Mankelow, J. M., M. A. Sen, D. E. Highley, S. F. Hobbs, et C. E. Edwards. 2007. *Collation of the results of the 2005 Aggregate Minerals Survey for England and Wales*. Communities and Local Government Publications.

Manninen, Sanni, et Niina Tanskanen. 1993. « Transfer of lead from shotgun pellets to humus and three plant species in a Finnish shooting range ». *Archives of Environmental Contamination and Toxicology* 24 (3): 410-14.

Marois, A., A. Gagnon, S. Thiboutot, G. Ampleman, et M. Bouchard. 2004. « Caractérisation des sols de surface et de la biomasse dans les secteurs d'entraînement, Base des Forces Canadiennes, Valcartier ». *Rapport technique DRDC Valcartier TR* 206: 171.

Matusik, Jakub, et Karolina Rybka. 2019. « Removal of Chromates and Sulphates by Mg/Fe LDH and Heterostructured LDH/Halloysite Materials: Efficiency, Selectivity, and Stability of Adsorbents in Single- and Multi-Element Systems ». *Materials* 12 (9): 1373. https://doi.org/10.3390/ma12091373.

Mazeas, Olivier. 2004. « Evaluation de l'exposition des organismes aux hydrocarbures aromatiques polycycliques (HAP) dans le milieu marin par le dosage des métabolites de HAP ». PhD Thesis.

McCarthy, Gregory J., David J. Hassett, et Jason A. Bender. 1991. « Synthesis, crystal chemistry and stability of ettringite, a material with potential applications in hazardous waste immobilization ». *MRS Online Proceedings Library (OPL)* 245.

McCormick, A. v, et A. T. Bell. 1989. « The solution chemistry of zeolite precursors ». *Catalysis Reviews—Science and Engineering* 31 (1-2): 97-127.

McKay, H., J. B. Hudson, et R. J. Hudson. 2003. « Woodfuel resource in Britain ». *Forestry Commission Report*.

Mehta, P. K., et D. Pirtz. 1978. « Use of rice hull ash to reduce temperature in high-strength mass concrete ». In *Journal Proceedings*, 75:60-63.

Mehta, Povindar K. 1977. « Properties of blended cements made from rice husk ash ». In *Journal Proceedings*, 74:440-42.

Mellor, Antony, et C. McCartney. 1994. « The effects of lead shot deposition on soils and crops at a clay pigeon shooting site in northern England ». *Soil Use and Management* 10 (3): 124-29.

Mench, Michel, Jaco Vangronsveld, Caroline Beckx, et Ann Ruttens. 2006. « Progress in assisted natural remediation of an arsenic contaminated agricultural soil ». *Environmental Pollution* 144 (1): 51-61.

Meng, Zilin, Fengzhu Lv, Xiaowei Li, Qian Zhang, Paul K. Chu, Sridhar Komarneni, et Yihe Zhang. 2016. « Simultaneous arsenate and alkali removal from alkaline wastewater by in-situ formation of Zn–Al layered double hydroxide ». *Microporous and Mesoporous Materials* 227: 137-43.

Miller, F. M. 1976. « Minor elements in cement clinker ». In *Paper No. 16, PCA Cement Chemist's Seminar*.

MINAØÍKOVÁ, MARTINA, et FRANTIŠEK ŠKVÁRA. 2006. « Fixation of heavy metals in geopolymeric materials based on brown coal fly ash ». *Ceramics- Silikáty* 50 (4): 200-207.

Miraoui, Mohamed. 2010. « Prétraitement et traitement des sédiments de dragage en vue d'une valorisation dans le génie civil ». PhD Thesis, Lille 1.

Mkahal, Zeinab, Yannick Mamindy-Pajany, Walid Maherzii, et Nor-Edine Abriak. 2022. « Recycling of Mineral Solid Wastes in Backfill Road Materials: Technical and Environmental Investigations ». *Waste and Biomass Valorization* 13 (1): 667-87.

Mo, Bing-hui, He Zhu, Xue-min Cui, Yan He, et Si-yu Gong. 2014. « Effect of curing temperature on geopolymerization of metakaolin-based geopolymers ». *Applied clay science* 99: 144-48.

Mohan, Rama, Jackie Spiby, G. S. Leonardi, Alan Robins, et Stephan Jefferis. 2006. « Sustainable waste management in the UK: the public health role ». *Public Health* 120 (10): 908-14.

Molle, Pascal. 2003. « Filtres plantés de roseaux: limites hydrauliques et rétention du phosphore ». PhD Thesis, Doctorat discipline Energétique génie des procédés, Université Montpellier II.

Molle, Pascal, A. Lienard, A. Grasmick, A. Iwema, et A. Kabbabi. 2005. « Apatite as an interesting seed to remove phosphorus from wastewater in constructed wetlands ». *Water Science and Technology* 51 (9): 193-203.

Montinaro, Selena, Alessandro Concas, Massimo Pisu, et Giacomo Cao. 2008. « Immobilization of heavy metals in contaminated soils through ball milling with and without additives ». *Chemical Engineering Journal* 142 (3): 271-84.

Monzó, J., J. Paya, M. V. Borrachero, et A. Córcoles. 1996. « Use of sewage sludge ash (SSA)-cement admixtures in mortars ». *Cement and Concrete Research* 26 (9): 1389-98.

Monzó, J., J. Payá, M. V. Borrachero, et I. Girbés. 2003. « Reuse of sewage sludge ashes (SSA) in cement mixtures: the effect of SSA on the workability of cement mortars ». *Waste Management* 23 (4): 373-81.

Mostarih, Rachid. 2006. « Elaboration de phases hydroxydes doubles lamellaires intercalant des anions sulfates: étude de leur évolution structurale, thermique et hygrométrique ». PhD Thesis, Université Blaise Pascal-Clermont-Ferrand II.

Moufti, Ahmed, et Mohammed Mountadar. 2004. « Lessivage des fluorures et des métaux à partir d'une cendre à charbon ». *Water Quality Research Journal* 39 (2): 113-18.

Mozaffari, E., J. M. Kinuthia, J. Bai, et Stan Wild. 2009. « An investigation into the strength development of wastepaper sludge ash blended with ground granulated blastfurnace slag ». *Cement and Concrete Research* 39 (10): 942-49.

Mozaffari, E., M. O'Farrell, J. M. Kinuthia, et S. Wild. 2006. « Improving strength development of wastepaper sludge ash by wet-milling ». *Cement and Concrete Composites* 28 (2): 144-52.

Mueller, A., S. N. Sokolova, et V. I. Vereshagin. 2008. « Characteristics of lightweight aggregates from primary and recycled raw materials ». *Construction and Building Materials* 22 (4): 703-12.

Murray, Kent, Ali Bazzi, Crystal Carter, Andrew Ehlert, Mike Kopec, Joanne Richardson, et Helene Sokol. 1997. « Distribution and mobility of lead in soils at an outdoor shooting range ». *Soil and Sediment Contamination* 6 (1): 79-93.

Nations Unis. 1999. « Rapport sur du groupe d'experts sur le problème des munitions et explosifs », 1999.

Němeček, Jiří. 2009. « Creep effects in nanoindentation of hydrated phases of cement pastes ». *Materials Characterization* 60 (9): 1028-34.

Neville, Adam. 2003. « Can we determine the age of cracks by measuring carbonation? Part 1 ». *Concrete international* 25 (12): 76-79.

Neville, Adam M. 2004. « Can we determine the age of cracks by measuring carbonation? Part 2 ». *Concrete international* 26 (1): 88-91.

Nikolić, Violeta, Miroslav Komljenović, Nataša Marjanović, Zvezdana Baščarević, et Rada Petrović. 2014. « Lead immobilization by geopolymers based on mechanically activated fly ash ». *Ceramics international* 40 (6): 8479-88.

Nishida, Katsunori, Yoshikazu Nagayoshi, Hitoshi Ota, et Hidekazu Nagasawa. 2001. « Melting and stone production using MSW incinerated ash ». *Waste management* 21 (5): 443-49.

Nocuń-Wczelik, Wies\lawa, et Jan Ma\lolepszy. 1995. « Application of calorimetry in studies of the immobilization of heavy metals in cementitious materials ». *Thermochimica acta* 269: 613-19.

Noppe, Karine. 1996. « Contamination métallique des sédiments des cours d'eau du bassin Artois-Picardie et son impact sur la contamination des chairs et des foies de poissons ». *Mémoire de DEA, Université Pierre et Marie Curie-Paris VI, 42p+ annexe*.

Novillo, Corina, D. Guaya, A. Allen-Perkins Avendaño, Chabaco Armijos, J. L. Cortina, et Iuliana Cota. 2014. « Evaluation of phosphate removal capacity of Mg/Al layered double hydroxides from aqueous solutions ». *Fuel* 138: 72-79.

Oggioni, G., R. Riccardi, et R. Toninelli. 2011. « The cement industry: Eco-eciency country comparison using data envelopment analysis ». *Journal of Statistics and Management Systems* 14 (6): 1067-1102.

Ogundiran, M. B., H. W. Nugteren, et G. J. Witkamp. 2013. « Immobilisation of lead smelting slag within spent aluminate—fly ash based geopolymers ». *Journal of Hazardous Materials* 248: 29-36.

Olfs, H.-W., L. O. Torres-Dorante, R. Eckelt, et H. Kosslick. 2009. « Comparison of different synthesis routes for Mg–Al layered double hydroxides (LDH): Characterization of the structural phases and anion exchange properties ». *Applied clay science* 43 (3-4): 459-64.

Oliva, J., Jordi Cama, J. L. Cortina, C. Ayora, et J. De Pablo. 2012. « Biogenic hydroxyapatite (Apatite II™) dissolution kinetics and metal removal from acid mine drainage ». *Journal of hazardous materials* 213: 7-18.

Olmo, I. Fernández, E. Chacon, et A. Irabien. 2001. « Influence of lead, zinc, iron (III) and chromium (III) oxides on the setting time and strength development of Portland cement ». *Cement and Concrete Research* 31 (8): 1213-19.

Oste, Leonard A., Jan Dolfing, Wei-chun Ma, et Theo M. Lexmond. 2001. « Effect of beringite on cadmium and zinc uptake by plants and earthworms: more than a liming effect? » *Environmental Toxicology and Chemistry: An International Journal* 20 (6): 1339-45.

Owens, P. L., et J. B. Newman. 1999. « Increasing the environmental acceptability of new EfW plants by integration with concrete aggregate manufacture ». *IWM SCIENTIFIC AND TECHNICAL REVIEW*, 21-26.

P. Molle, A. Liénard, A. Grasmick, A. Iwema. 2003. « Phosphorus retention in subsurface constructed wetlands: investigations focused on calcareous materials and their chemical reactions ». *Water Sci Technol 1 September 2003; 48 (5): 75–83. doi: https://doi.org/10.2166/wst.2003.0285*, 2003.

Palomo, A., et M. Palacios. 2003. « Alkali-activated cementitious materials: Alternative matrices for the immobilisation of hazardous wastes: Part II. Stabilisation of chromium and lead ». *Cement and concrete research* 33 (2): 289-95.

Palomo, Angel, M. W. Grutzeck, et M. T. Blanco. 1999. « Alkali-activated fly ashes: A cement for the future ». *Cement and concrete research* 29 (8): 1323-29.

Palomo, Ángel, E. Kavalerova, Ana Fernández-Jiménez, P. Krivenko, Inés García-Lodeiro, et O. Maltseva. 2015. « A review on alkaline activation: new analytical perspectives ».

Pan, Shih-Cheng, Dyi-Hwa Tseng, Chih-Chiang Lee, et Chau Lee. 2003. « Influence of the fineness of sewage sludge ash on the mortar properties ». *Cement and Concrete Research* 33 (11): 1749-54.

Pandey, Vimal Chandra, et Nandita Singh. 2010. « Impact of fly ash incorporation in soil systems ». *Agriculture, ecosystems & environment* 136 (1-2): 16-27.

Panfili, Frédéric. 2004. « Etude de l'évolution de la spéciation du zinc dans la phase solide d'un sédiment de curage contaminé, induit par phytostabilisation ». PhD Thesis, Université de Provence-Aix-Marseille I.

Pant, H. K., K. R. Reddy, et E. Lemon. 2001. « Phosphorus retention capacity of root bed media of sub-surface flow constructed wetlands ». *Ecological engineering* 17 (4): 345-55.

Pascual, C., B. Boos, O. Troesch, R. Beaurez, et M. Hermann. 1994. « Etude de l'évolution des propriétés physico-chimiques et mécaniques d'un stock de mâchefer ». *Environnement & technique*, n° 140: 86-92.

Péna, G., et B. Picot. 1991. « Métaux traces dans les sédiments d'une lagune méditerranéenne: l'étang de Thau ». *Oceanologica acta* 14 (5): 459-72.

Pera, Jean, et Achene Amrouz. 1998. « Development of highly reactive metakaolin from paper sludge ». *Advanced Cement Based Materials* 7 (2): 49-56.

Pereira, Vanessa J., Karl G. Linden, et Howard S. Weinberg. 2007. « Evaluation of UV irradiation for photolytic and oxidative degradation of pharmaceutical compounds in water ». *Water Research* 41 (19): 4413-23.

Perera, D. S., O. Uchida, E. R. Vance, et K. S. Finnie. 2007. « Influence of curing schedule on the integrity of geopolymers ». *Journal of materials science* 42 (9): 3099-3106.

Perez, Eduardo, Lijalem Ayele, Girum Getachew, Geolar Fetter, Pedro Bosch, Alvaro Mayoral, et Isabel Díaz. 2015. « Removal of chromium (VI) using nano-hydrotalcite/SiO2 composite ». *Journal of environmental chemical engineering* 3 (3): 1555-61.

Phair, J. W., et J. S. J. Van Deventer. 2002. « Effect of the silicate activator pH on the microstructural characteristics of waste-based geopolymers ». *International Journal of Mineral Processing* 66 (1-4): 121-43.

Phair, J. W., J. S. J. Van Deventer, et J. D. Smith. 2004. « Effect of Al source and alkali activation on Pb and Cu immobilisation in fly-ash based "geopolymers" ». *Applied geochemistry* 19 (3): 423-34.

Pitman, Rona M. 2006. « Wood ash use in forestry–a review of the environmental impacts ». *Forestry: An International Journal of Forest Research* 79 (5): 563-88.

Plowman, C., et G. J. Cabrera. 1981. « The influence of pulverised fuel ash on the hydration reactions of calcium aluminates ». In *Boston: Material research society–Effects on fly ash incorporation in cement and concrete: proceedings symposium and annual meeting (Diamonds, S.(éd)). Boston*, 71-81.

Pollmann, H. 1989. « Compounds with ettringite structure ». *Neues Jahrb. Mineral Abh.* 160: 133-58.

Poon, Chi Sun, A. I. Clark, R. Perry, A. P. Barker, et P. Barnes. 1986. « Permeability study on the cement based solidification process for the disposal of hazardous wastes ». *Cement and Concrete Research* 16 (2): 161-72.

Prasad, KVSK, P. Paradha Saradhi, et P. Sharmila. 1999. « Concerted action of antioxidant enzymes and curtailed growth under zinc toxicity in Brassica juncea ». *Environmental and experimental Botany* 42 (1): 1-10.

Prigent, Stephane. 2013. « Optimisation du traitement de l'azote et du phosphore des eaux usées domestiques adapté aux filtres plantés de roseaux », 230.

Prochaska, C.A., et A.I. Zouboulis. 2006. « Removal of Phosphates by Pilot Vertical-Flow Constructed Wetlands Using a Mixture of Sand and Dolomite as Substrate ». *Ecological Engineering* 26 (3): 293-303. https://doi.org/10.1016/j.ecoleng.2005.10.009.

Provis, John L., Grant C. Lukey, et Jannie SJ van Deventer. 2005. « Do geopolymers actually contain nanocrystalline zeolites? A reexamination of existing results ». *Chemistry of materials* 17 (12): 3075-85.

Prud'Homme, Elodie, Alexandre Autef, Najet Essaidi, Philippe Michaud, Basma Samet, Emmanuel Joussein, et Sylvie Rossignol. 2013. « Defining existence domains in geopolymers through their physicochemical properties ». *Applied Clay Science* 73: 26-34.

Quina, Margarida J., Marisa A. Almeida, Regina Santos, João M. Bordado, et Rosa M. Quinta-Ferreira. 2014. « Compatibility analysis of municipal solid waste incineration residues and clay for producing lightweight aggregates ». *Applied Clay Science* 102: 71-80.

Quina, Margarida J., João M. Bordado, et Rosa M. Quinta-Ferreira. 2014. « Recycling of air pollution control residues from municipal solid waste incineration into lightweight aggregates ». *Waste management* 34 (2): 430-38.

Rajamma, Rejini, Richard J. Ball, Luís AC Tarelho, Geoff C. Allen, João A. Labrincha, et Victor M. Ferreira. 2009. « Characterisation and use of biomass fly ash in cement-based materials ». *Journal of hazardous materials* 172 (2-3): 1049-60.

Rajamma, Rejini, Luciano Senff, M. J. Ribeiro, João A. Labrincha, R. J. Ball, Geoffry C. Allen, et V. M. Ferreira. 2015. « Biomass fly ash effect on fresh and hardened state properties of cement based materials ». *Composites Part B: Engineering* 77: 1-9.

Ramezanianpour, Ali A., E. Ghiasvand, I. Nickseresht, M. Mahdikhani, et F. Moodi. 2009. « Influence of various amounts of limestone powder on performance of Portland limestone cement concretes ». *Cement and Concrete Composites* 31 (10): 715-20.

Raujouan, P., et C. Le Guyader. 2010. « Enquête Dragage 2008-Analyse des données ». *Rapport CETMEF 34p*.

Reijnders, L. 2005. « Disposal, uses and treatments of combustion ashes: a review ». *Resources, Conservation and Recycling* 43 (3): 313-36.

Rives, Vicente, Margarita del Arco, et Cristina Martín. 2014. « Intercalation of drugs in layered double hydroxides and their controlled release: A review ». *Applied clay science* 88: 239-69.

Romero, S. 1999. « La gestion des sédiments de dragage des cours d'eau: Etat des lieux et recherche de nouvelles filières ». *Environnement & technique*, n° 188: 31-35.

Rooney, C. P., R. G. McLaren, et R. J. Cresswell. 1999. « Distribution and phytoavailability of lead in a soil contaminated with lead shot ». *Water, Air, and Soil Pollution* 116 (3): 535-48.

Rooney, Corinne P., Ronald G. McLaren, et Leo M. Condron. 2007. « Control of lead solubility in soil contaminated with lead shot: effect of soil pH ». *Environmental Pollution* 149 (2): 149-57.

Roseth, Roger. 2000. « Shell sand: A new filter medium for constructed wetlands and wastewater treatment ». *Journal of Environmental Science & Health Part A* 35 (8): 1335-55.

Rossetti, V. Alunno, et F. Medici. 1995. « Inertization of toxic metals in cement matrices: effects on hydration, setting and hardening ». *Cement and Concrete Research* 25 (6): 1147-52.

Rovnaník, Pavel. 2010. « Effect of curing temperature on the development of hard structure of metakaolin-based geopolymer ». *Construction and building materials* 24 (7): 1176-83.

Rowles, M. R., John V. Hanna, K. J. Pike, Mark E. Smith, et B. H. O'connor. 2007. « 29Si, 27Al, 1H and 23Na MAS NMR study of the bonding character in aluminosilicate inorganic polymers ». *Applied Magnetic Resonance* 32 (4): 663-89.

Rubin, G. James, Chris R. Brewin, Neil Greenberg, Jamie Hacker Hughes, John Simpson, et Simon Wessely. 2007. « Enduring consequences of terrorism: 7-month follow-up survey of reactions to the bombings in London on 7 July 2005 ». *The British Journal of Psychiatry* 190 (4): 350-56.

Ruttens, Ann, J. V. Colpaert, Michel Mench, J. Boisson, R. Carleer, et Jaco Vangronsveld. 2006. « Phytostabilization of a metal contaminated sandy soil. II: Influence of compost and/or inorganic metal immobilizing soil amendments on metal leaching ». *Environmental Pollution* 144 (2): 533-39.

Ryou, Jaesuk. 2004. « Examination of grinding techniques for the reuse of by-products of cement production ». *Materials Letters* 58 (3-4): 425-27.

Sá, Fernando Pereira de, Beatriz Nogueira Cunha, et Liliane Magalhães Nunes. 2013. « Effect of pH on the adsorption of Sunset Yellow FCF food dye into a layered double hydroxide (CaAl-LDH-NO3) ». *Chemical Engineering Journal* 215: 122-27.

Sakadevan, K., et H. J. Bavor. 1998. « Phosphate adsorption characteristics of soils, slags and zeolite to be used as substrates in constructed wetland systems ». *Water Research* 32 (2): 393-99.

« Samen werken we koolstofneutrale oplossingen uit ». s. d. ENGIE. Consulté le 8 mars 2022. https://corporate.engie.be/nl/home.

Sappin-Didier, Valérie. 1995. « Utilisation de composés inorganiques pour diminuer les flux de métaux dans deux agrosystèmes pollués: etude des mécanismes impliqués par l'emploi d'un composé de fer ». PhD Thesis, Bordeaux 1.

Scheetz, Barry E., et Russell Earle. 1998. « Utilization of fly ash ». *Current Opinion in Solid State and Materials Science* 3 (5): 510-20.

SCHNEIDER, Gregoire. 2001. « Le curage des sédiments des cours d'eau ». *Courrier de l'environnement de l'INRA*, n° 43: 146-47.

Schwartz, Joel, Philip J. Landrigan, Robert G. Feldman, Ellen K. Silbergeld, Edward L. Baker Jr, et Ian H. von Lindern. 1988. « Threshold effect in lead-induced peripheral neuropathy ». *The Journal of pediatrics* 112 (1): 12-17.

Scordia, Pierre-Yves. 2008. « Caractérisation et valorisation de sédiments fluviaux pollués et traités dans les matériaux routiers ». PhD Thesis, Ecole Centrale de Lille.

Segui, Pauline. 2011. « Elaboration de liants hydrauliques routiers à base de pouzzolane naturelle ou de cendre volante de papeterie ». PhD Thesis, Université de Toulouse, Université Toulouse III-Paul Sabatier.

Seo, Dong Cheol, Ju Sik Cho, Hong Jae Lee, et Jong Soo Heo. 2005. « Phosphorus retention capacity of filter media for estimating the longevity of constructed wetland ». *Water research* 39 (11): 2445-57.

Serpaud, B., R. Al-Shukry, M. Casteignau, et G. Matejka. 1994. « Adsorption des métaux lourds (Cu, Zn, Cd et Pb) par les sédiments superficiels d'un cours d'eau: rôle du pH, de la température et de la composition du sédiment ». *Revue des sciences de l'eau/Journal of Water Science* 7 (4): 343-65.

Shi, Wei-yu, Hong-bo Shao, Hua Li, Ming-an Shao, et Sheng Du. 2009. « Progress in the remediation of hazardous heavy metal-polluted soils by natural zeolite ». *Journal of Hazardous Materials* 170 (1): 1-6.

Shin, Hang-Sik, Jong-Oh Kim, Ja-Kong Koo, et Eung-Bai Shin. 1992. « Mixture Design Optimization Considering Three Disposal Options for Solidified Heavy Metal Sludges ». In *Stabilization and Solidification of Hazardous, Radioactive, and Mixed Wastes: 2nd Volume*. ASTM International.

Sigg, Laura, Philippe Behra, et Werner Stumm. 2001. *Chimie des milieux aquatiques*. Dunod.

Sim, Soo-Man, et Ki-Soo Kim. 2010. « Fabrication of lightweight aggregates from FRP Waste ». *Advanced Composite Materials* 19 (3): 289-97.

Sims, Ralph EH, Hans-Holger Rogner, et Ken Gregory. 2003. « Carbon emission and mitigation cost comparisons between fossil fuel, nuclear and renewable energy resources for electricity generation ». *Energy policy* 31 (13): 1315-26.

Singh, N. B., K. N. Bhattacharjee, et A. K. Shukla. 1995. « Effect of alkali bypass dust on the hydration of granulated blast furnace slag blended cement ». *Cement and concrete research* 25 (4): 883-92.

Sneddon, I. R., M. Orueetxebarria, M. E. Hodson, P. F. Schofield, et E. Valsami-Jones. 2006. « Use of bone meal amendments to immobilise Pb, Zn and Cd in soil: a leaching column study ». *Environmental pollution* 144 (3): 816-25.

Sokolova, S. N., et V. I. Vereshagin. 2010. « Lightweight granular material from zeolite rocks with different additives ». *Construction and Building Materials* 24 (4): 625-29.

Song, X. J., Marton Marosszeky, Michael Brungs, et Zhen-Tian Chang. 2005. « Response of geopolymer concrete to sulphuric acid attack ». In *Proceedings of World Congress Geopolymer*, 157-60.

Song, Yonghui, Peter G. Weidler, Ute Berg, Rolf Nüesch, et Dietfried Donnert. 2006. « Calcite-Seeded Crystallization of Calcium Phosphate for Phosphorus Recovery ». *Chemosphere* 63 (2): 236-43. https://doi.org/10.1016/j.chemosphere.2005.08.021.

Søvik, A.K., et B. Kløve. 2005. « Phosphorus Retention Processes in Shell Sand Filter Systems Treating Municipal Wastewater ». *Ecological Engineering* 25 (2): 168-82. https://doi.org/10.1016/j.ecoleng.2005.04.007.

Spuller, Cornelia, Harald Weigand, et Clemens Marb. 2007. « Trace metal stabilisation in a shooting range soil: Mobility and phytotoxicity ». *Journal of Hazardous Materials* 141 (2): 378-87.

Sreekrishnavilasam, Asha, Stephanie King, et Marika Santagata. 2006. « Characterization of fresh and landfilled cement kiln dust for reuse in construction applications ». *Engineering Geology* 85 (1-2): 165-73.

Srivastava, Shefali, Rubina Chaudhary, et Divya Khale. 2008. « Influence of pH, curing time and environmental stress on the immobilization of hazardous waste using activated fly ash ». *Journal of hazardous materials* 153 (3): 1103-9.

Stansley, W., et D. E. Roscoe. 1996. « The uptake and effects of lead in small mammals and frogs at a trap and skeet range ». *Archives of Environmental Contamination and Toxicology* 30 (2): 220-26.

Steins, Prune. 2014. « Influence des paramètres de formulation sur la texturation et la structuration des géopolymères ». PhD Thesis, Limoges.

Steins, Prune, Arnaud Poulesquen, Olivier Diat, et Fabien Frizon. 2012. « Structural evolution during geopolymerization from an early age to consolidated material ». *Langmuir* 28 (22): 8502-10.

Steins, Prune, Arnaud Poulesquen, Fabien Frizon, Olivier Diat, Jacques Jestin, Jérémy Causse, David Lambertin, et Sylvie Rossignol. 2014. « Effect of aging and alkali activator on the porous structure of a geopolymer ». *Journal of Applied Crystallography* 47 (1): 316-24.

Stene-Johansen, Kathrine, Tom Øystein Jonassen, et Kjell Skaug. 2005. « Characterization and genetic variability of Hepatitis A virus genotype IIIA ». *Journal of general virology* 86 (10): 2739-45.

Steveson, M., et K. Sagoe-Crentsil. 2005. « Relationships between composition, structure and strength of inorganic polymers ». *Journal of materials science* 40 (8): 2023-36.

Swanepoel, J. C., et C. A. Strydom. 2002. « Utilisation of fly ash in a geopolymeric material ». *Applied geochemistry* 17 (8): 1143-48.

Swenson, Edwin George, et Peter J. Sereda. 1968. « Mechanism of the carbonatation shrinkage of lime and hydrated cement ». *Journal of Applied Chemistry* 18 (4): 111-17.

Taha, Ramzi, Amer Al-Rawas, Ali Al-Harthy, et Ahmed Qatan. 2002. « Use of cement bypass dust as filler in asphalt concrete mixtures ». *Journal of materials in civil engineering* 14 (4): 338-43.

Takahashi, Hideo, Masato Shinkado, Hideshi Hirakida, et Shizushi Hasegawa. 1973. « 16. Fundamental Study on Solidification of Hazardous Industrial Wastes Containing Heavy Metals with Portland Cement ». In *The Cement Association of Japan. The 27th General Meeting, Technical Session*, 64-67.

Tan, W. F., L. A. Wang, C. Huang, et J. E. Green. 2013. « Municipal solid waste incineration fly ash sintered lightweight aggregates and kinetics model establishment ». *International Journal of Environmental Science and Technology* 10 (3): 465-72.

Tang, Chao-Wei. 2014. « Producing synthetic lightweight aggregates by treating waste TFT-LCD glass powder and reservoir sediments ». *Computers and Concrete* 13 (3): 325-42.

Tanner, M. Stuart. 1998. « Role of copper in Indian childhood cirrhosis ». *The American journal of clinical nutrition* 67 (5): 1074S-1081S.

Tao, Qi, Yuanming Zhang, Xiang Zhang, Peng Yuan, et Hongping He. 2006. « Synthesis and characterization of layered double hydroxides with a high aspect ratio ». *Journal of Solid State Chemistry* 179 (3): 708-15.

Tashiro, C., H. Takahashi, M. Kanaya, I. Hirakida, et R. Yoshida. 1977. « Hardening property of cement mortar adding heavy metal compound and solubility of heavy metal from hardened mortar ». *Cement and Concrete Research* 7 (3): 283-90.

Tay, Joo-Hwa, Sze-Yunn Hong, et Kuan-Yeow Show. 2000. « Reuse of industrial sludge as pelletized aggregate for concrete ». *Journal of Environmental Engineering* 126 (3): 279-87.

Tay, Joo-Hwa, Kuan-Yeow Show, et Sze-Yunn Hong. 2002. « Concrete aggregates made from sludge-marine clay mixes ». *Journal of materials in civil engineering* 14 (5): 392-98.

TCLP, EPA. 1992. « Toxicity Characteristic Leaching Procedure. Method 1311. Test Methods for Evaluating Solid Waste ». *US Environmental Protection Agency, Washington DC*.

Temuujin, J. V., Arie Van Riessen, et Ross Williams. 2009. « Influence of calcium compounds on the mechanical properties of fly ash geopolymer pastes ». *Journal of hazardous materials* 167 (1-3): 82-88.

TERRE, SOMMET PLANETE. 1992. « DÉCLARATION DE RIO SUR L'ENVIRONNEMENT ET LE DÉVELOPPEMENT PRINCIPES DE GESTION DES FORÊTS ». In *Conférence des Nations Unies sur l'environnement et le développement, Rio de Janeiro, Brésil*, 3-14.

Theiss, Frederick L., Sara J. Couperthwaite, Godwin A. Ayoko, et Ray L. Frost. 2014. « A review of the removal of anions and oxyanions of the halogen elements from aqueous solution by layered double hydroxides ». *Journal of colloid and interface science* 417: 356-68.

Thiery, Mickaël. 2006. « Modélisation de la carbonatation atmosphérique des matériaux cimentaires: prise en compte des effets cinétiques et des modifications microstructurales et hydriques ». *ETUDES ET RECHERCHES DES LABORATOIRES DES PONTS ET CHAUSSEES-SERIE OUVRAGES D'ART*, n° OA 52.

Thomas, M. D. A., et J. D. Matthews. 1991. *Durability studies of pfa concrete structures*. Building Research Establishment.

Thorbjornsen, Karen, et Jonathan Myers. 2007. « Identification of metals contamination in firing-range soil using geochemical correlation evaluation ». *Soil and Sediment Contamination: An International Journal* 16 (4): 337-49.

Tiruta-Barna, L., Z. Rakotoarisoa, et J. Mehu. 2006. « Assessment of the multi-scale leaching behaviour of compacted coal fly ash ». *Journal of hazardous materials* 137 (3): 1466-78.

Tokyay, Mustafa. 2016. *Cement and concrete mineral admixtures*. CRC Press.

Tran, Ngoc Thanh. 2009. « Valorisation de sédiments marins et fluviaux en technique routière ». *Université d'Artois*.

Tribout, Christelle, Bernard Husson, et Ange Nzihou. 2011. « Use of treated dredged sediments as road base materials: Environmental assessment ». *Waste and Biomass Valorization* 2 (3): 337-46.

Türk, TUĞBA, İBRAHİM Alp, et HACI Deveci. 2009. « Adsorption of As (V) from water using Mg–Fe-based hydrotalcite (FeHT) ». *Journal of hazardous materials* 171 (1-3): 665-70.

« UNPG ». s. d. Consulté le 19 avril 2022. https://www.unpg.fr/.

Van der Sloot, H. A., D. S. Kosson, et O. Hjelmar. 2001. « Characteristics, treatment and utilization of residues from municipal waste incineration ». *Waste Management* 21 (8): 753-65.

Van Jaarsveld, J. G. S., et J. S. J. Van Deventer. 1999. « The effect of metal contaminants on the formation and properties of waste-based geopolymers ». *Cement and Concrete Research* 29 (8): 1189-1200.

Van Jaarsveld, J. G. S., J. S. J. Van Deventer, et G. C. Lukey. 2004. « A comparative study of kaolinite versus metakaolinite in fly ash based geopolymers containing immobilized metals ». *Chemical Engineering Communications* 191 (4): 531-49.

Van Jaarsveld, J. G. S., J. S. J. Van Deventer, et A. Schwartzman. 1999. « The potential use of geopolymeric materials to immobilise toxic metals: Part II. Material and leaching characteristics ». *Minerals Engineering* 12 (1): 75-91.

Van Jaarsveld, J. G. S., Jannie SJ Van Deventer, et G. C. Lukey. 2002. « The effect of composition and temperature on the properties of fly ash-and kaolinite-based geopolymers ». *Chemical Engineering Journal* 89 (1-3): 63-73.

Vaysse, Christophe. 2001. « Caractérisation structurale d'hydroxydes doubles lamellaires contenant des anions oxométallates (Mo, W) ou acrylate intercalés ». PhD Thesis, Université Sciences et Technologies-Bordeaux I.

Vegas, Iñigo, J. Urreta, Moisés Frías, et R. García. 2009. « Freeze–thaw resistance of blended cements containing calcined paper sludge ». *Construction and Building Materials* 23 (8): 2862-68.

Vial, Stéphanie. 2005. « Immobilisation d'enzymes dans des hydroxydes doubles lamellaires. Réalisation de biocapteurs pour la détection de polluants organiques ». PhD Thesis, Université Blaise Pascal-Clermont-Ferrand II.

Villa, Raquel Vigil de la, Moisés Frías, María Isabel Sánchez de Rojas, Iñigo Vegas, et Rosario García. 2007. « Mineralogical and morphological changes of calcined paper sludge at different temperatures and retention in furnace ». *Applied Clay Science* 36 (4): 279-86.

Vohla, Christina, Reimo Alas, Kaspar Nurk, Sabrina Baatz, et Ülo Mander. 2007. « Dynamics of phosphorus, nitrogen and carbon removal in a horizontal subsurface flow constructed wetland ». *Science of the Total Environment* 380 (1-3): 66-74.

Vohla, Christina, Margit Kõiv, H. John Bavor, Florent Chazarenc, et Ülo Mander. 2011. « Filter Materials for Phosphorus Removal from Wastewater in Treatment Wetlands—A Review ». *Ecological Engineering* 37 (1): 70-89. https://doi.org/10.1016/j.ecoleng.2009.08.003.

Vohla, Christina, Elar Poldvere, Alar Noorvee, Valdo Kuusemets, et ÜLO MANDER. 2005. « Alternative filter media for phosphorous removal in a horizontal subsurface flow constructed wetland ». *Journal of Environmental Science and Health* 40 (6-7): 1251-64.

Volland, S., O. Kazmina, V. Vereshchagin, et M. Dushkina. 2014. « Recycling of sand sludge as a resource for lightweight aggregates ». *Construction and building Materials* 52: 361-65.

Wan, Dongjin, Huijuan Liu, Ruiping Liu, Jiuhui Qu, Shanshan Li, et Jian Zhang. 2012. « Adsorption of nitrate and nitrite from aqueous solution onto calcined (Mg–Al) hydrotalcite of different Mg/Al ratio ». *Chemical Engineering Journal* 195: 241-47.

Wan, Dongjin, Yongde Liu, Shuhu Xiao, Jing Chen, et Jian Zhang. 2015. « Uptake fluoride from water by caclined Mg-Al-CO3 hydrotalcite: Mg/Al ratio effect on its structure, electrical affinity and adsorptive property ». *Colloids and Surfaces A: Physicochemical and Engineering Aspects* 469: 307-14.

Wang, Jian, Dongjuan Kang, Xiaolin Yu, Maofa Ge, et Yuantao Chen. 2015. « Synthesis and characterization of Mg–Fe–La trimetal composite as an adsorbent for fluoride removal ». *Chemical Engineering Journal* 264: 506-13.

Wang, Shuangzhen, Larry Baxter, et Fernando Fonseca. 2008. « Biomass fly ash in concrete: SEM, EDX and ESEM analysis ». *Fuel* 87 (3): 372-79.

Wang, Wenwen, Jiabin Zhou, Gopal Achari, Jiaguo Yu, et Weiquan Cai. 2014. « Cr (VI) removal from aqueous solutions by hydrothermal synthetic layered double hydroxides: adsorption performance, coexisting anions and regeneration studies ». *Colloids and Surfaces A: Physicochemical and Engineering Aspects* 457: 33-40.

Wei, Yu-Ling, Chang-Yuan Lin, Shao-Hsiang Cheng, et H. Paul Wang. 2014. « Recycling steel-manufacturing slag and harbor sediment into construction materials ». *Journal of hazardous materials* 265: 253-60.

Wei, Yu-Ling, Chang-Yuan Lin, Kuan-Wei Ko, et H. Paul Wang. 2011. « Preparation of low water-sorption lightweight aggregates from harbor sediment added with waste glass ». *Marine pollution bulletin* 63 (5-12): 135-40.

Wei, Yu-Ling, Jing-Chiang Yang, Yong-Yang Lin, Shih-Yu Chuang, et H. Paul Wang. 2008. « Recycling of harbor sediment as lightweight aggregate ». *Marine Pollution Bulletin* 57 (6-12): 867-72.

Wesche, Karlhans. 1991. *Fly ash in concrete: properties and performance*. CRC Press.

Wheatley, A. D., et Steven Sadhra. 2004. « Polycyclic aromatic hydrocarbons in solid residues from waste incineration ». *Chemosphere* 55 (5): 743-49.

Wiebusch, Bernd, Masaaki Ozaki, Haruki Watanabe, et Carl Franz Seyfried. 1998. « Assessment of leaching tests on construction material made of incinerator ash (sewage sludge): investigations in Japan and Germany ». *Water science and technology* 38 (7): 195-205.

Wiles, Carlton C. 1987. « A review of solidification/stabilization technology ». *Journal of hazardous materials* 14 (1): 5-21.

Wilson, David C., Costas Velis, et Chris Cheeseman. 2006. « Role of informal sector recycling in waste management in developing countries ». *Habitat international* 30 (4): 797-808.

Wu, Xilin, Xiaoli Tan, Shitong Yang, Tao Wen, Hongli Guo, Xiangke Wang, et Anwu Xu. 2013. « Coexistence of adsorption and coagulation processes of both arsenate and NOM from contaminated groundwater by nanocrystallined Mg/Al layered double hydroxides ». *Water research* 47 (12): 4159-68.

Xiao, Chengqing, Lena Q. Ma, et Terry Sarigumba. 1999. « Effects of soil on trace metal leachability from papermill ashes and sludge ». Wiley Online Library.

Xintara, Charles. 1992. *Analysis paper: impact of lead-contaminated soil on public health*. US Department of Health and Human Services, Public Health Service.

Xu, Bo, et Yaolin Yi. 2022. « Treatment of Ladle Furnace Slag by Carbonation: Carbon Dioxide Sequestration, Heavy Metal Immobilization, and Strength Enhancement ». *Chemosphere* 287 (janvier): 132274. https://doi.org/10.1016/j.chemosphere.2021.132274.

Xu, Hua, et Jannie SJ van Deventer. 2003. « The effect of alkali metals on the formation of geopolymeric gels from alkali-feldspars ». *Colloids and Surfaces A: Physicochemical and Engineering Aspects* 216 (1-3): 27-44.

Xu, Hua, et J. S. J. Van Deventer. 2000. « The geopolymerisation of alumino-silicate minerals ». *International journal of mineral processing* 59 (3): 247-66.

Xu, Hua, et Jannie SJ Van Deventer. 2002. « Geopolymerisation of multiple minerals ». *Minerals engineering* 15 (12): 1131-39.

Xu, J. Z., Y. L. Zhou, Q. Chang, et H. Q. Qu. 2006. « Study on the factors of affecting the immobilization of heavy metals in fly ash-based geopolymers ». *Materials letters* 60 (6): 820-22.

Xue, Lihong, Bin Gao, Yongshan Wan, June Fang, Shengsen Wang, Yuncong Li, Rafael Muñoz-Carpena, et Linzhang Yang. 2016. « High efficiency and selectivity of MgFe-LDH modified wheat-straw biochar in the removal of nitrate from aqueous solutions ». *Journal of the Taiwan Institute of Chemical Engineers* 63: 312-17.

Yalçın, Nevin, et Vahdettin Sevinç. 2000. « Utilization of bauxite waste in ceramic glazes ». *Ceramics International* 26 (5): 485-93.

Yan, Liang-guo, Kun Yang, Ran-ran Shan, Tao Yan, Jing Wei, Shu-jun Yu, Hai-qin Yu, et Bin Du. 2015. « Kinetic, isotherm and thermodynamic investigations of phosphate adsorption onto core–shell Fe3O4@ LDHs composites with easy magnetic separation assistance ». *Journal of colloid and interface science* 448: 508-16.

Yan, Yubo, Xiuyun Sun, Fangbian Ma, Jiansheng Li, Jinyou Shen, Weiqing Han, Xiaodong Liu, et Lianjun Wang. 2014. « Removal of Phosphate from Etching Wastewater by Calcined Alkaline Residue: Batch and Column Studies ». *Journal of the Taiwan Institute of Chemical Engineers* 45 (4): 1709-16. https://doi.org/10.1016/j.jtice.2013.12.023.

Yang, Kun, Liang-guo Yan, Yan-ming Yang, Shu-jun Yu, Ran-ran Shan, Hai-qin Yu, Bao-cun Zhu, et Bin Du. 2014. « Adsorptive removal of phosphate by Mg–Al and Zn–Al layered double hydroxides: kinetics, isotherms and mechanisms ». *Separation and Purification Technology* 124: 36-42.

Yip, Christina K., Grant C. Lukey, et Jannie SJ Van Deventer. 2004. « Effect of blast furnace slag addition on microstructure and properties of metakaolinite geopolymeric materials ». *Ceramic Transactions* 153: 187-209.

Yoshida, Mari, Paulmanickam Koilraj, Xinhong Qiu, Tsuyoshi Hirajima, et Keiko Sasaki. 2015. « Sorption of arsenate on MgAl and MgFe layered double hydroxides derived from calcined dolomite ». *Journal of Environmental Chemical Engineering* 3 (3): 1614-21.

Yu, Qiangqiang, Yangqing Zheng, Yuanpeng Wang, Liang Shen, Haitao Wang, Yanmei Zheng, Ning He, et Qingbiao Li. 2015. « Highly selective adsorption of phosphate by pyromellitic acid intercalated ZnAl-LDHs: assembling hydrogen bond acceptor sites ». *Chemical Engineering Journal* 260: 809-17.

Yuan, Xiaoya, Yufei Wang, Jian Wang, Chao Zhou, Qi Tang, et Xiaobei Rao. 2013. « Calcined graphene/MgAl-layered double hydroxides for enhanced Cr (VI) removal ». *Chemical engineering journal* 221: 204-13.

Yue, Xianyang, Weizhen Liu, Zuliang Chen, et Zhang Lin. 2017. « Simultaneous removal of Cu (II) and Cr (VI) by Mg–Al–Cl layered double hydroxide and mechanism insight ». *Journal of Environmental Sciences* 53: 16-26.

Yunsheng, Zhang, Sun Wei, Chen Qianli, et Chen Lin. 2007. « Synthesis and heavy metal immobilization behaviors of slag based geopolymer ». *Journal of hazardous materials* 143 (1-2): 206-13.

Zeraoui, Ahmed. 2020. « Approche opérationnelle pour une gestion durable des sédiments de dragage dans des filières de génie civil ». PhD Thesis, Ecole nationale supérieure Mines-Télécom Lille Douai.

Zhang, Jianguo, John L. Provis, Dingwu Feng, et Jannie SJ van Deventer. 2008. « Geopolymers for immobilization of Cr6+, Cd2+, and Pb2+ ». *Journal of Hazardous materials* 157 (2-3): 587-98.

Zhang, Tao, Qiurong Li, Haiyan Xiao, Zhenyu Mei, Hongxiao Lu, et Yuming Zhou. 2013. « Enhanced fluoride removal from water by non-thermal plasma modified CeO2/Mg–Fe layered double hydroxides ». *Applied clay science* 72: 117-23.

Zhang, Xiangling, Lu Guo, Hualing Huang, Yinghe Jiang, Meng Li, et Yujie Leng. 2016. « Removal of phosphorus by the core-shell bio-ceramic/Zn-layered double hydroxides (LDHs) composites for municipal wastewater treatment in constructed rapid infiltration system ». *Water Research* 96: 280-91.

Zhang, Zhi-qing, Meng-chen Liao, Hong-Yan Zeng, Sheng Xu, Xiao-jun Liu, Jin-ze Du, Pei-han Zhu, et Qing-jun Huang. 2014. « Temperature effect on chromium (VI) removal by Mg/Al mixed metal oxides as adsorbents ». *Applied clay science* 102: 246-53.

Zhao, Xiaofeng, Haijun Zhang, Yuwen Ni, Xianbo Lu, Xueping Zhang, Fan Su, Jingfeng Fan, Daoming Guan, et Jiping Chen. 2011. « Polybrominated diphenyl ethers in sediments of the Daliao River Estuary, China: levels, distribution and their influencing factors ». *Chemosphere* 82 (9): 1262-67.

Zhao, Xin, Liangmiao Zhang, Pan Xiong, Wenjing Ma, Na Qian, et Wencong Lu. 2015. « A novel method for synthesis of Co–Al layered double hydroxides and their conversions to mesoporous CoAl2O4 nanostructures for applications in adsorption removal of fluoride ions ». *Microporous and Mesoporous Materials* 201: 91-98.

Zorić, Dmitar, Dušan Lazar, Ognjen Rudić, Miroslava Radeka, Jonjaua Ranogajec, et Helena Hiršenberger. 2012. « Thermal conductivity of lightweight aggregate based on coal fly ash ». *Journal of thermal analysis and calorimetry* 110 (1): 489-95.

Zoubeir, Lafhaj, Saliceto Adeline, Cohen Solal Laurent, Coudray Yoann, Huynh Trung Truc, et Anguoni Federico. 2007. « The use of the Novosol process for the treatment of polluted marine sediment ». *Journal of Hazardous Materials* 148 (3): 606-12.

ZRI, Abdeljalil, Nor Edine ABRIAK, et Mahfoud BENZERZOUR. s. d. « Etude de formulations d'un béton de sable à base de sable de dragage ».

Chapter 2:

Pilot-scale natural carbonation of waste paper fly ash for stabilization of Ba and Pb

Pilot-scale natural carbonation of waste paper fly ash for stabilization of Ba and Pb

Bader Bouzar [a, b, *], Yannick Mamindy-Pajany [a, b], Zeinab Mkahal [a, b]

[a] IMT Nord Europe, Institut Mines-Télécom, Centre for Materials and Processes, Environnement, F-59000 Lille, France.

[b] Univ. Lille, Univ., ULR 4515 – LGCgE, Laboratoire de Génie Civil et géo-Environnement, F-59000 Lille, France.

Article submitted to the International Journal of Environmental Science and Technology since July 12, 2022

ABSTRACT

The increase of energy valorization of paper sludge waste and biomass due to their high calorific value by incineration leads to an increase of waste paper fly ash (WPFA) quantities, which are in most cases considered as hazardous, and must be dealt with accordingly. The Alternative options for the management of WPFA, such as stabilization/solidification, vitrification or sintering, are not fully developed or either costly. In the present study, pilot-scale natural carbonation technology was used to reduce the hazardous nature of WPFA by improving the stabilization of metallic and metalloids trace elements (MMTE), especially Barium (Ba) and Lead (Pb) leaching. The natural carbonation of WPFA was found to be optimal at a water/solid ratio of 0.3 under natural temperature and humidity conditions. Batch leaching tests based on thermodynamic equilibrium were used to evaluate the solubility of the MMTE as a function of pH and at the natural pH of non-carbonated and carbonated WPFA. Thermogravimetry, X-ray diffraction, scanning electron microscope and energy dispersive spectroscopy analyses were performed to investigate the evolution of carbonation over time and its effect on the chemical and mineralogical properties of WPFA. After 7 days of natural carbonation, the leaching concentration of Ba and Pb was below the French legal limit. The leaching concentration of Ba and Pb from carbonated samples decreased 98.5% and 98 % respectively. The leaching and release potential behavior of carbonated WPFA were further evaluated using the four-step sequential extraction procedure proposed by the Commission of the European Communities Bureau of Reference (BCR). The speciation of MMTE was largely changed from the soluble substance to carbonated fraction because of the carbonation reaction. The percolation water collected during the carbonation process respects the discharge standards.

Keywords: Waste paper fly ash, Natural carbonation, Carbonation efficiency, Stabilization, Metallic and metalloids trace elements, Pilot-scale

1.Introduction

In France the paper industry uses 40% wood and 60% recycled paper and board as raw material (on average). In the case of wood, 70% originates directly from the forest and the remaining 30% may originate from the sawmill offcuts or from the recycling of transport pallets. In terms of the reprocessing percentage, France is in 6th position in Europe with 60% of paper and cardboard recycled. If one considers the tonnage of recycled products, France is in second place behind Germany. French paper manufacturers have to import some paper to cover their consumption. The development of this by-product is a consequence of the paper and cardboard industry's awareness of the need to preserve forest resources and to limit the landfilling of the various products resulting from the manufacture and recycling of paper. In 1992, France signed a commitment to sustainable forest management at the United Nations Conference on Environment and Development in Rio with 170 other countries. In line with this principle, paper recycling was developed, resulting in the production of new waste (pulp processing sludge and de-inking sludge). In 1992, France signed a commitment to sustainable forest management at the United Nations Conference on Environment and Development in Rio with 170 other countries. In

line with this principle, paper recycling was developed, resulting in the production of new waste (pulp processing sludge and de-inking sludge). The paper industry then had the idea of using these different residues with high calorific values as fuel for their boilers, thus providing hot water and electricity (cogeneration boiler) often much more than the paper mill itself, which constitutes an important recovery channel limiting the disposal of waste (M. PETITPAIN, 2016). After co-incineration of the residues with biomass, new waste is generated: waste paper fly ash (WPFA)
The WPFA are industrial by-products resulting from the combustion of both paper mill sludge and biomass (sawmill and wood pallet reprocessing residues). In France, only two paper mills out of twelve incorporate, in part, both types of sludge, from the cleaning of recycled paper, in their paper boilers as a substitute for biomass with a variable percentage (which can reach more than 60%) and generating ash at the end of the boiler mainly composed of silica, alumina, calcite and lime. The national production of WPFA is estimated at 200,000 tons of dry matter per year and varies from one plant to the other, depending mainly on the power of the boilers and the production. In parallel, the opening of several new plants, fueled only by biomass, is planned in the next few years.

The characteristics of WPFA depend on the type of sludge and other materials (such as sawmill and wood pallet reprocessing residues) that are supplied to the boilers, as well as the mode of operation of the boilers. He WPFA is mainly composed of calcium, silicon and aluminum: between 70 and 90 % of the material. Concentrations of other major elements are low (less than 2%) except for MgO, which can reach the content of 5%. Sulfate (SO_3) levels are below 1% (Bai et al. 2003; Frías et al. 2008; Vegas et al. 2009; Mozaffari et al. 2009). From a mineralogical point of view, WPFA are composed of quartz. Calcium is present in the form of sulfate (gypsum, hemihydrate) or oxide (CaO). Traces of calcium carbonates ($CaCO_3$) may be present where the lime has started to react with the CO_2 in the air. Quartz, gypsum and quicklime are the three main mineral phases present. Other studies have confirmed the possibility of clay minerals being present in WPFA, since these compounds are used in the composition of paper (Pera and Amrouz 1998; García et al. 2008; Frías et al. 2008). The presence of lime gives WPFA a high alkalinity; thus WPFA has a high chloride (Cl) content (typically 10-20%) which has a high complexing capacity for several metallic and metalloids trace elements (MMTE). Both of these factors result in an increased potential for leaching of MMTE, which is important for landfills. Only the study done by **Segui** (Segui 2011) considers the environmental aspect of a valorization of WPFA, the inorganic contaminants present in this fly ash are mainly zinc (1389 mg/kg), barium (1238 mg/kg) and lead (796 mg/kg), exceed the thresholds of the methodological guide which led to a limitation of their valorization.

The environmental impact of solid incineration residues is mainly related to their ability to release a certain quantity of chemical elements (Zhang et al. 2022), including soluble salts and MMTE, when in contact with water (Yao et al. 2022). The carbonation process has an important role in the immobilization of certain MMTE within the WPFA matrix. The initial pH of the WPFAs at the furnace outlet is generally between 11 and 13.5. At these pH values, all the amphoteric metals (Ba, Pb, Zn...) are in soluble hydroxide form. Carbonation induces a decrease in pH to 8-9. The pH range is that of a solution containing carbonate ions (CO_3^{2-}) and hydrogen carbonates (HCO^{3-}). At such a pH, the amphoteric metals become insoluble and are trapped in the matrix. This observation is verified by the studies carried out at BRGM (Bureau de recherches géologiques et minières) on the evolution of fly ash subjected to weathering, which underlines the importance of the carbonation process for the stabilization of certain metals (Pb, Zn, Cd) in these products (Baranger et al. 2002). According to several research, the leaching behavior of MMTE from industrial by-products can be reduced by different treatments, such as carbonation (Meima et al. 2002; Polettini and Pomi 2004; Todorovic and Ecke 2006; Costa et al. 2007) and maturation (Meima and Comans 1999; Chimenos et al. 2003), including lead (Pb) (Meima and Comans 1999; Chimenos et al. 2003; Ecke et al. 2003; Rendek et al. 2006a), copper (Cu) (Ecke et

al. 2003) and zinc (Zn) (Meima and Comans 1999; Chimenos et al. 2003; Ecke et al. 2003). The reaction process of carbonation can be described in a simplified manner by equation (1), (2). Carbonation can only occur in the presence of humidity, as carbon dioxide (CO_2) gas can hydrate to form carbonic acid:

$$CO_{2(g)} + H_2O_{(aq)} \longleftrightarrow H_2CO_{3\,(aq)} \longleftrightarrow 2H^{2+}{}_{(aq)} + CO_3^{2-}{}_{(aq)} \quad (1)$$

$$M^{2+}{}_{(aq)} + CO_3^{2-}{}_{(aq)} \longleftrightarrow MCO_{3(s)} \quad (2)$$

In this paper, the WPFA used were classified as hazardous waste. Considering the enormous amount of WPFA to be generated in the future by the large-scale combustion of paper mill sludge and biomass instead of coal, a low-cost environmental technology has to be applied in order to safely valorize WPFA in different civil engineering fields such as lightweight aggregates (Bouzar and Mamindy-Pajany 2022) or road construction (Mkahal et al. 2022) due to their pozzolanic and/or hydraulic properties (rich in CaO) which presents advantages for their use as a replacement for Portland cement.. Until now no researches have been reported for the WPFA treatment, especially by natural carbonation at pilot scale (industrial). Until now no researches have been reported for the WPFA treatment, especially by natural carbonation at pilot scale (industrial). In order to evolve the immobilization potential of Ba, Pb and Cl, a pilot scale natural carbonation process of WPFA was carried out. Thus, due to the high content and leaching concentration of Ba and Pb in WPFA, a relationship between carbon dioxide uptake and leaching concentration was investigated. For a simple technical operation, the experimental parameters such as the liquid/solid ratio (L/S) and the reaction time were fixed. The underlying reasons for the observed changes in the leaching of carbonate WPFA were interpreted on the basis of the ANC results, Thermogravimetry (TG) and differential thermal analysis (DTA), modified European Community Bureau of Reference (BCR) sequential extraction procedure, scanning electron microscope (SEM) and energy dispersive spectroscopy (EDS) analyses and X-ray diffraction (XRD). Specifically, the leaching evaluation of carbonated WPFA for the following components: Ba, Pb and Cl.

2. Materials and methods

2.1. Waste paper fly ash description

The type of ash used in this study is ash from biomass and waste paper sludge. The WPFA used was collected from the cyclone of a massive combustion incinerator located in the North-East of France, this thermal power plant generates more than 55,000 tons per year of WPFA. Once in the laboratory, the WPFA is steamed at 40°C until the mass is stabilized. The leaching of MMTE from WPFA was confirmed by Inductively coupled plasma atomic emission spectroscopy (ICP-AES) and the chemical composition was determined by X-ray Fluorescence (XRF), the results are presented in Table 1. The chemical composition of the WPFA is as follows: CaO 64.02 %; SiO_2 14.59 % and Al_2O_3 8.1 %. The results revealed that the concentration of Pb 7.35±0.6 mg/kg, Ba 178±6 mg/kg and Cl 1422±72 mg/kg were the most plentiful trace elements in the WPFA. According to the regulations in force, the environmental analysis of WPFA shows that it is considered as a hazardous waste.

Chemical composition by XRF	wt.%	Metallic and metalloids trace elements (MMTE)	Concentration ($mg.kg^{-1}$)
SiO_2	14.59	As	<0.11
Al_2O_3	8.4	Ba	178±6
MgO	1.74	Cd	<0.009
Fe_2O_3	0.8	Co	<0.009
CaO	64.02	Cr	<0.011
Na_2O	0.45	Cu	0.09±0.02
SO_3	1.57	Mo	0.08±0.02
TiO_2	0.7	Ni	<0.047

ZnO	0.22	Pb	7.35±0.6
Cl	0.8	Sb	<0.057
BaO	0.11	Se	<0.08
P_2O_5	0.35	Zn	1.1±0.2
K_2O	0.7	Cl	1422±72

Table 1. Chemical composition in major and MMTE of the WPFA.

2.2. Materials characterization

The particle size distribution of WPFA was determined using a dry-voice laser particle size analyzer. In this study, a Coulter LS 230 laser was used to determine the particle size between 0.04 µm and 2000 µm. The test was carried out in accordance with NF ISO 13320-1 (AFNOR 2000a). The counting of the cumulative percentages of particles is performed by analyzing the diffraction spots created by the particles when they cut the laser beam. The particle size distribution of WPFA was below 250 µm (Figure 1), which was optimum for this experiment. Median diameter is (d50=10µm).

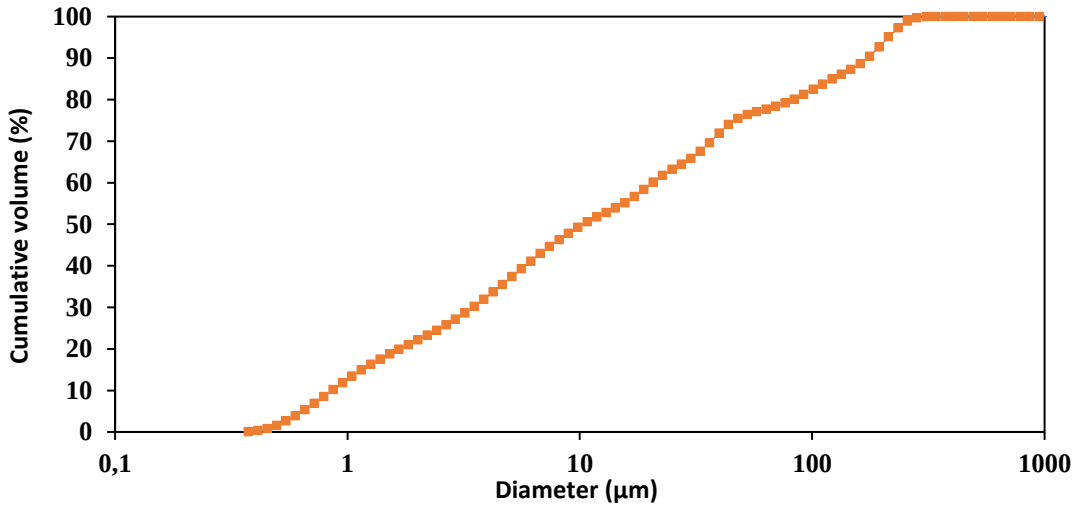

Figure 1. Granular distributions of WPFA.

The specific surface area was measured by the BET method using a Micromeritics stirring analyzer (3FLEX Surface Characterization) according to NF EN ISO-18757 (AFNOR 2006). Prior to analysis, the samples were degassed from nitrogen with a Smart Prep degasser (VacPrep 061) under nitrogen at 80°C for 8 hours to remove moisture from the sample surface and pores.

The specific density of WPFA was measured using a Micromeritics ACCUPYC 1330 Helium Pycnometer in accordance with standard NF EN 15326 (AFNOR 2009). The principle of which is based on the determination of the absolute volume occupied by a specific mass of material. The absolute volume of the sample is determined by sweeping the sample with helium gas at a fixed pressure. The method of calculation is based on the perfect gas relationship.

The Loss On Ignition (LOI) of WPFA was determined according to the NF EN 12879 (AFNOR 2000b) standard, 5g of samples were calcined at 550 °C for 3 hours. Subsequently, to avoid hydration, the sample was cooled in a desiccator with resin. A percentage of the organic material could be determined by the weight loss. **Table 2** illustrates the results of the physico-chemical characterization of WPFA.

Physical parameters	Standard	WPFA
Specific density (kg/m^3)	NF EN 1097-7	2980±8
Median diameter d_{50} (µm)	NF ISO 13320-1	10±0.1
Specific surface BET (m^2/kg)	NF EN ISO-18757	2261±3

pH	NF EN 14429	13.5±0.2
Conductivity (mS/cm)	EN 12457-2	11.3±2
Loss On Ignition (LOI) (%)	NF EN 12879	5.7±0.1

Table 2. Physical and chemical characterizations of WPFA

The XRF analysis was performed with a S4-PIONEER equipped with a 4 kW generator with a Rhodium anti-cathode. The instrument was capable of providing results in atomic mass percentages of the elements. The analyzed samples are ground and dried beforehand.

The mineral composition of WPFA before and after carbonation was determined by X-ray Diffraction (XRD). The analysis was performed on powders using a D8 Focus diffractometer from Bruker. The powder samples are placed on standard sample holders which are 1 to 2 mm deep, 25 mm in diameter and can hold approximately 1g of powder. The sample is arranged to have a flat surface in order to respect the 0-plane of the wafer for diffracted ray detection. The ray source is a monochromatized Cobalt ($\lambda K\alpha 1 = 1.74$ Å) with a Lynx Eye fast linear detector. The operating current is 20 mA and the voltage are 40kV. The samples were analyzed over an angular range from 10° to 80° with an acquisition step of 0.02° and a compaction time of 5s.

In order to quantify the consumption of portlandite and the formation of calcite after carbonation, thermogravimetric (TG) and differential thermal analysis (DTA) analyses were performed on a NETZSCH STA 409C thermobalance. The analyzed samples were pre-dried in an oven at 40°C to a constant mass. For each analysis, a quantity of 200 to 250 mg of dry powdered material is introduced into the apparatus and subjected to a linear temperature rise from ambient temperature to 1150°C at a rate of 3 °C/minute under an inert gas (argon) with a flow rate of 75 ml/min. At the end of the test, the processing software accompanying the apparatus allows the recovery of the TG Coubes and the DTA derivative.

To investigate the phase morphology present in the WPFA after carbonation, the Scanning electron microscope (SEM- Hitachi S-4300SE/N) and energy dispersive spectroscopy (EDS) observations were realized. The sample was introduced into the resin, then the solid powder was dispersed on a double-sided carbon tape with polishing. To ensure proper electron conduction in the SEM chamber, the samples were coated with carbon.

2.2. Pilot-scale natural carbonation processes

The pilot tests are conducted as described in Figure 2. The concept was to test carbonation on a sufficiently large scale and under variable wet and dry conditions, as governed by changing weather conditions. Firstly, the WPFA was hydrated in order to consume all the lime (CaO), then a tank with a percolation system was used. The tank was filled with gravel washed in a quarry (6/14 mm) from the region of Charleroi (Belgium), then a filtering geotextile was placed in order to let the rain water through. After manual de-agglomeration using a pestle of the hardened material, caused by hydration of lime ($Ca(OH)_2$), resulting in cementitious behavior and drying, 10 kg of WPFA was adequately mixed with 3 l of water in the mixer at the mass ratio of liquid to solid of 0.3 l/kg. Then the sample was spread in the tank on the geotextile. The liquid/solid ratio was monitored weekly.
During the weekdays, The WPFA was stirred to ensure carbon dioxide CO_2 penetration. The experiment lasted 3 months, during the reaction time, WPFA and percolation water were removed at (1, 3, 7, 15, 30, 60 and 90 days) and prepared for further analysis. During the experiment the WPFA received a significant pluviometry 178 mm, it was necessary to collect the percolation of water for analysis.

Figure 2. Pilot-scale natural carbonation processes

2.4 Leaching tests

The leaching behavior of MMTE in WPFA was studied under different carbonation times (1, 3, 7, 15, 30, 60 and 90 d) according to NF EN 12457-2 (AFNOR 2002). The leaching was performed with a ratio L/S=10 l/kg (Liquid/Solid), 90 g of WPFA was mixed with 900 ml of MilliQ water. The moisture content of the containment matrix to weigh the correct dry matter mass was determined at each time point. The samples were placed under agitation on a turntable (Heidolph Reax 20) at 10 rpm and 25 °C for 24 h. The mixture was then filtered through cellulose acetate membrane filters (0.45 µm). Acidified with 2 vol.% nitric acid, the MMTE concentrations of the leachate were analyzed by ICP-OES; The chloride (Cl^-), sulfate (SO_4^{2-}) and fluoride (F^-) concentration was determined through ion chromatography (IC). The temperature, conductivity and pH of the leachate are also recorded.

The physico-chemical stabilization of WPFA before and after carbonation under acid-base conditions was studied in accordance with standard NF EN 14429 (AFNOR 2015). The ANC-BNC test enables the leaching behavior of WPFA to be evaluated as a function of pH. Similar to batch leaching, the L/S ratio (L/kg of dry matter) is 10. A volume of nitric acid or sodium hydroxide at a determined concentration between 0.1 and 5 mol/l was added to the leachate. The samples were placed under agitation on a turntable (Heidolph Reax 20) at 10 rpm and 25 °C for 48 h. Then, the leachate (water + acid or base) was added in 3 steps (t_0, t_{0+30} min, t_{0+2h}), in order to reduce the swelling of the bottle resulting from the outgassing. The pH is verified and noted at 4 h, 44 h and 48 h after the start of the test. The first measurement verifies that the pH correction is satisfactory, and the subsequent measurements verify the stability of the pH. Following measurement of the final pH, the leachate was filtered through a cellulose acetate filter with a pore size of 0.45 µm. The MMTE concentrations of the leachate were analyzed by ICP-AES.

2.5. BCR (the Community Bureau of Reference) sequential extraction

Sequential extractions were performed in triplicate, based on the modified four-step BCR procedure (which determined the exchangeable water/acid soluble, reducible, oxidizable and residual fractions of the MMTE in the WPFA samples) (Manskinen et al. 2011; Gu et al. 2017) that has been proposed by the European Community Reference. (Now SMT: Standards, Measurements and Testing Program (Gu et al. 2017)). Approximately 1.5 g of WPFA before (WPFA0) and after carbonation (WPFA90) crushed <1 mm, was put in 125 mL polypropylene bottles, dissolved with different chemical reagents. Continuous agitation was maintained on a turntable (Heidolph Reax 20) at 10 rpm and 25 °C. The solid residues were separated by centrifugation at 5000 G for 20 min. Following the centrifugation, the supernatant was carefully collected and filtered on a cellulose acetate filter with a pore size of 0.45 µm in order to allow the necessary analyses (pH, metals and anions analyses). According to the protocol

Table 2, no rinsing of the samples was performed before starting the next extraction. The sequential extraction procedures are shown in Table 1 (Appendix).

3. Results and discussion

3.1. pH of WPFA after natural carbonation

The measured pH values of WPFA after natural carbonation for different times are presented in Figure 3. Natural carbonation was expected to decrease the basicity of WPFA, as unslaked lime ($Ca(OH)_2$) was transformed to calcite ($CaCO_3$). The WPFA original pH was 13.5±0.13, which is higher than the pH of a $Ca(OH)_2$ saturated solution, whereas the carbonated WPFA showed a decreased pH value (pH = 11.42±0.1) after 90 days, due to the consumption of $Ca(OH)_2$ during the carbonation process and the formation of $CaCO_3$.

In fact, the carbonation process can be divided into two steps. In the first step, the pH of WPFA changed slightly upon at $Ca(OH)_2$ depletion, and the second step occurs after the consumption of $Ca(OH)_2$ when the pH is below 12.5. In the first stage, the pH of naturally carbonated WPFA leachate decreased from 13.5±0.13 to 12.55±0.11 in 30 days. Then, with a sufficiently long carbonation time (90 d), the final pH of WPFA drops to 11.42±0.1.

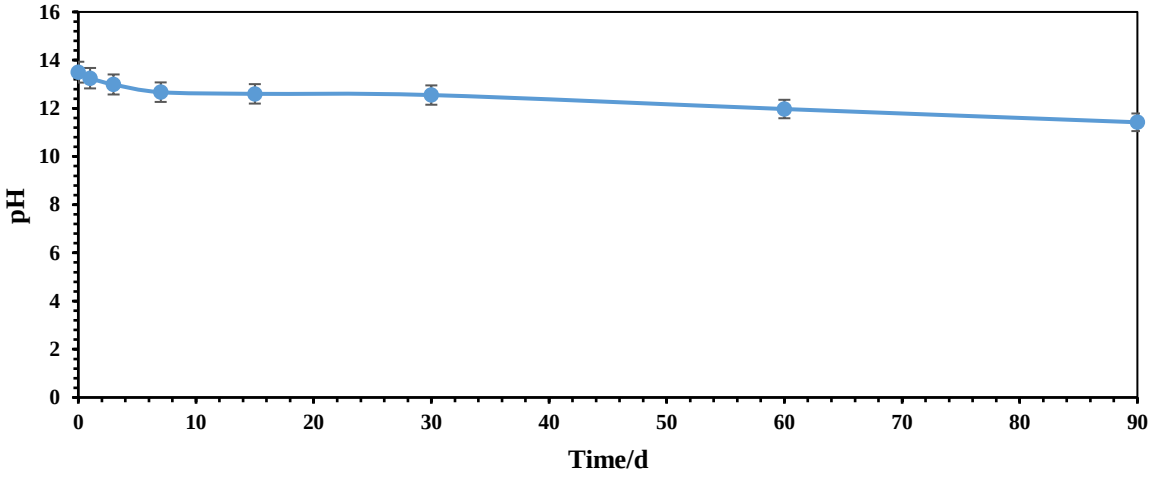

Figure 3. pH of the WPFA after natural carbonation for different times.

3.2 Influence of natural carbonation upon leaching

A most important criteria for landfilling or valorization of WPFA is the release of metallic trace elements MTE in the environment. The Landfill Regulation (BRGM) (2014) defines disposal standards for landfilled waste in three categories: “inert”, “non-hazardous” and “hazardous” in terms of stability and leachability (Table 2 Appendix). The MTE leachate and soluble salts from the untreated and carbonated WFPA were analyzed to identify elements of concern. The release of Ba^{2+}, Pb^{2+} and Cl^- from the original WPFA exceeded landfill thresholds (2014) and should be considered.

After the first days of carbonation (1, 3d), the MMTE concentration was lower than the original WPFA, and the Ba and Pb leachate concentrations were significantly lower after 7 days of natural carbonation. Figure 4 shows the Ba, Pb and Cl leached concentrations from the WPFA before and after natural carbonation for different times. The waste is considered hazardous due to the high leaching concentrations of Ba and Pb in the WPFA (BRGM) (2014). As illustrated in Figure 4, Ba concentration decreased from 178±6 mg/kg to 2.5±0.2 mg/kg (about 98.5%), and for Pb, the concentration decreased from 7.35±0.6 mg/kg to 0.15±0.06 mg/kg (about 98%) after 7 days of carbonation, below the inert waste identification standard limit. However, Cl leaching concentration decreased from 1422±72 mg/kg to

1031±52 mg/kg, but exceeded the regulatory limit, it was concluded that the toxicity of carbonated WPFA could be significantly reduced, thus reducing the risk to landfills and the environment. Due to the high alkalinity and pH of the WPFA, the MMTE leaching concentrations varied considerably with increasing reaction times. The Pb and Ba leaching concentrations in carbonate WPFA decreased with increasing reaction time, reaching a maximum of 90 days, 0.03±0.01 mg/kg, 0.15±0.05 mg/kg and 502±14 mg/kg for Pb, Ba and Cl respectively.

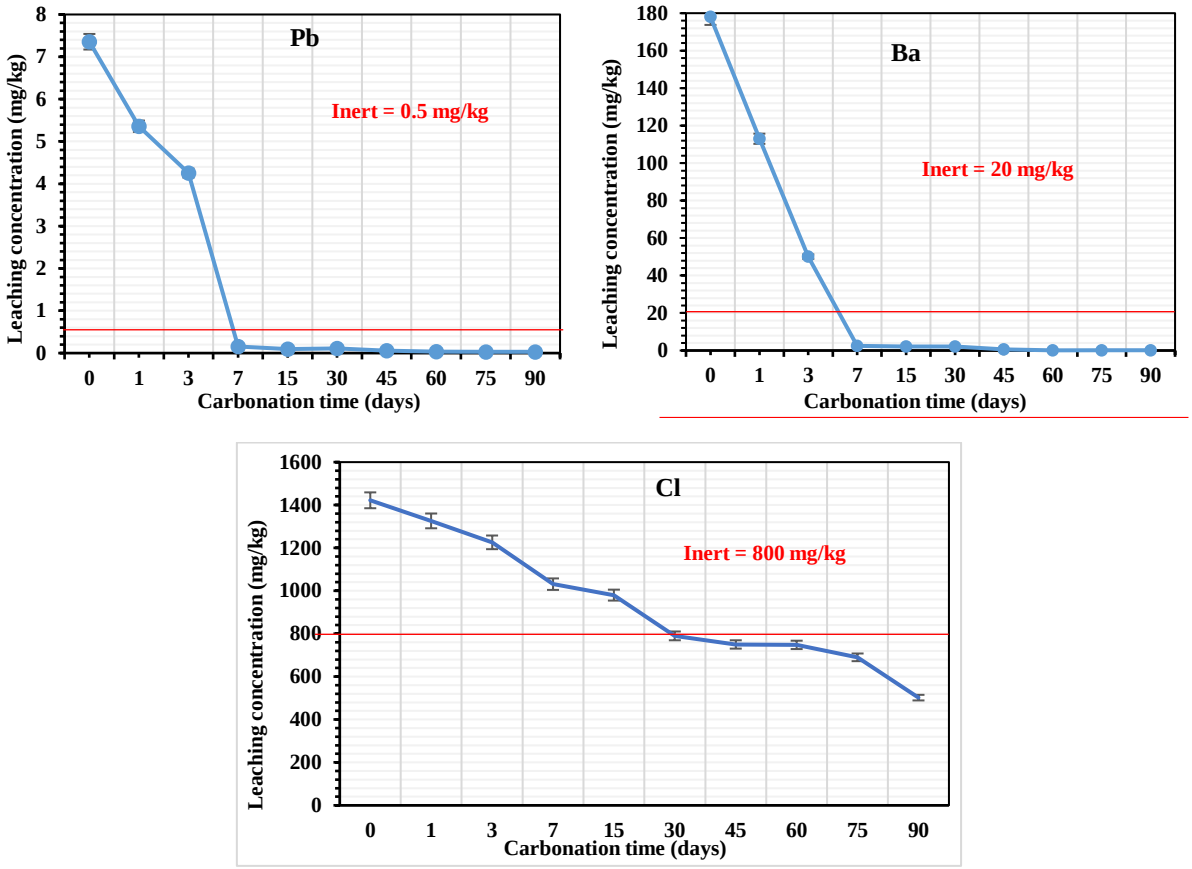

Figure. 4 The concentrations of Ba, Pb and Cl leached before and after natural carbonation

No quantifiable concentrations of Cu, Cd, or Zn were detected in the eluate. In addition, levels of As, Sb, and Se are below the inert landfill limit. In most cases, Mo is present at stable, non-reactive levels and is not affected by carbonation. Conversely, natural carbonation increased the leaching Cr in the WPFA without exceeding the inert waste limit (Table 3).

Several research studies on fly ash carbonation demonstrated that MTEs could be stabilized by carbonation, and the leaching concentration of certain MTEs in water or basic solution decreased. Since the MTEs were transformed into carbonate fractions, most of the MTEs became stable after carbonation (Ni et al. 2017), thus, the leaching concentration of Pb and Zn in water decreased by 95% and was below the French legal limit. Optimal water content would favor carbonation reactions, while the presence of excess water makes it difficult for CO_2 to diffuse and dissolve, limiting the carbonation reaction and leading to higher MTE leaching concentrations. Due to the soluble speciation of the phases, the fixation of certain MTE would be influenced. Several studies demonstrated that the leaching concentrations of Ba^{2+}, Cu^{2+}, Zn^{2+}, Pb^{2+} have few changes at pH 11 and 13. However, the MTE leaching concentrations have a significant increase in pH<9 and pH>13 (Komonweeraket et al. 2015; Zheng et al. 2016). In this study, the pH is between 13.5 and 11.42 before and after natural carbonation, the principal cause was that Ba^{2+} and Pb^{2+} reacted with CO_3^{2-} to form a carbonate precipitation; thus, the MMTE leaching

concentrations were decreased. The leaching concentrations of Cd, Cr, Cu, and Mo evolved for 90 days without exceeding the limits of inert waste identification standards (BRGM) (2014).

Increasing water content improves CO_2 uptake and dissolution to form CO_3^{2-}, while decreasing the pH of WPFA and the release of MMTEs such as Ca^{2+}, Ba^{2+} and Pb^{2+}. The increased water content (caused by rain) and decreased pH, accelerates the dissolution of Ba^{2+} and Pb^{2+} in the medium and react with CO_3^{2-} to precipitate barium carbonate ($PbCO_3$) and lead carbonate ($BaCO_3$) in the WPFA. Yet, high water content has a negative effect on the absorption and dissolution of CO_2, and thus leads to higher leaching concentrations of MMTE.

The effect of natural carbonation on the leachability of soluble salts was also evaluated. Chloride ions are present as potassium chloride (KCl) and sodium chloride (NaCl). It has been shown that the leaching of Cl^- is relatively fast due to the high solubility of KCl and NaCl; thus it is independent of the pH and uncontrolled from solubility limitations (Todorovic and Ecke 2006). As illustrated in Figureure 4, the results indicated that the level of Cl^- (1422±72 mg/kg) released from the WPFA was higher than the BRGM recommendations for inert waste (2014). After 30 days of carbonation the leaching of Cl^- decreases to reach a value below the regulatory limit (790±18 mg/kg) (Table 3).

Parameter (mg/kg)	T0	1d	3d	7d	15d	30d	60d	90d
As	<0.11	<0.11	<0.11	<0.11	<0.11	<0.11	<0.11	<0.11
Ba	178±6	113±4	50±2	2.5±0.2	2.1±0.2	2.09±0.2	0.17±0.05	0.15±0.05
Cd	<0.009	<0.009	<0.009	<0.009	<0.009	<0.009	<0.009	<0.009
Co	<0.009	<0.009	<0.009	<0.009	<0.009	<0.009	<0.009	<0.009
Cr	<0.011	0.11±0.05	0.11±0.05	0.28±0.06	0.2±0.05	0.33±0.08	0.46±0.04	0.41±0.03
Cu	0.09±0.02	0.15±0.04	0.03±0.01	<0.021	<0.021	0.049±0.01	0.039±0.02	0.03±0.01
Mo	0.08±0.02	0.92±0.1	0.09±0.1	0.13±0.3	0.08±0.02	0.43 ±0.12	0.43±0.15	0.48 ±0.1
Ni	<0.047	<0.047	<0.047	<0.047	<0.047	<0.047	<0.047	<0.047
Pb	7.35±0.6	5.36±0.5	4.25±0.4	0.15±0.06	0.09±0.04	0.11±0.04	0.03±0.01	0.03±0.01
Sb	<0.057	<0.057	<0.057	<0.057	<0.057	<0.057	<0.057	0.06±0.01
Se	<0.08	<0.08	<0.08	<0.08	<0.08	<0.08	<0.08	<0.08
Sn	<0.07	<0.07	<0.07	<0.07	<0.07	<0.07	<0.07	<0.07
V	<0.021	<0.021	<0.021	<0.021	<0.021	<0.021	<0.021	<0.021
Zn	1.1±0.2	0.23±0.4	0.18±0.4	0.04±0.01	0.03±0.01	0.03±0.01	0.03±0.01	0.06±0.02
Chlorides	1422±72	1326±73	1226±66	1031±52	980±37	790±18	748±21	502±14
Fluorides	1.1±0.5	-	-	-	-	-	-	-
Sulfates	208±25	206±27	201±31	193±18	163±19	150±9	165±11	159±8
Soluble fraction	3920±121	3980±130	3740±185	1007±93	598±52	400±59	215±16	221±13
Conductivity (mS.cm^{-1})	25.62±0.3	22.62±0.3	13.5±0.23	6.42±0.16	2.94±0.12	2.68±0.13	1.13±0.1	1.02±0.1
pH	13.5±0.13	13.25±0.18	12.99±0.14	12.67±0.13	12.6±0.1	12.55±0.11	11.97±0.1	11.42±0.1

''-'' No value detected

Table 3. Parameter (mg/kg) in the WPFA before and after natural carbonation at 1, 3, 7, 15, 30, 60 and 90 days

3.3. Percolation water analysis

The purpose of recovering the percolation of water is to observe the possibilities of the dissolution of chemical elements and their possible migration into the natural environment. Rainwater trickles down onto the pilot and is collected in a plastic drip tray thanks to a system of taps installed on the pipes which are designed to collect natural runoff water. This collection during the experimentation time allows samples to be taken for their chemical characterization. **Table 4** shows the element concentrations in the WPFA percolation waters during natural carbonation for different times.

Before emptying the tray, a check of compliance with the Decree of August 9, 2006 (consolidated version of July 30, 2014) relating to the levels to be considered during an analysis of discharges into surface water under respectively of section 2.2.3.0 of the nomenclature appended to article R.214-1 of the environment code must be carried out. The quality of the rejects is assessed according to the R1 levels of this nomenclature. The analysis results are lower than the R1 level (**Table 4).**

Contrary to the results conducted by Fernandez et al. (2004), who concluded that fly ash carbonation was the main factor in the decrease of chloride leaching. Chemical analysis of the percolation water revealed that the decrease in Cl^- leaching was not decreased in response to natural carbonation. The main cause of the decrease in Cl^- concentration was the presence of soluble substances in WPFA such as KCl and NaCl which were removed by rainwater, and collected in the percolation of water. Nevertheless, FA washing to eliminate salts has already been reported in a study that revealed high MMTE concentrations in the washed water, particularly Cr, Cu, Pb and Zn (Li et al. 2007). According to the results in Table 4, rainwater washing during the natural carbonation process has the same efficiency for chloride removal that the water washing process, According to the results in Table 4, rainwater washing during the natural carbonation process has the same efficiency advantages for chloride removal as the water washing process, while not conducting the critical MMTE such as Ba, Cu, Cr, Mo, Pb and Zn released on a large degree that was a problem during the water washing process (Li et al. 2007).

Concentration (mg/l)	3d	7d	15d	30d	60d	90d	R1 level (mg/d)
As	<0.11	<0.11	<0.11	<0.11	<0.11	<0.11	1245
Ba	0.11 ± 0.02	0.31 ± 0.09	0.01 ± 0.01	0.02 ± 0.05	0.009 ± 0.002	0.03 ± 0.01	***
Cd	<0.01	<0.009	<0.009	<0.009	<0.009	<0.009	120
Co	<0.01	<0.009	<0.009	<0.009	<0.009	<0.009	***
Cr	0.09±0.03	0.04±0.01	0.03±0.01	0.03±0.01	0.13±0.02	0.27±0.15	5100
Cu	0.15±0.03	0.66±0.1	0.37±0.08	0.23±0.04	<0.021	<0.021	1500
Mo	0.09±0.03	0.06±0.02	0.05±0.02	0.03±0.01	0.04±0.01	0.02 ± 0.01	***
Ni	<0.05	<0.047	<0.047	<0.047	<0.047	< 0.047	6000
Pb	0.25 ± 0.03	0.05 ± 0.02	0.04 ± 0.01	0.03 ± 0.01	0.03 ± 0.01	< 0.01	1800
Sb	<0.06	<0.057	<0.057	<0.057	<0.057	<0.057	***
Se	<0.08	<0.083	<<0.083	<0.083	<0.083	<0.083	***
Sn	<0.07	<0.074	<0.074	<0.074	<0.074	<0.074	***
V	0.03	0.316	0.217	<0.112	<0.021	<0.021	***
Zn	0.23	0.033	<0.064	<0.01	<0.01	<0.01	11 700
Chlorides	163±11	186±17	172±16	154±10	133±10	80±9	
Fluorides	-	-	-	-	-	-	***
Sulfate	-	-	-	-	-	-	***
Soluble fraction (mg/l)	374±22	100±11	598±89	400±72	200±19	182±13	**
Conductivity ($mS.cm^{-1}$)	9.51±0.2	4.97±0.4	2.33±0.15	2.07±0.18	1.2±0.09	0.5±0.1	***
pH	12.99±0.22	12.67±0.21	13.12±0.17	12.55±0.18	11.97±0.15	11.56±0.11	***
Percolation water (L)	4	9	12	12	8	31	***

‘’*’’ without environmental requirements, ‘’-‘’ No value detected**

Table 4. Parameter (mg/kg) in the percolation waters of the WPFA during natural carbonation for different time

3.5. Thermogravimetric analysis (TGA):

Figure. 5 shows the thermal characteristics of the WPFA before and after natural carbonation at 30, 60 and 90 days was examined by the Thermogravimetry (TG) and differential thermal analysis (DTA) (NETZSCH STA 449C). The TG curves are divided into three parts:

- The deshydroxylation of hydrates, depending on the degree of hydration, from 90 °C to about 300 °C depending on their nature;
- The deshydroxylation of lime ($Ca(OH)_2$) between 400 and 500 °C;
- The decarbonation of calcium carbonates ($CaCO_3$) between 550 °C and 950 °C;

The TG / DTA curves of raw WPFA shows little mass loss up to the temperature of 500 °C. This confirms what we got in XRD and X-ray fluorescence: a large amount of lime and a small amount of clay. After the temperature 550 ° C up to the temperature 900 °C, there is a great loss of mass due to decarbonation which means that our WPFA contains a considerable amount of calcite.

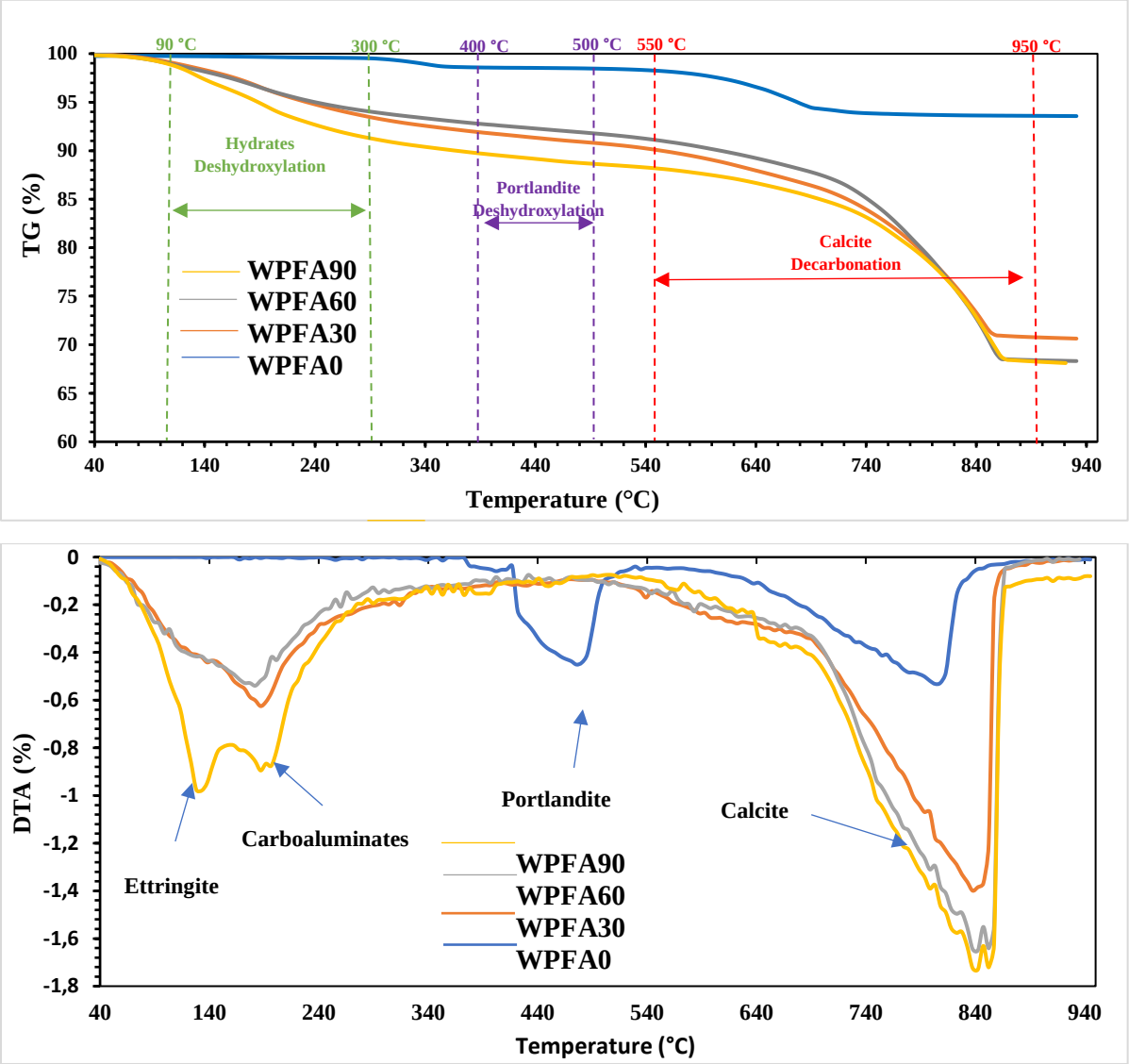

Figure 5. The thermal characteristics of the WPFA before and after natural carbonation at 30, 60 and 90 days.

The TG / DTA curves of the results for the periods of (30, 60 and 90 days) clearly show the three parts mentioned above. The effect of carbonation and lime consumption is noticeable by comparing WPFA0 and WPFA30 then WPFA60 and WPFA90. The loss of mass corresponding to the water of the composition of the hydrates is greater with the increase of the time of carbonation. The difference between WPFA30 and WPFA90 is the most obvious from this point of view. The curve obtained in case WPFA90 i.e. at 90 days of carbonation shows the highest consumption of lime and the greatest loss of mass due to deshydroxylation of hydrates. It turns out that the presence of silica (SiO_2) and alumina (Al_2O_3) at low percentages with calcium oxide (CaO) under these experimental conditions are those that

were responsible for the formation of hydrates (Ettringite and Carboaluminates) after 30, 60 and 90 days of carbonation. Subsequently, the evolution of lime consumption and hydrate formation over time seems significant. An increase in mass loss related to the water constituting hydrates between 30, 60 and 90 days is clearly identified. It is associated with a decrease in lime. Lime does participate in a hydration type reaction which is a priori not negligible.

We note the particularity of the curve WPFA90 from the point of view of carbonates with decomposition in two modes. This is observed when metastable forms of $CaCO_3$ are present (vaterite, aragonite). These polymorphs of calcite ($CaCO_3$) can then evolve to the most stable form which is calcite ($CaCO_3$). The formation of these phases depends in particular on temperature and humidity. Vaterite and argonite, which decompose rather around 640°C, are more abundant at low humidity and high temperature. Calcite ($CaCO_3$), on the other hand, decomposes rather towards 800°C in ATG and forms more rapidly at room temperature or below (Fernández Bertos et al. 2004; Li et al. 2007; Drouet 2010). The presence of high moisture metastable forms remains difficult to explain in this study.

In any case, the total amount of $CaCO_3$ in WPFA90 is high compared to other cases. There is therefore no doubt that lime was consumed for the formation of carbonates. In general, the amount of $CaCO_3$ in the samples is high due to its high presence in the WPFA even before carbonation (WPFA0). Regarding the effect of carbonation, the comparison of WPFA0, WPFA30, WPFA60 and WPFA90 confirms the highest consumption of lime associated with the formation of $CaCO_3$ over time. During the process of carbonation, it is probable that the CO_2 first dissolves into water and forms CO_3^{2-} in the presence of water; at the same time, Ba^{2+} and Pb^{2+} dissolve from the solid phase and react with CO_3^{2-}, forming the $PbCO_3$ and $BaCO_3$ (Yang et al. 2012)**.**

3.4. X-ray diffraction analysis

The XRD spectrum of WPFA obtained before and after carbonation is shown in Figureure 6. The analysis highlighting the crystallized phases therefore proves that the WPFA consists exclusively of CaO.

This corresponds to the very nature of class C fly ash. The main chemical elements present are calcite (CaCO3), calcium oxide (CaO), Gehlenite (Ca_2Al), and Quartz (SiO_2). But also, phases as calciumsilicate in particular which have effects by interaction with water and lime. Also, Rodriguez et al. (Rodríguez et al. 2013) suggests that WPFA, possessing crystallized calciumsilicate phases, may exhibit relatively high pozzolanic activity.

The most obvious differences between the diffractogram of original and carbonated WPFA are the increase in calcite peak intensity and the reduction of the lime/portlandite peaks. Untreated WPFA contains lime/portlandite and calcium hydroxide. These phases disappear after carbonation. There was also a lot of Si–Al–Ca-H hydrated phases identified in the carbonated ashes, including carboaliminate, ettringite and larnite. It should be noted that there are many chloride bearing phases, such as halite, sylvite and Ca(OH)Cl, in WPFA. These phases are the main components releasing chloride in leachates (Bodénan and Deniard 2003) and their high solubility leads to high concentrations of chloride in ash leachates.

Figureure 6 shows the XRD spectra obtained for the three-time frames 30, 60 and 90 days of carbonation for WPFA. It shows that the representative peaks of calcium hydroxide $Ca(OH)_2$ decreased in intensity between 30, 60, 90 days of carbonation. This supports the conclusions drawn by the TGA results regarding the consumption of lime to form calcite ($CaCO_3$). It is noted that the intensity of the quartz peaks remains unchanged, as reported in the study by Diamond (Diamond. S 1981) relative to the carbonation of fly ash rich in calcium. Finally, the presence of new compounds resulting from the

pozzolanic reaction is identified, the products probably formed being very little crystallized. For example, Ettringite were identified as $Ca_6Al_2(SO_4)_3(OH)_{12};26H_2O$ in the carbonated WPFA and as complex compounds in the carbonated samples.

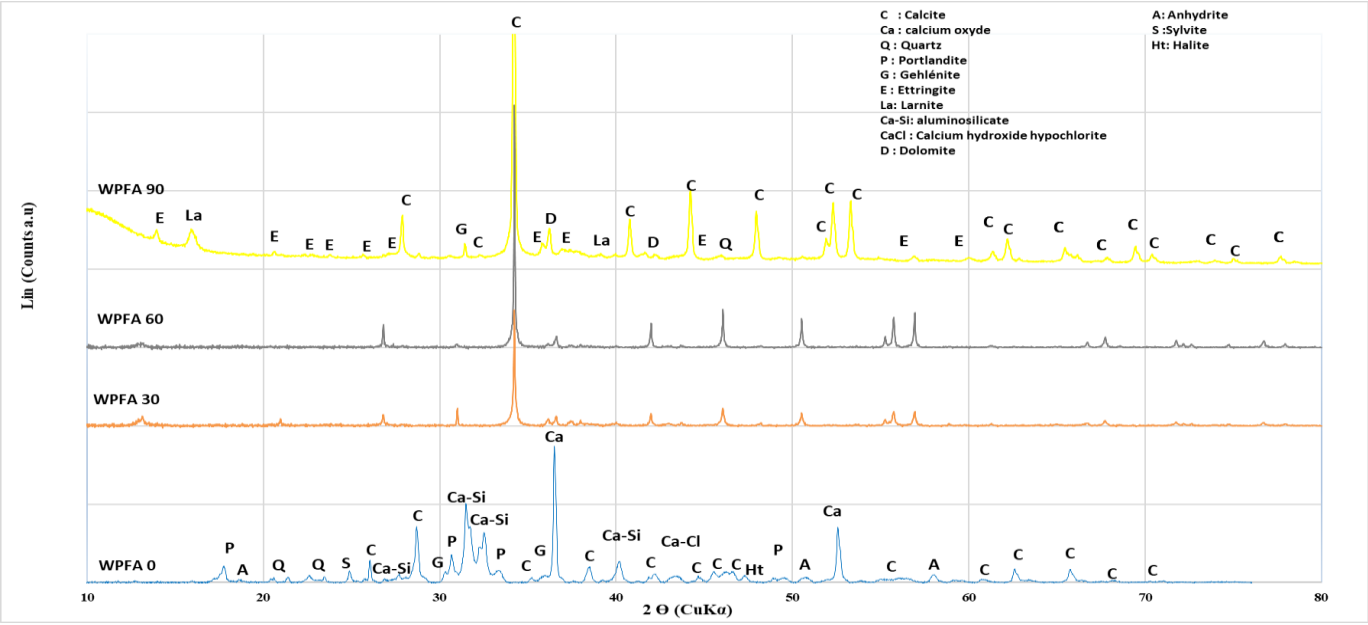

Figure.6 X-ray diffractograms of WPFA before and after natural carbonation at 30, 60 and 90 days.

Subsequently, it is also noted that the peaks of calcium oxide (CaO) and portlandite ($Ca(OH)_2$) were replaced by peaks of calcite ($CaCO_3$), which confirms that the carbonation reaction has taken place. The highest intensity $CaCO_3$ peaks are observed at 90 days of carbonation, which is quite consistent with the literature on polymorphs of calcium carbonate (Chabannes et al. 2015), The peaks associated with other polymorphs (vaterite, etc.), however, remain difficult to identify on the XRD spectra of this study because they often overlap with other low-intensity peaks.

The MTE as Pb and Ba mainly exist as oxide (PbO or BaO) in the WPFA. With carbonation CO_3^{2-} react with Pb^{2+} and Ba^{2+} to form other compounds, which could stabilize the MMTE in the WPFA. After carbonation, $PbCO_3$ and $BaCO_3$ are missing; for the trace amount, there is no detectable existence of Pb and Ba after the natural carbonation.

3.6. SEM-EDS analysis

The SEM-EDS showed that the calcium, silicon, aluminum and magnesium were the major constituents of WPFA samples untreated (Figure.7(a) and (c)) and treated (Figure.7f) which is in accordance with XRF results (Table 1). In fact, SEM-EDS data showed the presence of lime CaO and a little of $CaCO_3$ in the same particles of WPFA0 (Figure.7(a)). Quartz SiO_2 and iron oxides have been identified in WPFA0 (Figure.7(a)). These results are coherent with those obtained by TG-DTA (Figure.5) and XRD (Figure.6). Chlorides were identified in WPFA0 (Figure.6(c)). For MMTE, barium was principally presented as $BaSO_4$ (Figure.7(b)) in WPFA0. Zinc was identified in WPFA0 as Zn oxides and a little of copper was associated with aluminum (Figure.7(g)).

After carbonation, all MMTE were not identified by elemental mapping, maybe due to their weak concentrations in WPFA90 (less than 1000 mg/kg) (Bruder-Hubscher et al. 2002). The changes observed can be related to the formation of coating carbonate phases such as calcite $CaCO_3$ (Figure.7(b)) and barium carbonate $BaCO_3$ (Figure.7(e)). It is important to note that the identification of $BaSO_4$ in

WPFA90 indicates that only a part of barium has been carbonated (Figure.7(e) and (f)). Iron and chlorides were identified in WPFA90 as oxides (Figure.7(d), (e) and (f)).

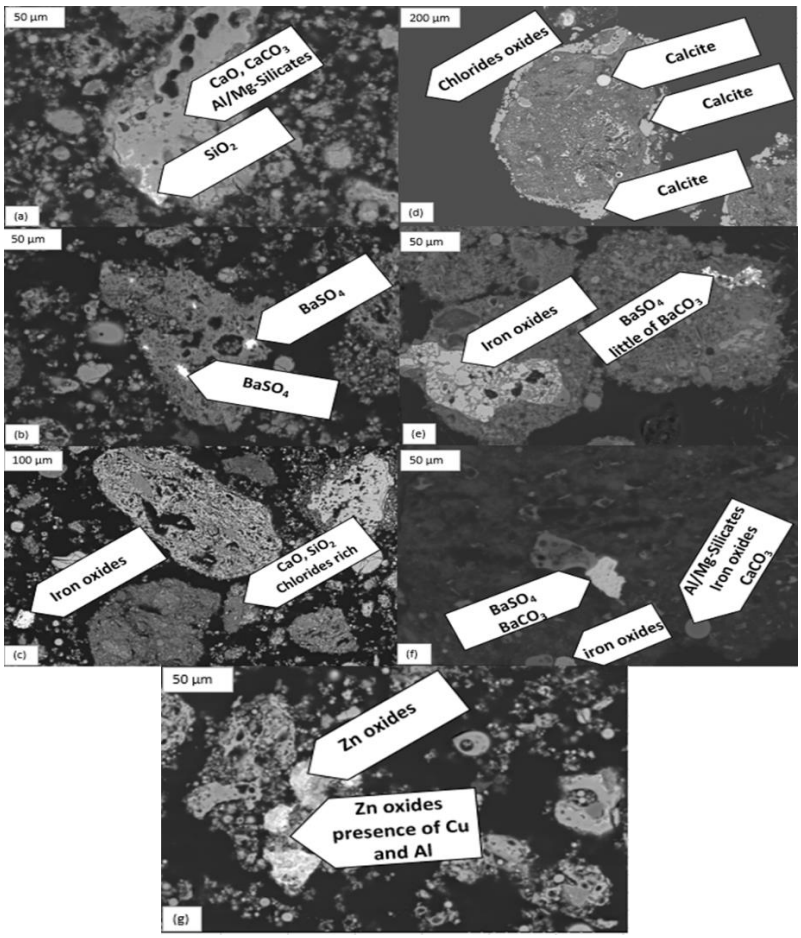

Figure.7 SEM micrographs of WPFA0 (a), (b) and (c) and of WPFA90 (d), (e) and (f).

3.7. Sequential extraction analysis

Since the results obtained by solid analysis were rather about the mineralogical phases containing major elements MEs and not a lot of information is available about the mineral trace elements MTEs, hence the importance of carrying out the sequential chemical extraction to determine the speciation of different metals (MEs and MTEs) present in the WPFA samples. The sequential extraction performed on WPFA is a stepwise sequential extraction. It makes it possible to determine the mineralogical phases that control the mobility and the retention of metals (MEs and MTEs) by determination of the extracted quantities of metals. The presence of metals in the four fractions was evaluated by comparing the concentration of each extract to the total concentrations, which was calculated to be 100% (Figure.8 and Figure.9).

3.7.1 Sequential extraction of MEs

The recoveries of MEs in each fraction were presented in Figure.8. There is no significant change in the speciation of Ca, Si, Fe and Mn before and after carbonation in the WPFA samples.

Calcium was weakly extracted in exchangeable water/acido-soluble fraction before and after carbonation. This indicated that the Ca was presented in the WPFA0 as calcite $CaCO_3$ which support the conclusions drawn by the TG-DTA and XRD (see. Figure.5 and Figure.6). In this fraction, soluble phases such as $CaCl_2$, $CaSO_4$ can also be leached. The highest extractability was in the reducible fraction F2 (>60%) representing metals bound to iron and manganese oxides (Tessier et al. 1979; Bruder-

Hubscher et al. 2002; Fuentes et al. 2008). In fact, these oxides existed between the particles or formed coatings on mineral surfaces. They are thermodynamically unstable in anoxic conditions and their reactivity depends on the degree of crystallinity (Cornu and Cloze 2000). The little increase of extractability of Ca in F3 after carbonation (10% for WPFA0 and 15% for WPFA90) maybe due to the formation of new phases such as ettringite $Ca_6Al_2(SO_4)_3(OH)_{12};26H_2O$ which is coherent with the results of XRD (Figure.6). About 4% of Ca was extracted from residual fraction F4 due to the presence of larnite (Ca_2SiO_4) which was also identified by XRD results in WPFA30 and WPFA90.

Silicium was extracted by the reducible F2 (17%) and the oxidizable fractions F3 (>80%). Si is bound to Iron/Mn oxyhydroxides and to sulfides. Only <1% of Si was found in the residual fraction F4. This indicated that the aqua regia was not efficient to dissolve the silicates phases (crystalline forms).

Iron was extracted with the highest percentage in the residual fraction F4 (>80%) in WPFA0, WPFA30 and WPFA90 which indicated that the Si is bound to silicate phases. The low amount of iron extracted from the reducible fraction indicated the low presence of iron oxyhydroxides.

On the other hands, *manganese* was extracted rather in the reducible fraction F2 with 61%, 52% and 48% in WPFA0, WPFA30 and WPFA90 respectively. The presence in F2 indicated that the Mn was presented as Mn oxyhydroxides (Gu et al. 2017; Gonzalez et al. 2019). Non-negligible amount was extracted in F4 before and after carbonation meaning that Mn is presented in crystalline forms.

The carbonation treatment has a milder effect on the speciation of *Aluminium*. In fact, the dominant fraction of Al was associated with the residual fraction F4 before (84%) and after treatment (61% in WPFA90) which means that, the Al is presented as alumina-silicate phases such as gehlenite (see. Figure.6). After carbonation, the extractability of Al was increased in F3 from 16% for WPFA0 to 38% for WPFA90. This indicated that the Al maybe presented as Al oxides and be bounded to sulfides. The formation of ettringite can explain this phenomenon.

For *sodium* and *potassium*, the most extractability fraction was F1 in WPFA0 which can be explained by their presence as soluble salts such as halite NaCl and sylvite KCl (Guerin 2000) and also maybe bounded to carbonates such as Na_2CO_3 and K_2CO_3. After carbonation, a significant decrease of Na and K amount in F1 compared to WPFA0 due to the leaching of these elements in percolation water. The extractability fraction of these elements in WPFA30 and WPFA90 due to the formation of Na/K-carbonates phases. The carbonation treatment also promotes the formation of crystalline phases such as Na/K-silicates phases.

Sulphur, most of S was extracted in F2 with 82% in WPFA0. 12% and 6% were extracted in F3 and F4 respectively. After carbonation, the distribution of S was remarkably changed especially in F1 and F2, 40% of S was extracted in F1 in WPFA90 after carbonation which may be due to the dissolution of ettringite, anhydrite $CaSO_4$ (Guerin 2000; Rendek 2006).

Magnesium was extracted in F3, F4 with the highest amount of 63% in F2 in WPFA0. After carbonation, no remarkable difference in the distribution of Mg was seen in F2 (35%), F3 (25%) and F4 (39%) in WPFA90. This indicated that the Mg can be presented such as Mg oxides, MgS ang Mg-silicates.

Phosphorus was mainly extracted by residual fraction F4 (95%) in WPFA0. This indicated that most of P was included in crystalline forms bound to silicates. After carbonation, P was extracted in F1 (40%) water exchangeable/acido-soluble fraction, F3 (18%) and F4 (83%). This indicated that the carbonation promotes the formations of new phases such as Whitlockite $Ca_9MgFe(PO_4)_6PO_3OH$. $KCaPO_4$ (Gunning 2011a), phases that are bound to carbonates such as $MgCaCO_3$ (Gunning 2011a) and sulfides, which control the leaching of P in WPFA90.

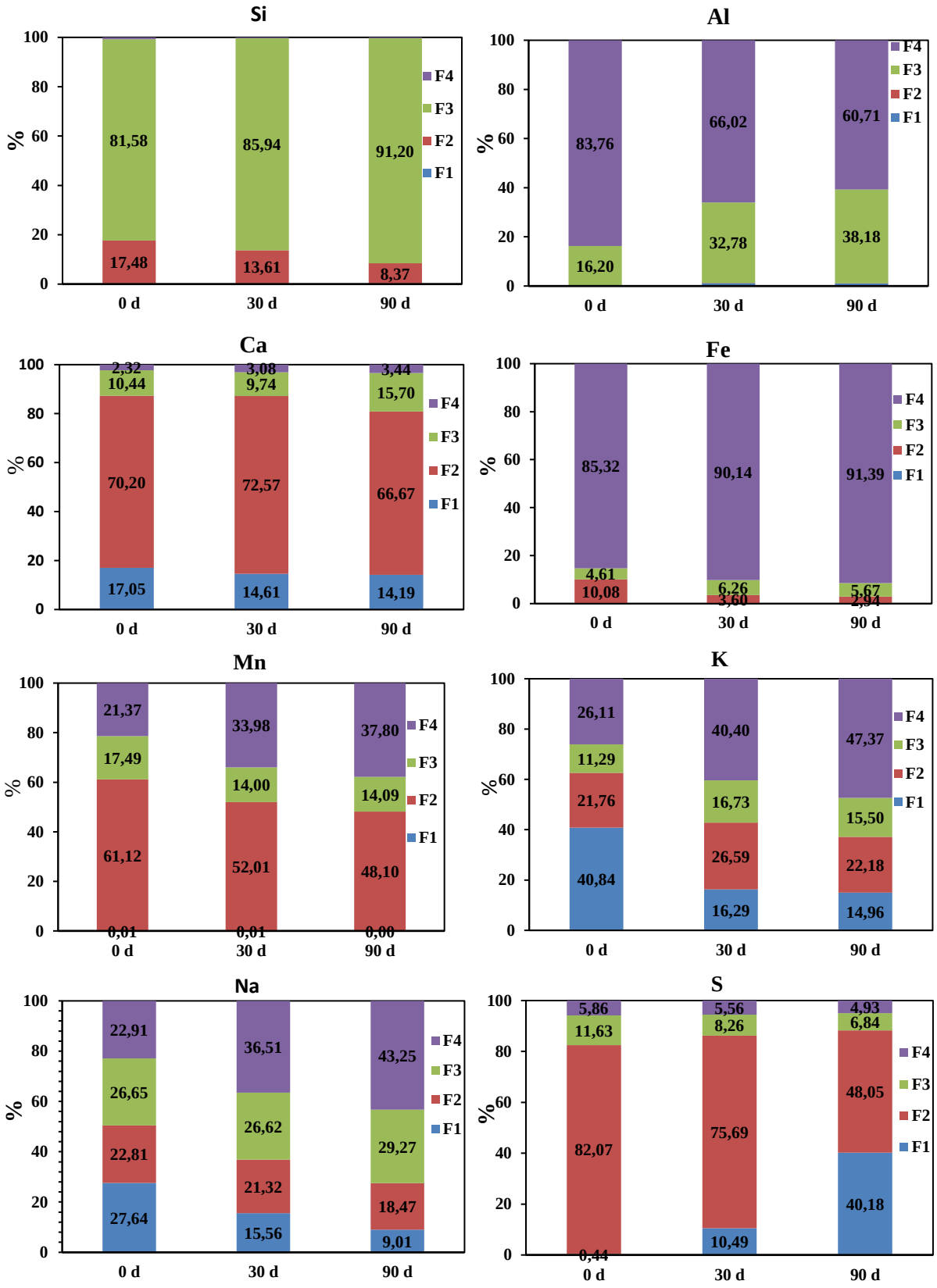
Si
100
80
60
40
20
0
%
81,58
17,48
85,94
13,61
91,20
8,37
0 d
30 d
90 d
F4
F3
F2
F1
Al
83,76
16,20
66,02
32,78
60,71
38,18
Ca
2,32
10,44
70,20
17,05
3,08
9,74
72,57
14,61
3,44
15,70
66,67
14,19
Fe
85,32
4,61
10,08
90,14
6,26
3,60
91,39
5,67
2,94
Mn
21,37
17,49
61,12
0,01
33,98
14,00
52,01
0,01
37,80
14,09
48,10
0,00
K
26,11
11,29
21,76
40,84
40,40
16,73
26,59
16,29
47,37
15,50
22,18
14,96
Na
22,91
26,65
22,81
27,64
36,51
26,62
21,32
15,56
43,25
29,27
18,47
9,01
S
5,86
11,63
82,07
0,44
5,56
8,26
75,69
10,49
4,93
6,84
48,05
40,18

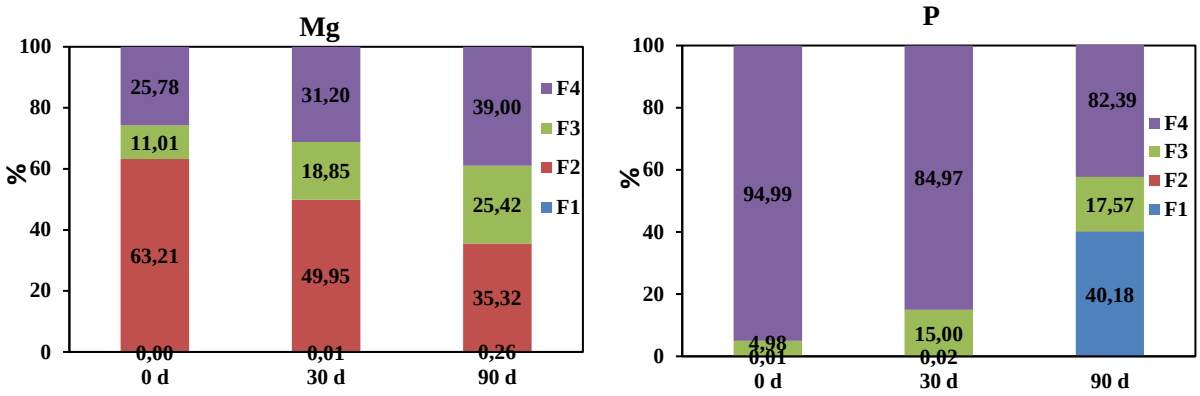

Figure 8. Percentage of MEs extracted fraction in WPFA0, WPFA30 and WPFA90 samples. F1-acido-soluble fraction; F2-reductible fraction; F3-oxidizable fraction; F4-residual fraction

3.7.2 Sequential extraction of MTEs

Figure.9 presented the speciation of different MTE in WPFA0, WPFA30 and WPFA90. There was clear that the carbonation treatment weakened affected the speciation of some elements in WPFA samples such as As, Cd, Ni and Se.

Barium, the F1-F4 ratios of Ba in WPFA0 was 18%, 7%, 26% and 79% respectively. This indicated that the Ba was principally included in crystalline minerals or within crystalline oxides (F4) and to sulfides as BaS or $BaSO_4$ (F3) and/or bound to organic matter. In fact, $BaSO_4$ was detected by SEM-EDS (see Figure. 7(b)). A little amount is bound to carbonates ($BaCO_3$) and also bound to the surfaces of solid by pH-dependent bounds which explains the leaching of Ba at natural pH. In fact, according to the results of ANC, an increase of released quantity of Ba in WPFA0 was seen at pH 12.7 (pH of F1). After carbonation, Ba was extracted from reducible fraction F2 in WPFA30 and WPFA90 rather than WPFA0. This indicated that the carbonation promotes the bounding to Mn/Fe-oxyhydroxides. The F1 ratio of Ba was not detected (0.5%) which explained the no leaching of Ba occurred according to leaching test 12457-2. In fact, the metals separating in F1 are thought to be the most labile and pose a greater risk to the environment (Jain 2004; Gu et al. 2017).

Chromium, the F2-F4 ratios of Cr in WPFA0 was 77%, 10% and 13% respectively. This indicated that the Cr was principally bound to Fe/Mn-oxyhydroxides or as Chromium oxides. Cr was not detected in F1 which can explain the very low leaching quantity of Cr (below the QL) in WPFA0 according to the leaching test 12457-2. In fact, the fraction F1 includes metals absorbed at the surface of solids by weak electrostatic interactions, metals which can be released by ion exchange processes (elements that are easily leachable) as well as metals precipitated and co-precipitated with carbonates (Nurmesniemi et al. 2008; Yao et al. 2013)**.** In the case of Cr, as the carbonation time further increased from 30 d to 90 d (Table 3), the F1 ratios increased to 6% and 14% respectively in WPFA30 and WPFA90. This indicates that the carbonation promotes the leaching of Cr by the formation of existing forms, which are easily leached such as Cr-Ettringite.

Molybdenu, the proportion of the acid-soluble fraction of Mo increased from 4% to 21% in WPFA0 and WPFA90 respectively indicating that the carbonation promotes the existing forms of Mo which were easily leached in a weak acidic environment (Tong et al. 2020). However, the residual fraction of Mo decreased with the carbonation time from 82% to 56% and 59% for WPFA0, WPFA30 and WPFA90 respectively. This result can be explained by the increase of Mo leaching from 0.08 mg/kg (<QL) in WPFA0 to 0.43±0.12 mg/kg and 0.48±0.1 mg/kg in WPFA30 and WPFA90 respectively.

Antimony, most of Sb is presented in the residual fraction before (95%) and after carbonation (89% and 88% for WPFA30 and WPFA90). This indicated that the Sb could be bound to silicate phases. The

proportion of acid-soluble fraction of Sb increased from 0.5% to 3% in WPFA0 and WPFA90 respectively which indicating that the carbonation promotes the absorption of Sb at the surface of solids by weak electrostatic interactions, thus increased the leaching of Sb from 0.057 mg/kg (<QL) to 0.06±0.01 mg/kg in WPFA90 according to the leaching test 12457-2.

Lead, the F1-F4 ratios of Pb in WPFA0 was 1%, 9%, 55% and 35%. Most of Pb was bound to sulfides and/or organic matter in oxidizing conditions and to alumina-silicates in residual fraction (Piredda 2011). In fact, the LOI in WPFA0 was 5.6% that indicated the presence of organic matter. After carbonation, Pb was detected only in F3 and F4 with an increase of the F4 ratio (66%) in WPFA90 and decrease of F3 ratio (33%) in WPFA90. The carbonation promotes the encapsulation of Pb in the silicate phases, which reduced its leaching. On the other hand, carbonation contributed to the formation of $PbCO_3$ (Gunning 2011b) (Schwartz and Ploethner 2000; Ecke 2003; Jianguo et al. 2009; Ni et al. 2017) which was not detected in F1 because the pH of F1 was not sufficient to dissolve the precipitation of $PbCO_3$.

Zinc was extracted principally in F2 (63%) in WPFA0 which indicated that the Zn is bound to Iron/Manganese-oxyhydroxides and/or presented as ZnO or $Zn(OH)_2$ (see Figure.7(g)). The proportion of F3 was increased from 20% to 31% and 32% in WPFA0, WPFA30 and WPFA90 respectively. This indicated that the Zn was bounded to sulfides (ZnS) and/or organic matter (Gunning 2011a)-(Yao et al. 2013). The proportion of residual fraction of Zn increased from 16% to 29% in WPFA0 and WPFA90 respectively which indicated that the Zn was encapsulated in the solid matrix or bounded by silicate phases and not available to be leached (Tong et al. 2020).

It is important to note that a series of isomorphous substitution can be formed through the isomorphism replacement, thus reducing the leaching amount of MMTE after carbonation(Lu et al. 2009; Lu et al. 2009; Zheng et al. 2016; Ni et al. 2017). On the other hand, the leaching concentrations could probably be reduced by sorption onto calcite $CaCO_3$, leading to coprecipitation (Ecke et al. 2003; Zhao et al. 2017; Ni et al. 2017).

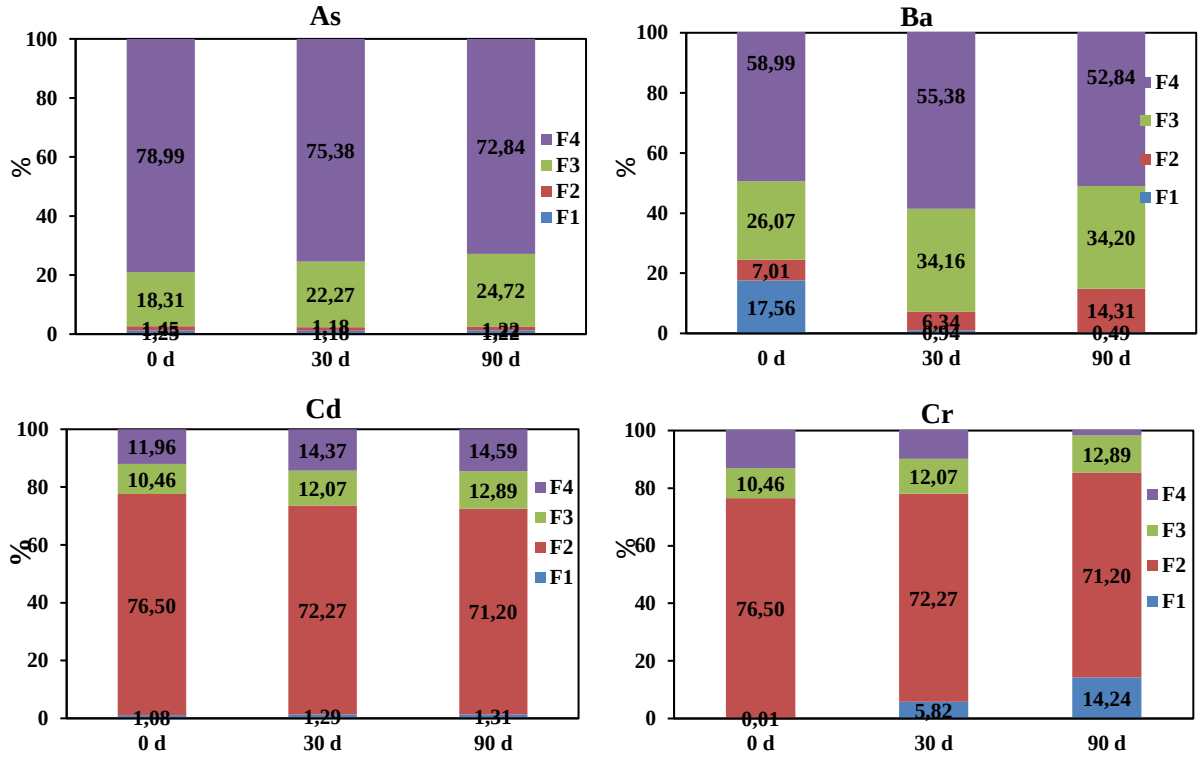

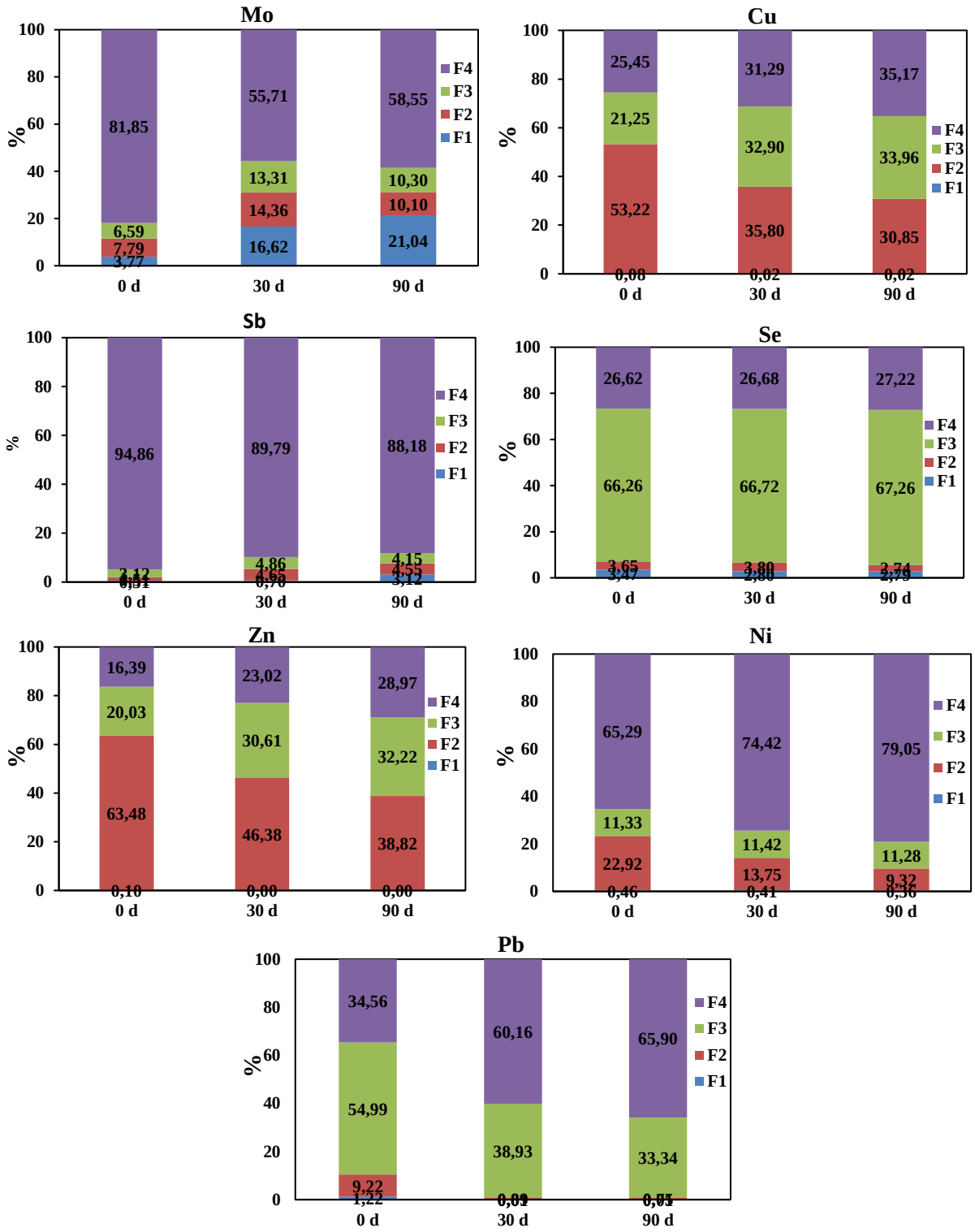

Figure.9 Percentage of extracted fraction of MTEs in WPFA0, WPFA30 and WPFA90 samples. F1-acido-soluble fraction; F2-reductible fraction; F3-oxidizable fraction; F4-residual fraction

3.8. Acid neutralizing capacity (ANC) analysis

3.8.1. Buffering reactions

The evolution of experimental pH of WPFA before and after natural carbonation at 30 and 90 days is shown in Figure.10. Results showed discrepancies at different pH of standard and carbonated WPFA while a general

agreement between the results of carbonated WPFA was observed as a function of acid addition expected from pH 8 to 5 and from 3 to 1. The ANC total, which corresponds to silicates, carbonates and (hydro)oxides, of standard fly ash was about 24 equi H^+/kg while it was about 19 and 18 equi H^+/kg for WPFA30 and WPFA90 respectively. On the other hand, to reach the pH 7.5 ($ANC_{7.5}$) which corresponds to the consumption of hydroxides (OH^-), carbonates (CO_3^{2-}) and soluble basic silicate hydrates (Johnson et al. 1995), the amount of acid adding decreases progressively with the carbonation times from 16 to 9 and 6.5 Equi H^+/kg at 0, 30 and 90 days respectively.

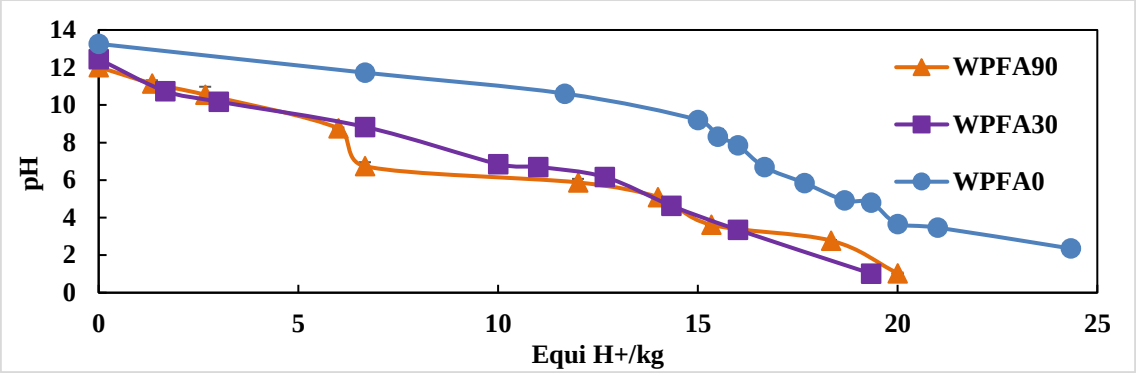

Figure.10 Evolution of WPFA pH before and after natural carbonation at 30 and 90 days from ANC test as function of acid (H+) adding. (L/S =10 L.kg-1, contact time = 48 h)

This indicated that the carbonation lowers the initial buffering capacity of the WPFA30 and WPFA90 relative to the WPFA0. The buffering capacity of WPFA90 is lower than WPFA30. In fact, the mineral assemblage in WPFA0 contained a higher quantity of phases that are responsible for buffering reactions in basic pH (pH >7.5) such as lime CaO and calcium hydroxide $Ca(OH)_2$ than WPFA30 and WPFA90. On the other hand, the quantity of acid which is needed to reduce the pH from 7.5 to 2, it was more important in WPFA90 > WPFA30 > WPFA0. This is indicated that the presence of calcite ($pH_{solubility}$ < 6) is higher in WPFA90 than WPFA30 and WPFA0. For pH below 7, the consummation of acid corresponds to the increase of major ions leaching such as Al, Fe, Si and Ca due to the dissolution of phases containing these elements (Figure.10) (Yan et al. 1998; Yan et al. 1998; Dijkstra et al. 2006).

The natural pH (without adding acid) of WPFA0 (13.5) decreases with the days of carbonation to attend 12.45 and 12.02 for WPFA30 and WPFA90 respectively. This phenomenon can be explained by the gradual consumption of lime CaO and portlandite $Ca(OH)_2$ to form ettringite, carbonated phases such as calcite ($CaCO_3$) and basic hydrated compounds (Meima and Comans 1997; Meima and Comans 1998; Polettini and Pomi 2004; Yao et al. 2010; Luo et al. 2019). These results are similar to those obtained with XRD and TG-DTA which showed that the quantity of CaO and $Ca(OH)_2$ decreased with the carbonation times while the quantity of carbonates increased. SEM-EDS also showed an important presence of calcite in WPFA90 than WPFA0 (Figure.7).

3.8.2. Leaching behavior of MMTE as a function of pH

The ANC results in Figure.10 and Figure.11 can be used to understand the mechanisms that control the leaching behavior of MTEs. At pH natural, all elements do not exceed the inert thresholds (IT) except for Ba and Pb. The leaching concentration of Ba (178±6 mg/kg) and Pb (7.35±0.6mg/kg) decreased markedly below the IT after carbonation to attend 0.15±0.05 mg/kg and 0.03±0.01 mg/kg in WPFA90 for Ba and Pb respectively. All MMTE and metalloids appear to follow the solubility curve of the WPFA0 after carbonation for all values of pH except for Ba and Pb at pH>10. Most of these elements, their leach is considerably only at pH<6. This is the case of As, Cd, Cu. Ni, Se and Zn. Santos et al,. (Santos et al. 2013) obtained the same results. This indicated that the leaching mechanism is dominated by the reduction of Basicity. In fact, their speciation was not significantly changed. These results are confirmed by those obtained by the sequential extraction (Figure.9).

Barium, there is a clear shift on the curve of WPFA30 and WPFA90 compared to WPFA0. For pH >10, its leaching concentration increased in WPFA0 while in WPFA30 and WPFA90, it decreased. This indicated that the $BaCO_3$ controlled the leaching of Ba in carbonated samples (Gunning 2011a; Santos et al. 2013) and $BaSO_4$ controlled the Ba leaching in WPFA0. For pH <10, the barium leaching is independent of pH. According to the results of sequential extraction and SEM-EDS, $BaSO_4$ and $BaCO_3$ controlled the behavior of Ba leaching (Figure.7 and Figure.9).

Chromium, the leaching behavior follows the curve of WPFA0 for WPFA30 and WPFA90 for all pH values, but the Cr leaching was more important in WPFA30 and WPFA90 than WPFA0. According to sequential extraction, Cr was presented an acido-soluble fraction (14%) in WPFA90 while it was not the case of WPFA0. On the other hand, the carbonation affects the speciation of Cr by reducing its presence in reducible fraction F2 in WPFA30 (5%) and WPFA90 (3%) compared to WPFA0 (7%). The higher leaching of Cr in treated samples than standard samples can be explained by the presence of more soluble form of chromium such as Cr(VI) unstable form than Cr(III) stable form. In fact, CrO_4^{2-} can substitute SO_4^{2-} in Ettringite (phase detected in WPFA30 and WPFA90) then in a lower pH, these phases are soluble and release chromates in solution (Piredda 2011; Blanc et al. 2018). These results are contrary to that obtained by Nilssonet all. (Nilsson et al. 2016), Rendek et al. (Rendek et al. 2006b) and Santos et al. (Santos et al. 2013) but are similar to those obtained by Peter (Gunning 2011a) and Piredda (Piredda 2011).

Lead, a strong correlation between the curves of Pb for all values of pH before and after carbonation except at natural pH. The curve showed that Pb is an amphoteric element. The concentration of Pb in WPFA0 was much higher than the inert thresholds (7.35±0.6 mg/kg) while after carbonation, Pb leaching was reduced by more than one hundred orders of magnitude and was 0.03±0.01 mg/kg in WPFA90 and below the quantify limit in WPFA30. The reduction of lead leaching can be explained by the encapsulation of Pb in the silicate phases according to sequential extraction (Figure.9) and to the formation of the lead carbonate (van Zomeren and Comans 2004). The leaching concentration, in all samples, was very low and below the inert thresholds for pH>6 while the leaching increased substantially for pH below 6 and exceeded the inert threshold.

Molybdenum, the leaching concentration of Mo was below the inert threshold 0.08±0.02, 0.43±0.12 and 0.48±0.1 mg/kg at natural pH for WPFA0, WPFA30 and WPFA90 respectively. The increased leaching of Mo can be explained by a possible replacement of SO_4^{2-} in the mineral by oxyanions such as MoO_4^{2-}. Piredda (Piredda 2011) obtained the same results. When the acid was added, the concentration of Mo in standard and treated samples increased significantly and exceeded the inert threshold for a pH between 11 and 6. The leaching concentration was maximum in this region of the pH to reach a value of 0.7±0.11 mg/kg for WPFA0, 0.9±0.15 mg/kg for WPFA30 and 0.7±0.09 mg/kg for WPFA90 at pH 8.3, 8.8 and 10.6 respectively. These values have increased by more than 7.2 and 1.5 orders of magnitude from the pH natural for WPFA0, WPFA30 and WPFA90 respectively. For pH<6, the leaching concentration of Mo reduced substantially to reach a value below the quantify limit in the three cases of WPFA. Under extreme acidic conditions (pH<2.5), the leaching of Mo is favored again and exceeds the inert threshold to reach 0.69±0.08 mg/kg for WPFA90. From the point of view of treatment of WPFA, the carbonation did not reduce the leaching concentration of Mo. On the other hand, under extreme basic conditions (pH>11.5) or pH between 6.5-2.5, the leaching concentration of Mo was the weakest and below the IT.

Copper, the leaching concentration of Cu decreased lightly in natural pH of WPFA30 (0.049±0.01 mg/kg) and WPFA90 (0.03±0.01 mg/kg) compared to WPFA0 (0.09±0.02 mg/kg). This can be explained by the retention mechanism of calcite for Cu (Gunning 2011a). The formation of calcite was detected by TG-DTA (Figure.5), XRD (Fi.6) and SEM-EDS (Figure.7). For pH lower 7, the

concentration leaching of Cu in WPFA30 and WPFA90 increased substantially from WPFA0 (Figure.11). According to the results of sequential extraction, the carbonation affects the repartition of Cu. In fact, Cu has more presence in oxidizable fraction and residual fraction in WPFA30 and WPFA90 than WPFA0. This can also be explained by the reduction of leaching of Cu in WPFA30 and WPFA90 at natural pH, Piredda (Piredda 2011) obtained the same results.

Antimony, a strong correlation between the curves of standard and treated WPFA in function of pH. No noticeable change was identified in the leaching concentration of Sb before and after carbonation. This indicated that the treatment had no effect on the mineral phases of Sb and it did not control the leaching behavior of Sb. For natural pH, the leaching concentration was below the IT (0.06±0.01 mg/kg) and QL (0.057 mg/kg) for WPFA0, WPFA30 and WPFA90. For pH<10.6, the leaching concentration of Sb in three WPFA increased and exceeded the IT to reach maximum values of leaching at pH 6.7 with 0.33±0.04 mg/kg, 0.52±0.05 mg/kg and 0.50±0.04 mg/kg for WPFA0. WPFA30 and WPFA90 respectively. A new significantly increasing leaching concentration of Sb was observed for pH below 3 in the case of standard and treated WPFA. The behavior of Sb for pH can be attributed to the dissolution of mineral phases that have a good sorption affinity for Sb like portlandite and ettringite (Cornelis et al. 2006; Gunning 2011a; Santos et al. 2013).

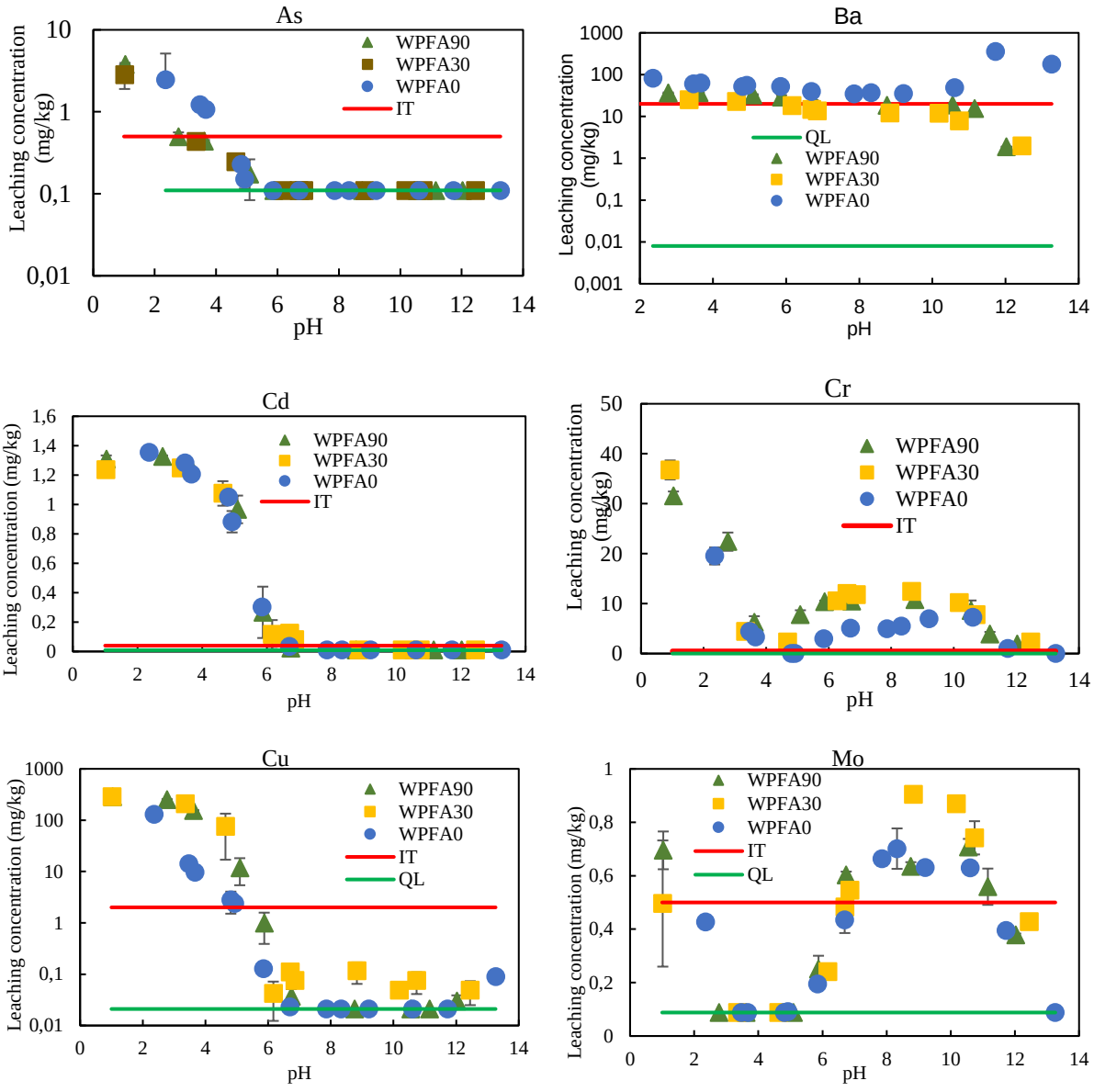

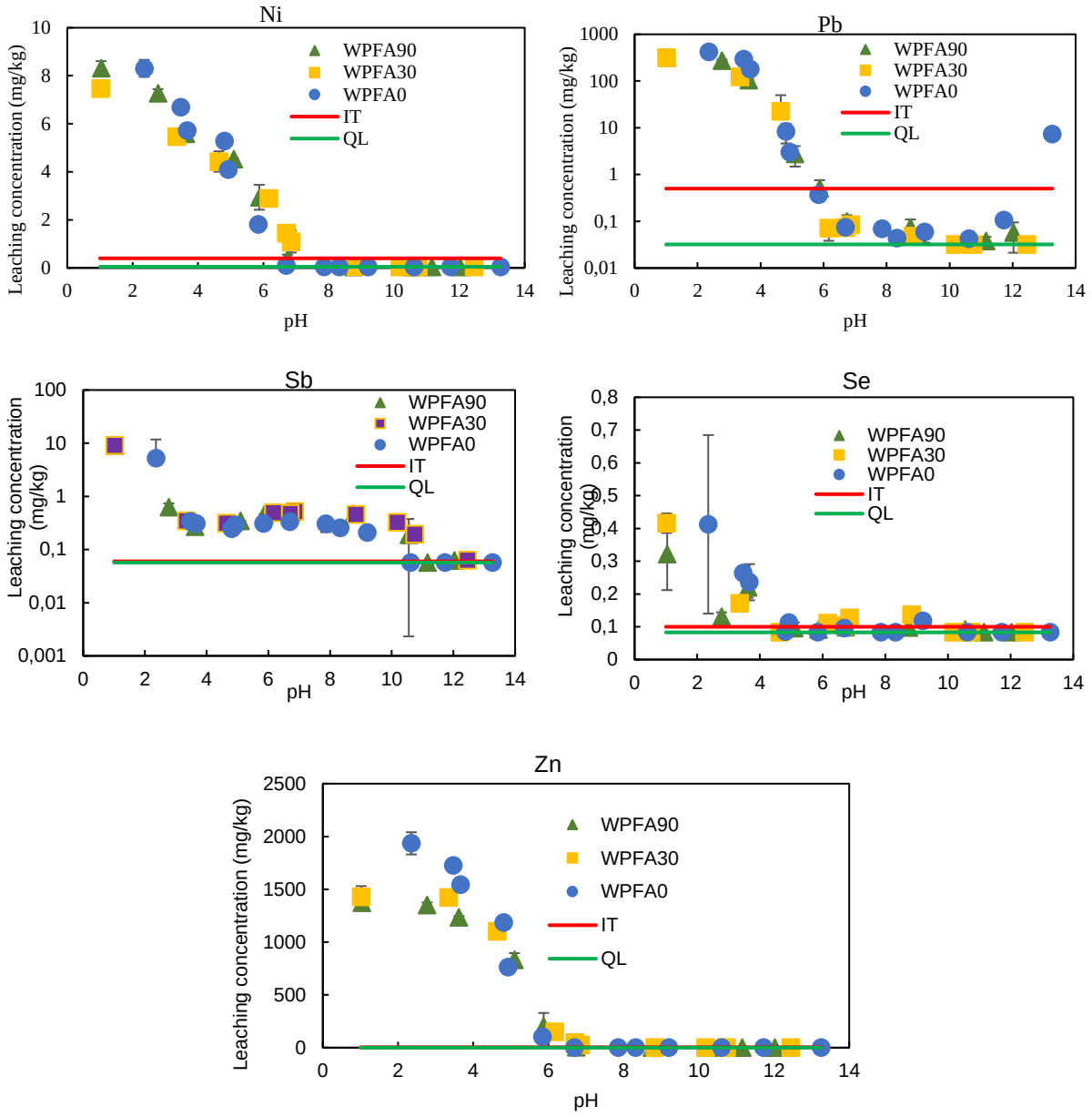

Figure 11. MTEs solubility as a function of pH (L/S ratio. 10 L.kg-1) of WPFA0, WPFA30 and WPFA90; IT: Inert thresholds. QL: Quantify limit.

4. Pilot scale application of natural carbonation

The natural carbonation allows to obtain an alternative material in accordance with the environmental requirements of the SETRA guide (2011) for a use in road technique. However, the application of the elaboration technology via natural carbonation on an industrial scale will require a humidification step allowing the lime hydration, a regular and frequent homogenization step (for a perfect hydration of the lime and a more efficient mixing with the atmospheric CO_2) and a time of exposure to the open air to allow a natural carbonation of the ash (minimum one week).

On the valorization platform, it will be essential to put in place the storage cells allowing regular mechanical turning of the ash piles, the percolation water generated must be collected by a drainage system at the bottom of the cell and treated before discharge into the collective network or the natural environment. Thus, the powdery nature of the ashes will require a protection of the cells against the flight of the fine particles.

5. Conclusion

This investigation constitutes a mineralogical approach to understand the phenomenology of carbonation and to consider the valorization of WPFA from thermal power plants in different engineering sector. The study systematically examined the effects of carbonation on the leaching of MMTE, in particular the leaching of Ba, Pb and Cl, compositional changes, phase content, pH, chemical speciation and acid neutralization capacity. The main findings are as follows:

- Experiments in real conditions demonstrate the feasibility of Ba and Pb stabilization by natural carbonation. Based on the demobilization of MMTE, the optimum final pH of the WPFA after 90 days of carbonation was 11.4.
- The XRD and SEM/EDS analyses revealed the disappearance of lime/portlandite and the formation of hydration products, including Ettringite, carboaluminates and carbonation products, including $CaCO_3$ and $BaCO_3$, which caused immobilization of Ba and Pb in the WPFA subjected to natural carbonation.
- The TG analyses revealed the consumption of portlandite and the formation of hydration products, aragonite, vaterite and calcite ($CaCO_3$) as carbonation proceeds.
- The results of the BCR analysis revealed that the carbonated WPFA possessed higher values of residual fraction (F4) of Ba and Pb than those standard conditions (without carbonation). In addition, the values of soluble fraction decreased and the values of exchangeable fraction (F1) increased in Ba and Pb after the carbonation.

References

AFNOR (2000a) NF ISO 13320-1, Laser diffraction methods

AFNOR (2006) NF EN ISO 18757, Determination of specific surface area pf ceramic powders by gas adsorption using the BET method

AFNOR (2009) NF EN 15326, Measurement of density and specific gravity

AFNOR (2000b) NF EN 12879, Characterization of sludges

AFNOR (2002) NF EN 12457-2, Leaching-Compliance test for leaching of granular wasre materials ans sludges

AFNOR (2015) NF EN 14429, Characterization of waste-leaching behaviour test-influence of pH on leaching with initial acid/base addition

Bai J, Chaipanich A, Kinuthia JM, O'Farrell M, Sabir BB, Wild S, Lewis MH (2003) Compressive strength and hydration of wastepaper sludge ash–ground granulated blastfurnace slag blended pastes. Cement and Concrete Research 33(8):1189–1202. https://doi.org/10.1016/S0008-8846(03)00042-5

Baranger P, Azaroual M, Freyssinet P, Lanini S, Piantone P (2002) Weathering of a MSW bottom ash heap: a modelling approach. Waste Management 22(2):173–179. https://doi.org/10.1016/S0956-053X(01)00066-6

Blanc D, Gonzalez L, Lupsea-Toader M, de Brauer C (2018) Mineralogical Evolution and Leaching Behaviour of a Heap of Bottom Ash as a Function of Time: Influence on Its Valorization. Waste Biomass Valor 9(12):2517–2527. https://doi.org/10.1007/s12649-018-0444-1

Bodénan F, Deniard P (2003) Characterization of flue gas cleaning residues from European solid waste incinerators: assessment of various Ca-based sorbent processes. Chemosphere 51(5):335–347. https://doi.org/10.1016/S0045-6535(02)00838-X

Bouzar B, Mamindy-Pajany Y (2022) Manufacture and characterization of carbonated lightweight aggregates from waste paper fly ash. Powder Technology :117583. https://doi.org/10.1016/j.powtec.2022.117583

Bruder-Hubscher V, Lagarde F, Leroy MJF, Coughanowr C, Enguehard F (2002) Application of a sequential extraction procedure to study the release of elements from municipal solid waste incineration bottom ash. Analytica Chimica Acta 451(2):285–295. https://doi.org/10.1016/S0003-2670(01)01403-9

Chabannes M, Garcia-Diaz E, Clerc L, Bénézet J-C (2015) Studying the hardening and mechanical performances of rice husk and hemp-based building materials cured under natural and accelerated carbonation. Construction and Building Materials 94:105–115. https://doi.org/10.1016/j.conbuildmat.2015.06.032

Chimenos JM, Fernández AI, Miralles L, Segarra M, Espiell F (2003) Short-term natural weathering of MSWI bottom ash as a function of particle size. Waste Management 23(10):887–895. https://doi.org/10.1016/S0956-053X(03)00074-6

Cornelis G, Van Gerven T, Vandecasteele C (2006) Antimony leaching from uncarbonated and carbonated MSWI bottom ash. Journal of Hazardous Materials 137(3):1284–1292. https://doi.org/10.1016/j.jhazmat.2006.04.048

Cornu S, Cloze B (2000) A critical review on sequential extraction and trace metal speciation in natural soils. Etude et Gestion des Sols (France)

Costa G, Baciocchi R, Polettini A, Pomi R, Hills CD, Carey PJ (2007) Current status and perspectives of accelerated carbonation processes on municipal waste combustion residues. Environ Monit Assess 135(1):55–75. https://doi.org/10.1007/s10661-007-9704-4

Diamond. S (1981) Proc. Of the 8th Int. Congress on the Chemistry of Cement

Dijkstra JJ, Van der Sloot HA, Comans RN (2006) The leaching of major and trace elements from MSWI bottom ash as a function of pH and time. Applied geochemistry 21(2):335–351

Drouet E (2010) Impact de la température sur la carbonatation des matériaux cimentaires: prise en compte des transferts hydriques. PhD Thesis, École normale supérieure de Cachan-ENS Cachan

Ecke H (2003) Sequestration of metals in carbonated municipal solid waste incineration (MSWI) fly ash. Waste Management 23(7):631–640. https://doi.org/10.1016/S0956-053X(03)00095-3

Ecke H, Menad N, Lagerkvist A (2003) Carbonation of Municipal Solid Waste Incineration Fly Ash and the Impact on Metal Mobility. Journal of Environmental Engineering 129(5):435–440. https://doi.org/10.1061/(ASCE)0733-9372(2003)129:5(435)

Fernández Bertos M, Simons SJR, Hills CD, Carey PJ (2004) A review of accelerated carbonation technology in the treatment of cement-based materials and sequestration of CO2. Journal of Hazardous Materials 112(3):193–205. https://doi.org/10.1016/j.jhazmat.2004.04.019

Frías M, García R, Vigil R, Ferreiro S (2008) Calcination of art paper sludge waste for the use as a supplementary cementing material. Applied Clay Science 42(1):189–193. https://doi.org/10.1016/j.clay.2008.01.013

Fuentes A, Lloréns M, Sáez J, Isabel Aguilar M, Ortuño JF, Meseguer VF (2008) Comparative study of six different sludges by sequential speciation of heavy metals. Bioresource Technology 99(3):517–525. https://doi.org/10.1016/j.biortech.2007.01.025

García R, Vigil de la Villa R, Vegas I, Frías M, Sánchez de Rojas MI (2008) The pozzolanic properties of paper sludge waste. Construction and Building Materials 22(7):1484–1490. https://doi.org/10.1016/j.conbuildmat.2007.03.033

Gonzalez ML, Blanc D, de Brauer C (2019) Multi-Analytical Approach and Geochemical Modeling for Mineral Trace Element Speciation in MSWI Bottom-Ash. Waste Biomass Valor 10(3):547–560. https://doi.org/10.1007/s12649-017-0075-y

Gu Z, Wu M, Li K, Ning P (2017) Variation of heavy metal speciation during the pyrolysis of sediment collected from the Dianchi Lake, China. Arabian Journal of Chemistry 10:S2196–S2204. https://doi.org/10.1016/j.arabjc.2013.07.053

Guerin L (2000) Devenir des polluants inorganiques contenus dans les résidus solides issus de la combustion des déchets ménagers. Spéciation et élaboration de tests de mobilité en vue de leur stockage ou de leur valorisation. PhD Thesis, These de doctorat, Universite de Toulon et du Var

Gunning PJ (2011a) Accelerated carbonation of hazardous wastes. PhD Thesis, University of Greenwich

Gunning PJ (2011b) Accelerated carbonation of hazardous wastes. PhD Thesis, University of Greenwich

Jain CK (2004) Metal fractionation study on bed sediments of River Yamuna, India. Water Research 38(3):569–578. https://doi.org/10.1016/j.watres.2003.10.042

Jianguo J, Maozhe C, Yan Z, Xin X (2009) Pb stabilization in fresh fly ash from municipal solid waste incinerator using accelerated carbonation technology. Journal of Hazardous Materials 161(2):1046–1051. https://doi.org/10.1016/j.jhazmat.2008.04.051

Johnson CA, Brandenberger S, Baccini P (1995) Acid neutralizing capacity of municipal waste incinerator bottom ash. Environmental science & technology 29(1):142–147

Komonweeraket K, Cetin B, Benson CH, Aydilek AH, Edil TB (2015) Leaching characteristics of toxic constituents from coal fly ash mixed soils under the influence of pH. Waste Management 38:174–184. https://doi.org/10.1016/j.wasman.2014.11.018

Li X, Bertos MF, Hills CD, Carey PJ, Simon S (2007) Accelerated carbonation of municipal solid waste incineration fly ashes. Waste management 27(9):1200–1206

Lu SG, Chen YY, Shan HD, Bai SQ (2009) Mineralogy and heavy metal leachability of magnetic fractions separated from some Chinese coal fly ashes. Journal of Hazardous Materials 169(1):246–255. https://doi.org/10.1016/j.jhazmat.2009.03.078

Luo H, Cheng Y, He D, Yang E-H (2019) Review of leaching behavior of municipal solid waste incineration (MSWI) ash. Science of The Total Environment 668:90–103. https://doi.org/10.1016/j.scitotenv.2019.03.004

M. PETITPAIN, (2016) Économie circulaire : Projet valorisation croisée de co-produits industriels. Accessed 5 May 2022

Manskinen K, Nurmesniemi H, Pöykiö R (2011) Total and extractable non-process elements in green liquor dregs from the chemical recovery circuit of a semi-chemical pulp mill. Chemical Engineering Journal 166(3):954–961. https://doi.org/10.1016/j.cej.2010.11.082

Meima JA, Comans RNJ (1999) The leaching of trace elements from municipal solid waste incinerator bottom ash at different stages of weathering. Applied Geochemistry 14(2):159–171. https://doi.org/10.1016/S0883-2927(98)00047-X

Meima JA, Comans RNJ (1997) Geochemical Modeling of Weathering Reactions in Municipal Solid Waste Incinerator Bottom Ash. Environ Sci Technol 31(5):1269–1276. https://doi.org/10.1021/es9603158

Meima JA, Comans RNJ (1998) Application of Surface Complexation/Precipitation Modeling to Contaminant Leaching from Weathered Municipal Solid Waste Incinerator Bottom Ash. Environ Sci Technol 32(5):688–693. https://doi.org/10.1021/es9701624

Meima JA, van der Weijden RD, Eighmy TT, Comans RNJ (2002) Carbonation processes in municipal solid waste incinerator bottom ash and their effect on the leaching of copper and molybdenum. Applied Geochemistry 17(12):1503–1513. https://doi.org/10.1016/S0883-2927(02)00015-X

Mkahal Z, Mamindy-Pajany Y, Maherzii W, Abriak N-E (2022) Recycling of Mineral Solid Wastes in Backfill Road Materials: Technical and Environmental Investigations. Waste Biomass Valor 13(1):667–687. https://doi.org/10.1007/s12649-021-01544-5

Mozaffari E, Kinuthia JM, Bai J, Wild S (2009) An investigation into the strength development of Wastepaper Sludge Ash blended with Ground Granulated Blastfurnace Slag. Cement and Concrete Research 39(10):942–949. https://doi.org/10.1016/j.cemconres.2009.07.001

Ni P, Xiong Z, Tian C, Li H, Zhao Y, Zhang J, Zheng C (2017) Influence of carbonation under oxy-fuel combustion flue gas on the leachability of heavy metals in MSWI fly ash. Waste Management 67:171–180. https://doi.org/10.1016/j.wasman.2017.05.023

Nilsson M, Andreas L, Lagerkvist A (2016) Effect of accelerated carbonation and zero valent iron on metal leaching from bottom ash. Waste Management 51:97–104. https://doi.org/10.1016/j.wasman.2015.12.028

Nurmesniemi H, Pöykiö R, Kuokkanen T, Rämö J (2008) Chemical sequential extraction of heavy metals and sulphur in bottom ash and in fly ash from a pulp and paper mill complex. Waste Manag Res 26(4):389–399. https://doi.org/10.1177/0734242X07079051

Pera J, Amrouz A (1998) Development of Highly Reactive Metakaolin from Paper Sludge. Advanced Cement Based Materials 7(2):49–56. https://doi.org/10.1016/S1065-7355(97)00016-3

Piredda M (2011) Stabilization of MSW combustion residues by accelerated carbonation treatment and their potential carbon dioxide sequestration

Polettini A, Pomi R (2004) The leaching behavior of incinerator bottom ash as affected by accelerated ageing. Journal of Hazardous Materials 113(1):209–215. https://doi.org/10.1016/j.jhazmat.2004.06.009

Rendek E (2006) Influence des procédés de la filière traitement thermique sur les caractéristiques et les évolutions bio-physico-chimiques des Mâchefers d'Incinération d'Ordures Ménagères (MIOM). PhD Thesis, Lyon, INSA

Rendek E, Ducom G, Germain P (2006a) Carbon dioxide sequestration in municipal solid waste incinerator (MSWI) bottom ash. Journal of Hazardous Materials 128(1):73–79. https://doi.org/10.1016/j.jhazmat.2005.07.033

Rendek E, Ducom G, Germain P (2006b) Carbon dioxide sequestration in municipal solid waste incinerator (MSWI) bottom ash. Journal of hazardous materials 128(1):73–79

Rodríguez O, Kacimi L, López-Delgado A, Frías M, Guerrero A (2013) Characterization of Algerian reservoir sludges for use as active additions in cement: New pozzolans for eco-cement manufacture. Construction and Building Materials 40:275–279. https://doi.org/10.1016/j.conbuildmat.2012.10.016

Santos RM, Mertens G, Salman M, Cizer Ö, Van Gerven T (2013) Comparative study of ageing, heat treatment and accelerated carbonation for stabilization of municipal solid waste incineration bottom ash in view of reducing regulated heavy metal/metalloid leaching. Journal of Environmental Management 128:807–821. https://doi.org/10.1016/j.jenvman.2013.06.033

Schwartz MO, Ploethner D (2000) Removal of heavy metals from mine water by carbonate precipitation in the Grootfontein-Omatako canal, Namibia. Environmental Geology 39(10):1117–1126. https://doi.org/10.1007/s002549900082

Segui P (2011) Elaboration de liants hydrauliques routiers à base de pouzzolane naturelle ou de cendre volante de papeterie. PhD Thesis, Université de Toulouse, Université Toulouse III-Paul Sabatier

Tessier A, Campbell PG, Bisson M (1979) Sequential extraction procedure for the speciation of particulate trace metals. Analytical chemistry 51(7):844–851

Todorovic J, Ecke H (2006) Demobilisation of critical contaminants in four typical waste-to-energy ashes by carbonation. Waste Management 26(4):430–441. https://doi.org/10.1016/j.wasman.2005.11.011

Tong L, He J, Wang F, Wang Y, Wang L, Tsang DCW, Hu Q, Hu B, Tang Y (2020) Evaluation of the BCR sequential extraction scheme for trace metal fractionation of alkaline municipal solid waste incineration fly ash. Chemosphere 249:126115. https://doi.org/10.1016/j.chemosphere.2020.126115

van Zomeren A, Comans RNJ (2004) Contribution of Natural Organic Matter to Copper Leaching from Municipal Solid Waste Incinerator Bottom Ash. Environ Sci Technol 38(14):3927–3932. https://doi.org/10.1021/es035266v

Vegas I, Urreta J, Frías M, García R (2009) Freeze–thaw resistance of blended cements containing calcined paper sludge. Construction and Building Materials 23(8):2862–2868

Yan J, Bäverman C, Moreno L, Neretnieks I (1998) Evaluation of the time-dependent neutralising behaviours of MSWI bottom ash and steel slag. Science of The Total Environment 216(1):41–54. https://doi.org/10.1016/S0048-9697(98)00133-8

Yang R, Liao W-P, Wu P-H (2012) Basic characteristics of leachate produced by various washing processes for MSWI ashes in Taiwan. Journal of Environmental Management 104:67–76. https://doi.org/10.1016/j.jenvman.2012.03.008

Yao J, Kong Q, Zhu H, Long Y, Shen D (2013) Content and fractionation of Cu, Zn and Cd in size fractionated municipal solid waste incineration bottom ash. Ecotoxicology and Environmental Safety 94:131–137. https://doi.org/10.1016/j.ecoenv.2013.05.014

Yao J, Li W-B, Tang M, Fang C-R, Feng H-J, Shen D-S (2010) Effect of weathering treatment on the fractionation and leaching behavior of copper in municipal solid waste incinerator bottom ash. Chemosphere 81(5):571–576. https://doi.org/10.1016/j.chemosphere.2010.08.038

Yao Z, Prabhakar AK, Cadiam Mohan B, Wang C-H (2022) An innovative accelerated carbonation process for treatment of incineration bottom ash and biogas upgrading. Waste Management 144:203–209. https://doi.org/10.1016/j.wasman.2022.03.033

Zhang P, Chen Z, Brown KG, Garrabrants AC, Delapp R, Meeussen JCL, van der Sloot HA, Kosson DS (2022) Impact of carbonation on leaching of constituents from a cementitious waste form for treatment of low activity waste at the DOE Hanford site. Waste Management 144:431–444. https://doi.org/10.1016/j.wasman.2022.04.009

Zhao S, Chen Z, Shen J, Kang J, Zhang J, Shen Y (2017) Leaching mechanisms of constituents from fly ash under the influence of humic acid. Journal of Hazardous Materials 321:647–660. https://doi.org/10.1016/j.jhazmat.2016.09.054

Zheng L, Wang W, Gao X (2016) Solidification and immobilization of MSWI fly ash through aluminate geopolymerization: Based on partial charge model analysis. Waste Management 58:270–279. https://doi.org/10.1016/j.wasman.2016.08.019

(2014) Coussy S. Bodénan. F. Claret. F. (2014) – Faisabilité de la stabilization physico-chimique des terres excavées dans la perspective d'un stockage en Installation de Stockage de Déchets Inertes ISDI). Rapport final. BRGM/RP-63698-FR. Accessed 9 May 2022

Chapter 3:

Manufacture and characterization of carbonated lightweight aggregates from waste paper fly ash

Powder Technology 406 (2022) 117583

Contents lists available at ScienceDirect

Powder Technology

journal homepage: www.journals.elsevier.com/powder-technology

Manufacture and characterization of carbonated lightweight aggregates from waste paper fly ash

Bader Bouzar [a,b,*], Yannick Mamindy-Pajany [a,b]

[a] IMT Nord Europe, Institut Mines-Télécom, Centre for Materials and Processes, Environnement, F-59000 Lille, France
[b] Univ. Lille, Univ., ULR 4515 – LGCgE, Laboratoire de Génie Civil et géo-Environnement, F-59000 Lille, France

HIGHLIGHTS

- LWA was manufactured from WPA without any agglomerating agents.
- The physical-chemical properties of LWA were improved after carbonation.
- The resulted LWA meet the requirements of NF EN -13,055-1.
- The microstructure of LWA was studied before and after carbonation.
- Influence of time, mode and rotation speed on the size of the manufactured LWA.

GRAPHICAL ABSTRACT

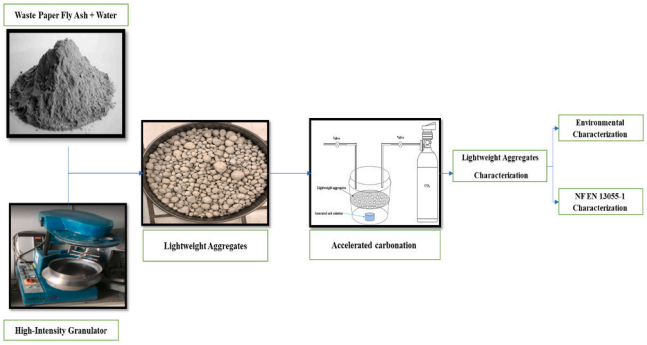

ARTICLE INFO

Keywords:
Waste paper fly ash
Accelerated carbonation
Lightweight aggregates
Stabilization
Metallic and metalloids trace elements

ABSTRACT

The combustion of biomass and waste paper sludge in a fluidized bed is ecologically profitable. However, a large amount of by-product with high hydraulic reactivity is produced and is considered as wastes. Most of the time the waste paper fly ash (WPFA) goes to landfills, therefore new utilization methods are necessary. In some countries, the high content of metallic and metalloids trace elements (MMTE) in WPFA, more specifically Barium (Ba) and Lead (Pb) makes its valorization difficult. In this paper, the Lightweight Aggregates (LWA) was produced from WPFA by granulating with water in high-intensity granulator. Since WPFA is rich in CaO, the addition of water promotes rapid setting and hydration compared to other types of ash. In this study, different granulation parameters were investigated, such as the rotation modes between the steel pan and the impeller, the rotation speed of the steel pan, the granulation time, in order to improve the mass percentage of the targeted LWA (2–16 mm). In order to evolve the immobilization potential of Ba and Pb, a carbonation process was performed, exposing the manufactured LWA to pure carbon dioxide (CO_2) gas at laboratory scale. The physical, morphological, thermal and mechanical characterizations were performed on LWA for use in mortars, concretes or civil engineering constructions.

Results have demonstrated the influence of the rotation mode between the steel pan and the on the distribution of WPFA inside the steel pan and the change in the growth rate of the granules can be observed. Increased

Abbreviations: Waste paper fly ash, WPFA; Lightweight aggregates, LWA; Metallic and metalloids trace elements, MMTE; Biomass fly ash, BFA; Loss on Ignition, LOI; Scanning Electron Microscopy with Energy Dispersive Spectroscopy, SEM-EDS.

* Corresponding author at: IMT Nord Europe, Institut Mines-Télécom, Centre for Materials and Processes, Environnement, F-59000 Lille, France.
E-mail addresses: bader.bouzar@imt-nord-europe.fr (B. Bouzar), yannick.mamindy@imt-nord-europe.fr (Y. Mamindy-Pajany).

https://doi.org/10.1016/j.powtec.2022.117583
Received 25 March 2022; Received in revised form 19 May 2022; Accepted 30 May 2022
Available online 3 June 2022

density and improved compressive strength with low porosity and water absorption were also found in LWA after carbonation. This was due to the occurrence of both a carbonation reaction and a hydration reaction. Furthermore, the results of thermogravimetry and SEM-EDS confirmed the formation of hydrated phases (ettringite, carboaluminates), also the formation of calcite in the pores and the external surface of the LWA. Regarding environmental aspects, the results have revealed that Ba and Pb were well immobilized in the solid matrix after carbonation.

1. Introduction

In France, the annual production of fly ash (FA) from paper sludge and waste biomass combustion has been estimated to be about 120,000 tons**.** Two of the twelve paper mills equipped with biomass boilers use paper mill sludge as a substitute for biomass up to 60% [1]. The physical-chemical properties of this ash depend mainly on the combustibles used by the boilers of the paper production and/or recycling plants. However, new wastes (pulp processing sludge and de-inking sludge) are produced during recycling operations, creating new challenges. For example, paper manufacturers have found combustible material for their boilers in these sludges (with high calorific value), which constitutes an important recovery channel limiting the need for disposal [1]. When these residues are co-incinerated with biomass, new waste is generated: Waste Paper Fly Ash (WPFA).

The amount of WPFA generated worldwide will likely continue to increase in the near future. The increasing demand for energy and the polluting nature of current fossil fuel sources demonstrate the need for new energy technologies, which offer greater efficiency with minimal environmental damages [2]. The process of energy production from biomass, which is already widely available, is considered to have a near-zero carbon dioxide (CO_2) impact [3], because the emissions produced during its use neutralize the CO_2 fixed in the biomass during its growth. The use of biomass for energy is based on the idea that it is a carbon-neutral fuel and will help reduce greenhouse gas emissions. The combustion of biomass for heat and power produces ash composed mainly of inorganic elements naturally present in the biomass. This FA is often disposed of in landfills, which is currently becoming unattractive due to costs and may not be possible in the future due to EU (European Union) policy instruments for a circular economy [4].

WPFA is different from coal FA because it is derived from different fuels [5]. WPFA is an industrial by-product of the energy industries and has significant potential for use as a pozzolanic mineral admixture and as an activator or binder for cement composite materials. Currently, WPFA is not yet widely used commercially, unlike coal FA. Most WPFA produced by power plants is either landfilled or recycled on fields or forests, and often this happens without any form of control [6]. The WPFA differs from coal FA primarily in its chemistry and mineralogy [7]. Compared to coal, WPFA contains a high content of calcium oxide (CaO), silica (SiO_2) and alumina (Al_2O_3) and low content of iron oxide (Fe_2O_3) [8]. The presence of unreacted lime gives the WPFA a high alkalinity, and the WPFA has a high chloride (Cl) content (typically 10–20%) which has a high complexing capacity for several metallic and metalloids trace elements (MMTE). Both of these factors have resulted in an increased potential for leaching of amphoteric trace elements, which is important when it comes to landfills. The WPFA are produced from wastes paper sludge and waste biomass, it contains high levels of hazardous elements such as Barium (Ba), Plomb (Pb) and Chlorides. The high levels of trace elements in the WPFA limit its reuse. This forces energy producers to transport the WPFA to landfills, leading to greater costs and environmental risks. A workaround would be recovering of MMTE from WPFA [9–12]. However, this is not economically or technologically feasible. For all these reasons, sustainable management must be established. The amount of FA is increasing and so is the cost of disposal. The development of innovative methodologies to convert WPFA into useful materials is essential to support the increasing use of biomass for energy production [7]. Therefore, granulation/carbonation is the next better option.

Raw materials used to produce artificial aggregates are becoming depleted and society is increasingly concerned about preserving natural resources by producing alternative materials. Therefore, there is a growing interest in using other natural sources such as sediments and FA for the production of artificial aggregates. Several studies have shown that in the field of civil engineering, FA can be used as a substitute for traditional aggregates, such as the use of coal FA or biomass in the manufacture of lightweight aggregates (LWA). Chen et al. [13], developed new aggregates based on FA and showed that they can replace 15% natural aggregates in concrete. In another study, Andrade et al. [14], produce aggregates by heat treatment of bottom ash, the results show that the higher the percentage of bottom ash aggregate in concrete, the worse the performance regarding moisture transport, However, the mechanical properties remain similar. However, the results of Liu et al. [15], showed that natural sand aggregates can be replaced by plastic granules. The increase in the percentage of plastic granules in concrete results in a higher energy absorption capacity compared to ordinary concrete. Thus, the impact resistance of recycled plastic concrete materials was higher than that of ordinary concrete. Some studies [16,17] use thermally modified FA as aggregates in particulate form, the result show that the strength and specific gravity of all aggregates decreased with increasing the FA content at the highest temperature. The dense structure of the aggregates can be the factor responsible for increasing the mechanical strength and specific gravity as well as decreasing the water absorption. Alqahtani et al. [18], use a thermoplastic matrix (linear low-density polyethylene) containing fillers: sand, quarry, red sand/dunes, FA to produce LWA. The aggregate produced was lightweight, with a density ranging from 510 to 750 kg/m^3 and absorption of from 2.7 to 9.81%. Other properties such as strength and thermal conductivity were comparable to aggregates of similar density. Finally, Franus et al. [19], have manufactured lightweight aggregates from fly ash, using a new method that replaces burner furnaces with microwave furnaces, The results concluded that compressive strength of lightweight aggregates increases with longer microwave heating time.

Agglomeration, or granulation, is defined as a process of increasing the average size of the particle distribution and in which these particles will be combined to form larger agglomerates, in which the original initial particle can still be identified [20,21] Agglomeration techniques can be broadly classified into two categories depending on whether the process is performed dry (by pressing technology, extrusion, etc.) or wet, in the presence of a granulation binder [22]. Since wet granulation is the method used in this paper, only wet granulation is discussed in detail, this is achieved by wetting with a binder and mixing the solid particles in a moving vessel, or a fluidized air bed, or a high shear mixer or other similar equipment. Regardless of the technology used, the granulation binder will be dispersed by contact and transfer in a mechanically created shear field [23]. The binder will thus contribute to the association of the particles with each other through a combination of capillary and viscous forces until a permanent bond is formed during the drying of the product by cementation or gelatinization, or by a chemical reaction with the solid substrate [24,25].

Wet granulation can be considered as a combination of three rate processes as defined by Iveson et al. [24],: wetting and nucleation when the binder is distributed throughout the powder mass forming initial nuclei, consolidation and growth when collisions between granules as well as between granules and initial powder particles result in increased

compaction and granule size, and attrition and breakage when granules deform or break under the action of shear and impact forces. Several processing conditions of high-intensity granulators play critical roles on the characteristics of fabricated granulates [23,26–34], such as operation speeds of the impeller and/or container, granulation time, chopper speed, etc.,

Carbonation is considered the most common chemical reaction that influences the performance of materials in the environment. The void spaces within the hydrated material fill up with water first. When the material dries in the open air, it becomes depleted of water and air partially fills the pores. Carbon dioxide present in the atmosphere can then diffuse through the gas phase into the pores of the material and dissolve into the pore solution. As the reactions (1), (2): the dissolved CO_2 passes from the form H_2CO_3 (carbonic acid) to HCO_3^- (bicarbonate ion) then to CO_3^{2-} (carbonate ion) which is the most abundant form when the pH is between 10 and 14. Indeed, when a solution is exposed to atmospheric CO_2, the gas dissolves and absorbs water in the form of carbonic acid (H_2CO_3) [35,36]:

$$CO_{2(g)} + H_2O_{(aq)} \leftrightarrow H_2CO_{3(aq)} \quad (1)$$

$$H_2CO_{3(aq)} \leftrightarrow 2H^{2+}{}_{(aq)} + {CO_3}^{2-}{}_{(aq)} \quad (2)$$

Fresh WPFA contains reactive alkaline constituents (mainly CaO/Ca$(OH)_2$) and exhibits a high leachability of MMTE (e.g. Ba, Pb) [37]. The carbonation reduces the mobility of the aforementioned MMTE in WPFA according to the reaction (3):

$$M^{2+}{}_{(aq)} + {CO_3}^{2-}{}_{(aq)} \leftrightarrow MCO_{3(s)} \quad (3)$$

Carbonation has many advantages such as the agglomeration of particles to form solid aggregates (the hardening of the matrix allows to obtain resistant finished materials) and the physical (pollutants) and chemical (formation of insoluble metal carbonates and pH decrease) stabilization. For all these reasons, the valorization of WPFA (rich in CaO) is particularly adapted to the carbonation process.

In order to develop the field of valorization of building materials based on WPFA within the sector of the Building and Public Works, it is necessary to carry out a methodology of characterization of the intrinsic properties of these by-products (the carbonated aggregates). For these purposes, the study of morphological, physical, chemical, mechanical and thermal characteristics of these aggregates is presented. In this perspective, the LWA manufacturing process and the influence of the granulation parameters on the granule properties will be mainly presented, then, in a second part, the process of accelerated carbonation of the manufactured aggregates. Finally, the aspects to evaluate fabricated granulates before and after carbonation include the particle size distribution, granule class, apparent density, actual density, organic matter content, leaching characteristics, % chloride (Cl), sulfates soluble in acid, % total sulfur, compressive strength, crushed particles, porosity, water adsorption and thermal conductivity were realized according to the standard EN 13055-1 [38].

2. Materials and methods

2.1. Waste paper fly ash used in lightweight aggregate production

The WPFA used in this study was collected from the cyclone of a mass-burning incinerator located in the North-East of France. The ash type used in this paper were biomass and waste paper sludge ash. The chemical composition was determined by X-Ray Fluorescence (XRF) and leaching of metallic and metalloids trace elements (MMTE) from the WPFA was confirmed by Inductively Coupled Plasma-Optical Emission Spectrometry (ICP-AES), the results are shown in Table 1. The chemical composition of WPFA is as follows: CaO 64.02%; SiO_2 14.59% and Al_2O_3 8.1%. The results revealed that the concentration of Pb 7.35 ± 0.6 mg/kg, Ba 178 ± 6 mg/kg and Cl 1422 ± 72 mg/kg were the most abundant

Table 1
Chemical composition in major and MMTE of the WPFA.

Chemical composition by XRF	wt%	Metallic and metalloids trace elements (MMTE)	Concentration (mg. kg^{-1})
SiO_2	14.59	As	<0.11
Al_2O_3	8.4	Ba	178 ± 6
MgO	1.74	Cd	<0.009
Fe_2O_3	0.8	Co	<0.009
CaO	64.02	Cr	<0.011
Na_2O	0.45	Cu	0.09 ± 0.02
SO_3	1.57	Mo	0.08 ± 0.02
TiO_2	0.7	Ni	<0.047
ZnO	0.22	Pb	7.35 ± 0.6
Cl	0.8	Sb	<0.057
BaO	0.11	Se	<0.08
P_2O_5	0.35	Zn	1.1 ± 0.2
K_2O	0.7	Cl	1422 ± 72

trace elements in the WPFA. The leaching of Ba, Pb and Cl from the WPFA exceeded the limit values for landfill (Inert: 0.5 mg/kg, 20 mg/kg and 800 mg/kg for Ba, Pb and Cl respectively) [39] and should be considered. The concentrations of copper (Cu), molybdenum (Mo) and zinc (Zn) in the WPFA are relatively low.

The physical and chemical properties of WPFA were determined through various characterization tests. Brunauer Emmett–Teller (BET) method was used to determine the specific surface area of the WPFA from nitrogen sorption experiments using an AGITENT Analyzer apparatus from Micromeritics in accordance with standard NF EN ISO-18757 [40], Physical adsorption results from relatively low forces (Van der Waals forces) between the gas molecules (adsorbate) and the sample surface (adsorbent). 1.5 g of dry sample was weighed and placed in the cell. The entire measuring cell was immersed in a nitrogen bath to maintain a constant temperature. Successive quantities of nitrogen were then introduced into the cell containing the sample, which had been degassed for 8 h at 80 °C. The adsorption/desorption isotherms were measured on the previously desorbed samples at 80 °C, 5 mbar. The residual pressure is used to calculate the specific surface area, which is directly related to the quantity of nitrogen adsorbed. The BET method used on WPFA allows reliable surface measurements (<10% error).

The specific density was measured using a Micromeritics ACCUPYC 1330 Helium Pycnometer in accordance with standard NF EN 1097–7 [41]. Three samples were prepared in order to promote consistency of results. The samples were dried at 105 °C to constant mass. Finally, a mass of approximately 1.5 g of sample was weighed and placed in a cell with a total volume of 3.5 cm3. The pycnometer performed several measurements on the same sample and the average of the measurements was recorded.

Particle size distribution was determined with laser diffraction Coulter LS12330 in accordance with standard NF EN ISO 13320-1 [42]. This instrument is used to determine the size of particles between 0.04 μm and 2000 μm. Following the granulation process, particle size analysis is performed to determine the particle size distribution of the manufactured aggregates. The test was carried out in accordance with the European standard NF EN 933–1 [43]. The particle size analysis was carried out by the dry method, using the sieves recommended by the European standard NF EN 933–2 [44]. The test represents the reference test for measuring the granulometry of aggregates. The sieves used are: 2, 4, 8, and 16 mm. Each sieve is weighed empty and then full in order to verify that the mass of each reject is less than the saturation mass of the sieve. The test is carried out 3 times for each lot of aggregate.

The conductivity and pH were determined use batch leaching tests made according to the standard NF EN 12457–2 [45]. Table 2 illustrates the results of the physical-chemical characterization of WPFA.

The WPFA used in this study conforms to the requirements of Class C as specified by ASTM C 618 (Class-C) [46] which is shown in Table 3.

Particle size distributions of the WPFA used in LWA production are illustrated in Fig. 1. It can be seen that the WPFA has a fine particle size

Table 2
Physical and chemical characterizations of WPFA.

Physical parameters	Standard	WPFA
Specific density (kg/m^3)	NF EN 1097–7	2980
Median diameter d_{50} (μm)	NF ISO 13320-1	10
Specific surface BET (m^2/kg)	NF EN ISO-18757	2261
pH	NF EN 14429	13.5
Conductivity (mS/cm)	EN 12457–2	11.3
Loss On Ignition (LOI) (%)	EN 12457–2	5.7

Table 3
Chemical properties of WPFA and specification requirements.

Properties %	ASTM C 618 (Class-C) %	WPFA used
$SiO_2 + Al_2O_3 + Fe_2O_3$	> 50	87.01
SO_3	< 5	1.57
$Na_2O + 0.658K_2O$	< 1.5	0.91
Moisture content	< 3	0
Loss on ignition	< 6	5.7

distribution (< 250 μm) and 50% of particles smaller than 10 μm.

2.2. Granulation process

The WPFA granules are fabricated in a 5 L Eirich high-intensity granulator (Eirich R-02) manufactured in Hardheim, Germany. Impeller, chopper and steel pan (container) are important components of this machine, as shown in Fig. 2. The chopper is a static tool which prevents deposit build-up on the vessel wall. The steel pan and the impeller can be operated in the counter-current and co-current flow modes. The impeller inside can rotate both at clockwise and anti-clockwise directions, while the steel pan (positioned horizontally) can only rotate in a clockwise direction. Thus, two different rotation modes can be generated when we combine the rotation directions of impeller and the steel pan in different ways: cross current rotation mode, where the pan rotate clockwise but the impeller rotate anti clockwise; counter current rotation mode, where both the pan and the impeller rotate clockwise.

The rotation speed of impeller has been kept constant: 3000 rpm for the period of nucleation formation and for the period of granulate growth, in order to study the effect of steel pan rotation speeds (85 rpm and 170 rpm). The granulation procedure employed in this study is as follows:

- Dry WPFA was weighed (1000 g), homogenized and added to the steel pan.
- After switching on the steel pan and the impeller, 300 g of tap water was sprayed via wash bottle on the WPFA. The time to add tap water is 90 s. Within this period of time, secondary units of nuclei come into birth, and we thus name it as the nucleation time.

Sprayed water was used as an agglomeration binder and coagulation so that the wet mixture (WPFA rich in CaO + water) was hydrated and transformed into LWA by the rolling motion and the effects of capillary attraction by an inclined turntable. During the granulation process, granulate starts to grow, and a period of 3 min was set as the granulating time. it is necessary to specify, surplus water caused bigger and irregular particles and insufficient water led to difficulty in granulation, as also confirmed by Chiou et al., [47]. To investigate the effect of granulation time and flow patterns within the steel pan on the properties of generated granulation, we varied the impeller rotates differently: counter current flow, cross current flow, then, the granulation time from 3 min to 9 min. After the granulation process, the granulates within the range between 2 and 16 mm were selected by the sieving process, then, each batch of LWA was sealed in air-tight plastic bags and stored at room temperature before were carbonated. The different granulation parameters are outlined in Table 4.

Fig. 2. Eirich high-intensity granulator.

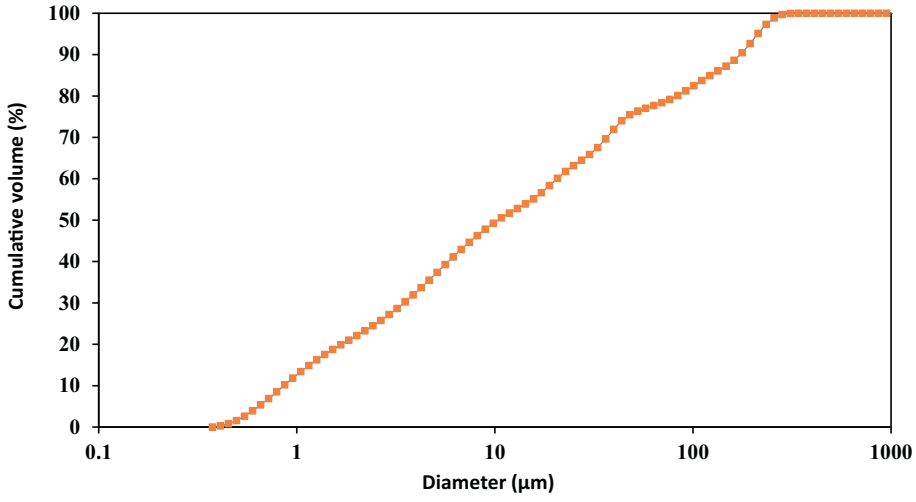

Fig. 1. Granular distributions of WPFA.

Table 4
The different granulation parameters of the WPFA.

Experimental	Rotation modes	Time (min)	Steel pan rotation speeds (rpm)
1	Cross current rotation	3	85
2	Cross current rotation	3	170
3	Counter current rotation	3	85
4	Counter current rotation	3	170
5	Cross current rotation	6	170
6	Cross current rotation	9	170

2.3. Lightweight aggregate carbonation process

Carbonation has many advantages such as hardening of the matrix to obtain resistant finished LWA, physical stabilization (of pollutants) and chemical stabilization (formation of insoluble metal carbonates $BaCO_3$/$PbCO_3$ and decrease of pH). To this observation, an accelerated carbonation process was developed allowing the reaction of $Ca(OH)_2$ portlandite/calcium oxide (CaO) as well as Ba and Pb from LWA with CO_2.

The CO_2 is transformed into carbonic acid which can then initiate reactions with calcium hydroxide compounds (portlandite or lime) to form calcium carbonates. The precipitation of carbonates (Calcite) causes the permanent fixation of CO_2.This process aims to carbonate LWA in an atmosphere enriched in carbon dioxide in order to generate inert aggregates. The manufactured LWA were treated with carbon dioxide (CO_2) in a pressure reaction vessel (see Fig. 3).

The LWA were mixed with sufficient tap water (ratio of liquid to solid of 0.3 L/kg) and then carbonated in a 100% carbon dioxide atmosphere held at 0.5 bar pressure for 72 h. Saturated sodium chloride solution maintained the relative humidity at 65% inside the reaction vessel. Maintaining humidity around this level is for efficient carbonation [48].

Analysis of LWA shape and morphology before and after carbonation was performed at high magnification using electron microscope (SEM-Hitachi S-4300SE/N), energy dispersive spectroscopy (EDS) observations and the Zeiss digital microscope.

2.4. Lightweight aggregate characterization

The characteristics of the manufactured LWA have a very important role on the properties and performances of concrete or mortar (injection mortar). In fact, the properties of concrete are largely influenced by the characteristics of its constituents. For this reason, in order to develop the field of the valorization of the LWA based on WPFA, we proceeded out tests of characterization of these LWA before and after carbonation, according to the standard EN 13055–1 [38]. Then we compared these characteristics with commercialized LWA from ARGEX.

The bulk densities ρ_{app} of the LWA were measured according to NF EN 1097–3 [49] with a 1-l container. The helium pycnometer method, in accordance with NF EN 1097–6, was used to obtain the absolute densities of the LWA. We determine the densities in order to verify the mineralogical regularity of the materials.

The porosity measurement of LWA was performed according to the NF P94–410-3 [50] standard, with a MicroActive AutoPore V 9600 2.00 mercury porosimeter.

The measurement of water absorption of LWA was made on three samples of 500 g immersed in water for 24 h in order to measure the capacity of a LWA to absorb water according to the standard NF EN 1097–6 [51]. This test is performed in order to consider the absorption of aggregates in the calculation of the water/cement ratio in concrete and to have an estimate of the ability of the LWA to influence the rheology of the concrete.

In order to evaluate the mechanical strength of LWA, bulk crushing tests were performed according to EN 13055–1 [38]. A sample of LWA compacted by vibration is compressed, with the help of a piston, in a cylinder of 100 mm height and 175 to 200 cm^2 of section. The speed of the plunger is 1 mm per minute and the test is completed when the plunger has reached 20 mm. The conventional strength of the LWA is defined as the quotient of the applied force required to achieve 20 mm of piston depression per cylinder cross-section.

The percentage of chloride, sulphate soluble in acid, total sulfur and the loss on ignition were determined according to standard NF EN 1744–1 [52]. The three methods of measuring the solubility of chloride, sulphate soluble in acid, total sulfur is determined gravimetrically, the sulphate content is expressed as a percentage of Sulfur trioxide per mass of LWA (% SO_3).

To measure the thermal conductivity of LWA, we used the steady-

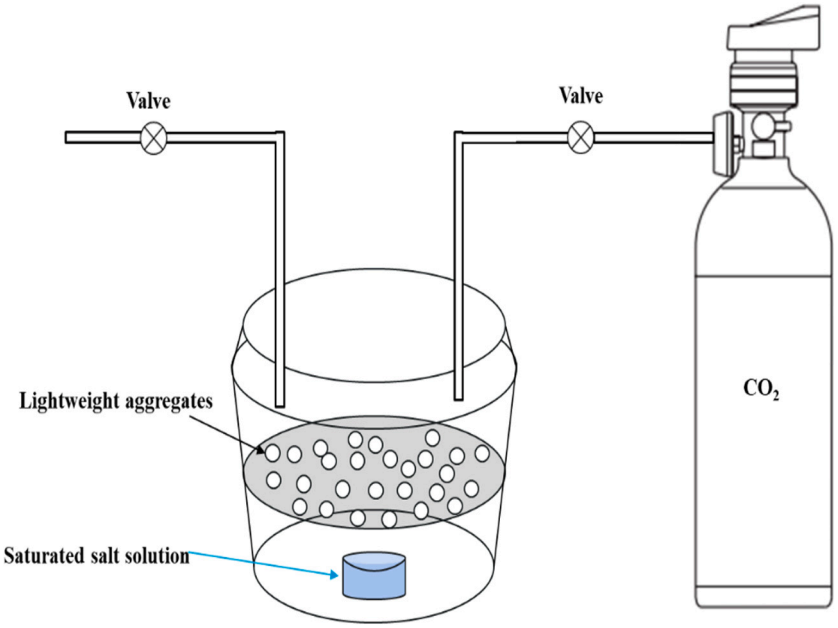

Fig. 3. LWA carbonation apparatus.

state hot plate method on 25x25x6 cm samples. The material sample to be studied is placed between two plates, hot and cold, and surrounded by insulation to avoid lateral losses of heat flow. Thermocouples are installed on the faces of the sample to measure the temperature differences. The upper plate hot is lowered until it is in contact with the material and the acquisition is launched.

3. Results and discussion

3.1. Effect of rotation speed of the steel pan

According to Iveson's theory of the granule formation process [27], granules form in two continuous stages, wetting/nucleus formation and the growth period. Apparently, a faster rotation speed of the plate creates more chances for solid powders to contact the sprayed liquid droplets; thus, a larger quantity of small nuclei can be formed. In the case of a low rotation speed, the liquid droplets can remain on the surface of the solid powders for a relatively longer period of time, which reduces the chances of the solid powders meeting the liquid droplets. During the next period of granule growth, these previously formed nuclei will have different ways of "growing" themselves: by attaching to other pre-formed nuclei (nuclei agglomeration) or by attracting free powder to their surface (powder attachment) [53]. In the case of a high rotation speed, more nuclei have been generated, and thus, these pre-formed nuclei are more likely to encounter each other (nuclei to nuclei attachment), and their growth tends to follow a nuclei agglomeration path; in the other case, the number of nuclei is limited, and thus, they are more likely to encounter fine powders [53].

Fig. 4 show size distribution for LWA fabricated under counter current rotation mode. Maintaining a constant rotation speed of impeller (3000 rpm) and rotation mode between the impeller and the steel pan (counter current rotation mode), we have produced LWA under two different rotation speeds of the steel pan (85 rpm and 170 rpm). The variation of rotation speeds of the steel pan has brought a difference to the growth rate, which has been proved by the investigation of the LWA size distribution (Fig. 4). Clearly, faster rotational speed shifts the size of the granules to larger values, indicating that the rate of increase in granule size is faster when they develop from agglomeration of the nuclei than from the attachment of the fine powder to the nuclei. In addition, it can be seen that a higher rotational speed (170 rpm) generates a higher yield of larger granules, while a lower rotational speed (85 rpm) favors the creation of a greater amount of smaller granules [53]. This will apparently vary the final granulates yield within a certain size range, which is interesting information for people who want to improve the granulates yield with certain sizes.

3.2. Effect of rotation modes

Two different rotation modes are available in the Eirich high-intensity granulator, they differentiate each other from the rotation directions of the impeller: cross current rotation and counter current rotation. When the machine operates in cross current rotation mode, powders are taking up the whole space and distribute homogeneously within the steel pan. While in the case of counter current rotation mode (both the impeller and the steel pan rotate in clockwise directions), due to gravity reason, powders tend to 'concentrate' more in the lower part of the steel pan [53].

Fig. 5 shows the size distribution of LWA fabricated under these two different rotation modes. Fig. 5 shows that despite the pan rotation speed differences (85 rpm and 170 rpm), granulates are larger from cross current rotation mode than from counter current rotation mode. This information also indicates that there are fewer powders in the upper part of the pan (where the liquid was added) for the counter-current rotation mode than for the cross-rotation mode; thus, fewer nuclei will be formed for the counter-current rotation mode, and the granules will grow in a way of powder attachment. Conversely, more nuclei will be formed in the cross-rotation mode, and the granulate will grow in a way of nuclei agglomeration mode. In other words, the generated granules are larger when the initial powders are homogeneously dispersed in the steel pan rather than relatively "concentrated" in the lower part of the steel pan. Since powder dispersion directly affects the chances of powders coming into contact with other powders, we can say that the better dispersion created by the cross-flow rotation mode creates more chances for cores to encounter other cores or loose powders (rapid incorporation), which is beneficial for a faster growth rate of the granules, and vice versa [53].

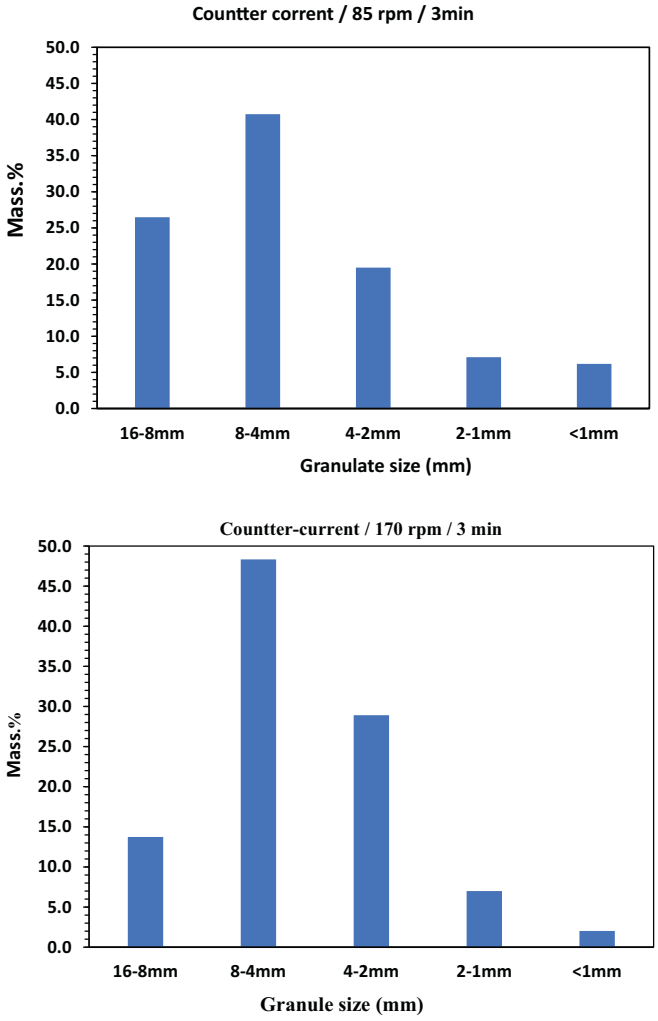

Fig. 4. Size distribution for LWA fabricated under counter current rotation mode.

3.3. Effect of granulation time

The rotation modes between impeller and steel pan and both the steel pan rotation speed affect the growing behavior of LWA, with the steel pan rotation speed controlled at 170 rpm and the rotation mode in cross current throughout (95% of LWA have a grain size between 2 and 16 mm), the size distribution of the LWA made under these conditions under different granulation time (3, 6 and 9 min) is shown in Fig. 6.

Increasing the granulation time from 3, 6 to 9 min improved the yield of the LWA with the size range < 4 mm (from 22.2 wt% to 95.5 wt%). However, increasing the granulation time to 9 min resulted in a decrease of targeted LWA yield to 80 wt% by forming more larger LWA within the size range of 4 mm to <1 mm.

The amount of LWA less than 1 mm is increasing from 1.9% to 6%, while the ratios of larger LWA (8-16 mm) are decreasing continuously.

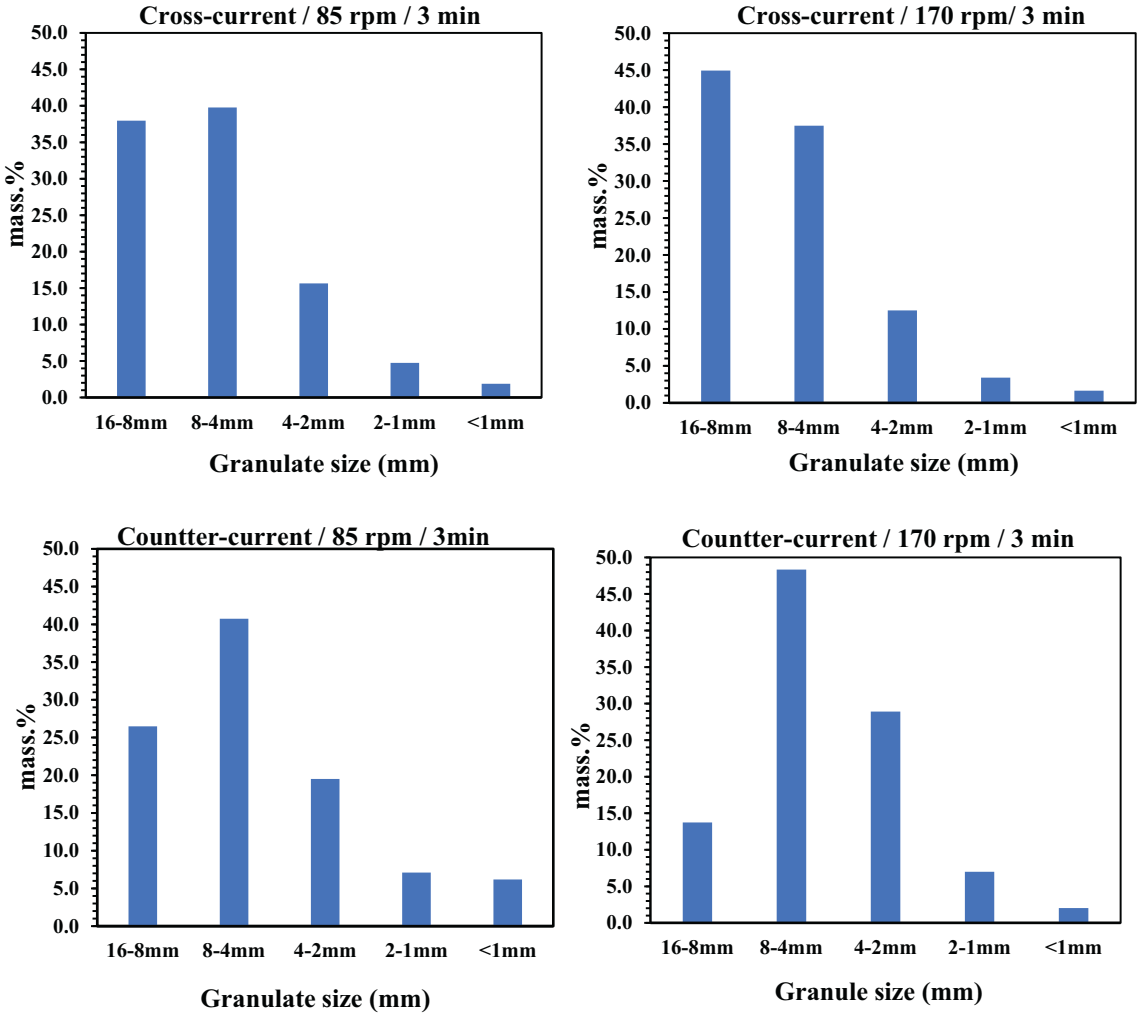

Fig. 5. Size distribution of LWA fabricated under different rotation modes.

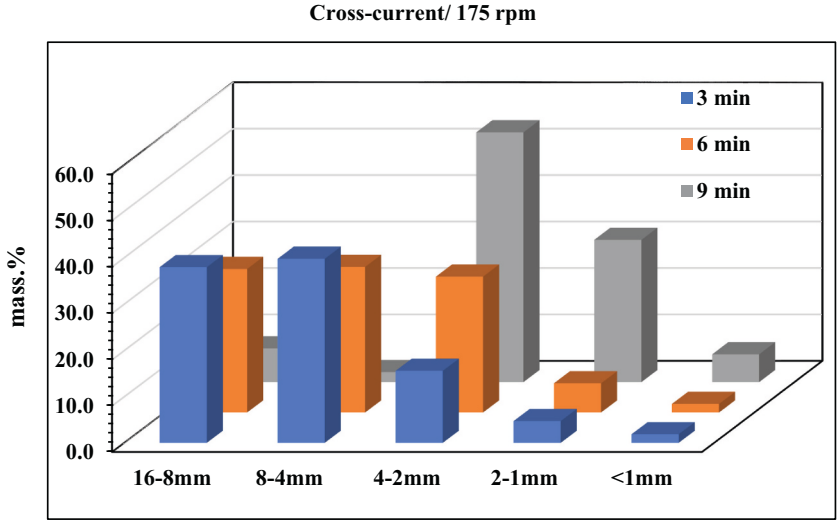

Fig. 6. Effect of the granulation time on the size distribution of LWA produced.

However, the size changes between 3 and 6 min are relatively smaller, whose relative mass ratio differences are between 1.1 and 1.8. The changes from 6 to 9 min are much larger, whose mass ratios rise to more than 10 times the difference in the case of LWA < 4 mm. Inversely to the trend observed in the study of the steel pan speed, the increase of granulation time resulted in the formation of smaller LWA, which was clearly shown in the diameters of the manufactured LWA in Fig. 6.

This is attributed to the hydraulic properties of the lime present in

the WPFA which hardens rapidly by mixing with water during the first 3 min of granulation. Apparently, with the increase of the granulation time (6 to 9 min), the LWA of diameters higher than 4 mm, undergo physical interactions on the one side with the turbine and on the other side with the other LWA, which results in the reduction of their sizes.

This information does not agree with the results reported in the research work done by Mangwandi et al., [30] in which the authors indicated that a longer granulation time could help consolidate the microstructure of the LWA formed. In contrast, Walker et al. showed that as the granulation time of lactose increased, an increase in mean particle size had been found [54].

3.4. Effect of carbonation

To investigate the effects of carbonation on the leachability, mechanical strength and the porous properties of the fabricated LWA, we have performed accelerated carbonation on the fabricated LWA under the following conditions: Cross-current/ 175 rpm / 3 min (95% of the manufactured LWA have average size distributions vary from 16 mm to 2 mm).

3.4.1. Thermogravimetric analysis (TGA)

Fig. 7 shows the thermal characteristics of the WPFA and the LWA before and after carbonation. The WPFA and the LWA before and after carbonation present a mass loss between 90 °C and 300 °C corresponds to the deshydroxylation of hydrates including ettringites and carboaluminates [55]. The mass losses corresponding to carboaluminates appeared in the case of carbonated LWA and non-carbonated LWA, and ettringite in the case of carbonated LWA, which confirms the hydraulic properties of our WPFA, since both portlandite participates in the hydration reaction and the carbonation reaction during the 3 days of the accelerated carbonation.

However, the mass loss observed between 400 °C and 500 °C corresponds to the deshydroxylation of Portlandite [56], the intensity and

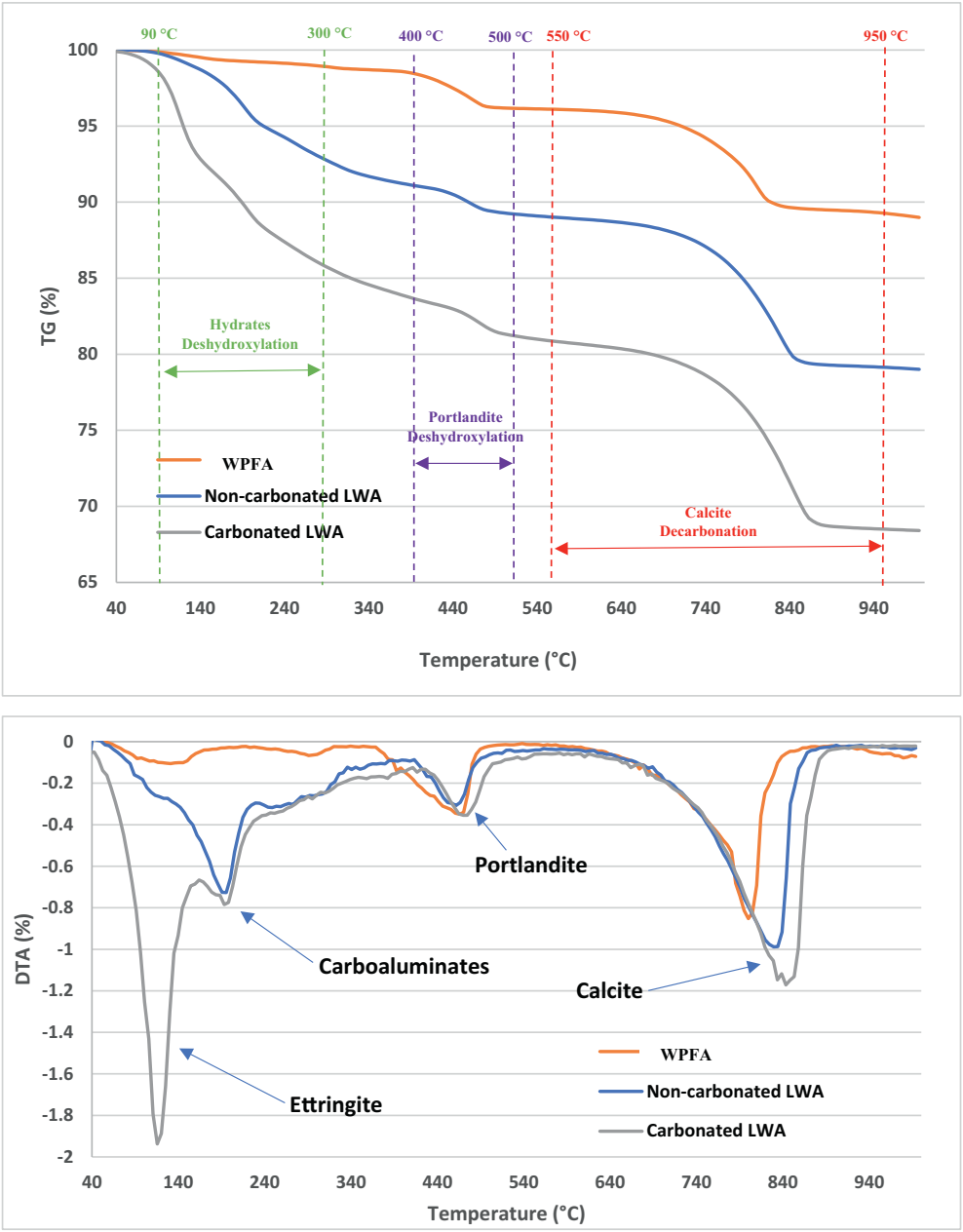

Fig. 7. The thermal characteristics of the WPFA and LWA before and after carbonation.

peak broadening in the case of carbonated LWA decreased compared to the WPFA. It is important to note that mass loss between 550 °C and 950 °C corresponds to the decarbonation of the calcites. This peak is more important in the carbonated LWA which is normal considering the carbonation process (100% CO_2). Confirming that lime and portlandite which represent major phases in the WPFA were transformed through carbonation to calcite.

In the study done by Dijkstra [55], the carbonation of both ashes was studied. During the carbonation, the quantity of reactive aluminates (mayenite) decreased by transformation into ettringite and carboaluminate [55], which reduces the risks of expansion since the expansive phases (ettringite, carboaluminate) are formed before the incorporation of LWA into concrete.

3.4.2. *Microstructure evolution before and after carbonation*

The surfaces of the LWA were used to determine the microstructure by using the Zeiss digital microscope (Fig. 8 a, b, c, d) and scanning electron microscope (SEM-EDS) (Fig. 8 e, f).

Morphological analysis revealed structural differences between carbonate and non-carbonate LWA. The non-carbonated LWA have an explicit porous structure in the middle of a granule while their surface layers are denser (Fig. 8 a, c). The black dots in the image are pores, which were most probably produced by the enclosure of air bubbles in the granulation procedure. The structure is very dense in general. Fig. 9a shows another SEM image with higher magnification than Fig. 8c. In this image also, it can be seen that the structure is very dense, A crack is also clearly visible in the figure, probably resulting from the splitting of the granule, thus, a significant porosity.

After carbonation (Fig. 8 b, d), as can be seen, the LWA have a clearly denser structure than the non-carbonated LWA structure. In addition, the surface is more irregular, indicating that precipitation may have formed during the carbonation process. The change in color and disappearance of pores after carbonation of the LWA may also be the result of the reaction between $Ca(OH)_2$ and carbon dioxide, eventually forming calcite between the particles and filling the pores.

Fig. 9 (a and b) shows a SEM image of the carbonated LWA before and after carbonation. At this level, it is possible to see a new layer that has precipitated on the surface that is probably calcite, as well as solid bridges between the precipitates, which bonds them together. The precipitation of calcite is the most probable binding mechanism due to the reaction between CaO and water as was mentioned in the literature review.

Only a few scientific studies can be found concerning the study of the inner and outer porosity/density of the LWA; similar results in relation to our date are mentioned, but not completely investigated by other scientists [57,58]. The authors observed that the porosity/density of the particles tended to decrease, which probably occurred due to the fact that the densification, consolidation and compaction of the particles increased with increasing granulation time. The others concluded that the densification process reduced the porosity of the granules and induced the migration of the binder to the surface of the granules. Thus, saturation was achieved due to the reduction of pore space by consolidation rather than due to pore filling promoted by the addition of binder.

SEM observations of the carbonated LWA show that the majority of the grains on the LWA have irregular shapes (Fig. 9 c and d) with the presence of a few spheres (Fig. 9 c). On the other side, the carbonated LWA have a less porous structure compared to the non-carbonated LWA. Importantly, ettringite is present in the form of needles about 10 μm long (Fig. 9 d). EDS observations of the carbonated LWA similarly confirm the presence of calcite (Fig. 9 e), and ettringite (Fig. 9 f). Consistent with the TGA results confirming the formation of hydrates including ettringite/carboaluminate (90–300 °C) and calcite (550–950 °C) in the carbonated LWA. Several authors have suggested the formation of ettringite

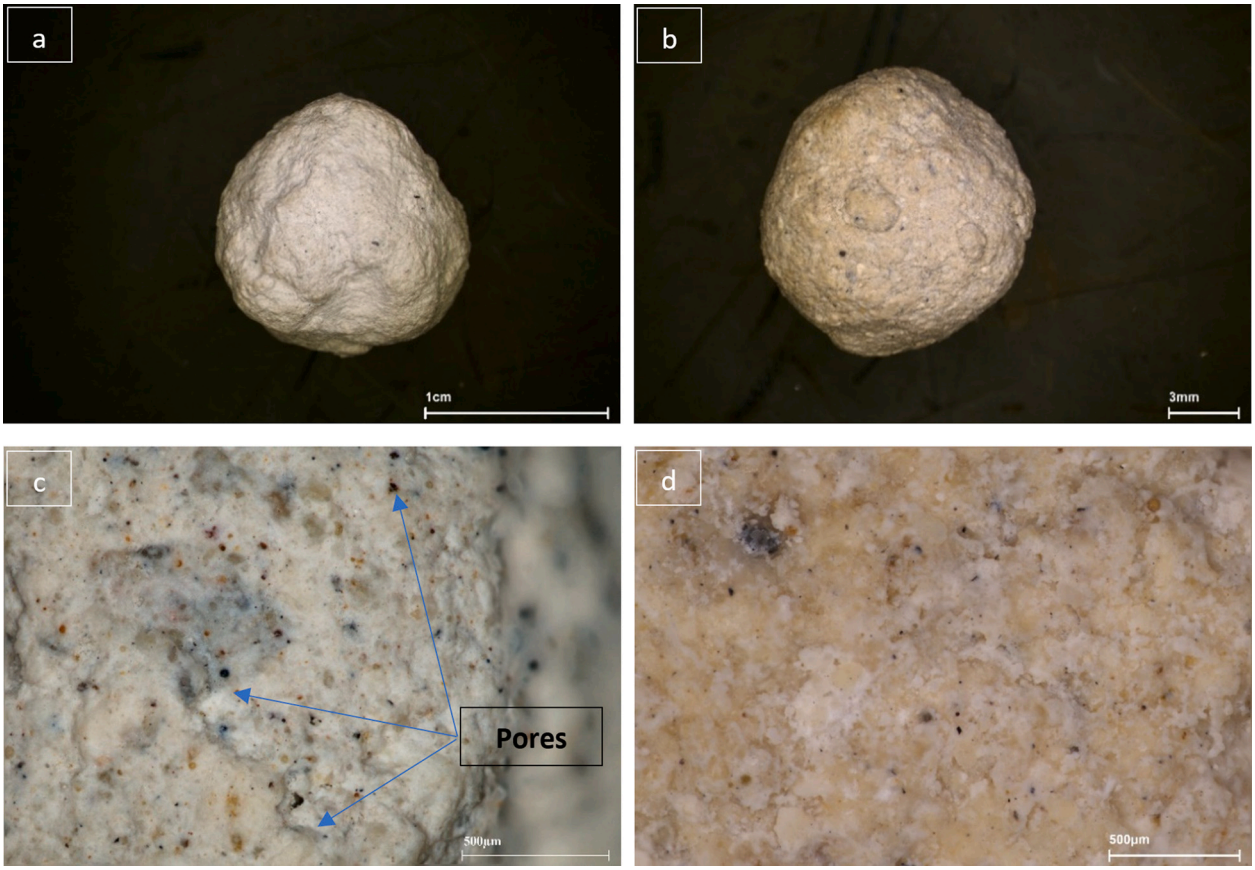

Fig. 8. Optical images of the LWA made by from WPFA before (a,c) and after (b,d) carbonation (Zeiss digital microscope).

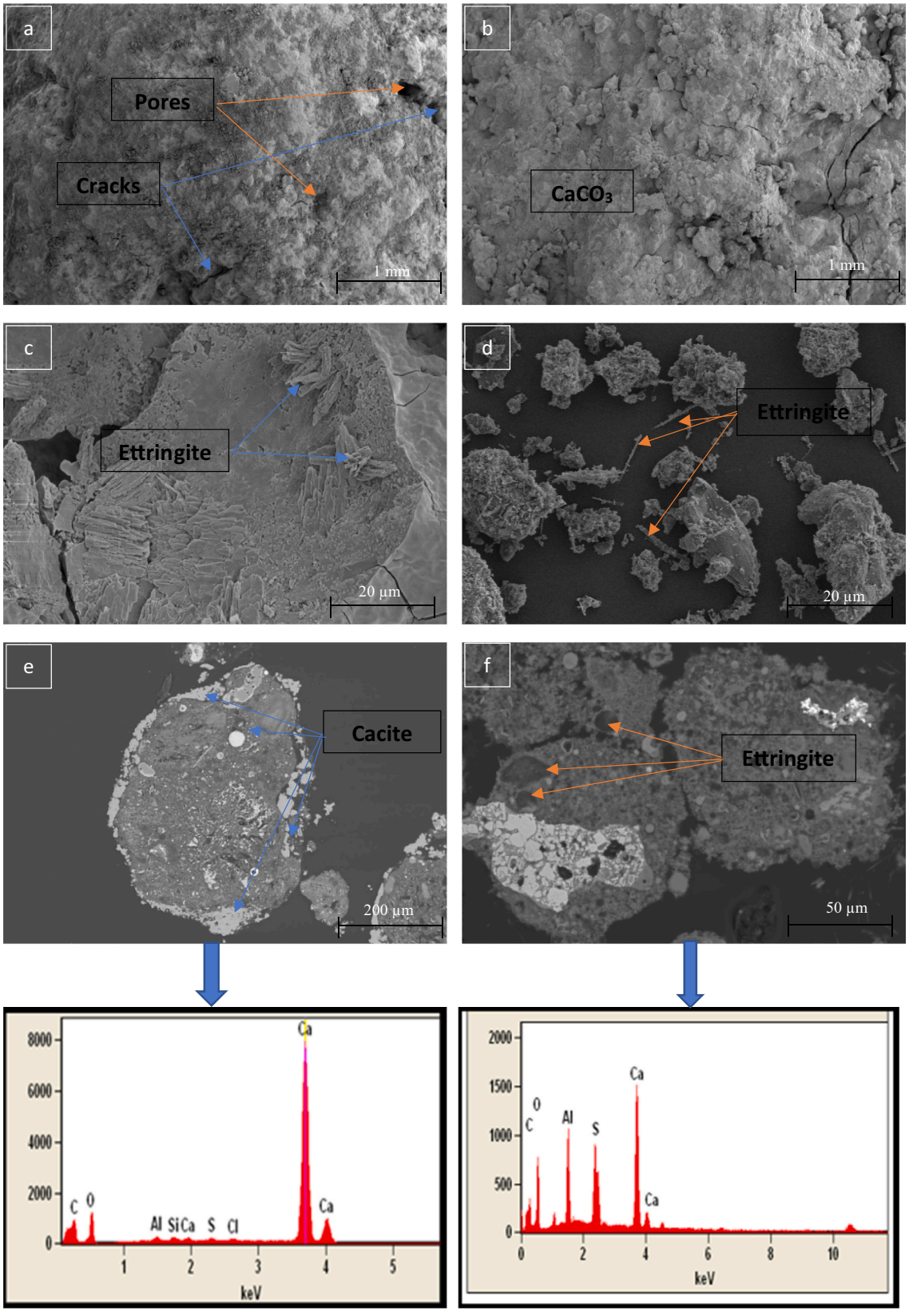

Fig. 9. SEM-EDS picture of the LWA before **(a)** and after **(b)**, **(c)**, **(d)**, **(e)**, **(f)** carbonation.

($Ca_6Al_2(SO_4)_3(OH)_{12}$. $26H_2O$) when WPFA is hydrated due to the presence of mayenite ($Ca_{12}Al_{14}O_{33}$), anhydrite ($CaSO_4$) and free lime (CaO) [55,59].

3.4.3. Influence of carbonation on leaching

Many studies have demonstrated that when LWA undergo carbonation, the immobilization of MMTE (such as Ba, Pb, Zn) is generally enhanced, minimizing the leachability of these elements [60,61]. Table 5 lists the concentrations of MMTE leached from WPFA, carbonated LWA and the legal limits (IWSI) for the use of LWA based on WPFA in civil engineering in France.

Since the chemical composition results (Table 5) showed that the WPFA had high amounts of Ba and Pb, an analysis of the concentration of these trace metal elements as well as other elements was performed on the eluates extracted from the leaching test performed on the carbonated LWA sample after crushing, according to standard 12,457–2.

The results displayed in Table 5 on the concentration of the MMTE eluate concentration in the WPFA corroborate that there is a predominance of Ba (178 ± 6 mg/kg) and Pb (7.35 ± 0.6 mg/kg) compared to the rest of the elements measured (Cu = 0.09 ± 0.02 mg/kg, Mo = 0.08 ± 0.02 mg/kg, Zn = 1.1 ± 0.2 mg/kg while As, Cr, Sb, and Se were not detected). When these results are compared to the leaching of carbonated LWA, it can be observed that carbonation seems to have favored a decrease in the leachability of certain elements, in particularly Zn <0.01 mg/ kg, Pb < 0.03 mg/kg and especially Ba = 0.3 ± 0.05 mg/kg. The leachability of Ba and Pb is 99% lower in the carbonated LWA than in the original WPFA, demonstrating that carbonation has played an important role in the immobilization of this element. It was also found that the leaching of calcium followed the same trend as Ba and Pb, the leaching is reduced after carbonation (from 10,839 ± 521 mg/kg to 451 ± 7 mg/kg) which confirms that the majority of calcium was carbonated. The calcium leaching is presented in Supplementary data (Table 1). The formation of $BaCO_3$, $PbCO_3$ and $ZnCO_3$, an insoluble barium, lead and zinc carbonate compounds, has been considered as the immobilization mechanism of Ba, Zn and Pb [62]. In addition, a few studies have reported the immobilization of Ba and Zn in type F FA with carbonation [58,59]. In a previous study [63], accelerated carbonation (100% CO_2) decreased the leaching of Pb and Zn by forming insoluble compounds such as $PbCO_3$ and $ZnCO_3$ which is consistent with what we assumed [62].

The leachability of sulfate and fluoride were below the legal leaching limit (IWSI) before and after carbonation. The chloride concentration exceeded the IWSI threshold even after carbonation, which indicates that the carbonation process has no influence on the immobilization of salts.

In general, cationic species immobilize well after accelerated carbonation. This behavior has been explained by the precipitation of elements as carbonates, since in a high pH environment, elements such as Ba and Pb would be hydroxic, they would not be able to precipitate as hydroxides. In this study, the original pH of the WPFA was 13.5, whereas that of the carbonated LWA showed a lower pH = 10.39 after only 3 days of carbonation, as a result of the rapid consumption of calcium hydroxide ($Ca(OH)_2$) during the carbonation process and the formation of calcite ($CaCO_3$). This result clearly demonstrates that the decrease in pH explains the behavior of Ba and Pb after carbonation. It also justifies the theory that pH decrease by carbonation is the dominant mode of stabilization [62].

In order to determine if the concentrations of these MMTE could be harmful to the environment, the results have been compared to the IWSI limits. As can be seen (Table 5), Ba and Pb are well below the maximum permitted values. This means that the eluates of these LWA do not represent a real threat to the environment, but on the contrary, they can be used safely from an environmental point of view.

Table 5
Concentration (mg/kg) of MMTE in WPFA and carbonated LWA.

Concentration (mg/kg)	IWSI	WPFA	Carbonated LWA
As	0.5	<0.11	<0.11
Ba	20	178 ± 6	0.3 ± 0.05
Cd	0.04	<0.009	<0.009
Cr	0.5	<0.011	<0.011
Cu	2	0.09 ± 0.02	0.09 ± 0.02
Mo	0.5	0.08 ± 0.02	0.09 ± 0.03
Ni	0.4	<0.047	<0.047
Pb	0.5	7.35 ± 0.6	<0.03
Sb	0.06	<0.057	<0.057
Se	0.1	<0.08	<0.08
Zn	4	1.1 ± 0.2	<0.01
Chlorides	800	1422 ± 72	1328 ± 48
Fluorides	10	1.1 ± 0.5	–
Sulfates	1000	208 ± 25	206 ± 27
Soluble fraction	4000	3920 ± 121	3980 ± 130
Conductivity ($mS.cm^{-1}$)	***	11.3 ± 0.2	11.8 ± 0.2
pH	***	13.5 ± 0.3	10.4 ± 0.3

4. Lightweight aggregates characterization

4.1. Absolute density, bulk density and apparent density

The absolute density, bulk density and apparent density are important factors when LWA properties are considered [64–66], the bulk density of common artificial LWA is generally between 300 kg/m^3 and 1300 kg/m^3, which is two to three times less than that of common aggregates. The results of the LWA are shown in Table 6. The various characterization methods have shown that the aggregates manufactured from the ash can be classified as LWA, as all fall within the set limits of loose bulk density (≤1.20 kg/m^3) and particle density ≤ 2.00 Mg/m^3 (BS EN 13055–1).

The Absolute density results of carbonated and non-carbonated LWA were found to be in the range of 2105–2370 kg/m^3 respectively. The carbonated LWA was found to be denser than the non-carbonated LWA and their density values are higher than the aggregates commercialized by Argex (550 kg/m^3), Similar trends in results were found for bulk density and apparent density. The enhancement in the density was due to $Ca(OH)_2$ from the WPFA reacting with CO_2 to produce a solid volume of Calcite ($CaCO_3$), leading to a reduction in porosity throughout the carbonation. In addition, $CaCO_3$ also improved the density of LWA due to its high density (2.71 kg/m^3) as compared to $Ca(OH)_2$ (2.24 kg/m^3).

4.2. Porosity and water absorption

Carbonated LWA have a lower porosity (21%) than non-carbonated LWA (29%). As the porosity decreases with carbonation time, the water absorption coefficient at 24 h decreases. Based on experimental results, a relationship between water adsorption and porosity was found, the higher the porosity, the more water is adsorbed.

As shown in Table 6, an absorption of 27.9% was measured for non-carbonated LWA. After 3 days of carbonation, the LWA reached about 21% water absorption. Overall, the manufactured LWA either before or after carbonation was comparable to the Argex aggregate in terms of porosity and density, although it had lower water absorption. Carbonation of the aggregates for 3 days resulted in a decrease in porosity, this confirmed what we obtained in the SEM images, a layer of calcite was formed and thus filling the pores.

The high porosity of LWA presents a problem when mixing them to produce concrete or mortar. Therefore, when using these eco-aggregates to formulate concrete or mortar, it is necessary to consider the water absorption by the aggregates. Lower porosity leads to lower water absorption. These results for water absorption agree with the results for density in which water absorption decreases with increasing density.

Table 6
Characterization of LWA according to the standard (NF EN 13055–1).

Technical specifications	Units	Standard	Non-carbonated LWA	Carbonated LWA	LWA(Argex)
Aggregate form	–	–	Round	Round	Round
Granular class	mm	EN 933–1	2–16	2–16	2–16
Absolute density	(kg/m^3) (±15%)		2105	2370	–
Bulk density	(kg/m^3) (±15%)	EN 1097–3	897	902	550
Apparent density	(kg/m^3) (±15%)	EN 1097–3	1024	1039	–
Compressive strength	MPa (±10%)	EN 13055–1	3.15	7.6	4.7
Crushed particles	% Weight (±15%)	EN 933–5	16.9	14.4	7
Chlorides	% Cl^-	EN 1744–1	0.52	0.49	<0.004
Sulfates soluble in acid	% SO_3	EN 1744–1	0.41	0.38	<0.05
Total Sulfur	%S	EN 1744–1	0.58	0.54	<0.04
Porosity	%	NF P94–410-3	29	21	–
Water absorption (24 h)	% (±10%)	EN 1097–6	27.9	19.8	27.3
Thermal conductivity	(W/m°C)	EN 12667	0.19	0.32	0.14
Loss On Ignition (LOI) (900 °C)	%	EN 1744–1	27.2	31.3	–

4.3. Compressive strength

The compressive strength of LWA is an important factor in concrete, as LWA are the weakest component of concrete [67]. Non-carbonated LWA have a lower bulk crushing strength (3.15 MPa) than ARGEX aggregates (4.7 MPa), as expected from the composition as well as the bulk and absolute density. The carbonated LWA tend to show higher mechanical performances superior (7.6 MPa) to the Non-carbonated LWA and the Argex aggregates. These results reflect the interest of carbonated aggregates in the field of civil engineering.

The effect of carbonation is very significant in type C of FA, this is due to the large amount of reactive CaO in WPFA, which reacts with water to form ($Ca(OH)_2$), the fact that the slaked lime containing aggregates were found to be resistant, and that exposure to 100% CO_2 promoted the development of resistance, indicates that the carbonation step is well optimized further to form $CaCO_3$ bridges. The strength increases significantly after carbonation, this confirms what we observed in SEM and TGA imaging, $Ca(OH)_2$ reacts with CO_2 forming solid calcite bridges in the particles which improves the compressive strength of the granules.

In a study by Bui et al. [68], the compressive strength of alkali-activated aggregates prepared from rice husk FA, blast furnace slag, and class F FA varied from 5.5 to 14.5 MPa. Gonzal et al. [65,66,69,70] have used several different precursors, such as FA, washing aggregate sludge, used motor oil, mining and industrial waste, then the aggregates are prepared by sintering in a rotary kiln. The bulk compressive strength of the aggregates is between 2 and 14 MPa.

Several studies have shown that the manufacture of artificial aggregates by granulating various wastes as raw materials with cement, leads to strengths between 1 and 7 MPa. Surprisingly, despite the different precursors and preparation methods used, the strength values are so similar to those previously studied. Ferrone et al., [71] has previously reported that commercial lightweight expanded clay aggregates (Leca) have compressive strengths varying from 0.7 to 4.5 MPa, depending on the size. This confirmed that LWA made from WPFA before and after carbonation have equivalent mechanical performance compared to aggregates made in other studies, also for commercial aggregates widely used (Argex) and can therefore replace them in civil engineering applications.

4.4. Thermal conductivity

The results presented in Table 6 show excellent thermal performances for the LWA before and after carbonation with a thermal conductivity of 0.19 W/m.°C and 0.32 W/m.°C respectively, similar to that of the Argex aggregate (0.14 W/m.°C).

The absolute density of LWA before carbonation was 2105 kg/m3, thus the porosity was higher (29%) which explains the high thermal performance of non-carbonated LWA. After carbonation, the porosity decreases (19.8%), because of the $CaCO_3$ formed at the surface and the absolute density value increases (2370 kg/m^3), this increase in density and the decrease in porosity led to a significant decrease in the insulating capacity of the aggregates. If the thermal conductivity of the aggregates depended only on their total porosity or on the density of the aggregates, the conductivity/density ratios of the different aggregates would be similar regardless of the nature of the aggregate.

This was also illustrated by Nguyen [72] in his studies on the characterization of insulating LWA; an order of magnitude conductivity of 0.4 W/m.°C was achieved. The author also presents the hypothesis that the denser external surface of the expanded shale aggregates can constitute a "thermal bridge" favoring the transfer of heat and thus lead to a slightly higher thermal conductivity of the aggregate, which is consistent with the results of this paper. According to Valore [73], the thermal conductivity of LWA depends mainly on its absolute density; thus, its honeycomb structure confers an interesting thermal conductivity and thermal expansion. As an example, the classic aggregate has a thermal conductivity of 1.75 W/m.°C while that of the LWA of expanded clay or expanded shale is between 0.10 and 0.80 W/m.°C [74]. This gives the LWA a higher thermal insulation. In addition, LWA has a high degree of fire resistance due to its low thermal conductivity and low coefficient of thermal expansion [75]. Fire resistance is not discussed in this study.

4.5. Loss on ignition

According to Table 6, the loss on ignition value of LWA before and after carbonation is 27.2% and 31.3% at 900 °C, respectively. At the same time, the loss on ignition at 900 °C was measured to explore the thermal instability of LWA before and after carbonation. It should be mentioned that the total mass loss observed in the loss on ignition only reflects the contribution of the residual organic matter. The mass loss from 0 to 550 °C due to the loss of bound water, organic matter and clays, between 350 and 550 °C corresponds to the deshydroxylation of portlandite, and when the temperature is higher than 550 °C up to 900 °C the mass loss corresponds well to the decarbonation of the different modes of calcium carbonates (aragonite, vaterite, calcite).

Based on the loss on ignition and TGA results, the percentage of organic matter in LWA before and after carbonation can be estimated using the following relationship:

$$\%\text{Organic matter} = \text{Total mass loss} - (\%\text{CSH deshydroxylation mass} + \%Ca(OH)_2 \text{ deshydroxylation mass} + \%CaCO_3 \text{ decarbonation mass})$$

The difference in mass loss at 900 °C of LWA due to hydrate formation, lime hydration and carbonate formation as we observed in the TGA. The percentage of organic matter seems to be similar before and after carbonation (5.76% before carbonation and 5.08% after

carbonation), which shows that carbonation has no influence on organic matter.

4.6. Solubility tests: acid-soluble sulphates and acid-soluble sulphates

The determination of the chemical and mineralogical composition in the LWA should be concentrated on the determination of % total sulfur, % chloride and % acid soluble sulfates. The percentages determined for chloride, total sulfur and acid soluble sulphates of the LWA before and after carbonation were similar (Table 6).

The content of acid soluble sulfates and chloride ions defines a designation of aggregates without a threshold being imposed. However, a maximum value of 0.01% and 0.8% respectively for the content of chloride ions and acid soluble sulfate are recommended [66].

In fact, a too high sulfate content leads to a risk of secondary ettringite formation or Candlot salt. The presence of chloride in LWA can cause premature corrosion in concrete or mortar after migration of ions. A high presence of chloride can also cause the formation of lime chloroaluminate or Friedel salt, which is expansive. It is determined according to the EN 1744–1 standard (Afnor, Norme NF EN 1744–1). Degradations can occur in concrete formulated with aggregates with a high sulfide content, sulfides can be transformed into sulfates by oxidation. The sulfates in turn can influence the setting and cause swelling (secondary ettringite) and thus lead to an increase in the porosity of concrete. This porosity can then have an important role in case of attack of the concrete by external agents such as sulphate or chloride solutions. Their presence is related to the operating environment of the structure, and a higher porosity facilitates the penetration of these aggressive elements towards the core of the materials and by increasing the reaction surfaces [66]. For this reason, carbonation was necessary to decrease the percentage of porosity. In fact, the contents of LWA are not very high and are clearly lower than those recommended by the standard.

5. Conclusion

This study shows the feasibility and optimization of granulation parameters, in order to fabricate LWA from WPFA (rich in CaO), by granulation with water in an Eirich high intensity granulator (Eirich R-02). An accelerated carbonation step was performed, exposing the manufactured LWA to pure carbon dioxide in order to evolve the immobilization potential of Ba and Pb, and to investigate the influence of carbonation on the physical, morphological, thermal and mechanical characterization of LWA.

- To adjusting the granulation parameters of the Eirich high intensity granulator to a constant impeller speed (3000 rpm), the rotation speed of the steel pan (170 rpm), the rotation mode between the impeller and the steel pan in cross current and a granulation time of 3 min, 95% of the LWA were produced with the target size (2 mm to 16 mm).
- WPFA exhibited high reactivity to carbon dioxide. Accelerated carbonation of the LWA reduced the leaching of Ba and Pb with removal percentages exceeding 98% for both elements. TGA and SEM-EDS results confirm the formation of calcite after accelerated carbonation, as well as the formation of hydrates (ettringite and carboaluminates) due to the hydraulic properties of WPFA.
- The characteristics of LWA before and after carbonation are evaluated according to the NF EN 13055–1 standard in order to confirm the possibility of valorizing these eco-materials in the manufacture of concrete. These aggregates present a relatively low density, classifying them in the category of LWA. This weight reduction is due to the high porosity of these aggregates, suggesting a significant capacity of water imprisonment for the hydration of cement. Moreover, after carbonation the percentage of porosity and water absorption decreased, thus, the mechanical strength was improved (7.6 MPa). Finally, the measurement of the thermal conductivity of LWA is interesting and would lead to an improvement of the thermal performance of concrete
- However, in order to improve the valorization of these waste types, it is essential to improve the performance of the manufactured LWA. Many research perspectives are also envisaged to extend this study. These prospects may concern: (i) Testing other binders, allowing the improvement of the physic-chemical properties; (ii) Realizing sorption tests at different temperatures to evaluate the temperature influence on the hygric behavior of LWA; (iii) Substituting partially or totally ordinary aggregates by LWA in concrete; (iv) Studying the coupling between carbonated and non-carbonated LWA in concrete.

CRediT authorship contribution statement

Bader Bouzar: Investigation, Methodology, Data curation, Writing – original draft. **Yannick Mamindy-Pajany:** Conceptualization, Methodology, Investigation, Data curation, Resources, Writing – original draft, Writing – review & editing, Validation, Supervision.

Declaration of Competing Interest

The authors declare that they have no known competing financial interests or personal relationships that could have appeared to influence the work reported in this paper. The manuscript has not been submitted to a preprint server prior to submission on Powder Technology.

The authors declare that no funds, grants, or other support were received during the preparation of this manuscript.

The authors have no relevant financial or non-financial interests to disclose.

All authors contributed to the study conception and design. Material preparation, data collection and analysis were performed by Bader Bouzar and Yannick Mamindy-Pajany.

Acknowledgements

The authors wish to acknowledge technical contributions of the chemistry pole of Institut Mines-Télécom. This research did not receive any specific grant from funding agencies in the public, commercial, or not-for-profit sectors.

Appendix A. Supplementary data

Supplementary data to this article can be found online at https://doi.org/10.1016/j.powtec.2022.117583.

References

[1] S. Ray, A.K. Mishra, A.S. Kalamdhad, Hydraulic performance, consolidation characteristics and shear strength analysis of bentonites in the presence of fly-ash, sewage sludge and paper-mill leachates for landfill application, J. Environ. Manag. 302 (janv. 2022) 113977, https://doi.org/10.1016/j.jenvman.2021.113977.
[2] M. Cox, H. Nugteren, M. Janssen-Jurkovičová, Combustion Residues: Current, Novel and Renewable Applications, John Wiley & Sons, 2008.
[3] A.A. Tortosa Masiá, B.J.P. Buhre, R.P. Gupta, T.F. Wall, Characterising ash of biomass and waste, Fuel Process. Technol. 88 (11) (déc. 2007) 1071–1081, https://doi.org/10.1016/j.fuproc.2007.06.011.
[4] D. Yao, et al., Carbon footprint and water footprint analysis of generating synthetic natural gas from biomass, Renew. Energy 186 (mars 2022) 780–789, https://doi.org/10.1016/j.renene.2022.01.014.
[5] S. Wang, L. Baxter, F. Fonseca, Biomass fly ash in concrete: SEM, EDX and ESEM analysis, Fuel 87 (3) (mars 2008) 372–379, https://doi.org/10.1016/j.fuel.2007.05.024.
[6] R. Rajamma, et al., Biomass fly ash effect on fresh and hardened state properties of cement based materials, Compos. Part B 77 (août 2015) 1–9, https://doi.org/10.1016/j.compositesb.2015.03.019.
[7] R. Rajamma, R.J. Ball, L.A.C. Tarelho, G.C. Allen, J.A. Labrincha, V.M. Ferreira, Characterisation and use of biomass fly ash in cement-based materials, J. Hazard. Mater. 172 (2) (déc. 2009) 1049–1060, https://doi.org/10.1016/j.jhazmat.2009.07.109.

[8] T.C. Esteves, R. Rajamma, D. Soares, A.S. Silva, V.M. Ferreira, J.A. Labrincha, Use of biomass fly ash for mitigation of alkali-silica reaction of cement mortars, Constr. Build. Mater. 26 (1) (janv. 2012) 687–693, https://doi.org/10.1016/j.conbuildmat.2011.06.075.
[9] S. Ehsan, S.O. Prasher, W.D. Marshall, A washing procedure to mobilize mixed contaminants from soil, J. Environ. Qual. 35 (6) (2006) 2146–2153, https://doi.org/10.2134/jeq2005.0474.
[10] M. Isoyama, S.-I. Wada, Remediation of Pb-contaminated soils by washing with hydrochloric acid and subsequent immobilization with calcite and allophanic soil, J. Hazard. Mater. 143 (3) (mai 2007) 636–642, https://doi.org/10.1016/j.jhazmat.2007.01.008.
[11] A. Moutsatsou, M. Gregou, D. Matsas, V. Protonotarios, Washing as a remediation technology applicable in soils heavily polluted by mining–metallurgical activities, Chemosphere 63 (10) (juin 2006) 1632–1640, https://doi.org/10.1016/j.chemosphere.2005.10.015.
[12] C.N. Mulligan, R.N. Yong, B.F. Gibbs, Remediation technologies for metal-contaminated soils and groundwater: an evaluation, Eng. Geol. 60 (1) (juin 2001) 193–207, https://doi.org/10.1016/S0013-7952(00)00101-0.
[13] H. Chen, C. Mangwandi, D. Rooney, Production of solid biofuel granules from drum granulation of bio-waste with silicate-based binders, Powder Technol. 354 (sept. 2019) 231–239, https://doi.org/10.1016/j.powtec.2019.05.074.
[14] L.B. Andrade, J.C. Rocha, M. Cheriaf, Evaluation of concrete incorporating bottom ash as a natural aggregates replacement, Waste Manag. 27 (9) (janv. 2007) 1190–1199, https://doi.org/10.1016/j.wasman.2006.07.020.
[15] F. Liu, Y. Yan, L. Li, C. Lan, G. Chen, Performance of recycled plastic-based concrete, J. Mater. Civ. Eng. 27 (2) (févr. 2015) A4014004, https://doi.org/10.1061/(ASCE)MT.1943-5533.0000989.
[16] N.U. Kockal, T. Ozturan, Characteristics of lightweight fly ash aggregates produced with different binders and heat treatments, Cem. Concr. Compos. 33 (1) (janv. 2011) 61–67, https://doi.org/10.1016/j.cemconcomp.2010.09.007.
[17] N.U. Kockal, T. Ozturan, Effects of lightweight fly ash aggregate properties on the behavior of lightweight concretes, J. Hazard. Mater. 179 (1) (juill. 2010) 954–965, https://doi.org/10.1016/j.jhazmat.2010.03.098.
[18] F.K. Alqahtani, M.I. Khan, G. Ghataora, S. Dirar, Production of recycled plastic aggregates and its utilization in concrete, J. Mater. Civ. Eng. 29 (4) (avr. 2017) 04016248, https://doi.org/10.1061/(ASCE)MT.1943-5533.0001765.
[19] M. Franus, R. Panek, J. Madej, W. Franus, The properties of fly ash derived lightweight aggregates obtained using microwave radiation, Constr. Build. Mater. 227 (déc. 2019) 116677, https://doi.org/10.1016/j.conbuildmat.2019.116677.
[20] M. Benali, V. Gerbaud, M. Hemati, Effect of operating conditions and physico–chemical properties on the wet granulation kinetics in high shear mixer, Powder Technol. 190 (1) (mars 2009) 160–169, https://doi.org/10.1016/j.powtec.2008.04.082.
[21] K.P. Hapgood, B. Khanmohammadi, Granulation of hydrophobic powders, Powder Technol. 189 (2) (janv. 2009) 253–262, https://doi.org/10.1016/j.powtec.2008.04.033.
[22] M. Singh, S. Shirazian, V. Ranade, G.M. Walker, A. Kumar, Challenges and opportunities in modelling wet granulation in pharmaceutical industry – a critical review, Powder Technol. 403 (mai 2022) 117380, https://doi.org/10.1016/j.powtec.2022.117380.
[23] L. Vandevivere, E. Van Wijmeersch, O. Häusler, T. De Beer, C. Vervaet, V. Vanhoorne, The effect of screw configuration and formulation variables on liquid requirements and granule quality in a continuous twin screw wet granulation process, J. Drug Deliv. Sci.Technol. 68 (févr. 2022) 103042, https://doi.org/10.1016/j.jddst.2021.103042.
[24] S.M. Iveson, J.D. Litster, K. Hapgood, B.J. Ennis, Nucleation, growth and breakage phenomena in agitated wet granulation processes: a review, Powder Technol. 117 (1) (juin 2001) 3–39, https://doi.org/10.1016/S0032-5910(01)00313-8.
[25] V. Chouk, G. Reynolds, M. Hounslow, A. Salman, Single drop behaviour in a high shear granulator, Powder Technol. 189 (2) (janv. 2009) 357–364, https://doi.org/10.1016/j.powtec.2008.04.019.
[26] P.K. Le, P. Avontuur, M.J. Hounslow, A.D. Salman, The kinetics of the granulation process: Right from the early stages, Powder Technol. 189 (2) (janv. 2009) 149–157, https://doi.org/10.1016/j.powtec.2008.04.018.
[27] P.B. Pathare, N. Baş, J.J. Fitzpatrick, K. Cronin, E.P. Byrne, Effect of high shear granulation process parameters on the production of granola cereal aggregates, Biosyst. Eng. 110 (4) (déc. 2011) 473–481, https://doi.org/10.1016/j.biosystemseng.2011.10.004.
[28] P. Pandey, J. Tao, A. Chaudhury, R. Ramachandran, J.Z. Gao, D.S. Bindra, A combined experimental and modeling approach to study the effects of high-shear wet granulation process parameters on granule characteristics, Pharm. Dev. Technol. 18 (1) (févr. 2013) 210–224, https://doi.org/10.3109/10837450.2012.700933.
[29] S.I.F. Badawy, M.M. Menning, M.A. Gorko, D.L. Gilbert, Effect of process parameters on compressibility of granulation manufactured in a high-shear mixer, Int. J. Pharm. 198 (1) (mars 2000) 51–61, https://doi.org/10.1016/S0378-5173(99)00445-7.
[30] C. Mangwandi, M.J. Adams, M.J. Hounslow, A.D. Salman, Effect of impeller speed on mechanical and dissolution properties of high-shear granules, Chem. Eng. J. 164 (2) (nov. 2010) 305–315, https://doi.org/10.1016/j.cej.2010.05.039.
[31] M. Bardin, P.C. Knight, J.P.K. Seville, On control of particle size distribution in granulation using high-shear mixers, Powder Technol. 140 (3) (févr. 2004) 169–175, https://doi.org/10.1016/j.powtec.2004.03.003.
[32] N. Rahmanian, A. Naji, M. Ghadiri, Effects of process parameters on granules properties produced in a high shear granulator, Chem. Eng. Res. Des. 89 (5) (mai 2011) 512–518, https://doi.org/10.1016/j.cherd.2010.10.021.
[33] M.X.L. Tan, K.P. Hapgood, Foam granulation: effects of formulation and process conditions on granule size distributions, Powder Technol. 218 (mars 2012) 149–156, https://doi.org/10.1016/j.powtec.2011.12.006.
[34] P.C. Knight, A. Johansen, H.G. Kristensen, T. Schæfer, J.P.K. Seville, An investigation of the effects on agglomeration of changing the speed of a mechanical mixer, Powder Technol. 110 (3) (juin 2000) 204–209, https://doi.org/10.1016/S0032-5910(99)00259-4.
[35] J.G. Jang, H.K. Lee, Microstructural densification and CO2 uptake promoted by the carbonation curing of belite-rich Portland cement, Cem. Concr. Res. 82 (avr. 2016) 50–57, https://doi.org/10.1016/j.cemconres.2016.01.001.
[36] A.M. Safhi, P. Rivard, A. Yahia, K. Henri Khayat, N.-E. Abriak, Durability and transport properties of SCC incorporating dredged sediments, Constr. Build. Mater. 288 (juin 2021) 123116, https://doi.org/10.1016/j.conbuildmat.2021.123116.
[37] L. Van Ginneken, V. Dutré, W. Adriansens, H. Weyten, Effect of liquid and supercritical carbon dioxide treatments on the leaching performance of a cement-stabilised waste form, J. Supercrit. Fluids 30 (2) (juill. 2004) 175–188, https://doi.org/10.1016/j.supflu.2003.07.004.
[38] AFNOR, EN 13055–1, Lightweight Aggregates for Concrete, Mortar and Grou, décembre 2002.
[39] Y. Mamindy-Pajany, C. Hurel, N. Marmier, M. Roméo, Arsenic (V) adsorption from aqueous solution onto goethite, hematite, magnetite and zero-valent iron: Effects of pH, concentration and reversibility, Desalination 281 (oct. 2011) 93–99, https://doi.org/10.1016/j.desal.2011.07.046.
[40] AFNOR, NF EN ISO 18757, Determination of Specific Surface Area PF Ceramic Powders by Gas Adsorption Using the BET method, juin 2006.
[41] AFNOR, NF EN 1097–7 “Tests for Mechanical and Physical Properties for Aggregates”, juin 2008.
[42] AFNOR, NF ISO 13320-1, Laser Diffraction Methods, septembre 2000.
[43] AFNOR, NF EN 933-1 “Test for Geometrical Properties of Aggregates”, mai 2012.
[44] AFNOR, NF EN 933–2 “Test for Geometrical Properties of Aggregates”, juin 2020.
[45] AFNOR, NF EN 12457–2, Leaching-Compliance Test for Leaching of Granular Wasre Materials ans Sludges, décembre 2002.
[46] AFNOR, ASTM C 618, Standard Specification for Coal Fly Ash and Raw or Calcined Natural Pozzolan for Use in Concrete, décembre 2002.
[47] I.-J. Chiou, K.-S. Wang, C.-H. Chen, Y.-T. Lin, Lightweight aggregate made from sewage sludge and incinerated ash, Waste Manag. 26 (12) (janv. 2006) 1453–1461, https://doi.org/10.1016/j.wasman.2005.11.024.
[48] M. Criado, A. Palomo, A. Fernández-Jiménez, Alkali activation of fly ashes. Part 1: effect of curing conditions on the carbonation of the reaction products, Fuel 84 (16) (nov. 2005) 2048–2054, https://doi.org/10.1016/j.fuel.2005.03.030.
[49] AFNOR, NF EN 1097–3 “Tests for Mechanical and Physical Properties of Aggregates”, août 1998.
[50] AFNOR, NF P 94–410-3 “Essais pour déterminer les propriétés physiques des roches”, mai 2001.
[51] AFNOR, EN 1097–6 “Tests for Mechanical and Physical Properties of Aggregates”, février 2022.
[52] AFNOR, NF EN 1744–1+A1 “Tests for Chemical Properties of Aggregates”, février 2014.
[53] Y. Liu, D. Scharf, T. Graule, F.J. Clemens, Granulation processing parameters on the mechanical properties of diatomite-based porous granulates, Powder Technol. 263 (sept. 2014) 159–167, https://doi.org/10.1016/j.powtec.2014.04.094.
[54] G.M. Walker, Chapter 4 Drum granulation processes, in: A.D. Salman, M. J. Hounslow, J.P.K. Seville (Eds.), Handbook of Powder Technology vol. 11, Elsevier Science B.V, 2007, pp. 219–254, https://doi.org/10.1016/S0167-3785(07)80039-X.
[55] J.J. Dijkstra, H.A. van der Sloot, R.N.J. Comans, The leaching of major and trace elements from MSWI bottom ash as a function of pH and time, Appl. Geochem. 21 (2) (févr. 2006) 335–351, https://doi.org/10.1016/j.apgeochem.2005.11.003.
[56] A. Bouchikhi, A.M. Safhi, P. Rivard, R. Snellings, N.-E. Abriak, Fluvial sediments as SCMs: characterization, pozzolanic performance, and optimization of equivalent binder, J. Mater. Civ. Eng. 34 (2) (2022) 04021430.
[57] F. Casini, G.M.B. Viggiani, S.M. Springman, Breakage of an artificial crushable material under loading, Granul. Matter 15 (5) (oct. 2013) 661–673, https://doi.org/10.1007/s10035-013-0432-x.
[58] R.F. Rodrigues, S.R. Leite, D.A. Santos, M.A.S. Barrozo, Drum granulation of single super phosphate fertilizer: effect of process variables and optimization, Powder Technol. 321 (nov. 2017) 251–258, https://doi.org/10.1016/j.powtec.2017.08.036.
[59] H.A. van der Sloot, R.N.J. Comans, O. Hjelmar, Similarities in the leaching behaviour of trace contaminants from waste, stabilized waste, construction materials and soils, Sci. Total Environ. 178 (1) (janv. 1996) 111–126, https://doi.org/10.1016/0048-9697(95)04803-0.
[60] S.-Y. Pan, E.E. Chang, P.-C. Chiang, CO2 capture by accelerated carbonation of alkaline wastes: a review on its principles and applications, Aerosol Air Qual. Res. 12 (5) (2012) 770–791, https://doi.org/10.4209/aaqr.2012.06.0149.
[61] E. Rendek, G. Ducom, P. Germain, Carbon dioxide sequestration in municipal solid waste incinerator (MSWI) bottom ash, J. Hazard. Mater. 128 (1) (janv. 2006) 73–79, https://doi.org/10.1016/j.jhazmat.2005.07.033.
[62] P.J. Gunning, C.D. Hills, P.J. Carey, Accelerated carbonation treatment of industrial wastes, Waste Manag. 30 (6) (2010) 1081–1090.
[63] H. Ecke, N. Menad, A. Lagerkvist, Carbonation of municipal solid waste incineration fly ash and the impact on metal mobility, J. Environ. Eng. 129 (5) (mai 2003) 435–440, https://doi.org/10.1061/(ASCE)0733-9372(2003)129:5(435.
[64] V. Ducman, A. Mladenovič, J.S. Šuput, Lightweight aggregate based on waste glass and its alkali–silica reactivity, Cem. Concr. Res. 32 (2) (févr. 2002) 223–226, https://doi.org/10.1016/S0008-8846(01)00663-9.

[65] B. González-Corrochano, J. Alonso-Azcárate, M. Rodas, F.J. Luque, J. F. Barrenechea, Microstructure and mineralogy of lightweight aggregates produced from washing aggregate sludge, fly ash and used motor oil, Cem. Concr. Compos. 32 (9) (oct. 2010) 694–707, https://doi.org/10.1016/j.cemconcomp.2010.07.014.
[66] B. González-Corrochano, J. Alonso-Azcárate, M. Rodas, J.F. Barrenechea, F. J. Luque, Microstructure and mineralogy of lightweight aggregates manufactured from mining and industrial wastes, Constr. Build. Mater. 25 (8) (août 2011) 3591–3602, https://doi.org/10.1016/j.conbuildmat.2011.03.053.
[67] P. Monteiro, Concrete: Microstructure, Properties, and Materials, McGraw-Hill Publishing, 2006.
[68] L.A. Bui, C. Hwang, C. Chen, K. Lin, M. Hsieh, Manufacture and performance of cold bonded lightweight aggregate using alkaline activators for high performance concrete, Constr. Build. Mater. 35 (oct. 2012) 1056–1062, https://doi.org/10.1016/j.conbuildmat.2012.04.032.
[69] B. González-Corrochano, J. Alonso-Azcárate, M. Rodas, Characterization of lightweight aggregates manufactured from washing aggregate sludge and fly ash, Resour. Conserv. Recycl. 53 (10) (août 2009) 571–581, https://doi.org/10.1016/j.resconrec.2009.04.008.
[70] B. González-Corrochano, J. Alonso-Azcárate, M. Rodas, Production of lightweight aggregates from mining and industrial wastes, J. Environ. Manag. 90 (8) (juin 2009) 2801–2812, https://doi.org/10.1016/j.jenvman.2009.03.009.
[71] C. Ferone, F. Colangelo, F. Messina, F. Iucolano, B. Liguori, R. Cioffi, Coal combustion wastes reuse in low energy artificial aggregates manufacturing, Materials 6 (11) (nov. 2013), https://doi.org/10.3390/ma6115000. Art. n° 11.
[72] L.H. Nguyen, A.-L. Beaucour, S. Ortola, A. Noumowé, Influence of the volume fraction and the nature of fine lightweight aggregates on the thermal and mechanical properties of structural concrete, Constr. Build. Mater. 51 (janv. 2014) 121–132, https://doi.org/10.1016/j.conbuildmat.2013.11.019.
[73] R.C. Valore, Calculations of U-values of hollow concrete masonry, Concr. Int. 2 (2) (févr. 1980) 40–63.
[74] T. Van Gerven, J. Moors, V. Dutré, C. Vandecasteele, Effect of CO2 on leaching from a cement-stabilized MSWI fly ash, Cem. Concr. Res. 34 (7) (juill. 2004) 1103–1109, https://doi.org/10.1016/j.cemconres.2003.11.022.
[75] M.S. Abrams, A.H. Gustaferro, Fire endurance of concrete slabs as influenced by thickness, aggregate type, and moisture, Portl. Cem. Assoc. R & D Lab. Bull. 0 (2021). Art. no No 223.

Chapter 4:

Innovative reuse of fly ashes for treatment of contaminated river sediments: Synthesis of Layered Double Hydroxides (LDH) and chemical performance assessments

Waste and Biomass Valorization
https://doi.org/10.1007/s12649-023-02056-0

ORIGINAL PAPER

Innovative Reuse of Fly Ashes for Treatment of a Contaminated River Sediment: Synthesis of Layered Double Hydroxides (LDH) and Chemical Performance Assessments

Bader Bouzar[1,2] · Yannick Mamindy-Pajany[1,2] · Charlotte Hurel[3]

Received: 15 September 2022 / Accepted: 20 January 2023

Abstract

Purpose This investigation presents a new valorization route of fly ash, based on the synthesis of layered double hydroxide (LDH) used as efficient and cost-effective adsorbent for the stabilization of contaminants in sediments.

Methods LDH were synthesized through an acid leaching method at constant pH followed by precipitation, applied on waste paper fly ash (WPFA) and biomass fly ash (BFA), obtained from industries of the Hauts de France region. The synthesized LDH (LDH_{WPFA} and LDH_{BFA}) were calcinated at 450 °C, their physico-chemical and adsorption properties were then compared before and after calcination, with a commercial hydrotalcite (HT).

Results The XRD diffractograms of synthesized LDH showed characteristic bands of hydrocalumite $Ca_4Al_2(OH)_{12}(Cl,CO_3,OH)_2{\cdot}4H_2O$ and paraalumohydrocalcite ($CaAl_2(CO_3)(OH)_4.6H_2O$) for LDH_{WPFA} and LDH_{BFA}, respectively. The FTIR spectra showed similar patterns to LDH containing interlamellar anions (CO_3^{2-} and OH^-) in the vicinity of 1360 cm^{-1} and 3600 cm^{-1}. The LDH morphology presented platelets and hexagonal block shapes with some octahedral forms. The batch and column adsorption results showed that more than 98% of Sb, Zn and SO_4^{2-} were stabilized when the sediment matrix was amended with 5% of calcinated LDH_{WPFA}, compared to untreated sediment, due to the negative charge of the surface.

Conclusion Synthesized LDH were able to stabilize both cationic species (by adsorption and electrostatic attraction), and anionic species (by anion exchange) inside the sediment matrix.

✉ Bader Bouzar
bader.bouzar@imt-nord-europe.fr

Yannick Mamindy-Pajany
yannick.mamindy@imt-nord-europe.fr

Charlotte Hurel
charlotte.hurel@univ-cotedazur.fr

[1] IMT Nord Europe, Centre for Materials and Processes, Environnement, Institut Mines-Télécom, F-59000 Lille, France

[2] Laboratoire de Génie Civil Et Géo-Environnement, Univ. Lille, Univ., ULR 4515—LGCgE, 59000 Lille, France

[3] Institut de Physique de Nice, UMR CNRS 7010 UNS, Université Côte d'Azur, Nice, France

Published online: 09 February 2023

Graphical Abstract

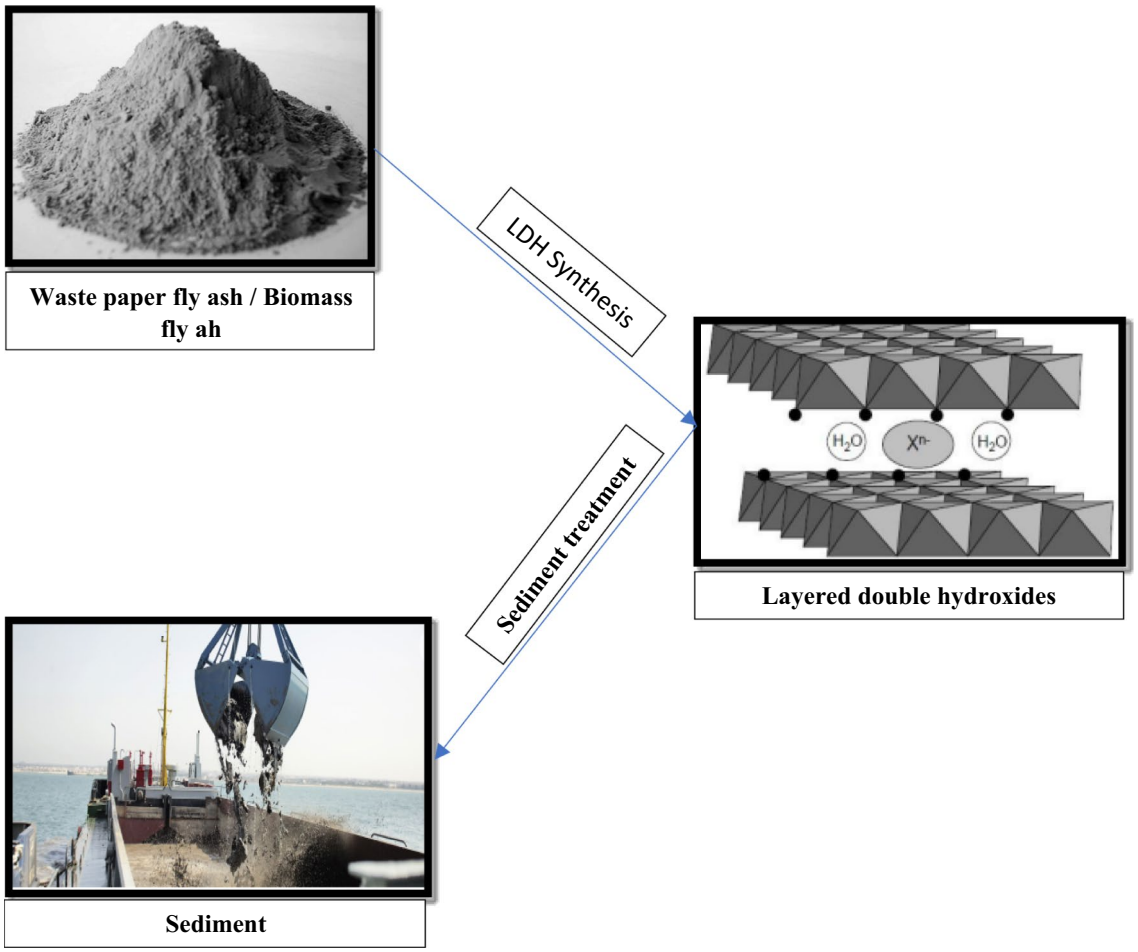

Keywords Sediment · Stabilization · Layered double hydroxide · Trapping mechanism · Surface adsorption · Anionic exchange · Metallic and metalloids trace elements

Statement of Novelty

LDHs were synthesized through an acid leaching at constant pH followed by precipitation applied to waste paper fly ash (WPFA) and biomass fly ash (BFA), originating from the industry in the Hauts de France region. X-ray diffraction (XRD), X-ray fluorescence (XRF), infrared (IR), scanning electron microscope (SEM) and zeta potential (ξ) were used to confirm the formation of LDH by comparison with commercial hydrotalcite. Batch and column adsorption results showed that amendment of river sediment with 5% of calcinated LDH_{WPFA} stabilized more than 98% of Sb, Zn, and SO_4^{2-} compared with untreated sediments. Cationic species were stabilized through electrostatic attraction and adsorption mechanisms, and anionic species were stabilized through anion exchange mechanism.

Introduction

Inland waterway navigation is a highly developed mode of transport in Europe. The European waterway network is estimated at about 20,000 km, and nearly 8500 km in France [1]. Inland waterway transport is considered as the most modern and most suitable for all kinds of products [1]. This mode of transport is reliable, economic and ecologic but the ship circulation is regularly disturbed by sediment accumulation that naturally occurs at the bottom of waterways, canals, rivers. The annual volume of dredged sediments is huge: about 600 Mm^3 in the world [2], 250 Mm^3 in Europe [3], 50 Mm^3 in France [4] among which more than 6 Mm^3 are river sediments [5]. The dredging activity is essential to maintain or restore the minimum draft to facilitate the ship circulation, the restoration of the natural environment

and the flood risk prevention. Therefore, the management of large amount of dredged sediments is an issue that would be worth addressing.

The physico-chemical complexity of sediments makes difficult their incorporation into management schemes in a scientific point of view. Indeed, sediments are composed of inert and reactive mineral phases (including metallic sulfides), organic matter with changing maturity degree, and a large diversity of metallic, organic and organometallic contaminants [6]. Depending on the degree of contamination, dumping of sediments at sea may be prohibited, and sediment valorization may also be problematic [6]. The management of dredged sediments represents a major environmental and economic challenge since sediment immersion undoubtedly pollute the aquatic and continental environment. To date, the alternative to disposal at sea has been storage on land, when possible, in a supervised storage center for contaminated sediments that meet the criteria established by the regulations [6].

Several techniques are used to reduce the hazardous nature of sediments such as stabilization with chemical additives and hydraulic binders, contaminant extraction, membrane separation or adsorption, leaching, flotation and thermal inserting [7, 8]. Among the methods for removing these contaminants from aqueous effluents, adsorption is considered as one of the most attractive technologies. Materials able to remove anionic pollutants are less numerous compared to those able to bind cationic pollutants. The development of adsorbents adapted to anionic species, with a low production cost and efficiency comparable to synthetic supports may be an answer to a systematic implementation of treatment units.

The use of mineral additives has been extensively studied for in situ treatment of contaminated sediments [9–11]. Förstner [10] compiled an inventory of the most commonly used minerals for in situ stabilization of sediments due to their stability, sorption capacity and low cost. Among them, industrial products (fly ash and red mud) and natural minerals (calcite, apatite, clay and zeolites) were the most promising additives [10]. Nevertheless, few studies have focused on the stabilization of dredged sediments with LDH.

Layered Double Hydroxides (LDH) of the hydrotalcite (HT) group are generally represented by the formula $[M^{II}_{1-y} L^{III}_{y} (OH)_2]^{y+} [X^{n-}]_{y/n}.zH_2O$. Several methods have been proposed for the synthesis of LDH with controlled structures and properties. Among them, conventional co-precipitation process via chemicals [12, 13], anion exchange [14], hydrothermal treatment [15], structural reconstruction [16] and electrochemical methods [17, 18]. Recently, LHD synthesis starting from industrial by-products such as oil shale ash [19], aluminum slag [20], blast furnace slag [21, 22] and coal fly ash [23] have been proposed as a possible valorization route of these by-products. LDH have capability to scavenge simple and complex anions (F^-, Cl^-, Br^-, I^-, ClO_4^-, BF_4^-, CrO_4^-, SO_4^{2-} [24, 25]) by anion exchange due to the flexibility of the interlayer space [26, 27] and the property is verified on Mg/Al LDH corresponding to natural hydrotalcites [28], this capacity has been applied in the field of soil or water remediation. Therefore, LDH have been widely studied as anionic adsorbent, especially towards nitrates in soils [29], water contaminants [28], or dyes in aqueous solution [27, 30]. The calcination treatment leads to the formation of a mixture of mixed oxides of divalent and trivalent metals which, through rehydration in the presence of a selected anionic species, results in a new LDH phase intercalated by the new anion species. Miyata et al. [31] were the first researchers to describe the ability of LDH phases to recover their original structure after calcination under peculiar thermal treatment conditions. Some have referred this as the "memory effect" of the LDH structure. Similarly, the calcination products are also susceptible to trap organic or inorganic anions through ion exchange and reconstruction reactions [32–35]. The efficiency of such compounds in the treatment of water polluted by nitrate, phosphate or chromate anions has already been demonstrated [36, 37], as well as the trapping of toxic molecules such as pesticides used in agriculture (MCPA82 ….) [38], and for the sorption of Ni on pyrophyllite [39].

The objective of this study was to investigate incorporation of LDH as amendments in a sediment matrix, in order to limit sulfate, metallic and metalloid trace elements (MMTE) (such as Cu, Sb, Zn) mobility from the sediment. For that, waste paper fly ash (WPFA) and biomass fly ash (BFA) were used for the first time as precursors for LDH synthesis. Then, LDH characterization was done by X-ray diffraction (XRD), X-ray fluorescence (XRF), Infrared (IR), Scanning Electron Microscope (SEM) and zeta potential (ξ), and compared with commercial hydrotalcite. Next, batch adsorption tests and column leaching tests were performed in order to assess the efficiency of LDH to limit mobility of sulfate and MMTE contained in the sediment matrix. Finally, after comparison with hydrotalcite, conclusions about the applicability of this proposed local circular economy scenario to a land storage context were proposed.

Materials and Methods

Sediment Description

Each year, approximately 4 Mm^3 of sediments are dredged in the Hauts-de-France region. This volume represents 8% of the total dredged sediments in France. The dredged river sediment sample used in this work has been collected from the city of Noyelles Sous Lens (SED_{NSL}). The SED_{NSL} sample was stored near from the industrial zone of Lens, in a storage area managed by Voies Navigables de France (VNF).

Table 1 Chemical composition in major of BFA and WPFA

Chemical composition by XRF	WPFA (wt.%)	BFA (wt.%)
SiO_2	14.59	16.19
Al_2O_3	8.4	2.46
MgO	1.74	3.81
Fe_2O_3	0.8	5.15
CaO	64.02	36.39
Na_2O	0.45	1.48
SO_3	1.57	9.24
TiO_2	0.7	0.67
ZnO	0.22	0.62
SrO	Traces	0.11
BaO	0.11	0.22
P_2O_5	0.35	2.29
K_2O	0.7	11.12
PbO	Traces	0.43
Cl	0.8	2.5

A sampling of about 100 kg is representative of 45,000 m^2 storage area. The SED_{NSL} was collected with a backhoe and placed in a non-filtering container. The dredged SED_{NSL} was de-agglomerated using a pestle of the hardened material after being collected in quarters and stored in hermetic bags in the laboratory in a climate-controlled room at 20 °C.

Synthesis of LDH From FA

Biomass fly ash (BFA) [40], and waste paper fly ash (WPFA) [41] were used as precursors for LDH synthesis. Both of them have been collected in the Hauts-de-France region, from the cyclone of an incinerator with massive combustion. The chemical composition of BFA and WPFA is reported in Table 1. The LDH synthesis was performed by an acid leaching method followed by precipitation [12]. Briefly fly ash was leached in hydrochloric acid (3 M) with a liquid/solid ratio = 20 l/kg for 2 h at 100 °C to completely dissolve the amorphous silica present in the ash. Then, the leachate was filtered through cellulose acetate membrane filters (0.45 µm) to remove the silica gel. The solution was heated until 65 °C, after which aliquots of sodium hydroxide (2 M) were gradually added until a final pH of 11.5 was obtained. The alkaline solution was stir-aged at 65 °C for 30 min, followed by hydrothermal treatment in a furnace at 70 °C for 12 h in a sealed container to crystallize the LDH. The two LDH samples were called LDH_{BFA} and LDH_{WPFA}. The resulting solid fraction was recovered by centrifugation for 15 min at 6000 rpm, then washed 3 times with MilliQ water to remove excess of sodium hydroxide. The product

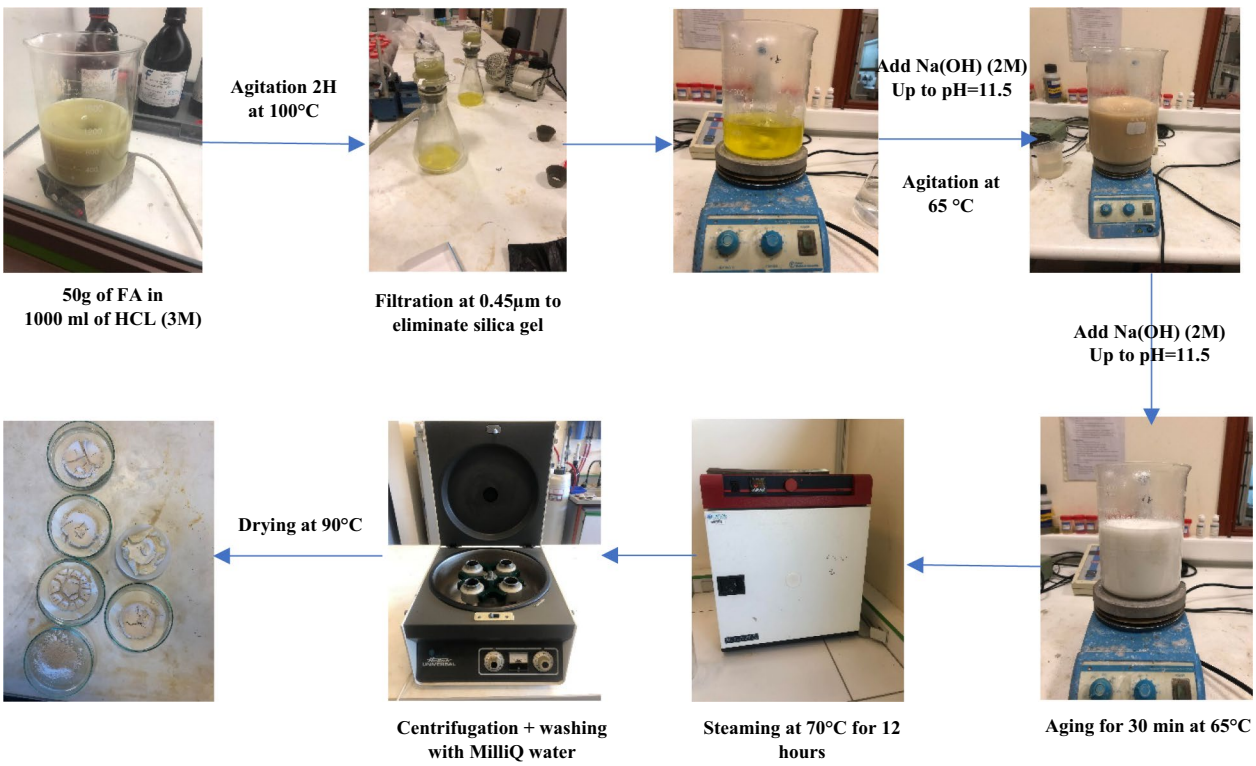

Fig. 1 Synthesis of LDH

was dried at 90 °C in an oven for 24 h and then crushed by the shredder. Figure 1 illustrates the synthesis steps of LDH.

For comparison, a commercial hydrotalcite ($Mg–Al–CO_3^{2-}$) (HT), known for its efficiency in the trapping and elimination of toxic minerals and organic pollutants was also investigated.

In order to increase the adsorption capacity of the synthesized LDH and commercial HT, these products were calcinated at 450 °C for 4 h. (HT calcination according to reaction 1).

$$Mg_6Al_2(OH)_{16}(CO_3).4H_2O \xrightarrow[4H]{\text{Calcination at } 450^{\circ}C} MgAl_2O_4 + 5MgO + CO_2 \uparrow \quad (1)$$

Materials Characterization

The particle size distribution was established on the SED_{NSL}, WPFA and BFA using Laser Coulter LS230 particle size analysis method according to standard NF ISO 13320–1 [42]. Laser particle size analysis allows the identification of particles with sizes between 0.04 µm and 2000 µm by assimilating particles to spheres. The analysis was performed in triplicates. The analysis of particles larger than 2 mm in the SED_{NSL} was carried out in accordance with the European standard NF EN 933–1[43]. The particle size analysis was done by the dry method, using the sieves recommended by the European standard NF EN 933–2 [44]. This test constitutes the reference for the measurement of the granulometry of SED_{NSL}. The sieves used are: 2, 4 and 8 mm.

The specific surface area of the studied materials was determined with the BET method using a Micromeritics stirring analyzer (3FLEX Surface Characterization) according to standard NF EN ISO 18757 [45]. Before the BET measurement, around 3 g of each sample was degassed under nitrogen at 80 °C for 8 h to remove moisture from the surface and the pores of the sample.

The specific density of the samples was measured by helium pycnometer from Micromeritics (ACCUPYC 1330) according to the standard NF EN 15326 [46]. The sample, dried at 40 °C, was introduced in powder form into a cell. Helium is injected which expels the air from the cell. The difference between the volume of the cell and the volume of helium injected, measured by pressure, is the volume of the material. The mass of the sample is measured and allows the calculation of the dry density. For each sample, 20 measurements at different pressures were performed.

The quantity of organic matter present in the samples was determined by a loss on ignition test, performed according to the European standard NF EN 12879 [47]. 5 g of the sample was weighed in small ceramic crucibles, then placed in an oven set at 550 °C for 3 h. The mass difference before and after the heating process was used to calculate the loss on ignition.

To determine the total content of anions (F^-, Cl^-, SO_4^{2-}) and MMTE, each sample was subjected to mineralization by microwave acid digestion followed by chemical analysis using ICP-AES (Agilent Technologies 5110) for MMTE and ion chromatography (IC: Dionex ICS-6000 EG) for anions. Two subsamples of SED_{NSL}, LDH_{BFA}, LDH_{WPFA}, HT were oven dried at 105 °C and then crushed with a RS 200-RETSCH vibratory disc crusher. Mineralization was performed with aqua regia: 250 mg of subsamples was placed in a CEM-MARS 5 microwave reactor at 1600 W, 0.5 mL of ultrapure water was added, then 1 mL of HNO_3 (> 68% Fisher) and finally 3 mL of HCl (37% Fisher). After the microwave oven cycle, the resulting digests were recovered in a container and the volume was completed with ultrapure water until a total volume of 100 mL was obtained (diluted 20 times). Then, the solution was filtered to 0.45 µm, in order to get rid of the colloidal fraction, and analyzed.

The XRF analysis was performed with a S4-PIONEER equipped with a 4-kW generator with a Rhodium anti-cathode. The samples were placed on a glass slide after being dried and crushed. Spectra of all the minerals cutting a transect on the samples were made. The results are expressed in atomic percentage of each element.

To verify the presence of the synthesized LDH structures, the thermogravimetric (TGA) and differential thermal analysis (DTA) analyses were performed on a NETZSCH STA 409 °C thermobalance. The analyzed samples were pre-dried in an oven at 40 °C to a constant mass. For each analysis, a quantity of 200 to 250 mg of dry powdered material is introduced into the apparatus and subjected to a linear temperature rise from ambient temperature to 1150 °C at a rate of 3 °C/minute under an inert gas (argon) with a flow rate of 75 ml/min. At the end of the test, the processing software accompanying the apparatus allows the recovery of the TG Curves and the derivative (DTA).

Mineralogical phase identification was performed by X-ray Diffraction (XRD) using a D8 Focus diffractometer from Bruker. The gram-sized samples were crushed and then analyzed by XRD using cobalt anticathode emitting rays of wavelength $\lambda K\alpha 1 = 1.74$ Å. Diffractograms were obtained from disoriented powders (placed the solids directly in a conventional sample carrier) with 2θ between 5 to 80° with the acquisition step of 0.03° and a compaction time of 5 s.

The microstructure and morphology of the different solid matrices were characterized with a scanning electron microscope (SEM- Hitachi S-4300SE/N) coupled to energy dispersive spectroscopy (EDS). The samples were impregnated with a resin in order to harden the material. The samples

were then polished to have a flat surface. In order to obtain a conductive surface and to avoid the accumulation of charges, the samples were covered with a layer of carbon following a metallization.

Fourier transform infrared spectroscopy (ATR-FTIR) measurements were performed using a Thermo Scientific Nicolet iS50 FT-IR spectrometer in a wavenumber range between 525 cm^{-1} and 4000 cm^{-1}. Sample powder was directly placed on the diamond ATR crystal. The acquisition program was Pike GladiATR.

The zeta potential (ξ) of the samples was measured using a zetasizer from Malvern (Nano-ZS). For that, a 10 g/L suspension of each sample was prepared in ultrapure water, and a small volume of suspension was transferred inside the DTS 1070 cell (Malvern). All the measurements were performed at ambient temperature and at equilibrium pH of the suspension.

Equilibrium Batch Leaching Tests

Batch leaching tests were performed according to EN 12457–2 [48]. The SED_{NSL} was sieved to 4 mm, the sample was relatively fine and therefore no crushing was necessary. For the leaching test, 90 g of dry SED_{NSL} sample was placed in a 2 L PTFE bottle, completed with adequate volume of MilliQ water to obtain a L/S (liquid to solid) ratio of 10 L/kg dry mass. This ratio has been fixed by the standard and ensures the reproducibility of the test and the comparison of the results of the test with environmental standards. The same preparation was repeated in the presence of 5%, 10%, and 15% in mass of LDH_{BFA}, or $LDH_{WPFA,}$ or HT. Since the SED_{NSL} collected in the field was moist, the volume of water added for the tests was calculated by taking into account the initial moisture of the sample. The mixture was then stirred on a rotary shaker (Heidolph Reax 20) for 24 h at a speed of 10 rpm and ambient temperature of 25 °C. After 24 h, the pH of the suspension was measured and the leachate was decanted for 30 min and filtered through cellulose acetate membrane filters (0.45 µm). After acidification of the solutions with HNO_3 (65%), the MMTE were analyzed by ICP-AES and the anions (fluorides, chlorides, sulfates) by ion chromatography (IC) [49].

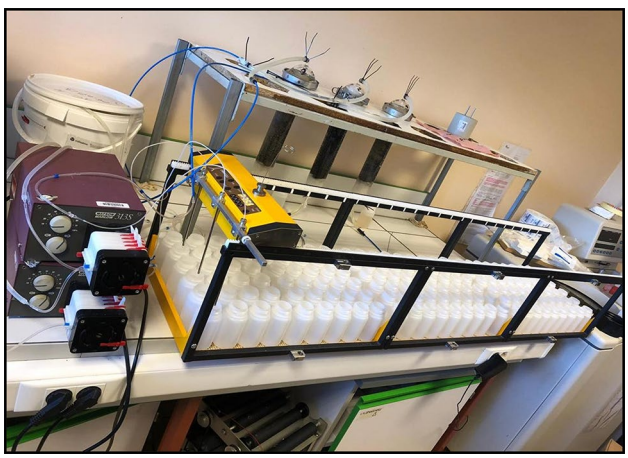

Fig. 2 Photography of dynamic up-flow percolation tests

Dynamic Up-Flow Percolation Tests

The leaching test in an ascending percolation column is based on the standard NF EN 14405 [50] and allows identifying the leached constituents under dynamic conditions. Glass columns with a 20 cm high and a 5 cm diameter was used. A dry mass of approximately 1 kg of SED_{NSL} was introduced in the first column. The others columns contained SED_{NSL} mixed with different mass percentage of LDH_{BFA}, $LDH_{WPFA,}$ HT (5%, 10%, 15%). All the experiments were performed twice, at the same time. To ensure an homogeneous compaction of the samples inside each column, 1/3 of the total amount of the sample was placed inside the column, then a 250 g weight was released twice at 10 cm high over the top of the sample surface. After that, 1/3 of the sample was added over the first compacted part, and the compaction operation was reproduced. Finally, the last 1/3 of the sample was added over the second-compacted part, and the compaction operation was reproduced. The test was carried out by saturating the column with water injected at the bottom of the column using a multichannel peristaltic Pump (Fig. 2). Once the column saturated, an equilibration period of 24 h was necessary in order to reach an initial equilibrium. After

Table 2 Chemical composition in major and MMTE of the SED_{NSL}

XRF data		Batch equilibrium leaching test		IWSI
Chemical composition	wt.%	Parameter	Concentration (mg. kg^{-1})	Concentration ($mg.kg^{-1}$)
SiO_2	53.04	As	< 0.11	0.5
Al_2O_3	12.8	Ba	0.2 ± 0.05	20
MgO	0.83	Cd	< 0.009	0.04
Fe_2O_3	4.15	Co	< 0.009	***
CaO	14.97	Cr	< 0.011	0.5
Na_2O	0.67	Cu	0.92 ± 0.3	2
SO_3	1	Mo	0.14 ± 0.02	0.5
TiO_2	0.67	Ni	0.17 ± 0.02	0.4
ZnO	0.17	Pb	< 0,03	0.5
K_2O	1.93	Sb	**0.13 ± 0.02**	0.06
P_2O_5	1.15	Se	< 0.08	0.1
K_2O	0.7	Zn	**5.24 ± 0.29**	4
		Sulfates	**13 937 ± 192**	1 000
		Fluorides	3 ± 0.15	10
		Chlorides	31 ± 1.5	800

Parameters exceeding the IWSI threshold are shown in bold

Table 3 Total content of MMTE in SED_{NSL}, LDH_{WPFA}, LDH_{BFA} and HT

Concentration MMTE ($mg.kg^{-1}$)	SED_{NSL}	LDH_{WPFA}	LDH_{BFA}	HT
As	19.3 ± 1.8	9.5 ± 0.3	76 ± 4	< 4.4
Ba	475 ± 11	267 ± 16	213 ± 12	7.8 ± 1.6
Cd	5.2 ± 1.8	2.7 ± 0.2	70 ± 5	< 0.4
Co	180 ± 0.5	7.1 ± 0.4	25 ± 1.3	< 0.3
Cr	91 ± 3	178 ± 21	383 ± 22	< 0.2
Cu	870 ± 7	169 ± 9	428 ± 24	4.8 ± 06
Mo	< 3.5	< 3.5	< 3.5	< 3.5
Ni	47 ± 1.2	81 ± 3	247 ± 10	< 1.9
Pb	476 ± 55	202 ± 15	1054 ± 12	< 1.3
Sb	6.9 ± 0.9	8.3 ± 0.4	26 ± 1.9	< 2.3
Se	4,3 ± 0,1	< 3.3	< 3.3	< 3.3
Zn	1952 ± 14	1069 ± 46	3236 ± 21	20 ± 1

Table 4 Physical and chemical characterizations of SED_{NSL}, LDH_{WPFA}, LDH_{BFA} and HT

Physical parameters	SED_{NSL}	LDH_{WPFA}	LDH_{BFA}	HT
Specific density (kg/m^3)	2.47	2.55	2.52	2.8
Specific surface BET (m^2/g)	4.37	81.79	89.23	117.18
Loss On Ignition (LOI) (%)	9.3	26.5	15.9	43.8
pH	6,95	12.53	12.18	11.13
Conductivity (mS/cm)	4.27	3.9	4.95	0.1

this period, the flow rate of the water injected at the bottom of the column was adjusted to 15 ± 2 cm/d (1177 cm^3/d or 0.01 cm^3/s).

The fractions were collected by an automatic fraction collector connected to the columns. The collected volume for each fraction was calculated on the basis of the L/S (l/kg) ratio of each fraction, i.e., eleven fractions ranging from an L/S (l/kg) ratio of 0.1 to 30 L/kg. The L/S (l/kg) ratio is calculated by considering the mass of water flowing through the column at a flow rate of 15 ± 2 cm/day and the mass of dry samples placed inside the column. The volume of leachate corresponding to each fraction was calculated from the amount of dry matter placed in the columns. Each collected liquid fraction was filtered through cellulose acetate syringe filters with a pore size of 0.45 µm and then acidified with HNO_3 (65%) before ICP-AES and IC analysis.

Acid Digestion by Microwave

The elemental analyses led to the determination of the total contents of trace elements (As, Cd, Cr, Cu, Ni, Pb, Zn…) contained in the SED_{NSL}, LDH_{WPFA}, LDH_{BFA} and HT (Table 2). The total concentrations of each chemical element provide an indication of the release of MMTEs from the leaching tests.

The XRF and mineralization results highlighted that major elements and inorganic pollutants present in the LDH and HT were in lower quantities than those present in the SED_{NSL} with the exception of Zn in LDH_{BFA}. The increase of Zn content in LDH_{BFA} is justified by the presence of ZnO in high quantities in the BFA before the synthesis of LDH (Table 3). Data from Table 4 confirm that the SED_{NSL} is highly polluted with Cu (870 ± 7 mg/kg), Sb (6.9 ± 0.9 mg/kg) and Zn (1952 ± 14 mg/kg), which explains the important release of these elements presented in Table 3. Due to their high concentrations in the sediment matrix, Cu, Sb, and Zn were selected as target pollutants to be stabilized in this study. Since the mercury (Hg) content is below the detection limit of the measuring device (< 3 µg/L), it does not appear in Tables 3 and 4. It should be noted that LDH_{WPFA} and LDH_{BFA} contained high levels of MTE, in particular Ba, Cr, Cu, Ni, Pb and Zn, which can be penalizing for the stabilization process from an environmental standpoint, generating side contamination.

The Specific Surfaces BET, Specific Density and Loss On Ignition

The specific density, specific surface area BET and loss on ignition of the samples are summarized in Table 4. LDH_{WPFA}, LDH_{BFA} as well as HT exhibited higher specific surface and specific density than SED_{NSL}. This was generally attributed to the irregular morphology and open porosity of the materials. The specific surface area values obtained by BET were: 4.37 m^2/g, 81.79 m^2/g, 89.23 m^2/g and 117.18 m^2/g for SED_{NSL}, LDH_{WPFA}, LDH_{BFA} and HT, respectively. The specific surface area is generally related to the shape, particle diameter and porosity. The specific surface area values of the two synthesized LDHs were comparable. However, commercial HT had a higher specific surface area than the synthesized LDHs, due to the optimal synthesis conditions. The different LDHs presented a finer particle size distribution than SED_{NSL}, and a higher specific surface area. This is explained by the marked presence of submicrometer size particles in LDH as well as the irregular surface condition of the grains. The low specific surface area value of SED_{NSL} could be attributed to its coarser grain size distribution.

The specific surface area of LDH decreased with increasing Loss On Ignition (LOI) (Table 4). The observed tendency in the present study seems to be in agreement with the results obtained by Malkawi et al. [51] on materials with LOI below 15%. In materials with LOI above 15%, Malkawi et al. [51] observed an increase in the specific surface. Malkawi et al. [51] explained that in lower organic matter

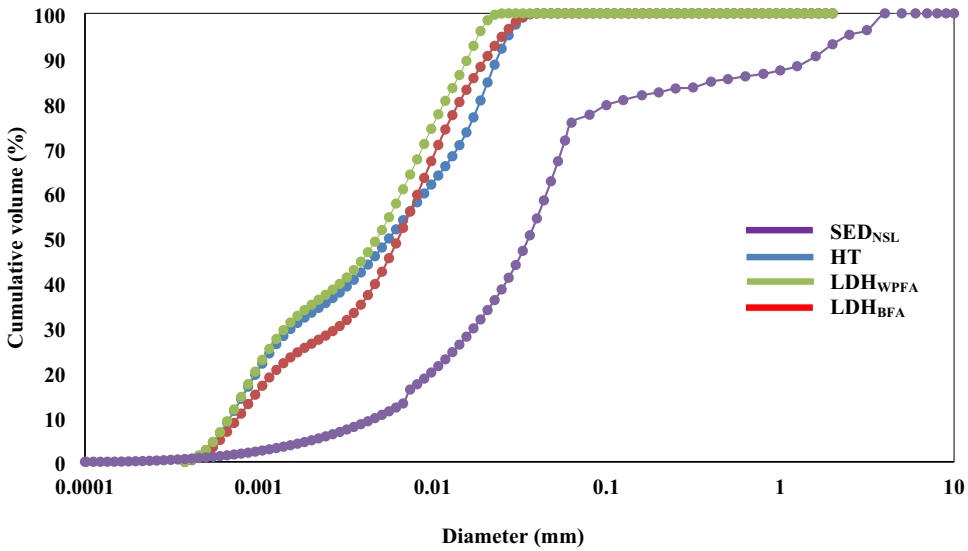

Fig. 3 Granular distributions of SED_{NSL}, LDH_{WPFA}, LDH_{BFA} and HT

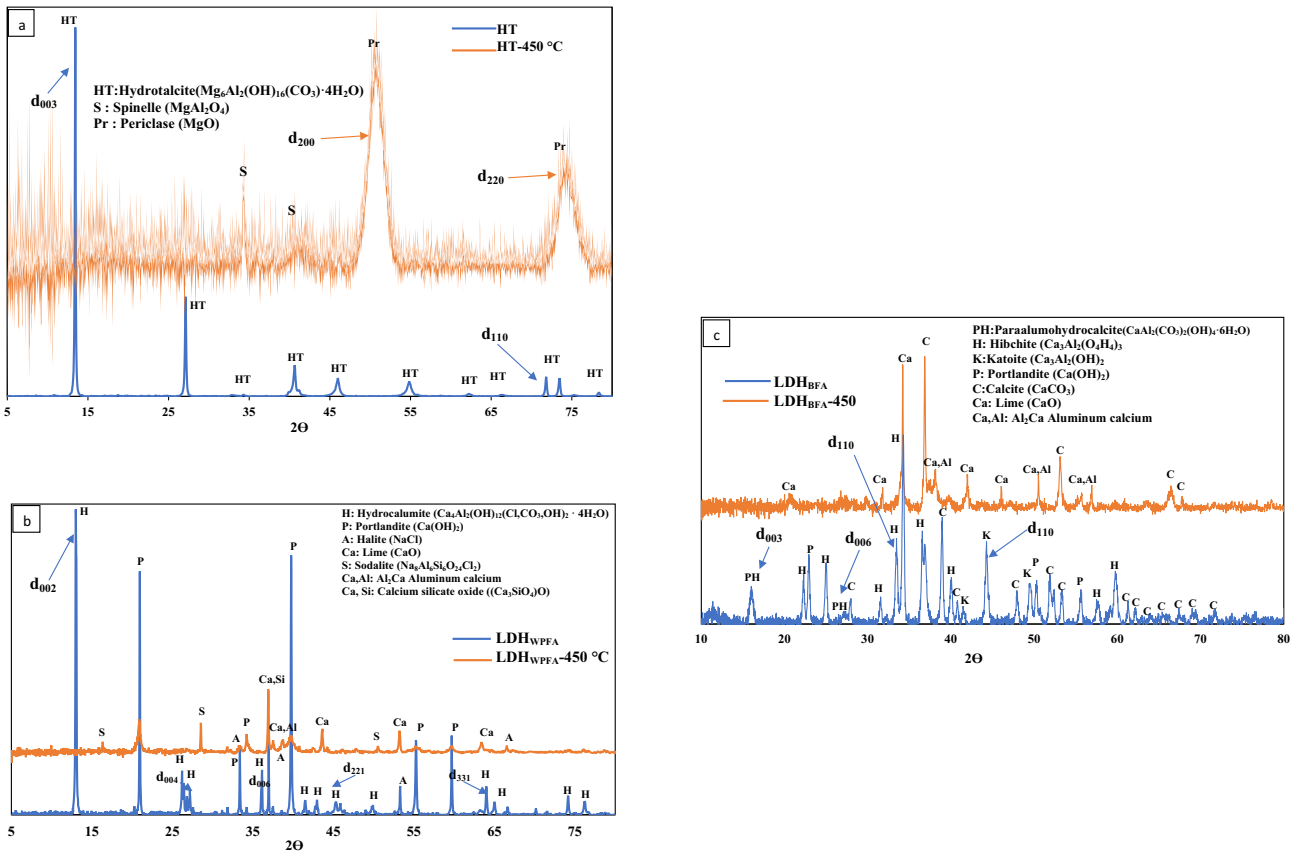

Fig. 4 Diffractogram of HT (**a**), LDH_{WPFA} (**b**) and LDH_{BFA} (**c**) powders before and after calcination at 450 °C

(OM) content, mixtures have a tendency to aggregate, which explained the decrease in specific surface.

Concerning specific density, the values reported in the literature varied over a fairly wide range depending on the source and oxide content of the initial fly ash [52]. The specific density values were: 2.47 m^2/g, 2.55 m^2/g, 2.52 m^2/g and 2.8 m^2/g for SED_{NSL}, LDH_{WPFA}, LDH_{BFA} and HT, respectively. There are relatively few data in the literature on these two characteristics to make comparisons with the LDHs under study. The investigation of Muriiti et al. [52]

gave a LDH density of 2.78 g/cm^3, thus confirming that the reduction of the particle size is a favorable factor for the adsorption kinetics of the pollutants, due to an increase of the specific surface and a higher dispersion of the solid.

The pH value of SED_{NSL} was neutral. However the different LDHs had a highly basic pH (> 11). The basic pH of LDHs favored the adsorption of anionic and cationic pollutants on LDH surface. The high electrical conductivity of SED_{NSL}, LDH_{WPFA} and LDH_{BFA} was caused by the leaching of dissolved salts in the pore water of the material during the wetting phases. In contrast, HT showed a low electrical conductivity (0.1 mS/cm), suggesting that LDH_{WPFA} and LDH_{BFA} were not sufficiently washed after synthesis (See Fig. 3).

X-ray Diffraction Analysis

The diffractograms of synthesized LDH_{WPFA} and LDH_{BFA} (Fig. 4b, c) and HT (Fig. 4a) showed high similarity with that of lamellar double hydroxides from the literature [52].

HT diffractogram (Fig. 4a) highlighted the presence of the main reflections characteristic of HT crystallizing in a hexagonal system, with a rhombohedral symmetry and a space group R-3 m in accordance with bibliographic data [53–56]; The results showed the presence of several symmetric peaks (001) towards the low values of 2 theta, the first diffraction peak (003) is related to the spacing of the layers (d_{003}) and allowed the calculation of the mesh parameter *c* using the formula $c = 3\ d_{003}$. On the other hand, the parameter *a* which designates the interatomic distance metal–metal was calculated by the formula $a = 2\ d_{110}$, with d_{110} the line (110) located in the vicinity of 70° in 2 theta [39, 57]. The interlamellar distance (d_{003} = 7.57 Å) agreed with the one reported by other authors for the same HT phase intercalated with carbonates [58]. According to the diffractogram presented in Fig. 4a for HT-450 calcinated phase, the HT structure was destroyed due to the dehydroxylation of the system, and the disappearance of water molecules and carbonate anions [56]. Only Periclase MgO and Spinel ($MgAl_2O_4$) were detected. The phase transformation was confirmed by the disappearance of reflections (003) and (110) and the appearance of two broad peaks (d_{200} = 2.1 Å and d_{220} = 1.44 Å) corresponding to the main reflections characteristic of Periclase (MgO) [59]. At this calcination temperature (T = 450 °C), the aluminum oxides were in an amorphous state and therefore not detectable [60, 61].

The diffractograms of the LDH_{WPFA} phases are presented in Fig. 4b. The general appearance of the diffractograms was typical of such materials (HT) [20, 62, 63]. The diffractograms showed intense and symmetrical peaks at low 2θ values as well as less intense and asymmetrical peaks at higher 2θ values. Among the (00L) lines, the first peak (002) had a relatively high intensity, which is consistent with [63]. Its positions (in 2θ) provided direct access to the values of the interlamellar (interfoliar) distances [dhkl = d (004) = 2d (006)], and to the monoclinic mesh parameter. In the series of the lines of type (hkl), the line (331) was easily observed on the diffractogram and its angular position allowed observing the arrangement of the metal cations in the hydrocalumite layers, and the mesh parameter a(Å) = 2d (331) which represented the Ca-Al distance [63]. Figure 4b confirmed the formation of LDH_{WPFA} in the form of a hydrocalumite ($Ca_4Al_2(OH)_{12}(Cl,CO_3,OH)_2{\cdot}4H_2O$) which differed from HT by the distortion of the octahedral layer due to the coordination of the Ca^{2+} ions bound to OH^- and H_2O. After calcination at 450 °C, the collapse of the LDH structure was observed by the disappearance of peaks corresponding to hydrocalumite. LDH_{WPFA}-450 presented new crystalline phases indexed Sodalite ($Na_8Al_6Si_6O_{24}Cl_2$) and lime (CaO) resulting from the dehydroxylation of portlandite. Aluminum oxides were in the amorphous state and therefore not detectable [63].

Figure 4c shows the diffractograms obtained for the LDH_{BFA} phases before and after calcination at 450 °C. The X-ray diffractograms of the Paraalumohydrocalcite ($CaAl_2(CO_3)_2(OH)_4 \cdot 6H_2O$) phase showed a general appearance characteristic of (LDH) type phases with notably the appearance of all the harmonic lines (00L) encountered in isotype compounds with a lamellar structure and indicate a hexagonal lattice, with a typical rhombohedral symmetry R-3 m. The LDH_{BFA} diffractogram showed LDHs as Paraalumohydrocalcite ($CaAl_2(CO_3)_2(OH)_4{\cdot}6H_2O$), Hibchite ($Ca_3Al_2(O_4H_4)_3$, and Katoite ($Ca_3Al_2(OH)_2$ showed numerous fine, intense, symmetrical reflections at low 2θ values for the (003), (006), (110), (113) planes and broader, less intense, and asymmetrical reflections at large angles. The diffractograms of LDH_{BFA}-450 °C showed that calcination modified the crystalline structure of LDH, by dehydration and decarbonization [64, 65] giving rise to a mixture of CaO and Al_2O_3 (amorphous). The calcination improved the texture and adsorption properties.

TGA

The XRD results of the different phases in LDH_{WPFA}, LDH_{BFA} and HT (Fig. 4) were confirmed by TGA analysis (Fig. 5a, b, c). TGA curves had a similar shape for the three samples, with a thermal degradation that occurred at the same temperature. three main processes can be highlighted from TGA curves: dehydration, dehydroxylation and release of the interlamellar anion.

The HT mass loss curve obtained follows the behavior for LDH phases studied on several researches [23, 52, 62]. From 20 °C to 560 °C, two endothermic phenomena occurred. The first mass loss corresponded to evaporation of adsorbed water, and the second one corresponded to dehydroxylation

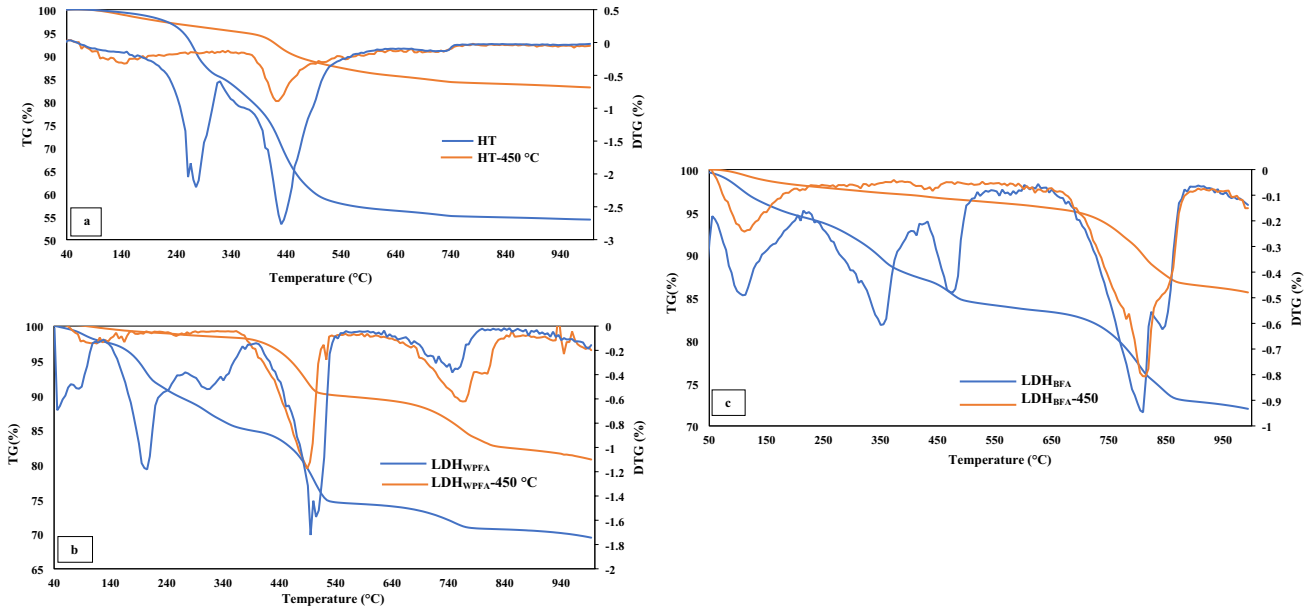

Fig. 5 Thermogravimetric analysis of HT (**a**), LDH_{WPFA} (**b**) and LDH_{BFA} (**c**) powders before and after calcination at 450 °C

of hydroxyl surface groups [62]. The mass loss occurring between 700 and 750 °C corresponded to layers dehydroxylation and intercalated anions decomposition (mainly OH^-). After calcination, the mass loss observed for HT-450 was much lower compared to HT, thus the peaks intensity corresponding to the Mg–Al phases of LDH structure were largely decreased. No further significant mass loss was observed above 560 °C for HT-450, while above 560 °C, HT structure could be converted to spinel ($MgAl_2O_4$), and possibly periclase (MgO) mixed oxide, as shown by XRD results [18, 52].

The TGA of LDH_{WPFA} and LDH_{WPFA}-450 °C are shown in Fig. 5b. The DTG curve provided a clearer appreciation of the temperatures at which mass losses occurred. Five major mass losses were observed between 40–105 °C, 140–253 °C, 280–337 °C, 440–530 °C and 645–785 °C. The first mass loss between 40 and 105 was due to evaporation of water molecules. The mass loss between 140 and 253 °C was due to loss of water molecules bound to LDH structure. From 253 °C, the degradation of the first mode of the hydrocalumite structure ($Ca_4Al_2(OH)_{12}(Cl,CO_3,OH)_2{\cdot}4H_2O$) started [63]. The mass loss between 260 and 337 °C corresponded to the collapse of the second mode of hydrocalumite (($Ca_4Al_2(OH)_{12}(Cl,CO_3,OH)_2{\cdot}4H_2O)_{,syn}$) [63]. The mass loss between 440 and 530 °C corresponded to the release of calcium hydroxide ($Ca(OH_2)$), and finally calcite release was characterized by a mass loss between 645 and 785 °C [63]. LDH_{WPFA}-450 °C showed two significant mass losses corresponding to release of $Ca(OH)_2$ (between 400 and 510 °C) and calcite (between 600 and 830 °C) [63]. No significant mass loss related to the two hydrocalumite modes were observed confirming the results from XRD.

The TGA of LDH_{BFA} and LDH_{BFA}-450 °C are shown in Fig. 5c. The thermal decomposition of LDH_{BFA} underwent five stages: The first stage (60–220 °C) decomposition corresponded to elimination of water from the interlayer, implying a slight shift in LDH layers. In the second stage (240–440 °C), the most rapid and important weight loss corresponded to an irreversible decomposition of the LDH structure that began to transform into amorphous CaO and Al_2O_3 phase. In the third stage (430 °C to 520 °C), CaO was formed due the dehydroxylation of portlandite, as shown in the XRD results (Fig. 4c). In the last stage (650 to 900° C), weight loss corresponded to continuous decomposition of calcite. LDH_{BFA}-450 °C showed one single mass loss, corresponding to calcite decomposition, that is consistent with XRD results (Fig. 4c).

FTIR

The IR spectra recorded for LDH_{WPFA}, LDH_{BFA} and HT before and after calcination were almost similar and all showed the characteristic bands of LDH (Fig. 6).

The IR spectrum of HT (Mg–Al–CO_3^{2-}) before and after calcination at 450 °C reported in Fig. 6a, showed the main molecular groups characteristic of a layered double hydroxide phase [66]. The bands around 3449 cm^{-1} were attributed to the vibrations of hydroxyl groups (νOH), including intercalated and physically adsorbed water molecules [38, 39]. The absorption bands with weak intensity located at about 2988 and 2900 cm^{-1} were assigned to symmetric and

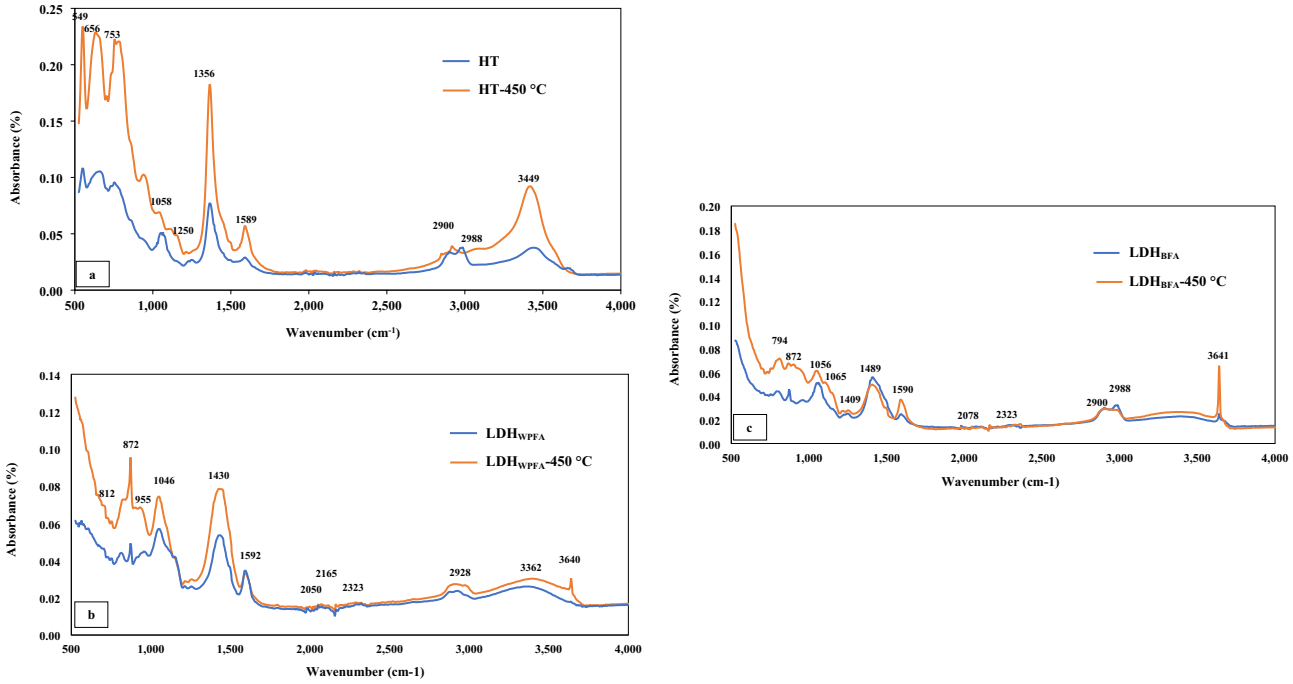

Fig. 6 FTIR spectra of HT (**a**), LDH_{WPFA} (**b**) and LDH_{BFA} (**c**) powders before and after calcination at 450 °C

asymmetric vibrations of the C–H bond, respectively [67, 68]. In the mid-spectrum, the intense band located at about 1589 cm^{-1} was assigned to the angular deformation vibrations of the intercalated water molecules (δH_2O) [69]. The carbonate anion was represented by the intense adsorption band located in 1365 cm^{-1} and 1250 cm^{-1} [70]. The adsorption bands below 800 cm^{-1} characterized the M–O–M and M–O metal–oxygen vibrations [71, 72]. For the HT-450 °C sample, the bands at about 1050 cm^{-1} and below 1000 cm^{-1} were attributed to the vibrations of the Mg–O groups [73]. The decrease in the intensity of the peaks characteristic of carbonate anions and water molecules confirmed that most of the species were eliminated during calcination at 450 °C and the detected bands were probably those of the adsorbed species on the surface.

The IR absorbance spectra of LDH_{WPFA} and LDH_{BFA} [Ca–Al–CO_3] before and after calcination at 450 °C are shown in Fig. 6b, c. The bands at approximately 3640 cm^{-1} and 2000 cm^{-1} were attributed to the vibrations of the free hydroxyl groups (νOH) or to the vibrations of the interlamellar water molecules linked to the hydroxyl groups by hydrogen bonds. The shoulders at 2323 cm^{-1}, 2165 cm^{-1}, 2078 cm^{-1} and 2050 cm^{-1} (Fig. 6b, c) corresponded to the interactions of water molecules with carbonate anions by hydrogen bonds [52]. The average band between 1590 cm^{-1} and 1592 cm^{-1} for LDH_{BFA} and LDH_{WPFA} respectively, were attributed to the deformation vibrations of the water O–H bond and to the deformation vibrations of the water molecules adsorbed between the layers, after calcination at 450 °C the intensity of the peak decreases. The vibrational band between 1409 cm^{-1} and 1430 cm^{-1} was assigned to the vibrational mode of free carbonates. The vibrational bands at low frequencies (below 1000 cm^{-1}) were assigned to metal–oxygen bonds. In the IR spectrum of LDH_{WPFA} and LDH_{BFA}, individual broad absorption bands appeared around 1046 cm^{-1}, 955 cm^{-1}, 872 cm^{-1}, and 812 cm^{-1} for LDH_{BFA} and 1065 cm^{-1}, 1056 cm^{-1}, 872 cm^{-1} and 794 cm^{-1} for LDH_{WPFA}. All the bands were related to the typical stretching vibrations of MO and MOH (M = Ca and Al) in LDH [48, 49]. After calcination at 450 °C, the intensity of the peaks decreased and at times disappeared, confirming the breakdown of the LDH structure and the appearance of oxides such as Al_2O_3 and CaO. The peaks observed in LDH_{BFA} at 564 cm^{-1} and 552 cm^{-1} corresponded to the vibrations of (–Si–O–Si) and (–Al–O) respectively [74].

SEM Analysis

The morphological study by scanning electron microscopy was performed on the different LDH before and after calcination at 450 °C. It was demonstrated that LDHs morphologies strongly depended on the composition of the fly ash used for LDH synthesis [52]. The particles of LDH before calcination were formed by the aggregation of small platelets arranged in a "desert rose" morphology as shown in the SEM pictures (Fig. 7). An increase in platelet size was

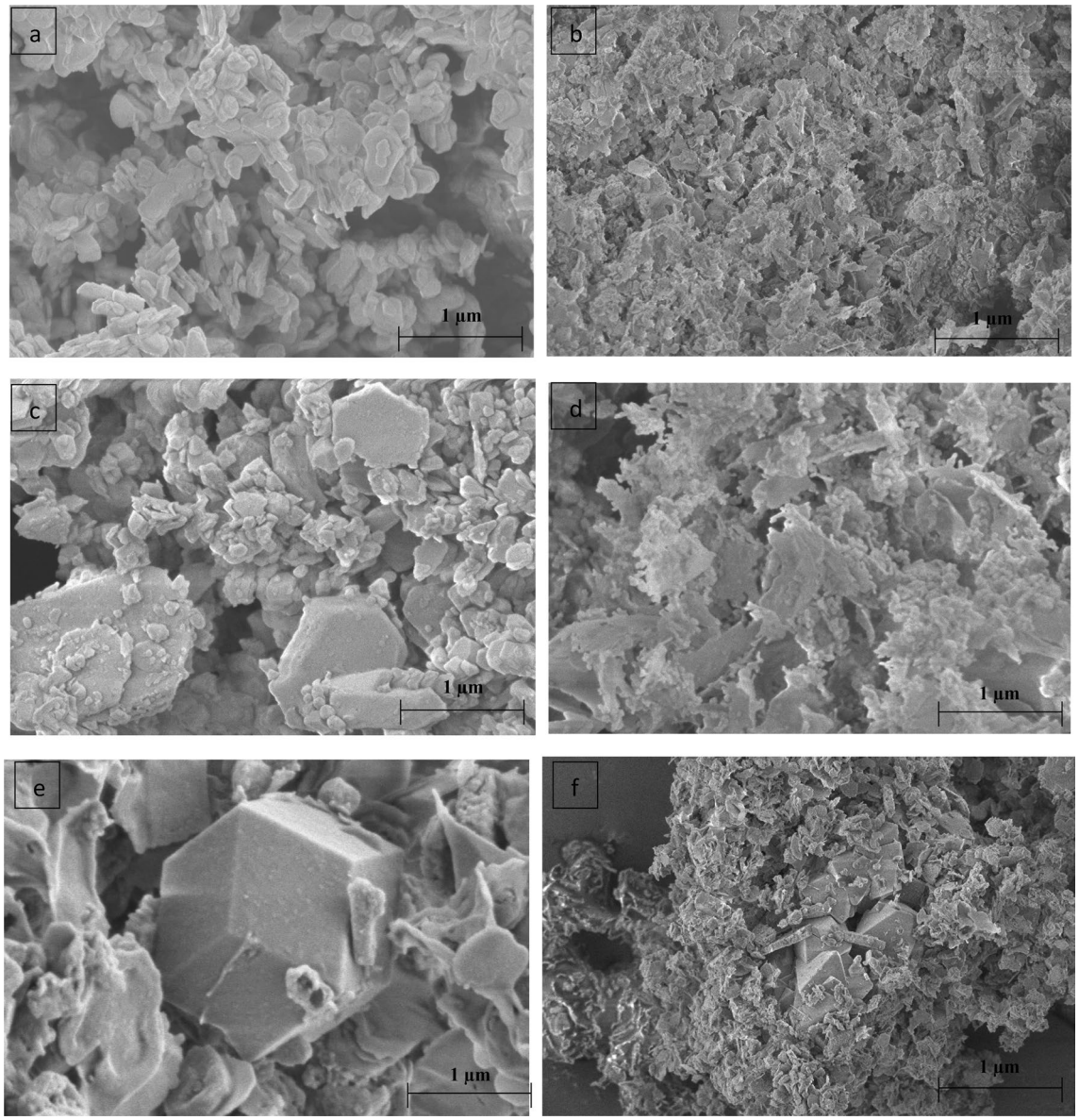

Fig. 7 SEM images of HT (**a**), HT-450 (**b**), LDH_{WPFA} (**c**), LDH_{WPFA}-450 (**d**), LDH_{BFA} (**e**), LDH_{BFA}-450 (**f**)

observed, correlated with an increase in Mg^{2+}/Al^{3+} ratio for HT, and Ca^{2+}/Al^{3+} ratio for LDH_{WPFA} and LDH_{BFA}. This increase in platelet size was related to the improvement of material crystallinity. HT particles presented a disc shape with diameter higher than one micrometer. Aggregation occurred by the principal faces and led to a piling up along the perpendicular axis to the faces forming individual particles, quite defined, of hexagonal form and monodispersed with size around 2 µm (Fig. 7a).

HT-450 particles were smaller and more homogeneous (Fig. 7a, b), due to water evaporation from the structure, followed by structure compaction that occurred during calcination. The picture in Fig. 7a confirmed the layered structure of HT. After calcination, the structure became amorphous (disappearance of the LDH structure, Fig. 7b), consistently with the XRD. Comparison of Fig. 7a and b, HT-450 was more porous than HT which is in agreement with the results from Lin et al. [75].

SEM pictures of LDH_{WPFA} and LDH_{BFA} exhibited a mixture of small and large block particles with hexagonal shape (Fig. 7c), and the presence of few octahedral shape crystallites in LDH_{BFA} (Fig. 7e). The crystallinity of these materials was low. According to Forano et al., [76]; the LDH structure is constructed from $Metal(OH)_6$ octahedral units that share their borders to form brucite-type sheets. The general formula can be expressed as $[M^{II}{}_{1-x}M^{III}{}_{x}(OH)_2][X^{q-}{}_{x/q}\ nH_2O]$ or $[M^{II}\text{-}M^{III-}{}_{X}]$ or $[M^{II}\text{–}M^{III}]$ ($[M^{II}{}_{1-x}M^{III}x(OH)_2]$ represents the sheet and $[X^{q-}{}_{x/q}\ nH_2O]$ the interlamellar domain) [76].

Rousselot et al. [77], reported that in hydrocalumite family (Ca^{II}/Al^{III}), LDH formed octahedra that opened on the interfoliar space in order to accept an additional coordination with a water molecule from the interlayer. Drici [39] showed that the Mg–Al-CO_3^{2-} phase presented a mixture of large and smaller blocks particles without any defined shape and some octahedral crystallites.

SEM pictures of LDH_{WPFA}-450 and LDH_{BFA}-450 (Fig. 7d, f) showed that mostly all the hexagonal structures were destroyed, associated with a textural change of the material and an increased porosity, as also shown by TGA and XRD analysis (Fig. 7d, f).

The LDH crystallites were generally hexagonal in morphology (Fig. 7), although in the case of LDH_{BFA} prior to calcination, octahedral shaped particles have been observed [78]. The morphology and particle size strongly depend on the synthesis conditions [79–82]. High-resolution microscopy allows to access to structural information. Lopez Salinas et al. [83] reported the presence of stacking or dislocation defects in high resolution micrographs of LDH Mg^{II}/Ga^{III} phase: the size of the interfoliar space is then larger at the edges of the crystallites than at the center of the crystallites, meaning that the sheets are weakly held at the edges of the crystallites. Such characteristics may result either from an inhomogeneous distribution of charges within the layer, or from a variation in the amount of water, or from a reorganization of the interfoliar anion [84].

The large specific surface developed by the different LDH and the pore volume (Table 2) were in good accordance with their morphologies observed with SEM.

Table 5 Zeta potential and pH value of LDH_{WPFA}, LDH_{BFA} and HT before and after calcination

	LDH_{WPFA}	LDH_{WPFA}-450	LDH_{BFA}	LDH_{BFA}-450	HT	HT-450
Zeta potential (mV)	−19.3 ± 0.9	−21.8 ± 1.2	−15.8 ± 0.7	−19.6 ± 1.3	−11.8 ± 0.3	−21.7 ± 0.5
pH	13.21	13.27	11.83	13.15	9.51	9.35

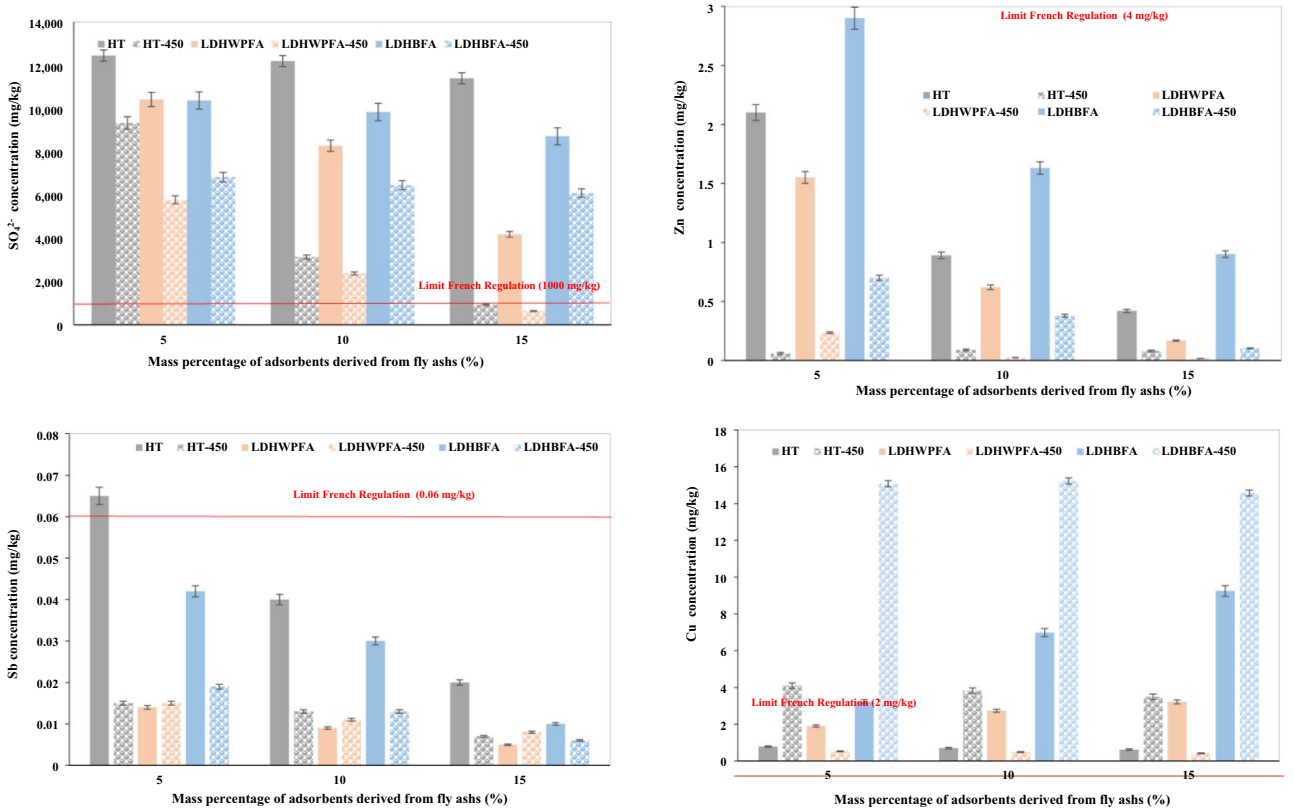

Fig. 8 Leaching concentration of Cu, Sb, Zn and SO_4^{2-} from SED_{NSL} after treatment with HT, HT-450, LDH_{WPFA}, LDH_{WPFA}-450, LDH_{BFA} and LDH_{BFA}-450 (Batch)

Zeta-Potential

The zeta potential of LDH_{WPFA}, LDH_{BFA}, and HT before and after calcination at 450 °C were measured at the equilibrium pH of a suspension with water (Table 5). The surface charges of LDHs and HT were negatives, and the equilibrium pH were basic for HT and HT-450 to highly basic for LDH_{WPFA} and LDH_{BFA} before and after calcination. Calcination moderately affected the pH of LDH_{WPFA} and HT suspensions, whereas an increase in pH was measured for LDH_{BFA} after calcination. Zeta potential was systematically more negative after calcination, indicating that the suspensions tended towards an increased stability.

Equilibrium Batch Leaching Tests

A batch leaching was performed following the standard NF EN 12457–2. The results of SED_{NSL} batch leaching tests with different mass percentage of HT, HT-450, LDH_{WPFA}, LDH_{WPFA}-450, LDH_{BFA} and LDH_{BFA}-450 are presented in Fig. 8. The results obtained in Table 3 indicated that Sb, Zn and SO_4 were the most abundant MMTE in the SED_{NSL}, with concentrations above the threshold limits of inert waste storage installations (IWSI). The SETRA [85] limit for the backfill ratio L/S = 10 l/kg (Batch) is presented by a red line for each element.

For a L/S ratio = 10 l/kg, the Sb, Zn and SO_4 leaching decreased as the percentage of LDH mass in the medium increased (from 5%, 10% to 15%). Sulfate was efficiently stabilized in the sediment matrix when 15% of HT, or LDH_{WPFA} or LDH_{BFA} was added. Sulfate released was respectively 11,400 ± 570 mg/kg, 4180 ± 209 mg/kg and 8720 ± 261 mg/kg, versus 13,937 ± 192 mg/kg for untreated SED_{NSL}. Nevertheless, released concentrations exceeded the IWSI threshold set at 1000 mg/kg (SO_4^{2-}). After sediment stabilization with 15% of HT-450 and LDH_{WPFA}-450, sulfate release strongly decreased compared to untreated $SED_{NSL,}$ reaching concentrations of 938 ± 467 mg/kg and 632 ± 31.6 mg/kg, respectively. This decrease represented a 1500% decrease compared to untreated $SED_{NSL,}$ and was below the IWSI threshold especially for LDH_{WPFA}-450 amendment.

Regarding Zn stabilization, the leaching decreased as the amendment ratio of LDH increased. A 5% LDH amendment was enough to reach a leaching concentration below IWSI threshold. The very efficient Zn stabilization by all the LDHs investigated is explained by their strong negative surface charge and their highly alkaline pH.

Sb stabilization was excellent when sediment was amended with HT or LDH. A 5% amendment was enough to efficiently immobilize Sb in the sediment matrix, in a lesser extent for HT. After 5% of amendment, Sb release was below the IWSI threshold and reached 0.065 ± 0.003 mg/kg, 0.015 ± 0.05 mg/kg, 0.014 ± 0.003 mg/kg, 0.015 ± 0.002 mg/kg, 0.042 ± 0.002 mg/kg, and 0.019 ± 0.005 mg/kg for HT, HT-450, LDH_{WPFA}, LDH_{WPFA}-450, LDH_{BFA}, and LDH_{BFA}-450 respectively (Table 1, 2, 3 Appendix). From 10 to 15% amendments, the Sb concentrations were lower than 0.04 mg/kg and 0.02 mg/kg respectively.

Cu was released from the matrix when HT and LDH_{WPFA}-450 were used, but the concentrations remained below the IWSI threshold. The maximum Cu releases were measured when HT-450 (4.1 ± 0.2 mg/kg), LDH_{WPFA} (3.21 ± 0.29 mg/kg), LDH_{BFA} (9.25 ± 0.33 mg/kg) and LDH_{BFA}-450 (15.23 ± 0.33 mg/kg), were used as amendments. As reported by Bekkouche [86], the calcination process modifies the mineral phases containing Cu and made them more soluble. This could explain Cu release when HT-450 LDH_{BFA}-450 were used. Cu release when LDH_{WPFA} and LDH_{BFA} were used as amendment can be due to (i) the initial Cu concentration in the sediment matrix, (ii) the alkaline pH of LDH that could locally enhance the solubility of Cu-minerals from the sediment matrix.

Comparison of Sb, Zn, and SO_4^{2-} concentrations in SED_{NSL} with the leaching thresholds for inert waste showed that untreated SED_{NSL} does not meet all of the criteria for inert landfill acceptance. Only LDH_{WPFA}-450 was able to reduce the leaching of Sb, Zn, and SO_4^{2-} below the regulatory limits without generating further contamination. The leaching results for the different MMTEs are presented in the Appendix (Tables 1, 2, 3).

Dynamic Up-Flow Percolation Tests

To understand the MMTE release in column percolation mode more thoroughly, pH and electrical conductivity were measured at different L/S (l/kg) ratios (Fig. 9). The batch leaching results revealed that amendment of SED_{NSL} with HT-450 and LDH_{WPFA}-450, all the Cu, Sb, Zn, SO_4^{2-} concentrations were inferior to the regulatory limits. For this reason, the leaching in column mode was realized only with HT-450 and LDH_{WPFA}-450. The SED_{NSL} treated with different mass percentages of HT-450 had slightly basic initial pH values (between 7.05 and 7.76). Similarly, to the untreated SED_{NSL}, the pH tended to decrease from 7.74 to 7.27 all along the duration of experiments. This pH decrease is generally explained by the sulfide oxidation reactions inside the SED_{NSL} [87]. Thus, amendment of HT-450 had no effect on the pH of the leached solution. In contrast, the pH of leached water when LDH_{WPFA}-450 was used as amendment was basic and tended to increase all along the experiment. The increase of mass percentage of LDH_{WPFA}-450 was accompanied by an increase in pH. When 5% of LDH_{WPFA}-450 was used, the pH of leached water ranged between 12.02 and 12.49. When 10% and 15% of LDH_{WPFA}-450 was used, the pH of leached water ranged from 12.07—12.67, due to

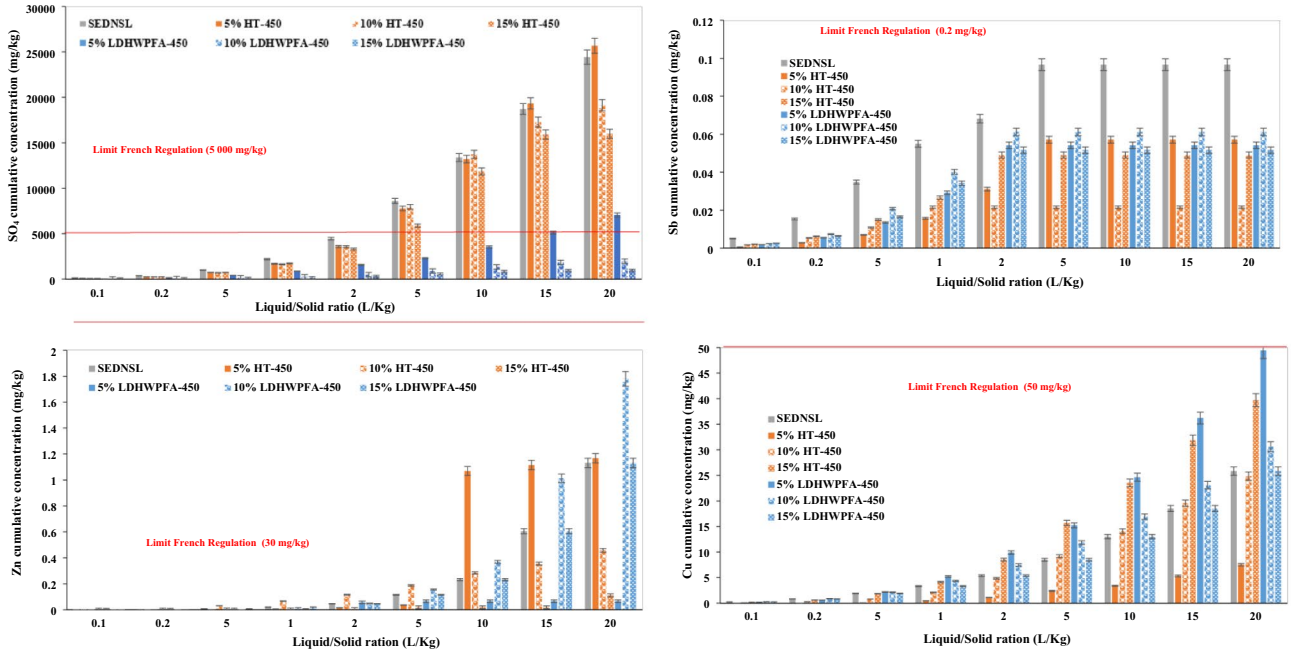

Fig. 9 Leaching concentration of Cu, Sb, Zn and SO_4^{2-} and the variation of pH and conductivity from SED_{NSL} after treatment with HT, HT-450, LDH_{WPFA} and LDH_{WPFA}-450 (Columns)

the presence of carbonate minerals ($CaCO_3$) and calcium oxide (CaO) [87].

The conductivity of the leached solutions was high at the beginning of the experiments with a value of about 3.53 mS/cm for the untreated SED_{NSL}. During the experiments, the conductivity decreased as a function of the ration (L/S) until it reached 0.69 mS /cm for the ratio L/S = 20 l/kg. When HT-450 or LDH_{WPFA}-450 were used as amendment, the electrical conductivity value decreased significantly at the beginning of the experiment (L/S = 0.1 l/kg), reaching 2.13 mS/cm and 1.83 mS/cm for 15% HT-450 and 15% LDH_{WPFA}-450 respectively. At the end of the experiment, the conductivity reached similar values than untreated SED_{NSL}: 0.73 mS/cm and 0.71 mS/cm for 15% HT-450 and 15% LDH_{WPFA}-450, respectively. The decrease in electrical conductivity of the leached solutions was attributed to the leaching of soluble salts into the interstitial water of the SED_{NSL} during the first phases of the experiments. Thus, a large portion of the SO_4^{2-} was stabilized and trapped in the LDH lattice. The cumulative concentrations of Cu, Sb, Zn and SO_4^{2-} in the leachate from the column experiments are presented as a function of the L/S (l/kg) ratio in Fig. 9. The limit of the backfill or shoulder covered fixed by SETRA [85] for the ratio L/S = 10 l/kg and presented with a red line for each element.

The percolation test results show that the release of MMTE present in the SED_{NSL}, increases rapidly with the increase of the ratio (L/S). The high conductivity of the solution and sulfide oxidation process are at the origin of the fast-leaching kinetics of the pollutants. The high mobilization of pollutants (Cu, Mo, Sb, Zn) during column percolation tests was correlated to the high salinity of the leached solutions. Indeed, the presence of major cationic (Ca^{2+}, Mg^{2+}, K^+) and anionic elements (Cl^-, SO_4^{2-}, NO_3^-) favors the desorption of pollutants from the SED_{NSL} surface [88, 89]. This process has already been reported during oxidation of anoxic sediments in the laboratory and in river dredging sediments [90]. When SED_{NSL} was amended with LDH_{WPFA}-450 or LDH_{WPFA}-450, dissolved MMTE were released in a lower extent and the oxidation reaction kinetics were lower. The decrease of MMTE and SO_4^{2-} mobility could be explained by the weak conductivity of the solution, the adsorption of some cationic pollutants at the surface of the LDHs (negatively charged surface) and the SO_4^{2-} trapping between the interlayer by anionic exchange with OH^- [91].

To evaluate the stabilization efficiency of SED_{NSL} with HT-450 and LDH_{WPFA}-450, the MMTE concentrations measured in the leachates of the stabilized samples were compared with those obtained for untreated SED_{NSL}. The leaching rate of Ba, Cu, Mo, Sb, Se and Zn in SED_{NSL} for a L/S = 10 l/kg ratio corresponded to 0.18%, 1.49%, 8.57%, 1.39%, 1.27%, 0.01% of the total contents measured in SED_{NSL} respectively. The rates were particularly low for most pollutants (< 1.5%), except for Mo which was mobilized at 8.57%. The low mobility of cationic pollutants (Ba,

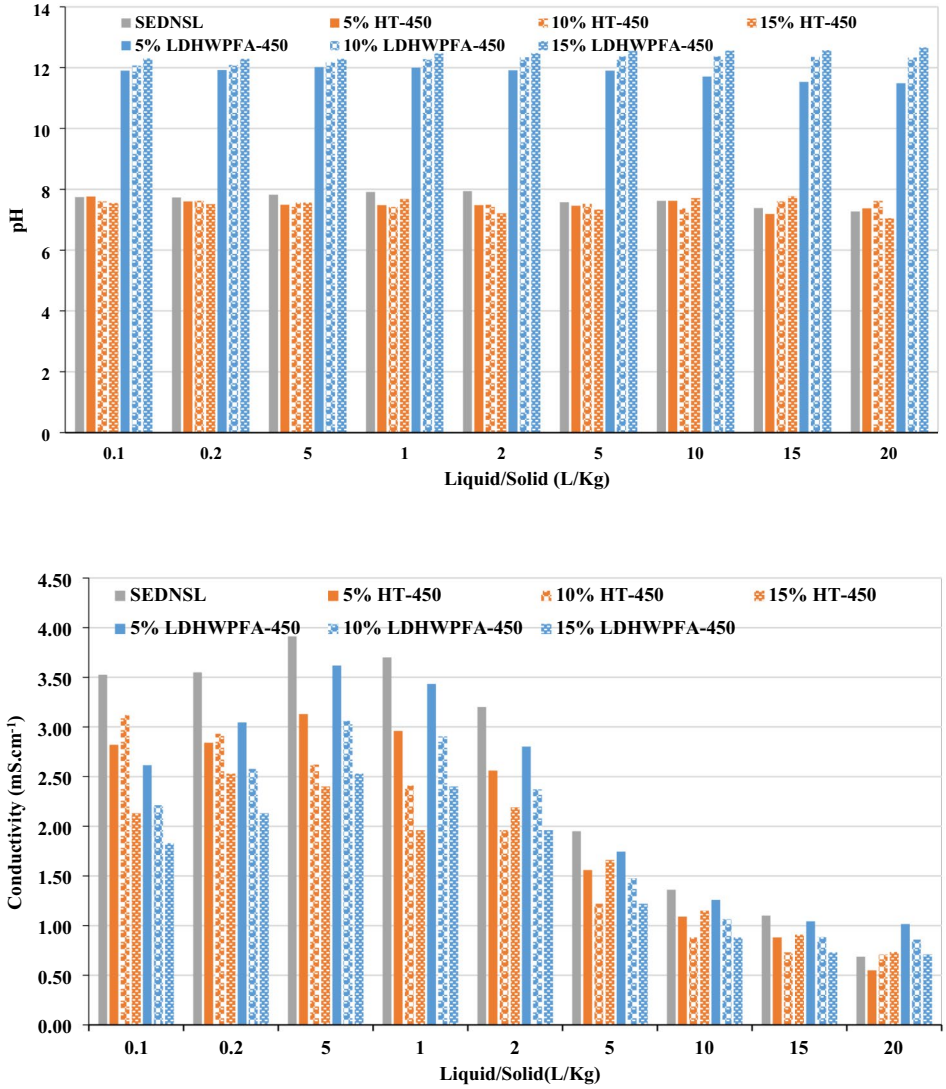

Fig. 9 (continued)

Cu, Pb, Zn) can be explained by the alkaline pH of the SED_{NSL} which favors adsorption and precipitation processes on the surface of minerals. After treatment of SED_{NSL} with HT-450 and LDH_{WPFA}-450, the dissolved concentrations of most MMTE (especially Sb, Zn, and SO_4^{2-}) decreased with the increase of mass percentage of each LDH (5%, 10% and 15%). In contrast, the dissolved Cu concentration increased in the leachate.

Amendments with HT-450 (10% and 15%) and LDH_{WPFA}-450 (5%, 10% and 15%) significantly decreased the SO_4^{2-}concentration in the leachate compared to the untreated SED_{NSL} (13 373 mg/kg). The dissolved SO_4^{2-}concentration decreased in the following order (ratio L/S = 10 l/kg): 5% HT-450 (13 208 mg/kg) > 10% HT-450 (13 735 mg/kg) > 15% HT-450 (11 844 mg/kg) > 5% LDH_{WPFA}-450 (3 529 mg/kg) > 10% LDH_{WPFA}-450 (1 320 mg/kg) > 15% LDH_{WPFA}-450 (842 mg/kg). HT-450 and LDH_{WPFA}-450 (at 5% of amendment) were effective in trapping Sb since Sb concentration in the leachates was reduced even at low percentage of addition. The dissolved Sb concentration decreased in the following order (ratio L/S = 10 l/kg): 10% LDH_{WPFA}-450 (0.061 mg/kg) > 5% HT-450 (0.057 mg/kg) > 5% LDH_{WPFA}-450 (0.054 mg/kg) > 15% LDH_{WPFA}-450 (0.051 mg/kg) > 15% HT-450 (0.049 mg/kg) > 10% HT-450 (0.021 mg/kg). Zn leaching decreased mainly in the SED_{NSL} stabilized with HT-450. On the other hand, an increase in Zn mobility was measured when SED_{NSL} was stabilized with 10% and 15% LDH_{WPFA}-450, but Zn leached concentration remained significantly below the SETRA threshold (30 mg/kg). The mobility of Cu was increased after SED_{NSL} amendment. This was in good agreement with the results from

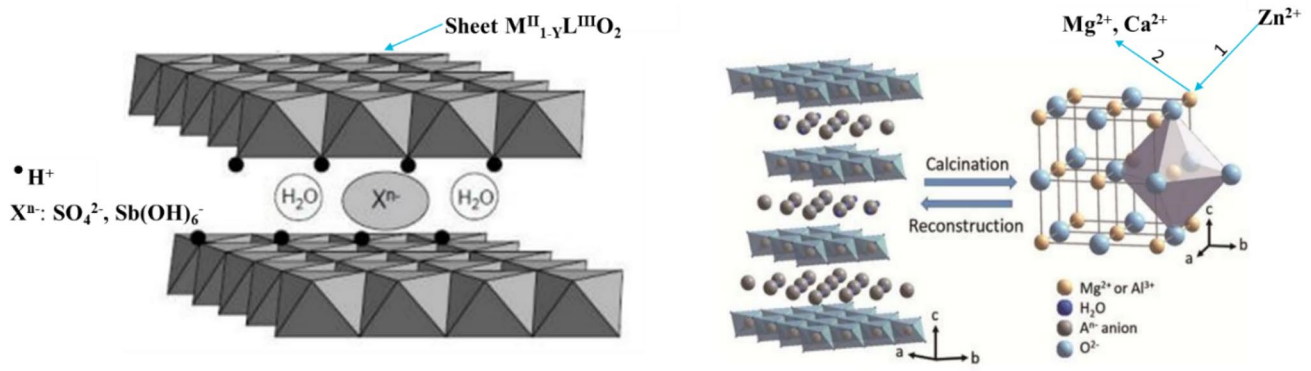

Fig. 10 Physico–chemical mechanism of chemical elements [93]

the batch test. Cu leaching was higher when LDH_{WPFA}-450 was used as amendment probably due to the pH increase in these conditions (> 12). Thus, the total copper content in SED_{NSL} and LDH_{WPFA} are (870 ± 7 mg/kg) and (169 ± 9 mg/kg) respectively. Thee dissolved Cu concentration was not constant at the end of the experiment and continued to increase in the leachates.

The results of the SED_{NSL} treatment column tests clearly demonstrated the effect of HT-450 and LDH_{WPFA}-450 on the dissolved concentrations of MMTE and SO_4^{2-} in the treated SED_{NSL} leachates. For all the studied elements, dissolved concentrations were significantly lower in SED_{NSL} stabilized with LDH_{WPFA}-450 compared to untreated SED_{NSL}. Thus, the SED_{NSL} stabilized with LDH_{WPFA}-450 released lower concentrations of MMTE and SO_4^{2-} compared to SED_{NSL} stabilized with HT-450, and below the threshold of engineered fill or paved shoulders (set at 50 mg/kg, 0.2 mg/kg, 30 mg/kg and 5000 mg/kg for Cu, Sb, Zn and SO_4^{2-} respectively. The concentrations of the MMTEs are presented in the Appendix (Table 4, 5, 6, 7, 8 and 9).

Trapping Mechanism

Geochemical stabilization is a widely used treatment technique in contaminated sediments since it is an easy-to-implement process to recover or store contaminated waste. LDH are one of the most used amendments to immobilize several pollutants by precipitation, complexation and adsorption [92]. Figure 10 shows the different trapping mechanisms of Sb, Zn and SO_4^{2-} during SED_{NSL} treatment by the different LDH. [93].

Zinc (Zn)

The main mechanisms of Zn trapping by the different LDHs before and after calcination at 450 °C include surface adsorption, precipitation and surface complexation [94]. Zn can easily combine with the different LDHs during SED_{NSL} treatment, due to the presence of hydrogen bonds and exchangeable ions on the surface. The different LDHs also contained hydroxyl groups that could combine with Zn. Thus, the negatively charged surface facilitated the complexation of Zn with LDH surface. According to the study carried out by Guan et al., [95], the Zn^{2+} interactions may be attributed to (i) precipitation of Zn^{2+} and negatively charged ions (such as OH^- and CO_3^{2-}), (ii) surface complexation of Zn by functional groups (OH single bond), (iii) incorporation of Zn^{2+} by the substitution of Ca^{2+} or Mg^{2+} ions into the LDH structure. During the adsorption process, interactions also occured simultaneously. Owing to the large specific surface area and surface functional groups of LDH, surface complexation can be predominant and rapid (Fig. 10).

Park et al. indicated that the surface-induced precipitation could be a major mechanism of metal-cation adsorption by LDH, which occurs due to localized high pH values and the released carbonate ions available to metal cations [96]. The negative charge of LDH layers could attract cationic ions in aqueous solution to induce the formation of metal hydroxides. To confirm this process, the comparison of LDH pH before (Table 4) and after (Table 1, 2, 3 Appendix) the treatment was performed. The results revealed a slight decrease in pH of the solution after treatment with LDH_{WPFA} and HT, meaning that Zn^{2+} adsorption by LDH_{WPFA} and HT was able to generate $Zn(OH)_2$ precipitate under these extremely basic pH conditions. Meanwhile, the pH of the leachates from SED_{NSL} treated with LDH_{BFA} were all between 12.34 and 12.45 (Table 2 Appendix). Consequently, the adsorption of Zn^{2+} by LDH_{BFA} could not generate $Zn(OH)_2$ precipitate. The presence of hydroxide groups (OH^-) and carbonate (CO_3^{2-}) was confirmed by XRD, TGA, and FTIR results, indicating that Zn^{2+}immobilization could occur according to (2):

$$3Zn^{2+} + 2CO_3^{2-} + 2OH^- \rightarrow Zn_3(CO_3)_2(OH)_2 \quad (2)$$

Batch and column leaching tests revealed that the different LDHs (before and after calcination) showed excellent

performances for Zn^{2+} immobilization since the released concentrations were below the IWSI and SETRA thresholds. The different LDHs had a relatively high specific surface area, abundant functional groups containing cations and a well-hierarchical pore structure. The high surface area enhanced the capture of free Zn^{2+} ions by the LDHs due to the Van der Waals forces and electrostatic attraction [97]. The collapse of the lamellar structure and the formation of metal oxides after calcination promoted the dissolution of major functional groups such as Ca–O, –OH, Mg–O in the medium, i.e. the O-containing functional groups could lead to the complexation of Zn^{2+}. $^{+}$ [98].

Zn^{2+} trapping can be produced by substitution of Ca^{2+} and or Mg^{2+} ions in the LDH layers, which changed from a Friedel salt to a hydrotalcite-type structure, according to the reaction (3) and (4):

$$Mg_6Al_2(OH)_6(CO_3).4H_2O + Zn^{2+} \rightarrow Zn - Mg5\ Al_2(OH)_6(CO_3).4H_2O + Mg^{2+} \quad (3)$$

$$Ca_4Al_2(OH)_{12}\ (Cl, CO_3, OH)_2 + Zn^{2+} \rightarrow Zn - Ca_3Al_2(OH)_{12}(Cl, CO3, OH)_2 + Ca^{2+} \quad (4)$$

After calcination at 450 °C, the Zeta potential results showed that the surface charge always remained negative, meaning that Zn can still be trapped by complexation or adsorption mechanisms on the surface. For LDH_{WPFA}, LDH_{WPFA}-450, LDH_{BFA} and LDH_{BFA}-450, the XRD and TGA results indicated the presence of calcite promoting zinc carbonate ($ZnCO_3$) precipitation.

Sulfate (SO_4^{2-})

Three kinds of trapping mechanisms have been proposed for the sorption of sulfate anions onto LDH surface, including anion exchange, electrostatic attraction and precipitation. Previous studies have reported that anions such as sulfate are most likely adsorbed onto the LDH surface by electrostatic attraction and anion exchange in the interlayer region [99, 100]. In addition, favorable anion adsorption occured when the pH of LDH was above the SED_{NSL} pH. When the non-calcinated LDHs were used for SED_{NSL} stabilization, the surface of LDHs was negatively charged, making the electrostatic attraction more complicated but favoring the anion exchange that occurred between SO_4^{2-} and OH^- groups [101] (Fig. 10). According to the results reported by Theiss et al. [24] after sulfate trapping, the LDH surface was rendered non-porous, which could be attributed to the precipitation of calcium and/or aluminum sulfate. Another study [102] demonstrated some evidences of sulfate substitution with chloride and carbonate in the LDH interlayer after adsorption. This indicates that ion exchange can readily occur between sulfate and interlayer anions.

LDH_{BFA} has the lowest adsorption capacity, probably due to its low specific surface area compared to others LDH. From Figs. 8 and 9 LDH_{WPFA} has a higher adsorption capacity compared to HT. The different mechanisms of SO_4^{2-} removal are the important reason for the difference in removal behavior between uncalcined and calcined samples. In the presence of non-calcinated LDH_{WPFA}, SO_4^{2-} removal reaction primarily involved the exchange of SO_4^{2-} anions by the anion present in the interlayer. In calcinated LDH_{WPFA}, the adsorption mechanism involved the rehydration of mixed metal oxides and the simultaneous intercalation of SO_4^{2-} species into the interlayer to rebuild the original Ca–Al structure.

The OH groups were present on the calcinated LDH surface and also resulted from the hydration of CaO or MgO in aqueous solution. Sulfate anions can therefore exchange with OH^- groups and complex on the surface of LDH. According to the results of LDHs physico-chemical characterization and batch and column test results, a number of factors can explain the ability of LDH_{WPFA}-450 to more efficiently scavenge SO_4^{2-} compared to the others LDHs. The first factor was the basic pH value, confirming hydration of CaO in aqueous solution and precipitation of gypsum according to reaction (5):

$$Ca(OH)_2 + SO_4^{2-} \rightarrow CaSO_4 + 2OH^- \quad (5)$$

It should be noted that several trapping mechanisms occur simultaneously such as; precipitation of $CaSO_4$, anionic exchange of SO_4^{2-} with OH^- groups and complexation on the surface (Fig. 10). The studies carried out by Letshwenyo et al,. [103] showed that sulfate adsorption by two kinds of LDH prepared by co-precipitation method (LDH $4Mg_2Al.NO_3$ and LDH $8Mg_2Al.NO_3$) engaged two kinds of reactions, the first one corresponding to SO_4^{2-} surface complexation on LDH, and the second one corresponding to anionic exchange with NO_3.

Antimony (Sb)

The batch and column test results showed an excellent capacity of non-calcinated and calcinated HT, LDH_{WPFA} and LDH_{BFA} to stabilize Sb from SED_{NSL}. However, Sb trapping in LDH structures can occur according to two different mechanisms: surface adsorption, or anion exchange. Given the negatively charged surface of the LDHs, electrostatic attraction between the negatively charged $Sb(OH)_6^-$ and the negatively charged surface sites was not favored. For this reason, surface adsorption should be excluded as a significant trapping mechanism for Sb.

Owing to the lack of surface sites to adsorb $Sb(OH)_6^-$, anionic exchange with OH^- groups in the interlayer regions of the LDHs would be the main process for Sb trapping. Since Sb exists in the Sb(III) or Sb(V) oxidation degree, the leaching results showed that more than 98% of Sb was trapped in the LDH lattices, this confirms that Sb was present in the $Sb(OH)_6^-$ form under basic pH conditions, and most of the $Sb(OH)_6^-$ was trapped in the interleaf region by substituting the OH^- groups.

As shown in the results of XRD, FX and FTIR, after calcination of LDH at 450 °C, new phases appeared and the interlayer structure collapsed. The phases change directly implied a change in Sb trapping mechanism. The formation of periclase (MgO), spinel ($MgAl_2O_4$) or Sodalite ($Na_8Al_6Si_6O_{24}Cl_2$) structure in the case of HT-450 and LDH_{WPFA} respectively, resulted in the incorporation of Sb into the layer structure during its during reconstruction [104]. Furthermore, HT-450 will not allow Sb sorption reactions by anion exchange, as the OH- groups are dehydroxylated after calcination. Ardau et al,. [99] tested the removal of Sb from wastewater by calcinated HT (presence of periclase) and concluded that Sb trapping occurred mainly through a rapid adsorption on the surface, while the reconstruction of the layer structure from the periclase form slowed down Sb removal. Hence, Sb removal mainly occurred by anion exchange in the interlayer space and by incorporation into the reconstructed layered structure, rather than by only anion exchange.

Based on the results of batch and column tests and the physicochemical characterizations of LDH, several factors can explain the ability of LDH_{WPFA} and LDH_{BFA} to more efficiently trap Sb, compared to HT. The most important one was the basic pH value, which promoted the hydration of CaO in aqueous solution and the precipitation of calcium antimonate according to reaction (6):

$$Ca(OH)_2 + 2Sb(OH)_6^{2-} \rightarrow Ca(Sb(OH)_6)_2 + 2(OH)^- \quad (6)$$

Conclusion

The main objective of this research was the synthesis and characterization of LDH from WPFA and BFA which were used as amendments to stabilize Sb, Zn and SO_4^{2-} in SED_{NSL}. From this study, the following conclusions can be drawn.

- The treatment of fly ashes by acid leaching followed by precipitation allowed the formation of layered phases showing high similarities with layered double hydroxides. The main resulting phases were HT ($Mg_6Al_2(OH)_{16}(CO_3).4H_2O$), Hydrocalumite ($Ca_4Al_2(OH)_{12}(Cl,CO_3,OH)_2{\cdot}4H_2O$) and Paraalumohydrocalcite ($CaAl_2(CO_3)_2(OH)_4{\cdot}6H_2O$) for HT, LDH_{WPFA} and LDH_{BFA} respectively. Calcination of theses materials at 450 °C resulted in destruction of LDH lattices.
- LDHs presented FTIR spectra identical to all HT phases. Identification of the vibrational bands revealed the presence of interlamellar anions, hydroxylated groups and lattice structure related to octahedral layers.
- The SEM analyses revealed a platelet morphology of LDH phases which is characteristic of lamellar double hydroxides with hexagonal blocks with some octahedral shape.
- The thermogravimetric analysis of the LDHs revealed three typical decomposition steps of the layered double hydroxides: dehydration, dehydroxylation leading to the destruction of the layered framework, decomposition of the layered compounds into oxide and spinel. The decomposition being usually preceded by the elimination of the interlamellar anion.
- The use of LDHs as amendment to stabilize MMTE and sulfate in the sediment matrix was efficient. The quality of the leachates from SED_{NSL} was significantly improved when using LDHs as amendments and the amount of released pollutants decreased by 50 to 99%. Among the different LDHs tested, LDH_{WPFA}-450 was the most efficient to immobilize the pollutants du to the higher Ca/Al ratio of the initial WPFA matrix, compared to BFA matrix.
- From the batch leaching experiments, amendment of SED_{NSL} with 15% of HT-450 or LDH_{WPFA}-450 was enough to stabilize Sb, Zn and SO_4^{2-}. The resulting leachates had concentrations below the SETRA threshold without generating further contamination. From the column leaching experiments, only 5% of LDH_{WPFA}-450 amendment allowed the stabilization of SED_{NSL}. The resulting leachates had concentrations below the SETRA threshold for recovery or storage.
- The pollutant removal rate reached 97% and 99% for HT-450 and LDH_{WPFA}-450, respectively.
- Anion exchange, electrostatic attraction and surface complexation were the main mechanisms for Sb, Zn and SO_4^{2-} trapping.

Synthesis of LDH from fly ash stemming from industries is a promising route for the reduction of industrial ultimate waste volumes. Calcinated LDHs, have demonstrated to be an interesting alternative, at reduced cost, to be used for stabilization by adsorption of MMTE and sulfate in sediment matrix.

Supplementary Information The online version contains supplementary material available at https://doi.org/10.1007/s12649-023-02056-0.

Acknowledgements The authors wish to acknowledge technical contributions of the chemistry pole of Institut Mines-Télécom and Institut de Physique de Nice. This research did not receive any specific grant from funding agencies in the public, commercial, or not-for-profit sectors.

Funding The authors have not disclosed any funding.

Data Availability This manuscript has data included as electronic supplementary material.

Declarations

Conflict of interest The authors declare that they have no known competing financial interests or personal relationships that could have appeared to influence the work reported in this paper.

References

1. É. Ruin, Les enjeux du transport fluvial. Métropolitiques, 2013
2. R. Boutin, Amélioration des connaissances sur le comportement des rejets en mer de produits de dragage de type vase: phénomènes à court terme et dans le champ proche, PhD Thesis, Lyon, INSA, 1999.
3. SedNet. European Sediment Network. https://sednet.org/(consulté le 15 mai 2022).
4. C. Alzieu, *Dragages et environnement marin: état des connaissances = Dredging and marine environment: state of the art*. 1999. Consulté le: 15 mai 2022. [En ligne]. Disponible sur: https://www.vliz.be/en/imis?refid=17902
5. Tran, N.T.: Valorisation de sédiments marins et fluviaux en technique routière. Université d'Artois, Arras (2009)
6. Mkahal, Z., Mamindy-Pajany, Y., Maherzii, W., Abriak, N.-E.: Recycling of mineral solid wastes in backfill road materials: technical and environmental investigations. Waste Biomass Valor **13**, 667–687 (2022). https://doi.org/10.1007/s12649-021-01544-5
7. Levacher, D., Dhervilly, P.: Déshydratation mécanisée in situ de sédiments fraîchement dragués ou mis en dépôts: le projet SEDIGATE® I, XIèmes Journées Nationales Génie Côtier-Génie Civil. Sables d'Olonne, France (2010)
8. Agostini, F., Skoczylas, F., Lafhaj, Z.: About a possible valorisation in cementitious materials of polluted sediments after treatment. Cement Concrete Compos. **29**, 270–278 (2007). https://doi.org/10.1016/j.cemconcomp.2006.11.012
9. Yu, G., Lei, H., Bai, T., Li, Z., Yu, Q., Song, X.: In-situ stabilisation followed by ex-situ composting for treatment and disposal of heavy metals polluted sediments. J. Environ. Sci. **21**, 877–883 (2009). https://doi.org/10.1016/S1001-0742(08)62357-8
10. Förstner, U.: Geochemical techniques on contaminated sediments-river basin view. Environ. Sci. Pollut. Res. **10**, 58–68 (2003). https://doi.org/10.1065/espr2003.01.145
11. Qian, G., Chen, W., Lim, T.T., Chui, P.: In-situ stabilization of Pb, Zn, Cu, Cd and Ni in the multi-contaminated sediments with ferrihydrite and apatite composite additives. J. Hazard. Mater. **170**, 1093–1100 (2009). https://doi.org/10.1016/j.jhazmat.2009.05.093
12. Tao, Q., Zhang, Y., Zhang, X., Yuan, P., He, H.: Synthesis and characterization of layered double hydroxides with a high aspect ratio. J. Solid State Chem. **179**, 708–715 (2006). https://doi.org/10.1016/j.jssc.2005.11.023
13. Bocher, F., Géhin, A., Ruby, C., Ghanbaja, J., Abdelmoula, M., Génin, J.-M.R.: Coprecipitation of Fe(II–III) hydroxycarbonate green rust stabilised by phosphate adsorption. Solid State Sci. **6**, 117–124 (2004). https://doi.org/10.1016/j.solidstatesciences.2003.10.004
14. Olfs, H.-W., Torres-Dorante, L.O., Eckelt, R., Kosslick, H.: Comparison of different synthesis routes for Mg–Al layered double hydroxides (LDH): characterization of the structural phases and anion exchange properties. Appl. Clay Sci. **43**, 459–464 (2009). https://doi.org/10.1016/j.clay.2008.10.009
15. Hutson, N.D., Attwood, B.C.: High temperature adsorption of CO2 on various hydrotalcite-like compounds. Adsorption **14**, 781–789 (2008). https://doi.org/10.1007/s10450-007-9085-6
16. Chibwe, K., Jones, W.: Synthesis of polyoxometalate pillared layered double hydroxides via calcined precursors. Chem. Mater. **1**, 489–490 (1989)
17. Elbasuney, S.: Surface engineering of layered double hydroxide (LDH) nanoparticles for polymer flame retardancy. Powder Technol. **277**, 63–73 (2015). https://doi.org/10.1016/j.powtec.2015.02.044
18. Tamura, H., Chiba, J., Ito, M., Takeda, T., Kikkawa, S.: Synthesis and characterization of hydrotalcite-ATP intercalates. Solid State Ionics **172**, 607–609 (2004). https://doi.org/10.1016/j.ssi.2004.04.035
19. Zhang, H., et al.: Synthesis of a hydrotalcite-like compound from oil shale ash and its application in uranium removal. Coll. Surf. A **444**, 129–137 (2014). https://doi.org/10.1016/j.colsurfa.2013.12.054
20. Galindo, R., López-Delgado, A., Padilla, I., Yates, M.: Synthesis and characterisation of hydrotalcites produced by an aluminium hazardous waste: a comparison between the use of ammonia and the use of triethanolamine. Appl. Clay Sci. **115**, 115–123 (2015). https://doi.org/10.1016/j.clay.2015.07.032
21. Kuwahara, Y., Ohmichi, T., Kamegawa, T., Mori, K., Yamashita, H.: A novel conversion process for waste slag: synthesis of a hydrotalcite -like compound and zeolite from blast furnace slag and evaluation of adsorption capacities. J. Mater. Chem. **20**(24), 5052–5062 (2010). https://doi.org/10.1039/C0JM00518E
22. Kuwahara, Y., Tsuji, K., Ohmichi, T., Kamegawa, T., Mori, K., Yamashita, H.: Transesterifications using a hydrocalumite synthesized from waste slag: an economical and ecological route for biofuel production. Catal. Sci. Technol. **2**(9), 1842–1851 (2012). https://doi.org/10.1039/C2CY20113E
23. Volli, V., Purkait, M.K.: Preparation and characterization of hydrotalcite-like materials from flyash for transesterification. Clean Techn. Environ. Policy. **18**(2), 529–540 (2015). https://doi.org/10.1007/s10098-015-1036-4
24. Theiss, F.L., Couperthwaite, S.J., Ayoko, G.A., Frost, R.L.: A review of the removal of anions and oxyanions of the halogen elements from aqueous solution by layered double hydroxides. J. Coll. Interface Sci. **417**, 356–368 (2014). https://doi.org/10.1016/j.jcis.2013.11.040
25. Châtelet, L., Bottero, J.Y., Yvon, J., Bouchelaghem, A.: Competition between monovalent and divalent anions for calcined and uncalcined hydrotalcite: anion exchange and adsorption sites. Coll. Surf. A: Physicochem. Eng. Asp. **111**(3), 167–175 (1996). https://doi.org/10.1016/0927-7757(96)03542-X
26. Wang, J., Kang, D., Yu, X., Ge, M., Chen, Y.: Synthesis and characterization of Mg–Fe–La trimetal composite as an adsorbent for fluoride removal. Chem. Eng. J. **264**, 506–513 (2015). https://doi.org/10.1016/j.cej.2014.11.130
27. Extremera, R., Pavlovic, I., Pérez, M.R., Barriga, C.: Removal of acid orange 10 by calcined Mg/Al layered double hydroxides from water and recovery of the adsorbed dye. Chem. Eng. J. **213**, 392–400 (2012). https://doi.org/10.1016/j.cej.2012.10.042
28. Goh, K.-H., Lim, T.-T., Dong, Z.: Application of layered double hydroxides for removal of oxyanions: a review. Water Res. **42**(6), 1343–1368 (2008). https://doi.org/10.1016/j.watres.2007.10.043

29. Halajnia, A., Oustan, S., Najafi, N., Khataee, A.R., Lakzian, A.: The adsorption characteristics of nitrate on Mg–Fe and Mg–Al layered double hydroxides in a simulated soil solution. Appl. Clay Sci. **70**, 28–36 (2012). https://doi.org/10.1016/j.clay.2012.09.007
30. de Sá, F.P., Cunha, B.N., Nunes, L.M.: Effect of pH on the adsorption of sunset yellow FCF food dye into a layered double hydroxide (CaAl-LDH-NO3). Chem. Eng. J. **215–216**, 122–127 (2013). https://doi.org/10.1016/j.cej.2012.11.024
31. Miyata, S.: Anion-exchange properties of hydrotalcite-like compounds. Clays Clay Miner. **31**(4), 305–311 (1983). https://doi.org/10.1346/CCMN.1983.0310409
32. Goswamee, R.L., Sengupta, P., Bhattacharyya, K.G., Dutta, D.K.: Adsorption of Cr(VI) in layered double hydroxides. Appl. Clay Sci. **13**(1), 21–34 (1998). https://doi.org/10.1016/S0169-1317(98)00010-6
33. Kagunya, W., Chibwe, M., Jones, W.: Synthesis and structural characterisation of LDH-organic intercalates. Mole. Cryst Liq. Cryst. Sci. Technol. Sect. A Mole. Cryst. Liq. Cryst. **244**(1), 155–160 (1994). https://doi.org/10.1080/10587259408050097
34. Kameda, T., Yoshioka, T., Uchida, M., Miyano, Y., Okuwaki, A.: New treatment method for dilute hydrochloric acid using magnesium-aluminum oxide. BCSJ **75**(3), 595–599 (2002). https://doi.org/10.1246/bcsj.75.595
35. Kameda, T., Yabuuchi, F., Yoshioka, T., Uchida, M., Okuwaki, A.: New method of treating dilute mineral acids using magnesium–aluminum oxide. Water Res. **37**(7), 1545–1550 (2003). https://doi.org/10.1016/S0043-1354(02)00374-3
36. Parker, L.M., Milestone, N.B., Newman, R.H.: The use of hydrotalcite as an anion absorbent. Ind. Eng. Chem. Res. **34**(4), 1196–1202 (1995)
37. Houri, B., Legrouri, A., Barroug, A., Forano, C., Besse, J.-P.: Use of the ion-exchange properties of layered double hydroxides for water purification. Collect Czech. Chem. Commun. **63**(5), 732–740 (1998). https://doi.org/10.1135/cccc19980732
38. Inacio, J., Taviot-Guého, C., Forano, C., Besse, J.P.: Adsorption of MCPA pesticide by MgAl-layered double hydroxides. Appl. Clay Sci. **18**(5), 255–264 (2001). https://doi.org/10.1016/S0169-1317(01)00029-1
39. N. Drici. 2015. Hydroxydes doubles lamellaires, synthèse, caractérisation et propriétés. PhD Thesis, Université Sorbonne Paris Cité
40. Bouzar, B., Mamindy-Pajany, Y.: Immobilization study of As, Cr, Mo, Pb, Sb, Se and Zn in geopolymer matrix: application to shooting range soil and biomass fly ash. Int. J. Environ. Sci. Tech. https://doi.org/10.1007/s13762-023-04788-x
41. Bouzar, B., Mamindy-Pajany, Y.: Manufacture and characterization of carbonated lightweight aggregates from waste paper fly ash. Powder Technol. (2022). https://doi.org/10.1016/j.powtec.2022.117583
42. AFNOR. 2000. NF ISO 13320–1, Laser diffraction methods.
43. AFNOR. 2012. NF EN 933–1 "Test for geometrical properties of aggresgates".
44. AFNOR. 2020. NF EN 933–2 "Test for geometrical properties of aggresgates".
45. AFNOR. 2006. NF EN ISO 18757, Determination of specific surface area pf ceramic powders by gas adsorption using the BET method.
46. AFNOR. 2009. NF EN 15326, Measurement of density and specific gravity.
47. AFNOR. 2000. NF EN 12879, Characterization of sludges.
48. AFNOR. 2002. NF EN 12457–2, Leaching-Compliance test for leaching of granular wasre materials ans sludges.
49. Bouzar, B., Mamindy-Pajany, Y.: Phosphorus removal from real and synthetic wastewater using biomass bottom ash. Int. J. Environ. Sci. Technol. (2022). https://doi.org/10.1007/s13762-022-04451-x
50. AFNOR. 2017. NF EN 14405, Characterization of waste — Leaching behaviour test — Up-flow percolation test (under specified conditions).
51. Husein Malkawi, A.I., Alawneh, A.S., Abu-Safaqah, O.T.: Effects of organic matter on the physical and the physicochemical properties of an illitic soil. Appl. Clay Sci. **14**(5), 257–278 (1999). https://doi.org/10.1016/S0169-1317(99)00003-4
52. Muriithi, G.N., Petrik, L.F., Gitari, W.M., Doucet, F.J.: Synthesis and characterization of hydrotalcite from South African coal fly ash. Powder Technol. **312**, 299–309 (2017). https://doi.org/10.1016/j.powtec.2017.02.018
53. Barriga, C., Gaitán, M., Pavlovic, I., Ulibarri, M.A., Hermosîn, M.C., Cornejo, J.: Hydrotalcites as sorbent for 2,4,6-trinitrophenol : influence of the layer composition and interlayer anion. J. Mater. Chem. **12**(4), 1027–1034 (2002). https://doi.org/10.1039/B107979B
54. Lakraimi, M., Legrouri, A., Barroug, A., Roy, A.D., Besse, J.P.: Preparation of a new stable hybrid material by chloride–2,4-dichlorophenoxyacetate ion exchange into the zinc–aluminium–chloride layered double hydroxide. J. Mater. Chem. **10**(4), 1007–1011 (2000). https://doi.org/10.1039/A909047I
55. Aramendía, M.A., et al.: Thermal decomposition of Mg/Al and Mg/Ga layered-double hydroxides: a spectroscopic study. J. Mater. Chem. **9**(7), 1603–1607 (1999). https://doi.org/10.1039/A900535H
56. Reichle, W.T.: Synthesis of anionic clay minerals (mixed metal hydroxides, hydrotalcite). Solid State Ion. **22**(1), 135–141 (1986). https://doi.org/10.1016/0167-2738(86)90067-6
57. Khan, A.I., O'Hare, D.: Intercalation chemistry of layered double hydroxides: recent developments and applications. J. Mater Chem. **12**(11), 3191–3198 (2002). https://doi.org/10.1039/B204076J
58. George, G., Saravanakumar, M.P.: Facile synthesis of carbon-coated layered double hydroxide and its comparative characterisation with Zn–Al LDH: application on crystal violet and malachite green dye adsorption—isotherm, kinetics and Box-Behnken design. Environ. Sci. Pollut. Res. **25**(30), 30236–30254 (2018). https://doi.org/10.1007/s11356-018-3001-3
59. Crepaldi, E.L., Tronto, J., Cardoso, L.P., Valim, J.B.: Sorption of terephthalate anions by calcined and uncalcined hydrotalcite-like compounds. Coll. Surf. A: Physicochem. Eng. Asp. **211**(2), 103–114 (2002). https://doi.org/10.1016/S0927-7757(02)00233-9
60. You, Y., Zhao, H., Vance, G.F.: Hybrid organic–inorganic derivatives of layered double hydroxides and dodecylbenzenesulfonate: preparation and adsorption characteristics. J. Mater. Chem. **12**(4), 907–912 (2002). https://doi.org/10.1039/B106811C
61. Fernandez, J.M., Ulibarri, M.A., Labajos, F.M., Rives, V.: The effect of iron on the crystalline phases formed upon thermal decomposition of Mg-Al-Fe hydrotalcites. J. Mater. Chem. **8**(11), 2507–2514 (1998). https://doi.org/10.1039/A804867C
62. Deng, L., Shi, Z.: Synthesis and characterization of a novel Mg–Al hydrotalcite-loaded kaolin clay and its adsorption properties for phosphate in aqueous solution. J. Alloys Compd. **637**, 188–196 (2015)
63. Gevers, B.R., Labuschagné, F.J.: Green Synthesis of Hydrocalumite (CaAl-OH-LDH) from Ca(OH)2 and Al(OH)3 and the parameters that influence its formation and speciation. Crystals (2020). https://doi.org/10.3390/cryst10080672
64. You, Y., Zhao, H., Vance, G.F.: Surfactant-enhanced adsorption of organic compounds by layered double hydroxides. Coll. Surf. A: Physicochem. Eng. Asp. **205**(3), 161–172 (2002). https://doi.org/10.1016/S0927-7757(01)01137-2
65. You, Y., Zhao, H., Vance, G.F.: Adsorption of dicamba (3,6-dichloro-2-methoxy benzoic acid) in aqueous solution by

calcined–layered double hydroxide. Appl. Clay Sci. **21**(5), 217–226 (2002). https://doi.org/10.1016/S0169-1317(01)00102-8
66. Rives, V., Kannan, S.: Layered double hydroxides with the hydrotalcite-type structure containing Cu2+, Ni2+ and Al3+. J. Mater. Chem. **10**(2), 489–495 (2000). https://doi.org/10.1039/A908534C
67. Leaustic, A., Babonneau, F., Livage, J.: Structural investigation of the hydrolysis-condensation process of titanium alkoxides Ti (OR) 4 (OR= OPr-iso, OEt) modified by acetylacetone 1 study of the alkoxide modification. Chem. Mater. **1**(2), 240–247 (1989)
68. Smith, M.B.: March's advanced organic chemistry: reactions, mechanisms, and structure. Wiley, New Jersey (2020)
69. Aramendía, M.A., Boráu, V., Jiménez, C., Marinas, J.M., Porras, A., Urbano, F.J.: Synthesis and characterization of MgO-B 2 O 3 mixed oxides prepared by coprecipitation; selective dehydrogenation of propan-2-ol. J. Mater. Chem. **9**(3), 819–825 (1999). https://doi.org/10.1039/A807536K
70. Aramendía, M.Á., Borau, V., Jiménez, C., Marinas, J.M., Romero, F.J., Urbano, F.J.: Synthesis and characterization of a novel Mg/In layered double hydroxide. J. Mater. Chem. **9**(10), 2291–2292 (1999)
71. Pausch, I., Lohse, H.-H., Schürmann, K., Allmann, R.: Syntheses of disordered and Al-rich hydrotalcite-like compounds. Clays Clay Miner. **34**(5), 507–510 (1986). https://doi.org/10.1346/CCMN.1986.0340502
72. Reichle, W.T.: Catalytic reactions by thermally activated, synthetic, anionic clay minerals. J. Catal. **94**(2), 547–557 (1985). https://doi.org/10.1016/0021-9517(85)90219-2
73. Kooli, F., Depège, C., Ennaqadi, A., de Roy, A., Besse, J.P.: Rehydration of Zn-Al Layered double hydroxides. Clays Clay Miner. **45**(1), 92–98 (1997). https://doi.org/10.1346/CCMN.1997.0450111
74. Forano, C., Costantino, U., Prevot, V., Gueho, C.T.: Layered Double Hydroxides (LDH). In: Bergaya, F., Lagaly, G. (eds.) Developments in Clay Science. Elsevier, Amsterdam (2013)
75. Lin, Y., Fang, Q., Chen, B.: Perchlorate uptake and molecular mechanisms by magnesium/aluminum carbonate layered double hydroxides and the calcined layered double hydroxides. Chem. Eng. J. 237, 38–46 (2014). https://doi.org/10.1016/j.cej.2013.10.004
76. C. Forano, T. Hibino, F. Leroux, et C Taviot-Guého. 2006. Chapter 131 Layered Double Hydroxides. In: F Bergaya, B K G Theng, et G Lagaly (Éds), Developments in Clay Science, Elsevier, Amstersdam
77. Rousselot, I., Taviot-Guého, C., Leroux, F., Léone, P., Palvadeau, P., Besse, J.-P.: Insights on the structural chemistry of hydrocalumite and hydrotalcite-like materials: investigation of the series Ca2M3+(OH)6Cl·2H2O (M3+: Al3+, Ga3+, Fe3+, and Sc3+) by X-ray powder diffraction. J. Solid State Chem. **167**(1), 137–144 (2002). https://doi.org/10.1006/jssc.2002.9635
78. Prinetto, F., Ghiotti, G., Graffin, P., Tichit, D.: Synthesis and characterization of sol–gel Mg/Al and Ni/Al layered double hydroxides and comparison with co-precipitated samples. Microporous Mesoporous Mater. **39**(1), 229–247 (2000). https://doi.org/10.1016/S1387-1811(00)00197-9
79. Faour, A., Prévot, V., Taviot-Gueho, C.: Microstructural study of different LDH morphologies obtained via different synthesis routes. J. Phys. Chem. Solids **71**(4), 487–490 (2010). https://doi.org/10.1016/j.jpcs.2009.12.018
80. Kloprogge, J.T., Hickey, L., Frost, R.L.: The effects of synthesis pH and hydrothermal treatment on the formation of zinc aluminum hydrotalcites. J. Solid State Chem. **177**(11), 4047–4057 (2004). https://doi.org/10.1016/j.jssc.2004.07.010
81. León, M., Díaz, E., Bennici, S., Vega, A., Ordóñez, S., Auroux, A.: Adsorption of CO2 on hydrotalcite-derived mixed oxides: Sorption mechanisms and consequences for adsorption irreversibility. Ind. Eng. Chem. Res. **49**(8), 3663–3671 (2010). https://doi.org/10.1021/ie902072a
82. Sharma, S.K., Kushwaha, P.K., Srivastava, V.K., Bhatt, S.D., Jasra, R.V.: Effect of hydrothermal conditions on structural and textural properties of synthetic hydrotalcites of varying Mg/Al ratio. Ind. Eng. Chem. Res. **46**(14), 4856–4865 (2007). https://doi.org/10.1021/ie061438w
83. López Nieto, J.M., Dejoz, A., Vazquez, M.I.: Preparation, characterization and catalytic properties of vanadium oxides supported on calcined Mg/Al-hydrotalcite. Appl. Catal. A: Gener. **132**(1), 41–59 (1995). https://doi.org/10.1016/0926-860X(95)00153-0
84. López-salinas, E., Torres-garcía, E., García-sánchez, M.: THERMAL BEHAVIOR OF HYDROTALCITE-LIKE [Mg1−xGax(OH)2](CO3)x/2·mH2O AS A FUNCTION OF GALLIUM CONTENT. J. Phys. Chem. Solids **58**(6), 919–925 (1997). https://doi.org/10.1016/S0022-3697(96)00210-7
85. Acceptabilité de matériaux alternatifs en technique routière - Evaluation environnementale, *Cerema*. http://www.cerema.fr/fr/centre-ressources/boutique/acceptabilite-materiaux-alternatifs-technique-routiere (consulté le 8 mars 2022).
86. M. Bekkouche. 2014. Synthèse, Caractérisation d'hydroxydes lamellaires type Cu-M (M= Al, Fe) et application dans le traitement de l'eau. Mémoire de magister, université des Sciences et de la technologie-Mohamed.
87. Mamindy-Pajany, Y., Hurel, C., Geret, F., Roméo, M., Marmier, N.: Comparison of mineral-based amendments for ex-situ stabilization of trace elements (As, Cd, Cu, Mo, Ni, Zn) in marine dredged sediments: a pilot-scale experiment. J. Hazard. Mater. **252–253**, 213–219 (2013). https://doi.org/10.1016/j.jhazmat.2013.03.001
88. Lions, J., van der Lee, J., Guérin, V., Bataillard, P., Laboudigue, A.: Zinc and cadmium mobility in a 5-year-old dredged sediment deposit: experiments and modelling. J Soils Sedim. **7**(4), 207–215 (2007). https://doi.org/10.1065/jss2007.05.226
89. Garnier, J.-M., Ciffroy, P., Benyahya, L.: Implications of short and long term (30 days) sorption on the desorption kinetic of trace metals (Cd, Zn Co, Mn, Fe, Ag, Cs) associated with river suspended matter. Sci. Total Environ. **366**(1), 350–360 (2006). https://doi.org/10.1016/j.scitotenv.2005.07.015
90. Isaure, M.-P., et al.: Quantitative Zn speciation in a contaminated dredged sediment by μ-PIXE, μ-SXRF, EXAFS spectroscopy and principal component analysis. Geochim. Cosmochim. Acta **66**(9), 1549–1567 (2002). https://doi.org/10.1016/S0016-7037(01)00875-4
91. Guimarães, D., et al.: Precipitation of a layered double hydroxide comprising Mg2+ and Al3+ to remove sulphate ions from aqueous solutions. J. Environ. Chem. Eng. **7**(1), 102815 (2019). https://doi.org/10.1016/j.jece.2018.102815
92. Dong, Y., Kong, X., Luo, X., Wang, H.: Adsorptive removal of heavy metal anions from water by layered double hydroxide: a review. Chemosphere **303**, 134685 (2022). https://doi.org/10.1016/j.chemosphere.2022.134685
93. L. Zhao. 2016. Développement et mise en oeuvre de nouveaux matériaux adsorbants d'anions à base de ferrihydrite ou d'Hydroxydes Doubles Lamellaires intégrés dans un gel d'alginate. PhD Thesis, Limoges, 2016.
94. Mohammadi, M., Mohammadi Torkashvand, A., Biparva, P., Esfandiari, M.: Synthesis ratios of Mg-Al and Zn-Al layered double hydroxides efficiency and selectivity in nitrate removal

from solution. Global J. Environ. Sci. Manag. **5**(4), 485–500 (2019). https://doi.org/10.22034/GJESM.2019.04.08
95. Guan, X., et al.: Application of functionalized layered double hydroxides for heavy metal removal: a review. Sci. Total Environ. **838**, 155693 (2022). https://doi.org/10.1016/j.scitotenv.2022.155693
96. Park, M., et al.: Reactions of Cu2+ and Pb2+ with Mg/Al layered double hydroxide. Appl. Clay Sci. **37**(1), 143–148 (2007). https://doi.org/10.1016/j.clay.2006.12.006
97. Fang, Q., et al.: Application of layered double hydroxide-biochar composites in wastewater treatment: recent trends, modification strategies, and outlook. J. Hazard. Mater. **420**, 126569 (2021). https://doi.org/10.1016/j.jhazmat.2021.126569
98. Lyu, P., Wang, G., Cao, Y., Wang, B., Deng, N.: Phosphorus-modified biochar cross-linked Mg–Al layered double-hydroxide composite for immobilizing uranium in mining contaminated soil. Chemosphere **276**, 130116 (2021). https://doi.org/10.1016/j.chemosphere.2021.130116
99. Ardau, C., Frau, F., Lattanzi, P.: Antimony removal from aqueous solutions by the use of Zn-Al sulphate layered double hydroxide. Water Air Soil Pollut. **227**(9), 344 (2016). https://doi.org/10.1007/s11270-016-3048-z
100. Matusik, J., Rybka, K.: Removal of chromates and sulphates by Mg/Fe LDH and heterostructured LDH/halloysite materials: efficiency, selectivity, and stability of adsorbents in single- and multi-element systems. Materials (2019). https://doi.org/10.3390/ma12091373
101. Mahjoubi, F.Z., Khalidi, A., Abdennouri, M., Barka, N.: Zn–Al layered double hydroxides intercalated with carbonate, nitrate, chloride and sulphate ions: synthesis, characterisation and dye removal properties. J. Taibah Univ. Sci. **11**(1), 90–100 (2017). https://doi.org/10.1016/j.jtusci.2015.10.007
102. Halajnia, A., Oustan, S., Najafi, N., Khataee, A.R., Lakzian, A.: Adsorption–desorption characteristics of nitrate, phosphate and sulfate on Mg–Al layered double hydroxide. Appl. Clay Sci. **80**, 305–312 (2013)
103. Letshwenyo, M.W., Mokokwe, G.: Phosphorus and sulphates removal from wastewater using copper smelter slag washed with acid. SN Appl. Sci. **3**(12), 854 (2021). https://doi.org/10.1007/s42452-021-04843-7
104. Cao, Y., Guo, Q., Liang, M., Sun, W.: Sb(III) and Sb(V) removal from water by a hydroxyl-intercalated, mechanochemically synthesized Mg-Fe-LDH. Appl. Clay Sci. **196**, 105766 (2020). https://doi.org/10.1016/j.clay.2020.105766

Chapter 5:

Immobilization study of As, Cr, Mo, Pb, Sb, Se and Zn in geopolymer matrix: application to shooting range soil and biomass fly ash.

International Journal of Environmental Science and Technology
https://doi.org/10.1007/s13762-023-04788-x

ORIGINAL PAPER

Immobilization study of As, Cr, Mo, Pb, Sb, Se and Zn in geopolymer matrix: application to shooting range soil and biomass fly ash

B. Bouzar[1,2] · **Y. Mamindy-Pajany**[1,2]

Received: 24 August 2022 / Revised: 19 December 2022 / Accepted: 18 January 2023

Abstract

The objective of this study was to investigate the feasibility of physico–chemical stabilization of Cr (24 ± 0.9 mg/kg), Mo (3.7 ± 0.4 mg/kg), Pb (20 ± 1.2 mg/kg), Se (1.1 ± 0.14 mg/kg) and Zn 17 ± 1.5 mg/kg) from a biomass fly ash (BFA) and Pb (1.3 ± 0.06 mg/kg), Sb (7.57 ± 0.09 mg/kg) from a shooting range soil (SRS) in a geopolymer elaborated from flash metakaolins. For that purpose, different geopolymer formulations were elaborated using three types of flash metakaolins. Following the formulation step, the geopolymers were subjected to an accelerated carbonation step in the liquid phase before the study of the material properties. To understand the behavior of metallic and metalloid trace elements (MMTEs) in the different matrices of the present study, leaching tests with water and as a function of pH were performed. Thermogravimetry, X-ray diffraction, scanning electron microscopy and energy-dispersive spectroscopy analyses were performed to study the evolution of geopolymerization and accelerated carbonation and their effects on the physico–chemical and mineralogical properties. The physico–chemical stabilization of As, Cr, Mo, Pb, Sb, Se and Zn by geopolymerization followed by an accelerated carbonation step resulted in reduced release levels for these elements. Metakaolin R was particularly efficient in trapping the different elements with a release level below the IWSI threshold, attaining concentrations of Cr (0.48 ± 0. 04 mg/kg), Mo (0.45 ± 0.13 mg/kg), Pb (< 0.032 mg/kg), Se (< 0.083 mg/kg) and Zn 17 ± 1.5 mg/kg) from a BFA and Pb (0.22 ± 0.02 mg/kg), Sb (0.03 ± 0.01 mg/kg) from an SRS. The study results clearly demonstrate the effectiveness of geopolymerization/carbonation stabilization processes for the trapping of As, Cr, Mo, Pb, Sb, Se and Zn over a wide pH range. It is also shown that the composition of the metakaolin significantly influences the efficiency of this type of process.

Keywords Geopolymer · Metallic and metalloid trace element · Physico–chemical stabilization · Accelerated carbonation · Shooting range soil · Biomass fly ash

Introduction

Metallic and metalloid trace elements (MMTEs) from various industrial processes and shooting ranges represent a major environmental problem through soil and groundwater contamination (Sorvari et al. 2006). The contamination of shooting range soils is characterized by the presence of large amounts of metallic lead and also of Sb, Cu, Zn, Ni and As, which also need to be considered. The contamination of shooting range soils is characterized by the presence of large amounts of metallic lead and also of Sb, Cu, Zn, Ni and As, which also need to be considered. Lead is the main component of bullets; it constitutes 93.1% of the bullet mass. Antimony, which acts as a hardener for Pb, represents 1.9% of the bullet's mass (Laporte-Saumure et al. 2010). These quantities of metallic lead from the use of bullets have been deposited on the soil of shooting ranges all over the world. The corrosion or alterations lead to the mobilization of metals in cationic and anionic form causing high levels of Pb, Cu, Sb and Zn pollution in the soils (Clausen et al. 2011; Ma et al. 2007; Strømseng et al. 2009). Shooting range soils are classified as hazardous waste under the Resource Conservation and Recovery Act of 1976, which requires sustainable management of these materials (Heier et al. 2009). The materials have recently become a focal

Editorial responsibility: Hari Pant.

✉ B. Bouzar
bader.bouzar@imt-nord-europe.fr

[1] Institut Mines-Télécom, Centre for Materials and Processes, Environnement, IMT Nord Europe, 59000 Lille, France

[2] LGCgE, Laboratoire de Génie Civil Et Géo-Environnement, Univ. Lille, ULR 4515, 59000 Lille, France

Published online: 28 January 2023

point of public concern because Pb loading in shooting range soils is in excess of 10,000 mg/kg (Ma et al. 2007; Liu et al. 2013), exceeding by an order of magnitude the environmental threshold values set by the US Environmental Protection Agency (US EPA) and National Environmental Protection Measure in Australia (NEPMs).

Biomass fly ash (BFA) usually comes from wood waste from forests, farm waste or food waste. The ash generally ends up in one of two manners, disposed of in landfills or reused as a secondary raw material. The most common option is disposal in specialized landfills that receive only hazardous residues (Thi et al. 2015; Nanda and Berruti 2021; Lausselet et al. 2016). BFA_s are essentially composed of calcium, silicon and aluminum: between them, they represent between 70 and 90% of the materials (Mozaffari et al. 2009; 2006; Bouzar and Mamindy-Pajany 2022a, b; Bouzar and Mamindy-Pajany 2022a, b; Jurado-Contreras et al. 2022; Teixeira et al. 2022). The concentrations of other major elements are small (below 2%) except for MgO, which can reach a content of 5%. Sulfate (SO_3) levels are below 1% except for the ash studied by Bai et al. (Mozaffari et al. 2009) (1.1%). The high values (between 14.5 and 23.5%) of loss on ignition reflect the decarbonation of the calcite present and also the combustion of unburned organic compounds initially contained in the wood waste. In most cases, the BFA is environmentally hazardous and is stabilized and disposed of in special landfills (Class I and II). The large investments are required for such treatment oblige companies to find alternatives to treatment (François and Criado 2007). Some countries prefer treatment of ash prior to landfill due to environmental protection.

Currently, in some countries, a small percentage of these wastes is used mainly for the manufacture of concrete, cement and brick products (Mkahal et al. 2022; Zouch et al. 2022; Bouchikhi et al. 2021); the remainder is as mentioned below put in landfill, which is an unsatisfactory solution both from the ecological and economic point of view. The disposal of hazardous waste requires a physico–chemical stabilization step to limit the release of toxic elements into the environment. This management strategy is widespread in France and in Europe with variable levels of efficiency depending on the nature of the contaminated matrices. Studies have shown that geopolymer binders can permanently trap MMTE and ensure a certain stability under aggressive conditions for several months or even years (Davidovits 2013).

The geopolymer binders are a class of semi-crystalline aluminosilicate materials, generally synthesized at ambient or mildly elevated temperature from aluminates and silicates solubilized in a medium (Pacheco-Torgal et al. 2008). Indeed, geopolymers are composed of aluminum and silica tetrahedra interconnected by oxygen. A polymeric structure Al–O–Si and Si–O–Si constitutes the main bonds of the geopolymer. Moreover, cations such as Na^+, K^+ and Ca^{2+} must be present in the structure to ensure neutrality. According to Davidovits (2013), these binders allow the stabilization of toxic waste. Also, several parameters influence the performance of the binders such as temperature, molar ratios SiO_2/Al_2O_3; Na_2O/SiO_2; Na_2O/Al_2O_3; H_2O/Na_2O, nature and concentration of alkaline solutions. Therefore, it appears essential to develop materials that allow the incorporation of wastes such as metakaolin-based geopolymers, obtained by calcination of kaolinite clay. Metakaolin, a natural material rich in silica and alumina, is produced from the calcination (around 700 °C) of raw kaolin, which contains kaolinite as its main mineral. It is an amorphous metastable material with a high reactivity. The reaction with alkaline solutions leads to the formation of a geopolymer with high mechanical performances. The alkaline activation of metakaolin involves the rupture of Si–O–Si, SiO–Al and Al–O–Al covalent bonds due to the high concentration of OH- ions in the medium leading to the passage of aluminate ions and silicates in solution forming Si–OH and AlOH groups. The condensation of these chemical species leads to the formation of an amorphous aluminosilicate gel named NASH (Na_2O-Al_2O_3-SiO_2-H_2O). The interest of geopolymers in different applications has increased, in particular for waste encapsulation.

Two possibilities exist for the immobilization of MMTE. One possibility is physical immobilization by capturing the toxic elements in the empty pore space in the solid matrix. Another possibility is the immobilization of MMTE by replacing them with a component of the same valence. The function of the positively charged elements (M^{2+}) will be to compensate the negative charge of aluminum. MMTEs such as Pb or Zn… have two cations (divalent), which is identical to Ca. The assumption was that MMTE could replace Ca during the structuring of the matrix. Ca^{2+} would behave similarly to Na^+, i.e., it would compensate the negative charge of the aluminum ion (Fang and Kayali 2013), which forms a tetravalent hydroxide ($Al(OH)_4$). A study carried out using silicate-rich Waste Incineration Fume Treatment Residues (WIFTR) for geopolymer synthesis showed that Pb immobilization can differ according to the pH. The leaching of Pb was significantly elevated when the pH was below 4.8 (Srivastava et al. 2008). The study conducted by Hassam et al. (2016) using kaolins for geopolymer synthesis to test the immobilization capacity of lead (Pb) and zinc (Zn) proved the immobilization capacity of lead (Pb) from the Amizour waste.

The state of knowledge on the formulation of geopolymers as remediation binders for MMTE has shown the exclusive use of standard metakaolins as a source of aluminates and silicates. In the present study, new metakaolins with different characteristics were selected to study the physicochemical stabilization of inorganic elements. The novelty

of the present study was to formulate geopolymer matrices followed by an accelerated carbonation process to simultaneously stabilize Sb and Pb in SRS and Cr, Mo, Pb, Se and Zn in BFA using commercial flash metakaolin of varying compositions. To date and to our knowledge, no study has investigated the stabilization of range soil and biomass fly ash using geopolymer/accelerated carbonation technology. The aim of this research is to produce a geopolymer with high chemical resistance and high physical properties, in order for these geopolymer matrices to be the most promising storage matrices for future industrial applications.

Materials and methods

Material description

The SRS was collected on the shooting range sites of the military base of Meucon (France), from a depth between 0 and 30 cm. In order to carry out the required tests, the SRS was dried in the oven at 40 °C until a constant mass was obtained. Subsequently, it was sieved through the 4, 3.15 and 2 mm sieves, eliminating at the same time the bullet fragments (Figure 1 Appendix). Subsequently, the SRS was crushed in a SK 300-RETSCH flail crusher using the < 250 µm sieve. The MMTE leaching and chemical composition of the SRS were determined by inductively coupled plasma atomic emission spectrometry (ICP-AES) and X-ray fluorescence (XRF), respectively. The characterization results of the SRS indicate a predominance of silicon content expressed as SiO_2 (69%). Other elements are also detected, notably aluminum expressed as Al_2O_3 (16.23%), K_2O (5.91%) and Fe_2O_3 (1.42%). Finally, other elements are found in a minor quantity (< 1%) including TiO_2, CaO and MgO. The predominance of silicon and aluminum in the SRS is rather favorable to the geopolymerization reaction. Nevertheless, their presence at high levels does not predict their solubility in alkaline media. The leaching results show that the concentration of Sb (7.57 ± 0.09 mg/kg) exceeds the threshold for Hazardous Waste Storage Installations (HWSI), while Pb (1.3 ± 0.06 mg/kg) exceeds the threshold for Inert Waste Storage Installations (IWSI) (Table 1 Appendix). The releases of the other MMTE and the anions are below the IWSI thresholds. It should be observed that in the leachate water pH was 9.7, which is relatively high for a matrix mainly composed of quartz. The pH is explained by the alkalinity brought by the residues of the shooting bullet fragments, which hydrolyze in the presence of water.

The BFA was collected in the Hauts-de-France region from the cyclone of a mass combustion incinerator. The chemical composition and leaching of MMTE presented in Table 1 show the BFA is mainly composed of CaO (41.4%), SiO_2 (15.2%), K_2O (10.1%), Fe_2O_3 (3.81%) and Al_2O_3 (2.46%). However, Cr (24 ± 0.9 mg/kg), Zn (17 ± 1.5 mg/

Table 1 Chemical composition in major and MMTE of SRS, BFA, MK (S), MK (R) and MK (P)

XRF data						Batch equilibrium leaching test		
Chemical composition	SRS (wt.%)	BFA (wt.%)	MK (S) (wt.%)	MK (R) (wt.%)	MK (P) (wt.%)	Parameter	SRS ($mg.kg^{-1}$)	BFA ($mg.kg^{-1}$)
SiO_2	68.78	16.19	60.1	57.32	54.97	As	< 0.11	< 0.11
Al_2O_3	16.23	2.46	31.54	28.33	37.59	Ba	0.02 ± 0.01	2.9 ± 0.15
MgO	0.49	3.81	–	0.33	–	Cd	< 0.009	< 0.009
Fe_2O_3	1.42	5.15	1.43	7.58	1.72	Co	< 0.009	< 0.009
CaO	0.56	41.39	0.7	–	0.42	Cr	< 0.004	**24 ± 0.9**
Na_2O	3.5	1.48	–	–	–	Cu	0.1 ± 0.02	0.14 ± 0.02
SO_3	–	9.24	–	–	–	Mo	< 0.09	**3.7 ± 0.4**
TiO_2	0.16	0.67	1.17	1	1.5	Ni	< 0.047	0.11 ± 0.02
ZnO	–	0.62	–	–	–	Pb	**1.3 ± 0.06**	**20 ± 1.2**
SrO	–	0.11	–	–	–	Sb	**7.57 ± 0.09**	< 0.06
BaO	–	0.22	–	–	–	Se	< 0.083	**1.1 ± 0.14**
P_2O_5	0.45	2.29	–	–	–	Zn	< 0.01	**17 ± 1.5**
K_2O	5.91	11.12	0.36	0.6	0.12	Sulfates	206 ± 16	**$24\,000 \pm 238$**
PbO	0.32	0.43	–	–	–	Fluorides	4.9 ± 0.4	**14 ± 1.5**
Cl	–	2.5	–	–	–	Chlorides	31 ± 2	**$15\,000 \pm 190$**
						pH	9.7 ± 0.15	12.8 ± 0.2
						Conductivity ($mS.cm^{-1}$)	0.12 ± 0.01	15 ± 0.5

The bold characters are the problematic elements to be studied

kg), Se (1.1 ± 0.14 mg/kg), Pb (20 ± 1.2 mg/kg) Mo (3.7 ± 0.4 mg/kg), sulfates (24 000 ± 238 mg/kg), fluorides (14 ± 1.5 mg/kg) and chlorides (15 000 ± 190 mg/kg) were the most abundant elements in BFA. In the first approach, BFA was potentially hazardous.

Commercial flash metakaolins are derived from the calcination of clay in the temperature ranges 600–850 °C. Three metakaolins are used: standard metakaolin (S), iron-rich metakaolin (R) and clay-rich metakaolin (P). The chemical composition analysis (Table 1) shows that the silicon content measured as SiO_2 varies between 55 and 60% of the analyzed samples' mass composition. For aluminum, the content of Al_2O_3 varies between 28 and 38%, while the content of Fe_2O_3 varies between 1 and 8%. The other elements detected are inferior to 2% and expressed with contents of CaO, MgO, TiO_2 and K_2O oxides.

Geopolymer synthesis/accelerated carbonation

The reagents used to activate the geopolymerization reaction are NaOH (20 wt% of the activation solution) and Na_2SiO_3 (80 wt%). The sodium silicate is a FISHER commercial solution (SiO_2/Na_2O molar ratio = 2.2; 14.6% Na_2O; 30.8% SiO_2 and 54.6% H_2O). NaOH powder of 98.8% purity was used to prepare the activation solution. Na_2SiO_3 was added, with the objective of increasing the concentration of soluble silicates and increasing the reaction rate. The two reagents were mixed in a glass container by a magnetic agitator for 6 h; then, the solution was rested in a plastic bottle for 24 h. Then, the alkaline solution was mixed in a mixer with metakaolin and SRS or BFA at a rotational speed of 300 rpm for about 3 min. The obtained paste was filled into test tubes in prismatic form 4*4*16 cm. Subsequently, the specimens were placed on the vibrating table to eliminate the air bubbles introduced during the procedure. The specimens manufactured were in accordance with the standard NF EN 196–1 (AFNOR (NF EN 196-1) 2016) with a water/binder ratio equal to 0.45 for SRS and 0.8 for BFA. The specimens are of prismatic form and were made in triplicate.

After 7 days of curing at room temperature (20 °C), mortar specimens were carbonated in the laboratory. For this purpose, glass reactors were filled with Milli-Q water saturated at 100% with sodium bicarbonate ($NaHCO_3$) and the specimens were agitated for 7 days with a magnetic bar. Following the carbonation step, the specimens were dried at 20 °C in the air for 4 days in order to perform the compression tests and environmental analyses. Table 2 represents the quantities of the constituents used for the formulation of the specimens. Figure 1 summarizes the experimental program followed for the formulation and characterization of the geopolymer matrices.

Characterization methods

The particle size distribution of SRS and BFA was determined using a dry-voice laser particle size analyzer. In this study, a Coulter LS 230 laser (Douai, France) was used to determine the particle size between 0.04 µm and 2000 µm. The test was carried out in accordance with NF ISO 13320-1 (AFNOR 2000a).

The Brunauer–Emmett–Teller (BET) method was used to determine the specific surface area of the materials from nitrogen sorption experiments using an AGITENT Analyzer apparatus from Micromeritics (3FLEX Surface Characterization, Douai, France) in accordance with standard NF EN ISO-18757 (AFNOR 2006). Physical adsorption results from relatively low forces (van der Waals forces) between the gas molecules (adsorbate) and the sample surface (adsorbent). 1.5 g of dry sample was weighed and placed in the cell. The entire measuring cell was immersed in a nitrogen bath to maintain a constant temperature. Successive quantities of nitrogen were then introduced into the cell containing the sample, which had been degassed for 8 h at 80 °C. The adsorption/desorption isotherms were measured on the previously desorbed samples at 80 °C for 5 mbar. The residual pressure is used to calculate the specific surface area, which is directly related to the quantity of nitrogen adsorbed. The BET method used on materials allows reliable surface measurements (< 10% error).

Table 2 Quantities of the constituents used for the specimen's formulation

	G-S-SRS	G-R-SRS	G-P-SRS	G-S-BFA	G-R-BFA	G-P-BFA
12 M NaOH solution (g)	81	81	81	162	162	162
Na_2SiO_3 (g)	324	324	324	648	648	648
Activation solution ($NaOH + Na_2SiO_3$) (g)	405	405	405	810	810	810
SRS (g)	675	675	675	–	–	–
BFA (g)	–	–	–	675	675	675
MK(S) (g)	225	–	–	225	–	–
MK(R) (g)	–	225	–	–	225	–
MK(R) (g)	–	–	225	–	–	225

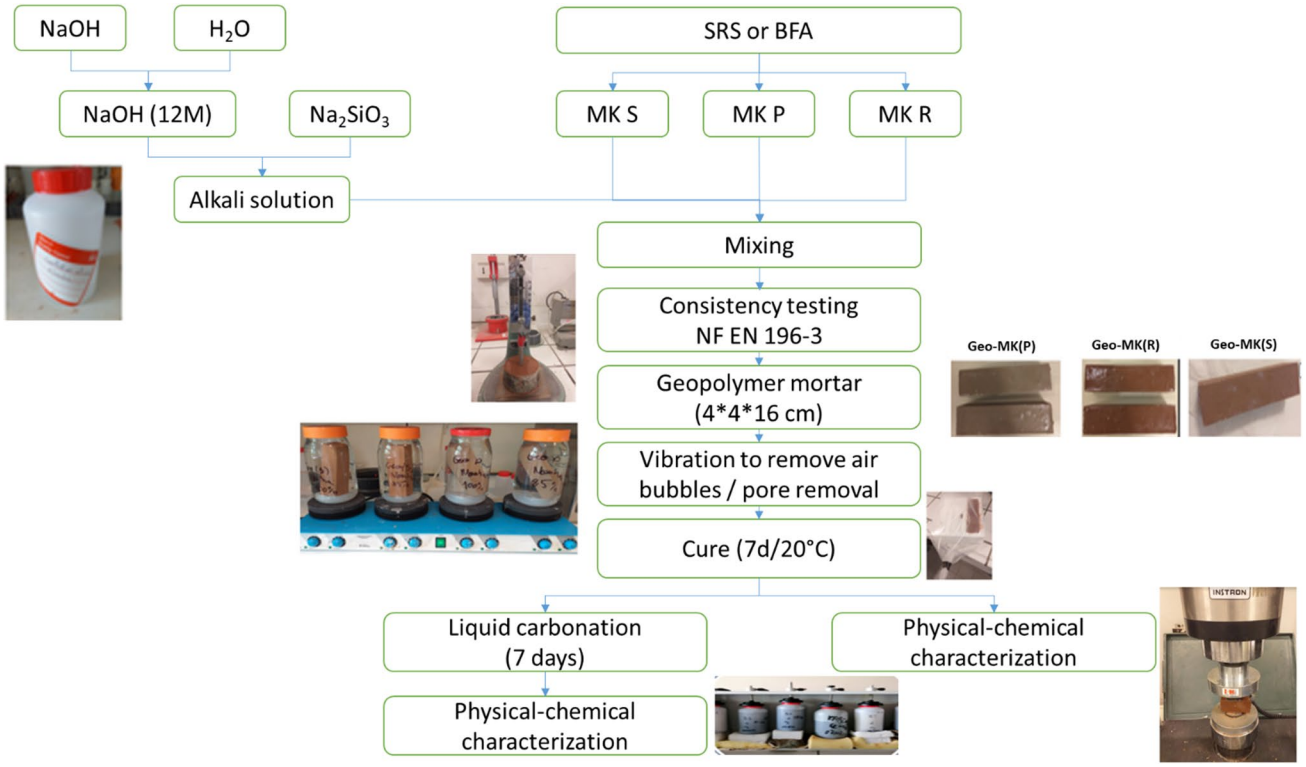

Fig. 1 Experimental program followed for the formulation and characterization of the geopolymer matrices

The specific density was measured using a Micromeritics ACCUPYC 1330 Helium Pycnometer (Douai, France) in accordance with standard NF EN 1097-7 (AFNOR 2008). Three samples were prepared in order to promote the consistency of results. The samples were dried at 105 °C to constant mass. Finally, a mass of approximately 1.5 g of the sample was weighed and placed in a cell with a total volume of 3.5 cm^3. The pycnometer performed several measurements on the same sample, and the average of the measurements was recorded.

The loss on ignition (LOI) of SRS and BFA was determined according to the NF EN 12879 (AFNOR 2000b) standard; 5 g of samples was calcined at 550 °C for 3 h. Subsequently, to avoid hydration, the sample was cooled in a desiccator with resin. A percentage of the organic material could be determined by the weight loss.

The compressive strength of the 4*4*16 cm prismatic specimens was determined using the 15 ton INSTRON 5500 R (Douai, France) with a load rate of 144 kN/min according to NF EN 196-1(AFNOR (NF EN 196-1) 2016). The tests were carried out on at least three specimens for each term in order to ensure the reproducibility of the results.

The XRF analysis was performed with a S4-PIONEER (Douai, France) equipped with a 4-kW generator with a rhodium anti-cathode. The instrument was capable of providing results in atomic mass percentages of the elements. The analyzed samples are crushed and dried previously.

The mineral composition of SRS and BFA before and after synthesis was determined by X-ray diffraction (XRD). The analysis was performed on powders using a Bruker D8 focus diffractometer (Douai, France). The ray source was a monochromatized cobalt ($\lambda K\alpha 1 = 1.74$ Å) with a Lynx Eye fast linear detector. The operating current is 20 mA and the voltage is 40 kV. The samples were analyzed over an angular range of 10° to 80° with an acquisition step of 0.02° and a compaction time of 5 s.

In order to quantify certain physical or chemical transformations occurring in a material such as oxidation, dehydration, decomposition, phase changes, thermogravimetric (TG) and differential thermal analysis (DTA), analyses were performed on a NETZSCH STA 409C thermobalance (Douai, France). The analyzed samples were pre-dried in an oven at 40 °C to a constant mass. For each analysis, a quantity of 200 to 250 mg of dry powdered material is introduced into the apparatus and subjected to a linear temperature rise from ambient temperature to 1150 °C at a rate of 3 °C/minute under an inert gas (argon) with a flow rate of 75 ml/min. At the end of the test, the processing software accompanying the apparatus allows the recovery of the TG Coubes and the DTA derivative.

To study the phase morphology present in SRS and BFA before and after synthesis, observations were made by scanning electron microscope (SEM- Hitachi S-4300SE/N) and energy-dispersive spectroscopy (EDS) (Douai, France). The sample was introduced into the resin, and then, the solid powder was dispersed on a double-sided carbon band with polishing.

The leaching behavior of MMTE in SRS and BFA before and after synthesis was studied according to NF EN 12457–2 (AFNOR 2002). The leaching was performed with a ratio L/S = 10 l/kg (liquid/solid); 90 g of WPFA was mixed with 900 ml of Milli-Q water. The moisture content of the containment matrix to weigh the correct dry matter mass was determined at each time point. The samples were placed under agitation on a turntable (Heidolph Reax 20) at 10 rpm and 25 °C for 24 h. The mixture was then filtered through cellulose acetate membrane filters (0.45 µm). Acidified with 2 vol.% nitric acid, the MMTE concentrations of the leachate were analyzed by inductively coupled plasma atomic emission spectroscopy (ICP-AES, 5100 Agilent Technologies, Douai, France); The chloride (Cl^-), sulfate (SO_4^{2-}) and fluoride (F^-) concentration was determined through ion chromatography (IC-Dionex ICS 6000, Douai, France). The temperature, conductivity and pH of the leachate are also recorded.

The physico–chemical stabilization of SRS and BFA before and after synthesis under acid–base conditions was studied in accordance with standard NF EN 14429 (AFNOR 2015). The ANC-BNC test enables the leaching behavior of SRS and BFA to be evaluated as a function of pH. Similar to batch leaching, the L/S ratio (L/kg of dry matter) is 10. A volume of nitric acid or sodium hydroxide at a determined concentration between 0.1 and 5 mol/l was added to the leachate. The samples were placed under agitation on a turntable (Heidolph Reax 20) at 10 rpm and 25 °C for 48 h. Then, the leachate (water + acid or base) was added in 3 steps (t_0, t_{0+30} min, $t_{0+2\,h}$), in order to reduce the swelling of the bottle resulting from the outgassing. The pH is verified and noted at 4 h, 44 h and 48 h after the start of the test. The first measurement verifies that the pH correction is satisfactory, and the subsequent measurements verify the stability of the pH. Following measurement of the final pH, the leachate was filtered through a cellulose acetate filter with a pore size of 0.45 µm. The MMTE concentrations of the leachate were analyzed by ICP-AES (ICP-AES, 5100 Agilent Technologies, Douai, France).

Results and discussion

Material particle size

According to the result obtained by laser diffraction technique, the particle size distribution of SRS, BFA, MK(S), MK(R) and MK(P) is shown in Fig. 2. The purity and fineness of the materials are necessary to obtain maximum reactivity and high mechanical performance. The higher fineness, the larger contact area with the reaction medium, promotes the geopolymerization reaction (Hajimohammadi and van Deventer 2016). For this reason, among others, the shooting range soil was finely crushed before being used in the formulations. For this particular reason, the SRS was finely crushed before being used in the formulations. As shown in Fig. 2, 60% of the particles in the crushed SRS belong to the particle size class of clays (≤ 2 µm) and silts (0.002–0.02 mm). The granular distributions of metakaolins (R), (P) and (S) presented in Fig. 2 show clearly that the three types of metakaolins have a relatively similar clay-silt granular distribution, with a maximum particle size of approximately 195 µm, 234 µm, and 246 µm for MK(S), MK(R) and MK(P), respectively.

In comparison with SRS and the different metakaolins, BFA has a fine particle size. BFA had a maximum particle size of approximately 47.9 µm. Particles smaller than 2 µm accounted for about 13% by volume, and the amount of particles smaller than 63 µm was about 100%. BFA had a median diameter (D50) of 8.4 µm.

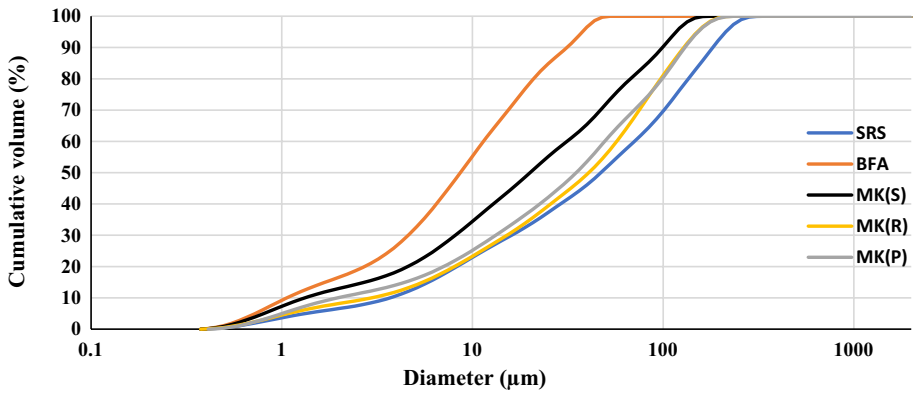

Fig. 2 Granular distributions of SRS, BFA, MK(S), MK(R) and MK(P)

The specific surfaces BET, specific density and loss on ignition

The specific density, specific surface area BET and loss on ignition of SRS and BFA are summarized in Table 3. The specific surface of BFA was relatively high, which was attributed to their particular fineness. It was confirmed by the particle size analysis (Fig. 2). The specific surface values obtained using BET are 1.40 and 25.24 m^2/g for SRS and BFA, respectively. Relatively few data are available in the literature on this characteristic to establish comparisons with BFA or SRS. The specific surface of biomass fly ash reported in the study of Bai et al. (2003) is similar to the present study; biomass fly ash has specific surface, which generally varied between 8.5 m^2/g and 89 m^2/g, although it can also be below or above in some cases (Wesche 2014), depending mainly on the type of biomass. The specific surface has a major influence on the reactivity of the material.

Table 3 Physical characterizations of SRS and BFA

Physical parameters	SRS	BFA
Specific density (kg/m^3)	2.72	2.54
Specific surface BET (m^2/g)	1.40	25.24
Loss on ignition (LOI) (%)	0.89	2.13

According to results in Table 3, the specific density of SRS (2.72 kg/m3) was significantly similar to the specific density of normalized sand (about 2.7 kg/m^3) (Hyodo et al. 2017). The BFA has a specific density of 2.52 kg/m^3, Bai et al. (2003), to report an identical value of the specific density from their biomass ash, which is equal to 2.52 kg/m^3. Although the comparison of the specific density of SRS and BFA was not obvious due to the different nature of the two materials, such difference can be explained by the fact that BFA (2.13%) has a higher organic matter content than SRS (0.89%). Indeed, the absolute density of organic matter is approximately 1.2 to 1.5 kg/m^3. The presence of organic matter in the material decreases the density. Thus, the specific density varies according to the mineralogical composition of the material; the presence of Fe and Pb in the SRS increases significantly the specific density of the material.

Mechanical performances

The compression strengths of the manufactured mortars are calculated statistically after 6 tests conducted to rupture. The tests were performed at 7 day curing times after manufacture. Figure 3 shows the results of the 7-day compressive strengths for geopolymer mortars before and after carbonation for SRS (a) and BFA (b).

Overall, the mortars' strength increases after carbonation with sodium bicarbonate (NaHCO3). The compressive

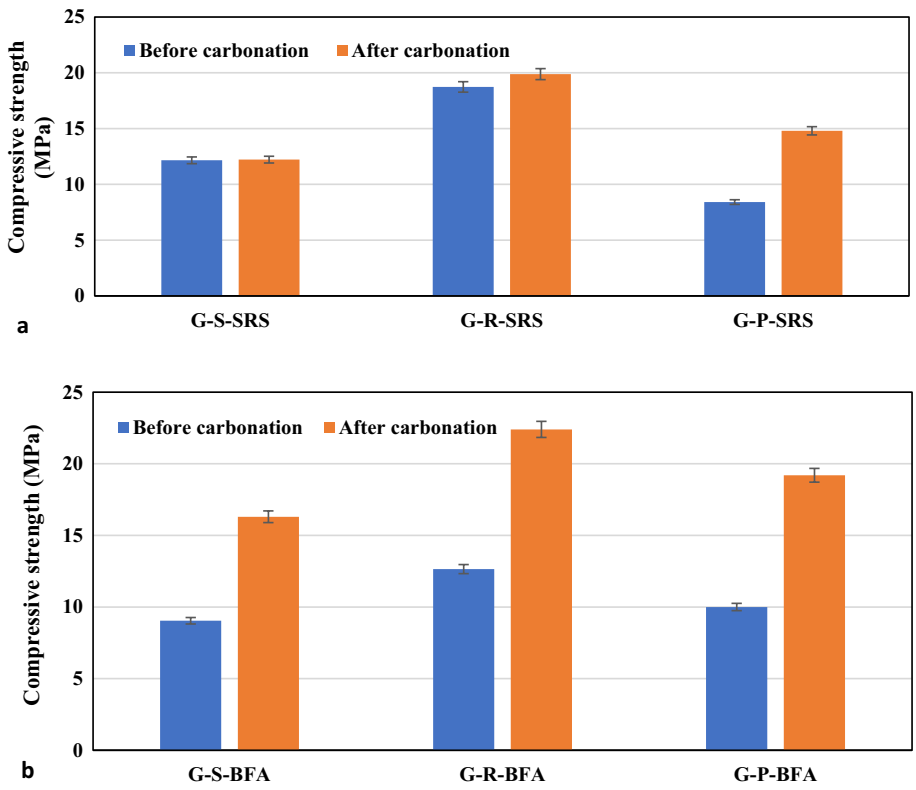

Fig. 3 Compressive strength of the different formulations of SRS **a** and BFA **b** before and after carbonation

strength increased from 8.41 MPa to 14.8 MPa for G-P-SRS and from 18.74 MPa to 19.88 MPa for G-R-SRS. Concerning G-S-SRS, the compressive strength was almost stable before and after carbonation (i.e., 12.16 MPa—12.2 MPa); it implied that under such storage conditions, the carbonation of G-S-SRS in this time interval does not provide mechanical strength benefit. The higher compressive strength obtained in the G-R-SRS case compared to G-S-SRS and G-P-SRS can be explained by the influence of the metakaolin type used. The increase in mechanical performance after carbonation for G-R-SRS and G-P-SRS is attributed to the precipitation of carbonates in the pores of the geopolymers, which contributes to increasing their compactness and therefore the compressive strength.

Regarding the geopolymers manufactured from BFA, under the same curing conditions (7 days/20 °C), the higher compressive strength obtained by G-R-SRS (15.65 MPa) was compared to G-S-SRS (9.04 MPa) and G-P-SRS (10 MPa). One more time, the metakaolin-type effect is highlighted with a significantly improved reactivity in G-R-SRS and G-P-SRS. The carbonation of the different geopolymers resulted in a noticeable strength grain, 16.3 MPa, 22.4 MPa and 19.2 MPa for G-S-SRS, G-R-SRS and G-R-SRS, respectively. It shows that the carbonation of geopolymers based on BFA is favored with $NaHCO_3$. Indeed, the presence of CaO in the original BFA favors the formation of $CaOH_2$ by hydration, followed by the release of Ca^{2+} in the reaction medium, and the subsequent precipitation of $CaCO_3$ (Bouzar and Mamindy-Pajany 2022a, b) in the pores of the geopolymers contributes to the improvement of the mechanical performance after carbonation compared to the SRS-based geopolymers.

According to several studies [39]–[42], [43], geopolymers are characterized by high mechanical strengths compared to a classical hydration reaction. However, for materials rich in calcium (such as BFA), the reaction will probably lead to the formation of structures composed of NASH, Si–O-Ca-O in addition to Si–O-Al-O; thus, the formation of CSH and CAH is due to the hydraulic power of the material, which increases the mechanical strength (Bouchikhi et al. 2021). In the presence of significant amounts of calcium, it has also been observed in the formation of a gel C-A-S–H (calcium aluminosilicate hydrate) (Puertas et al. 2011; Garcia-Lodeiro et al. 2011; Hong and Glasser 2002). Thus, according to the research of Chindaprasirt et al. (Chindaprasirt et al. 2013), which used for the synthesis of geopolymers residues rich in calcium, it may appear to the formation of an ettrengite phase $[Ca_6Al_2(SO_4)_3\ (OH)_{12}.26H_2O]$ existing in different forms (Stark et Bollmann 2000) that contributes to the improvement of mechanical performance.

Environmental analysis

In order to study the mobility of MMTE, leaching tests were performed on geopolymer mortars before and after carbonation. The results presented in Table 4 (G-SRS) demonstrate that the leaching of lead in the different geopolymer types before carbonation was relatively high and exceeded the threshold for classification as non-hazardous waste, which was equal to 10 mg/kg. After carbonation with sodium bicarbonate solution, the media pH decreases from 12.46 ± 0.15 to 9.43 ± 0.15 and the lead concentration decreases from 42 ± 1.8 mg/kg to 0.6 ± 0.13 mg/kg and from 37 ± 1.5 mg/kg to 0.77 ± 0.02 mg/kg in the carbonated G-S-SRS and G-S-SRS matrices, respectively, yet remains above the IWSI threshold. However, lead was stabilized in the carbonated G-R-SRS geopolymer matrix to reach a value of 0.22 ± 0.02 mg/kg, which is inferior to the IWSI threshold. In fact, there is no general agreement on the entrapment mechanism since it is not well understood. The study of Jarrsveld et al. (1998) indicated that the Pb stabilization was performed by the adsorption mechanism, i.e., electrostatic interactions allowed the substitution of ionic species at the adsorption surface to ensure electroneutrality. Another study has suggested the lead contributed to compensating the negative charge of aluminum by providing the charge balance through the cation exchange mechanism (CEC) instead of Na, which allowed stabilization in the matrix (Nikolić et al. 2018). The pH is an important factor in the lead release. The pH of carbonated mortars has been reduced to 9.37 ± 0.15 after carbonation. During the process, a chemical carbonation reaction stabilizes the lead to form cerussite ($PbCO_3$), which is insoluble and thus reduces lead leaching (Cao et al. 2003a, b).

For the carbonated G-R-SRS and G-P-SRS, the amount of antimony released in the leachate was reduced from 27 ± 1.1 mg/kg to values between 0.03 ± 0.01 and 1.43 ± 0.01 mg/kg, respectively. For the carbonated G-S-SRS, the antimony concentration decreased from 33 ± 1.4 mg/kg to 1.15 ± 0.18 mg/kg after carbonation. A significant reduction of antimony leaching was achieved although the leached concentration remains above the IWSI threshold of 0.06 mg/kg for G-S-SRS and G-R-SRS. However, the immobilization of Pb and Sb is provided when the geopolymer is manufactured from MK(R) followed by carbonation. Antimony is relatively soluble in alkaline media and its mobility may be controlled by different mechanisms such as the formation of iron antimonate ($FeSbO_4$ or $Fe_2O_3Sb_2O_5$), adsorption on iron oxides/hydroxides or the formation of calcium antimonate ($Ca_2Sb_2O_7$) (Cornelis et al. 2012). This explains the effectiveness of the geopolymer based on MK(R) rich in Fe.

Concerning the other MMTE, no exceedance of the IWSI thresholds was observed before and after

Table 4 Geopolymer leaching behavior before and after carbonation

Parameter	G-S-SRS ($mg.kg^{-1}$)	G-R-SRS ($mg.kg^{-1}$)	G-P-SRS ($mg.kg^{-1}$)	Carbonated G-S-SRS ($mg.kg^{-1}$)	Carbonated G-R-SRS ($mg.kg^{-1}$)	Carbonated G-P-SRS ($mg.kg^{-1}$)
As	0.14 ± 0.03	0,13	< 0.11	< 0.11	< 0.008	< 0.11
Ba	0.02 ± 0.01	0.05 ± 0,01	0.02 ± 0.01	< 0.008	< 0.008	< 0.008
Cd	< 0.009	< 0.009	< 0.009	< 0.009	< 0.009	< 0.009
Co	< 0.009	< 0.009	< 0.009	< 0.009	< 0.009	< 0.009
Cr	< 0.004	< 0.004	< 0.004	< 0.004	< 0.004	< 0.004
Cu	< 0.003	< 0.003	< 0.003	< 0.003	< 0.003	< 0.003
Mo	< 0.09	< 0.09	< 0.09	< 0.09	< 0.09	< 0.09
Ni	< 0.047	< 0.047	< 0.047	< 0.047	< 0.047	< 0.047
Pb	**42 ± 1.8**	**16 ± 0.9**	**37 ± 1.5**	**0.6 ± 0.13**	**0.22 ± 0.02**	**0.77 ± 0.02**
Sb	**33 ± 1.4**	**27 ± 1.1**	**27 ± 1.1**	**1.15 ± 0.18**	**0.03 ± 0.01**	**1.43 ± 0.01**
Se	< 0.083	< 0.083	< 0.083	< 0.083	< 0.083	< 0.083
Zn	< 0.01	< 0.01	< 0.01	< 0.01	< 0.01	< 0.01
Sulfates	209 ± 16	216 ± 11	201 ± 8	363 ± 15	396 ± 11	359 ± 7
Fluorides	**12 ± 0.4**	**12 ± 0.4**	**14 ± 0.4**	4.9 ± 0.4	5.3 ± 0.2	5.8 ± 0.2
Chlorides	31 ± 2	38 ± 3	35 ± 4	39 ± 3	32 ± 3	38 ± 4
pH	12.37 ± 0.15	12.28 ± 0.14	12.46 ± 0.15	9.43 ± 0.15	9.37 ± 0.15	9.3 ± 0.15
Conductivity ($mS.cm^{-1}$)	0.9 ± 0.02	0.9 ± 0.02	0.8 ± 0.02	0.4 ± 0.02	0.3 ± 0.02	0.5 ± 0.02
Parameter	G-S-BFA ($mg.kg^{-1}$)	G-R-BFA ($mg.kg^{-1}$)	G-P-BFA ($mg.kg^{-1}$)	Carbonated G-S-BFA ($mg.kg^{-1}$)	Carbonated G-R-BFA ($mg.kg^{-1}$)	Carbonated G-P-BFA ($mg.kg^{-1}$)
As	< 0.11	< 0.11	< 0.11	< 0.11	< 0.11	< 0.11
Ba	< 0.008	< 0.008	< 0.008	0.03	0.04	0.05
Cd	< 0.009	< 0.009	< 0.009	< 0.009	< 0.009	< 0.009
Co	< 0.009	< 0.009	< 0.009	< 0.009	< 0.009	< 0.009
Cr	**4.4 ± 0.35**	**1.5 ± 0.2**	**5.1 ± 0.1**	**0.59 ± 0.02**	**0.48 ± 0.04**	**1.18 ± 0.05**
Cu	< 0.021	< 0.021	< 0.021	< 0.003	< 0.003	< 0.003
Mo	**2.01 ± 0.1**	**2.07 ± 0.11**	**2.7 ± 0.1**	**1.1 ± 0.1**	**0.45 ± 0.13**	**1.3 ± 0.2**
Ni	< 0.047	< 0.047	< 0.047	< 0.047	< 0.047	< 0.047
Pb	**< 0.032**	**< 0.032**	**< 0.032**	**< 0.032**	**< 0.032**	**< 0.032**
Sb	**0.1 ± 0.03**	**1.5 ± 0.02**	**1.4 ± 0.02**	< 0.008	< 0.008	< 0.008
Se	**0.73 ± 0.06**	**0.71 ± 0.04**	**0.7 ± 0.05**	**< 0.083**	**< 0.083**	**< 0.083**
Zn	**< 0.01**	**< 0.01**	**< 0.01**	**< 0.01**	**< 0.01**	**< 0.01**
Sulfates	**17 033 ± 326**	**16 798 ± 311**	**15 319 ± 303**	**16 734 ± 299**	**17 064 ± 301**	**16 989 ± 326**
Fluorides	**34 ± 3**	**25 ± 2**	**29 ± 2**	**26 ± 1.5**	**38 ± 2**	**34 ± 1.8**
Chlorides	**2 431 ± 89**	**2 500 ± 91**	**2 177 ± 77**	**2 450 ± 66**	**2 540 ± 69**	**2 480 ± 61**
pH	13.5 ± 0.1	13.5 ± 0.1	13.4 ± 0.1	8.6 ± 0.15	8.8 ± 0.15	8.8 ± 0.15
Conductivity ($mS.cm^{-1}$)	11.1 ± 0.3	10.4 ± 0.2	10.1 ± 0.02	11 ± 0.1	11.8 ± 0.02	10.9 ± 0.02

The bold characters are the problematic elements to be studied

carbonation. The reason for this discrepancy is the limited presence of MMTE in the constituents of the geopolymer formulations (MK and SRS). For the anionic compounds, the results show a higher fluoride content before carbonation in the different geopolymers with values exceeding the IWSI threshold (12 ± 0.4 mg/kg G-S-SRS/G-R-SRS and 14 ± 0.4 mg/kg in G-P-SRS). After carbonation, however, the release of fluoride was reduced and stabilized below the IWSI threshold.

In Table 4 are shown the amounts of MMTE released from the different geopolymers based on BFA before and after carbonation. The different manufactured geopolymers present a high immobilization of the different pollutant's problematic in the raw BFA (Cr, Mo, Se, Pb, Zn, Cl, SO_4). In

the different geopolymers, either before or after carbonation, neither Pb nor Zn was detected by ICP-AES, demonstrating a high immobilization capacity of metal cations compared to the raw waste. The pH of the leachate after carbonation decreases from 13.5 ± 0.1 to 8.6 ± 0.15, and the pH was still basic, but was closer to neutral. The decrease in pH of the leaching solution was probably due to the carbonation reaction. Nevertheless, the large variation in alkalinity and pH after carbonation had no influence on the immobilization of Pb and Zn, which were not detected.

The Cr had a similar pattern to Pb and Zn; the release of Cr decreases from 24 ± 0.9 mg/kg in raw BFA to 5.1 ± 0.1 mg/kg, 4.4 ± 0.35 mg/kg and 1.5 ± 0.2 mg/kg for G-P-BFA, G-S-BFA and G-R-BFA, respectively, but the concentration released remains above the IWSI threshold. After carbonation, the Cr mobility was significantly reduced, attaining concentrations of 1.3 ± 0.2 mg/kg, 1.1 ± 0.1 mg/kg and 0.45 ± 0.13 mg/kg for G-P-BFA, G-S-BFA and G-R-BFA, respectively. The difference between the behaviors of Pb and Cr observed in the samples could be explained by the differences of their incorporation in the geopolymeric matrix or by the inhomogeneity of the raw waste. At present, no research has explained a similar phenomenon. It is probably that Cr was present in two forms (Cr^{3+} and Cr^{6+}) in the raw BFA, and the combination of the geopolymerization reaction and carbonation allowed the stabilization of the cationic (Cr^{3+}) and oxoanionic (Cr^{6+}) forms. According to several researchers (Fernández Olmo et al. 2001; Glasser 1997; Yousuf et al. 1995), Cr is incorporated chemically in O-S–O or C-S–H by the substitution of Si since the ionic radius of both elements is almost identical. Thus, the study carried by Chen et al. (Chen et al. 2009) confirms that the carbonation accelerates the incorporation of Cr in silicate matrices by complexation. Cr compounds would probably not combine stoichiometrically with silicates, but a species of variable composition of the general formula yCr(OH)-zSiO could be formed.

The different matrices of the manufactured geopolymers allowed to significantly decrease the concentration of Mo and Se; however, the concentrations remain relatively high and exceed the threshold of classification as inert waste, which is equal to 0.1 mg/kg and 0.5 mg/kg for Se and Mo, respectively. After carbonation, the concentration of Mo and Se decreases in the G-S-BFA and G-P-BFA matrices but remains above the IWSI threshold. In contrast, Mo and Se were stabilized well in the carbonate G-S-BFA matrix to reach a value of 0.45 ± 0.13 mg/kg for Mo, which is below the IWSI threshold. However, the release of Se was below the limit of quantification. These results show that the presence of Fe has an important influence on the precipitation of Se and Mo, potentially generating precipitates in the form of $FeSeO_4$ or $FeMoO_4$ that subsequently adsorb or co-precipitate with iron hydroxides (Mamindy-Pajany et al. 2013). The release of anionic species such as SO_4 and Cl has decreased significantly, although the concentration remains above the non-hazardous waste threshold for the different geopolymers.

Geopolymers based on MK(R) rich in iron in the Hematite form (Figure 2 Appendix) have a significant effect on the pollutant mobility since it reduces the release of both cationic and anionic species. Due to the amphoteric properties of the surface sites (Cornell and Schwertmann 2003), iron oxides are effective sorbents for anionic (As, Mo) and cationic (Cd, Cu, Ni and Zn) contaminants. On the surface of the mineral, adsorption occurs by surface complexation (Stumm 1992). The basic pH of geopolymer (between 9 and 13) favors the presence of negative and positive surface charges on hematite because the PZC (point of zero charge) of this mineral varies between pH 9 and 13 (Marmier et al. 1993; Duc et al. 2003; Jeon et al. 2003; Mamindy-Pajany et al. 2011).

Geopolymer characterization

Comparison of the different MMTE concentrations in the raw SRS and raw BFA with the leaching thresholds of inert waste shows that both untreated wastes do not fulfill all the acceptance criteria for inert landfills. Only geopolymers based on MK(R) after carbonation are capable of reducing the leaching of MMTE below the regulatory limit without generating additional contamination. For this purpose, only the G-R-BFA and G-R-SRS geopolymers before and after were characterized to understand the mechanisms of entrapment of the different MMTE.

Thermogravimetric analysis

Figure 4 shows the results of thermogravimetric analysis on raw BFA and SRS and two formulations of the geopolymers G-R-BFA and G-R-SRS before and after carbonation. The thermogravimetric analysis results presented enable the identification of different constituents according to several temperature intervals corresponding to mass losses:

- 90–300 °C: Dehydroxylation of hydrates (CSH, CAH, ettringite) according to the hydration degree and according to their nature;
- 105–150 °C: Condensation of NaOH and formation of Na_2O as well as to the existence of water molecules absorbed by gels or hydrogen bonds;
- 150–230 °C: Condensation of silanol groups Si–OH;
- 230–550 °C: Dehydration of mineral hydroxides of type M(OH)n such as calcium hydroxide (portlandite) and magnesium hydroxide;
- 550–950 °C: Decarbonation of calcium carbonates ($CaCO_3$) between 550 and 950 °C;

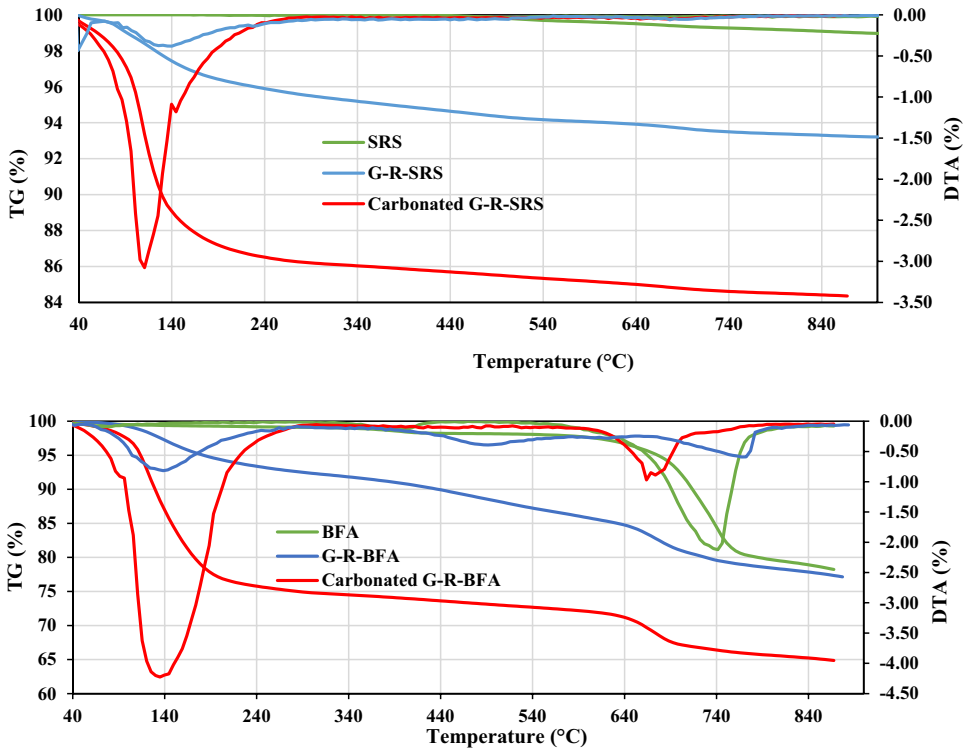

Fig. 4 The thermal characteristics of SRS, BFA, G-R-BFA and G-R-SRS before and after carbonation

The TGA analysis of BFA and raw SRS highlights two mass losses corresponding to the dehydroxylation of portlandite and the decarbonation of calcite. Both mass losses are more important in the BFA rich in calcium, which is in accordance with the results of the FX (Table 1). However, both geopolymers G-R-BFA and G-R-SRS show similar mass losses before and after carbonation. Two important peaks were observed; the first peak between 50 and 300 °C corresponds to the dehydroxylation of hydrates (CSH and ettringite) of the geopolymer matrices with a higher mass loss for the carbonated geopolymers, which means that the hydration reaction has continued during the carbonation process. The leaching results presented in Table 4 are in agreement with the thermogravimetric analyses; the decrease of sulfate leaching in the different geopolymers was proportional with the formation of ettringite ($Ca_6Al_2(SO_4)_3(OH)_{12}$-$26H_2O$) (Nozahic et al. 2012). As has been reported in the literature, several works (Zouch et al. 2022; Bouchikhi et al. 2021; Mkahal et al. 2022) have confirmed that hydrate formation is the origin of immobilization in certain MMTE. It has been shown that CSH and ettringite have a major role in the stabilization/solidification process (Bouchikhi et al. 2021; Mkahal et al. 2022). The main mechanism of MMTE retention within the hydrates was substitution and inclusion in the crystal lattice.

Over the temperature ranges 105–150 °C and 150–230 °C, the amount of H_2O released is more important since it is related to several types of hydrates formed as indicated above and more particularly to the hydration of Si–O–Si → 2(Si–OH) siloxane groups (Rashid et al. 2011). Also, it may be related to the formation of complexes between hydroxides on the surface of geopolymers as well as to the complexation of Ca and Mg with other hydrates, in particular with silanol in solution or in metastable Si- and Al-based phases (Rashid et al. 2011).

The second mass loss between 550 and 950 °C corresponds to the decomposition of calcium carbonates $CaCO_3$. The amount of calcite is higher in carbonated G-P-BFA compared to non-carbonated G-P-BFA; however, no change was observed in this temperature interval for G-P-SRS before and after carbonation, due to the low amount of CaO (0.56%) in raw SRS (Table 1). The decrease in calcite content in G-P-BFA compared to raw BFA appears due to a dilution effect during formation (MK(P) + BFA + alkaline solution).

X-ray diffraction (XRD)

Figure 5 shows the XRD spectra of raw SRS and raw BFA as well as the geopolymers G-R-SRS and G-R-BFA before and after carbonation. The XRD results show the presence of quartz (SiO_2) in SRS as a main phase, which is consistent with the results of the FX analysis. Also note the presence of albite ($NaAlSi_3O_8$), lead-antimony alloy (Pb-Sb) and metallic lead (Pb). The presence of lead in various forms was explained by the existence of residues/fragments of shooting bullets. The results also reveal some minority phases such as muscovite ($KAl_2(SiAl)_4O_{10}(OH)_2$). It should also be noted

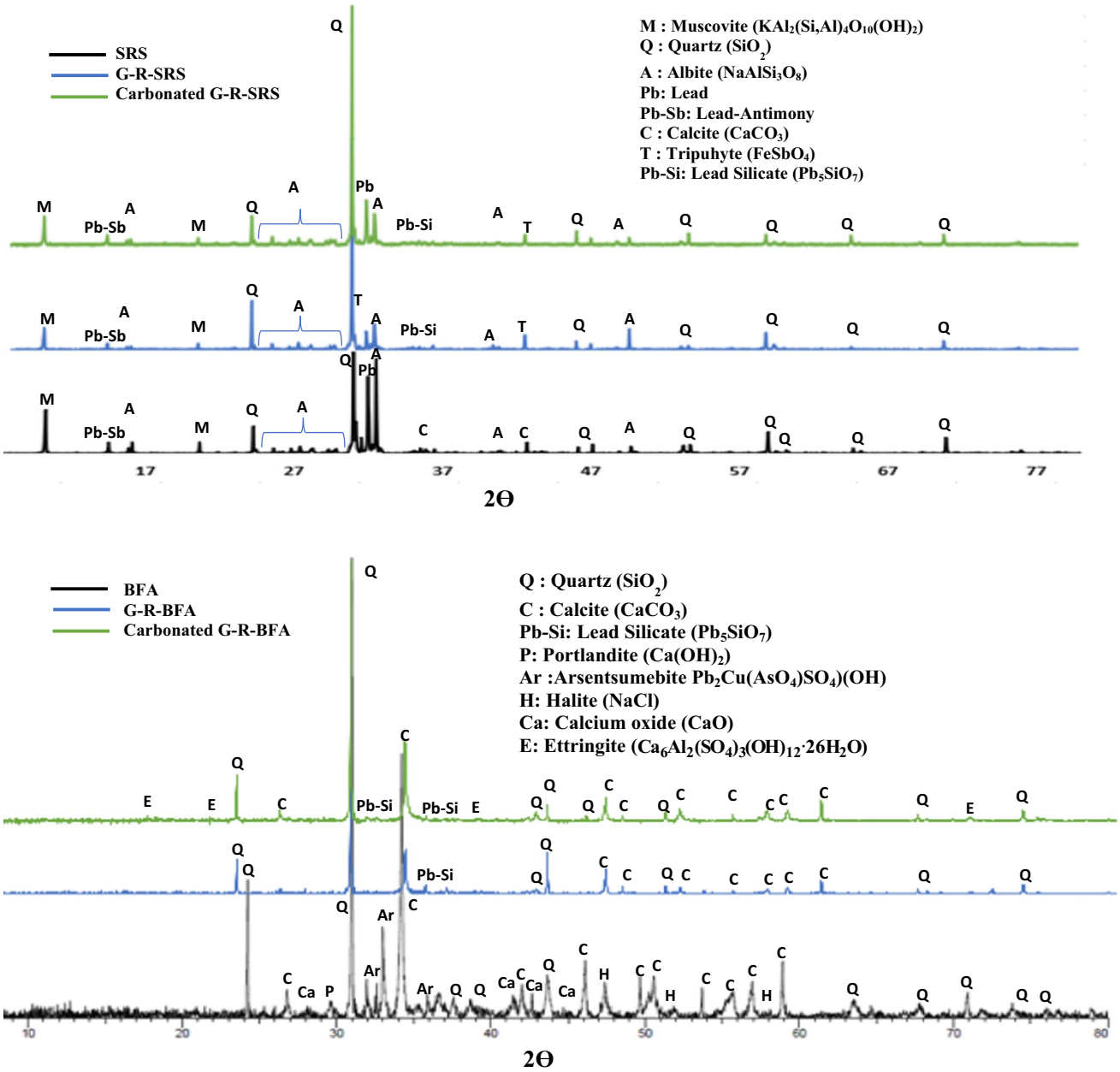

Fig. 5 Diffractograms of SRS, BFA, G-R-BFA and G-R-SRS before and after carbonation

that the silicon and aluminum present in the SRS enter in the composition of crystalline phases, which results in a lower availability for the geopolymerization reaction.

Before carbonation of the geopolymers G-R-SRS, mineralogical phases similar to those observed in the SRS are detected (albite, quartz, muscovite, Pb and Pb-Sb alloy). After carbonation, the geopolymer matrices contain carbonates in the form of calcite ($CaCO_3$). This result confirms the hypothesis of a precipitation of carbonates in the porosity of the geopolymeric matrices, which would explain the increase in mechanical performances previously observed. It should also be noted that the intensity of the Pb and Pb-Sb peaks decreased after carbonation, which suggests a transformation of lead into carbonates. Nevertheless, the carbonate compound was not detected in X-ray diffraction due to the high detection thresholds. Antimony is relatively soluble in slightly alkaline media, and its mobility can be controlled by different mechanisms such as the formation of iron antimonate ($FeSbO_4$ or $Fe_2O_3Sb_2O_5$). In the formulations of the G-R-SRS geopolymers, the compound $FeSbO_4$ was detected. This result can be explained by the presence of hematite in the MK(R) (Figure 2 Appendix), which allows a

higher trapping of antimony in the formulated geopolymer matrices.

However, the BFA was highly crystallized with intense peaks and with a minor amorphous portion. The XRD results show that the raw BFA has seven phases of which quartz is the phase with the most intense peaks, followed by the calcite phase. The BFA was particularly rich in calcium; this was reflected by the presence of portlandite ($Ca(OH)_2$), calcium oxide (CaO) and several calcite peaks. Three peaks corresponding to halite are present with low intensities, whose peaks emerge a few from the bottom. Thus, the presence of an arsentsumebite phase ($Pb_2Cu(AsO_4)SO_4)(OH)$ was probably the source of Pb and SO_4^{2-} in the BFA. The other problematic elements (Cr, Zn, Se and Mo) are not detected by XRD.

The DRX analysis confirms the results obtained in ATG and highlights the appearance and the increase of the peaks intensities corresponding to ettringite and calcite after carbonation. The G-R-BFA geopolymers before and after accelerating carbonation show similar peaks yet with different intensities, more precisely at the calcite level. The main mineral phases identified are quartz, calcite and lead silicate (Pb_5SiO_7). It appears from the XRD diffractograms that a clear disappearance of the peaks corresponds to arsentsumebite ($Pb_2Cu(AsO_4)SO_4)(OH)$, and the appearance of new peaks corresponds to lead silicate (Pb_5SiO_7), which confirms that the inclusion of Pb in the geopolymeric lattice, the intensity of the peak increases after the carbonation process. The same tendency was observed for halite (NaCl), except that no phase containing chlorides appeared in the geopolymer diffractograms. The disappearance of halite (NaCl) peaks and the appearance of ettringite ($Ca_6Al_2(SO_4)_3(OH)_{12}0.26H_2O$) peaks well confirm the entrapment of chlorides and sulfate in the geopolymer lattice, which is in agreement with the leaching results (Table 4).

Scanning electron microscopy and energy-dispersive x-ray spectrometer (SEM–EDS)

The SEM–EDS observations shown in Fig. 6 illustrate the main phase morphologies in the raw SRS and BFA as well as the phases formed in all the specimens after the geopolymer formulation. SEM–EDS characterization of raw SRS reflects the presence of Pb and Sb as Pb-Sb alloy (Fig. 6a). Pb and Sb are found as discrete particles variably altered, mainly by oxidation or carbonation. This observation was consistent with previous studies (Vantelon et al. 2005; Dermatas et al. 2006; Rooney et al. 2007; Hardison et al. 2004; Cao et al. 2003a, b; Lin et al. 2001, 1995), which demonstrated that the major alteration products found on the corroded surfaces of Pb particles in soils from shooting sites and are rapidly transformed into potentially more soluble Pb phases, among those are cerussite ($PbCO_3$), hydrocerussite ($Pb_3(CO_3)_2(OH)_2$), guillotine (PbO), and occasionally anglesite ($PbSO_4$) and hydroxypyromorphite ($Pb_{10}(PO_4)_6(OH)_2$). The SEM–EDS images of SRS show the presence of quartz as the majority phase along with the presence of K/Al/Si and Na/Al/Si, which appear to be muscovite and albite as confirmed by XRD. The SEM observations presented in Fig. 6c and e illustrate the main morphologies of the phases formed after the formulation of G-R-SRS geopolymers before and after accelerating carbonation, respectively. Figure 6c and e shows that geopolymerization allows the formation of N-A-S-H-type phase responsible for matrix strengthening (Rashid et al. 2011) (Fig. 3). The N-A-S–H hydration gel present in carbonated G-R-SRS (Fig. 6 e) has a denser texturing than the phase present in non-carbonated G-R-SRS (Fig. 6 c), as evoked in the TGA results (Fig. 4) due to the continuity of the geopolymerization reaction during the accelerated carbonation process. Other phases that contain Pb and Sb are also present notably in carbonate G-R-SRS. The association of Si with Pb is most probably related to soils, since Pb-Si–O-Si-minerals such as lead silicate (Pb_5SiO_7) exist in highly specific environments and also contain Fe and Mg, respectively. The results also reveal the presence of a minority Fe/Sb phase that appears to be tripuhyite ($FeSbO_4$).

The SEM–EDS characterization of raw BFA showed that calcium, silicon, sulfur and potassium were the main BFA constituents (Fig. 6b), which agreed with the XRF results (Table 1). In fact, SEM–EDS data showed the presence of $CaCO_3$ and minor $Ca(OH)_2$ in the same BFA particles (Fig. 6b). SiO_2 quartz and iron oxides were identified in the BFA (Fig. 6b). The results are consistent with those obtained by TG–DTA (Fig. 4) and XRD (Fig. 5). Chlorides were identified in the BFA. For MMTE, Pb was mainly presented as $PbSO_4$ (Fig. 6 b) in the BFA. Zinc was identified in the BFA as Zn oxides and Cr was associated with silicon and iron (Fig. 6b). After geopolymerization, Mo, Zn, SO_4 and Cl were identified by elemental characterization and were bound principally to hydration products such as silica gel (NASH) and ettringite. Other phases that contain Pb and sulfate are also present notably in G-R-SRS before and after carbonation in the form of arsentsumebite $Pb_2Cu(AsO_4)SO_4)(OH)$ (Fig. 6d and f). Further changes were observed related to the formation of carbonate coating phases such as calcite $CaCO_3$ (Fig. 6f). It is important to note that ettringite was not identified by SEM–EDS, possibly due to system heterogeneity.

Acid/base neutralization capacity test

The mobilization of MMTE associated with mineral species and/or OM was controlled by several phenomena such as adsorption/desorption, precipitation/dissolution, oxidation/reduction, resulting from physicochemical changes in the medium such as ionic strength, redox conditions, and pH

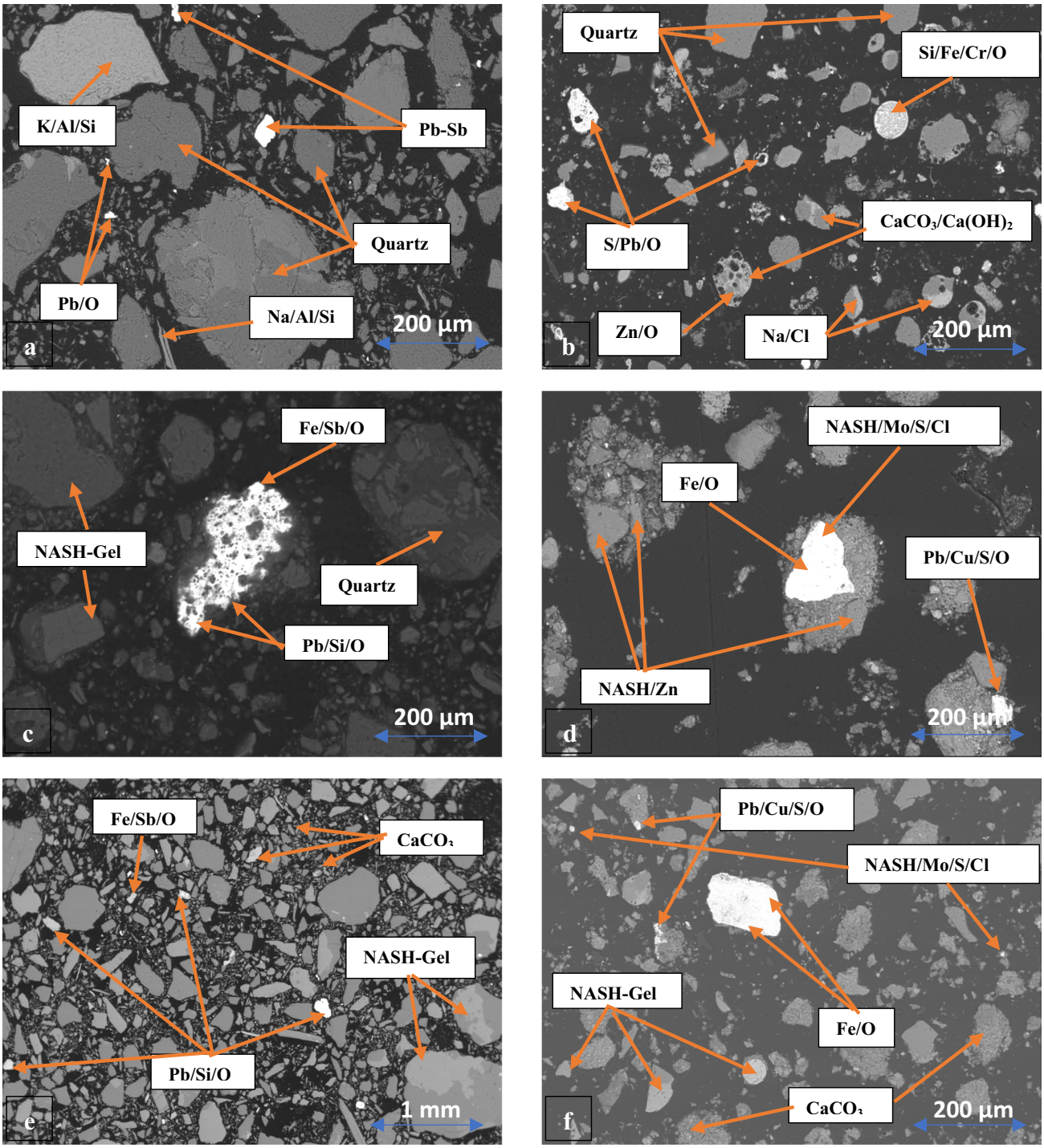

Fig. 6 SEM observations and EDX analyses of SRS (**a**), BFA (**b**), G-R-SRS (**c**), G-R-BFA (**d**), carbonated G-R-SRS (**e**) and carbonated G-R-BFA (**f**)

(Ciesielski et al. 2007; Deschamps et al. 2006; Lions 2004; Chatain 2004; Alloway 2012; Deneux-Mustin et al. 2003). Among the three parameters, the variation of pH was the most important for the MMTE mobility, since the speciation of the metal changes with the pH and influences the fixation on the solid phase (Blanchard 2000). The target pollutants are the problematic elements identified in the characterization of raw SRS (Pb and Sb) and raw BFA (Cr, Mo, Se, Pb and Zn) (Table 1). The leaching results as a function of SRS and BFA pH as well as the G-R-SRS and G-R-BFA geopolymers before and after carbonation are reported in Figs. 7 and 8.

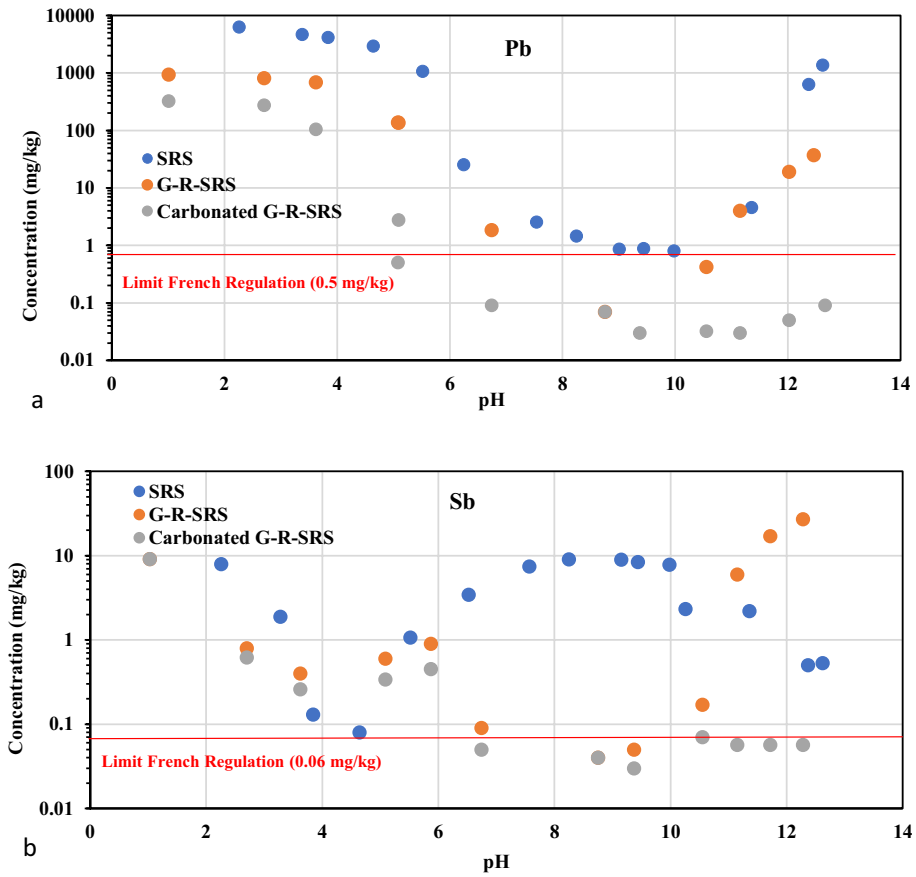

Fig. 7 Evolution of Pb and Sb mobilization in the SRS, G-R-SRS and carbonated G-R-SRS

SRS, G-R-SRS, carbonated G-R-SRS

Pb has amphoteric properties, which render it soluble in acidic and basic media (Fig. 7a). This character was highlighted through its release under acidic pH conditions below 6 to reach a maximum amount equal to 6286 mg/kg, 937 mg/kg and 322 mg/kg / for SRS, G-R-SRS and carbonated G-R-SRS, respectively. In basic medium, a maximum value of 1361 mg/kg, 37 mg/kg and 0.09 mg/kg is reached for pH > 11 for SRS, G-R-SRS and carbonated G-R-SRS, respectively. The results found are consistent with the literature. The pH controls the leaching of elements to the amphoteric hydroxide such as lead. As a result, the leaching of lead is minimal at intermediate pH values corresponding to the hydroxide stability ranges, yet it increases at acidic and basic pH conditions (Sorlini et al. 2017). At natural pH equilibrium conditions of the SRS, lead leaching will be decreased compared to extreme pH values. However, Pb salting out was lower in G-R-SRS and carbonated G-R-SRS, respectively, throughout the pH range (2–14) compared to raw SRS. The Pb trapping in the geopolymeric matrix and also the $PbCO_3$ precipitation should be the origin of the decrease of the salting out as confirmed in the results obtained in XRD and SEM–EDS.

Sb shows a different pH behavior for SRS and G-R-SRS before and after carbonation (Fig. 7b). For SRS, between pH 8 and 10 the amount released was maximal and could reach 9.93 mg/kg. For pH > 10, the amount released decreases to a minimum value of 0.5 mg/kg for a pH value of 12.62. In this extremely basic pH domain, the sorption of oxyanions such as $Sb(OH)^-_4$ on iron oxyhydroxides (HFO) is favored, which leads to the decrease of its release (Sorlini et al. 2017). However, for a pH < 3 the amount of Sb released increases to a maximum value of 7.9 mg/kg. In this strongly acidic pH range, the iron oxides are solubilized, which leads to a release of Sb. A high correlation between the G-R-SRS and carbonated G-R-SRS versus pH curves up to pH = 10.55. Several notable changes were identified in the leaching concentration of Sb before and after carbonation, specifically in a basic pH range. For G-R-SRS, the Sb leaching increases to reach 27 mg/kg at pH 12.28 (natural pH after the geopolymer formulation); a decrease in pH leads to a decrease in Sb leaching until a minimum is reached at pH 9.37 (0.05 mg/kg). This indicates that the geopolymer treatment had an effect on the mineral phases of Sb and controlled the leaching behavior of Sb. After accelerating carbonation, an effect on the pH-dependent leaching behavior was clearly identified, compared to SRS and G-R-SRS; the leaching minimum

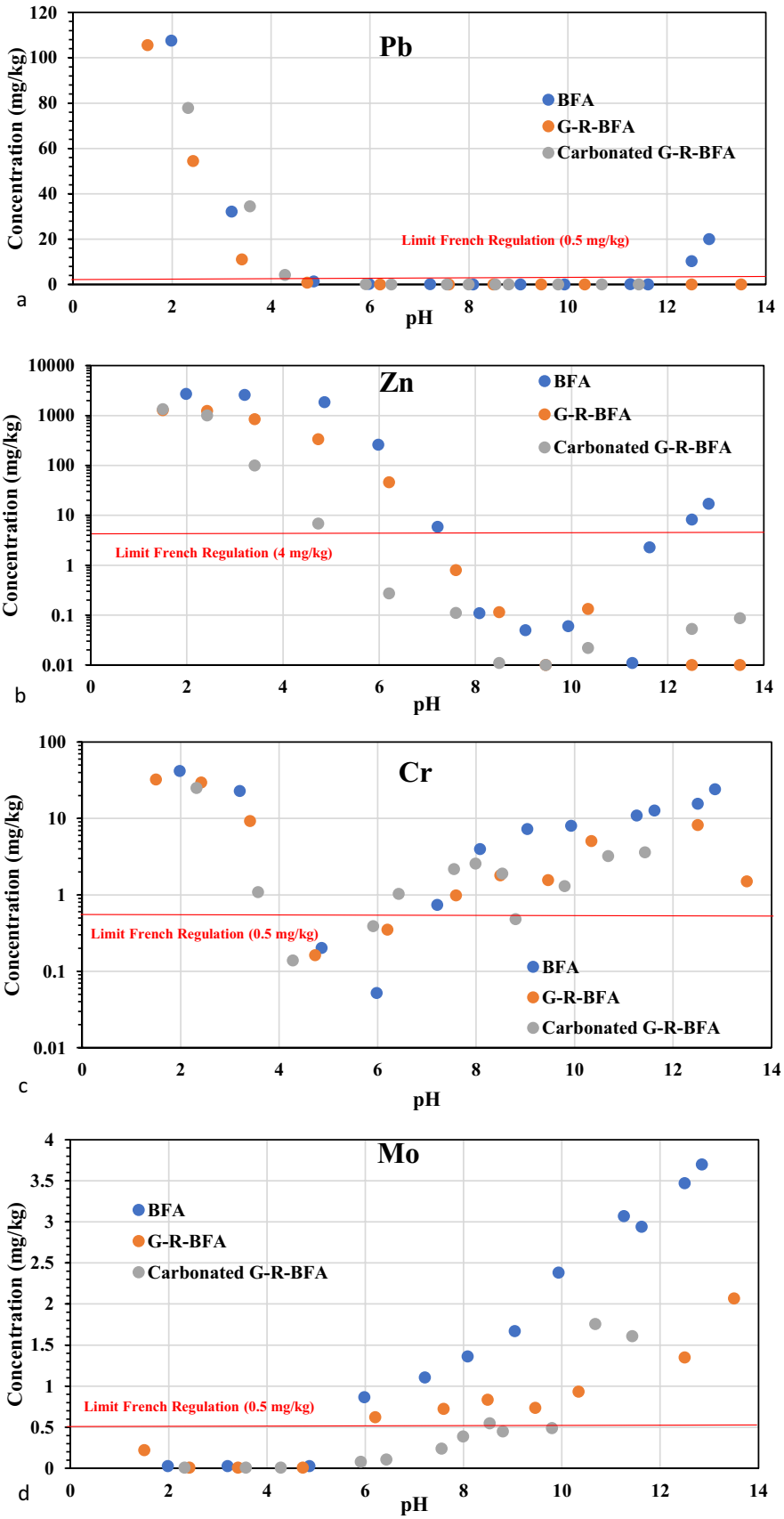

Fig. 8 Evolution of Pb, Zn, Cr, Mo and Se mobilization in the BFA, G-R-BFA and carbonated G-R-BFA

Fig. 8 (continued)

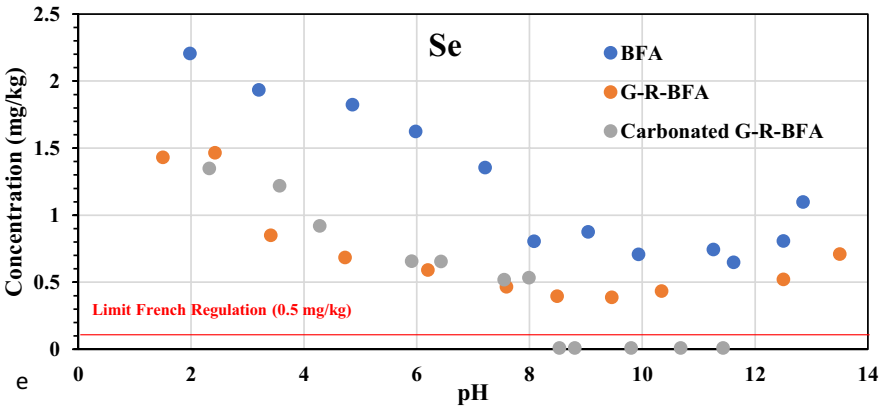

at alkaline pH was significantly reduced (0.057 mg/kg). Alternatively, Sb leaching at acidic pH was considerably reduced in carbonated G-R-SRS (0.62 mg/kg at pH 2.7). The pH behavior of Sb can be attributed to the dissolution of mineral phases that have high sorption affinity for Sb such as portlandite and ettringite (Cornelis et al. 2008; Guo et al. 2006; Santos et al. 2013).

BFA, G-R-BFA, carbonated G-R-BFA

Pb shows a quasi-similar behavior for BFA, G-R-BFA and carbonated G-R-BFA (Fig. 8a). The analysis of the solubilization curves, in extremely acidic medium (pH < 4), shows that lead was much more soluble in BFA than in G-R-BFA and carbonated G-R-BFA. In addition, solubilization in extremely basic medium (pH > 12) was more moderate, of the order of 20 mg/kg for BFA and of the order of 0.01 mg/kg for G-R-BFA and carbonated G-R-BFA. In agreement with the sequential extraction results of certain studies (Harvey et al. 2010; Renou et al. 2009; Kadıoğlu et al. 1995), the solubilization of Pb for pH values inferior to pH 4 can be induced by the presence of lead carbonates and sulfides, as well as by the presence of Pb, complexed to OM, trapped in the CSH, NASH and lime particles. The potential control of Pb by OM and sulfur compounds (sulfides and/or sulfate) should therefore be considered. The mobilization of Pb in raw BFA for pH values higher than 12 reveals its amphoteric character. The absence of lead mobilization for G-R-BFA and carbonated G-R-BFA, in extremely basic medium (pH > 12), despite its amphoteric character, suggests that it is precipitated as basic lead carbonate, such as $PbCO_3$, favored in the physico–chemical conditions induced by the accelerated carbonation treatment (Bouzar and Mamindy-Pajany 2022a, b; Chen et al. 2009) or arsentsumebite $Pb_2Cu(AsO_4)SO_4)(OH)$ and lead silicate (Pb_5SiO_7) as shown in the XRD and SEM–EDS results.

Zn shows similar pH behavior for G-R-BFA and carbonated G-R-BFA (Fig. 8b). The solubilization of zinc, for pH values below 6, approaches that of Pb, suggesting that Zn was bound to carbonate carrier phases. According to the results of sequential extractions reported by Cazalet (Cazalet 2012), zinc is divided between all fractions (exchangeable, reducible, oxidizable and residual). As a result, it was relatively difficult to associate zinc with mineral species. However, the absence of zinc mobilization in G-R-BFA and carbonated G-R-BFA compared to raw BFA under extremely basic conditions (pH > 12), despite its amphoteric character, confirms the trapping of Zn in the geopolymeric matrix and precipitation as basic carbonate such as hydrozincite ($Zn_5(CO_3)_2(OH)_6$) or zinc hydroxide after carbonation (Hlaváčková 2005).

Cr shows a different solubility depending on the pH range, with a higher solubilization in acidic medium (pH < 3.5) for the different matrices (Fig. 8c). However, the solubility increases from pH 7 for the different samples, although it remains inferior in G-R-BFA and carbonated G-R-BFA compared to the raw BFA, which means that the Cr was well trapped in the geopolymeric matrix. The higher leaching of Cr in raw BFA compared to G-R-BFA and carbonated G-R-BFA can be explained by the presence of more soluble form of chromium such as the unstable form of Cr(VI) compared to the stable form of Cr(III). Indeed, CrO_4^{2-} can replace SO_4^{2-} in ettringite (phase detected in G-R-BFA and carbonated G-R-BFA) and then in a lower pH; such phases are soluble and release chromates in solution (Piredda 2011; Blanc et al. 2018). Two main mechanisms can control the mobility of Cr(VI): Reduction of the latter to Cr(III) mainly by organic matter and Fe and adsorption on Fe and Mn oxides and clay minerals. However, adsorption is not efficient for alkaline pH and is significantly decreased by competing anions.

The Mo solubility was minimal at acidic pH values (pH < 6) for the different samples (Fig. 8d). It increases progressively to reach maximum values exceeding the inserting threshold for extremely basic pH (> 12). The leaching concentration was maximum in this pH region to reach values of 3.7 mg/kg, 2.07 mg/kg and 1.61 mg/kg for BFA, G-R-BFA and carbonated G-R-BFA, respectively. From the

BFA processing viewpoint, geopolymerization and accelerated carbonation reduced the leaching concentration of Mo. Moreover, under acidic conditions (pH < 6), the leaching concentration of Mo was the minimum and below 0.5 mg/kg. However, carbonated G-R-BFA allows the trapping and stabilization of Mo below IWSI threshold in a large pH range between 2 and 10.

The Se solubility is strongly dependent on the system pH with a maximum of release in acidic medium 2.2 mg/kg, 1.43 mg/kg and 1.35 mg/kg for BFA, G-R-BFA and carbonated G-R-BFA (Fig. 8e). This could be explained by the chemistry of Se and in particular the existence of oxyanions when this element is in dissolved form (Laperche et al. 2003; Bisson et al. 2006). However, the Se release decreases with increasing pH, and the concentration remains almost stable between pH 8 and 12. It should be noted that the pH has a determining role in the leaching behavior of Se by favoring the mobility of this oxyanion under alkaline conditions. Thus, the decrease of the pH value related to the formulation of geopolymeric mortars followed by an accelerated carbonation in aqueous media to contribute to the reduction of Se mobility in the whole pH range.

The pH can change the form in which MMTE exist in solution and influence their solubility. Thus, most often, an increase in pH will result in the MMTE precipitating as insoluble metal oxides or hydroxides (TESSIER et al. 1990; Serpaud et al. 1994). Conversely, a decrease in pH will be accompanied by the dissolution of (oxy)-hydroxide phases and modification of the adsorption equilibria (Fig. 9). The pH variations also have an influence on the interaction between MMTE and OM. The carboxylic acid functions of humic substances are sensitive to increases in pH, whose conjugated bases are available sites for MMTE binding. The pH is mainly controlled by the biological activities, the buffering capacity of the system, or the exchangeable ions.

The major environmental issue concerning the application is chemical durability. Acid leaching of MMTE can occur when the structure is in contact with runoff water. According to the results obtained in the leaching versus pH, BFA and SRS were not releasing a large amount of MMTE at natural pH, after the geopolymerization/ accelerated carbonation process. The release of the various MMTEs was below the IWSI threshold.

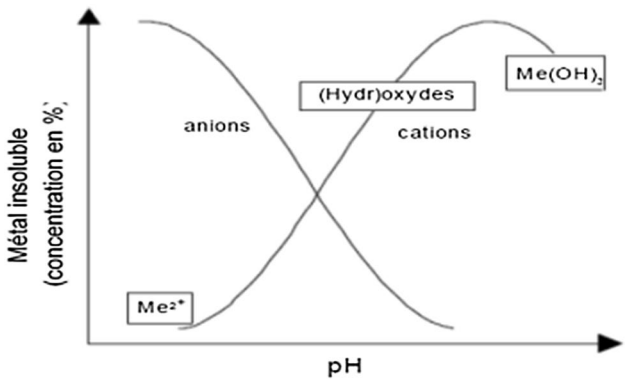

Fig. 9 Anion and cation solubility versus pH at the surface of solids. Me: metal

After leaching as a function of pH, the cationic elements always retain their amphoteric form as their leaching is excessively high in the extremely basic and acidic pH. After geopolymerization it can be observed that the leaching of cations has decreased compared to the raw material over the whole pH range, which means that a large part of the cations have been introduced into the geopolymeric matrix and still reach the IWSI threshold. After carbonation the leaching is lower in the pH range above 5 and the cation leaching is below the IWSI threshold; this means that a large part of the cations are stabilized as MCO_3, considering that the dissolution pH of carbonate is between 6 and 5, below pH 5 the leaching becomes higher. In contrast, in the acidic pH the Pb release was 6200 mg/kg in the SRS and decreased to 322 mg/kg in the carbonate geopolymers, which shows that Pb is well trapped in the geopolymeric matrix.

Concerning the anionic compounds, the release pattern was similar in the extremely acidic pH range with a higher release in the raw materials. At extremely basic pH, the anion release was still above the IWSI threshold even after geopolymerization; then after carbonation, the anionic compounds remained stable below the threshold for the basic pH range except for Cr and Mo in carbonated G-R-BFA. These results show that geopolymerization/accelerated carbonation allows enlarging the stabilization range of the different MMTE present in SRS and BFA.

The aim of this research work is to produce a geopolymer that will have high chemical resistance and excellent physical properties. In view of the first results obtained, geopolymers are the most promising storage matrices for future industrial applications. As this work is exploratory, the first results have been obtained, which will allow other scientific research to continue this promising path of geopolymers for the immobilization of MMTE from waste.

Conclusion

The research study presented in this paper is entirely in the context of the stabilization of MMTE such as, Cr, Mo, Pb, Sb, Se and Zn from SRS and BFA. For this purpose, a stabilization study by geopolymerization/accelerated carbonation was performed in order to evaluate its impact on the release of these elements in the leachate water. The geopolymer matrices were formulated by alkaline activation of SRS and BFA; various types of metakaolins (S, R, P) were used as aluminosilicate sources. The immobilization efficiency of

the different MMTEs was determined on the basis of leaching tests. The experimental results of this study led to the following conclusions:

- Before carbonation, the release of MMTE in the different geopolymer matrices was high (except for Pb and Zn in G-R-BFA) with an exceeding of the IWSI threshold. The geopolymers elaborated on the basis of MK R allows to significantly reduce the quantity of MMTE released.
- Upon further carbonation step, the pH of the carbonated geopolymers decreased to 9.37 ± 0.15 and 8.8 ± 0.15 for G-R-SRS and G-S-BFA, respectively, which led to the immobilization of MMTE in the MK R-based geopolymer matrix.
- Performing the mechanical tests on the geopolymers before accelerating carbonation, the highest compressive strength obtained after 7 days was obtained on the MK R-based geopolymer. The accelerated carbonation of the geopolymer increased its mechanical performance.
- TGA and SEM–EDS analysis results showed the presence of NASH-gel and ettringite after the geopolymer elaboration. Thus, the presence of silicate phase which contains Pb, Mo, Cr, S and Zn. In addition to the increased percentage of calcite in the geopolymers after accelerating carbonation.
- DRX analyses showed a decrease in Pb and Pb-Sb peak intensities for SRS and Pb carrier phase peak intensity for BFA, suggesting a change in lead speciation in the geopolymer matrices before and after carbonation. In G-R-SRS rich in hematite (MK R), antimony was stabilized with iron by forming $FeSbO_4$. Thus, the trapping of Pb as lead silicate (Pb-Si) for G-R-SRS and G-R-BFA before and after carbonation.

In summary, the highest environmental and mechanical performance was observed for the geopolymer formulated with MK R. Therefore, this metakaolin seems to be particularly effective for the formulation of geopolymer matrices capable of trapping MMTE.

Supplementary Information The online version contains supplementary material available at https://doi.org/10.1007/s13762-023-04788-x.

Acknowledgements The authors wish to acknowledge technical contributions of the chemistry pole of Institut Mines-Télécom. This research did not receive any specific grant from funding agencies in the public, commercial, or not-for-profit sectors.

Author contributions All authors contributed to the study conception and design. Material preparation, data collection and analysis were performed by Bader Bouzar and Yannick Mamindy-Pajany.

Funding The authors declare that they have no known competing financial interests or personal relationships that could have appeared to influence the work reported in this paper. The authors declare that no funds, grants, or other support were received during the preparation of this manuscript. The authors have no relevant financial or non-financial interests to disclose.

Declarations

Conflict of interests The authors declare no competing interests.

References

AFNOR (NF EN 196-1) (2016) Methods of testing cement — Part 1: Determination of strength

AFNOR (2002) NF EN 12457-2, Leaching-Compliance test for leaching of granular wasre materials ans sludges

AFNOR (2006) NF EN ISO 18757, Determination of specific surface area pf ceramic powders by gas adsorption using the BET method

AFNOR (2015) NF EN 14429, Characterization of waste-leaching behaviour test-influence of pH on leaching with initial acid/base addition

AFNOR (2000a) NF ISO 13320-1, Laser diffraction methods

AFNOR (2000b) NF EN 12879, Characterization of sludges

Alloway BJ (2012) Heavy metals in soils: trace metals and metalloids in soils and their bioavailability. Springer Science Business Media

Bai J, Chaipanich A, Kinuthia JM, O'Farrell M, Sabir BB, Wild S, Lewis MH (2003) Compressive strength and hydration of wastepaper sludge ash-ground granulated blastfurnace slag blended pastes. Cem Concr Res 33(8):1189–1202. https://doi.org/10.1016/S0008-8846(03)00042-5

Bisson M, Houeix N, Hulot C, Lacroix G, Lefevre JP, Leveque S, Magaud H, Morin A (2006) Arsenic et ses dérivés inorganiques. INERIS, fiches de données toxicologiques et environnementales des substances chimiques

Blanc D, Gonzalez L, Lupsea-Toader M, de Brauer C (2018) Mineralogical evolution and leaching behaviour of a heap of bottom ash as a function of time: influence on its valorization. Waste and Biomass Valorization 9(12):2517–2527. https://doi.org/10.1007/s12649-018-0444-1

Blanchard C (2000) Caractérisation de la mobilisation potentielle des polluants inorganiques dans les sols pollués. PhD Thesis, Lyon, INSA

Bouchikhi A, Mamindy-Pajany Y, Maherzi W, Albert-Mercier C, El-Moueden H, Benzerzour M, Peys A, Abriak N (2021) Use of residual waste glass in an alkali-activated binder – structural characterization, environmental leaching behavior and comparison of reactivity. J Build Eng 34:101903. https://doi.org/10.1016/j.jobe.2020.101903

Bouzar B, Mamindy-Pajany Y (2022b) Manufacture and characterization of carbonated lightweight aggregates from waste paper fly ash. Powder Techno. https://doi.org/10.1016/j.powtec.2022.117583

Bouzar B, Mamindy-Pajany Y (2022a) Phosphorus removal from real and synthetic wastewater using biomass bottom ash. Int J Environ Sci Technol. https://doi.org/10.1007/s13762-022-04451-x

Cao X, Ma LQ, Chen M, Hardison DW, Harris WG (2003a) Lead transformation and distribution in the soils of shooting ranges in Florida, USA. Sci Total Environ 307(1):179–189. https://doi.org/10.1016/S0048-9697(02)00543-0

Cao X, Ma LQ, Chen M, Hardison Jr DW, Harris WG (2003b) Weathering of lead bullets and their environmental effects at outdoor shooting ranges. J Environ Qual 32(2):526–534. https://doi.org/10.2134/jeq2003.5260

Cazalet ML (2012) Caractérisation physico-chimique d'un sédiment marin traité aux liants hydrauliques: Évaluation de la mobilité potentielle des polluants inorganiques. PhD Thesis, INSA de Lyon

Chatain V (2004) Caractérisation de la mobilisation potentielle de l'arsenic et d'autres constituants inorganiques présents dans les sols issus d'un site minier aurifère. PhD Thesis, INSA LYON

Chen Q, Zhang L, Ke Y, Hills C, Kang Y (2009) Influence of carbonation on the acid neutralization capacity of cements and cement-solidified/stabilized electroplating sludge. Chemosphere 74(6):758–764. https://doi.org/10.1016/j.chemosphere.2008.10.044

Chindaprasirt P, Thaiwitcharoen S, Kaewpirom S, Rattanasak U (2013) Controlling ettringite formation in FBC fly ash geopolymer concrete. Cement Concr Compos 41:24–28. https://doi.org/10.1016/j.cemconcomp.2013.04.009

Ciesielski H, Guérin-Lebourg A, Proix N (2007) Effets du pH sur l'extraction des éléments traces métalliques dans les sols. Étude Et Gestion Des Sols 14(1):7–30

Clausen JL, Bostick B, Korte N (2011) Migration of lead in surface water, pore water, and groundwater with a focus on firing ranges. Crit Rev Environ Sci Technol 41(15):1397–1448. https://doi.org/10.1080/10643381003608292

Cornelis G, Anette Johnson C, Van Gerven T, Vandecasteele C (2008) Leaching mechanisms of oxyanionic metalloid and metal species in alkaline solid wastes: a review. Appl Geochem 23(5):955–976. https://doi.org/10.1016/j.apgeochem.2008.02.001

Cornelis G, Van Gerven T, Vandecasteele C (2012) Antimony leaching from MSWI bottom ash: modelling of the effect of PH and carbonation. Waste Manage 32(2):278–286. https://doi.org/10.1016/j.wasman.2011.09.018

Cornell R, Schwertmann U (2003) The iron oxides–structure, properties, occurrences and uses 2nde edition. Wiley-VCH Verlag, Weinheim

Davidovits J (2013) Geopolymer cement. A review. Geopolymer Institute, Technical Papers 21:1–11

Deneux-Mustin S, Roussel-Debet S, Mustin C, Henner P, Munier-Lamy C, Colle C, Berthelin J, Garnier-Laplace J, Leyval C 2003 Mobilité et transfert racinaire des éléments en traces(influence des micro-organismes du sol)

Dermatas D, Shen G, Chrysochoou M, Grubb DG, Menounou N, Dutko P (2006) Pb speciation versus TCLP release in army firing range soils. J Hazard Mater 136(1):34–46. https://doi.org/10.1016/j.jhazmat.2005.11.009

Deschamps T, Benzaazoua M, Bussière B, Belem T, Mbonimpa M. (2006) Mécanismes de rétention des métaux lourds en phase solide: cas de la stabilisation des sols contaminés et des déchets industriels. VertigO-la revue électronique en sciences de l'environnement 7 (2)

Duc M, Lefevre G, Fedoroff M, Janine Jeanjean JC, Rouchaud F-R, Dumonceau J, Milonjic S (2003) Sorption of selenium anionic species on apatites and iron oxides from aqueous solutions. J Environ Radioact 70(1):61–72. https://doi.org/10.1016/S0265-931X(03)00125-5

Fang Y, Kayali O (2013) The fate of water in fly ash-based geopolymers. Constr Build Mater 39:89–94. https://doi.org/10.1016/j.conbuildmat.2012.05.024

Fernández Olmo I, Chacon E, Irabien A (2001) Influence of lead, Zinc, Iron (III) and Chromium (III) oxides on the setting time and strength development of portland cement. Cem Concr Res 31(8):1213–1219. https://doi.org/10.1016/S0008-8846(01)00545-2

François D, Criado C (2007) Monitoring of leachate at a test road using treated fly ash from municipal solid waste incinerator. J Hazard Mater 139(3):543–549. https://doi.org/10.1016/j.jhazmat.2005.02.019

Garcia-Lodeiro I, Palomo A, Fernández-Jiménez A, Macphee DE (2011) Compatibility studies between N-A-S-H and C-A-S-H Gels. Study in the ternary diagram Na2O–CaO–Al2O3–SiO2–H2O. Cem Concr Res 41(9):923–931. https://doi.org/10.1016/j.cemconres.2011.05.006

Glasser FP (1997) Fundamental aspects of cement solidification and stabilisation. J Hazard Mater Fundam Aspects Solid/stab 52(2):151–170. https://doi.org/10.1016/S0304-3894(96)01805-5

Guo G, Zhou Q, Lene QM (2006) Availability and assessment of fixing additives for the in situ remediation of heavy metal contaminated soils: a review. Environ Monit Assess 116(1):513–528. https://doi.org/10.1007/s10661-006-7668-4

Hajimohammadi A, van Deventer JSJ (2016) Dissolution behaviour of source materials for synthesis of geopolymer binders: a kinetic approach. Int J Min Process 153:80–86. https://doi.org/10.1016/j.minpro.2016.05.014

Hardison WD Jr, Ma LQ, Luongo T, Harris WG (2004) Lead contamination in shooting range soils from abrasion of lead bullets and subsequent weathering. Sci Total Environ 328(1):175–183. https://doi.org/10.1016/j.scitotenv.2003.12.013

Harvey OR, Harris JP, Herbert BE, Stiffler EA, Haney SP (2010) Natural organic matter and the formation of calcium-silicate-hydrates in lime-stabilized smectites: a thermal analysis study. Thermochim Acta 505(1):106–113. https://doi.org/10.1016/j.tca.2010.04.007

Hassam T, Braham LA, Mouhoub S (2016) Elaboration des géopolymères pour l'encapsulation d'un rejet de Pb/Zn. PhD Thesis, Université Abderrahmane Mira-Bejaia

Heier LS, Lien IB, Strømseng AE, Ljønes M, Rosseland BO, Tollefsen KE, Salbu B 2009 Speciation of Lead, Copper, Zinc and Antimony in Water Draining a Shooting Range—Time Dependant Metal Accumulation and Biomarker Responses in Brown Trout (Salmo Trutta L.). Science of The Total Environment, Thematic Papers: Selected papers from the 2007 Wetland Pollutant Dynamics and Control Symposium, 407 (13): 4047-55. https://doi.org/10.1016/j.scitotenv.2009.03.002

Hlaváčková P (2005) Evaluation du comportement du cuivre et du zinc dans une matrice de type sol à l'aide de différentes méthodologies. PhD Thesis, Lyon, INSA.

Hong S-Y, Glasser FP (2002) Alkali Sorption by C-S-H and C-A-S-H gels: part II role of alumina. Cement Concr Res 32(7):1101–1111. https://doi.org/10.1016/S0008-8846(02)00753-6

Hyodo M, Yang Wu, Aramaki N, Nakata Y (2017) Undrained monotonic and cyclic shear response and particle crushing of silica sand at low and high pressures. Can Geotech J 54(2):207–218. https://doi.org/10.1139/cgj-2016-0212

Jeon B-H, Dempsey BA, Burgos WD, Royer RA (2003) Sorption kinetics of Fe(II), Zn(II), Co(II), Ni(II), Cd(II), and Fe(II)/Me(II) onto hematite. Water Res 37(17):4135–4142. https://doi.org/10.1016/S0043-1354(03)00342-7

Jurado-Contreras S, Bonet-Martínez E, Sánchez-Soto PJ, Gencel O, Eliche-Quesada D (2022) Synthesis and characterization of alkali-activated materials containing biomass fly ash and metakaolin: effect of the soluble salt content of the residue. Arc Civ Mech Eng 22(3):121. https://doi.org/10.1007/s43452-022-00444-2

Kadıoğlu YY, Karaca S, Bayrakçeken S (1995) Kinetics of pyrite oxidation in aqueous suspension by nitric acid. Fuel Process Technol 41(3):273–287. https://doi.org/10.1016/0378-3820(94)00101-X

Laperche V, Bodénan F, Dictor MC, Baranger Ph. 2003. Guide méthodologique de l'arsenic, appliqué à la gestion des sites et sols pollués . Rapport BRGM RP-52066-FR

Laporte-Saumure M, Martel R, Mercier G (2010) Evaluation of physicochemical methods for treatment of Cu, Pb, Sb, and Zn in Canadian small arm firing ranges backstop soils. Water Air Soil Pollut 213(1):171–189. https://doi.org/10.1007/s11270-010-0376-2

Lausselet C, Cherubini F, del Serrano GA, Becidan M, Strømman AH (2016) Life-cycle assessment of a waste-to-energy plant in Central Norway: current situation and effects of changes in waste

fraction composition. Waste Manage 58:191–201. https://doi.org/10.1016/j.wasman.2016.09.014
Lin Z, Comet B, Qvarfort U, Herbert R (1995) The chemical and mineralogical behaviour of Pb in shooting range soils from Central Sweden. Environ Pollut 89(3):303–309. https://doi.org/10.1016/0269-7491(94)00068-O
Lin HK, Man XD, Walsh DE (2001) Lead removal via soil washing and leaching. JOM 53(12):22–25. https://doi.org/10.1007/s11837-001-0007-x
Lions J (2004). Etude hydrogéochimique de la mobilité de polluants inorganiques dans des sédiments de curage mis en dépôt: expérimentations, étude in situ et modélisations. PhD Thesis
Liu R, Gress J, Gao J, Lena QM (2013) Impacts of Two Best Management practices on Pb weathering and leachability in shooting range soils. Environ Monit Assess 185(8):6477–6484. https://doi.org/10.1007/s10661-012-3039-5
Ma LQ, Hardison DW, Harris WG, Cao X, Zhou Q (2007) Effects of soil property and soil amendment on weathering of abraded metallic Pb in shooting ranges. Water Air Soil Pollut 178(1):297–307. https://doi.org/10.1007/s11270-006-9198-7
Mamindy-Pajany Y, Hurel C, Marmier N, Roméo M (2011) Arsenic (V) adsorption from aqueous solution onto goethite, hematite, magnetite and zero-valent iron: effects of PH, concentration and reversibility. Desalination 281:93–99. https://doi.org/10.1016/j.desal.2011.07.046
Mamindy-Pajany Y, Hurel C, Geret F, Roméo M, Marmier N (2013) Comparison of mineral-based amendments for ex-situ stabilization of trace elements (As, Cd, Cu, Mo, Ni, Zn) in marine dredged sediments: a pilot-scale experiment. J Hazar Mater 252–253:213–219. https://doi.org/10.1016/j.jhazmat.2013.03.001
Marmier N, Dumonceau J, Fromage F, Chupeau J (1993) Experimental study and surface-complexation modelling of trivalent lanthanide ion sorption on haematite. Comptes Rendus De L'academie Des Sciences. 317(3):311–317
Mkahal Z, Mamindy-Pajany Y, Maherzii W, Abriak N-E (2022) Recycling of mineral solid wastes in backfill road materials: technical and environmental investigations. Waste Biomass Valorization 13(1):667–687. https://doi.org/10.1007/s12649-021-01544-5
Mozaffari E, O'Farrell M, Kinuthia JM, Wild S (2006) Improving strength development of wastepaper sludge ash by wet-milling. Cement Concr Compos 28(2):144–152
Mozaffari E, Kinuthia JM, Bai J, Wild S (2009) An investigation into the strength development of wastepaper sludge ash blended with ground granulated blastfurnace slag. Cem Concr Res 39(10):942–949. https://doi.org/10.1016/j.cemconres.2009.07.001
Nanda S, Berruti F (2021) Municipal solid waste management and landfilling technologies: a review. Environ Chem Lett 19(2):1433–1456. https://doi.org/10.1007/s10311-020-01100-y
Nikolić V, Komljenović M, Džunuzović N, Miladinović Z (2018) The influence of Pb addition on the properties of fly ash-based geopolymers. J Hazard Mater 350:98–107. https://doi.org/10.1016/j.jhazmat.2018.02.023
Nozahic V, Amziane S, Torrent G, Saïdi K, De Baynast H (2012) Design of green concrete made of plant-derived aggregates and a pumice-lime binder. Cement Concr Compos 34(2):231–241. https://doi.org/10.1016/j.cemconcomp.2011.09.002
Pacheco-Torgal F, Castro-Gomes J, Jalali S (2008) Alkali-activated binders: a review: part 1. Historical background, terminology, reaction mechanisms and hydration products. Constr Build Mater 22(7):1305–1314. https://doi.org/10.1016/j.conbuildmat.2007.10.015
Piredda M (2011) Stabilization of MSW combustion residues by accelerated carbonation treatment and their potential carbon dioxide sequestration
Puertas F, Palacios M, Manzano H, Dolado JS, Rico A, Rodríguez J (2011) A model for the C-A-S-H gel formed in alkali-activated slag cements. J Eur Ceram Soc 31(12):2043–2056. https://doi.org/10.1016/j.jeurceramsoc.2011.04.036
Rashid I, Daraghmeh N H, Al Omari MM, Chowdhry BZ, Leharne SA, Hodali HA, Badwan AA (2011) Chapter 7–Magnesium Silicate . In Profiles of Drug Substances, Excipients and Related Methodology, édité par Harry G. Brittain, 36:241-85. Academic Press. https://doi.org/10.1016/B978-0-12-387667-6.00007-5
Renou S, Poulain S, Givaudan JG, Sahut C, Moulin P (2009) Lime treatment of stabilized leachates. Water Sci Technol 59(4):673–685. https://doi.org/10.2166/wst.2009.014
Rooney CP, McLaren RG, Condron LM (2007) Control of lead solubility in soil contaminated with lead shot: effect of soil PH. Environ Pollut 149(2):149–157. https://doi.org/10.1016/j.envpol.2007.01.009
Santos RM, Mertens G, Salman M, Cizer Ö, Van Gerven T (2013) Comparative study of ageing, heat treatment and accelerated carbonation for stabilization of municipal solid waste incineration bottom ash in view of reducing regulated heavy metal/metalloid leaching. J Environ Manage 128:807–821. https://doi.org/10.1016/j.jenvman.2013.06.033
Serpaud B, Al-Shukry R, Casteignau M, Matejka G (1994) Adsorption des métaux lourds (Cu, Zn, Cd et Pb) par les sédiments superficiels d'un cours d'eau: rôle du pH, de la température et de la composition du sédiment. Revue Des Sciences De L'eau/journal of Water Science 7(4):343–365
Sorlini S, Collivignarelli MC, Abbà A (2017) Leaching behaviour of municipal solid waste incineration bottom ash: from granular material to monolithic concrete. Waste Manage Res 35(9):978–990
Sorvari J, Antikainen R, Pyy O (2006) Environmental contamination at finnish shooting ranges—the scope of the problem and management options. Sci Total Environ 366(1):21–31. https://doi.org/10.1016/j.scitotenv.2005.12.019
Srivastava S, Chaudhary R, Khale D (2008) Influence of PH, curing time and environmental stress on the immobilization of hazardous waste using activated fly ash. J Hazard Mater 153(3):1103–1109. https://doi.org/10.1016/j.jhazmat.2007.09.065
Stark J, Bollmann K (2000) Delayed ettringite formation in concrete. Nordic Concr Res Publ- 23:4–28
Strømseng AE, Ljønes M, Bakka L, Mariussen E (2009) Episodic discharge of lead, copper and antimony from a norwegian small arm shooting range. J Environ Monit 11(6):1259–1267. https://doi.org/10.1039/B823194J
Stumm W (1992) Chemistry of the solid-water interface: processes at the mineral-water and particle-water interface in natural systems. John Wiley
Teixeira ER, Camões A, Branco FG (2022) Synergetic effect of biomass fly ash on improvement of high-volume coal fly ash concrete properties. Constr Build Mater 314:125680. https://doi.org/10.1016/j.conbuildmat.2021.125680
Tessier A, Campbell PGC, Carignan R (1990) Influence du pH sur la spéciation et la biodisponibilité des métaux. Influence Du pH Sur La Spéciation Et La Biodisponibilité Des Métaux 2:69–73
Thi NBD, Kumar G, Lin C-Y (2015) An overview of food waste management in developing countries: current status and future perspective. J Environ Manage 157:220–229. https://doi.org/10.1016/j.jenvman.2015.04.022
Van Jaarsveld JGS, Van Deventer JSJ, Lorenzen L (1998) Factors affecting the immobilization of metals in geopolymerized flyash. Metall and Mater Trans B 29(1):283–291. https://doi.org/10.1007/s11663-998-0032-z
Vantelon D, Lanzirotti A, Scheinost AC, Kretzschmar R (2005) Spatial distribution and speciation of lead around corroding bullets in a shooting range soil studied by micro-x-ray fluorescence and absorption spectroscopy. Environ Sci Technol 39(13):4808–4815. https://doi.org/10.1021/es0482740

Wesche K (ed) (2014) Fly ash in concrete: properties and performance. CRC Press, London. https://doi.org/10.1201/9781482267051

Yousuf M, Mollah A, Vempati RK, Lin T-C, Cocke DL (1995) The interfacial chemistry of solidification/stabilization of metals in cement and pozzolanic material systems. Waste Manage 15(2):137–148. https://doi.org/10.1016/0956-053X(95)00013-P

Zouch A, Mamindy-Pajany Y, Bouchikhi A, Abriak N-E, Ksibi M (2022) Valorization of marine sediments in geopolymer mortars: physico-mechanical, microstructural and environmental investigations at laboratory scale. J Mater Cycles Waste Manage 24(3):1109–1123. https://doi.org/10.1007/s10163-022-01382-0

Chapter 6:
Phosphorus removal from real and synthetic wastewater using biomass bottom ash

International Journal of Environmental Science and Technology
https://doi.org/10.1007/s13762-022-04451-x

ORIGINAL PAPER

Phosphorus removal from real and synthetic wastewater using biomass bottom ash

B. Bouzar[1,2] · **Y. Mamindy-Pajany**[1,2]

Received: 28 March 2022 / Revised: 5 July 2022 / Accepted: 22 July 2022

Abstract

The biomass bottom ash (BBA_S) from Roubaix and Lens (France) with different physical–chemical characteristics was used as reactive filters for phosphorus (P) removal. The principal objective of our study was to evaluate the P removal potential with the two BBA_S, and batch tests were performed to determine the influence of several parameters including the origin and type of BBA_S, particle size, chemical composition, initial P concentration, contact time and water quality (real wastewater, synthetic wastewater) on P removal performance. Then, a series of laboratory scale column tests were performed with real wastewater doped to 30 mg P/l during the 8 months of experiments. To determine the mechanisms of P removal by the two BBA_S, a monitoring of pH, calcium concentration and P concentration was performed using a fraction collector. In addition, a series of physical–chemical analyses such as XRD, SEM–EDS and sequential extraction were performed before and after 8 months of filter operation. The maximum phosphorus removal capacity (PRC) of the real wastewater solutions (100 mg P/l) in batch ranged from 1.56 to 1.96 mg P/g after 7 days of contact for BBA_L and BBA_R, respectively. The maximum P removal capacities in the columns varied from 4.15 to 9.72 g P/kg material after 8 months of experimentation for BBA_L and BBA_R, respectively. The results of XRD, SEM–EDS, sequential extraction confirm that the main mechanism of P removal was through precipitation of Ca-P (as hydroxyapatite). The P removal performance of the real wastewater was mainly related to the particle size, specific surface area and CaO dissolution of each BBA_S. However, the results show that wastewater treatment plants represent an important source of Ca^{2+} ions to further promote the precipitation of hydroxyapatite on the surface, resulting in increased P removal efficiency.

Keywords Biomass bottom ash · Hydroxyapatite precipitation/crystallization · Phosphorus removal · Wastewater treatment

Introduction

Phosphorus (P) is an essential element for modern industry and agriculture. It is therefore omnipresent in domestic, industrial and agricultural wastewater discharges. For a long time, P contained in wastewater was considered only as a harmful element to be treated in order to limit eutrophication problems in receiving aquatic environment (Cabanes 2006). For the last decade, P has been considered as an essential resource with a major economic interest (Cordell 2010).

The source of P is phosphate rock mining resources that are finite and non-renewable. Recent estimates indicate that mineral reserves would cover global demand for several decades to a few centuries (Cordell et White 2015). However, the majority of these reserves are located in a few countries: Morocco, China and the USA concentrate 70% of the world's reserves of P mineral resources. This creates a high dependence on imports and long-term insecurity for countries with a high demand for P. Over the past decade, the P present in wastewater has been increasingly considered as a secondary source of P that should be exploited (Kasprzyk et Gajewska 2019; de-Bashan et Bashan 2004; Chen et al. 2015; Mandel et al. 2019). The P in wastewater is mainly from metabolic discharges (urine). Inorganic P in the form of orthophosphates or phosphates ($P–PO_4$) represents 60 to 85% of total P (Pt sum of inorganic and organic P). Inorganic P is also

Editorial responsibility: Fatih ŞEN.

✉ B. Bouzar
bader.bouzar@imt-nord-europe.fr

[1] Institut Mines-Télécom, Centre for Materials and Processes, Environnement, IMT Nord Europe, 59000 Lille, France

[2] Univ., ULR 4515 –LGCgE, Laboratoire de Génie Civil et géo-Environnement, University of Lille, 59000 Lille, France

Published online: 04 August 2022

found as polyphosphates and organic P as phospho-lipids or polynucleotides (Stricker et Heduit 2009). In domestic effluents, total P is present in different forms and may originate from human metabolism, laundry, industrial and agricultural discharges. The daily amount of P discharged by wastewater treatment plants (WWTPs) in population equivalent is about 2.5 g $Pt.PE^{-1}.d^{-1}$ (Prigent 2013).

In view of the current challenges, the elimination of P from water treatment plants is an imperative point to be ensured. In wastewater treatment plants, effluent P removal can be achieved in two different ways. It is possible to let the micro-organisms in the aeration tanks operate, which will assimilate and eliminate part of the P. However, when this solution is not possible, the operator is required to apply a physical–chemical treatment by adding reactive that will allow the precipitation of P (dephosphatation). The process of dephosphatation consists of fixing P ions in or on solids which are then separated from the effluent (de-Bashan et Bashan 2004). Depending on the method used, the solids may be in the form of an insoluble metal salt precipitate, substances with a high chemical affinity for P, bacterial biomass or plant biomass. The present dephosphatation technique used in France in WWTPs consists of adding metal salts such as $FeCl_3$ or $AlCl_3$ or $Ca(OH)_2$ to form insoluble phosphate precipitates. However, it is essential to have a separation step to eliminate this precipitate formed, either at the inlet or at the outlet of the WWTP. In addition, several studies (Esser et al 2004) have demonstrated that the use of $FeCl_3$ can lead to P release when this precipitate is under reducing conditions due to the chemical instability of iron phosphate.

The use of reactive materials for P retention on a solid phase through adsorption and/or precipitation mechanisms is an alternative to maintain the extensive character of the classical French system (constructed wetlands) (Akratos et Tsihrintzis 2007). A bibliographic synthesis of 64 scientific papers concerning materials used for P removal was carried out by Vohla et al. (2011b). Various types of materials rich in calcium have been used in P removal processes to precipitate hydroxyapatite ($Ca_{10}(PO_4)_6OH_2$) using low cost materials, among these materials are steel slag (Kostura et al 2005; Kim et al. 2006; Korkusuz et al 2005), magnetite minerals (Karapinar et al 2004), limestone and calcite concrete (Song et al. 2006; Molle et al 2003), natural wastes and industrial by-products (Yan et al. 2014), fly ash and red mud (Karaca et al. 2006; Yan et al. 2014; Li et al. 2006), these materials have been developed as low-cost adsorbents to remove P from wastewater, and the removal rates vary between 40 and 90%.

In this study, biomass bottom ash (BBA_S) (rich in calcium) was used as a reactive substrate without any physical or chemical pretreatment to treat WWTP. Therefore, the passage of water containing P on these reactive filters aims to allow the recovery of wastewater with a total P concentration lower than the authorized limit for discharges (European Union (EU) effluent standards ≤ 0.5 mg P/l). Thus, the phosphorus removal capacity (PRC) of two BBA_S from thermal power plants in the Hauts-de-France region was studied. Static batch tests were first performed, which determined the equilibrium time and the phosphate removal capacity. Then, column tests were realized, in order to show the phosphorus removal capacity at a laboratory scale.

A comparative study on P removal performance in column was performed. Both filters were operated under the same experimental conditions: real wastewater doped with an initial concentration of P input at 30 mg P/L, flow rate (0.5 L/d) hydraulic retention time of 24 h, ambient temperature. This permitted to compare the results of the two filters in order to evaluate the influence of the type, size and composition of the BBA_S on the P removal performance. Then, an in-depth study on the P removal mechanisms was realized. Several physicochemical and mineralogical analyses, including X-ray diffraction (XRD), X-ray fluorescence (XRF), scanning electron microscopy (SEM), energy-dispersive X-ray (EDX) and sequential extractions, were used to investigate the mechanisms of P trapping in the BBA_S used as reactive filters. Indeed, it is important to understand the reactions that lead to P removal with BBA_S, not only in relation with the performance of filtration systems, but also with the potential risks associated with their subsequent fate. For example, reuse in agriculture is one of the most interesting applications, due to the calcium, silicate and magnesium content of these substrates, replacing lime as a source of calcium and adsorbed P as a nutrient.

Materials and methods

Characterization of biomass bottom ash

In this study, biomass bottom ash from Roubaix (BBA_R) and biomass bottom ash from Lens (BBA_L) used as reactive filters resulting from the combustion of biomass used in French thermal power plants. The mass composition of chemical elements of the two BBA_S measured by X-ray fluorescence. The mobility of MMTE was measured after the leaching of both BBA_S according to NF EN 12457–2. The leaching was performed with a ratio L/S = 10 l/kg (liquid/solid); 90 g of BBA_S was mixed with 900 ml of synthetic wastewater. The samples were placed under stirring on a turntable (Heidolph Reax 20) at 10 rpm and 25 °C for 24 h. The mixture was then filtered through cellulose acetate membrane filters (0.45 µm). Before chemical analysis by an inductively coupled plasma optical emission spectrometer (ICP-OES 5100 Agilent Technologies), the solutions were acidified with 2 vol.% nitric acid. The accuracy of the

measurement, determined using standard solutions (diluted from 1000 mg/L of SPEX CertiPre elemental standards), is ± 2%.

The specific surface area was measured by the BET method using a Micromeritics stirring analyzer (3FLEX Surface Characterization) according to NF EN ISO-18757. Prior to analysis, the samples were degassed from nitrogen with a Smart Prep degasser (VacPrep 061) under nitrogen at 80 °C for 8 h to remove moisture from the sample surface and pores.

The specific density of both BBA_S was measured using a Micromeritics ACCUPYC 1330 Helium Pycnometer in accordance with standard NF EN 15326. The principle of which is based on the determination of the absolute volume occupied by a specific mass of material. The absolute volume of the sample is determined by sweeping the sample with helium gas at a fixed pressure. The method of calculation is based on the perfect gas relationship.

The XRF analysis was performed with a S4-PIONEER equipped with a 4-kW generator with a rhodium anticathode. The instrument was capable of providing results in atomic mass percentages of the elements. The analyzed samples are ground and dried beforehand.

Batch test

Synthetic and real wastewater were used for preparing P containing solutions with five different concentrations of P (5 mg P/L; 10 mg P/L; 20 mg P/L; 50 mg P/L; 100 mg P/L). Synthetic solutions were obtained by dissolving K_2HPO_4 in synthetic wastewater. Real wastewater having 2.63 and 8.21 mg P/l and 183–189 mg Ca/l was doped with P until reaching the same concentrations as synthetic solutions.

Batch tests were performed to determine the equilibrium PRC_S. First, a preliminary kinetic study was carried out to determine the time necessary for the establishment of the physical–chemical equilibrium between BBA_S and an aqueous solution of P (during 0.25, 1, 4, 24, 48, 72, 168 h). Once the adsorption kinetics were determined, the experiments were realized in triplicates in order to determine the PRC_S of the two materials concerned. A liquid/solid ratio (L/S) of 20 l/kg was used for this experiment: 10 g of BBA_S (dried at 40 °C) was introduced with 200 mL of P (K_2HPO_4) solutions at different concentrations (5 mg P/L; 10 mg P/L; 20 mg P/L; 50 mg P/L; 100 mg P/L) into 250-mL HDPE (high density polyethylene) flasks. For each concentration, seven triplicates solutions corresponding to a contact time were prepared in order to respect the L/S ratio during the whole reaction time. The elution was performed at room temperature 20 °C (± 2 °C), at 10 rpm. After 24 h, the pH and conductivity of the solutions are measured directly in the flasks. Then, the solutions in contact with the BBA_S are collected using 20-mL Terumo® syringes and filtered on cellulose membrane filters (0.45 µm). Acidified with nitric acid at 2 vol%, MMTE present in the solutions (specifically P and Ca) were analyzed by inductively coupled plasma optical emission spectrometer (ICP-OES). In this study, the removal efficiency and PRC of both BBA_S were calculated for the different concentrations at 1 and 7 days. The PRCs (mg P/g BBA_S) are calculated from Eq. (1) and (2):

$$\text{Removal Efficiency} = \frac{(\text{Pin} - \text{Pe}) * 100}{\text{Pin}} \quad (1)$$

$$\text{PRC} = \frac{(\text{Pin} - \text{Pe})V}{\text{M}} \quad (2)$$

where P_{in} is the initial P concentration (mg P/L), P_e is the residual P concentration of the solution after 1 and 7 days of P removal (mg P/L), M is the mass of BBA_S (g), and V is the volume of the solution (L).

Columns test

Figure 1 shows the experimental setup which was used for the laboratory-scale column tests. Four columns of 1.5L and 50 mm in diameter were fed continuously since start-up. Based on the annual average concentrations measured in the wetland effluent, a concentration of 30 mg P/L was set for the column tests. Each column is filled with 300 g of BBA_S. At the top and bottom of the column, a glass fiber filter of the same diameter as the column is placed in contact with the BBA_S used before closing the estimates (the columns were made in duplicate). A 25-L tank was used to prepare the synthetic P effluent (KH_2PO_4, 30 mg P/L real wastewater). Every week, the effluent was renewed. The P-doped real wastewater was sent through a peristaltic pump (MASTERFLEX) at the bottom of the column at a flow rate of 0.35 mL/min to obtain a flow time close to 0.5 l/d (hydraulic

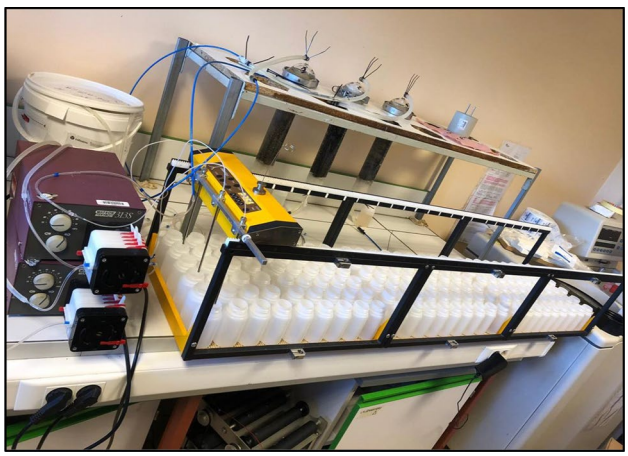

Fig. 1 Photography of the columns of reactive materials

retention time of 24 h and temperature ambient). Up-flow feeding was preferred to minimize dead volume in the columns. Treated effluent was discharged by gravity through flexible hoses directly to a fraction collector. The solutions were acidified with 2 vol% nitric acid and analyzed by ICP-OES to quantify the P and Ca at the outlet of the different columns (Bouzar et Mamindy-Pajany 2022).

The adsorption capacity of the column Qc (g P/kg), which represents the amount of P accumulated on the material, is determined by following Eq. (3):

$$\mathrm{Qc} = \frac{D}{\mathrm{M}} \int (\mathrm{Co} - C)\mathrm{d}t \tag{3}$$

where D is daily flow rate (l/d), M is the mass of the substrate in the column (g), C_0 is the P concentration of the inlet effluent (mg P/l), and C is the P concentration of the outlet effluent (mg P/l).

In order to study the influence of type, particle size and composition of each BBA_S, thus to understand the mechanism of P trapping by both BBA_S, 50 g of each BBA_S was recovered at the end of the experiment, dried at 40 °C and crushed for physical–chemical analyses (X-ray diffraction (XRD), scanning electron microscopy (SEM), energy-dispersive X-rays (EDX) and sequential extractions).

Investigation of P removal mechanisms

Two methods were used to study the mechanisms of P removal with BBA_S in the experimental setups, one based on monitoring of purification performance and the second on selective analysis techniques. The first method consists of comparing the monitoring of parameters such as pH, calcium and P over time. The second method involves selective techniques such as SEM–EDS, DRX and sequential extraction. The surface of the raw BBA_S was first analyzed. Then the P removal mechanisms with the BBA_S used in the columns were compared.

The samples were previously dried at 40 °C for 72 h and covered with a carbon layer before observation by SEM–EDS (SEM- Hitachi S-4300SE/N). EDS analyses permitted qualitative analysis of the SEM observations at 15 kV. X-ray diffraction (XRD) was also used before and after dephosphatation on the BBA_S used as reactive filters.

Table 2 Physical characterizations of BBA_R and BBA_L

Materiel	Particle size (mm)	Absolute density (g/cm^3)	Apparent density (g/cm^3)	Specific surface (m^2/g)
BBA_R	0–20	2.77 ± 0.03	1.28 ± 0.04	1,81 ± 0.01
BBA_L	0–2	2.65 ± 0.04	1.44 ± 0.02	0.90 ± 0.05

The technique allows the identification of P-Ca, P-Al and/or P-Fe crystal forms. An XRD diffractometer and D8 Focus diffractometer from Bruker with Cukα radiation of 5 to 80 degrees 2-theta were used.

The sequential extraction procedure of P (Headley 2003) was used to quantify the fractions of different P compounds in the BBA_S before and after 8 months of filter operation (to saturation of both BBA_S with P). The sequential extraction procedure used is consisted of four steps; approximately 20 g of the BBAs before and after dephosphatation was transferred in 250-mL polypropylene bottle and solubilized with different chemical reagents under continuous stirring, which determined the weakly bound P, iron and aluminum bound phosphate (Fe/Al ~ P), calcium bound phosphate (Ca ~ P) and acid-soluble organic phosphate (ASOP, Porg-acid) fractions of the contaminants in the BBA_S samples. The sequential extraction procedures are shown in Table 1.

Sequential extraction was performed according to EN 12,457–2 with an extraction solution to BBA_S ratio of 10L/kg and a duration of 16 h except for the last step. Following (Headley 2003), a wash with 25 ml of KCl (1 M) was realized after each step in order to recover the P re-adsorbed on the surface of the BBA_S. All extractions were performed in duplicate.

Results and discussion

Characterization of biomass bottom ash

The particle size of both BBA_S was considered large enough to prevent the risk of clogging the filters especially in the case of column tests, as was observed in a previous study (Chazarenc 2007). Table 2 shows the particle size of BBA_R was 0–20 mm, while the particle size

Table 1 Sequential extraction procedure

Extraction	Reagents	Extraction conditions (nominal target phases)
Step 1	Sodium bicarbonate (200 mL, 0.5 mol.L^{-1}, 16 h, room temperature)	Exchangeable, weakly bound P
Step 2	Sodium hydroxide (200 mL, 0.1 mol.L^{-1},, 16 h, room temperature)	Iron an aluminum bound phosphate (Fe/Al ~ P)
Step 3	Hydrochloric acid (200 mL, 1 mol.L^{-1}, 16 h, room temperature)	Calcium bound phosphate (Ca ~ P)
Step 4	Hydrochloric acid (50 mL, 12 mol.L^{-1}, in a 20 min water bath at 80 °C)	Soluble organic phosphate (SOP, Porg-acid)

of BBA_L is 0–2 mm. Thus, the absolute density of BBA_R and BBA_L varies from 2.88 ± 0.03 g/cm^3 to 2.65 ± 0.04 g/cm^3, respectively. The specific surface BET of BBA_R was about 0.9 ± 0.04 m^2/g, while the apparent density of BBA_L was about 1.81 ± 0.02 m^2/g. In all the experimental tests, the two BBA_S were used as reactive filters without any physical (crushing) or chemical pretreatment to treat the WWTP.

The results obtained showed a different chemical composition between the two BBA_S for the following elements: SiO_2, CaO, MgO, P_2O_5. The chemical composition of SiO_2 and CaO is significantly different between the BBA_S. Indeed, the mass percentage of CaO in BBA_R is 27.7% higher than in BBA_L. On the other hand, the SiO_2 content is lower in the BBA_R by 46.63% compared to BBA_L. The leaching results revealed that Cr and Mo were the most abundant MTEs in BBA_S, and exceeded the limit values for landfills (inert) and should be considered. (Table 3).

Batch test

Influence of initial concentration and contact time on P removal

The P-removal efficiency using synthetic wastewater, for both filters, is shown in Fig. 2 (BBA_R (a) and BBA_L (b). An increase in the percentage removal of P for the different concentrations (5, 10, 20, 50, 100 mg P/l) is clearly observed with time until equilibrium was reached for both BBA_S (Fig. 2a, b). Furthermore, the percentage of P removal at time t increases strongly with increasing initial P concentration in the BBA_R (Fig. 2a). The P adsorption capacity in BBA_L surprisingly shows a different pattern (Fig. 2b) than that observed for the removal rate for BBA_R. The BBA_L shows a high P removal capacity at low initial concentrations 5 mg P/l (100% after 7 days) compared to the BBA_R (52.8% after 7 days). However, the percentage P removal of

Table 3 Concentration of metallic and metalloids trace elements in BBA_R and BBA_L

Chemical composition by XRF	BBA_R (wt.%)	BBA_L (wt.%)	Metallic and metalloids trace elements (MMTE)	BBA_R (mg.kg^{-1})	BBA_L (mg.kg^{-1})
SiO_2	38.71	85.34	As	< 0.11	< 0.11
Al_2O_3	4.16	2.83	Ba	3.87 ± 0.05	2.05 ± 0.03
MgO	2.99	0.5	Cd	< 0.01	< 0.01
Fe_2O_3	2.57	1.14	Cr	0.91 ± 0.12	0.76 ± 0.09
CaO	30.36	2.66	Cu	0.51 ± 0.08	0.02 ± 0.01
Na_2O	0.81	0.54	Mo	0.68 ± 0.11	0.09 ± 0.03
SO_3	0.25	0.25	Ni	< 0.047	< 0.047
TiO_2	0.33	0.17	Pb	0.09 ± 0.02	0.03 ± 0.02
MnO	0.39	0.13	Sb	< 0.057	< 0.057
SrO	0.11	***	Se	< 0.08	< 0.08
BaO	0.13	***	Zn	1.71 ± 0.2	0.01 ± 0.01
P_2O_5	2.52	0.23	pH	12.1 ± 0.2	11.3 ± 0.2
K_2O	9.4	0.54	Conductivity (µS/cm)	2900 ± 63	490 ± 16

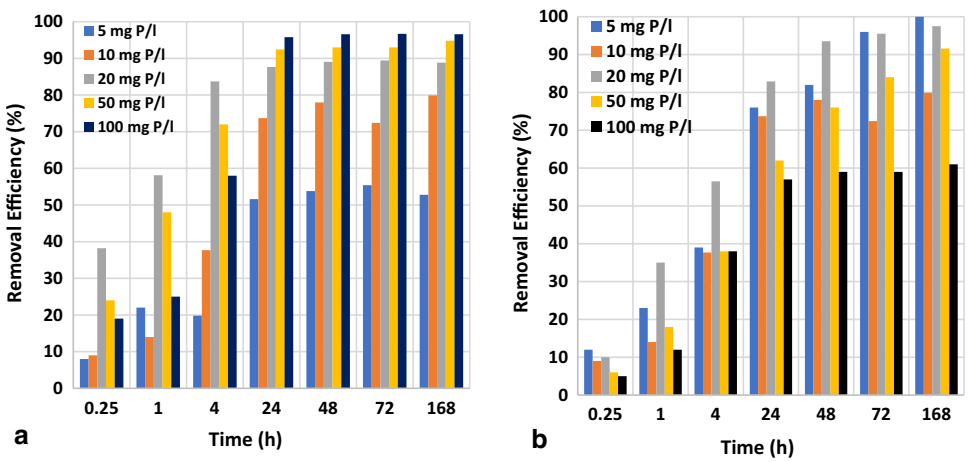

Fig. 2 P-removal efficiency using synthetic wastewater, for both filters (BBA_R (**a**) and BBA_L (**b**))

BBA_L (61% after 7 days) is lower compared to BBA_R (96.8% after 7 days) at higher initial concentrations 100 mg P/l. The adsorption has two stages: in the first minutes of the experiment, the sorption was rapid and thereafter the adsorption rate decreased until equilibrium was reached. The equilibrium time clearly depends on the initial P concentration and the reactive filter used, equilibrium is reached in about 4 h for low concentrations (5, 10, 20 mg P/l) and 24 h for higher concentrations (50 and 100 mg P/l), these results are valid whatever the BBA_S or the synthetic solution used (synthetic wastewater or real wastewater).

The rapid adsorption of P at the start of the experiment may be explained by the high number of available sorption sites; the adsorption rate decreases quite rapidly with time (after 24 h). Several hypotheses are possible to explain this result (i) the relatively high initial concentration in solution combined with attractive forces between phosphate in solution and ions already adsorbed on the solid surface, (ii) the progressive decrease of the number of available sorption sites with time and (iii) the progressive saturation of the external sorption sites of the BBA_S and the adsorption process of P in the internal pores which decreases the sorption rate. Similar results have been reported in previous studies for the adsorption of P on a double lamellar calcium iron hydroxide (Wu et al. 2012) and an iron (III) chromium (III) hydroxide (Namasivayam et Prathap 2005). Interestingly, the P removal percentages at 100 mg P/l are less than 100% which helps to determine the maximum P adsorption capacity for these two BBA_S.

Influence of water quality on P removal

Figure 3 presents the P-removal efficiency using real wastewater, for both filters (BBA_R (a) and BBA_L (b)). As shown in Fig. 3, the composition of the solution has an impact on the capacity of P removal by the reactive filters. Regardless of the initial concentration, the BBA_R and BBA_L immersed in the real wastewater solution (Fig. 3a, b) trapped about 40% more P in the first few hours of reactions than those in synthetic wastewater (Fig. 2a, b). The largest discrepancy was between the synthetic wastewater solution and the real wastewater, which contains the highest concentration of calcium promoting the precipitation of hydroxyapatite on the reactive filter surface as already reported by (Bowden et al. 2009). According to the pH, Ca^{2+} and P concentration of the solution, several Ca-P precipitates can be formed: tricalcium phosphate (TCP), amorphous calcium phosphates (ACP), dicalcium phosphate (DCP) and hydroxyapatite (Valsami-Jones 2001). In general, this indicates that the use of more calcium-rich water will allow for more efficient P scavenging. Using real wastewater doped with different initial P concentrations, P removal efficiencies increased (from 20 to 40%) as a function of increasing reaction time and initial P concentration for BBA_R. Similarly, to BBA_L, P removal efficiencies were still above 90% for low concentrations (5, 10 and 20 mg P/l), and above 60% for higher initial concentrations (50 and 100 mg P/l). The decrease in P concentrations was observed with a decrease in Ca^{2+} concentrations of the solutions (from 183 to 122 mg Ca^{2+}/l) and pH values from 12.11 to 9.8 and from 11.54 to 10.32 for BBA_R and BBA_L, respectively. This seems to confirm that the primary mechanism of P removal was HAP precipitation.

However, the removal capacity of P by BBA_R remains always more important than BBA_L; this is explained with the important specific surface of BBA_R (1.81 ± 0.01 m^2/g) compared to BAA_L (0.90 ± 0.05 m^2/g), as well as the chemical composition (BBA_R richer in calcium than BBA_L).

P-removal capacity (PRC)

The PRCs of BBA_R and BBA_L at 1 and 7 days are presented in Fig. 4. The PRC of BBA_R and BBA_L was determined at a low dose of adsorbent (10 g) for which the removal of P from the solution was not complete over the concentration range studied. The sorption of P on BBA_R and BBA_L is

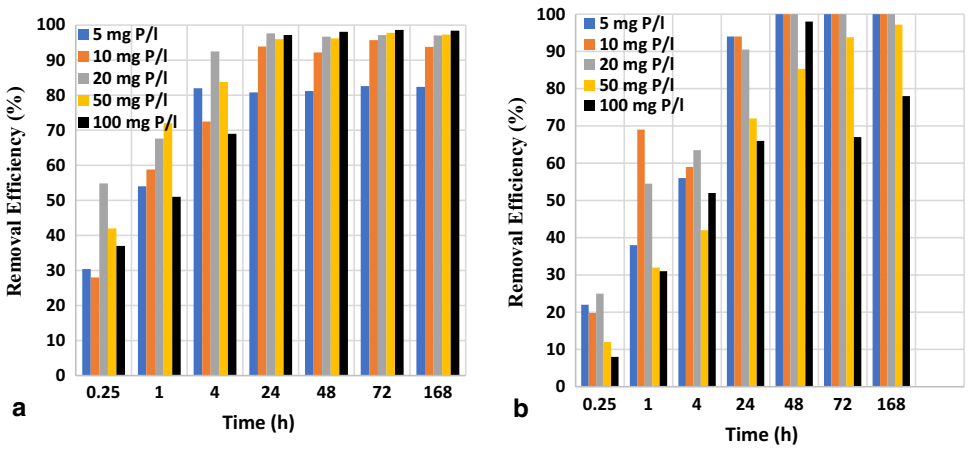

Fig. 3 P-removal efficiency using real wastewater, for both filters (BBA_R (**a**) and BBA_L (**b**))

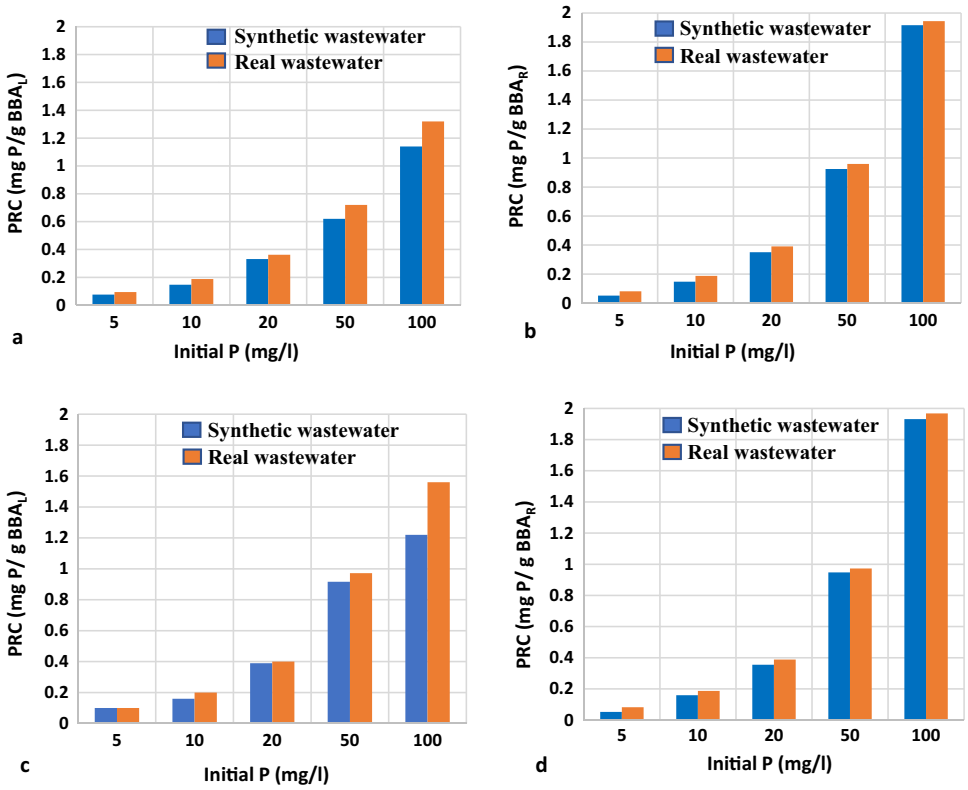

Fig. 4 Mean PRCs after 1 (**a**, **b**) and 7 (**c**, **d**) days of P removal from synthetic wastewater and real wastewater

clearly different depending on the solution used (synthetic wastewater or real wastewater).

The PRC for BBA_L, as in most of the literature, shows a saturation point beyond which increasing the reaction time (1 and 7d) does not result in a significant increase in the sorption capacity of P (Fig. 4a, c) (Boeykens et al. 2017). On the contrary, the PRCs obtained for BBA_R do not show a saturation level, which does not allow to evaluate the maximum sorption capacity on the basis of PRC calculation. While infrequent, such behavior has already been reported in the literature during studies on the sorption of P by several materials used in engineered wetlands such as bauxite, limestone, zeolite, expanded clay aggregate (Drizo et al. 1999) or slag (Xue et al 2009). The sorption capacity varies as follows: $BBA_R > BBA_L$. A possible explanation for the higher reactivity of BBA_R could be the higher specific surface area than BBA_L. The variations of the measured PRC values confirm that this quantity is significantly dependent on the initial concentration of P. Indeed, a variation of a factor of 20 Ce, this one (from 5 to 100 mg P/l) induces an almost equivalent variation of the value of PRC passing from 0,1 to 1,22 mg P/g BBA_L in synthetic wastewater and from 0,1 to 1,56 mg P/g BBA_L in real wastewater. Also, the PRC value is increasing from 0.05 to 1.93 mg P/g BBA_R in synthetic wastewater and from 0.08 to 1.96 mg P/g BBA_R in real wastewater.

The PRC increases with the concentration of P at equilibrium (Ce). According to the classification of (Limousin et al. 2007), this type of appearance suggests that adsorption proceeds by progressive occupation of the available sites until their saturation, i.e., establishment of the monolayer. This observation agrees with previous studies carried out on bauxite and a mixture of sand and dolomite (Drizo et al. 1999) (Prochaska et Zouboulis 2006). According to these authors, when P adsorbs specifically on a surface, the electrical charge of the surface increases and the reaction with an additional P molecule becomes more limited. The maximum adsorption capacity value (PRC_{max}) determined from Fig. 4 is 1.96 mg P/g BBA_R and 1.56 mg P/g BBA_L in $WWTP_S$.

The maximum adsorption capacity for both BBA_S is higher than that determined for hydroxyapatite, which is 0.41 mg/g for a P concentration of 150 mg P/l (Bellier et al 2006). It should be noted that hydroxyapatite has already been used for real wastewater P removal on a pilot scale (Molle et al 2003). This PRC_{max} value for both BBA_S is obtained by varying the P concentration up to 100 mg P/l. Similar results have been previously reported in studies related to P adsorption on a mixture of iron hydroxide and eggshell waste (Mezenner et Bensmaili 2009), lanthanum-doped activated carbon fibers or a mixed Fe (III) and Cr (III) hydroxide (Namasivayam et Prathap 2005). Yet the PRC value obtained for an initial phosphate ion concentration of 5 mg P/l was 0.08 mg P/g BBA_R. Thus, it is clear that increasing the initial concentration results in an increase in sorption by a factor of 25 for BBA_R and a factor of 16 for

BBA_L. However, such experimental conditions of P concentration (100 mg P/l) do not reflect the conditions encountered in real wastewater, i.e., ion concentrations between 2 and 8 mg P/l (Deronzier et Choubert 2004).

Particle size and specific surface effect on P removal

One of the most important parameters for the sorption capacity of a material is the specific surface area. The larger the specific surface area, the higher the adsorption capacity. It is possible to observe that the granulometry has a very important impact on the P removal capacity of the material. The contact surfaces, more important for the finer materials, thus make it possible to increase the dissolution of CaO, and thus a possible precipitation while supporting the accessibility of the reaction sites.

Overall, the P removal performance of both BBA_S seemed to be related to the increase in CaO content. However, the granulometry of the two BBA_S being an index of the specific surface, confirms that this parameter has a very significant impact on the capacity of P elimination by adsorption on the surface of the material.

Although the comparison of the two BBA_S physical properties on P removal is not straightforward, a correlation between particle size and specific surface area for P removal is clearly observed on the initial phase of the reaction. As shown in Figs. 2, 3 and 4, the BBA_L with a compact particle size between 0 and 2 mm, having higher removal capacity when the concentration of P was relatively high (5 mg P/l, 10 mg P/l and 20 mg P/l), adsorbed up to 40% more than the BBA_R with a diameter of 0–20 mm at these concentrations. With increasing P concentration in the medium as well as increasing reaction time, CaO dissolution becomes more important and favoring Ca-P (HAP) precipitation rather than adsorption to the surface. The particle size, and thus the reaction surface area involved, may have an impact on the apparent reaction rates and the mechanism of P entrapment.

In contrast to the BBA_L filter, the BBA_R large filter showed significantly high values for P removal (> 95% for the 50 mg P/l and 100 mg P/l concentrations). This suggests that the removal of P at higher concentrations (50 mg P/l and 100 mg P/l) is mainly related to the filter reagent composition and reaction time, and the main mechanism was HAP precipitation.

According to the present study, during the first hours of reaction and at lower P concentrations in the reaction medium (5 mg P/l, 10 mg P/l and 20 mg P/l), the smaller the material particle size, the P removal mechanism is achieved by adsorption to the surface. With increasing reaction time, and at higher P concentrations (50 mg/P and 100 mg P/L), P removal seems to be related to the increase of CaO dissolution in the medium followed by HAP precipitation. The study by Barca et al. 2012 confirms this hypothesis.

In addition, the measured specific density of BBA_R (2.88 $g.cm^{-3}$) is higher than BBA_L (2.65 $g.cm^{-3}$). Note that the higher density for BBA_R is related to its Fe_2O_3 content. This mineral is the heaviest in the material with a density of 5.24 $g.cm^{-3}$. Therefore, the BBA_R has a higher density than BBA_L.

Columns test

pH evolution

The pH measured at the inlet and outlet of the columns over time is presented in Fig. 5. The pH (pH of the real wastewater solution doped at a concentration of 30 mg P/l) at the inlet was constant when the synthetic effluent was fed to the real wastewater (8.06 ± 0.2). The maximum threshold of the effluent discharge standard to the receiving environment is defined by a red line. French regulations require a pH at the

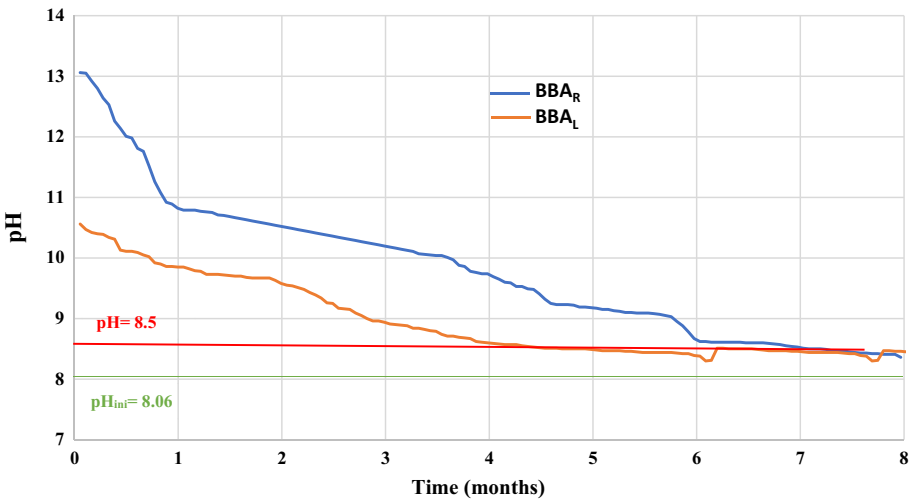

Fig. 5 Evolution of effluent pH at the outlet of the BBA_R and BBA_L columns as a function of time (maximum discharge standard represented by the red line)

outlet of a real wastewater treatment plant of between 5.5 and 8.5. However, this parameter is well above the discharge limit for both BBA_S.

An increase in outlet pH is observed during the first hours of real effluent feeding for both BBA_S. Then, a decrease of the outlet pH is observed as a function of time on all the columns during the whole experimental period. Overall, the pH at the outlet of the BBA_R column (pH = 13.06 at t0) is maintained higher than on the BBA_L column (pH = 10.4 at t0). Also, the pH value at the outlet is higher than 10 over a period of 3.7 months for BBA_R and 23 days for BBA_L. This study shows a strong reactivity of BBA_R compared to BBA_L characterized by an increase of the pH of the effluent from the reactive filters above an estimated temperature of 22 °C. However, the pH at the outlet of BBA_R and BBA_L was 13.06 and 10.4, respectively, during the first hours of reaction and tends to decrease over time to values between 8.7 and 8.5 after 8 months of feeding. The origin, the granulometry and the composition of the material had then an influence on the pH parameter.

This increase in pH, relative to P-Ca precipitation at the outlet of the reactive filters of both BBA_S, has also been reported in the literature (Weber et al, 2007) (Bird et Drizo 2010). On the other hand, the use of reactive filters (BBA_L) does not show an increase in pH at the outlet as for the reactive filter (BBA_R) in the first months of feeding, which can certainly be related to the manufacturing process, the composition and the calcium form included in the material. The pH values measured at the outlet of the columns as a function of time respect the standards for real wastewater discharge in France after 8 months of feeding, i.e., $5.5 \leq pH \leq 8.5$. To buffer the pH increase, some authors propose the use of methods such as aeration (Vohla et al. 2011) or CO_2 injection (Claveau-Mallet et al, 2012). The use of a buffer tank at the outlet of the reactive filter allowing the decrease of pH through the diffusion of atmospheric CO_2 is also considered.

Ca^{2+} concentration evolution

Figure 6 shows the evolution of the cumulative concentration of Ca^{2+} ions in solution as a function of time for an initial P solution at 30 mg P/l. The calcium concentration of the inlet effluent was 183 ± 9 mg Ca/l. Nearly zero values of cumulative calcium at the outlet of the BBA_R and BBA_L reactive filters are observed during the first days of the experiment (Fig. 6). This result shows an increased calcium consumption with BBA_R and BBA_L, which can certainly be related to the P purification performance. Then an increase in cumulative calcium is observed over time. The release of calcium at the exit of the reactive filters is more important for BBA_L than for BBA_R during the 8 months of the experiment, confirming the reactivity of BBA_R and the consumption of calcium to form Ca-P precipitates. This increase in Ca^{2+} ion concentrations at the exit of the column could be attributed to the progressive saturation of the surface sites with calcium phosphate by limiting the precipitation of additional solid compounds (HAP) on the surface of BBA_S.

The release of calcium from BBA_L and BBA_R significantly influenced the alkalinity of the aqueous solution (pH > 10) at the start of the experiment. Although pH values and Ca^{2+} concentrations represent important parameters in the precipitation of calcium phosphate, the formation of this precipitate is indicated in reaction (3):

$$5Ca^{2+} + 3PO_4^{3-} + OH^- \rightarrow Ca_5(PO_4)_3(OH) \downarrow \quad (4)$$

As calcium concentration increased in the aqueous phase, a decrease in pH over time was also observed (Fig. 5). This observation confirms the reaction between Ca^{2+} ions, P and OH^- to form $Ca_5(PO_4)_3(OH)$ precipitates as a major mechanism for P removal (Yamada et al. 1986) (Blanco et al. 2016). However, the increase in Ca^{2+} concentration can be explained by the decrease in surface sites with time for (HAP) precipitation, thus the relatively high accumulation

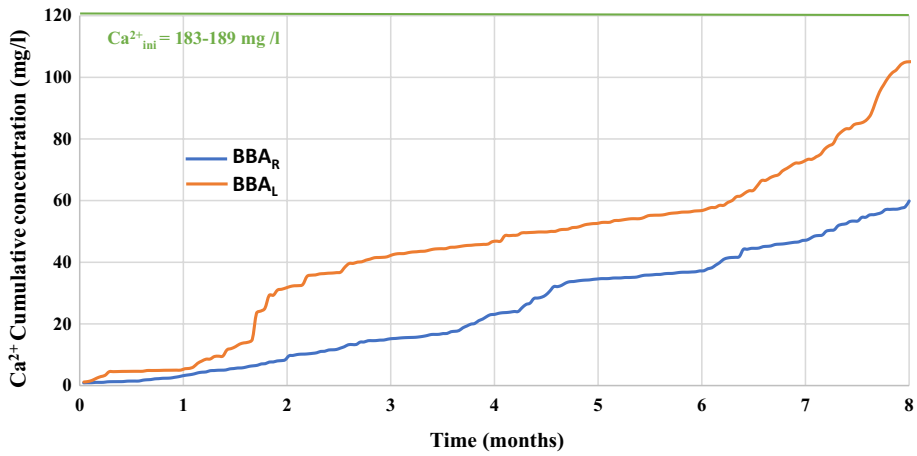

Fig. 6 Cumulative $Ca.^{2+}$ concentration in the effluent versus time for BBA_R and BBA_L (P solution at 30 mg P/l, real wastewater)

of Ca^{2+} ion from real wastewater that does not participate in P removal in the columns.

P concentration evolution

The results of the monitoring of the cumulative P evolution versus time of BBA_R and BBA_L are reported in Fig. 7. The P concentration of the inlet effluent was constant over time. The input concentration over all eight months was 30 ± 0.5 mg P/l. Firstly, it is proposed to compare the physical–chemical parameters measured on the two columns. In general, the P removal efficiency on the columns is directly linked to two parameters: the pH and the calcium concentration. The results obtained show a significant removal of P throughout the treatment period, which is relatively strong during the first four months of the experiment. Both BBA_S contain iron, calcium, aluminum and magnesium oxides, which probably explains the high P removal in agreement with previous experiments performed in batch (Arias et al. 2001; Vohla et al. 2011).

The variation of the P concentration at the column outlet for BBA_R and BBA_L is to be related for the same reasons as those mentioned during the pH monitoring: the influence of the Ca^{2+} and OH^- concentration, the type of material and the granulometry used. The removal efficiency of both filters was 100% during the first four months. Then, the efficiency decreased as a function of time until the material was saturated with P. In addition, the finer particle size filter (BBA_L 0–2 mm) had a lower average total P removal rate (79%) than the BBA_R 0–20 mm filter (91.5%), which is inconsistent with the high specific surface area of BBA_L (Drizo et al. 1999; Prigent 2013); P removal is mainly related to the composition of the BBA_S. The adsorption capacities (Q_C) calculated for the 960 days (8 months) of testing for both filters are ~ 4.15 and 9.72 g P/kg for BBA_L and BBA_R, respectively.

The particle size (0–20 mm) of BBA_R has a higher exchange surface than BBA_L (0–2 mm) used in the second column. As a result, the reactivity of BBA_R was characterized by higher pH (Fig. 5) and higher calcium ion release (Fig. 6) (Comeau et al. 2006) compared to BBA_L. The accumulation capacity of P in BBA_R is the highest at the term of the experimental following and reaches 9.72 g $P.kg^{-1}$ of material without the output concentration exceeding 0.5 mg P/L during the first 5 months. Under similar operating conditions, according to (Claveau-Mallet et al 2012), Canada 5–10 mm FAE slag accumulates a minimum of 6.2 g P/kg1 of material. Even at this level of accumulation, about 0.9 times lower than our study, no increase in P concentration at the column outlet was observed during the first 5 months. It is also important to mention the calcium concentration of the real effluent is lower than in our study (151 mg Ca/l), which most probably contributes to optimize the P treatment. The results obtained in this study respect the limit values and daily flows of the pollutants in France according to the regulation of the discharges and emissions of the classified installations for the environmental protection.

We notice that the Ca^{2+} concentrations increase with time at the column outlet of the BBA_L and BBA_R. The P concentrations are almost null in the first months for the two BBA_S, reflecting abatement rates of 100% for an initial concentration (30 mg P/L). Despite the different physical–chemical properties, a correlation between Ca^{2+} and P concentrations at the column outlet was evident, and the precipitation of HAP on the surface of the material seems to be the main mechanism of P removal for both BBA_S.

Our study demonstrates that BBA_R and BBA_L have a P accumulation capacity comparable to other column studies (Drizo et al. 1999; Comeau et al. 2006; Claveau-Mallet et al. 2012). The P accumulation capacity of the columns ranged from 4.15 to 9.72 g P/kg material after 8 months of experimentation for BBA_L and BBA_R, respectively. (Drizo et al. 1999) observed a saturation of the Canadian EAF slag from 3.65 g P/kg material with a stay time in the column of 24 h. However, the P input concentration of

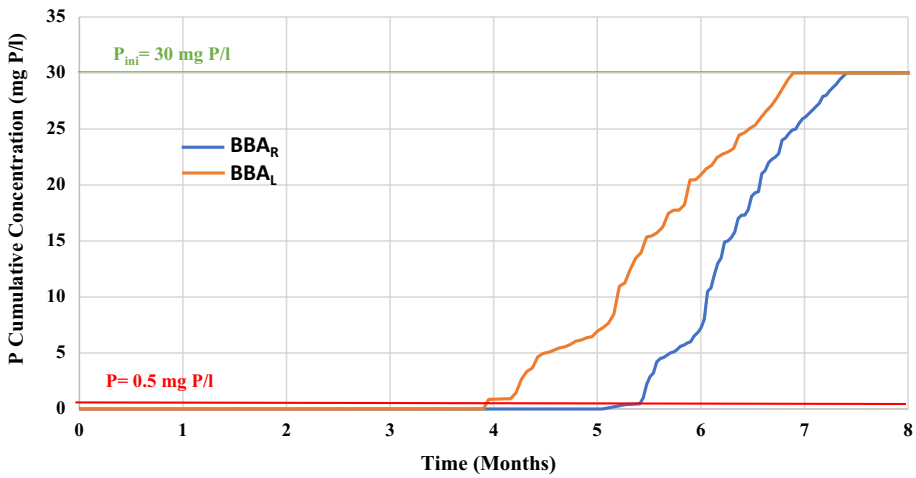

Fig. 7 Evolution of the P concentration versus time at the outlet of the BBA_R and BBA_L columns (PO_4-P solution at 30 mg P/l, real wastewater)

350–400 mg P/L (up to 15 times higher than in our study) and the physical–chemical properties of the material have certainly led to this difference in P accumulation. Indeed, the P concentration of the input effluent partly conditions the P-Ca (HAP, OCPs, TCPs, DCPs, etc.) and/or P-Fe, P-Al reaction mechanisms and thus the P accumulation capacity of the reactive material (Molle et al 2003). Many studies agree that the main mechanism of P removal in fly ash and bottom ash is a process of adsorption and precipitation (HAP) on the filter (Molle et al. 2003; Vohla et al. 2011; Johansson Westholm 2006). However, the higher the specific surface area of the material, the greater the adsorption and the more the dissolution of the material will be favored (Molle et al. 2012). Therefore, the granulometry, thus the specific surface area, is an important parameter to consider.

Our results demonstrate that Ca-rich alkaline filter materials are indeed effective and inexpensive filter materials for P removal from real wastewater. The only potential problem with the use of Ca-rich alkaline material is the unintentionally high pH (> 11) of the treated water. However, (Liira et al. 2009) showed that treated water can be effectively neutralized to pH 7–8 using a peat filter bed installed after the hydrated ash filter.

Characteristics of the reagent filter

X-ray diffraction (XRD)

The X-ray diffractograms of the BBA_R and BBA_L samples are shown in Fig. 8. The BBA_R consists of four main minerals well crystallized. These include quartz (SiO_2) and silicate minerals: akermanite Ca,Na,Mg,Fe(Si_2O_7), silicate calcium ($CaSiO_3$) and potassium aluminum silicate ($K(AlSiO_4)$), together with the presence of calcite and a phosphate phase (ferrowylliete ($Na_2FeAl(PO_4)_3$). However, quartz is the only mineral phase detected for BBA_L. The presence of these mineral phases agrees with the elemental chemical composition of the two slate BBA_S reported in Table 2.

After 8 months of operation of the filters (BBA_R or BBA_L) in columns, precipitates covering the surface of the BBA_S were analyzed by XRD. Figure 8 indicates the probable presence of hydroxyapatite (HAP) crystals growing on the surfaces of the BBA_S, as suggested by the slopes in correspondence of the characteristic HAP peaks. The results confirmed the presence of $CaCO_3$ (calcite) crystals and calcium (Ca^{2+}) covering the BBA_R surface, as indicated by the position of the peaks. This result is evidence that P in real wastewater was co-precipitated with calcium on the

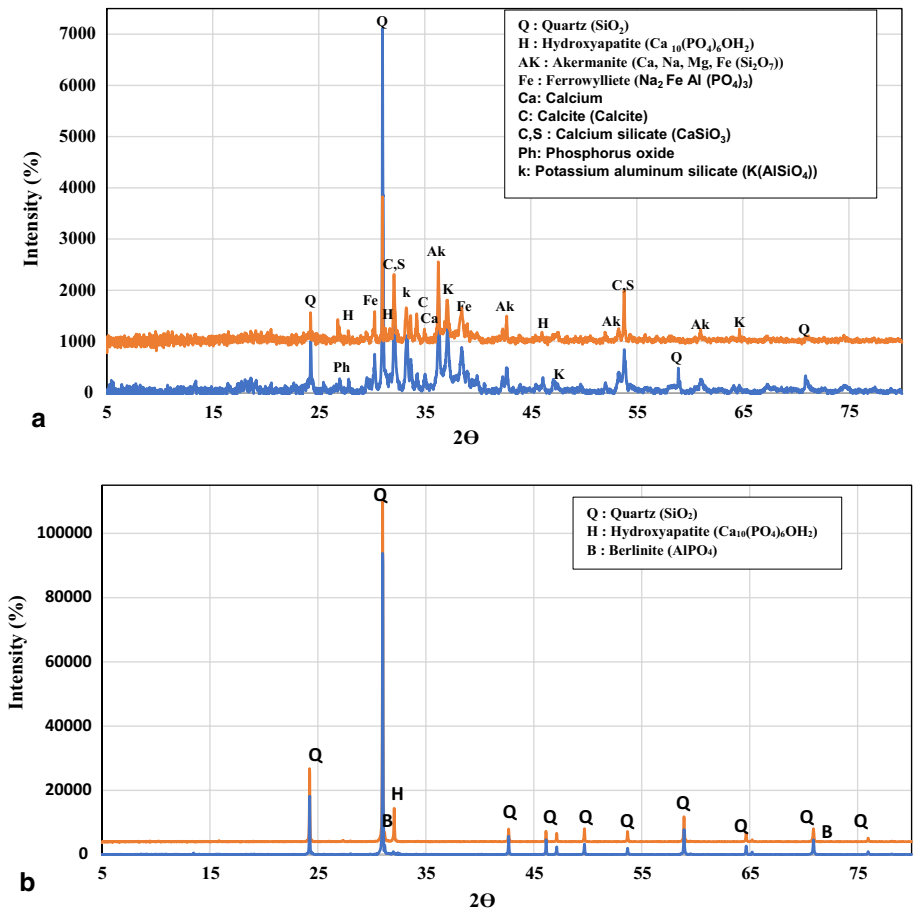

Fig. 8 X-ray analysis of BBA_R **a** and BBA_L **b** before and after 8 months of dephosphatation

surface of BBA_R and calcium in real wastewater to form HAP ($Ca_{10}(PO_4)_6OH_2$) (Yan et al. 2014) which was verified by XRD analysis, while the calcium existing in BBA_R was found as calcite ($CaCO_3$). The column results showed a high P trapping potential by BBA_R compared to BBA_L; it implied that the high calcium content in BBA_R to increase the phosphate adsorption associated with the ability of calcium to form HCO_3-Ca-HPO_4 on carbonate sites (Haddad et al. 2015). In addition, the study by (Krogstad et al. 2005) claimed that a material with high CaO or $CaCO_3$ content would remove more P than a material with low calcium content.

However, two phosphate phases were detected after 8 months of operation of BBA_L as reactive filters. Since BBA_L is less rich in calcium than BBA_R, the intense HAP peak observed may be explained by several hypotheses: calcium ions and P present in the real wastewater precipitated on the surface of BBA_L (i), the formation of insoluble phosphate precipitates at the beginning of the reaction (berlinite $AlPO_4$), then a cationic exchange between calcium and aluminum is established with the increase of the calcium concentration (ii). The presence of berlinite ($AlPO_4$) shows that several mechanisms of P sorption are involved.

(Valsami-Jones 2001) suggests that Ca-P initially precipitates in an amorphous form and then initiates recrystallization into a more thermodynamically stable HAP. It is coherent with the conclusions of (Bowden et al. 2009) who found that a series of Ca-P minerals are present on the surface of BOF slag during water filtration, and these minerals develop in progression from less stable forms to the more stable HAP. The "recrystallized" HAP crystals can then provide seeds for further HAP crystallization (Kim et al. 2006). These other mechanisms of P trapping by co-precipitation with $CaCO_3$ and HAPs on seeds may have a significant effect on the long-term P removal efficiency of the filter.

Scanning electron microscopy, energy-dispersive x-ray spectrometer (SEM–EDS)

In an effort to comprehend the surface properties and adsorption/precipitation/crystallization mechanisms of P-Ca, the morphology of BBA_R and BBA_L before and after 8 months of operation as reactive filters was examined by scanning electron microscopy (Fig. 9). Images obtained at 20 µm magnification (Fig. 9a, b) reveal a morphology characteristic of a dense structure that agrees with the relatively high specific surface area of BBA_R compared to BBA_L determined by BET.

Before the experiments, the surface of BBA_R was mainly composed of Si, Al, Ca and O (Fig. 9a). However, the surface of BBA_L is composed mainly of Fe and Si in the form of quartz (Fig. 9b). A P-rich iron/calcium compound was visualized by SEM on the surface of the iron oxyhydroxides of BBA_R and BBA_L (Fig. 9c, d) on the surface. Comparatively between the EDX analyses in Fig. 9(a, b) and Fig. 9(c,d), the amount of accumulated P is higher on the surface of BBA_R and BBA_L after the 8 months (Fig. 9c, d). SEM–EDX and XRD analyses confirmed the presence of oxygen, phosphorus, calcium, iron as a finely distributed crystalline layer covering the surface of BBA_R and BBA_L, indicating the

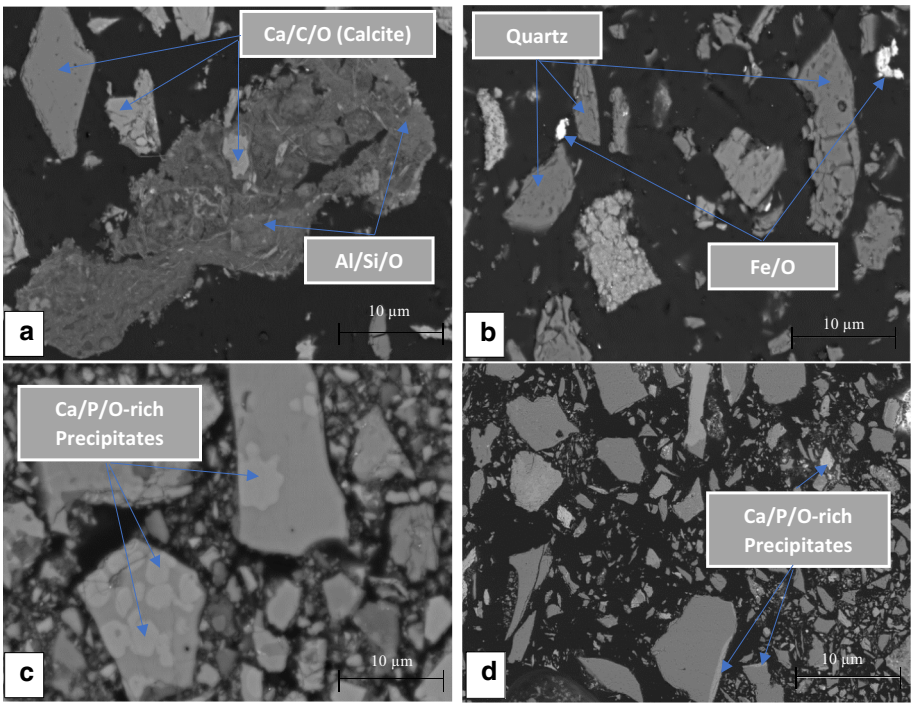

Fig. 9 SEM observations and EDX analyses. **a** Surface of BBA_R before P removal; **b** surface of BBA_L before P removal; **c** surface of BBA_R after P removal; **d** surface of BBA_L after P removal

crystallization/precipitation of HAPs. Kim et al. (2006) observed a similar form of HAP crystals precipitated on the surface of EAF and BOF slag.

SEM–EDX analyses also showed the presence of crystals mainly consisting of C, O and Ca (calcite $CaCO_3$), These analytical results seemed to indicate the co-precipitation of Ca-P with $CaCO_3$, the $CaCO_3$ crystals providing adsorption sites for the Ca-P precipitates. This was consistent with our XRD results which revealed the presence of calcite in the BBA_R prior to the experiments, then the precipitation of HAP after the 8 months of filter operation. The incorporation of P into the growing $CaCO_3$ crystals has been confirmed by several authors (House et Donaldson 1986) (Plant et House 2002) also allowing further reduction of P concentration in the solution. Other studies have noted the formation and precipitation of HAP_S on the surface of reactive filters based on hydrated and carbonated fly ash (Kaasik et al. 2008) (Liira et al. 2009), which is confirmed in the present study by the precipitation of Ca-P on the surface of BBA_R and BBA_L.

Several P removal mechanisms described by researchers in experiments performed at different scales, the mechanism of P immobilization in BBA_R and BBA_L seems to be as follows: (i) increase of Ca^{2+} and OH^- concentrations of solutions by dissolution of CaO from BBA_S, (ii) decrease of P, OH^- and Ca^{2+} concentrations of solutions by precipitation of HAP_S, (iii) crystallization and/or adsorption of HAP_S on the BBA_S surface (Liira et al. 2009) (Freeman et Rowell 1981) (Kõiv et al. 2010).

The sequential extraction of P

Figure 10 shows the results of sequential P extractions for BBA_R and BBA_L. 6.60 g P/kg and 0.39 g P/kg were totally extracted from BBA_R and BBA_L, respectively, before use as filter reagents. These results confirm that BBA_R is richer in P than BBA_L, as demonstrated in the XRF results (Table 1). The P in BBA_R was mainly bound to calcium (F3 = 51%) and in the stable residual compounds (F4 = 47%); however, in BBA_L the P was distributed between the exchangeable fraction (F1 = 12% weakly bound), calcium (F3 = 75%) and the residual fraction (F4 = 14%).

After 8 months of operation of the BBA_R and BBA_L filters the amount of totally extracted P increased from 6.60 g P/kg to 14.34 g P/kg and from 0.39 g P/kg to 3.13 g P/kg for the BBA_R and BBA_L, respectively, indicating P accumulation on both filters. A significant increase in the fraction of weakly bound P and Ca-bound P was observed when BBA_R was used as the reactive filter, indicating the presence and formation of Ca-P precipitate on the filter surface as shown by the SEM results; thus, an increase in P in stable residual fraction confirms precipitation followed by recrystallization of Ca-P as HAP which is the most stable form. However, the major increase in BBA_L was observed for the weakly bound P fraction, the Al/Fe bound P fraction and the Ca bound fraction which seems to approve the XRF (BBA_L richer in Fe) and DRX (presence of hydroxyapatite and Berlinite $AlPO_4$) results.

The sequential extraction results in Fig. 10 show that the P bound to Fe and Al fractions was negligible compared to other P fractions in the BBA_R, and it is possible that the high pH (> 8.5) favored the precipitation and crystallization of HAP as reported by (Kim et al. 2006). According to Stumm and Morgan (1996) chemical equilibrium ratios of P in aqueous solution, the basic pH favors precipitation of Ca-P rather than adsorption onto Fe and Al hydroxides. The major mechanism when the pH is basic could be the formation of P-Ca (pH > 8.5) and the formation of P-Fe/Al when the pH is acid (pH < 8.5). Indeed, it has been highlighted in the literature (Fytianos et al, 1998; Streat et al 2008) that the adsorption of P on the surface of ferric oxides is favored for acid pH. The surface of the material is then positively

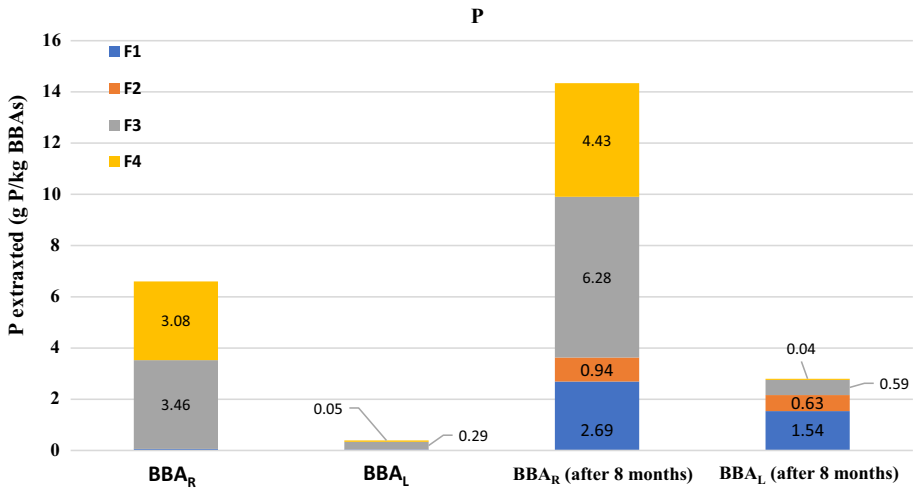

Fig. 10 P fractionation experiments: P fractions extracted from BBA_R and BBA_L before and after 8 months of filter operation. Average values from triplicates

charged which allows a strong attraction with negatively charged species.

The results of the P extractions indicated that approximately 7.75 g P/kg and 2.74 g P/kg were accumulated on BBA_R and BBA_L tested as reactive filters, respectively. However, the amount of P accumulated on both BBA_S from the P extractions was less than that based on the calculation of the adsorption capacity of each column (Qc). A similar difference has also been reported in other P removal studies with reactive filters (shell sand and Filtralite P®) with vertical flow (Søvik et Kløve 2005; Ádám et al. 2007). According to Ádám et al. (2007) this difference is attributed to the precipitation accumulation of Ca-P at the bottom of the filters that was not used for sequential extraction in the columns. Thus, the CaO content of both BBA_S resulted in higher hydration followed by carbonation (presence of $CaCO_3$ peaks in BBA_R (Fig. 8) in BBA_R, resulting in a decrease in pore size (Wang et al, 2010)). This decrease in pore size is expected to disfavor the homogeneous accumulation of Ca-P precipitate over the entire filter volume, explaining the difference between the P extractions and the calculation of the adsorption capacity of each column (Qc).

P removal mechanism

The general principle of real wastewater dephosphatation used in the present study, consists in the accumulation of P within a filter composed of either BBA_L or BBA_R which have a high chemical affinity for this element. It has been shown that the physical properties of the reactive filter are also important to consider. Indeed, its specific surface is a significant parameter, because the trapping mechanisms are surface phenomena. The particle shape, particle size and porosity will define the specific surface (Cucarella et Renman 2009).

Since the mechanisms acting within these filters are variable and not always well established, it is generally agreed to refer to sorption. The term refers to a combination of adsorption, ion exchange and precipitation (Cucarella et Renman 2009). Results from XRD, SEM–EDS and sequential extraction show that the three active elements for P sorption are iron (Fe), aluminum (Al) and calcium (Ca) (Johansson Westholm 2006). The P removal mechanisms by Fe and Al are quite similar, while the action of Ca is different.

For calcium-rich BBA_R, generally the dominant P removal mechanism was precipitation (Vohla et al. 2011). A study by Comeau et al. (2006) reports that electrostatic bonding to calcium-containing molecules is also possible, as shown in Fig. 11. Calcium found in the form of CaO, $CaSO_4$ or $CaCO_3$, will progressively solubilize to precipitate orthophosphate ions (Chen et al. 2015) The product formed is usually hydroxyapatite (Comeau et al. 2006).

Figure 11 illustrates the mechanism of orthophosphate scavenging by Ca^{2+} from CaO. The initial phase formed during the calcium phosphate precipitation depends on the physico-chemical characteristics of the solution, especially the alkaline pH. Once dissolved, Ca^{2+} ions, metal ions and phosphate ions present in the effluent will form complexes by nucleation. The Ca/P molar ratio has a direct consequence on the precipitation rate and on the amplitude of the reaction. For a Ca/P molar ratio of the solution of 1.67, the homogeneous precipitation becomes effective for a pH of 8.5–9. The calcium phosphate precipitate is present mainly on the surface of the two BBA_S where the calcite grains are located. This precipitate can be formed in place of calcite, which was shown by XRD (Fig. 8a). Nucleation and crystal growth are the limiting steps. Thus, HAP is most readily formed on reactive surfaces under super-saturated conditions (Cabanes 2006).

The solubility diagram of calcium phosphates presented by Cabanes (2006) shows that hydroxyapatite (HAP), of chemical composition $Ca_5(PO_4)_3(OH)$, is the compound which is thermodynamically the most stable and the most insoluble. However, the pH, temperature, calcium and P concentrations are all parameters affecting the nature of the precipitated phosphates. According to Comeau et al (2006), bottom ash also has the ability to precipitate atmospheric CO_2 into carbonates, which may also represent a limit on

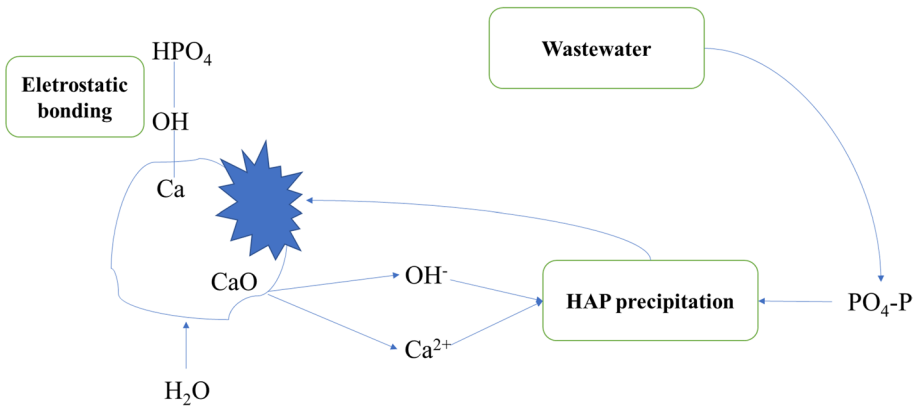

Fig. 11 Illustration of HAP precipitation mechanism

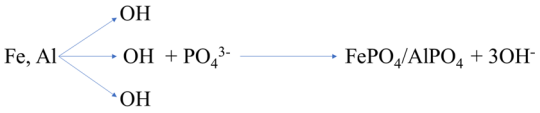

Fig. 12 Electrostatic attraction of a phosphate ion to a sesquioxide

their potential use. Competition may then occur between the calcium carbonates, HAP and other precipitates formed.

On the other hand, it has been shown that the forms of Fe and Al with the most affinity for P are the oxyhydroxides, also referred to as sesquioxides (KARAM 2012). Metal sesquioxides are composed of a compact assembly of oxygen and/or hydroxyl (OH^-) ions that contain metal ions in their octahedral cavity (Dubus 1997). Iron oxide (Fe_2O_3) and aluminum oxide (Al_2O3) are examples of sesquioxides. In wet environments, numerous studies have shown that oxyhydroxides may interact with phosphate ions by replacing one of their hydroxyl groups with an orthophosphate anion (Dubus 1997; KARAM 2012). The XRF compositional characterization showed both BBA_S contain significant amounts of Fe_2O_3 and Al_2O_3, and after the 8 months of dephosphatation, SEM–EDS and XRD results confirm the presence of Fe/Al-P precipitated phases (ferrowylliete (Na_2 Fe Al $(PO_4)_3$)) in the BBA_R and berlinite ($AlPO_4$) in the BBA_L.) Fig. 12 illustrates the described reaction.

Overall, P removal appears to improve with increasing CaO content, decreasing BBA_S size and increasing reaction time, most probably because the contact time between BBA_S and solution was lengthened, promoting CaO dissolution and Ca-P precipitation. The present study shows a difference in terms of scavenging mechanisms. While the major mechanism of P removal involves the precipitation/crystallization of calcium phosphate (P-Ca)/hydroxyapatite in the column, iron phosphate (P-Fe) nodules were certainly formed by adsorption and then by precipitation on the surface of the iron oxy/hydroxides present on the two BAA_S used as reactive filters. Interrogations still remain on the laboratory scale (Batch) as to the concomitance of the P-Ca/P-Fe reactions or on the predominance of an adsorption mechanism during the initial period of contact and of a precipitation mechanism when the contact time is longer.

Conclusion

This study was devoted to the comparison of P removal performance with two biomass bottom ash (BBA_S) as reactive filters, in batch and column reactors. The influence of origin, particle size, chemical composition, initial P concentration, CaO dissolution, water quality and pH on P removal performance was investigated for both BBA_S at laboratory scale.

The removal of P was first studied in a batch reactor. In particular, an increase of the removal rate was observed with an increase of the initial concentration and the contact time (7 days). The influence of different physicochemical parameters on P removal was clarified. In particular, it was observed, for both materials, a strong increase of the phosphorus removal capacity (PRC) when Ca^{2+}-rich real wastewater is used, to finally reach a constant maximum value when the removal rate is below 100%.

The study realized in column reactor reveals, in a most interesting manner, a low rate of clogging and pH values at the column outlet in agreement with the discharge standards after 8 months of experimentation. For an initial column inlet concentration of 30 mg P/l, maximum P removal capacities in the columns varied from 4.15 to 9.72 g P/kg after 8 months of experimentation for BBA_L and BBA_R, respectively. Furthermore, monitoring of Ca^{2+} ion concentrations and pH revealed the mechanism of P removal over time. Thus, the very low P concentration at the column outlet and at the start of the experiment increases with time. A correlation between P concentration and Ca^{2+} ion concentrations as a function of pH was established. The order of efficiency of the reactive filters is as follows: $BBA_R \geq BBA_L$ in agreement with the results obtained in a "batch" reactor.

The results of the different physical–chemical characterizations XRD, SEM–EDS and sequential extraction before and after the operation of the two BBA_S as reactive filters confirm that the removal of P from the real wastewater is realized with different trapping mechanism (adsorption, precipitation, etc.). However, the main mechanism occurs in three steps: (i) dissolution of CaO from BBA_S providing OH^- and Ca^{2+} ions and directly increasing the pH of the solution; (ii) precipitation of Ca-P on the filter surfaces at basic pH ($pH < 8.5$); (iii) accumulation and recrystallization of Ca-P in the form of HAP which is the most stable form.

Acknowledgements The authors wish to acknowledge technical contributions of the chemistry pole of Institut Mines-Télécom. This research did not receive any specific grant from funding agencies in the public, commercial or not-for-profit sectors.

Author's contribution All authors contributed to the study conception and design. Material preparation, data collection and analysis were performed by BB and YM-P. BB contributed in conceptualization, investigation, methodology, data curation, writing—original draft, writing—review & editing, validation, YM-P contributed to conceptualization, methodology, investigation, data curation, resources, writing—original draft, writing—review & editing, validation, supervision.

Funding The authors declare that no funds, grants or other supports were received during the preparation of this manuscript.

Data availability Not applicable.

Declarations

Conflict of interest The authors declare no competing interests. The authors declare that they have no known competing financial interests or personal relationships that could have appeared to influence the work reported in this paper. The authors have no relevant financial or non-financial interests to disclose.

Ethical approval The authors confirm that the manuscript has not been submitted to journal for simultaneous consideration and has not been previously published. Results collection, selection and processing performed personally. Authors' institution informed about this submission.

Consent to participate Not applicable.

Consent for publication Not applicable.

References

Ádám K, Krogstad T, Vråle L, Søvik AK, Jenssen PD (2007) Phosphorus retention in the filter materials shellsand and filtralite P®—batch and column experiment with synthetic P solution and secondary wastewater. Ecol Eng 29(2):200–208. https://doi.org/10.1016/j.ecoleng.2006.09.021

Akratos CS, Tsihrintzis VA (2007) Effect of temperature, HRT, vegetation and porous media on removal efficiency of pilot-scale horizontal subsurface flow constructed wetlands. Ecol Eng 29(2):173–191. https://doi.org/10.1016/j.ecoleng.2006.06.013

Arias CA, Del Bubba M, Brix H (2001) Phosphorus removal by sands for use as media in subsurface flow constructed reed beds. Water Res 35(5):1159–1168. https://doi.org/10.1016/S0043-1354(00)00368-7

Barca C, Gérente C, Meyer D, Chazarenc F, Andrès Y (2012) Phosphate removal from synthetic and real wastewater using steel slags produced in Europe. Water Res 46(7):2376–2384. https://doi.org/10.1016/j.watres.2012.02.012

De-Bashan LE, Bashan Y (2004) Recent advances in removing phosphorus from wastewater and its future use as fertilizer (1997–2003). Water Res 38(19):4222–4246. https://doi.org/10.1016/j.watres.2004.07.014

Bellier N, Chazarenc F, Comeau Y (2006) Phosphorus removal from wastewater by mineral apatite. Water Res 40(15):2965–2971. https://doi.org/10.1016/j.watres.2006.05.016

Bird SC, Drizo A (2010) EAF steel slag filters for phosphorus removal from milk parlor effluent: the effects of solids loading, alternate feeding regimes and in-series design. Water 2(3):484–499. https://doi.org/10.3390/w2030484

Blanco I, Molle P, de Miera LES, Ansola G (2016) Basic oxygen furnace steel slag aggregates for phosphorus treatment. Evaluation of its potential use as a substrate in constructed wetlands. Water Res 89:355–365. https://doi.org/10.1016/j.watres.2015.11.064

Boeykens SP, Piol MN, Legal LS, Saralegui AB, Vázquez C (2017) Eutrophication Decrease: phosphate adsorption processes in presence of nitrates. J Environ Manag 203:888–895. https://doi.org/10.1016/j.jenvman.2017.05.026

Bouzar B, Mamindy-Pajany Y (2022) Manufacture and characterization of carbonated lightweight aggregates from waste paper fly ash. Powder Technol Juin. https://doi.org/10.1016/j.powtec.2022.117583

Bowden LI, Jarvis AP, Younger PL, Johnson KL (2009) Phosphorus removal from waste waters using basic oxygen steel slag. Environ Sci Technol 43(7):2476–2481. https://doi.org/10.1021/es801626d

Cabanes F (2006) Déphosphatation des effluents : précipitation et valorisation du phosphore , 219

Chen T-H, Wang J-Z, Wang J, Xie J-J, Zhu C-Z, Zhan X-M (2015) Phosphorus removal from aqueous solutions containing low concentration of phosphate using pyrite calcinate sorbent. Int J Environ Sci Technol 12(3):885–892. https://doi.org/10.1007/s13762-013-0450-6

Claveau-Mallet D, Wallace S, Comeau Y (2012) Model of phosphorus precipitation and crystal formation in electric arc furnace steel slag filters. Environ Sci Technol 46(3):1465–1470. https://doi.org/10.1021/es2024884

Comeau Y, Brisson J, Chazarenc F (2006) Déphosphatation d'effluents piscicoles par marais artificiel et lit absorbant en série et par bioréacteur à lit mobile absorbant, 2006

Cordell D (2010) Sustainability Implications of Global Phosphorus Scarcity for Food Security, 241

Cordell D, White S (2015) Tracking phosphorus security: indicators of phosphorus vulnerability in the global food system. Food Secur 7(2):337–350. https://doi.org/10.1007/s12571-015-0442-0

Cucarella V, Renman G (2009) Phosphorus sorption capacity of filter materials used for on-site wastewater treatment determined in batch experiments–a comparative study. J Environ Qual 38(2):381–392. https://doi.org/10.2134/jeq2008.0192

Deronzier G, et Choubert J (2004) Traitement du phosphore dans les petites stations d'épuration à boues activées. Comparaisons techniques et économiques des voies de traitement biologique et physico-chimique. 2004, Document technique FNDAE, n°29. édition

Drizo A, Frost CA, Grace J, Smith KA (1999) Physico-chemical screening of phosphate-removing substrates for use in constructed wetland systems. Water Res 33(17):3595–3602. https://doi.org/10.1016/S0043-1354(99)00082-2

Dubus I (1997) La rétention du phosphore dans les sols: principe d'étude, modélisation, mécanismes et compartiments du sol impliqués. *Documents scientifiques et techniques- ORSTOM, Centre de Nouméa*

Esser D, Ricard B, Fernades N, Merlin G (2004) Physical-chemical phosphorus removal in vertical flow reed bed treatment plants. International conference on wetland systems for water pollution control. Avignon, France. 2004

Chazarenc F, Brisson J, Comeau Y (2007) Slag columns for upgrading phosphorus removal from constructed wetland effluents. Water Sci Technol 56(3):109–115. https://doi.org/10.2166/wst.2007.499

Freeman JS, Rowell DL (1981) The adsorption and precipitation of phosphate onto calcite. J Soil Sci 32(1):75–84. https://doi.org/10.1111/j.1365-2389.1981.tb01687.x

Fytianos K, Voudrias E, Raikos N (1998) Modelling of phosphorus removal from aqueous and wastewater samples using ferric iron. Environ Pollut 101(1):123–130. https://doi.org/10.1016/S0269-7491(98)00007-4

Haddad K, Jellali S, Jaouadi S, Benltifa M, Mlayah A, Hamzaoui AH (2015) Raw and treated marble wastes reuse as low cost materials for phosphorus removal from aqueous solutions: efficiencies and mechanisms. C R Chim 18(1):75–87. https://doi.org/10.1016/j.crci.2014.07.006

House WA, Donaldson L (1986) Adsorption and coprecipitation of phosphate on calcite. J Colloid Interface Sci 112(2):309–324. https://doi.org/10.1016/0021-9797(86)90101-3

Johansson Westholm L (2006) Substrates for phosphorus removal—Potential benefits for on-site wastewater treatment? Water Res 40(1):23–36. https://doi.org/10.1016/j.watres.2005.11.006

Kaasik A, Vohla C, Mõtlep R, Mander Ü, Kirsimäe K (2008) Hydrated calcareous oil-shale ash as potential filter media for phosphorus removal in constructed wetlands. Water Res 42(4–5):1315–1323. https://doi.org/10.1016/j.watres.2007.10.002

Karaca S, Gurses A, Ejder M, Acikyildiz M (2006) Adsorptive removal of phosphate from aqueous solutions using raw and calcinated dolomite. J Hazard Mater 128(2–3):273–279. https://doi.org/10.1016/j.jhazmat.2005.08.003

Karam A (2012) COMPTE RENDU DE RECHERCHE EN SCIENCE DU SOL

Karapinar N, Hoffmann E, Hahn HH (2004) Magnetite seeded precipitation of phosphate. Water Res 38(13):3059–3066. https://doi.org/10.1016/j.watres.2004.04.042

Kasprzyk M, Gajewska M (2019) Phosphorus removal by application of natural and semi-natural materials for possible recovery according to assumptions of circular economy and closed circuit of P. Sci Total Environ 650:249–256. https://doi.org/10.1016/j.scitotenv.2018.09.034

Kim E-H, Lee D-W, Hwang H-K, Yim S (2006) Recovery of phosphates from wastewater using converter slag: kinetics analysis of a completely mixed phosphorus crystallization process. Chemosphere 63(2):192–201. https://doi.org/10.1016/j.chemosphere.2005.08.029

Kõiv M, Liira M, Mander Ü, Mõtlep R, Vohla C, Kirsimäe K (2010) Phosphorus removal using ca-rich hydrated oil shale ash as filter material—the effect of different phosphorus loadings and wastewater compositions. Water Res 44(18):5232–5239. https://doi.org/10.1016/j.watres.2010.06.044

Korkusuz EA, Beklioğlu M, Demirer GN (2005) Comparison of the treatment performances of blast furnace slag-based and gravel-based vertical flow wetlands operated identically for domestic wastewater treatment in Turkey. Ecol Eng 24(3):185–198. https://doi.org/10.1016/j.ecoleng.2004.10.002

Kostura B, Kulveitová H, Leško J (2005) Blast furnace slags as sorbents of phosphate from water solutions. Water Res 39(9):1795–1802. https://doi.org/10.1016/j.watres.2005.03.010

Krogstad T, Sogn TA, Asdal Å, Sæbø A (2005) Influence of chemically and biologically stabilized sewage sludge on plant-available phosphorous in soil. Ecol Eng 25(1):51–60. https://doi.org/10.1016/j.ecoleng.2005.02.009

Li Y et al (2006) Phosphate removal from aqueous solutions using raw and activated red mud and fly ash. J Hazard Mater 137(1):374–83. https://doi.org/10.1016/j.jhazmat.2006.02.011

Liira M, Kõiv M, Mander Ü, Mõtlep R, Vohla C, Kirsimae K (2009) Active filtration of phosphorus on ca-rich hydrated oil shale ash: does longer retention time improve the process? Environ Sci Technol 43(10):3809–3814. https://doi.org/10.1021/es803642m

Limousin G, Gaudet J-P, Charlet L, Szenknect S, Barthès V, Krimissa M (2007) Sorption Isotherms: a review on physical bases, modeling and measurement. Appl Geochem 22(2):249–275. https://doi.org/10.1016/j.apgeochem.2006.09.010

Mandel A, Zekker I, Jaagura M, Tenno T (2019) Enhancement of anoxic phosphorus uptake of denitrifying phosphorus removal process by biomass adaption. Int J Environ Sci Technol 16(10):5965–5978. https://doi.org/10.1007/s13762-018-02194-2

Mezenner NY, Bensmaili A (2009) Kinetics and thermodynamic study of phosphate adsorption on iron hydroxide-eggshell waste. Chem Eng J 147(2–3):87–96. https://doi.org/10.1016/j.cej.2008.06.024

Molle P, Harouiya N, Prost-Boucle S, Morlay C, Esser D, Martin S, Besnault S (2012) Déphosphatation des eaux usées par filtres plantés garnis de phosphorites. Recommandations pour le développement de la filière. Recommandations pour le développement de la filière. https://epnac.irstea.fr, 2012

Namasivayam C, Prathap K (2005) Recycling Fe(III)/Cr(III) hydroxide, an industrial solid waste for the removal of phosphate from water. J Hazard Mater 123(1–3):127–134. https://doi.org/10.1016/j.jhazmat.2005.03.037

Molle P, Liénard A, Grasmick A, Iwema A (2003) Phosphorus retention in subsurface constructed wetlands: investigations focused on calcareous materials and their chemical reactions. Water Sci Technol 48(5):75–83. https://doi.org/10.2166/wst.2003.0285

Plant LJ, House WA (2002) Precipitation of calcite in the presence of inorganic phosphate. Colloids Surf A 203(1–3):143–153. https://doi.org/10.1016/S0927-7757(01)01089-5

Prigent S (2013) Optimisation du traitement de l'azote et du phosphore des eaux usées domestiques adapté aux filtres plantés de roseaux, 230

Prochaska CA, Zouboulis AI (2006) Removal of phosphates by pilot vertical-flow constructed wetlands using a mixture of sand and dolomite as substrate. Ecol Eng 26(3):293–303. https://doi.org/10.1016/j.ecoleng.2005.10.009

Song Y, Weidler PG, Berg U, Nüesch R, Donnert D (2006) Calcite-seeded crystallization of calcium phosphate for phosphorus recovery. Chemosphere 63(2):236–243. https://doi.org/10.1016/j.chemosphere.2005.08.021

Søvik AK, Kløve B (2005) Phosphorus retention processes in shell sand filter systems treating municipal wastewater. Ecol Eng 25(2):168–182. https://doi.org/10.1016/j.ecoleng.2005.04.007

Streat M, Hellgardt K, Newton NLR (2008) Hydrous ferric oxide as an adsorbent in water treatment. Process Saf Environ Prot 86(1):21–30. https://doi.org/10.1016/j.psep.2007.10.009

Stricker AE, et Heduit A (2009) Phosphore des eaux usées: état des lieux et perspectives, 55

Headley TR, Huett DO, Davison L (2003) Seasonal variation in phosphorus removal processes_within reed beds-mass balance investigations. Water Sci Technol 48(5):59–66. https://doi.org/10.2166/wst.2003.0281

Valsami-Jones, E (2001) Mineralogical controls on phosphorus recovery from wastewaters, 2001, Mineralogical Magazine, 65(5), 611–620. édition

Vohla C, Margit Kõiv H, Bavor J, Chazarenc F, Mander Ü (2011) Filter materials for phosphorus removal from wastewater in treatment wetlands—a review. Ecol Eng 37(1):70–89. https://doi.org/10.1016/j.ecoleng.2009.08.003

Stumm W, Morgan JJ (1996) Aquatic Chemistry–Chemical Equilibria and Rates in Natural Waters, 1996

Wang G, Wang Y, Gao Z (2010) Use of steel slag as a granular material: volume expansion prediction and usability criteria. J Hazard Mater 184(1–3):555–560. https://doi.org/10.1016/j.jhazmat.2010.08.071

Weber D, Drizo A, Twohig E, Bird S (2007) Upgrading constructed wetlands phosphorus reduction from a dairy effluent using EAF slag filters. Water Sci Technol 56(3):135–143

Wu Y, Yu Y, Zhou JZ, Liu J, Chi Y, Xu ZP, et Qian G (2012) Effective Removal of Pyrophosphate by Ca–Fe–LDH and Its Mechanism. Chem Eng J 179 (janvier): 72-79. https://doi.org/10.1016/j.cej.2011.10.053

Xue Y, Hou H, Zhu S (2009) Characteristics and mechanisms of phosphate adsorption onto basic oxygen furnace slag. J Hazard Mater 162(2–3):973–980. https://doi.org/10.1016/j.jhazmat.2008.05.131

Yamada H, Kayama M, Saito K, Hara M (1986) A fundamental research on phosphate removal by using slag. Water Res 20(5):547–557. https://doi.org/10.1016/0043-1354(86)90018-7

Yan Y, Sun X, Ma F, Li J, Shen J, Han W, Liu X, Wang L (2014) Removal of phosphate from etching wastewater by calcined alkaline residue: batch and column studies. J Taiwan Inst Chem Eng 45(4):1709–1716. https://doi.org/10.1016/j.jtice.2013.12.023

General conclusion

The management of industrial wastes and by-products is an important issue from both an economic and environmental point of view. According to their contamination level, the storage is costly and all alternative solutions could be more cost-effective. In addition, their reuse or re-employment could help preserve non-renewable natural resources, which is important in a context of climate emergency. Consequently, and in a sustainable development approach, the stabilization and/or identification of new valorization routes becomes a necessity. The civil and environmental engineering sector represents an interesting and viable field for the valorization of mineral wastes in the form of natural, recycled or even artificial aggregates.

The objective of this thesis work was to propose new approaches for the management of various mineral wastes within the sustainable development framework:

- Stabilization of Ba and Pb in WPFA by natural carbonation through a pilot scale.
- The preparation and characterization of lightweight aggregates from WPFA.
- The synthesis of LDH from two fly ashes WPFA and BFA and the treatment of a river sediment with the synthesized LDH.
- Stabilization of two hazardous wastes (SRS and BFA) in a geopolymer matrix and their technical and environmental performance assessment.
- The valorization of the two BBA_S as reactive filters for the retention of P from wastewater in treatment plants.

Firstly, the use of natural carbonation of WPFA as a treatment method to reduce the leaching of Ba and Pb was highly effective. The study systematically examined the effects of carbonation on material mineralogy, pollutant leaching, pH, pollutant speciation and acid neutralization capacity. The results obtained for this treatment have shown that natural carbonation significantly decreased the leaching of Ba and Pb below the IWSI threshold after only 7 days of treatment. During the carbonation process, the pH of WPFA decreased from 13.5 to 11.42 after 90 days. Considering that the WPFA was rich in CaO (64.02%), there is a consumption of lime/portlandite and the formation of hydration products such as ettringite, carboaluminate and carbonation products mainly $CaCO_3$ and $BaCO_3$ phases. Contrary to $BaCO_3$, the $PbCO_3$ was not identified by XRD and SEM/EDS, potentially due to their low concentrations. The XRD and SEM/EDS results were confirmed by TGA analyses, which showed that as carbonation time increases, portlandite consumption and hydrate formation becomes more important. Thus, the TGA results showed the presence of three different modes of calcium carbonates (aragonite, vaterite and calcite). The BCR sequential extraction procedure provided useful information for environmental risk assessment. Specifically, the BCR allowed an estimate of the MMTE that would be mobilized under different environmental conditions. The BCR results revealed that natural carbonation had a significant effect on the MMTE fractions in steps 1 and 2. The carbonated WPFA had higher values of the residual fraction (F4) of Ba and Pb than the standard conditions (without carbonation). In addition, the soluble fraction values decreased and the exchangeable fraction (F1) values increased for Ba and Pb after carbonation.

Secondly, the characterization of WPFA showed that the hydraulic properties of this industrial by-product are favorable to a valorization as lightweight aggregates due to the presence of the hydraulic phases such as mayenite and calcium silicate, in addition to lime. Therefore, WPFA was used for the production of lightweight aggregates by granulation with water in an Eirich high intensity granulator (Eirich R02). Several lightweight aggregate manufacturing optimizations were tested to improve the mass percentage of the targeted LWA (2-16 mm). The Liquid/Solid ratio (L/S) was set at 0.3 l/kg in order to completely hydrate the CaO. Subsequently, the turbine rotation speed was kept constant: 3000

rpm for the nucleation formation period and for the granulation growth period, in order to study the effect of the steel pan rotation speeds (85 rpm and 170 rpm), the rotation modes between the steel pan and the turbine (Countter corrent and Cross-current), and the granulation time (3, 6 and 9 min). The size distribution results of the LWAs produced with these two different rotation modes and different granulation times showed that by adjusting the granulation parameters of the Eirich high intensity granulator to a constant turbine speed (3000 rpm), steel pan rotation speed (170 rpm), rotation mode between turbine and steel pan in cross current and a granulation time of 3 min, 95% of the LWAs were produced with the target size (2 mm to 16 mm). In order to stabilize and decrease the mobility of Ba and Pb, and thus improve the physico-chemical properties of the fabricated LWAs, an accelerated carbonation protocol (under CO_2 pressure) was performed. The leaching results showed that the accelerated carbonation reduced the mobility of Ba and Pb with stabilization percentages exceeding 98% for both elements. SEM/EDS and TGA results confirmed the hydrate formation such as carboaluminates and ettringite due to the hydraulic properties of WPFA, and the formation of calcite precipitates as a layer on the surface and in the pores of LWA. The LWA characteristics are evaluated according to the NF EN 13055-1 standard in order to assess the influence of accelerated carbonation on the LWA characteristics and subsequently the possibility to valorize these eco-materials in concrete manufacturing. The characterization results showed the manufactured aggregates have low density and fitted well into the LWA category, the low density was due to the high porosity in the LWA, also confirming the significant water absorption capacity. After carbonation, the porosity percentage and water absorption decreased, which can be explained by the precipitation of calcite in the pores. The mechanical strength results of LWA were quite interesting and varied between 3.15 MPa and 7.6 MPa respectively before and after carbonation. Finally, the results of thermal conductivity are highly encouraging (between 0.19 W/m.°C and 0.32 W/m.°C before and after carbonation) and allows the improvement of thermal performance when introducing LWA in concrete.

Chapter 4 is dedicated to the study of river sediment from Noyelles-Sous-Lens. The immobilization processes of MMTE and anionic compounds was studied in the NSL sediment by LDH synthesized from WPFA and BFA Firstly, two LDHs were synthesized from WPFA and BFA by the acid leaching method followed by precipitation, a calcination step at 450°C was carried out in order to improve the adsorption capacity of LDHs. The characterization of the different LDH before and after the calcination at 450°C showed the formation of the new phases. The XRD of LDH_{WPFA} and LDH_{BFA} revealed the presence of the phases similar to HT, the main phases were in the form of Hydrocalumite $Ca_4Al_2(OH)_{12}(Cl,CO_3,OH)_2{\cdot}4H_2O$) and Paraalumohydrocalcite ($CaAl_2(CO_3)_2(OH)_4{\cdot}6H_2O$) for LDH_{WPFA} and LDH_{BFA} respectively. However, after calcination, the double lamellar structure collapsed in the different LDHs. The FTIR and SEM characterization results confirm the results obtained in the XRD, the FTIR characterization of the two synthesized LDHs show identical spectra to all the HT type phases. The vibrations corresponding to octahedral layer lattices, hydroxyl groups and interlamellar anions have been identified. Moreover, SEM imaging revealed the presence of hexagonal blocks and some octahedral shape, thus the presence of a characteristic morphology of double lamellar hydroxides (the platelet morphology). After the physicochemical characterization of the different LDH before and after calcination at 450°C, the LDH were used as adsorbent amendment to stabilize Sb, Zn and SO_4^{2-} in the SED_{NSL}. Geochemical stabilization as a batch and column treatment process was used in SEDNSL with the different LDH percentages. The results revealed that the different LDHs improve the quality of SED_{NSL} by decreasing the release of MMTE from 50 to 99%. Generally, the LDH synthesized from WPFA was the most effective, it is explained by the initial chemical composition which has a higher Ca/Al ratio compared to BFA which improved the lamellar structure. Batch leaching revealed that only HT-450 and LDH_{WPFA}-450 and from 15% addition can stabilize both Sb, Zn and SO_4^{2-} from SED_{NSL} below IWSI thresholds. However, LDH_{WPFA}-450 was the only amendment allowing the stabilization of

different MMTE and anionic compounds under SETRA thresholds for SED_{NSL} in column tests. Only 5% addition of LDH_{WPFA}-450 in column mode allows to have removal rates of problematic elements around 97% and 99%. Anion exchange, electrostatic attraction and surface complexation were the main mechanisms for the trapping of Sb, Zn and SO_4^{2-}. These investigations concluded that LDHs and in particular their calcination products, may be a low-cost alternative for sediment stabilization processes.

Chapter 5 was devoted to the encapsulation of SRS and BFA in a geopolymeric matrix. Both wastes present a hazardous character in view of release of various MMTE and anionic compounds such as As, Cr, Mo, Pb, Sb, Se and Zn. The stabilization approach combines geopolymerization (7 days) and accelerated carbonation (7 days) processes in order to trap and reduce the release of toxic elements in the aqueous medium. Three metakaolins were used as aluminosilicate sources (i) standard metakaolin (S), (ii) Fe-rich metakaolin (R), (iii) clay-rich metakaolin (P). Then the geopolymer matrices were formulated by alkaline activation (Alkaline solution: water+NaOH+Na_2SiO_3). The immobilization efficiency of the different MMTEs was determined on the basis of leaching tests. The experimental results showed that after geopolymerization, the extremely basic pH (>12.5) imposed by the alkaline solution increase the release of MMTE into the different geopolymers. After that the accelerated carbonation cure was applied, the pH of the mixture decreased and reached values below 10 which led to the more efficient immobilization of MMTE in the geopolymer matrix. The results of batch leaching tests showed that geopolymers based on MK R were more efficient than other metakaolin, either before or after carbonation, and allowed the stabilization of MMTE below the IWSI threshold after the accelerated carbonation phase. Based on the compressive strengths of the geopolymers before carbonation, the highest compression after 7 days was obtained by geopolymers based on MK R, after accelerated carbonation the compressive strengths increased for the different formulations, however, the formulation based on MK R always presents the highest strengths. Based on the results obtained in the compression and leaching tests, the physico-chemical characterizations were carried out only on the geopolymer based on MK R before and after carbonation. The TGA and SEM-EDS analyses results showed the presence of NASH-gel and ettringite after the geopolymer elaboration. The TGA and SEM-EDS analysis results showed the presence of NASH-gel and ettringite after the geopolymer elaboration. The SEM/EDS revealed the presence of the silicate phase which contains Pb, Mo, Cr, S and Zn. In addition to the increase in the calcite percentage in the geopolymers after accelerated carbonation. These results were confirmed by the results obtained in the XRD, a decrease in the intensity of the Pb and Pb-Sb peaks for SRS and of the Pb carrier phase for BFA, which suggests a change in the speciation of lead in the geopolymer matrices before and after carbonation. In the G-R-SRS rich in hematite (MK R), antimony was stabilized with iron forming $FeSbO_4$. In addition, Pb is trapping as lead silicate (Pb-Si) for G-R-SRS and G-R-BFA before and after carbonation. However, the leaching results versus pH for G-R-SRS and G-R-BFA indicate that both are not stable at extremely basic or acidic pH.

The last chapter studied the phosphorus ion removal by two types of BBA_S. The objective was to use them as filter media for wastewater phosphorus removal. Indeed, the high cost and the complexity of the classical processes (biological treatments and chemical precipitations) have led to the need to search for alternative technologies for the treatment of domestic wastewater that are reliable, simple to set up and inexpensive. The two BBA_S were used without any physical or chemical pre-treatment, the choice of the two BBA_S was then justified by their chemical composition, being rich in iron, aluminium, calcium and magnesium (oxyhydr)oxide with a high affinity for phosphorous ions. The novelty of the study lies on the one side in the multi-scale approach of the reactivity of the geomaterials, from the batch reactor to the column reactor and on the other side in the approach of the reaction mechanisms carried out by combining the study of the intrinsic physicochemical properties of the materials with the global analysis of the species released in solution. Several parameters were studied in order to understand the P trapping mechanisms on each filter such as material origin, particle size, chemical composition, initial

P concentration, CaO dissolution, water quality and pH. The P removal was first studied in batch reactors, with several parameters studied such as water quality (real and synthetic wastewaters), initial concentration and contact time. The batch results showed an increase in the P removal rate with increasing initial concentration and contact time (7 days). In particular, it was observed, for both materials, a strong increase of the phosphorus removal capacity (PRC) when real wastewater rich in Ca^{2+} was used, to finally reach a maximum value when the removal rate was below 100%. Based on the batch reactor results, some parameters were set to perform column tests such as water quality (real wastewater), flow rate (0.5 l/d) and initial P concentration (30 mg P/l). For an initial column input concentration of 30 mg P/l, the maximum P removal capacities in the columns ranged from 4.15 to 9.72 g P/kg after 8 months of experimentation for BBA_L and BBA_R, respectively. Thus, the pH values at the column outlet agreed with the discharge standards after 8 months of experimentation. A correlation between P concentration and Ca^{2+} ion concentrations versus pH was established, the Ca^{2+} concentration at the beginning of the experiment at the column outlet was very low which confirmed the precipitation of Ca-P compounds on the reactive filters, then with the increase of the reaction time the reactive surface sites of each filter were no longer available which generated the increase of the Ca^{2+} concentration at the column outlet until the inlet concentration equaled the outlet concentration. The efficiency order of the reactive filters was as follows: $BBA_R \geq BBA_L$ in agreement with the results obtained in a batch reactor and column tests. After 8 months of operation of the two BBA as reactive filters, homogeneous substrates were recovered in order to make the different physicochemical characterizations. The results of XRD, SEM-EDS and sequential extraction confirm that P was trapped in the BBA_S according to several trapping mechanisms mainly adsorption and precipitation. However, the main mechanism proceeds in three steps: **(i)** dissolution of CaO from BBA_S providing OH^- and Ca^{2+} ions and directly increasing the pH of the solution; **(ii)** precipitation of Ca-P on the filter surfaces at basic pH ($pH < 8.5$); **(iii)** accumulation and recrystallization of Ca-P as HAP, which is the most stable form.

Perspectives

The prospects envisaged at the term of this thesis are initially the study and the understanding of the behavior of various MMTE and toxic compounds in the solid matrixes after ageing under reuse or elimination conditions. Indeed, the sustainability of stabilization techniques should be checked prior applying these technologies at large scale in the field.

Natural carbonation tests at small scale have revealed interesting results for the stabilization of Pb and Ba in WPFA with leaching thresholds under IWSI. It is necessary in a first step to test the natural carbonation pathways by optimizing several parameters such as relative humidity, temperature, L/S ratio and CO_2 pressure. This approach can help to optimize and improve the efficiency of this process before its application at large scale under natural conditions.

The reuse of WPFA as lightweight aggregates showed acceptable performances, however, it is essential to improve the technical performances of manufactured LWAs. For example, (i) the use of various binders or agglomerating agents to improve the physicochemical properties, (ii) the partial or total substitution of ordinary aggregates by LWA in concrete formulations, and (iii) the use of mixtures of carbonated and non-carbonated LWA in concrete formulations.

Ashes as WPFA and BFA are suitable to stabilize pollutants in SED_{NSL} following their processing into LDHs with interesting stabilization performances. However, it is essential to optimize the synthesis parameters such as aging time and temperature, pH during the aging step, as well as crystallization time and temperature in order to improve the properties of synthesized LDHs. Subsequently, the LDHs have demonstrated their suitability for stabilizing Sb, Zn, and SO_4 in the SED_{NSL}. However, many questions remain open, including the long-term fate of the contaminants and the reversibility of the adsorption mechanisms after treatment and under specific storage conditions.

The encapsulation of the two hazardous wastes SRS and BFA in the carbonated geopolymer matrixes has shown the technical feasibility of this approach. Nevertheless, few studies are available on this topic and it will be desirable to carry out an in-depth characterization of the microstructure as well as the speciation of MMTE in geopolymer matrixes in order to estimate their long-term efficiency in this process. Thus, it is essential to test various curing times ranging from 28 to 90 days in order to examine the evolution of the mechanical strength and mobility of MMTE. Chemical sequential extractions can bring some additional information about the speciation of MMTE after immobilization through the geopolymer matrix.

Ashes have shown very interesting results and performances in the field of wastewater treatment for phosphorus (P) removal. The results have showed the capacity of P trapping by the two BBA_S in equilibrium batch and dynamic column reactors without any physicochemical pretreatment. However, in order to improve the description of the evolution of P species within the BBA_S over time, it would be essential to continue investigations by identifying the speciation of P by various ways (for example by using sequential extraction and surface spectroscopic analyses). In addition, it is interesting to test the two materials as reactive filters at pilot scale in wastewater treatment plant. This experiment will allow testing the efficiency of materials under field conditions with natural levels of P. Furthermore, it would be interesting to make a more detailed economic profitability study of the two BBA_S. In order to optimize the use of this tertiary treatment, it would be interesting to extend this study to the removal of other pollutants, in particular MMTE (Ag^+, Cr^{3+}, Cu^{2+}, Zn^{2+} Cd^{2+}, Ni^{2+}, Pb^{2+}, etc.) from wastewater by these geomaterials at different scales of investigation (batch, column, and field).

Appendix

Extraction	Reagents	Extraction conditions (nominal target phases)
Step 1	Acetic acid (60 mL, 0.11 mol.L^{-1}, 24 h, room temperature)	Exchangeable, water and acid-soluble (carbonates)
Step 2	Hydroxylammonium chloride (60 mL, 0.1 mol.L^{-1}, adjusted by HCl to pH 2, 24 h, room temperature)	Easily reduced (iron/manganese oxyhydroxides)
Step 3	Hydrogen peroxide (hydrogen peroxide solution 8.8 mol.L^{-1} adjusted by HNO_3 to pH 2, 15 mL, 2 h, 90 °C followed by hydrogen peroxide solution 8.8 mol.L^{-1} adjusted by HNO_3 to pH 2, 15 mL, 1 h, 90 °C, then by ammonium acetate solution 1 mol.L^{-1} adjusted by HNO_3 to pH 2, 75 mL, 24 h, room temperature)	Oxidizable (organic matter and sulfides)
Step 4	Aqua regia	Residual fraction

Table 1. Sequential extraction procedure

Components	inert	Non-hazardous	hazardous
As	0.5	2	25
Ba	20	100	300
Cr	0.5	10	5
Cu	2	50	70
Mo	0.5	10	30
Pb	0.5	10	50
Sb	0.06	0.7	5
Se	0.1	0.5	7
Zn	4	50	200
Cl	800	15 000	25 000
F	10	150	500
SO_4	1 000	20 000	50 000

Table 2. Leaching limit values for the acceptance of wastes in landfills Regulation (BRGM,2017) (mg/kg)

Major components (mg/kg)	WPFA	Carbonated LWA
Al	0.5±0.1	0.2±0.1
Ca	10 839 ± 521	451±7
Fe	<0.02	<0.02
K	2 990± 39	2839± 34
Mg	<0.13	<0.13
Mn	<0.014	<0.014
Na	891±13	739±16
P	<0.17	<0.17
S	9±0.4	2.1±0.3
Si	2±0.3	1.2±0.2

Table 1. Concentration of Major components in WPFA Carbonated LWA

Parameter (mg/kg)	SED_{NSL}	5% HT	10% HT	15% HT	5% HT-450	10% HT-450	15 % HT-450
As	<0.11	<0.11	<0.11	<0.11	<0.11	<0.11	<0.11
Ba	0.2±0.01	0.2±0.01	0.18±0.009	0.15±0.008	0.3±.009	0.3±0.01	0.3±0.01
Cd	0.013	<0.009	<0.009	<0.009	<0.009	<0.009	<0.009
Cr total	<0.004	<0.004	<0.004	<0.004	<0.004	<0.004	<0.004
Cu	0.9±0.04	0.7±0.03	0.7±0.03	0.6±0.03	**4.1±0.2**	**3.8±0.19**	**3.49±0.17**
Mo	0.14±0.007	0.14±0.007	0.13±0.006	0.16±0.008	0.1±0.009	0.17±0.008	0.14±0.007
Ni	0.17±0.008	0.16±0.0081	0.97±0.04	<0.04	<0.04	<0.04	<0.04
Pb	<0.03	<0.03	<0.03	<0.03	<0.03	<0.03	<0.03
Sb	**0.13±0.01**	**0.065±0.01**	**0.04±0.01**	**0.02±0.01**	**0.015±0.01**	**0.03±0.01**	**0.07±0.1**
Se	<0.08	<0.08	<0.08	<0.058	<0.058	<0.058	<0.058
Zn	**5.2±0.2**	**2.1±0.1**	**0.8±0.04**	**0.42±0.02**	**<0.01**	**<0.01**	**<0.01**
Chlorides	31±1.5	33±1.6	32±1.6	36±1.8	31±1.5	32±1.6	36±1.8
Fluorides	3±0.15	2±0.1	3±0.15	1±0.05	4±0.2	2±0.1	6±0.3
Sulphates	**13937±192**	**12 450±622**	**12 200±610**	**11 400±570**	**9 332±466**	**3 129±156**	**938±46**
Soluble fraction (mg/kg)	**24 260±1213**	**22 270±1113**	**22 950±1147**	**24 830±1241**	**15 320±766**	**8 032±401**	**2 103±105**
Conductivity ($mS.cm^{-1}$)	4.2±0.1	2.2±0.1	1.9±0.09	1.8±0.09	1.7±0.08	1.15±0.05	0.95±0.047
pH	6.95±0.2	7.25±0.2	7.65±0.2	7.92±0.2	10.03±0.2	10.45±0.2	10.89±0.2

Table 1. MMTE concentration leached from SED_{NSL} after treatment with HT and HT-450 (Batch).

Parameter (mg/kg)	SED_{NSL}	5% LDH_{WPFA}	10% LDH_{WPFA}	15% LDH_{WPFA}	5% LDH_{WPFA}-450	10% LDH_{WPFA}-450	15% LDH_{WPFA}-450
As	<0.11	<0.11	<0.11	<0.11	<0.11	<0.11	<0.11
Ba	0.2±0.01	0.2±0.01	0.3±0.016	0.6±0.03	0.18±0.009	0.16±0.008	0.1±0.007
Cd	0.013	<0.009	<0.009	<0.009	<0.009	<0.009	<0.009
Cr total	<0.004	0.05±0.002	0.1±0.005	0.09±0.004	<0.04	<0.04	<0.04
Cu	0.9±0.04	1.9±0.2	**2.7±0.25**	**3.2±0.2**	0.5±0.02	0.4±0.02	0.4±0.02
Mo	0.14±0.007	0.3±0.01	0.39±0.019	0.41±0.02	0.16±0.008	0.16±0.008	0.17±0.008
Ni	0.17±0.008	0.05±0.002	0.1±0.005	0.21±0.01	0.05±0.004	0.05±0.002	0.05±0.002
Pb	<0.03	<0.03	0.09±0.004	**0.49±0.02**	<0.03	<0.03	<0.03
Sb	**0.13±0.006**	**0.014±0.03**	**0.009±0.001**	**0.005±0.001**	**0.015±0.002**	**0.011±0.004**	**0.005±0.001**
Se	<0.08	<0.058	<0.058	<0.058	<0.058	<0.058	<0.058
Zn	**5.2±0.2**	**0.16±0.008**	**0.6±0.03**	**1.5±0.07**	**0.6±0.03**	**0.3±0.01**	**0.1±0.005**
Chlorides	31±1	102±3	209±11	294±15	98±2	219±12	301±17
Fluorides	3±0.15	2±0.1	6±0.3	2±0.1	6±0.3	5±0.25	4±0.2
Sulphates	**13937±192**	**10 420±521**	**8 282±414**	**4 180±209**	**5 770±288**	**2 369±118**	**632±31**
Soluble fraction (mg/kg)	**24 260±1213**	**19 963±998**	**12 498±624**	**9 369±468**	**11 203±560**	**6 398±319**	**1 820±91**
Conductivity ($mS.cm^{-1}$)	4.2±0.1	5.75±0.2	3.91±0.1	2.75±0.1	10±0.5	6.4±0.3	3±0.1
pH	6.95±0.2	10.94±0.4	11.92±0.3	12.3±0.1	11.98±0.3	12.34±0.2	12.45±0.2

Table 2. MMTE concentration leached from SED_{NSL} after treatment with LDHWPFA and LDHWPFA-450 (Batch).

Parameter (mg/kg)	SED_{NSL}	5% LDH_{BFA}	10% LDH_{BFA}	15% LDH_{BFA}	5% LDH_{BFA}-450	10% LDH_{BFA}-450	15% LDH_{BFA}-450
As	<0.11	<0.11	<0.11	<0.11	<0.11	<0.11	<0.11
Ba	0.2±0.01	0.14±0.004	0.25±0.007	0.39±0.011	0.18±0.005	0.166±0.004	0.15±0.004
Cd	0.013	<0.009	<0.009	<0.009	<0.009	<0.009	<0.009
Cr total	<0.004	0.03±0.0009	0.07±0.002	0.07±0.002	<0.04	<0.04	<0.04
Cu	0.9±0.04	**3.2±0.2**	**6.8±0.38**	**9.25±0.33696**	**15±0.4**	**15.2±0.4**	**14.5±0.4**
Mo	0.14±0.007	0.2±0.008	0.3±0.009	0.3±0.01	0.16±0.04	0.16±0.04	0.17±0.005
Ni	0.17±0.008	<0.04	<0.04	0.05±0.01	0.08±0.002	0.05±0.01	0.05±0.01
Pb	<0.03	<0.03	<0.03	0.04±0.01	<0.03	<0.03	<0.03
Sb	**0.13±0.006**	**0.042±0.001**	**0.03±0.009**	**0.01±0.003**	**0.019±0.005**	**0.01±0.005**	**0.006±0.001**
Se	<0.08	**0.08±0.002**	<0.058	<0.058	<0.058	<0.058	<0.058
Zn	**5.2±0.2**	**2.9±0.5**	**1.6±0.4**	**0.9±0.1**	**0.7±0.1**	**0.4±0.1**	**0.1±0.05**
Chlorides	31±1.55	**5 394±161**	**9 452±283**	**16 328±489**	**5 693±170**	**10 034±301**	**1 7 691±530**
Fluorides	3±0.15	4±0.12	2±0.06	6±0.1	5±0.2	4±0.1	3±0.09
Sulphates	**13937±192**	**10 370±311**	**9 841±295**	**8 720±261**	**6 827±204**	**6 458±93**	**6083±182**
Soluble fraction (mg/kg)	**24 260±1213**	**29 234±547**	**36 789±443**	**43 468±344**	**25 203±336**	**38 327±429**	**45 269±398**
Conductivity ($mS.cm^{-1}$)	4.27±0.1	13.9±0.4	18.9±0.5	21.6±0.6	12.7±0.3	17.3±0.5	24.9±0.7
pH	6.95±0.2	9.7±0.3	10.54±0.3	11.12±0.2	11.98±0.3	12.34±0.15	12.45±0.16

Table 3. MMTE concentration leached from SED_{NSL} after treatment with LDH_{BFA} and LDH_{BFA}-450 (Batch).

Parameter (mg/kg)	0.1	0.2	5	1	2	5	10	15	20
As	<0.11	<0.11	<0.11	<0.11	<0.11	<0.11	<0.11	<0.11	<0.11
Ba	0.01	0.03	0.08	0.17	0.29	0.56	0.88	1.30	1.78
Cd	<0.09	<0.09	<0.09	<0.09	<0.09	<0.09	<0.09	<0.09	<0.09
Cr total	<0.04	<0.04	<0.04	<0.04	<0.04	<0.04	<0.04	<0.04	<0.04
Cu	0.27	0.81	1.9	3.3	5.3	8.4	13	18.5	25.8
Mo	0.06	0.02	0.04	0.08	0.12	0.16	0.2	0.3	0.5
Ni	0.001	0.005	0.01	0.04	0.08	0.14	0.23	0.35	0.46
Pb	<0.04	<0.04	<0.04	<0.04	<0.04	<0.04	<0.04	<0.04	<0.04
Sb	0.01	0.01	0.03	0.05	0.06	0.09	0.09	0.09	0.09
Se	<0.04	0.001	0.007	0.01	0.03	0.05	0.05	0.05	0.05
Zn	0.005	0.002	0.007	0.02	0.04	0.1	0.2	0.6	1.1
Chlorides	1	3	8	9	13	21	29	33	35
Fluorides	0.5	0.9	1.6	2.9	3	3	3	3.1	3.1
Sulphates	122	370	990	2 188	4 433	8 593	13 373	18 711	24 429
Conductivity ($mS.cm^{-1}$)	3.53	3.55	3.91	3.70	3.20	1.95	1.36	1.10	0.69
pH	7.74	7.73	7.82	7.91	7.94	7.57	7.62	7.38	7.27

Table 4. MMTE cumulative concentrations leached from SED_{NSL} (Column)

Parameter (mg/kg)	0.1	0.2	0.5	1	2	5	10	15	20
As	<0.11	<0.11	<0.11	<0.11	<0.11	<0.11	<0.11	<0.11	<0.11
Ba	0.009	0.02	0.07	0.14	0.25	0.38	0.61	0.88	1.2
Cd	<0.09	<0.09	<0.09	<0.09	<0.09	<0.09	<0.09	<0.09	<0.09
Cr total	<0.04	<0.04	<0.04	<0.04	<0.04	<0.04	<0.04	<0.04	<0.04
Cu	0.003	0.01	0.08	0.4	1.1	2.4	3.4	5.3	7.5
Mo	0.001	0.005	0.01	0.05	0.09	0.17	0.3	0.4	0.6
Ni	<0.09	<0.09	<0.09	<0.09	<0.09	<0.09	<0.09	<0.09	<0.09
Pb	<0.09	<0.09	<0.09	<0.09	<0.09	<0.09	<0.09	<0.09	<0.09
Sb	0.006	0.002	0.006	0.02	0.03	0.05	0.05	0.05	0.05
Se	0.01	0.01	0.01	0.01	0.01	0.01	0.01	0.01	0.01
Zn	0.002	0.002	0.03	0.05	0.01	0.03	1.06	1.1	1.1
Chlorides	2	3	7	9	14	20	28	36	42
Fluorides	0.3	0.9	1 .3	1.7	2.3	2.4	2.8	2.8	2.9
Sulphates	81	250	714	1 684	3 584	7 764	13 208	19 337	2 5683
Conductivity (mS.cm^{-1})	2.82	2.84	3.13	2.96	2.56	1.56	1.09	0.88	0.55
pH	7.76	7.6	7.49	7.48	7.48	7.46	7.62	7.19	7.37

Table 5. MMTE cumulative concentrations leached from SED_{NSL} after treatment with 5% HT-450 (Column).

Parameter (mg/kg)	0.1	0.2	0.5	1	2	5	10	15	20
As	<0.11	<0.11	<0.11	<0.11	<0.11	<0.11	<0.11	<0.11	<0.11
Ba	0.01	0.04	0.1	0.19	0.3	0.6	0.9	1.4	2
Cd	<0.09	<0.09	<0.09	<0.09	<0.09	<0.09	<0.09	<0.09	<0.09
Cr total	0.007	0.002	0.04	0.06	0.01	0.01	0.02	0.02	0.03
Cu	0.08	0.29	0.7	2.1	4.8	9.1	14.07	19.5	24.8
Mo	0.005	0.01	0.03	0.07	0.14	0.25	0.4	0.4	0.4
Ni	0.001	0.01	0.05	0.01	0.03	0.03	0.03	0.03	0.03
Pb	<0.03	<0.03	<0.03	<0.03	<0.03	<0.03	<0.03	<0.03	<0.03
Sb	<0.03	<0.03	<0.03	<0.03	<0.03	<0.03	<0.03	<0.03	<0.03
Se	0.001	0.005	0.01	0.02	0.02	0.02	0.02	0.02	0.02
Zn	0.005	0.001	0.03	0.06	0.11	0.18	0.28	0.35	0.45
Chlorides	1.9	3.9	7	9.3	12	19	31	38	40
Fluorides	0.3	0.9	1 .3	1.7	2.3	2.4	2.8	2.8	2.9
Sulphates	75	248	688	1 627	3 554	7 945	13 736	17 276	19 136
Conductivity (mS.cm^{-1})	3.12	2.93	2.62	2.41	1.96	1.22	0.88	0.73	0.71
pH	7.6	7.62	7.56	7;42	7.49	7.52	7.37	7.6	7.62

Table 6. MMTE cumulative concentrations leached from SED_{NSL} after treatment with 10% HT-450 (Column).

Parameter (mg/kg)	0.1	0.2	0.5	1	2	5	10	15	20
As	<0.11	<0.11	<0.11	<0.11	<0.11	<0.11	<0.11	<0.11	<0.11
Ba	0.01	0.03	0.08	0.17	0.32	0.62	1.02	1.5	2.02
Cd	<0.09	<0.09	<0.09	<0.09	<0.09	<0.09	<0.09	<0.09	<0.09
Cr total	0.007	0.002	0.05	0.01	0.01	0.02	0.03	0.04	0.05
Cu	0.19	0.62	1.8	4.14	8.5	15.6	23.5	31.8	39.7
Mo	0.02	0.01	0.03	0.07	0.13	0.24	0.3	0.5	0.5
Ni	0.09	0.002	0.002	0.012	0.03	0.03	0.03	0.03	0.03
Pb	<0.03	<0.03	<0.03	<0.03	<0.03	<0.03	<0.03	<0.03	<0.03
Sb	<0.03	<0.03	<0.03	<0.03	<0.03	<0.03	<0.03	<0.03	<0.03
Se	0.002	0.006	0.01	0.02	0.0	0.04	0.04	0.04	0.04
Zn	0.0002	0.0002	0.001	0.001	0.004	0.01	0.01	0.01	0.1
Chlorides	2	3	7	9	14	20	28	36	42
Fluorides	0.3	0.9	1 .3	1.7	2.3	2.4	2.8	2.8	2.9
Sulphates	72	250	720	1 722	3 294	5 880	11 844	15 916	15 994
Conductivity ($mS.cm^{-1}$)	2.13	2.53	2.40	1.96	2.19	1.66	1.15	0.91	0.73
pH	7.55	7.51	7.56	7.68	7.21	7.33	7.71	7.77	7.05

Table 7. MMTE cumulative concentrations leached from SED_{NSL} after treatment with 15% HT-450 (Column).

Parameter (mg/kg)	0.1	0.2	0.5	1	2	5	10	15	20
As	<0.11	<0.11	<0.11	<0.11	<0.11	<0.11	<0.11	<0.11	<0.11
Ba	0.005	0.03	0.04	0.1	0.1	0.2	0.5	0.78	1
Cd	<0.09	<0.09	<0.09	<0.09	<0.09	<0.09	<0.09	<0.09	<0.09
Cr total	<0.04	<0.04	<0.04	<0.04	<0.04	<0.04	<0.04	<0.04	<0.04
Cu	0.1	0.5	2.1	5.2	9.8	15.2	24.6	36. 4	49.4
Mo	0.01	0.02	0.07	0.1	0.2	0.4	0.6	1	1.2
Ni	0.02	0.007	0.03	0.09	0.18	0.2	0.4	0.5	0.7
Pb	<0.03	<0.03	<0.03	<0.03	<0.03	<0.03	<0.03	<0.03	<0.03
Sb	<0.03	<0.03	<0.03	<0.03	<0.03	<0.03	<0.03	<0.03	<0.03
Se	0.001	0.005	0.01	0.02	0.05	0.05	0.05	0.05	0.05
Zn	0.1	0.3	0.01	0.05	0.05	0.06	0.06	0.06	0.06
Chlorides	1.9	3.9	7	9.3	12	19	31	38	40
Fluorides	0.3	0.9	1.3	1.7	2.3	2.4	2.8	2.8	2.9
Sulphates	35	146	403	861	1 563	2 291	3 529	5 112	7 043
Conductivity ($mS.cm^{-1}$)	2.61	3.05	3.62	3.43	2.80	1.74	1.26	1.04	1.02
pH	11.9	11.92	12.02	12	11.91	11.9	11.71	11.53	11.49

Table 8. MMTE cumulative concentrations leached from SED_{NSL} after treatment with 5% LDH_{WPFA}-450 (Column).

Parameter (mg/kg)	0.1	0.2	0.5	1	2	5	10	15	20
As	<0.11	<0.11	<0.11	<0.11	<0.11	<0.11	<0.11	<0.11	<0.11
Ba	0.01	0.03	0.08	0.1	0.3	1.1	3.7	7.4	11.4
Cd	<0.09	<0.09	<0.09	<0.09	<0.09	<0.09	<0.09	<0.09	<0.09
Cr total	<0.04	<0.04	<0.04	<0.04	<0.04	<0.04	<0.04	<0.04	<0.04
Cu	0.2	0.8	2.1	4.3	7.4	11.8	16.9	23	30.6
Mo	0.01	0.03	0.07	0.13	0.7	0.3	0.43	0.5	0.8
Ni	0.005	0.01	0.04	0.1	0.2	0.3	0.45	0.62	0.8
Pb	<0.03	<0.03	<0.03	<0.03	<0.03	<0.03	<0.03	<0.03	<0.03
Sb	0.004	0.01	0.02	0.05	0.07	0.10	0.16	0.16	0.16
Se	0.002	0.007	0.02	0.04	0.06	0.06	0.06	0.06	0.06
Zn	0.001	0.001	0.001	0.007	0.04	0.15	0.36	1.01	1.7
Chlorides	2	3	7	9	14	20	28	36	42
Fluorides	0.3	0.9	1 .3	1.7	2.3	2.4	2.8	2.8	2.9
Sulphates	17	48	127	251	481	875	1 320	1 831	1 971
Conductivity (mS.cm^{-1})	4.27	2.58	3.06	2.90	2.37	1.48	1.06	0.88	0.86
pH	12.07	12.09	12.18	12.28	12.34	12.37	12.37	12.35	12.33

Table 9. MMTE cumulative concentrations leached in column tests from SED_{NSL} after treatment with 10% LDH_{WPFA}-450

Parametre (mg/kg)	0.1	0.2	0.5	1	2	5	10	15	20
As	<0.11	<0.11	<0.11	<0.11	<0.11	<0.11	<0.11	<0.11	<0.11
Ba	0.01	0.04	0.1	0.3	0.7	2.5	7.6	16.7	28.7
Cd	<0.09	<0.09	<0.09	<0.09	<0.09	<0.09	<0.09	<0.09	<0.09
Cr total	<0.04	<0.04	<0.04	<0.04	<0.04	<0.04	<0.04	<0.04	<0.04
Cu	0.2	0.8	1.9	3.3	5.3	8.4	13	18.5	25.8
Mo	0.006	0.02	0.04	0.08	0.12	0.16	0.2	0.38	0.56
Ni	0.005	0.01	0.03	0.07	0.13	0.21	0.35	0.50	0.71
Pb	0.001	0.005	0.01	0.05	0.16	0.52	1.16	2.56	4.4
Sb	0.005	0.01	0.03	0.05	0.06	0.09	0.09	0.09	0.09
Se	0.002	0.006	0.01	0.03	0.05	0.05	0.05	0.05	0.05
Zn	0.0005	0.002	0.007	0.02	0.04	0.1	0.23	0.6	1.1
Chlorides	1.9	3.9	7	9.3	12	19	31	38	40
Fluorides	0.3	0.9	1 .3	1.7	2.3	2.4	2.8	2.8	2.9
Sulphates	7	23	66	157	297	559	842	937	953
Conductivity (mS.cm^{-1})	1.83	2.13	2.53	2.40	1.96	1.22	0.88	0.73	0.71
pH	12.3	12.29	12.29	12.47	12.48	12.55	12.56	12.57	12.67

Table 10. MMTE cumulative concentrations leached in column tests from SED_{NSL} after treatment with 15% LDH_{WPFA}-450

Immobilization study of As, Cr, Mo, Pb, Sb, Se and Zn in geopolymer matrix: application to shooting range soil and biomass fly ash

Figure 1. Bullet fragments in shooting range soil (SRS)

Components	inert	Non-hazardous	hazardous
As	0.5	2	25
Ba	20	100	300
Cr	0.5	10	5
Cu	2	50	70
Mo	0.5	10	30
Pb	0.5	10	50
Sb	0.06	0.7	5
Se	0.1	0.5	7
Zn	4	50	200
Cl	800	15 000	25 000
F	10	150	500
SO_4	1 000	20 000	50 000

Table 1. Leaching limit values for the acceptance of wastes in landfills (BRGM, 2017) (mg/kg).